

**Protection and release of small molecules
via chemiluminescent protection groups
(CLPG)**



Inaugural-Dissertation

zur

Erlangung des Doktorgrades

der Mathematisch-Naturwissenschaftlichen Fakultät

der Universität zu Köln

Vorgelegt von

Tim Lippold

aus Neuss

Köln, 2023

Tag der mündlichen Prüfung: 15.03.2024

Erstgutachter: Prof. Dr. Axel G. Griesbeck

Zweitgutachter: Prof. Dr. Stephanie Kath-Schorr

„Come forth into the light of things,

let nature be your teacher.”

William Wordsworth, “The Tables Turned”, 1798.

Danksagung

Als erstes möchte ich mich herzlichst bei meinem Doktorvater Herrn Prof. Dr. *Axel G. Griesbeck* für die Aufnahme in seinen Arbeitskreis und die Möglichkeit diese Arbeit mit einem für mich faszinierendem Thema anzufertigen bedanken.

Frau Prof. Dr. *Stephanie Kath-Schorr* danke ich herzlich für die freundliche Übernahme des Zweitgutachtens dieser Arbeit.

Ich bedanke mich bei allen ehemaligen Mitarbeitern des Arbeitskreises: Dr. *Murat Atar*, Dr. *Diana But*, Dr. *Christina Bold*, Dr. *Angelika Eske*, Dr. *Florian Gaida*, Dr. *Sven Hohenberg*, Dr. *Jens Lefarth*, Dr. *Melissa Renner*, Dr. *Moritz Vollmer* und Dr. *Banu Öngel* für die schöne und entspannte Zeit. Letzterer danke zusätzlich ich für die musikalische und durchgedrehte Zeit im Labor 212. Ohne dich war es deutlich langweiliger im Labor. Besonders möchte ich dem „harten Kern“, also Dr. *Carolina Fendinger*, *Seyma Bozkuş* und *Matthias Spilles*, sowie *Jan van Stiphoudt* danken. Jedes Mittagessen, sowie die Nachmittags-Kaffee Besprechungen inklusive der vielen (un-)wissenschaftlichen Gespräche brachten immer sowohl neue Denkanstöße, als auch Erheiterungen. Zudem werde ich mir die Konferenz in Amsterdam dank euch sehr gut in Erinnerung behalten! Es verleitet immer wieder zum Schmunzeln, wenn man vom „Rolls Royce akquirieren“ oder dem „Bushalte-Boxsack/Oh meine Ohren!“ spricht. Und wo wir bei Konferenzen sind: meine „letzte“ Konferenz in Japan war eine schöne und prägende Erfahrung. Ein jeder von euch Dreien hat hier wirklich gefehlt und was verpasst!

Ein großer Dank gilt *Matthis Jonen*, *Linda Jütten*, *Matthias Spilles*, und *Dominik Albat*, welche sich allesamt Zeit genommen haben, um diese Arbeit Korrektur zu lesen.

Auch dem ehemaligen und aktuellen Arbeitskreis Goldfuß, dazu gehörend: Dr. *Florian Dato*, Dr. *Eric Brüllingen*, Dr. *Falco Fox*, Dr. *Elnaz Hobbollahi*, Dr. *Florian Wolf*, *Nadine Dernbach*, *Francesca Fortugno*, *Denis Sartakov*, *Saskia Thuns* und *Xiaochen Wang* danke ich für eine entspannte und kooperative Atmosphäre auf der roten Etage.

Ebenso möchte ein herzliches Dankeschön an meinen „AK Lippold“ ausrichten, welcher einen großen und essentiellen Beitrag zu dieser Arbeit geleistet haben. Zu diesem gehören: *Lea Luxenberger*, *Hooman Ghazi Zahedi*, *Nils Siefert*, *Robert Herzhoff* (*Großes Dankeschön für die DFT-Berechnungen!*), *Meike Kreuter*, *Uxue Agirre*, *Eva Van Doeselar*, *Leonie Wilczek*, *Satishbhai Badarukhiya*, *Julia Kosopalova*, *Anna Keimer* und *Sophie Lüggert*. Ich danke euch aus tiefstem Herzen; ohne euch wäre diese Dissertation nicht möglich gewesen.

Dr. *Jörg Neudörfl* danke ich für die Strukturaufklärung mittels Röntgenbeugung und Herrn *Michael Neihls* für die Aufnahme der Massen-Spektren und die schnelle Bestimmung der exakten Massen. Ebenso danke ich der gesamten NMR-Abteilung: Dr. *Nils Schlörer*, Dr. *Dolores Díaz Hernandez*, Dr. *Daniel Friedrich*, Dr. *Philipp Hegemann*, *Daniela Nauman* und *Kathrin König* für die Messung sämtlicher Proben.

Dietmar Rutsch, *Andreas Wallraf*, *Thomas Dautert* und der gesamten Werkstatt von Herrn *Hartmann* danke ich dafür, dass sie bei jeglichen technischen und digitalen Problemen sofort zur Stelle waren und den täglichen Betrieb des Labors gewährleistet haben.

Ein großer Dank gilt den guten Arbeitskollegen aus der „AC“ *Niko Flosbach* und *Dr. Laura Straub* aus dem *AK Wickleder*, welche sämtliche zeitabhängigen Lumineszenz-Messungen für meine Proben durchführten. Ebenso danke ich *Theresa Gehlich*, die sich bei jeglichen Fragen und Problemen zum Thema „Enzym-Experimente“ immer Zeit für mich nahm.

Des Weiteren möchte ich den Menschen danken die mir das tägliche „Feierabend-Leben“ außerhalb des Labors versüßt haben. Zu diesen gehören: *Henning Jonas* und *Matthis Jonen*; mit euch beiden ist jedes Unternehmen eine Garantie für viele chaotische, wahnsinnige und humorvolle Momente. Die spontanen Unternehmungen, Partys sowie die gemeinsamen „Corona-Nachmittage“ mit Fußball (auch wenn ich diesen Sport hasse) und erfrischender Limonade, fühlten sich immer so an als würde man mit seinen Brüdern unterwegs sein. *Dana Barnett*; den Berlin-Trip 2019 werde ich für immer in Erinnerung behalten und die Zocker- und Zeichensessions ermöglichten es auch der kreativen Hälfte des Gehirns mal tätig zu werden. *Sascha Schäfer*, *Benedict Witulski* und *Christopher Seabreeze*; die Pandemie hatte unseren Kontakt stark reduziert. Dennoch konnten wir ab und an eine gemeinsame Mittagspause genießen oder uns privat treffen und über unsere gemeinsame Studentenzeit sinnieren. Oder wie unfassbar schwer wir es doch als Doktoranden/Masteranden haben/hatten.

(Nochmals) *Robert Herzhoff*, *William Pappas* (aka the insane Aussie guy), sowie einem Großteil des *AK Meerholzes* danke ich für die Integration in die ausschweifenden Mittwoch-Feierabend Runden, wo wir uns immer einen gemütlichen Platz am „Mäuerchen“ zum Entspannen sichern konnten. Mit den Herren *Dominik Albat* und *Lars Hemmersbach* war es regelmäßig möglich sich privat oder direkt in der Uni zu treffen, um sich gepflegt über chemische Synthesprobleme und den sonstigen Wahnsinn im Labor zu beschweren. Das ein oder andere Getränk hat dabei auch geholfen. *Linda Jütten* und *Katharina von Schoeler* (inklusive ihrem wundervollen Freund *Oguzhan* „Oma gib Handtasche“ *Kara*); der rituelle „Date-Donnerstag“ geprägt von exotischem Essen, schlechten Fernsehserien und

ausschweifenden Konversationen mit euch sorgte jedes Mal für Vorfreude und war ein kurzer Urlaub für die Seele. An meinen großartigen Nachbarn bzw. halben WG-Partner *Oliver Morawietz*: Ich bin dankbar, dass du mein „Flurnachbar“ wurdest. Seit nun 10 Jahren kennen wir uns und die sporadischen Unternehmungen, sowie ein ritueller und exzellent schmeckender Sonntags-Kaffee mit ausschweifenden und stundenlangen Konversationen war immer etwas Besonderes!

Ein herzlichstes Dankeschön ist meinem *Freundesklan* gewidmet, den ich teilweise seit meiner Zeit im Kindergarten kenne. Zu diesen gehören die „Freunde auf Lebenszeit“: *Sven Schneider, Stanislav Fischer, Alexander Turobin, Helena Geibel, Nicolas Treese, Daniel Heckhausen, Philip Bernardy, Maximilian Pell, Aileen Sondermann* sowie *Michael* und *Frauke Birkhoff*. Unabhängig davon wie lange man sich nicht gesehen hat, ein Treffen mit euch lässt einen glauben als „wäre es erst gestern gewesen“. Mögen wir auch in der Zukunft weiterhin immer aufeinander bauen können. Komme was da wolle!

Abschließend möchte ich meiner kleinen aber feinen Familie danken: meinen Eltern *Karin* und *Martin Lippold*, meiner Stiefmutter *Gisela Lippold*, meiner „zweiten Mutter“ *Dorothea Kreischer* (inklusive ihrer wundervollen Familie), meinen Cousins *Ella* und *Sierra Lippold*, meiner Tante *Anne Lippold*, sowie der gesamten Familie *Axmacher* und *Mutz*. Ich bin glücklich euch alle zu haben und danke euch vom ganzen Herzen, dass ihr immer an mich geglaubt und mich motiviert habt.

Abbreviations

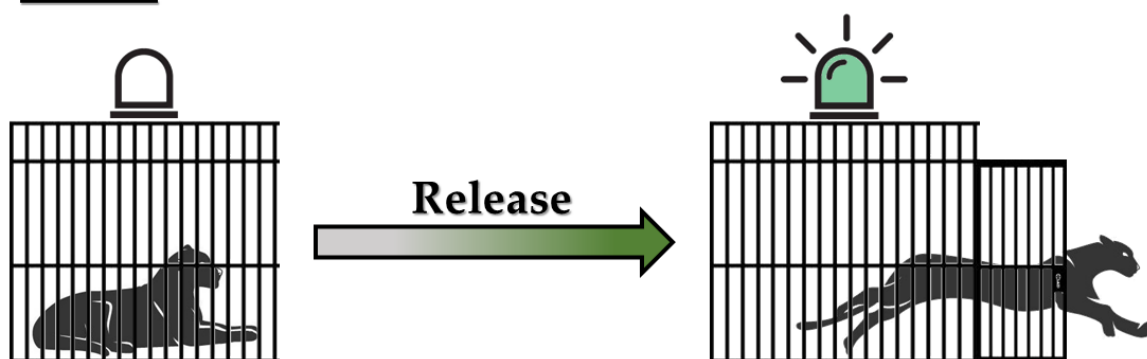
λ	wavelength	HMBC	heteronuclear multiple bond correlation
ν	frequency	HR-MS	high resolution mass spectrometry
δ	chemical shift	HRP	horse radish peroxidase
ϵ	molar absorption coefficient	Hz	Hertz
Φ	quantum yield	IC	internal conversion
AcOH	acetic acid	ISC	intersystem crossing
ATP	adenosine triphosphate	IR	infrared
AMP	adenosine monophosphate	J	joule
BL	bioluminescence	J	coupling constant
c	concentration	LG	leaving group
<i>c</i> -Hex	cyclohexane	M	molar
CIEEL	chem.-initiated electron-exchange luminescence	MeCN	acetonitrile
CL	chemiluminescence	min	minute
CLPG	chemiluminescent protection group	MP	melting point
CTIL	charge-transfer-induced luminescence	NMR	nuclear magnetic resonance
COSY	correlated spectroscopy	PG	protection group
CSI	chlorosulfonyl isocyanate	PPG	photoremovable protection group
d	day	PP ₁	inorganic pyrophosphate
DBU	diazabicycloundecene	ppm	parts per million
DCM	dichloromethane	R _f	retardation factor
DMSO	dimethylsulfoxide	rt	room temperature
E	energy	SET	single electron transfer
EBT	electron back transfer	TFA	trifluoroacetic acid
EDTA	ethylenediaminetetraacetic acid	TLC	thin layer chromatography
Et ₂ O	diethylether	UV	ultraviolet
EtOAc	ethylacetate	Vis	visible light
Eq.	equation	VR	vibronic relaxation
eq.	equivalent		
ESI	electron-spray ionisation		
ET	electron transfer		
eV	electronvolt		
FG	fluorescent group		
FPG	fluorescent protection group		
GAM	glyoxylic acid monohydrate		
GP	general procedure		
h	hour		
HEI	high energy intermediate		

Kurzzusammenfassung

In der synthetischen Chemie sind Schutz und selektive Entschützung von funktionellen Gruppen äußerst wichtige Prozesse. Bei der Entschützung wird die Schutzgruppe (engl. **PG**) entfernt und die ursprüngliche Reaktivität wiederhergestellt. Die lichtinduzierte Entschützung, entweder durch direkte Absorption oder durch photokatalytische Methoden, beinhaltet die elektronische Anregung des PG-FG-Paares und die anschließende Freisetzung des Substrats. Diese Gruppen werden als photodegradierbare (oder “photoreleasable”) Schutzgruppen (engl. **PPG**) bezeichnet.

In dieser Arbeit wurden 2-Cumaranone, insbesondere solche mit Harnstoff-, Carbamat- und Thiolcarbamat-Substrukturen, wobei letztere in dieser Arbeit zum ersten Mal beschrieben wurden, im Hinblick auf die Bandbreite der Substrate untersucht, die mit einem Cumaranon geschützt werden können, inklusive einer Studie der Lumineszenz und des Entschützungsprozesses für das Konzept der chemolumineszenten Schutzgruppen (engl. **CLPG**).

CLPG:



Mittels ^1H - und ^{13}C -NMR wurde die Zersetzungsreaktion der Cumaranone im Detail untersucht, um eine effiziente Freisetzung und die Natur der Nebenprodukte zu ermitteln. Zusätzlich wurden Zeitintervall-Lumineszenzmessungen durchgeführt, um das Abklingen der Chemolumineszenz sowie die Änderungen der Absorptions- und Fluoreszenzeigenschaften der während der Entschützung gebildeten neuen Produkte zu verfolgen.

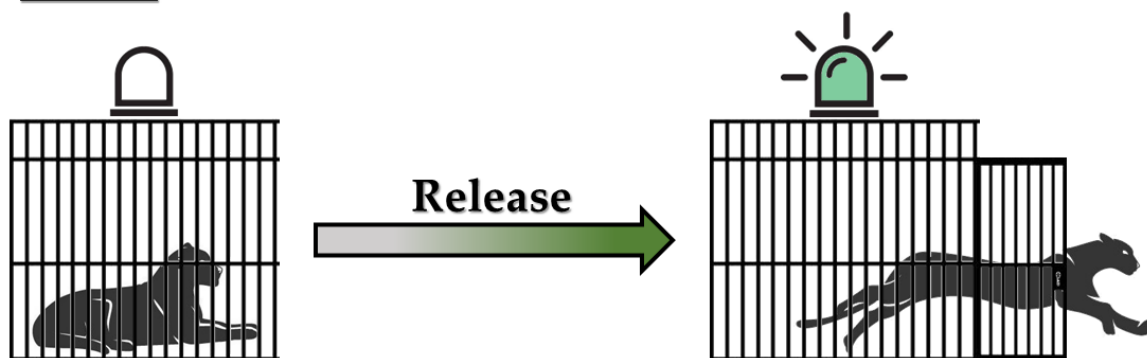
Der besondere Vorteil von CLPGs ist die In-situ-Kontrolle der Syntheseschritte, da die deutlich sichtbare Chemolumineszenz die erfolgreiche und vollständige Spaltung der PG nachweist. Darüber hinaus wäre es im Hinblick auf bildgebende Verfahren, z.B. für medizinische Anwendungen, möglich, eine Verbindung sowohl räumlich als auch zeitlich innerhalb eines biologischen Systems zu bestimmen.

Abstract

In synthetic chemistry, protection and selective deprotection of functional groups are highly important tools. The protecting group (**PG**) is removed in the deprotection step and the original reactivity is recovered. A light-induced removal, either by direct absorption or by photocatalytic methods, involves the electronic excitation of the PG-FG couple and subsequent cargo release. These groups are named photoremovable (or photoreleasable) protecting groups (**PPG**).

In this work, 2-coumaranones, especially those with an urea-, carbamate- and thiolcarbamate-substructure, with the latter being described for the first time in this work, were thoroughly investigated in terms of the range of substrates that can be protected with a coumaranone together with a detailed analysis of the luminescence and the deprotection process for the concept of chemiluminescent protection groups (**CLPG**).

CLPG:



Via ^1H - and ^{13}C -NMR, the decomposition reaction of the coumaranones was investigated in detail in order to determine an efficient release and byproducts. Additionally, time interval luminescence measurements were performed tracing the decay of the chemiluminescence as well as the changes of absorption and fluorescence properties of the new products formed during the deprotection.

The main advantage of CLPGs is the in-situ control of synthesis steps, since the clearly visible chemiluminescence verifies the successful and complete cleavage of the PG. Furthermore, in terms of imaging techniques, e.g., for medical applications, it would allow determination of a compound in space and time (“spatiotemporal”) within a cell or tissue.

Table of contents

1. Introduction	1
2. State of knowledge	2
2.1 The chemistry of protection groups in organic synthesis	2
2.2 History and development.....	2
2.3 Orthogonality of protection groups: Classification and lability	6
2.3.1 Acid-labile PGs ^[1-3]	6
2.3.2 Base-labile PGs ^[1-3]	8
2.3.3 Oxidation-labile PGs ^[1-3]	10
2.3.4 Reduction-labile PGs ^[1-3]	10
2.3.5 Cleavage of PGs by heavy metals or transition metal catalysis ^[1-3]	12
2.3.6 Fluoride-labile PGs ^[1-3]	13
2.3.7 Enzyme-labile PGs ^[1-3]	15
2.3.8 “Two-Stage” and “Safety Catch” PGs ^[2,3]	16
2.3.9 Photolabile PGs ^[50-52]	17
2.4 Photophysical processes and luminescence ^[113-115]	24
2.4.1 Jablonski diagram ^[114,116]	25
2.4.2 Franck-Condon-Principle ^[113-115]	27
2.4.3 Types of luminescence ^[117]	28
2.5 Definition and evolution of bioluminescence ^[124]	29
2.6 Bioluminescent reactions ^[124,137]	32
2.6.1 BL reactions involving a peroxo HEI.....	33

2.6.2 BL reactions involving a dioxetanone HEI	39
2.7 Definition and history of chemiluminescence ^[115,137]	43
2.7.1 Quantum yield, intensity and efficiency of CL-processes ^[115,137,220]	44
2.7.2 Chemiexcitation: CIEEL and CTIL mechanism ^[137]	45
2.7.3 Types of chemiluminescent reactions.....	48
3. Task and motivation	56
4. Results and discussion.....	58
4.1 Protection and deprotection of amines	58
4.1.1 General protection protocol of amines	59
4.1.2 Investigations of urea-coumaranones via NMR ^[300]	65
4.1.3 CL of urea-coumaranones ^[300]	73
4.1.4 Conclusions on the chemistry of urea-coumaranones ^[300]	79
4.2 Protection and deprotection of alcohols	82
4.2.1 General protection protocol of alcohols	82
4.2.2 Investigations of carbamate-coumaranones via NMR ^[300]	86
4.2.3 CL of carbamate-coumaranones ^[300]	91
4.2.4 Conclusions on the chemistry of carbamate-coumaranones ^[300]	96
4.3 Protection and deprotection of thiols.....	97
4.3.1 General protection protocol of thiols.....	97
4.3.2 Investigations of thiolcarbamate-coumaranones via NMR	101
4.3.3 CL of thiolcarbamate-coumaranones.....	103
4.3.4 Conclusions on the chemistry of thiolcarbamate-coumaranones	108

4.4 Decomposition with HRP and urease.....	109
4.4.1 CL with HRP.....	112
4.5 Theoretical calculations on the photophysical properties of 409A	117
5. Summary and outlook	120
6. Experimental section	128
6.1 General experimental requirements.....	128
6.1.1 Analysing methods	128
6.2 General procedures.....	131
6.3 Experimental section	136
6.3.1 Synthesis of urea derivatives	136
6.3.2 Carbamate and <i>S</i> -organyl thiocarbamate syntheses.....	171
6.3.3 Protection of Substrates with Coumaranones.....	190
6.3.4 Decomposition experiments	255
7. Analytical data and spectra.....	273
7.1 NMR spectra of selected compounds	273
7.1.1 Urea, carbamate and thiol carbamate precursors.....	273
7.1.2 Compounds protected by coumaranones.....	293
7.1.3 Decomposition experiments	326
7.1.3 CL and photoluminescence spectra of coumaranone compounds.....	336
8. Literature	338
9. Appendix	365
9.1 Data of X-ray crystal measurements	365

10. Erklärung zur Dissertation.....	367
11. Curriculum vitae.....	368

1. Introduction

When dealing with polyfunctionalised substrates, the individual reactivity of similar functional groups must be differentiated and selectively switched off and on so that unwanted side reactions are prohibited. Especially the syntheses of rather complex target molecules established the systematic introduction and cleavage of protecting groups (PG), accompanied by the release of the protected molecule (Figure 1). There are multiple options for the protection of every known functional group, that can be cleaved in various ways.

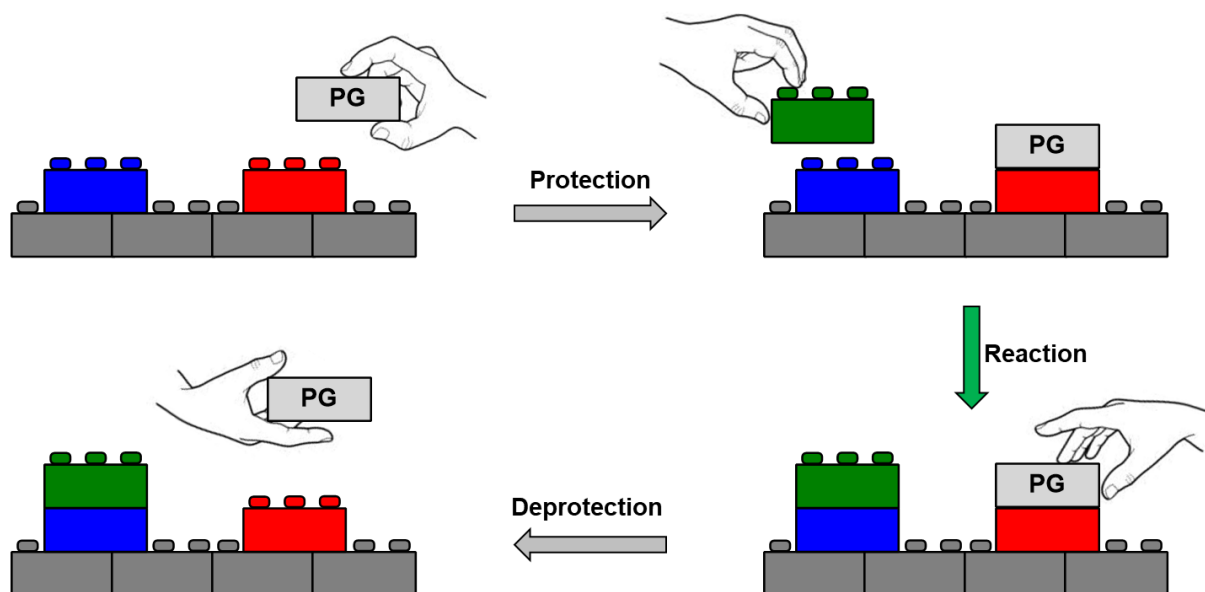


Figure 1: Simplified scheme for the concept and application of a protective group. One functional group is protected and therefore inhibited for the subsequent reaction. Afterwards the protective group is removed again and the synthesis route is complete.

Considering that PGs require additional steps in an often multi-step synthesis, the requirements for the latter are high to ensure a simple and efficient introduction and removal. Besides cost efficiency, stability and easy identification by spectroscopic methods, the selectivity of the cleavage of a PG is a particularly important aspect. Depending on its lability the usage of acids/bases, reductants/oxidants or enzymes has to result in a high yield of the deprotected substrate. In addition to chemical methods, there are also physical methods such as visible or UV light for photoremovable protecting groups (PPG) that enable the release of PGs when they interact with electromagnetic radiation, which increases the possibilities for an optimal synthesis route.

2. State of knowledge

2.1 The chemistry of protection groups in organic synthesis

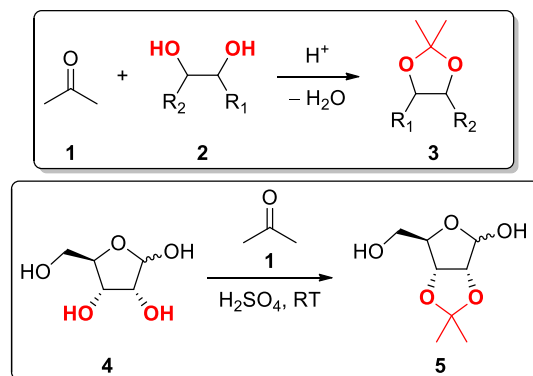
The term protecting group (PG) is defined as a substituent within a molecule that inhibits the reactivity of a functional group to prevent an undesired side reaction at that specific site. Standard requirements that must be met for a PG to be considered efficient are: I) Selective protection of a functional group with high yield; II) High stability towards the intended reactions and work-up procedures; III) Selective removal with cheap, available and preferably non-toxic reagents; IV) It must not generate a new stereogenic centre, but instead a derivative that can be easily separated from its byproducts upon formation or cleavage. V) The PG should not have many functional groups itself to avoid further possible side reactions.^[1-3] In any multistep synthesis, the best options are those that do not involve the use of PGs because of the minimum of two additional reaction steps (formation and cleavage). The chemistry of PGs therefore represents an important discipline within organic chemistry and is still critically discussed, improved and further developed until today.

2.2 History and development

With the use of increasingly complex structures and the increasing difficulty of targeted synthesis of specially designed building blocks, pharmaceuticals and natural products, the use and demand for PGs increased. A single PG can never completely fulfil all needed requirements for the same functional group in different substrates. Therefore, there are a large number of different PGs for a given functional group in order to generate several derivatives that are stable under certain reaction conditions.

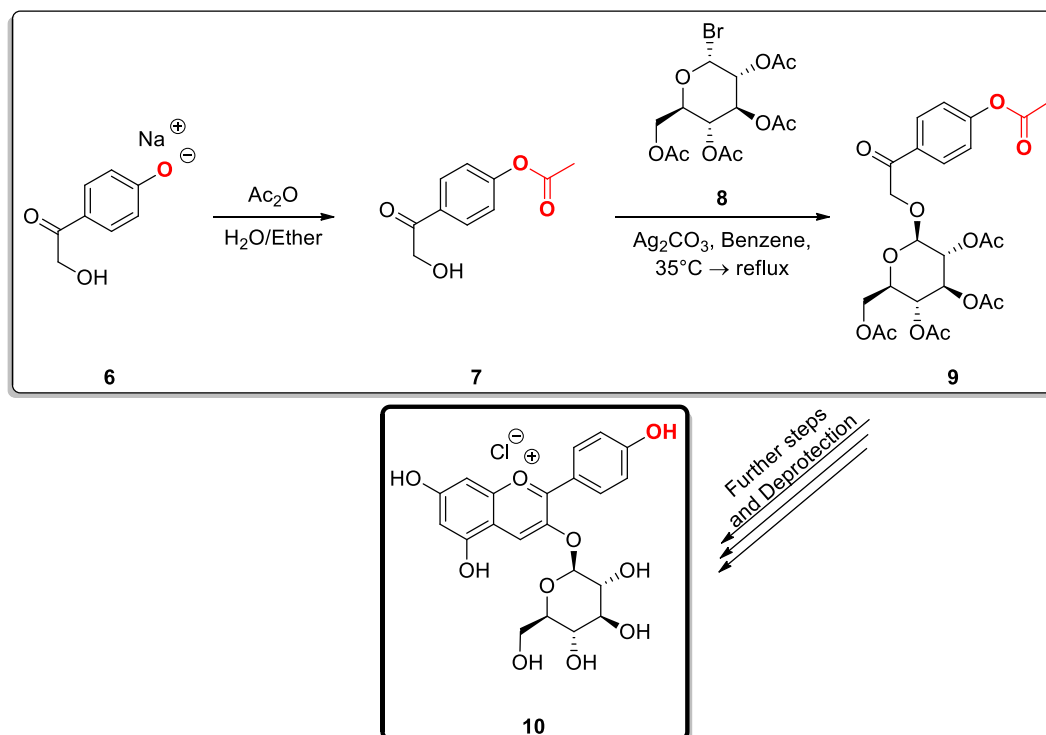
At the end of the 19th century a lot of literature was published discussing the synthesis of carbohydrate derivatives with the discover of selective protection of hydroxy and 1,2-diol groups. In particular, the work of *Emil Fischer*, who made enormous contributions to carbohydrate and purine chemistry in the 19th and 20th centuries^[4,5] and was awarded with the Nobel prize in 1902, has shown that it was possible to produce mono-, di- or triacetonide derivatives of various sugars using acetone (**1**)^[6,7] in a mildly acidic environment and to selectively synthesise either diacetonide or monoacetonide of a particular carbohydrate.^[8] In addition to the already known acetylated sugars, the acetal derivatives were more easily accessible and could in part be selectively protected and deprotected, which enabled, for example, the synthesis of benzylated sugars.^[9] This would lead to the targeted elaboration of

the acetal/ketal protecting group, which is still preferably used to protect 1,2- or 1,3-diols of carbohydrates (Scheme 1).^[10]



Scheme 1: Reactions for the synthesis of 1,3-dioxolanes, (Top) Illustration of the general protection of a i.e., 1,2-diol **2** using acetone (**1**); (Bottom) Selected example of the protection of D-ribose (**4**) with acetone (**1**) in sulfuric acid by Kim et al.^[11]

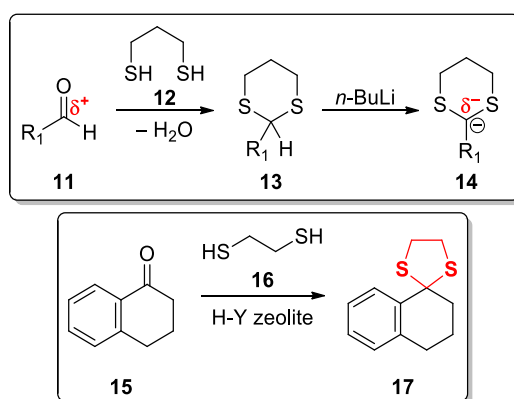
Another famous example is the synthesis of callistephin chloride (**10**), in which the sodium salt of 4-(2-hydroxyacetyl)phenol (**6**) was selectively protected with acetic anhydride to give the corresponding acetate **7** (Scheme 2).^[12] The aliphatic hydroxyl group remained free and was substituted with acetate-protected bromine glucoside **8** in the presence of silver carbonate. Further reaction and deprotection steps gave the desired product **10**.



Scheme 2: Synthesis of callistephin chloride (**10**).^[12]

The growing interest in the total synthesis of vitamins, steroids, antibiotics, or alkaloids is related to the increasingly sophisticated and targeted use of protecting groups. In the period from the 1940s to the 1970s, *Robert B. Woodward* (Nobel Prize winner 1965) established several total syntheses of various natural products^[13–15] in which the introduction and deprotection of PGs was implemented and optimised, with the production of the vitamin B₁₂ (cobalamin) molecule in collaboration with *Albrecht Eschenmoser* as the culmination of his research.^[16,17]

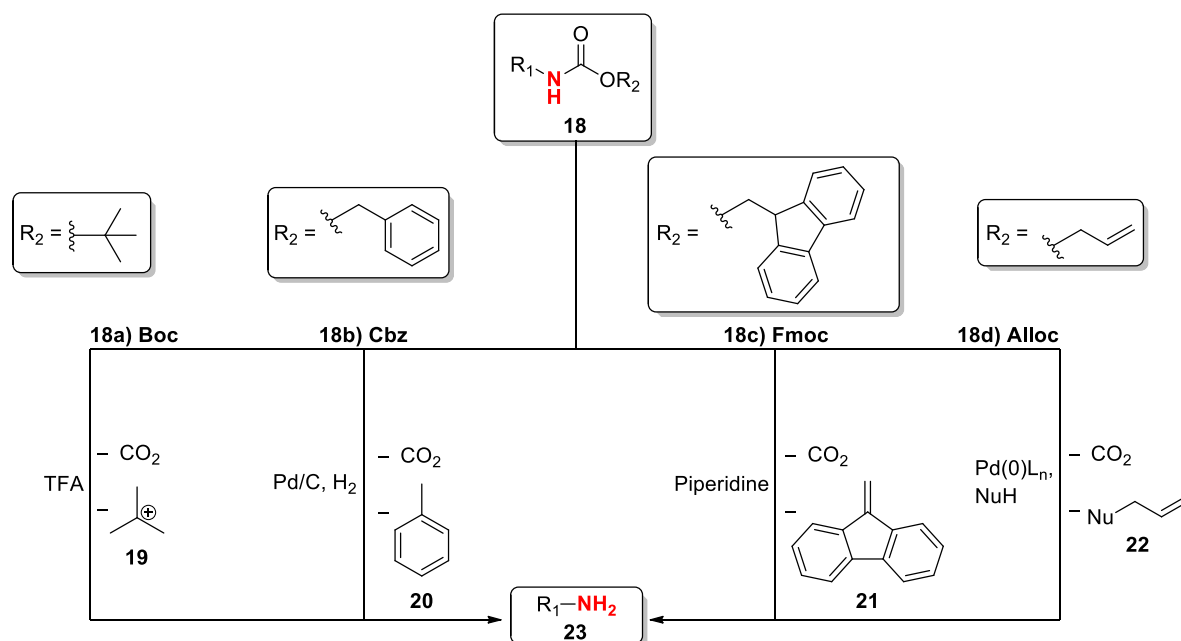
In 1965, *Elias James Corey* (Nobel Prize winner 1990) and *Dieter Seebach* investigated 1,3-dithianes as potential PGs for carbonyl groups and also developed the concept of "Umpolung" (Scheme 3).^[18,19] In addition to the advantageous ability to convert aldehydes into potent nucleophiles, *S,S*-acetals/ketals are more resistant towards hydrolysis than their *O,O*-counterparts^[2] and have a good stability to acidic and alkaline reaction conditions, which makes them a viable option for protecting carbonyl groups to this day.^[20]



Scheme 3: (Top) Illustration of the Umpolung of an aldehyde **11**, using propane-1,3-dithiol (**12**). The obtained 1,3-dithiane **13** can be deprotonated yielding the carbanion **14** and thus switching the polarity of the carbon atom^[18]; (Bottom) Selected example of the protection of 1-tetralone (**15**) with H-Y zeolite by Kumar et al.^[21]

In addition to organic chemical research, the development of PGs also led to significant breakthroughs in peptide synthesis, which played an increasingly important role in biochemistry and medicine and opened the way to more efficient and selective synthesis methods. Since amines are strongly nucleophilic and basic groups, great efforts were made to develop PGs for this functional group, leading to a huge variety of options.^[1,2]

A large number of amino-PGs are based on the backbone of carbamates, which can be easily produced with the help of chloroformates or (pyro)carbonates. The driving force of deprotection is based on the release of CO₂, which is achieved by various options (Scheme 4).^[2]



Scheme 4: Illustration of the different deprotection options of carbamate protected amines (18).^[1,2] a) Boc-PG (*tert*-butyloxycarbonyl), cleaved by protonolysis; b) Cbz-PG (benzyloxycarbonyl), cleaved by hydrogenolysis; c) Fmoc-PG (9-fluorenylmethoxycarbonyl), cleaved by β -elimination with piperidine; d) Alloc-PG (allyloxycarbonyl), cleaved by metal-assisted nucleophilic substitution.^[22] CO₂ is released in all reactions.

The large variety of carbamate alternatives allows a selective cleavage, so that the right PG is available depending on the planned synthesis. Beginning in 1963^[23], *Robert Bruce Merrifield* (Nobel Prize winner 1984) took advantage of these PGs for amine groups and developed the solid-phase peptide synthesis (SPPS). This method is based on successive reactions of amino acids, preferably protected by carbamate PGs immobilised on a solid matrix, resulting in a repetitive mechanism in which each coupling is followed by deprotection.^[24] This major breakthrough revolutionised the automated synthesis of peptides and today plays a central role in medical research and development, especially in the development of new peptide drugs that can fulfil specific biological functions. Targeted modifications of the peptide structure can improve properties such as stability, efficacy and selectivity.^[25]

2.3 Orthogonality of protection groups: Classification and lability

The entire repertoire of available protective groups is divided into orthogonal groups. The orthogonality of PGs means that when using multiple PGs of a different type, each protecting group can be cleaved individually and in any order by the different cleavage reagents without attacking a PG of another orthogonal group (Figure 2).

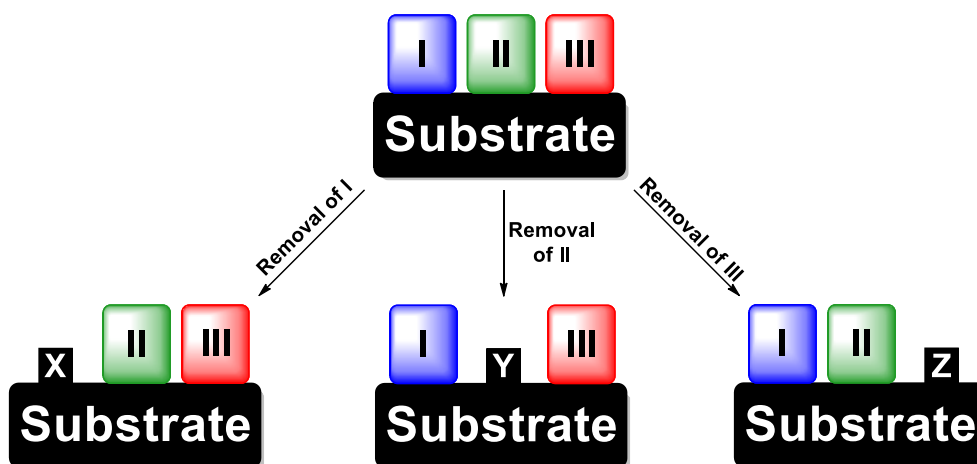


Figure 2: Concept of orthogonal PGs. A substrate with three different functional groups (X, Y and Z) is protected by different PGs (blue, green and red). According to the principle of orthogonality, each PG can be selectively cleaved in a specific order without removing any other PG. Modified according to [3].

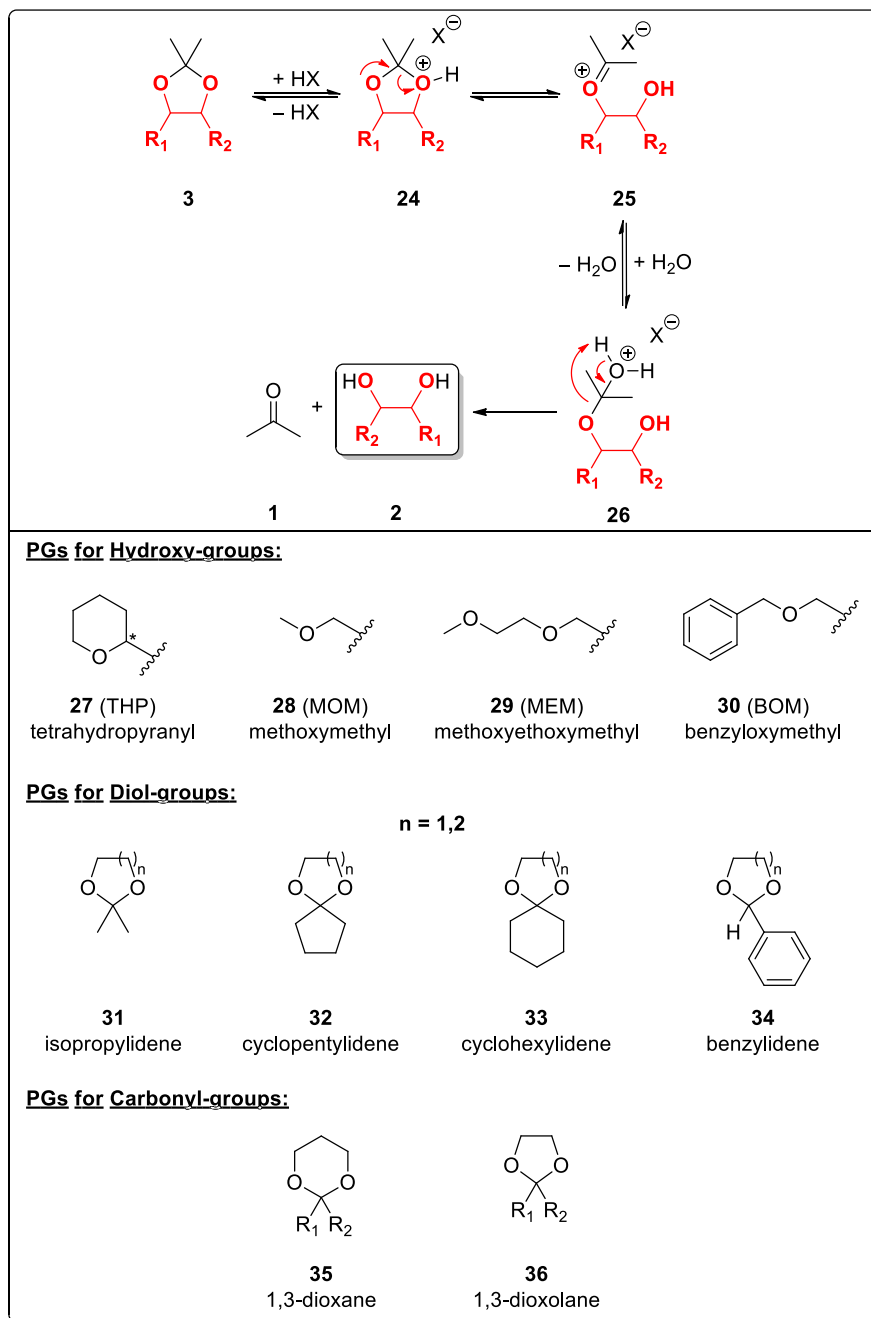
Overall, there are many orthogonal sets, which in turn can be divided into further subclasses. In the following, these sets are briefly introduced, explained and the deprotection mechanism is illustrated with classic examples.

2.3.1 Acid-labile PGs^[1-3]

In general, many PGs can be considered acid labile, depending on the applied acid and conditions for the deprotection so that those with mild conditions are preferred and commonly used in synthesis. The orthogonal set of acid labile PGs can be divided into two subclasses: a) *O,O*-acetals and b) PGs that enable the formation of stable carbenium ions.

The first subclass of *O,O*-acetals are PGs, which are formed and cleaved in acidic environments. Acyclic acetals are primarily used to protect hydroxy groups and are less stable than cyclic acetals, which are preferred for carbonyl compounds as well as for 1,2- or 1,3-diols, depending on which functional group needs to be shielded (Scheme 5). Deprotection is initiated by protonation or Lewis acids and produces a resonance-stabilised oxonium ion that

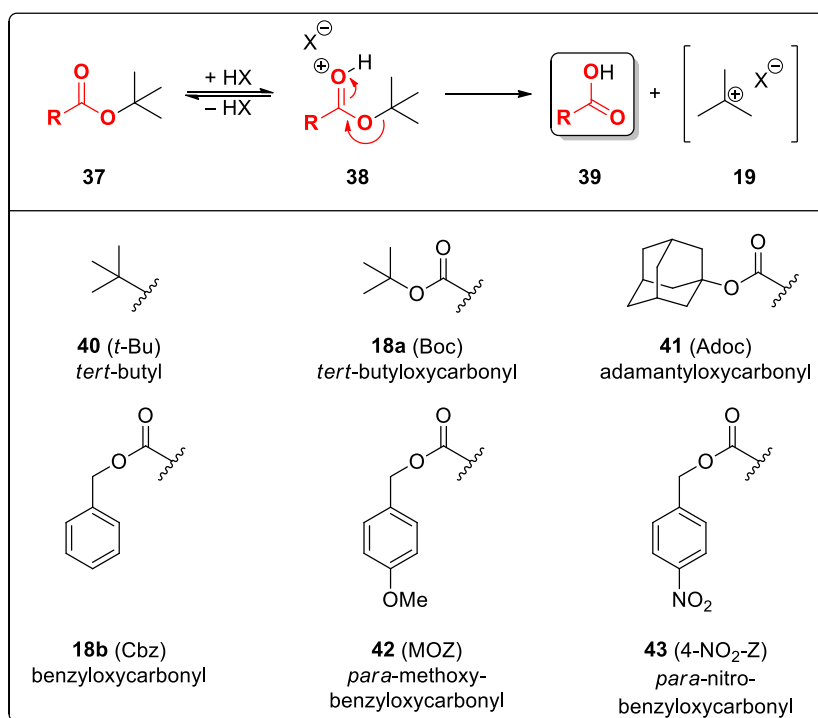
decomposes in the presence of water (or other nucleophiles) into two alcohols/a diol and a carbonyl compound.



Scheme 5: (Top) Hydrolysis mechanism of a diol protected as an acetal **3**. An acidic environment initiates the decomposition, generating the oxonium ion intermediate **25** and after the addition of water yielding acetone (**1**) and the diol **2**; (Bottom) Examples of acid labile *O,O*-acetals for alcohols, carbonyl-groups and diols. Modified according to [2,3].

The second subclass represents PGs that are heterolytically cleaved at a C–O bond of an ether, ester or urethane (e.g., Boc-PG) in an acidic environment, producing the deprotected substrate and a stabilised tertiary alkyl or benzyl carbenium ion (Scheme 6, Top). These are widely used for the protection of alcohols, thiols, amines and esters. Due to the wide range of groups and their varying labilities, different acids can be used which, if several acid-labile

PGs are present, can enable selective deprotection due to the required acid strength. Furthermore, the specific substitution of benzylic PGs leads to an increased or decreased stability of the obtained carbenium ion and thus has an influence on its lability (Scheme 6, bottom).

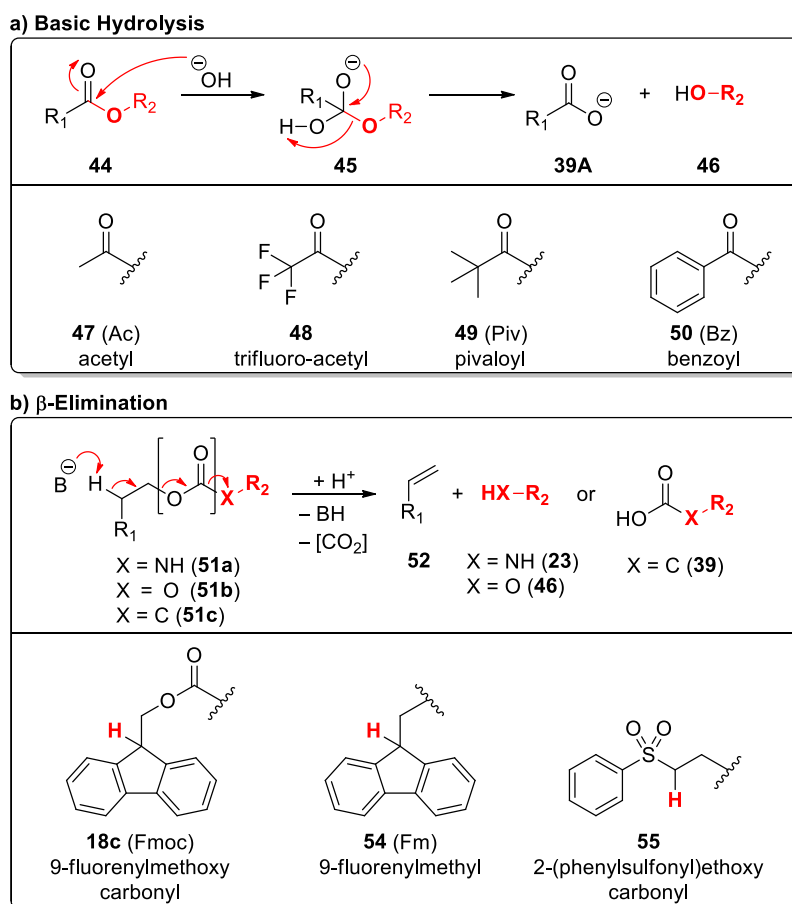


Scheme 6: (Top) Hydrolysis mechanism of a i.e., *tert*-butyl protected carboxylic acid **37**. An acidic environment initiates the decomposition, yielding the free acid **39** and the *tert*-butyl cation (**19**); (Bottom) Examples of acid labile PGs which are mainly used for the protection of alcohols and amines that generate CO₂ (except **40**) and stable cations. Modified according to [2,3].

2.3.2 Base-labile PGs^[1-3]

Similar to acid-labile PGs there are two subclasses for base-labile PGs consisting of a) deprotection via direct basic hydrolysis or b) deprotection via base-induced β -elimination. The mechanistic consideration for both subclasses differs due to the function of the base, which acts either as a nucleophile or a deprotonating base. Carboxylic acids are preferably protected as alkyl esters using alcohols. Vice versa many ester/amide derivatives of alcohols, thiols and amines are easily synthesised which can be very finely tuned in terms of their hydrolysis rate by adjusting the steric and electronic properties depending on the reaction conditions (Scheme 7a). This allows selective cleavage of one base-labile PG, while others remain intact due to the vastly different hydrolysis/reaction rates, with differences of up to

1:100.000.^[26] Due to the low leaving group potential of amines and the therefore required aggressive reaction conditions, the corresponding amides are rarely used for basic hydrolysis. An exception are phthalimides, which have a much higher electrophilicity. Following the *Gabriel* synthesis, the use of hydrazine enables the quick release of primary amines.

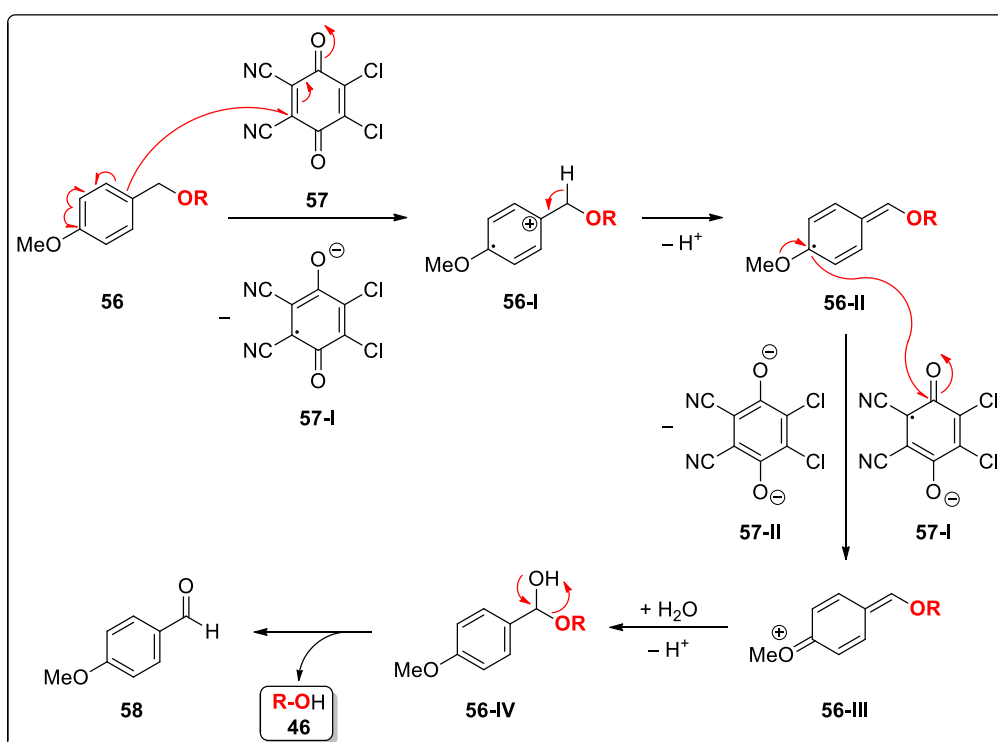


Scheme 7: (Top, upper part) Basic hydrolysis of an ester **44**. The saponification yields the free deprotonated acid **39A** and the alcohol **46**; (Top, lower part) Examples of base-labile PGs, which can be hydrolysed; (Bottom, upper part) β -elimination of a PG. If X represents a hetero atom the carboxyl group is part of the PG and removed via decarboxylation; (Bottom, lower part) Examples of base-labile PGs that are cleaved via β -elimination. Modified according to ^[2,3].

The other base-labile PG set is not directly hydrolysed, but deprotonated and cleaved by β -elimination (Scheme 7b). The abstraction of a proton is made possible by the fact that the resulting carbanion benefits from the stabilising effects of the aromatic system or electron accepting groups within the PGs, making it a viable option for amines, alcohols and, when using the Fm-PG **54**, carboxylic acids^[27].

2.3.3 Oxidation-labile PGs^[1-3]

There is only a small number of oxidation-labile PGs and their use is therefore limited. Alcohols and diols protected as electron-rich methoxy-substituted benzyl ethers are readily oxidised by dichlorodicyanoquinone (DDQ, **57**)^[28] or cerium (IV) ammonium nitrate (CAN)^[29] (Scheme 8). The rates of cleavage vary greatly depending on the ether used, which can be exploited in syntheses. Another important class of oxidation labile-PGs are *S,S*-acetals, which have a high stability towards hydrolysis and various nucleophiles. The oxidation of the sulfur atoms facilitates cleavage and therefore allows a selective deprotection in the presence of *O,O*-acetals.

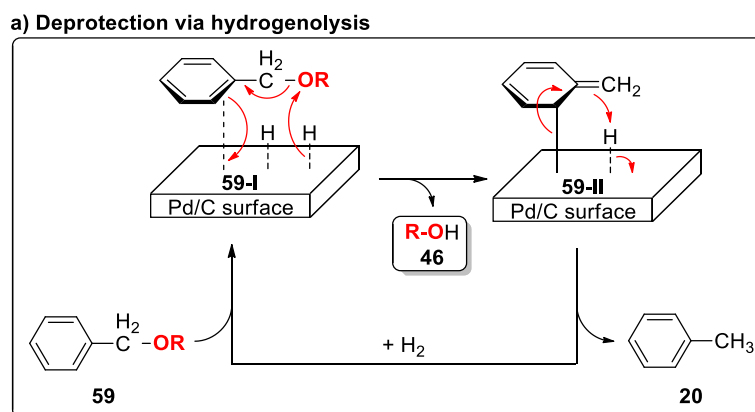


Scheme 8: Illustration of the oxidation of a methoxy-substituted benzyl ether **56** with DDQ (**57**). After two SET processes and the addition of water, the ether **56** is oxidised to the corresponding aldehyde **58**, releasing the former protected alcohol **46**. Modified according to ^[2,3].

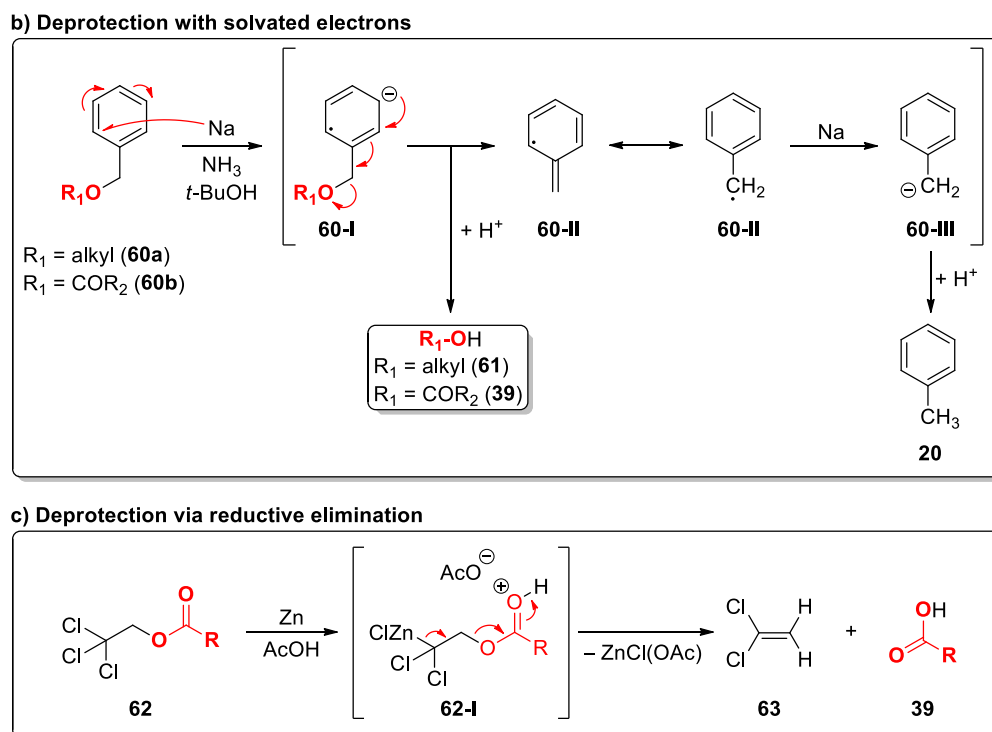
2.3.4 Reduction-labile PGs^[1-3]

This orthogonal set consists of a large number of PGs that can be removed by various reductive conditions. Altogether, there are three groups of subclasses depending on the reaction conditions, the reducing agent and the associated different cleavage mechanism: a) deprotection by hydrogenolysis, b) by reduction with a dissolved metal and c) by reductive

elimination. Deprotection by hydrogenolysis is a preferred method of choice because of the mild conditions and high tolerance to many functional groups. The benzyl-PG used to protect alcohols, carboxylic acids, amines and diols in the form of ethers, carbonates, esters, carbamates and benzylidene acetals is easily cleaved in the presence of hydrogen and a transition metal such as Pd (Scheme 9).



Scheme 9: Illustration of the hydrogenolysis of a benzyl ether. The benzyl ether **59** coordinates to the surface of palladium (**59-I**). Hydrogen is bound to the metal by oxidative addition. The alcohol **46** is split off by addition of a hydride to the oxygen atom, which shifts electron density towards the aromatic moiety (**59-II**). After reductive elimination, toluene (**20**) is released and the cycle repeats. Modified according to [2].



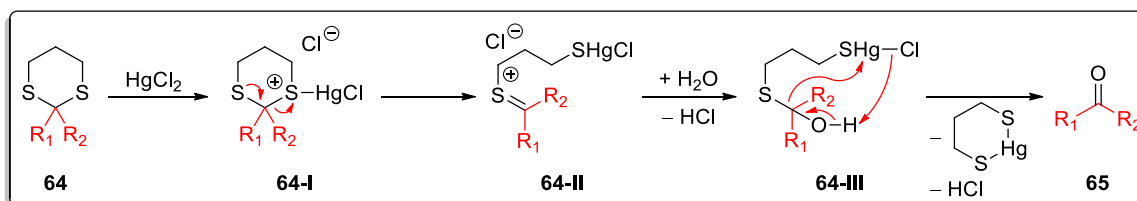
Scheme 10: (Top) Illustration of the deprotection of the benzyl-PG using solvated electrons. With 2 mol of sodium the reduction via SET-processes yields the released alcohol **61** or carboxylic acid **39** and toluene (**20**); (Bottom) Reductive elimination of a trichloro ethyl protected carboxylic acid **62**. Zinc is used as an electron donor, resulting in the decomposition of **62-I** into the olefin **63** and the free acid **39**. Modified according to [2].

In addition, many small organic molecules can be used as a hydrogen source for catalytic transfer hydrogenation.^[30] Depending on the substitution of the benzyl-PG the rate of hydrogenolysis can be influenced. When a substrate is protected by a benzyl ether and the previously mentioned oxidation-labile methoxy-substituted benzyl ether (Chapter 2.3.3), Raney nickel enables selective cleavage of the former.^[31] In a different manner the benzyl-PG can also be cleaved using solvated electrons as reductive agents (Scheme 10). Dissolved alkali metals in liquid ammonia with an additional proton source generate the diene radical anion **60-I** which gives the corresponding alcohol **61** or carboxylic acid **39** and toluene (**20**) after aqueous work-up. Due to the harsh reaction conditions, this method is rarely used, as this type of reduction has a low tolerance towards various functional groups.

The last subclass consists of PGs with a 2-haloethyl scaffold and are cleaved by reductive elimination with e.g., zinc in acetic acid or electrochemical processes (Scheme 10). The mechanism involves a β -elimination and is therefore similar to that of the base-labile PGs (Chapter 2.3.2). This principle can be applied to alcohols, protected as carbonates^[32] and ethers^[33], amines, protected as carbamates^[32], and carboxylic acids, protected as esters^[34].

2.3.5 Cleavage of PGs by heavy metals or transition metal catalysis^[1-3]

In general, the use of metals as catalysts and electrophilic auxiliaries allows a specific and targeted removal procedure for this orthogonal set. The aforementioned *S,S*-acetals (Chapter 2.3.3) can be readily hydrolysed with equimolar amounts of heavy metal salts of Ag(I), Cu(II), Hg(II) and Tl(III) or other effective Lewis acids.

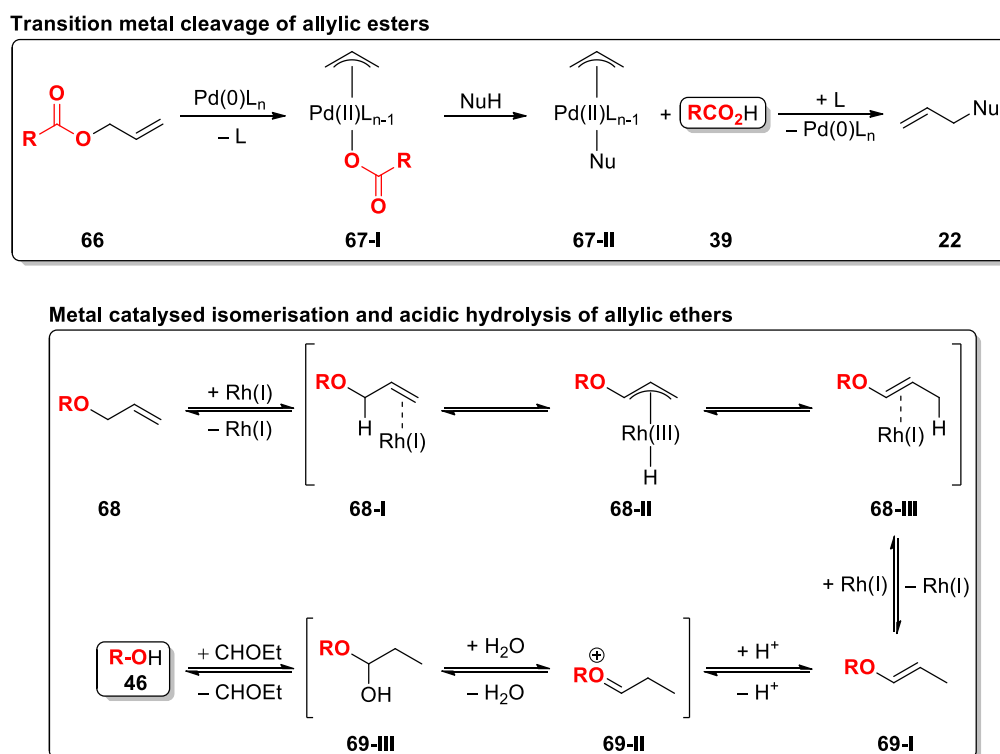


Scheme 11: Illustration of the deprotection of a 1,3-dithiane **64** with HgCl_2 . Modified according to ^[2].

Because of the deprotection processes requiring harsh reaction conditions and the use of toxic components, more environmentally friendly options are still being developed, among which removal via light has been studied.^[35] The removal of PGs in general represents a less invasive method and will be discussed in chapter 2.3.9.

PGs containing the allyl group can be cleaved by transition metal catalysis with Pd(0), Rh(I) or Ir(I) under mild conditions, with remarkable tolerance to many functional groups. The allyl

group of esters, carbamates, carbonates and phosphates is separated from the protected group by a nucleophilic attack of the metal, resulting in a π -complex and a stabilised anionic species (Scheme 12, Top). Allyl transfer is completed by the nucleophilic attack of mild agents such as morpholine and C-H-acidic compounds.



Scheme 12: (Top) Illustration of the deprotection of allyl-protected carboxylates with Pd(0). The oxidative addition leads to the intermediate **67-I**. Subsequent attack of a mild nucleophile gives the deprotected compound **39** and the allyl byproduct **22**; (Bottom) Metal-catalysed isomerisation of an allyl-protected alcohol. Rh(I)-mediated isomerisation of the double bond and acidic hydrolysis yield the deprotected alcohol **46**. Modified according to [2].

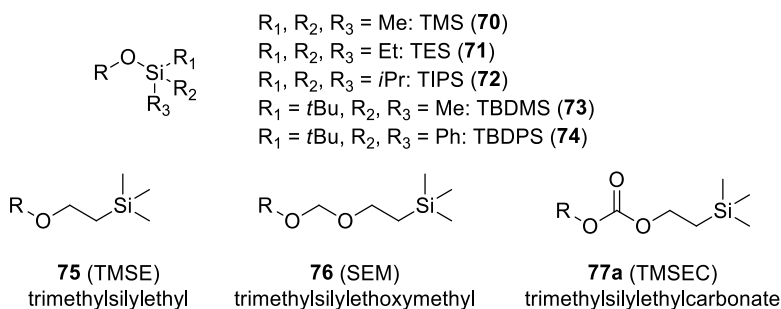
Allyl ethers are cleaved by double bond isomerisation with Rh(I) or Pd/C to give the acid-labile prop-1-enyl system (Scheme 12, Bottom, **69-I**). Mild acidic hydrolysis yields the deprotected alcohol and propionaldehyde. Stable allyl ethers can in turn be cleaved by oxidation with osmium tetroxide and ozone or by isomerisation with strong, non-nucleophilic bases such as potassium *tert*-butoxide.^[36,37]

2.3.6 Fluoride-labile PGs^[1-3]

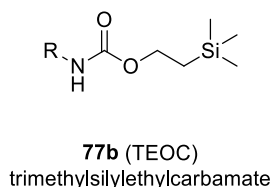
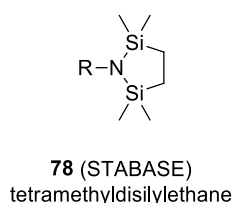
The sixth orthogonal group consists of silicon-based PGs that are frequently used in organic syntheses. The high affinity between silicon and fluorine is exploited for deprotection, resulting in selective and efficient removal. While trialkylsilyl-protected alcohols are among the most optimised and used PGs, the protection of amines, esters and 1,3-diols is rarely used

because few PGs have been developed for these functional groups and many of the corresponding derivatives are very labile (Scheme 13).

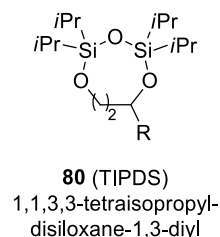
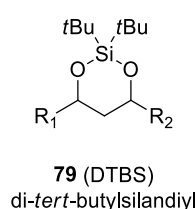
PGs for Hydroxy-groups:



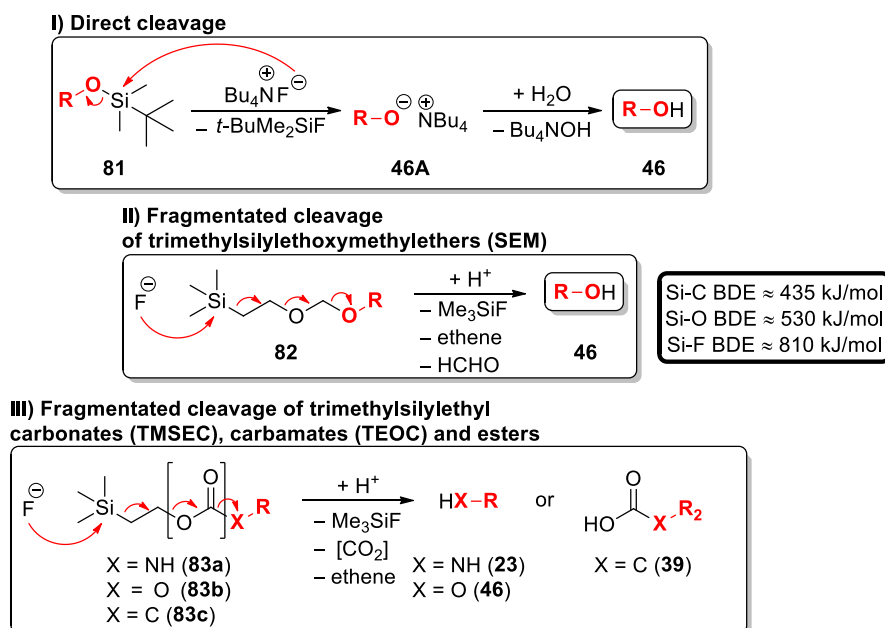
PGs for Amine-groups:



PGs for 1,3-Diols:



Scheme 13: Examples of fluoride-labile PGs for alcohols, amines and 1,3-diols. Modified according to [3].



Scheme 14: (Top, I) Direct cleavage of a trialkylsilyl protected alcohol **81**; (Middle, II) Fragmentated cleavage of a trimethylsilyl ethoxy methyl ether (SEM); (Bottom, III) Fragmentated cleavage of a trimethylsilylethyl carbonates, carbamates and esters. If X represents a hetero atom the carboxyl group is part of the PG and removed via decarboxylation. The bond dissociation energies are given in the bold square in kJ/mol. Modified according to [2,3].

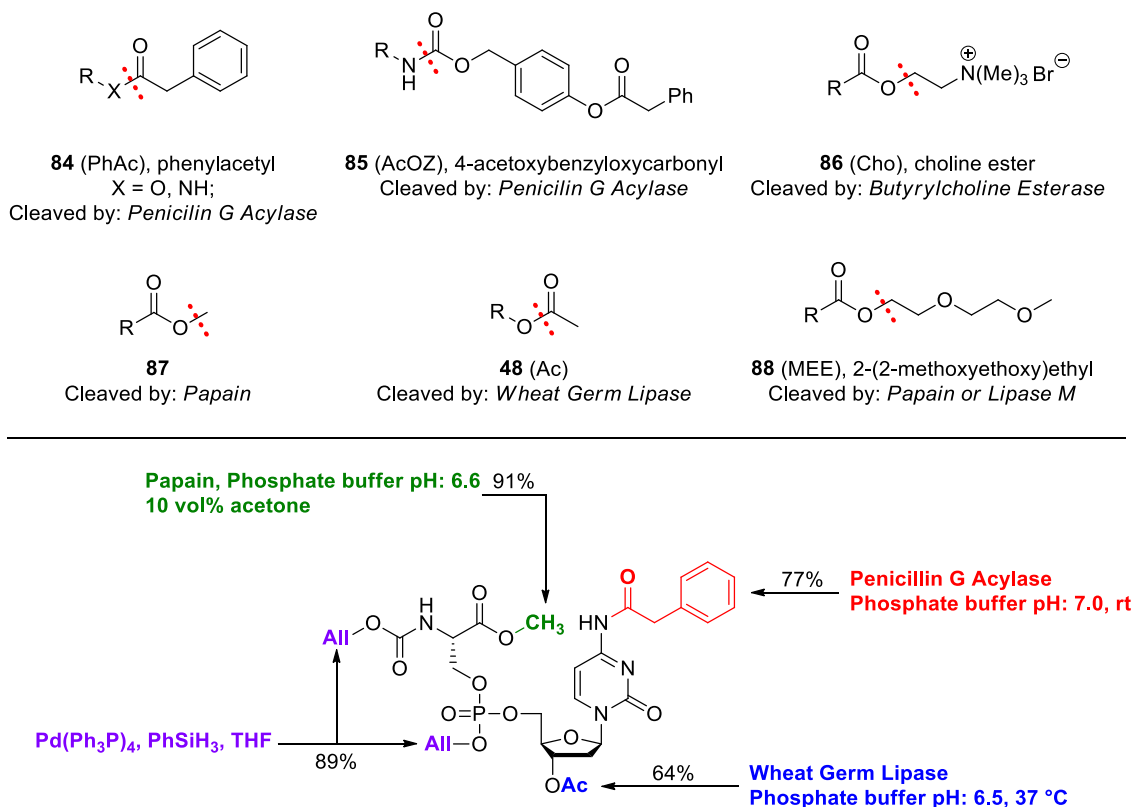
Removal of trialkylsilyl ethers is accomplished by direct cleavage initiated by the nucleophilic attack of fluoride, shifting the electron density towards the oxygen atom, yielding the

alcoholate which is subsequently protonated (Scheme 14, I). The larger the substituents are the higher the steric demand leading to lower reaction rates of deprotection.^[38]

Another strategy is fragmented cleavage, which is achieved by using 2-(trialkylsilyl)ethyl substituents. This deprotection mechanism therefore proceeds in an analogous way to the aforementioned β -elimination mentioned in the chapters 2.3.2 and 2.3.4. The nucleophilic attack of the fluoride ion leads to successive fragmentation of ethers^[39], but also esters^[40,41], carbamates^[42] and carbonates^[43], producing the deprotected substrate, trialkylsilyl fluoride, ethene, formaldehyde and, in the case of the latter two, carbon dioxide (Scheme 14, II and III).

2.3.7 Enzyme-labile PGs^[1-3]

Deprotection by enzymes allows highly selective removal of various PGs under mild conditions, by using a buffer system and a pH range of 5 to 9 at room temperature or low heating up to 40 °C. In addition to water, organic solvents are also tolerated in many cases.

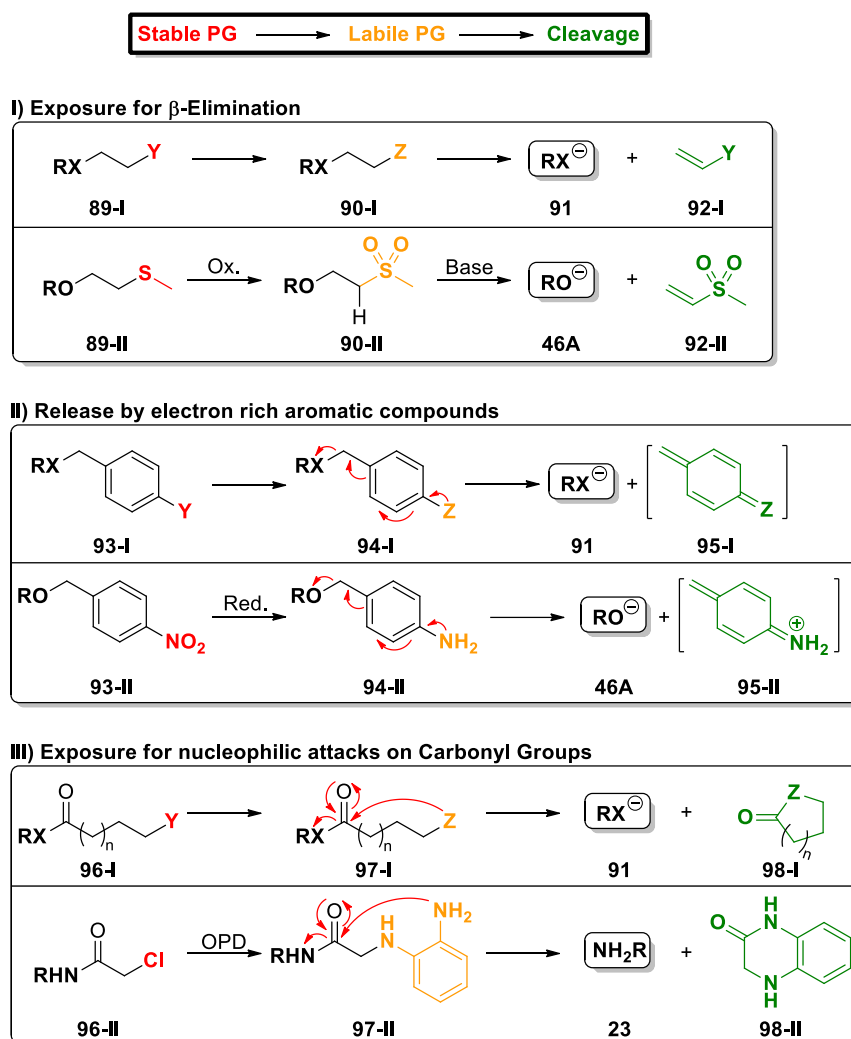


Scheme 15: (Top) Examples of PGs that can be cleaved with the corresponding enzyme; (Bottom) Multifunctional nucleopeptide protected by different PGs. Orthogonal deprotection is achieved by highly selective enzymes and hydrogenolysis under mild conditions, resulting in good yields and avoiding undesired side reactions. Modified according to [2,3].

Although enzymes cleave PGs that could also be cleaved by other options, the high and efficient regio- and chemoselectivity remains unsurpassable in many cases under the given reaction conditions. Therefore, this method is especially preferred in the synthesis of multifunctional substrates such as carbohydrates, peptides, nucleosides and other biologically relevant compounds, due to the effective orthogonal deprotection of the PGs (Scheme 15).^[44] The targeted development of enzyme-labile PGs and the investigation of enzymatic deprotection of already known PGs has increased the availability and possibilities for orthogonal (de)protection, especially of amines, alcohols and carboxylic acids. It has thus become an established and preferred method since the 20th century.

2.3.8 “Two-Stage” and “Safety Catch” PGs^[2,3]

In organic chemistry syntheses, some PGs must withstand a wide range of conditions before actual deprotection takes place. In contrast, removal may occur too early due to high lability to certain conditions. The "two-step" strategy circumvents this problem by using chemically stable PGs that can be converted to a labile counterpart and can be easily removed by e.g., β -elimination. The additional reaction step is associated with a higher effort, but can be used with regard to an optimised orthogonal deprotection. The thioether **89-II** itself has a high tolerance in acidic and basic environments, but oxidation of sulphur to the corresponding sulfone **90-II** allows the PG to be removed (Scheme 16, I).^[45-47] Besides oxidation, there are other options such as the use of Lewis acids, exhaustive alkylation of amines to obtain electrophilic ammonium salts, substitution reactions with alkyl halides and the isomerisation of robust allyl ethers to hydrolytically enol ethers (Chapter 2.3.5). Another common strategy is the “Safety Catch”^[47] method and involves the conversion of a stable PG into an activated intermediate prior to cleavage. One example is the reduction of aromatic compounds, which is accompanied by subsequent cleavage (Scheme 16, II).^[48] In case of the third example (Scheme 16, III), a stable PG is converted into a reactive species, which then performs an intramolecular attack on an electrophilic centre and causes the cleavage of the PG. Starting with the substitution of chlorine with *o*-phenylenediamine (OPD) the resulting derivative **97-II** nucleophilically attacks the carbonyl carbon yielding the deprotected substrate **23** and 3,4-dihydroquinoxalin-2(1*H*)-one (**98-II**).^[49] Hence, the reduction of nitro and azide substituents, condensation reactions of carbonyl compounds with hydrazine or the substitution of α -halide acetates with thiourea also became viable options for the "Safety Catch" method.

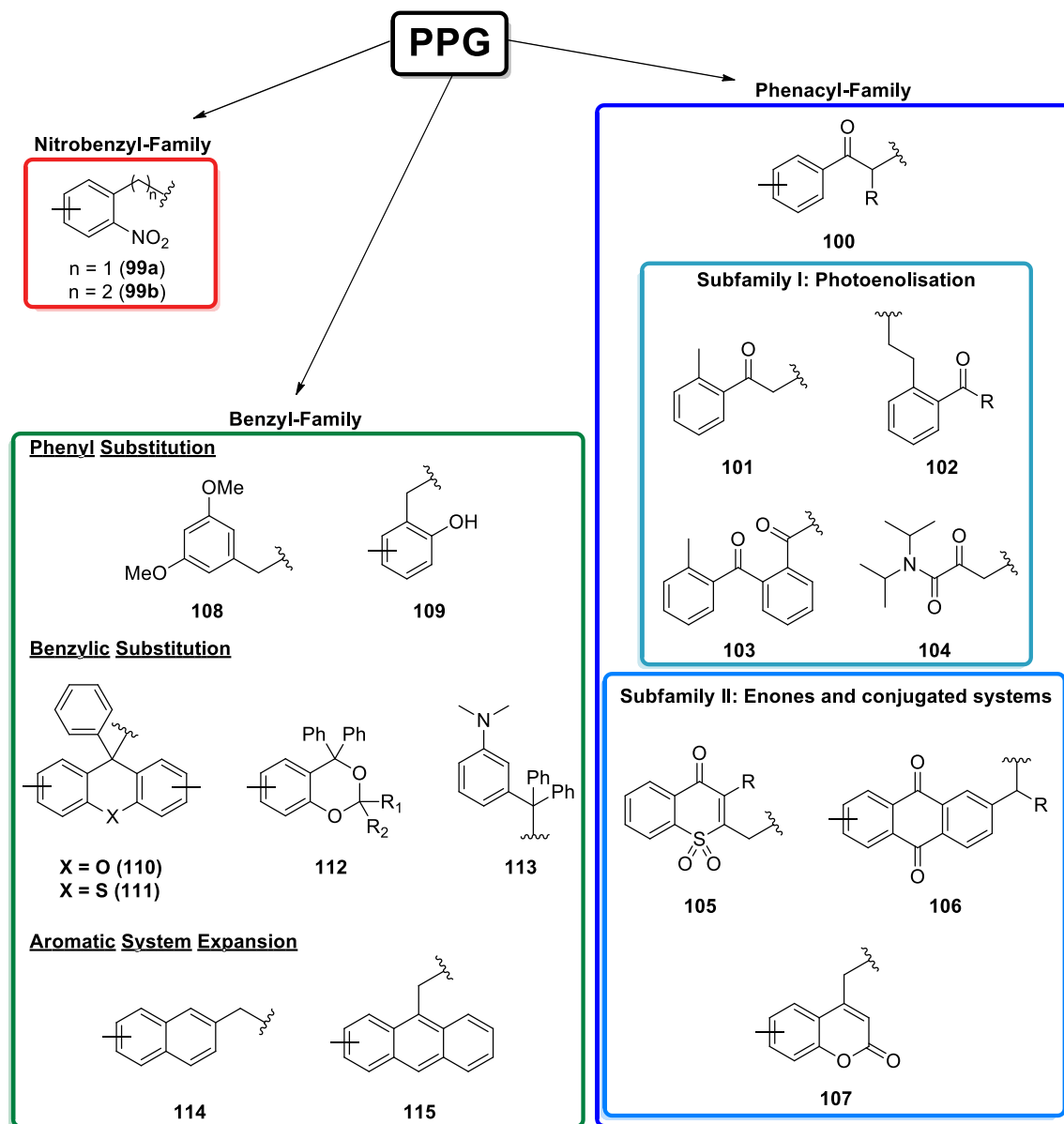


Scheme 16: Illustration of the principle of "Two-Stage" and "Safety Catch" PGs; I) The stable PG **89** is converted to the labile derivative **90**, which is cleaved by β -elimination; II) The stable PG **93** is converted to the labile derivative **94**, which is cleaved by electron density shift; III) The stable PG **96** is converted to the labile derivative **97**, which is cleaved by an intramolecular substitution reaction. Modified according to [2,3].

2.3.9 Photolabile PGs^[50-52]

Summarising the previous orthogonal groups of PGs, the corresponding deprotection includes acidic or basic hydrolysis, oxidative, reductive, electrophilic or nucleophilic auxiliaries, or the use of enzymes, which offer an enormous range of viable options. However, besides all these (bio-)chemical approaches, the use of light as a deprotecting agent is a special case that is not yet fully exploited. These photolabile PGs (PPGs) are cleaved by irradiation of a substrate alone, so that no further reagents are required, and have an intrinsic (chromatic) orthogonality to a certain degree due to the different excitation wavelengths used for the corresponding PPGs. In general, the basic scaffold of these PGs is based on a chromophore with unsaturated,

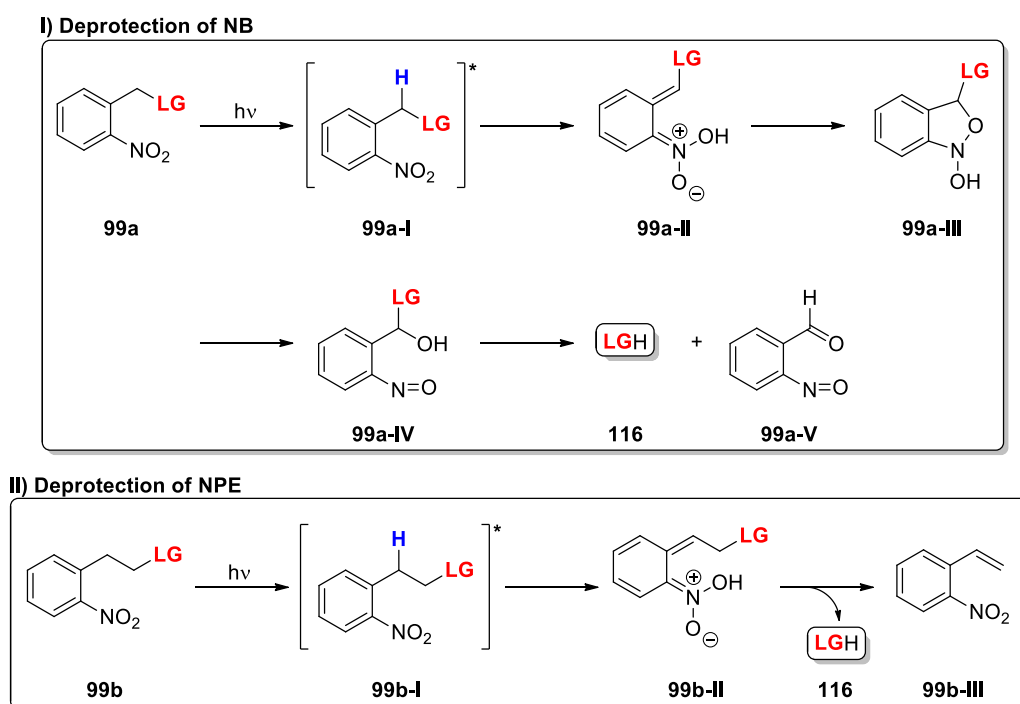
aromatic systems including substituents such as carbonyl and/or nitro groups, which allow $n \rightarrow \pi^*$ transitions. Over the last 60 years, the application and diversity of PPGs has been refined. Overall, there are three major subclasses: a) the nitrobenzyl (NB), b) the phenacyl and c) the benzyl family (Scheme 17).



Scheme 17: Overview of the most important PPG families: nitrobenzyl family (red box); benzyl family with various derivatives (green box); phenacyl family (blue box) with its two subfamilies of compounds that prefer photoenolisation (cyan box); and enones and other derivatives (light blue box).

In addition to these categories, many other derivatives and analogues have been developed for the protection of a specific functional group and for applications in biological research. The first subclass of NB derivatives represents a preferred option in organic synthesis because of the easy introduction and the various functional groups that can be released from them,

including phenols, thiols, carbamates, carbonates, carboxylic acids and phosphates. The NB deprotection has been intensively studied and is illustrated in Scheme 18.^[53–55] Irradiation of **99a** leads to the excited substrate **99a-I** which undergoes a 1,5-transfer of a benzylic hydrogen atom to generate the crucial *aci*-nitro intermediate **99a-II**. An irreversible cyclisation and subsequent ring-opening gives compound **99a-IV**, which decomposes to the aldehyde **99a-V** and releases the protected substrate **116**.

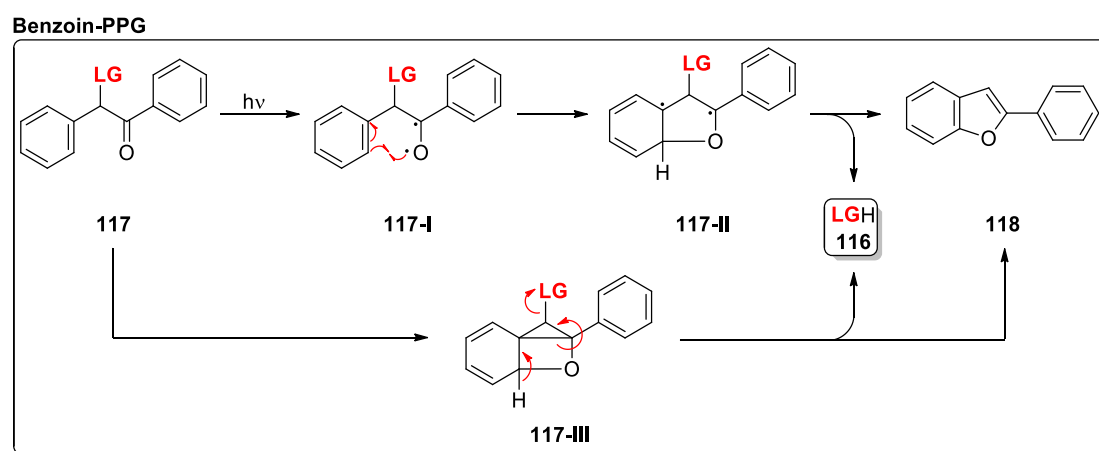


Scheme 18: I) Mechanism of NB deprotection; II) Mechanism of NBE deprotection. Modified according to ^[50].

The leaving group potential influences both the quantum yield and the reaction rate. Therefore, unfavourable leaving groups such as amines and alcohols are released much slower compared to, for example, phosphates. Another major problem is the resulting nitrosobenzaldehyde **99a-V**, which has a stronger absorption than the NB-PPG and thus reduces the overall efficiency of deprotection.^[54] In addition, secondary photoreactions^[54] of **99a-V** lead to a variety of byproducts that can further inhibit the photoreaction and interact with other substrates or biological systems.^[56,57] Optimisation strategies included modification of the aromatic ring and substitution in the benzylic position, with the latter intended for an efficient release of amino acids.^[58] 1997 Hasan et al. published the 2-(2-nitrophenyl)ethyl (NPE, **99b**) PPG.^[59] In a similar fashion to its NB derivative the excited species **99b-I** undergoes a 1,5-hydrogen transfer to generate the *aci*-nitro species **99b-II**. Subsequent decomposition yields the liberated substrate **116** and nitrostyrene **99b-III**. When

compared to NB PPG derivatives, the NPE group releases stable leaving groups faster and has higher quantum yields.^[59–61]

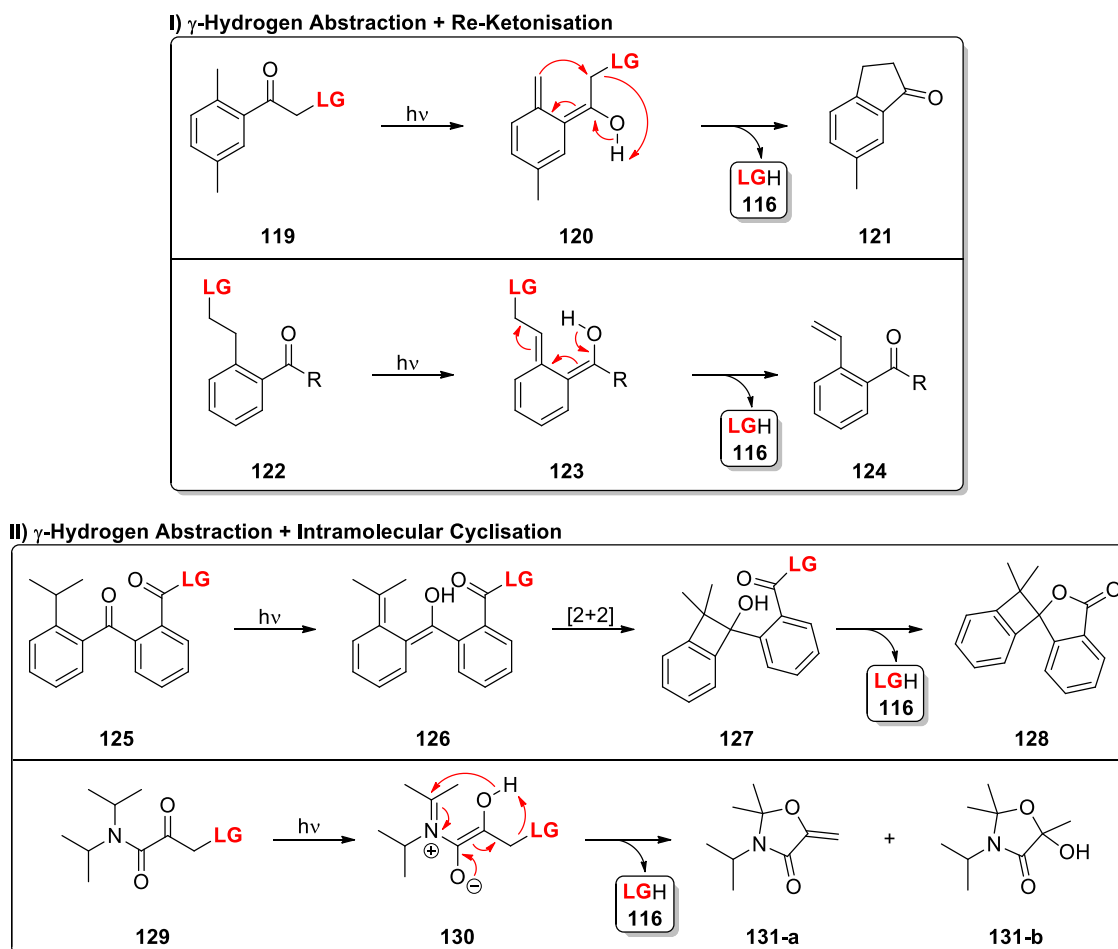
The phenacyl family consists of various carbonyl-based PPGs, whose deprotection mechanism may differ depending on the PPG backbone, leaving group, and reaction conditions.^[62–65] The phenacyl PPG contains the protected substrate in α -position, which can be efficiently released upon photolysis. *Sheehan* and *Wilson* investigated benzoin derivatives for the usage as potential PPGs^[66,67] which proved to be a viable option for the release of various functional groups.^[68–70] Several mechanisms involving either radical cyclisation or intramolecular [2+2] Paternò-Büchi were proposed (Scheme 19).^[71–74]



Scheme 19: Photolysis of benzoin PPGs. The upper path shows a cyclisation via radical steps, while the lower path proceeds via an intramolecular [2+2] Paternò-Büchi. Modified according to^[51].

Givens et al. designed the *p*-hydroxyphenacyl (*p*HP) PPG whose deprotection mechanism involves a photo-Favorskii rearrangement^[75–79], shows no secondary photoreactions and releases good leaving groups in high yields^[80–82]. The first subfamily of phenacyl PPGs involves the release of potent leaving groups such as phosphates^[83], sulfonates^[83], carboxylates^[84–86], carbonates^[87] and carbamates^[88] via photoenolisation through γ -hydrogen abstraction. Depending on its overall structure, the enol can react in different ways. If ketonisation occurs, the leaving group is either intramolecularly substituted or eliminated (Scheme 20, I).^[85,86,89] Using the benzophenone derivative **125** *Gudmundsdottir* et al. enabled the deprotection of alkoxides through intramolecular lactonisation (Scheme 20, II).^[90] The mechanism is initiated by photoenolisation which yields enol **126**. After an intramolecular [2+2] cycloaddition the tertiary alcohol **127** nucleophilically attacks the adjacent carbonyl group to obtain lactone **128** and the released alkoxide in good yields. Structurally deviating from the phenacyl scaffold but with a similar mechanism, *Steinmetz* et al. investigated the photoenolisation of ketoamides with the leaving group attached to the α -carbon atom.^[91,92]

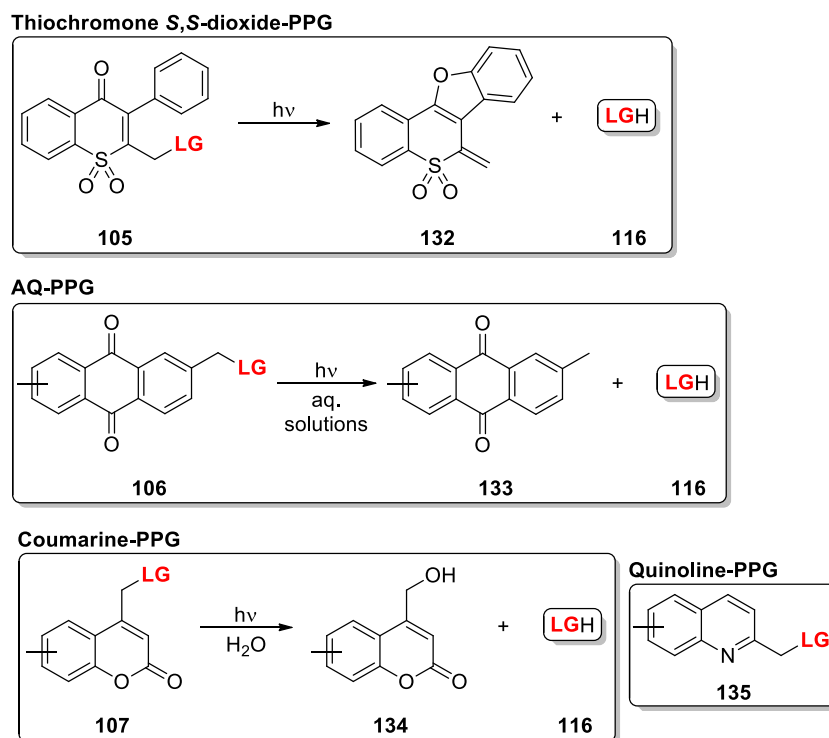
Irradiation of compound **129** gives the zwitterionic species **130** which upon intramolecular cyclisation releases the protected substrate (Scheme 20, II).



Scheme 20: Removal of PPGs via photoenolisation of carbonyl groups. The light induced γ -hydrogen abstraction either leads to a re-ketonisation (I) or an intramolecular cyclisation (II). Modified according to ^[50].

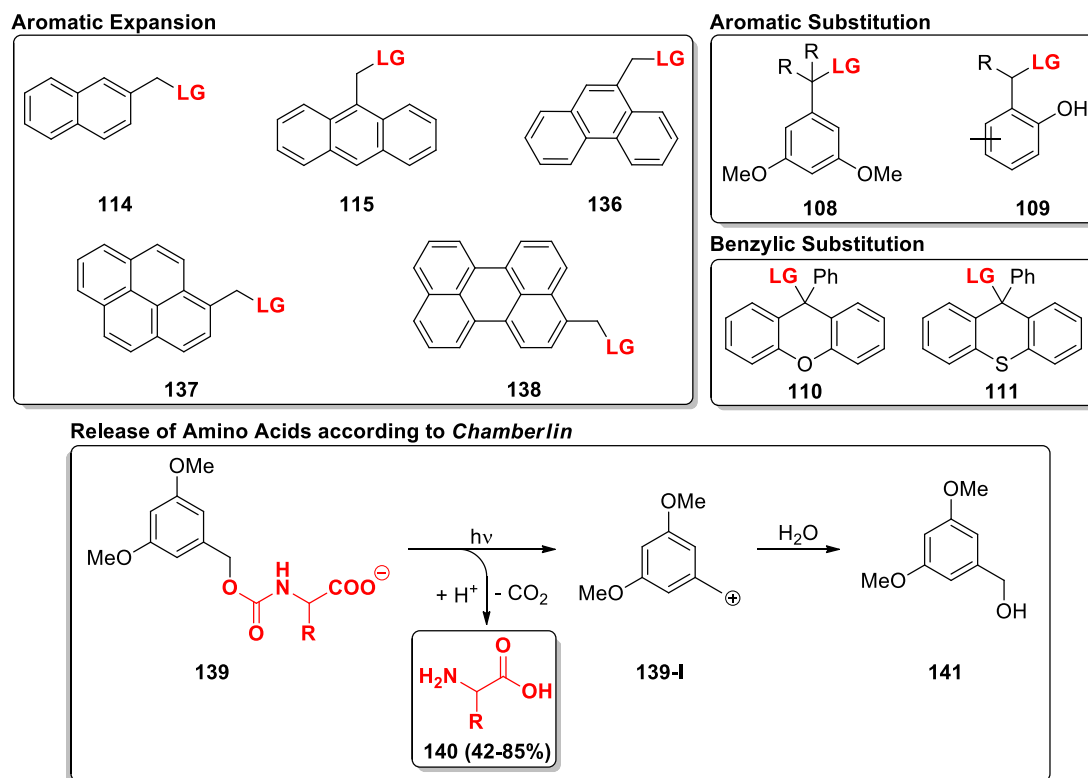
As for the second subfamily of phenacyl PPGs, the basic structure of thiochromone *S,S*-dioxide (**105**), (2-anthraquinonyl)methyl (AQ, **106**) and coumarin PPGs (**107**) is still related to that of the phenacyl scaffold, but also has its own features such as enones and an extended conjugated system with additional electron acceptors (Scheme 21). Especially the coumarin-PPG (**107**) as well as the quinoline-PPG (**135**), which represents its nitrogen containing analogue, became particularly interesting for biological and medical research as they show efficient release of phosphates, carboxylates and diols.^[82,93] The AQ-PPG (**106**) has been established as a PG for the protection and release of alcohols^[94], carboxylic acids^[95,96], ketones/aldehydes^[97] and cyclic adenosine monophosphate (cAMP).^[98] The photodeprotection mechanism has been thoroughly investigated. A solvent-dependent reduction to the corresponding dihydroxy anthracene via the formation of a ketyl-radical and subsequent release of the substrate with 2-methylanthraquinone (**133**) as the byproduct is

proposed.^[99] *Kakiuchi et al.* reported that UV-irradiation of thiochromone *S,S*-dioxide protected substrates in deuterated solvents allows rapid and quantitative release of various phosphates, amines, alcohols and carboxylic acids accompanied by the formation of the tetracyclic byproduct **132** which shows a strong fluorescence at 440 nm with a quantum yield of $\Phi = 0.85$.^[100–102]



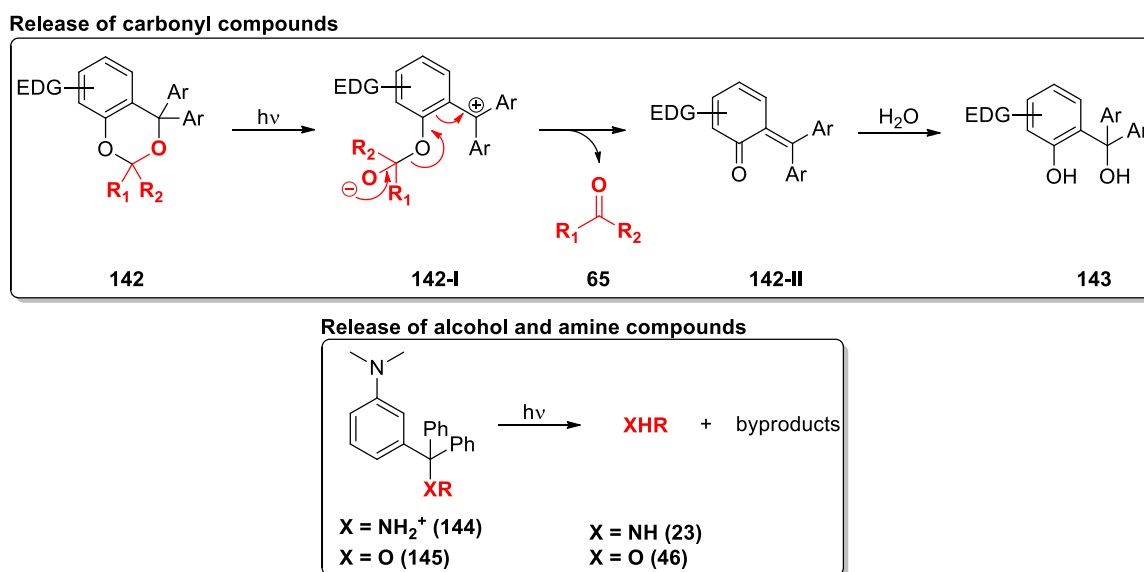
Scheme 21: Overview and reaction equations for the deprotection of the thiochromane *S,S*-dioxide- (**105**), AQ- (**106**) and coumarin-PPG (**107**). Next to the coumarin-PPG (**107**) the corresponding nitrogen containing quinoline-PPG (**135**) is illustrated. Modified according to ^[51,99,100].

The last major family of PPGs are the benzyl-based compounds (Scheme 22, top). The general mechanism involves the heterolytic cleavage of the benzylic C–X bond and is strongly dependent on the choice of solvent. The first report on this type of PPG was published in 1962 by *Barltrop and Schofield*, who studied the photolysis of benzyl-protected glycine carbamate.^[103] This reaction was improved by *Chamberlin* using the 3,5-dimethoxybenzyl derivative **108** as PPG for the protection and release of glycine, methionine, phenylglycine, serine and ϵ -Cbz-lysine with yields from 42 to 85% (Scheme 22, bottom).^[104] This substitution effect was thoroughly investigated by *Zimmermann et al.*^[105] The expansion of the aromatic system (**114**, **115**, **136–138**) and substitution at the benzyl position (**110**, **111**) have increased the availability of this PPG family.



Scheme 22: (Top) Benzyl-type PPGs. (Bottom) Selected example of the cleavage of amino acids from the 3,5-dimethoxybenzyl PPG by *Chamberlin*.^[104] Modified according to ^[50,51].

Recently new trityl-based compounds with methoxy (e.g., **142**) or dimethylamino (e.g., **144** and **145**) substituents have been developed and optimised for the targeted protection and effective release of carbonyl compounds^[106–108], alcohols^[109–111] and amines^[112] (Scheme 23).



Scheme 23: (Top) Mechanism of photochemical deprotection of carbonyl compounds. (Bottom) Illustration of the removal of dimethylaminotrityl (DMATr) protected alcohols and amines. The latter have to be protonated in order to be cleaved of the PG. Modified according to ^[50].

Overall, it can be stated that PPGs represent a valuable addition to other orthogonal sets of PGs. The chromophore-based structures possess their very own chromatic orthogonality and enable a neutral (de-)protection protocol for efficient reactions, comparable to that of enzyme and metal catalysis labile PGs.

2.4 Photophysical processes and luminescence^[113–115]

The term *luminescence* is defined as the emission of light due to a preceding energy input which causes electronic excitation that is not solely caused by high temperatures. This type of radiation is therefore referred to as "cold light" and lies in the range from the near ultraviolet through the visible to the infrared. The amount of energy of the emitted photon is equal to the energy difference between two different energetic states (Equation 1):

$$h \cdot \nu = \Delta E \quad (\text{Eq. 1})$$

h = Planck's constant [J·s], ν = frequency [s^{-1}], ΔE = difference of energy [J].

In accordance with *Stokes' rule*, the wavelength of the emitted light tends to be greater or at least equal to the wavelength of the exciting radiation. However, when a luminescent substance absorbs extra energy from the vibrational energy of its structure due to thermal effects, there can be an exception from this rule, leading to an *anti-Stokes* luminescence.

Electronic excitation can occur during the interaction of light with matter through the absorption of a photon in the range from ultraviolet (UV) to visible (Vis) light, which is termed *photoluminescence*. The subsequent emission of light proceeds via *fluorescence* or *phosphorescence*. Shorter wavelengths such as X-rays can cause the ionisation of atoms, while infrared light only causes molecular excitation in the form of rotational and vibronic excitation (Table 1).

Table 1: Electromagnetic spectrum from γ -rays to radio waves in nanometres including the technical use and corresponding values in Hz, eV and kJ/mol.^[113,116]

	γ -Rays	X-Rays	Ultraviolet	Visible			Infrared	Micro Waves	Radio Waves
	<i>Nuclear excitation</i>	<i>Ionisation</i>	<i>Electronic excitation</i>				<i>Vibration/Rotation</i>	<i>EPR</i>	<i>NMR</i>
λ [nm]	10^{-3} - 10^{-2}	10^{-2} - 10^1	10^1 - 10^2	380	580	780	10^3 - 10^6	10^6 - 10^9	10^9 - 10^{13}
ν [Hz]	$3 \cdot 10^{20}$ - 10^{19}	$3 \cdot 10^{19}$ - 10^{16}	$3 \cdot 10^{16}$ - 10^{15}	$8 \cdot 10^{14}$	$5 \cdot 10^{14}$	$4 \cdot 10^{14}$	$3 \cdot 10^{14}$ - 10^{11}	$3 \cdot 10^{11}$ - 10^8	$3 \cdot 10^8$ - 10^4
E [eV]	10^6 - 10^5	10^5 - 124	124 - 12	3.26	2.14	1.59	$1.2 \cdot 10^{-3}$	10^{-3} - 10^{-6}	10^{-6} - 10^{-10}
E $\left[\frac{\text{kJ}}{\text{mol}}\right]$	10^8 - 10^7	10^7 - 10^4	10^4 - 10^3	315	206	153	120 - 0.12	0.12 - 10^{-4}	10^{-4} - 10^{-8}

The absorption efficiency of a photon with the wavelength λ can be described by the *Lambert-Beer* law, which states that the process depends on the molar absorption coefficient $\varepsilon(\lambda)$, the concentration of the sample c and the absorption path length d (Equation 2):

$$A(\lambda) = \log \frac{I_{\lambda}^0}{I_{\lambda}} = \varepsilon(\lambda) \cdot c \cdot l \quad (\text{Eq. 2})$$

$A(\lambda)$ = Absorbance, $I_{\lambda}^0/I_{\lambda}$ = Light intensity before/after absorption [W/m^2], $\varepsilon(\lambda)$ = molar absorption coefficient [$\text{L/mol}\cdot\text{cm}$], c = concentration [mol/L], l = Thickness of sample [cm].

2.4.1 Jablonski diagram^[114,116]

When an electron **absorbs** a defined amount of energy which corresponds to the energetic difference between two states, it causes the excitation of the latter to a higher energy state ($S_{n>0}$). According to *Kasha's* rule this electron then undergoes non-radiative transitions, such as **vibrational relaxation (VR)**, and interactions with its environment and gradually returns to the lowest vibrational state of the excited state. Consequently, an emitted photon always has a lower frequency than the absorbed one, since emission occurs only after the molecule has released a small amount of thermal energy to its environment. In addition to **VR**, the electron can transition from the lowest vibrational state of an excited state to an isoenergetic vibrational state of a subsequent, lower state ($S_n \rightarrow S_{n-1}$) with the same multiplicity, which is called **internal conversion (IC)**. Alternatively, it can relax into a less excited vibrational state within the ground state (S_0) by radiative transfer. This process occurs rapidly and is permissible in terms of spin because the excited electron and the other electron in the ground state have different spins, resulting in singlet multiplicity. In this scenario, the emission of a photon is called **fluorescence**. Subsequently, the electron returns to the lowest vibrational state of S_0 via non-radiative transitions.

Table 2: Timescale of different photochemical processes.^[114]

Process	Time Scale [s]
Absorption	10^{-15}
Vibrational Relaxation	$10^{-12} - 10^{-10}$
Internal Conversion	$10^{-11} - 10^{-9}$
Intersystem Crossing	$10^{-10} - 10^{-8}$
Fluorescence Lifetime	$10^{-10} - 10^{-7}$
Phosphorescence Lifetime	$10^{-6} - 1$

Another classification of luminescence is **phosphorescence**. Similar to fluorescence, an electron is excited to a higher excited singlet state. After relaxing to the lowest vibrational state within the excited singlet state, the electron transitions to an isoenergetic vibrational state within an excited triplet state (T_1). This transition involves a spin change of the electron (which is partially allowed due to spin-orbit coupling), which is called **Intersystem Crossing (ISC)**. Subsequently, the electron relaxes into the lowest vibrational state of the excited triplet state. Since the electron now assumes a lower energy state and must reverse its spin to return to the singlet ground state (S_0), **phosphorescence** is of longer duration but also emits less energy than **fluorescence** (see Table 2). The different luminescence processes are illustrated and explained by a *Jablonski*-diagram shown in Figure 3.

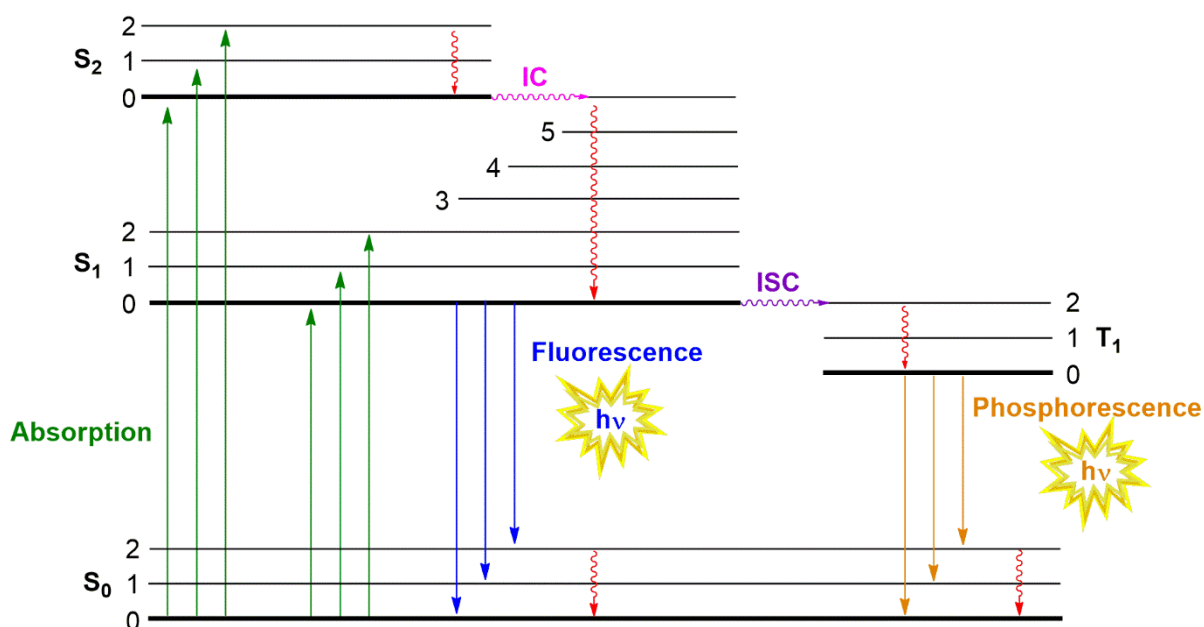


Figure 3: Illustration of a *Jablonski*-diagram. The absorption of a photon allows the excitation of an electron into an excited state S_2 or S_1 (green arrows). Through non-radiative transitions (red wavy arrows) the electron loses energy through oscillations and reaches the vibrational ground state of an excited state. Other non-radiative and isoenergetic transitions where the electron leaves the vibrational ground state of an excited state and enters a highly excited vibrational state of a lower excited or ground state are the *internal conversion* (IC, pink) or *inter system crossing* (ISC, purple). In the latter case the electron changes its spin and enters an excited triplet state. The transition from S_1 to S_0 is called **fluorescence** (blue arrows). The transition from T_1 to S_0 is called **phosphorescence** (orange arrows). The energy is released as photons. Modified according to [114,116].

2.4.2 Franck-Condon-Principle^[113–115]

The probability of an electronic transition can be explained with the *Franck-Condon*-principle. According to the *Born-Oppenheimer*-approximation the movement of nuclei and electrons can be distinguished from each other due to their size and mass. Thus, electrons move faster than nuclei and electronic transitions do not change the geometry of the molecule.

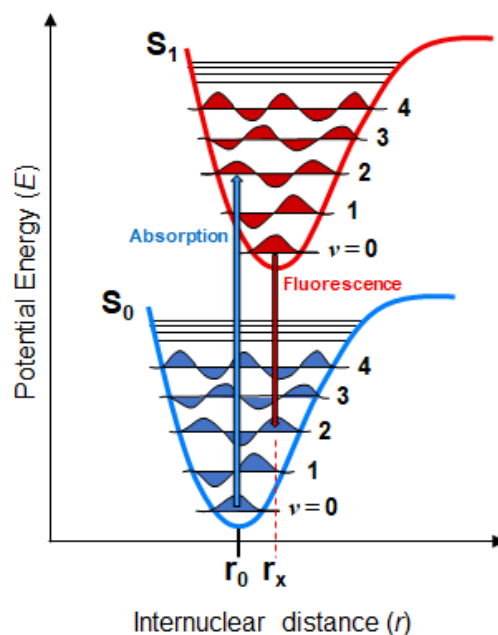


Figure 4: Diagram of the vertical transitions according to the *Franck-Condon*-principle with the potential energy of the molecule E plotted against the internuclear distance r . The function is described with the *Morse*-potential. The most intensive transition occurs from the vibrational ground state $\nu = 0$ of the electronic ground state to the vertical above existing excited vibrational state $\nu = 2$ of the excited electronic state (Absorption, blue arrow). Same case exists for the emission (red arrow). Other transitions can be observed but have a lesser intensity. Modified according to ^[113,114].

Each energetic state can be described with a potential energy curve (*Morse*-potential), which is subdivided in different vibrational states, starting with the vibrational ground state 0 to 1, 2, 3 etc. (Figure 4). Each of the vibrational states is described with a wave function. Therefore, the transition probability is equivalent to the integral overlap. The electronic transitions are illustrated as a vertical line between two different energetic states (**vertical transition**). Often the potential function of the excited state is, in comparison to the ground state, shifted towards greater atom distances, since excited electronic states have a higher antibonding character.

By means of the *Franck-Condon*-principle the characteristics of an absorption- and fluorescence spectrum can be explained. Different wavelengths can cause electronic excitations into different vibrational states. Afterwards through non-radiative relaxations the electron enters the vibrational ground state of an excited state. The emission of fluorescence is therefore always independent of the stimulation wavelength and is lower in energy than the

absorption. The energy difference between the absorption peak with the longest wavelength and the emission peak with the shortest wavelength is called “*Stokes-Shift*” (Figure 5).

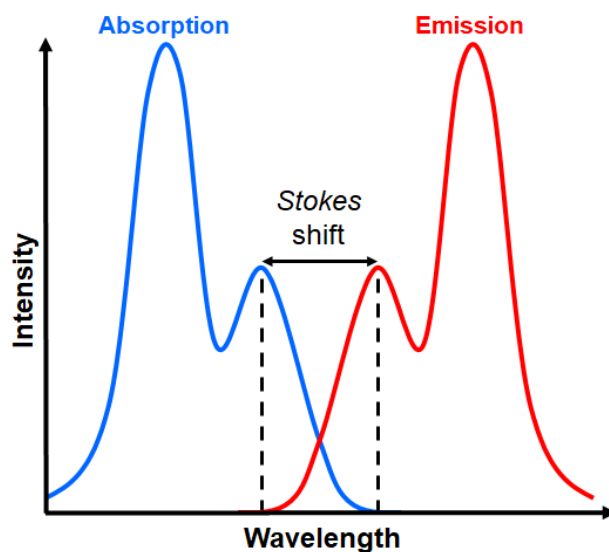


Figure 5: Overlay of an absorption and fluorescence spectrum; the intensity is plotted against the wavelength. The absorption and fluorescence lines are mirror-inverted due to the similar energy differences. The vibrational relaxations of the excited electron cause a bathochromic shift of the fluorescence towards the absorption. The difference between the absorption peak with the longest wavelength and the emission peak with the shortest wavelength gives the “*Stokes shift*”. Modified according to ^[114].

2.4.3 Types of luminescence^[117]

Electronic excitation can occur in various ways and is consequently differentiated according to the energy source (Figure 6). While electronic excitation is possible by photons in the UV and visible range, as in the case of *photoluminescence*, it can also be achieved by ionising radiation (X-rays, α -rays, β -rays, γ -rays) or particles of radioactive isotopes (radioisotopes). This type of luminescence is termed *radioluminescence*. Besides electromagnetic radiation the appliance of an electric current passed through e.g., a doped semiconductor can induce an *electroluminescence* (EL) by the recombination of the excited electron with a hole in the valence band. A special case of electroluminescence is *cathodoluminescence*, in which a high-energy electron beam (primary electrons) causes inelastic scattering within a sample/crystal. The subsequent emission of secondary electrons and X-rays leads to the excitation of valence electrons in the conduction band, again emitting a photon through radiative recombination with a hole. In the case of *mechanoluminescence*^[118] light emission results from a mechanical action such as rubbing, crushing and scratching (*triboluminescence*,

TL)^[119], fracturing (*fractoluminescence*)^[120], application of pressure (*piezoluminescence*)^[121] or sound waves (*sonoluminescence*).^[122] *Thermoluminescence* differs from incandescence in that the latter is caused only by a rise in temperature. When crystalline materials absorb electromagnetic radiation, it is possible that the corresponding excited states remain trapped within the lattice. A rise in temperature enables vibronic excitation in the crystal and thus the interaction of phonons with the excited states, so that decay through the emission of photons is enabled.

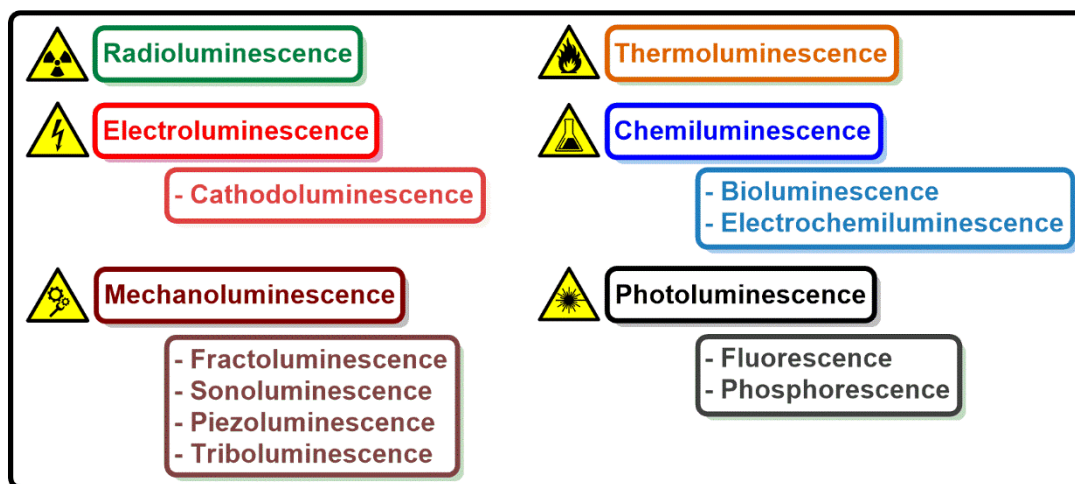


Figure 6: Overview of the different types of luminescence. Below some luminescence classes, subtypes are shown in lighter colours.

Chemiluminescence (CL) is a generic term for emission of light as the result of a chemical reaction. A subtype of CL is *bioluminescence* (BL) where a living organism produces light by itself or with the additional help of a symbiont through chemical processes. *Electrochemiluminescence* (ECL)^[123] on the other hand is based on the generation of reactive species at the electrode surface. These species cause the formation of excited states via electron transfer (ET) reactions which emit light. In the following chapters the phenomena of CL and BL will be discussed and described in more detail.

2.5 Definition and evolution of bioluminescence^[124]

As already stated in the previous chapter BL is defined as a characteristic trait of a living organism that can produce light itself or through the additional help of symbionts. This luminescence is based on chemical processes and therefore categorised as a CL. The phenomenon of BL has already been known to mankind for more than three and a half millennia, which can be traced back to the first mentioning of “glow worms” and “fireflies” in

ancient writings of Asian civilisations. Literature of *Aristotle* (384-322 B.C.) shows a further understanding of cold light emitted from fungi. Later on, *Pliny the Elder* (A.D. 23-79) even mentioned bioluminescent clams, jellyfishes and lantern fishes in his *Historia Naturalis*.^[125,126] During the end of the 19th century, the French pharmacologist *Raphaël Dubois* (1849-1929) discovered that the luminescence of click beetles (*pyrophorus*) was linked to the oxidation of a specific compound (defined by him as *luciferin*) which was catalysed by an enzyme (defined by him as *luciferase*).^[127]

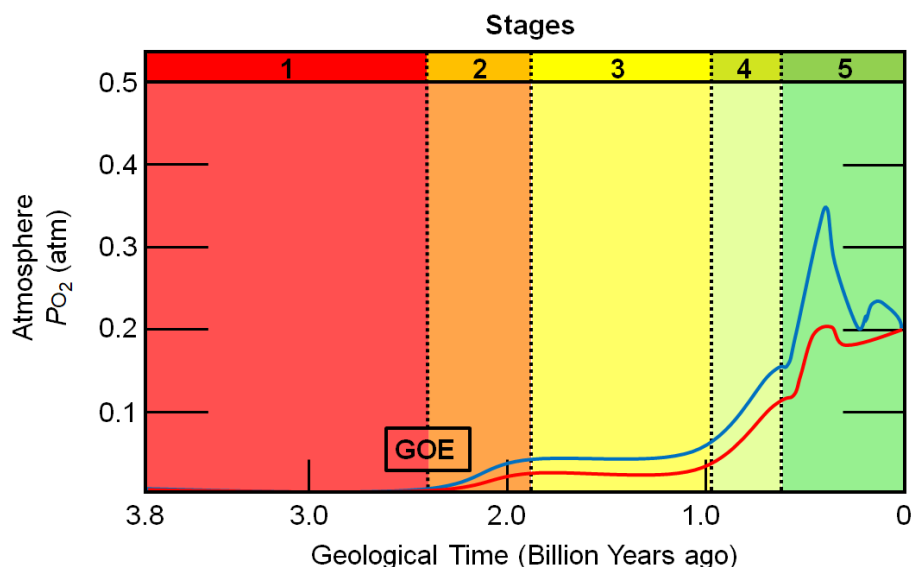


Figure 7: Illustration of the estimated evolution of O₂ enrichment within Earth's atmosphere. Stage 1 (3.85 - 2.45 billion years ago): Earliest known life forms emerge with almost no oxygen present. Oceans were mainly anoxic; Stage 2 (2.45 - 1.85 billion years ago): O₂ is produced but absorbed by oceans and rocks; Stage 3 (1.85 - 0.85 billion years ago): O₂ content is static and oceans are mildly oxygenated; Stage 4 (0.85 - 0.54 billion years ago): O₂ begins to accumulate in the atmosphere, oceans remain mostly anoxic or euxinic; Stage 5 (0.54 billion years ago - present): Peak of oxygen concentration in the atmosphere and subsequent decrease to 0.2 atm. Oceans are oxygenated as well. The curves indicate the upper (blue) and lower (red) limits of the estimated range, respectively. Modified according to ^[128].

Taking the entire fauna into account, bioluminescence is found in fungi, bacteria, insects, centipedes, crustaceans and fish. The exact evolutionary origins of bioluminescence remain uncertain. One hypothesis is based on the change of Earth's atmosphere. The prebiotic atmosphere (second atmosphere of Earth) consisted mainly of nitrogen (N₂), carbon dioxide (CO₂) and small amounts of hydrogen-based gases (e.g., H₂, NH₃, CH₄)^[129] before the *Great Oxygen Event* (GOE)^[130] occurred during the Paleoproterozoic era and transformed the reducing atmosphere into a highly oxidising one (Figure 7).

The first signs of life appeared about 3.8 billion years ago.^[131] These microorganisms adapted to the anaerobic environment, giving rise to a variety of microbial ecosystems based on the consumption of minerals and small molecules consisting of nitrogen, sulphur and hydrogen

through various metabolic pathways, including anoxygenic photosynthesis.^[132] Recent studies suggest that at least 3 billion years ago, the first organisms emerged that developed oxygenic photosynthesis during the Archaic era.^[133–135] Water thus became an essential energy resource and was oxidised to molecular oxygen in this process. In the course of evolution cyanobacteria became the predominant species responsible for the increased production of molecular oxygen, leading to its accumulation in minerals, oceans and eventually in the atmosphere, which culminated to the GOE (Figure 8).

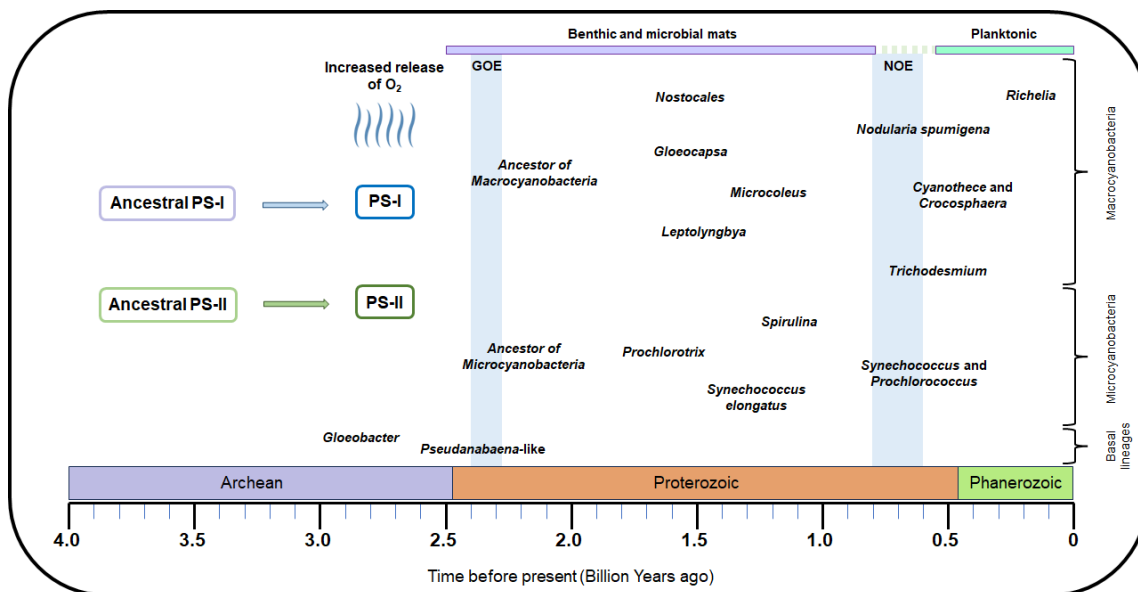


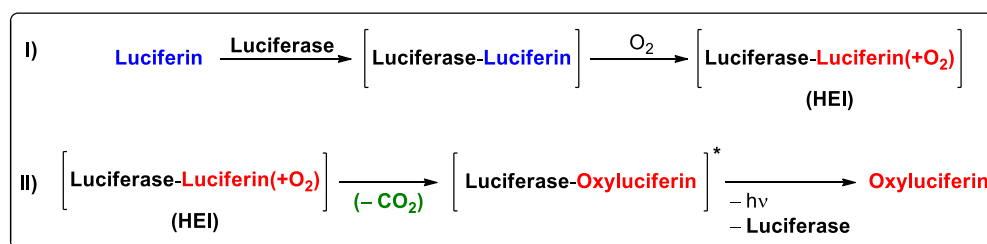
Figure 8: Timeline of the emergence of the first biological photosystems (PS) and cyanobacterial lineages. The respective species are categorised according to their size (basal lineage, micro- and macrocyanobacteria). GOE = Great oxygen event; NOE = Neoproterozoic oxidation event. It is assumed that early forms of water oxidation were performed by ancestral homodimeric photosystems (Ancestral PS-I and -II). Towards the late Archean era the heterodimeric photosystems PS-I and PS-II were inherited by the most recent common ancestor of cyanobacteria and shared by all extant oxygenic phototrophs. The majority of cyanobacteria species formed after the GOE, while marine planktonic cyanobacteria evolved mainly after the NOE. Modified according to ^[133].

Since heterotrophic organisms that existed at that time were initially adapted to an environment devoid of oxygen, the resulting enrichment of the latter caused evolutionary pressure that led to the extinction of many organisms, but also the development of aerobic metabolism and protective mechanisms against oxidation. One of these mechanisms for the detoxification of oxygen was bioluminescence. This hypothesis gains support from the fact that various organisms can produce light through different reactions, indicating that this feature evolved independently multiple times.^[136] All of these reactions ultimately depend on the presence of molecular oxygen and are catalysed by enzymes classified as luciferases. Because of the increasing oxygen levels, especially during the Neoproterozoic oxidation event (NOE), and the optimisation of methods and enzymes to counter oxygen, the

luciferin/luciferase systems became obsolete for this specific purpose. Instead of being lost through natural selection these biochemical reactions of various species living across Earth evolved and were optimised for a wide array of defensive and offensive functions. The utility includes: attracting mates or prey, communication, stunning, distracting or misdirecting predators (e.g., via the autotomy of a luminescent body part), burglar alarm (making the predator visible for its own predators), and camouflage.

2.6 Bioluminescent reactions^[124,137]

Every chemical reaction of BL-systems involves the oxidation of luciferin which is catalysed by luciferases. Due to the broad diversity of bioluminescent organisms, many different luciferine/luciferase systems with varying reaction mechanisms exist. In general, the reaction can be expressed in the following way (Scheme 24):



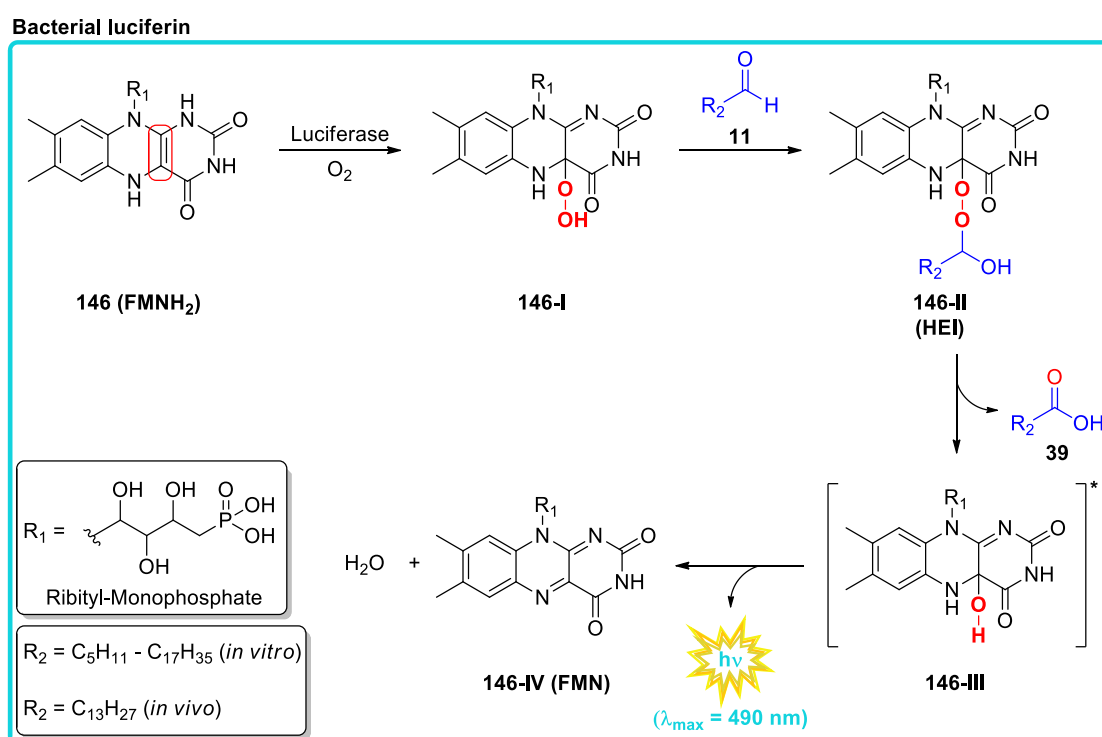
Scheme 24: Illustration of the general reaction progress of BL processes. HEI = High energy intermediate. I) Luciferin is bound to luciferase and subsequently oxidised with molecular oxygen, generating a HEI; II) The HEI is unstable and decomposes in a defined way (e.g., decarboxylation) and yields an oxyluciferin excited species. After the emission of a photon and the separation of luciferase and oxyluciferin the reaction is complete.

The whole reaction takes place within the pocket of the enzyme. In order to enable the emission of light the reaction mechanism involves the formation of a high energy intermediate (HEI), which represents an unstable species that is capable of releasing enough energy through the breakage of O–O bonds and the subsequent formation of stronger C–O bonds, including the release of byproducts such as CO₂. Thus, the decomposition leads to the corresponding oxyluciferin product and the emission of a photon. Though the enzyme itself is essential, the reaction mechanism can further depend on additional cofactors such as adenosine triphosphate (ATP) and magnesium or calcium ions. The following chapter gives a general overview of different bioluminescence systems depending on the structure of the HEI. It should be noted that some systems have not been fully understood or elucidated to date, which is why some of the following schemes illustrate reaction mechanisms that are still under discussion.

2.6.1 BL reactions involving a peroxy HEI

2.6.1.1 BL of bacteria^[124,137]

Bioluminescent bacteria are a versatile and widespread species and can live freely or in a symbiotic relationship with marine and terrestrial organisms such as fish, squids and worms as hosts. The bacteria gain nutrients and a space to colonise and the host gains a luminescence that is used for different situations. Besides symbiosis, saprophytic and parasitic behaviour are also possible.^[138] Although there are many different bioluminescent bacterial species, they all share the same biochemical reaction which involves a reduced flavin mononucleotide (**146**, FMNH₂) and an aliphatic aldehyde (Scheme 25).



Scheme 25: Mechanism of the bacterial BL. Reduced riboflavin mononucleotide (**146**) is oxidised with molecular oxygen catalysed by luciferase. The obtained peroxide **146-I** reacts with an aldehyde **11**, producing an acid compound **39** and flavin-hydroxide **146-III** as the emitting species. Upon relaxation, a photon with a wavelength of 490 nm is emitted. Modified according to ^[124].

Luciferase catalyses the oxidation of both substrates, which first leads to the flavin-peroxide **146-I**. The addition of the aldehyde **11** gives the peroxy-hemiacetal **146-II**, which is the HEI of this reaction, and decomposes to the corresponding fatty acid **39** and the flavin-hydroxide **146-III**. The latter represents the emitter of this reaction^[139] and relaxes to its ground state and emits a photon with a wavelength of 490 nm. The elimination of water yields flavin mononucleotide (**146-IV**, FMN) and represents the final product. The fatty acid obtained in this process was identified as myristic acid when the reaction is carried out *in vivo*, but

aldehydes with a chain length of 6 to 18 carbon atoms also cause light emission *in vitro*. Even though the mechanism shown in scheme 25 is generally accepted, different approaches including SET processes^[140,141] and a dioxirane species^[142] are still discussed, whereby the latter is considered inconsistent because of the many unstable intermediates.^[139,143]

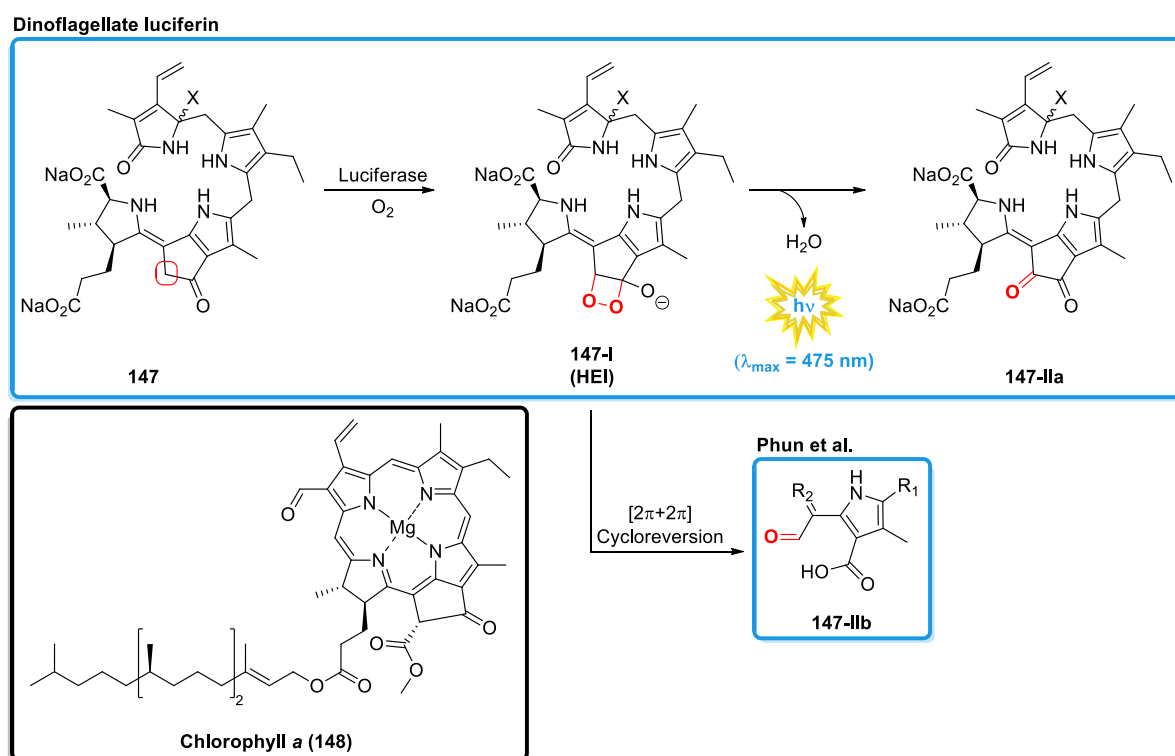
In addition to blue-green light emission, some bacterial strains have red- or blue-shifted emissions. Due to the involvement of an additional protein, the emission of *Photobacterium fischeri* Y-1 has a maximum at 540 nm (caused by the yellow fluorescent protein (YFP))^[144], while the emission of *Photobacterium phospherum*, *fischeri* and *leioognathi* is blue-shifted with a maximum at 475 nm (caused by the blue fluorescent protein (BFP), later called lumazine protein (LumP)).^[145,146] The biological relevance as well as the energy transfer mechanisms of these different emission wavelengths remain unresolved.

2.6.1.2 BL of dinoflagellates^[124,137]

Dinoflagellates are single-celled eukaryotes, that live mainly in marine and freshwater areas and make up a large part of the phytoplankton. Their name literally means "whirling whip", which is due to their appearance. Bioluminescent dinoflagellates are mainly found in the oceans. The BL reaction occurs through the deformation of the cell membrane, triggered by mechanical stimulation, e.g., by fast movements of fish, boats or breaking waves^[147], resulting in the emission of bright blue light with a wavelength maximum at 470-475 nm.^[124,148] Because of these observations and studies, it is assumed that the BL serves as a mechanism to disrupt the feeding behaviour of predators^[149] or as a burglar alarm which reveal the presence of the primary predator to secondary predators.^[150] Dinoflagellates can become abundant due to excess nutrients (e.g., marine pollution), resulting in small or large algal blooms and explaining the phenomenon of large areas of the oceans glowing green-blue during wave cycles. Besides the bright BL, larger algal blooms can provide a useful food source for higher organisms, but can also have fatal consequences. These harmful algal blooms (HAB) or red tides (due to the discolouration of the sea surface)^[151] can block sunlight, leading to oxygen depletion, and depending on the type of algae, accumulate toxins that can lead to mass mortality of marine life and birds, and can also be fatal to humans through direct exposure or consumption of fish and seafood enriched with the toxins.^[152,153]

The BL reaction of dinoflagellates is still to debate. In general, it involves an open-chained tetrapyrrole **147** and resembles the structure of chlorophyll *a* (**148**).^[154] The formation of the HEI **147-I** is enabled through deprotonation at the α -position to the keto-function of the

cyclopentapyrrolone moiety and the subsequent reaction of the corresponding anion with oxygen. The exact structure of the HEI is still a hypothesis. *Nakamura et al.*^[155] discussed an acyclic peroxide, but new theoretical calculations propose a dioxetanolate intermediate^[156], as shown in Scheme 26. In the case of the latter the subsequent cleavage of the O–O bond yields an excited *gem*-diol(ate). that upon emission of a photon eliminates water and leads to the final product **147-IIa**.



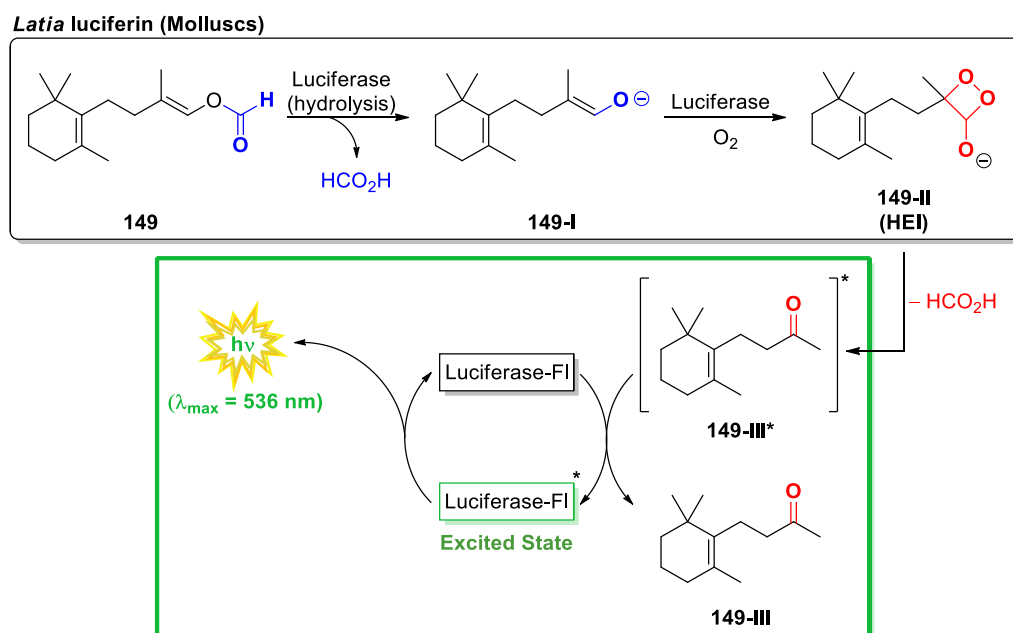
Scheme 26: (blue boxes) Mechanism of the dinoflagellate BL, the red square indicates the moiety of the molecule that is oxidised; (black box) Structure of chlorophyll *a* (**148**). The luciferin is an open-chained tetrapyrrole **147** which is oxidised with molecular oxygen catalysed by luciferase. The obtained dioxetanolate **147-I** may eliminate water, leading to the formation of product **147-IIa**^[156] or undergoes a $[2\pi+2\pi]$ cycloreversion which yields **147-IIb**.^[157] The emitting species is still controversial. The wavelength of the photon has a maximum at 475 nm. Modified according to ^[124,137].

It is worth mentioning that *in vitro* experiments showed that the emission of the dinoflagellate BL matches the fluorescence of the luciferin **147**, while **147-IIa** is not fluorescent. Therefore, an energy transfer between these two compounds has been proposed.^[158] Instead of an excited *gem*-diolate *Phun et al.*^[157] propose a $[2\pi+2\pi]$ cycloreversion which gives an oxopropenylpyrrole carboxylic acid **147-IIb** in its excited state and also represents the final product after the emission of a photon.

2.6.1.3 BL of *Latia neritoides*^[124,137,159]

The species *Latia neritoides* is a freshwater limpet endemic to the North Island of New Zealand and belongs to the phylum of molluscs. It is the only known terrestrial gastropod that can produce light. When disturbed or attacked by predators it releases a luminous green mucus, which indicates a defensive purpose of the BL.^[160]

Overall, the BL of this species has only been marginally studied and is therefore not completely understood. The reaction involves the luciferine (*E*)-2-methyl-4-(2,6,6-trimethylcyclohex-1-en-1-yl)but-1-en-1-yl formate (**149**) and a glycoprotein luciferase. A second protein (purple protein) is present as well but not directly required for the emission of the BL and fluorescence red instead of green. *Shimomura* (Nobel Prize winner 2008) mentions the possibility that the purple protein could act as an activator or enhancer.^[161] Though the reaction produces light, both the luciferin and its oxidised form **149-III** do not show fluorescence in the visible range.^[162] The light emitter itself remains unknown, but it is assumed that a flavin-like chromophore is bound to the luciferase, as its fluorescence is similar to the emission of the luciferin-luciferase system.^[161–164]



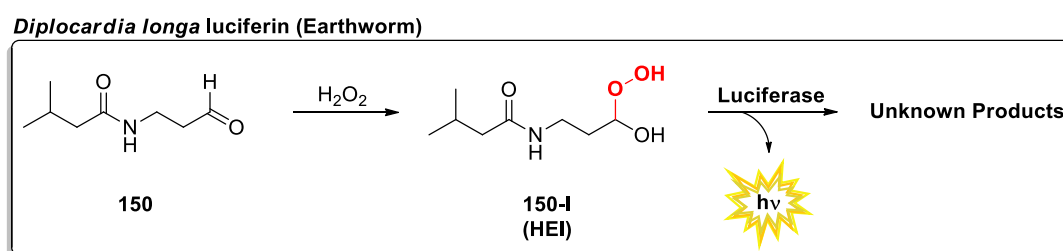
Scheme 27: Mechanism of the *Latia* BL. (black box) Hydrolysis and subsequent oxidation of *latia* luciferin **149** with molecular oxygen catalysed by luciferase; (green box) Assumed energy transfer of **149-III*** to a chromophore bound to luciferase and emission of a photon with a wavelength of 536 nm. Modified according to ^[162,164].

The proposed mechanism by *Ohmiya et al.*^[162,164] involves the hydrolysis of the ester yielding formic acid and alkoxide **149-I** (Scheme 27). Similar to the BL mechanism of dinoflagellates (see Chapter 2.6.1.2, **147-I**), the subsequent oxidation yields the HEI in form of a

dioxetanolate **149-II**. The decomposition yields a second equivalent of formic acid and the excited ketone compound **149-III*** which transfers its energy to a luciferase bound chromophore and emits a photon ($\lambda_{\text{max}} = 536 \text{ nm}$).

2.6.1.4 BL of *Diplocardia longa*^[124,137,165]

In general, many luminescent earthworms across the Earth are known to mankind, with the BL of *Diplocardia longa* (and *Friderica heliota*, Chapter 2.6.2.2) being one of most extensively studied. This earthworm species is native to the region of southern Georgia, USA, and grows up to 60 cm long and 1 cm wide. The luminescence of *D. longa* is localised in large cells in the coelomic fluid, which can be excreted from the body orifices when the worm is disturbed or stimulated. A bioluminescent mucus is formed only after cell lysis^[166], while the body of the worm itself does not luminesce. In general, the purpose of earthworm BL remains uncertain but a defensive mechanism^[167] and the attraction of mates^[168] have been suggested.



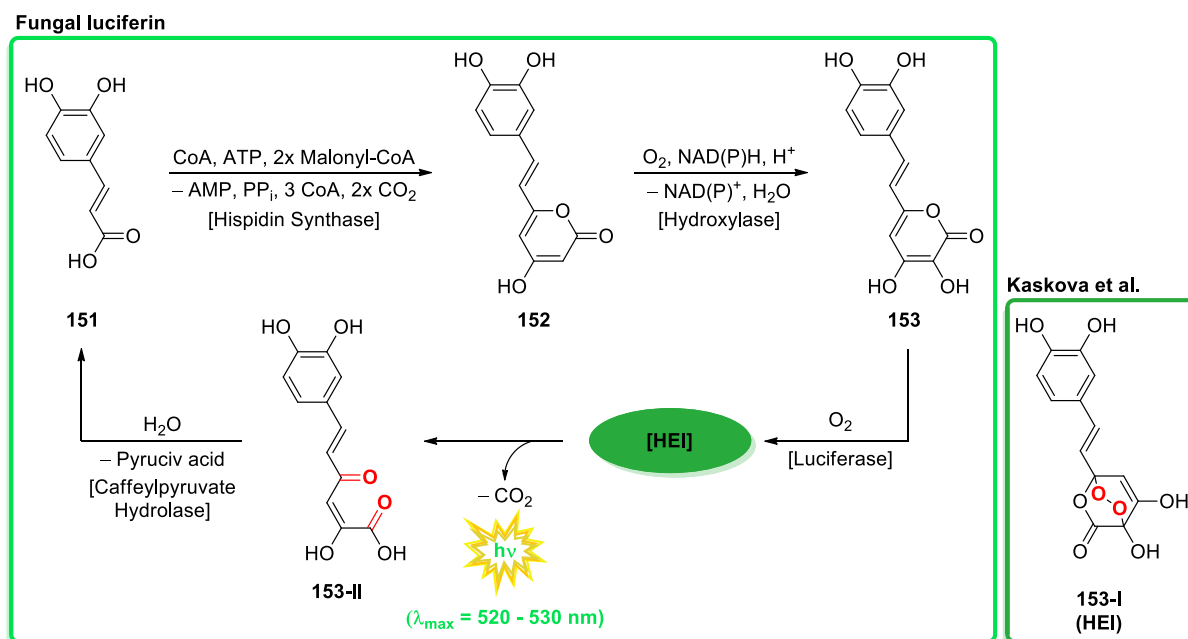
Scheme 28: Mechanism of the BL of *D. longa*. The luciferin **150** generates a geminal hydroperoxyl alcohol **150-I**, which is used for a subsequent reaction catalysed by luciferase. The structure of the corresponding oxyluciferin as well as the emitting species remain unknown. Modified according to ^[137,165].

The luciferin of this reaction is *N*-isovaleryl-3-amino-propanal (**150**, Scheme 28).^[169] In contrast to the previous BL reactions, this oxidation uses hydrogen peroxide instead of molecular oxygen. Although it has been shown that the reaction itself occurs without oxygen in the atmosphere, it is required during cell lysis. When worms expel the coelomic fluid in an oxygen-free atmosphere, no emission was observed. It is therefore assumed that when the cells are ruptured, an oxidase enzyme is released that generates hydrogen peroxide from oxygen.^[170] The latter is used for the subsequent BL reaction, suggesting that the luciferase is a peroxidase enzyme that oxidises the aldehyde to the corresponding acid. However, the emitting species has not yet been clarified. Overall, the luciferin **150** (or derivatives of it) has been found in 13 different earthworm species with varying emission maxima ranging from

500–570 nm.^[171,172] Luciferase also shows high substrate selectivity, leading to the hypothesis of a uniform BL mechanism for many earthworm species.

2.6.1.5 BL of fungi^[124,137]

Recent studies have summarised a collection of 109 luminescent fungal species on Earth, classified into four distinct evolutionary lineages.^[173] Independent of species the greenish emission maxima range from 520–530 nm^[174] which suggests that they all share a common BL reaction mechanism.^[175] Depending on the species the emission of light can occur in different or multiple regions of the fungus e.g., the mycelia, fruit bodies or rhizomorphs so that the luminescence appears to have different purposes.^[176] 3-Hydroxyhispidine (**153**) is the luciferin responsible for the observed green bioluminescence (Scheme 29).^[177,178]



Scheme 29: (light green box) Mechanism of the fungal BL; (dark green box) Proposed HEI intermediate **153-I** by Kaskova *et al.*^[179] Overall four different enzymes are involved which enable a recycling process. After formation of lactone **152** and hydroxylation, the oxidation of luciferin **153** yields the oxyluciferin **153-II** and a photon. Modified according to ^[173,180].

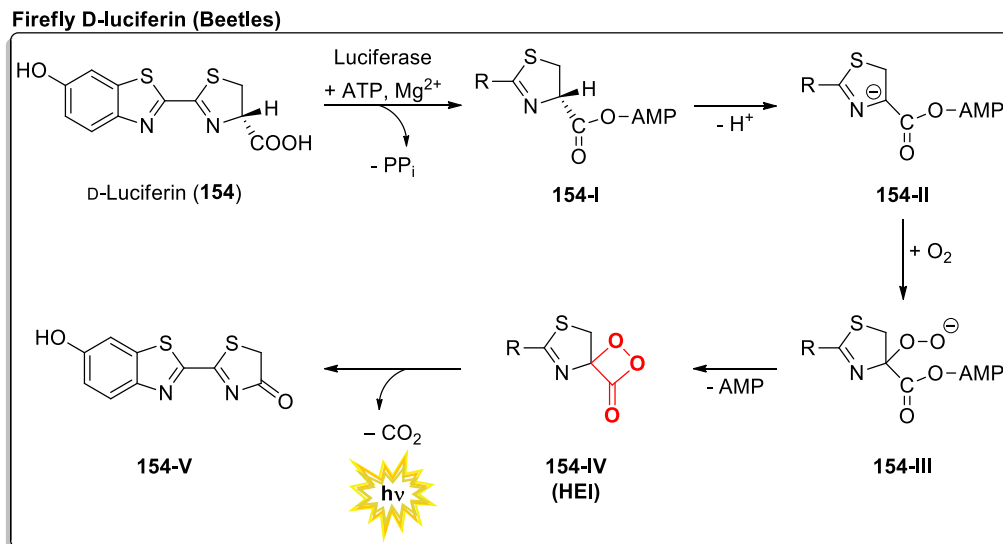
Most bioluminescent fungi have a common synthetic pathway involving four different enzymes that use caffeic acid (**151**) as a precursor. Formation of hispidine (**152**) followed by hydroxylation yields the luciferin, which is oxidised with molecular oxygen. After decarboxylation of the HEI, the exact structure of which is not yet clear, the corresponding oxyluciferin **153-II** is obtained, which can be degraded back to **151** by caffeoylpyruvate hydrolase.^[179,180] An endoperoxide **153-I** was recently proposed as the crucial HEI.^[179]

2.6.2 BL reactions involving a dioxetanone HEI

2.6.2.1 BL of fireflies^[124,137]

The most classic example for a BL in literature and other media is that of fireflies. It is also the best studied in terms of its reaction mechanism, the biosynthesis of luciferin and the study of the structures and sequences of luciferases.

Though termed fireflies (Lampyridae), they belong to the order of beetles (Coleoptera) instead to that of flies (Diptera). In addition to Lampyridae, the families of Phengodidae, Elateridae, Rhagophthalmidae and Sinopyrophoridae (recently recognised)^[181,182] together contain over 2000 bioluminescent species.^[183] The emission of light is used for communication and the attraction of prey or mates, including the known phenomena of large groups flashing together in unison. It is assumed that all beetle species share the same luciferin and the same reaction mechanism for their BL.^[184] Studies showed that the emission wavelength was not dependent on additional proteins or the luciferin but the structural differences of the luciferases.^[185,186] A famous example is the railroad worm *Phrixothrix hirtus*, which is capable of green/yellow BL along its body and red BL localised on its head using the same luciferin.^[187]



Scheme 30: Mechanism of the firefly BL. Luciferase requires ATP and Mg²⁺ as cofactors. After deprotonation and subsequent oxidation with molecular oxygen at the α -position of the luciferin adenylate, dioxetanone **154-IV** is obtained. Its decarboxylation yields the oxyluciferin **154-V** and a photon. Modified according to ^[124].

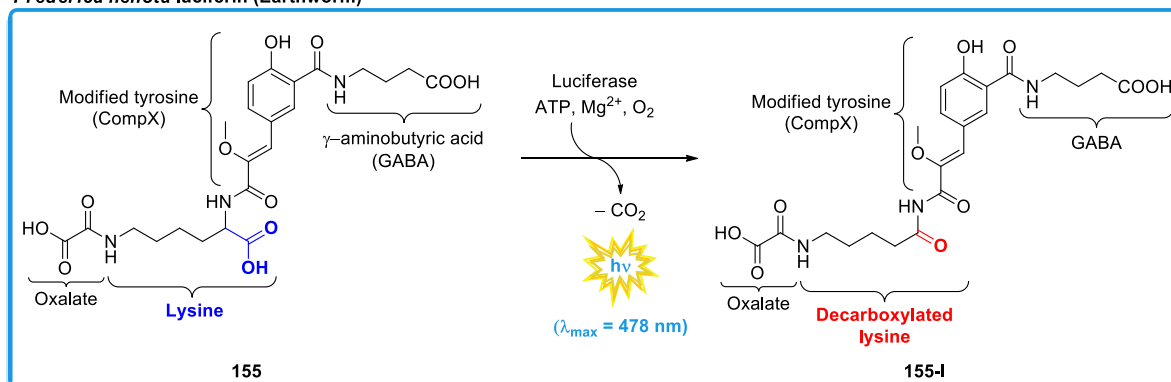
The firefly luciferin comprises a 6-hydroxybenzothiazole moiety connected with a 4-carboxy-4,5-thiazole ring (Scheme 30, **154**). The quantum yield of this reaction amounts to 41%.^[188] In this biochemical process, luciferase requires ATP and Mg²⁺ as cofactors for the transformation of firefly luciferin to the corresponding oxyluciferin **154-V**. The first step

involves the consumption of ATP for the formation of luciferyl adenylate **154-I** and pyrophosphate. The α -carbon of the resulting ester group in the intermediate is then deprotonated. Subsequently the carbanion **154-II** reacts with molecular oxygen, leading to the peroxide anion **154-III**, which substitutes the AMP rest of the ester and yields the firefly dioxetanone **154-IV** as the HEI. The latter was proven by the work of *Shimomura et al.* in 1977.^[189] However, the exact formation of the 1,2-dioxetanone remains unresolved. One hypothesis suggests that a basic side chain (supposedly a histidine residue *His245*) within the enzyme cavity deprotonates the luciferin to obtain the carbanion **154-II**. The oxidation then proceeds via SET-processes, involving a superoxide (O_2^-).^[190] Alternatively, the dioxygen molecule itself abstracts a hydrogen atom from the anionic intermediate, resulting in a hydroperoxide radical (HO_2^{\cdot}), which then recombines with the formed radical intermediate to give the HEI.^[191]

2.6.2.2 BL of *Friderica heliota*^[137]

First discovered in 1990, the bioluminescent earthworm *Friderica heliota* inhabits the soil of the Siberian forests. In comparison to *D. longa* (Chapter 2.6.1.4) *F. heliota* is very small in size (15-20 mm) with its body being semi-transparent. Additionally, the BL is located within the epidermal cells^[192] instead of expelled coelomic fluid, showing a blue emission ($\lambda_{\max} = 478$ nm).^[193]

Friderica heliota luciferin (Earthworm)



Scheme 31: Mechanism of the BL of *F. heliota*. Luciferase requires ATP and Mg^{2+} as cofactors. Similar to the BL of fireflies, luciferin **155** is oxidised, producing a dioxetanone. Subsequent decarboxylation gives the oxyluciferin **155-I** and the emission of blue light. Modified according to ^[194].

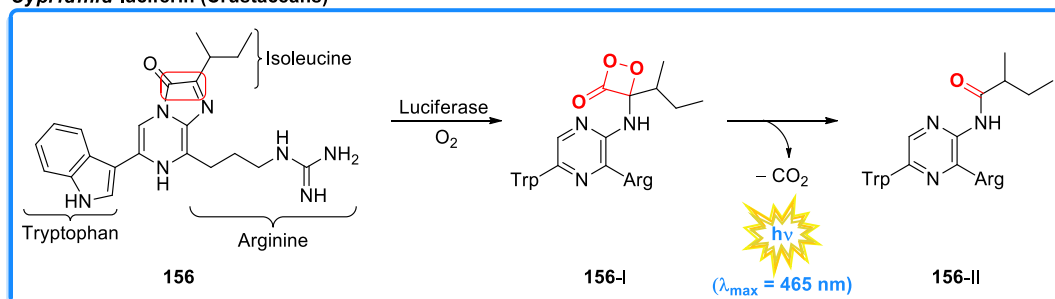
The reaction mechanism as well as the structure of luciferin **155** were elucidated by *Yampolsky et al.*^[192] The proposed mechanism is similar to that of the firefly (Chapter 2.6.2.1) and involves the formation of a luciferin adenylate on the lysine side chain (Scheme 31).^[194]

Oxidation at the α -carbon with oxygen yields a dioxetanone as HEI, which decarboxylates to give **155-I**. It is assumed that the CompX part is responsible for the photon emission.^[165,194] Recent theoretical calculations suggest that the oxidation of the penta-anionic derivative of **155** (with the three carboxylic acids, α -carbon of lysine and phenol-OH deprotonated) is initiated by SET processes.^[195]

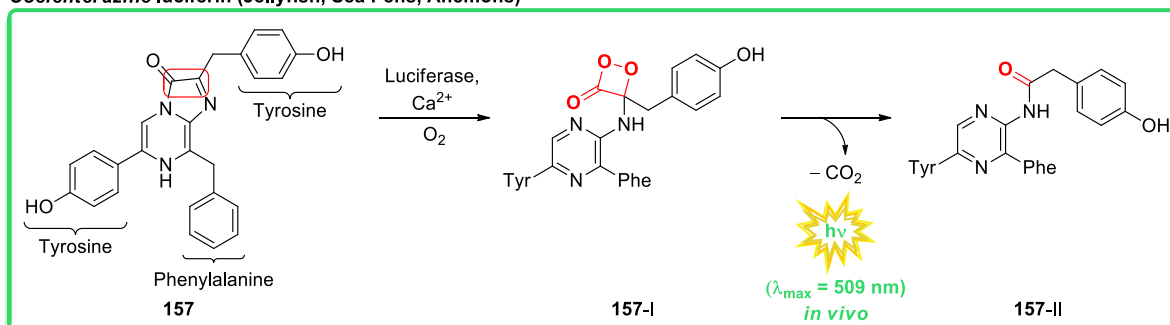
2.6.2.3 BL of cypridinid and coelenterazine systems^[124,137]

Cypridinid luciferin **156** is found in numerous species belonging to the family of ostracods (Cypridinidae). One of the best known and studied species is *Vargula hilgendorfi* (formerly known as *Cypridina hilgendorfi*^[196]), which is native to the southern coast of Japan. Since firefly species occur in Japan as well, its inhabitants termed it “*umi-hotaru*”, which literally means “sea-firefly”. It generally grows to only 3 mm in length and prefers shallow waters for its nocturnal foraging. Predators are repelled or intimidated by the secretion of a luminous fluid, allowing *V. hilgendorfi* to escape. Similar to fireflies, males of the species *Photeros annecohenae* are known to produce pulses of light in order to attract females.^[197]

Cypridinid luciferin (Crustaceans)

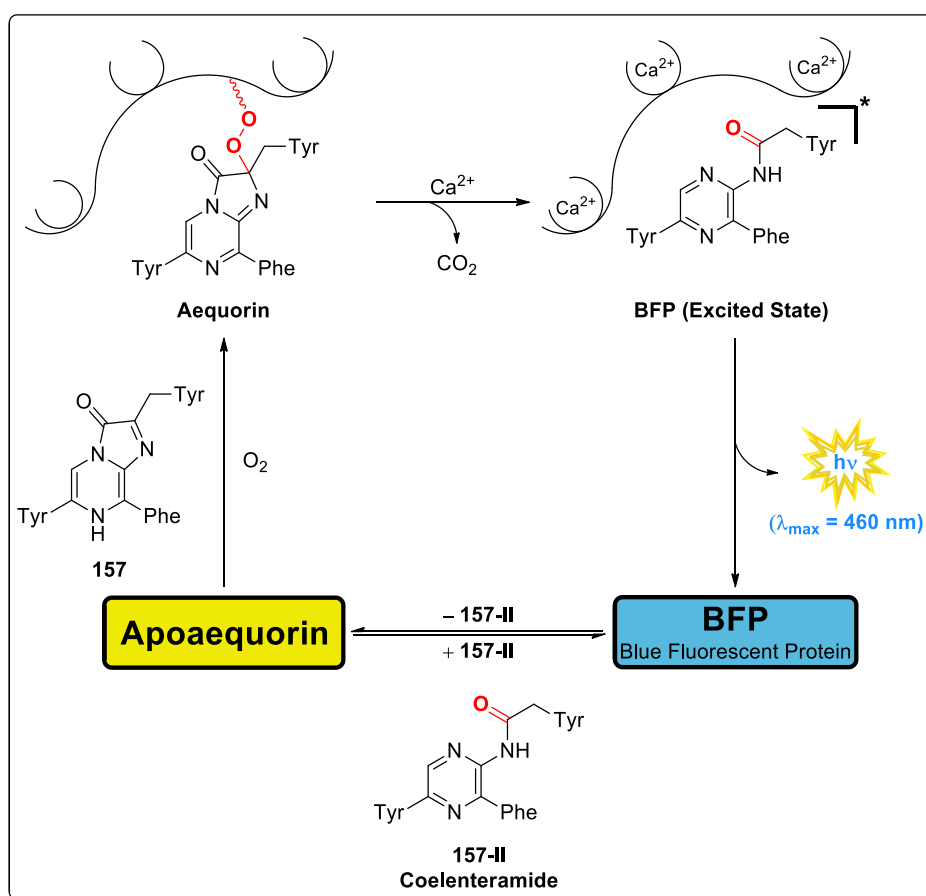


Coelenterazine luciferin (Jellyfish, Sea Pens, Anemons)



Scheme 32: (Top) Mechanism of BL with cypridinid luciferin; (Bottom) Mechanism of BL with coelenterazine luciferin. Both mechanisms involve luciferins with an imidazopyrazinone scaffold and a 1,2-dioxetanone as HEI. Coelenterazine BL additionally requires Ca²⁺ as cofactor. Modified according to ^[124].

Coelenterazine luciferin **157** on the other hand is found in numerous marine species such as jellyfishes, sea pens and anemones (Coelenterata), crustaceans and squids. Due to its ability to quench reactive oxygen species, it is also an important compound of the diet for non-luminescent marine life. Similar to bacteria (Chapter 2.6.1.1) some species such as *Renilla reniformis* (soft coral) and *Aequorea victoria* (jellyfish) possess a photoprotein as well as a red-shifting green fluorescent protein (GFP).^[198] Light emission peaks *in vivo* at 509 nm due to an energy transfer from the excited oxyluciferin to the GFP and turns blue in the absence of the latter.^[164] Hence the photoproteins themselves are termed blue fluorescent proteins (BFP). Cypridinide and coelenterazine luciferin both share an imidazopyrazinone core structure, differing only in their amino acid side chains (Scheme 32). In both cases, these systems generate a 1,2-dioxetanone as HEI^[199–201], resulting in the emission of blue (or green) light with good quantum yields.^[202,203] The BL of cypridinids requires only luciferin, luciferase and oxygen^[204], whereas the BL of Coelenterates involves photoproteins (e.g., aequorin^[201] and obelin^[205]) that require calcium ions to convert to luciferases and activate the reaction of coelenterazine with dioxygen leading to the HEI (Scheme 33).



Scheme 33: BL mechanism of *A. victoria*. without GFP. Apoaequorin binds the peroxy-luciferin to form the aequorin protein. Ca²⁺ acts as cofactor and activates the enzymatic function of aequorin, leading to the decarboxylation of the luciferin and the emission of blue light. Modified according to ^[164].

2.7 Definition and history of chemiluminescence^[115,137]

CL is defined as an emission of electromagnetic radiation originating from atoms or molecules, which achieve an excited electronic state through an exergonic chemical reaction. The emitted radiation ranges from the ultraviolet (UV) over the visible to the infrared (IR) region. When compared photochemical and CL reactions are complementary to each other. In a photochemical reaction, a photon is absorbed to excite a reagent, while in a CL reaction, the reagent enters an excited state through an exergonic thermal process leading to photon emission. Therefore, spontaneous exergonic reactions can release enough energy to produce electronically excited species that can decay by emitting a photon.

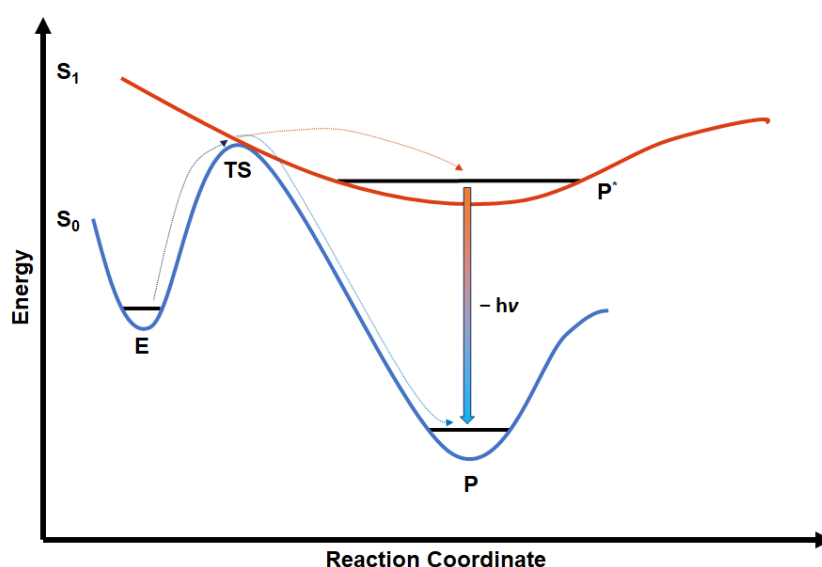


Figure 9: Energy profile diagram of a CL-reaction. The blue line represents the hyper surface of the electronic ground state (S_0) and red line that of the first excited state (S_1). The dashed blue and red arrows show the possible reaction paths. E starting material, P^* excited product, P product, TS transition state. Modified according to ^[115].

Figure 9 shows the energy profile diagrams of a CL reaction. Every point along the reaction coordinate represents a certain arrangement of the nuclei from the reagent E to the product P. During a CL reaction, the energy-rich reagent enters the excited state S_1 , potentially resulting in light emission. Consequently, thermodynamically highly unstable reagents, relative to their corresponding products (P), are particularly favoured for the phenomena of chemiluminescence.^[126]

The first scientifically documented chemiluminescence was accidentally discovered in 1669 by the German alchemist *Heinrich Hennig Brand*.^[206] By boiling urine, *Brand* first caused the sodium ammonium hydrogen phosphate dissolved in the urine to form polymeric sodium metaphosphate, which was then reduced by carbon-based charred products, producing carbon

monoxide, sodium biphosphate and elemental phosphorus in the form of a gas, the latter solidifying into white waxy phosphorus.^[115,207] The yellowish-green light is produced by the oxidation of the white phosphorus by molecular atmospheric oxygen and partly by water due to atmospheric humidity, creating the short-lived HPO molecules and the (PO)₂*-excimer, both of which emit visible light.^[208] In 1877, the Polish chemist *Radziszewski* discovered the first artificial organic chemiluminescence with lophine, which reacts with oxygen in an alkaline solution.^[209] Subsequently, interest in chemiluminescence reactions and their applications grew, from the *Trautz-Schorigin* reaction^[210,211] to the synthesis and characterisation of lucigenin^[212] and luminol^[213] (still used in modern forensics, etc.) to the chemiluminescence of peroxyoxalates^[214] (a reaction used for glow sticks), singlet oxygen^[215], 1,2-dioxetanes^[216-218] and the recent CL system of 2-coumaranones^[219]. It is important to emphasise the interdisciplinary nature of the phenomenon of CL (and BL). Current research and applications span the fields of biology, chemistry and medicine, which underlines its versatility and benefits to humanity.

2.7.1 Quantum yield, intensity and efficiency of CL-processes^[115,137,220]

Efficient CL emission requires specific conditions to be met. The energy needed for electronic excitation must come from a chemical reaction. According to the Planck-Einstein formula (Equation 3):

$$E = h\nu \text{ or } E = \frac{hc}{\lambda} \quad (\text{Eq. 3})$$

$E = \text{energy [J]}$, $h = \text{Planck-constant [Js]}$, $\nu = \text{frequency [Hz]}$, $c = \text{speed of light constant [m/s]}$, $\lambda = \text{wavelength [m]}$.

the enthalpy change of the reaction must fall within the 168 to 294 kJ/mol range to produce visible light emission. In 1964, *Chandross* and *Sonntag* proposed that this energy release must occur rapidly in a confined volume, all in a single reaction step.^[221]

$$\phi_{CL} = \phi_R \phi_{ES} \phi_F \quad (\text{Eq. 4.1})$$

$$\phi_{CL} = \phi_R \phi_{ES} \phi_{ER} \phi_F \quad (\text{Eq. 4.2})$$

$\phi_{CL} = \text{quantum yield of chemiluminescence reactions}$, $\phi_R = \text{chemical yield of molecules that are not excited}$, $\phi_{ES} = \text{yield of primarily electronically excited molecules}$, $\phi_{ER} = \text{energy-transfer-yield of primarily electronically excited molecules to the fluorophore}$, $\phi_F = \text{fluorescence quantum yield of the emitting species}$.

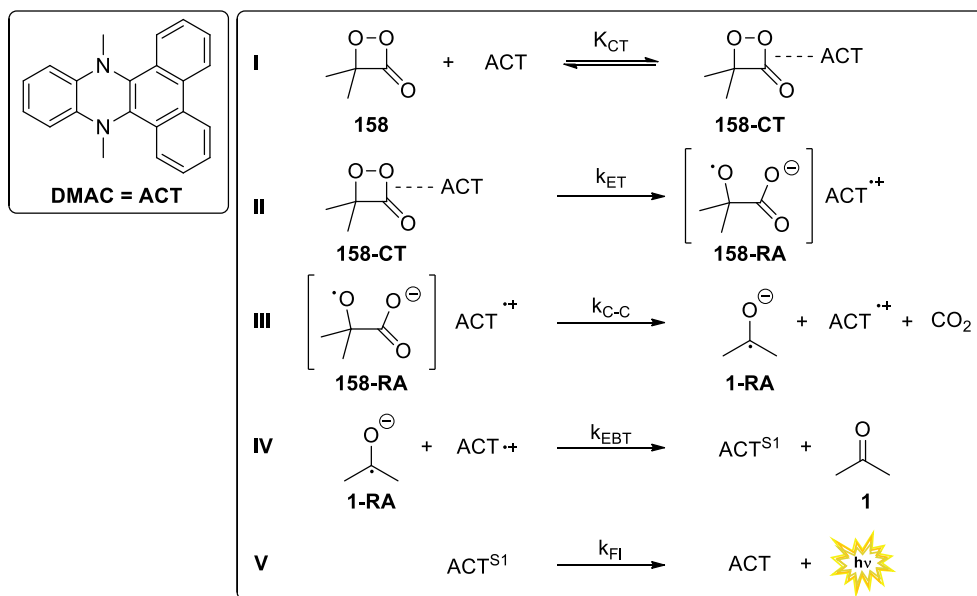
When the vital reaction involves multiple bonds, a concerted mechanism becomes indispensable. To evaluate the effectiveness of a CL reaction, the quantum yield can be calculated, representing a ratio between zero (0%, indicating no light emission) and 1.0 (100%). For direct CL equation 4.1 and for indirect (sensitised) CL, equation 4.2 is applicable. In situations where the quantum yield of a CL reaction falls short, introducing a suitable fluorophore to the reaction mixture becomes a viable strategy. The energy from the excited species gets transferred to the fluorophore, allowing the observation of distinctive fluorescence as an indirect or sensitised CL emission.

2.7.2 Chemiexcitation: CIEEL and CTIL mechanism^[137]

In analogy to BL systems, most of the CL reactions involve oxidation processes which generate cyclic peroxides as HEI. In total, three mechanisms are considered for chemiexcitation: I) Uncatalysed thermal decomposition; II) catalysed decomposition of cyclic peroxides involving ET and III) catalysed intramolecular decomposition of cyclic peroxides with electron-rich substituents. Since the uncatalysed pathways mainly lead to triplet excited states, which results in a low emission rate and cannot explain the observed quantum yields in BL processes, two catalysed chemical excitation mechanisms have been established that provide a more comprehensive explanation for the efficiency of these reactions.

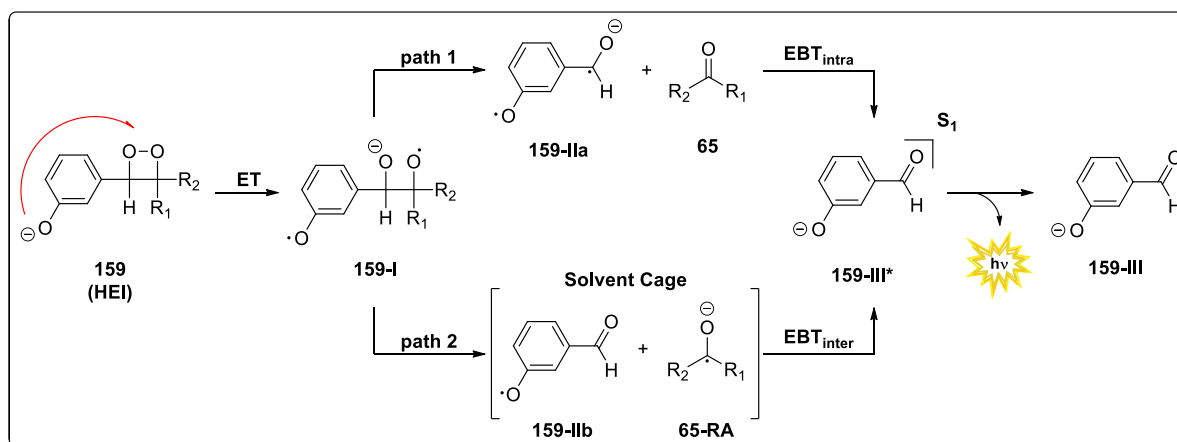
The first mechanism is known as "chemically initiated electron exchange luminescence" (CIEEL).^[222-224] This is a bimolecular decomposition process supported by several experimental results showing that the addition, amount and structure of aromatic hydrocarbons correlates with a higher decomposition rate of a cyclic peroxide.^[225] In the following, the mechanism with 1,2-dimethyldioxetanone (**158**) and 9,14-dimethyl-9,14-dihydro-dibenzo[*a,c*]phenazine (DMAC) as activator is presented according to *Schuster's* experiment (Scheme 34).^[226] The CIEEL mechanism begins with the formation of a charge transfer complex **158-CT** between a 1,2-dioxetanone and the activator (ACT). ET from the activator to the O–O- σ^* orbital initiates the dissociation of the peroxide bond, which leads to the formation of a radical carboxylate anion **158-RA** and a radical activator cation. Calculations have shown that ET is favoured by stretching the O–O bond. Subsequently, the C–C bond is cleaved and the radical carboxylate anion decomposes into a radical carbonyl anion **1-RA** and a neutral species (in this case CO₂). The radical anion **1-RA** and radical activator cation remain in close proximity in a solvent cage, giving rise to a neutral carbonyl

species **1** and the activator in its first excited singlet state by electron back transfer (EBT). In the final phase, this excited activator species returns to its ground state by emitting a photon.



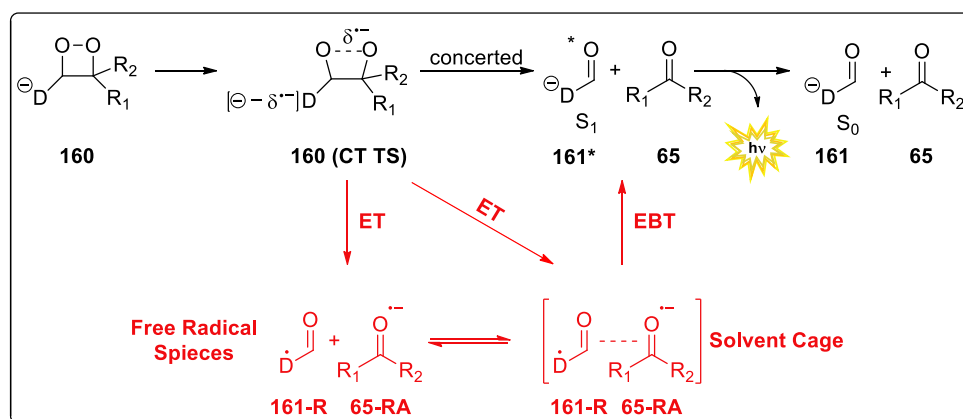
Scheme 34: CIEEL mechanism of **158** with DCAM as activator (ACT). Step I: CT complex formation of **158-CT**; Step II: ET occurs, triggering the dissociation of the peroxide bond; Step III: Cleavage of the C-C bond, yielding carbonyl radical anion **1-RA**, an ACT radical cation and CO_2 ; Step IV: EBT gives the neutral carbonyl species **1** and leads to singlet excitation of the ACT; Step V: light emission and relaxation of the ACT to its ground state. Modified according to [226].

However, the existence and efficiency of intermolecular EBT in the CIEEL mechanism is still controversial. The solvent-cage theory was analysed via solvent viscosity dependency and led to the conclusion of an intermolecular mechanism.^[227–229] In a study by *Baader et al.* the peroxyoxalate system, which can only occur intermolecularly (Chapter 2.7.3.1), and dioxetane systems (Chapter 2.7.3.3) were compared to each other.



Scheme 35: Decomposition of phenoxy-substituted 1,2-dioxetanes via the CIEEL mechanism. After deprotection, the obtained phenolate **159** initiates the cleavage of the O–O bond, which then undergoes an intra- (path 1) or intermolecular (path 2) catalysed dissociation. EBT yields the excited species **159-III*** which emits a photon. Modified according to [137].

Using apolar solvent mixtures from pure toluene to 90 % DPM (viscosity increase by a factor of 4.6), the CL quantum yields of two different dioxetane systems was raised by a factor of 2.2 and 2.6, respectively, while that of the peroxyoxalate was enhanced by a factor of 9.4. This minor increase for the dioxetane-systems has been used to argue for an intramolecular mechanism.^[230] Scheme 35 illustrates both possible mechanisms with 1,2-dioxetanes that are activated by phenolates.

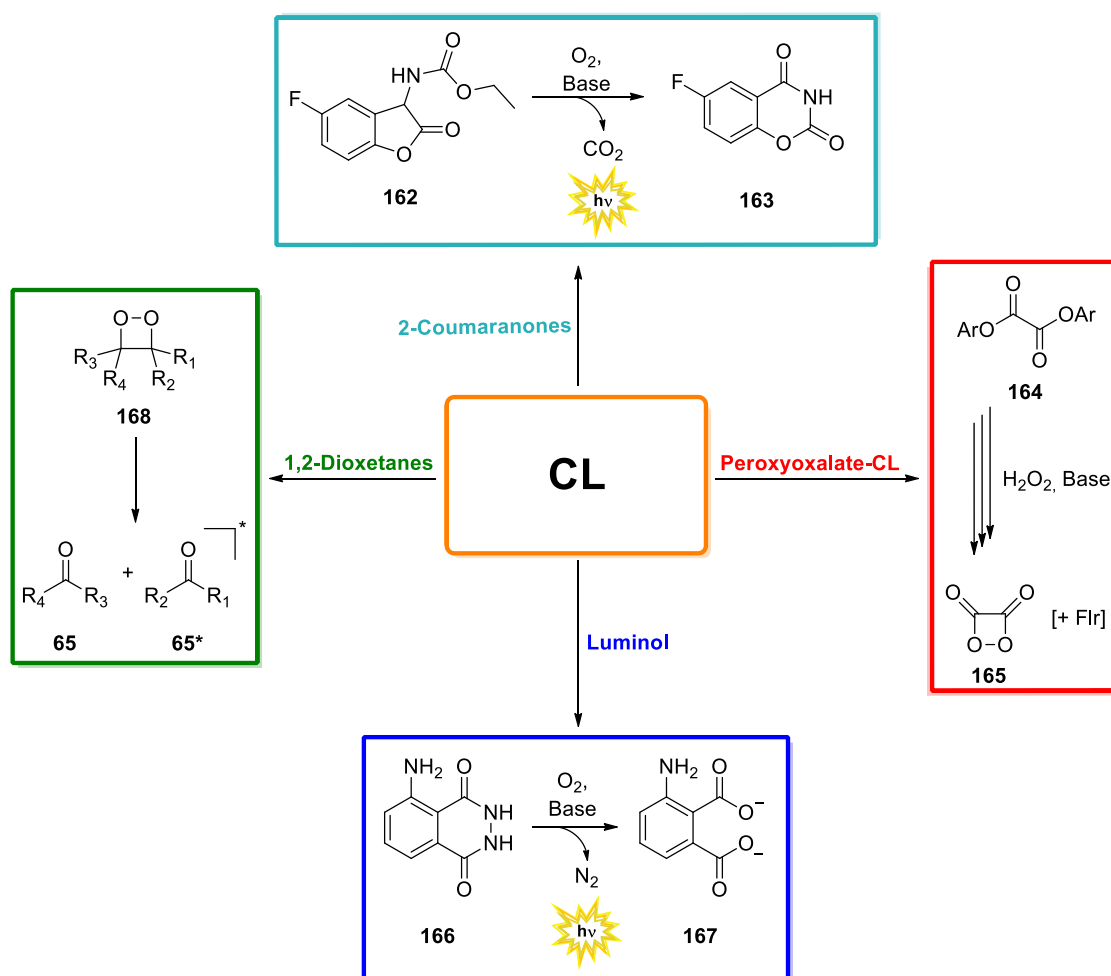


Scheme 36: Charge transfer-induced luminescence mechanism (CTIL) for the catalysed decomposition of a 1,2-dioxetanone **160** with an electron rich group (D) presented in black. The chemical induced electron exchange (CIEEL) mechanism is presented in red. Modified according to ^[231].

Because of this controversy, *Wilson et al.* proposed another mechanism^[232,233], called charge transfer induced luminescence (CTIL).^[231,234] In contrast to the CIEEL mechanism no complete electron transfer occurs and decomposition of the O–O bond is achieved by a partial charge-transfer from the activator to the peroxide, which yields the products **161** and **65** without the formation of radical ion pairs (Scheme 36). In this model, the activator is part of the dioxetane species **160** and must be an ionisable electron-rich group. Charge transfer (CT) and charge back transfer (CBT) occur gradually and in a concerted way with simultaneous cleavage of the O–O and C–C bonds. The CTIL mechanism is supported by theoretical simulations on firefly^[235,236] and sea-firefly^[237] dioxetanones. However, computational and experimental data, including the BL of coelenterazine and cypridinid, suggest that neutral rather than anionic dioxetanones are involved in the chemiexcitation step and that the chemiexcitation profiles of the neutral dioxetanones are more favourable.^[238–241]

2.7.3 Types of chemiluminescent reactions

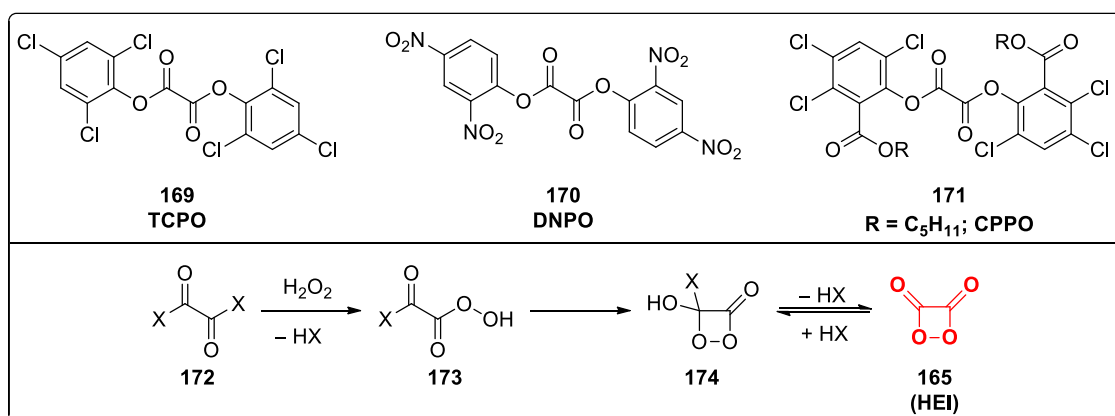
Although CL and BL reactions have been extensively studied and researched, there is still a need for new and efficient CL systems for analytical and practical applications. Even minor changes to potentially efficient CL systems can lead to a significant reduction in the intensity of light emission or even render them non-functional. Therefore, compounds such as luminol continue to be used in current scientific fields as they are still the best options. In the following chapters, four viable CL systems, namely the peroxyoxalate reaction, luminol, 1,2-dioxetanes and 2-coumaranones (Scheme 37), are briefly discussed in terms of their synthesis, CL mechanism and benefits to society.



Scheme 37: General overview of the best-known CL-systems. These include the peroxyoxalate reaction (red), luminol (blue), 1,2-dioxetanes (green) and 2-coumaranones (cyan). Flr = fluorescent compound.

2.7.3.1 Peroxyoxalate-CL^[115,242,243]

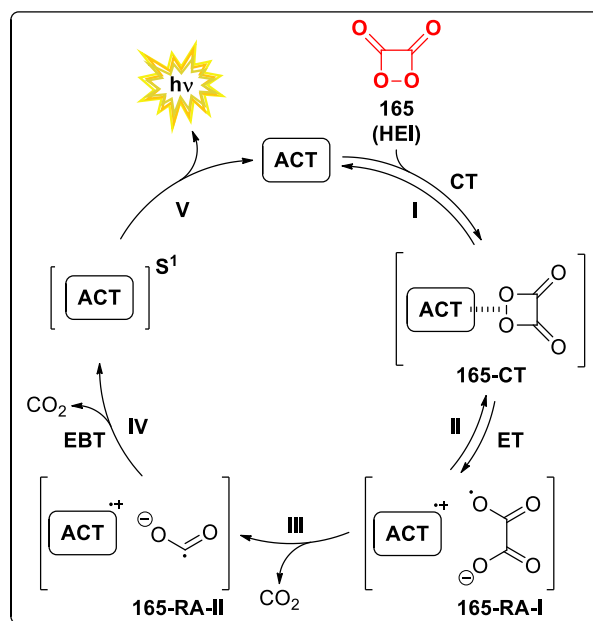
The peroxyoxalate reaction represents a sensitised CL and is well known because of its usage for glow sticks. These devices are a helpful and cheap source of light especially in emergency situations. It was also established as a viable tool for bioimaging and therapeutics.^[244] The reaction was first described by *Chandros* in 1963.^[214] When oxalyl chloride, oxalic anhydrides or oxalate derivatives are combined with hydrogen peroxide it gives a HEI. However, the reaction itself does not produce light by itself and hence requires the addition of a fluorescent dye. This allows the emission all visible colours. Research by *Rauhut et al.* and the Cyanamid Company focused on the synthesis of various oxalic acid derivatives in order to optimise the quantum yields.^[245–247] He established a correlation between the substitution of the phenols and the CL quantum yield, as well as a correlation between substitution and emission lifetime. The best results were achieved with oxalate derivatives containing aryl rests with electron withdrawing groups (Scheme 38, top). Nowadays, mainly *bis*-(2,4,6-trichlorophenyl)oxalate (TCPO, **169**), *bis*(2,4-dinitrophenyl)oxalate (DNPO, **170**) and *bis*[2,4,5-trichloro-6-(pentyl-oxycarbonyl)phenyl]oxalate (CPPO, **171**) are used. By optimising the reaction conditions oxalic anhydrides^[248] as well as oxalate ester^[245] and amide^[249] systems can reach quantum yields between 15% and 35%.



Scheme 38: (Top) Illustration of TCPO (**169**), DNPO (**170**) and CPPO (**171**); (Bottom) Formation of 1,2-dioxetanedione (**165**). Hydrogen peroxide (H_2O_2) acts as a nucleophile and reacts with an oxalic acid derivative **172**, generating the corresponding oxalic peracid **173**. Ring-closure leads to the formation of 1,2-dioxetanone **174**. Elimination of HX gives the HEI **165**. Modified according to ^[242].

The mechanistic details of this CL reaction were investigated (Scheme 39) with a major focus on the determination of the HEI. Via infrared spectroscopy (IR) the quantitative decomposition of ester groups was detected within 4 minutes after the addition of H_2O_2 . The CL itself, however, remained visible for much longer. It could also be delayed by adding the

fluorescent agent later. These results lead to the proposition of dioxetanedione (**165**) as a metastable intermediate.^[245] MS^[250] and NMR^[251,252] (including ab initio calculations) investigations of the peroxyoxalate-CL added new important details and led to formulation of a reaction mechanism (Scheme 38, bottom), but there has been no clear evidence for the assumed HEI.



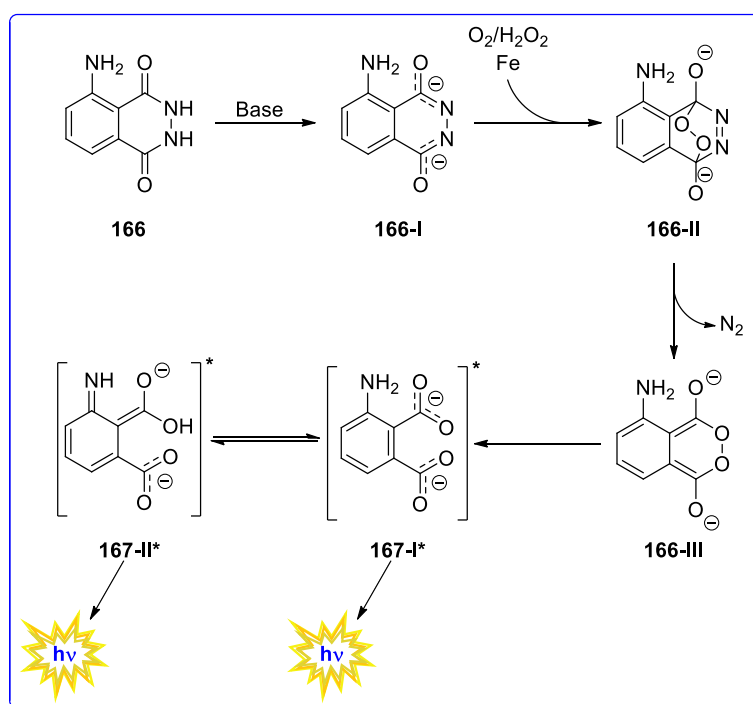
Scheme 39: Chemiexcitation of the peroxyoxalate CL. Step I: charge transfer complex formation of **165-CT**; Step II: ET (or partial CT) occurs, triggering the dissociation of the peroxide bond; Step III: Concerted C-C bond cleavage of **165-RA-I** and loss of CO₂; Step IV: an EBT (or CBT) gives a singlet excited ACT species and the release of a second equivalent of CO₂; Step V: light emission and relaxation of the ACT to its ground state. Modified according to ^[242].

Experimental^[253,254] and theoretical^[255] data confirm, that the decomposition mechanism of cyclic peroxides involves ET or CT. Lower quantum yields correlate with higher steric hindrance within the CT-complexes, showing that the additional planarity of the sp²-hybridised carbonyl groups facilitates the interaction between ACT and HEI during CT-complex formation. In 2021, 52 years after its first postulation by *Rauhut et al.*, a kinetic study by *Baader et al.* proved that dioxetanedione (**165**) represents the HEI of the peroxyoxalate reaction.^[256]

2.7.3.2 Luminol^[137]

As one of the most prominent CL compounds, luminol (**166**) was first mentioned by the German chemist *Schmitz* in 1902.^[257] The first important observation was made in 1928 by *Albrecht*^[213], who found that blood enhanced the CL of luminol in an alkaline solution of

hydroperoxide. This was later confirmed by another experiment with luminol in the presence of haematin^[258] and quickly established luminol as an important tool for detecting blood at crime scenes in the late 1940s.^[259,260] Further publications discussed the optimisation of the CL of luminol and its derivatives^[261,262] as well as its use for the detection of proteins and ions in cellular assays.^[263,264] Luminol needs to be oxidised, preferably in the presence of a catalyst such as a transition metal, to trigger CL, but the exact mechanism is not yet clear. There are several routes for the oxidation of luminol, depending on the reaction conditions used. In aprotic solvents such as DMSO, a strong base can generate the luminol dianion **166-I**, which subsequently reacts with molecular oxygen.^[265,266] In aqueous solutions, the proposed mechanisms involve a series of oxidation and deprotonation steps that result in reactions with hydrogen peroxide or superoxide radicals.^[267,268] The generally accepted mechanism involves the formation of an endoperoxide **166-II** (Scheme 40). Due to the neighbouring aniline moiety, a CIEEL chemiexcitation has been proposed involving ET processes from the former to the σ^* -orbital of the O-O bond.^[269] Overall, similarities with fungal BL can be seen (chapter 2.6.1.5).



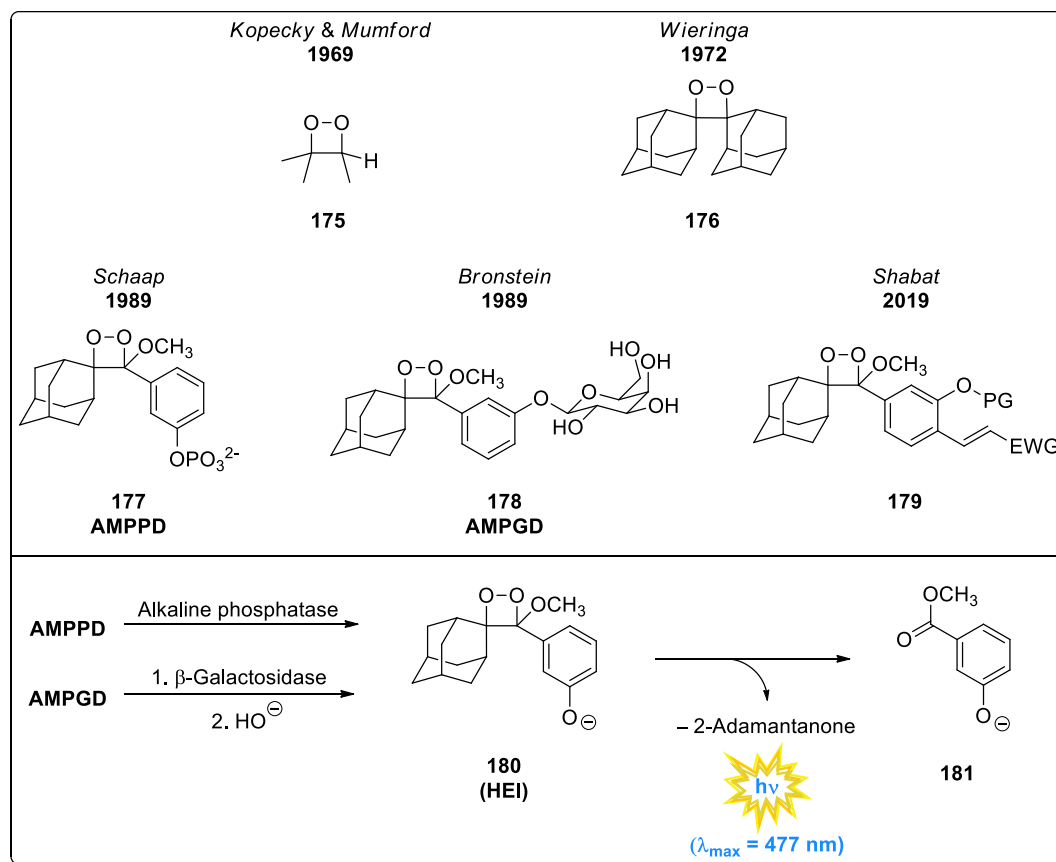
Scheme 40: Proposed mechanism for the oxidation and CL of luminol **166** In an alkaline solution the dianion **166-I** is generated, which in the presence of a catalyst (e.g., iron) is oxidised to the corresponding endoperoxide **166-II**. Upon release of nitrogen the cyclic peroxide **166-III** is obtained. Both structures **167-I*** and **167-II*** are considered for light emission depending on the solvent. Modified according to ^[137].

Once endoperoxide **166-II** is formed, ring opening occurs with relatively low thermal energy, producing the cyclic peroxide **166-III** by splitting off nitrogen gas and subsequently entering

the excited state. The exact structure of the HEI is still controversial, as both the endoperoxide **166-II** and the cyclic peroxide **166-III** are potential intermediates that could produce excited states upon decomposition. In luminol experiments by *White et al.* the occurrence of different emission maxima in water (424 nm) and in DMSO (485 nm) was discovered, which was attributed to the formation of two different excited structures (**167-I*** and **167-II***).^[270] It is assumed that the long wavelength band in aprotic solvents is due to photo tautomerism, in which an intramolecular proton transfer from the amino group to the neighbouring carboxyl group takes place in the excited state, which is inhibited in protic solvents by intermolecular hydrogen bonds to the carboxylate group.^[271]

2.7.3.3 1,2-Dioxetanes^[137,243]

As an important and unstable intermediate, 1,2-dioxetanes play a central role in numerous CL reactions. The stability and properties of these cyclic systems can vary greatly depending on the substituents.



Scheme 41: (Top) Illustration of 1,2-dioxetanes from various publications, EWG electron withdrawing group; (Bottom) Enzymatic triggering of AMPPD (**177**) and AMPGD (**178**) forming the phenolate (**180**), which upon decomposition releases light and yields ester (**181**). Modified according to ^[115].

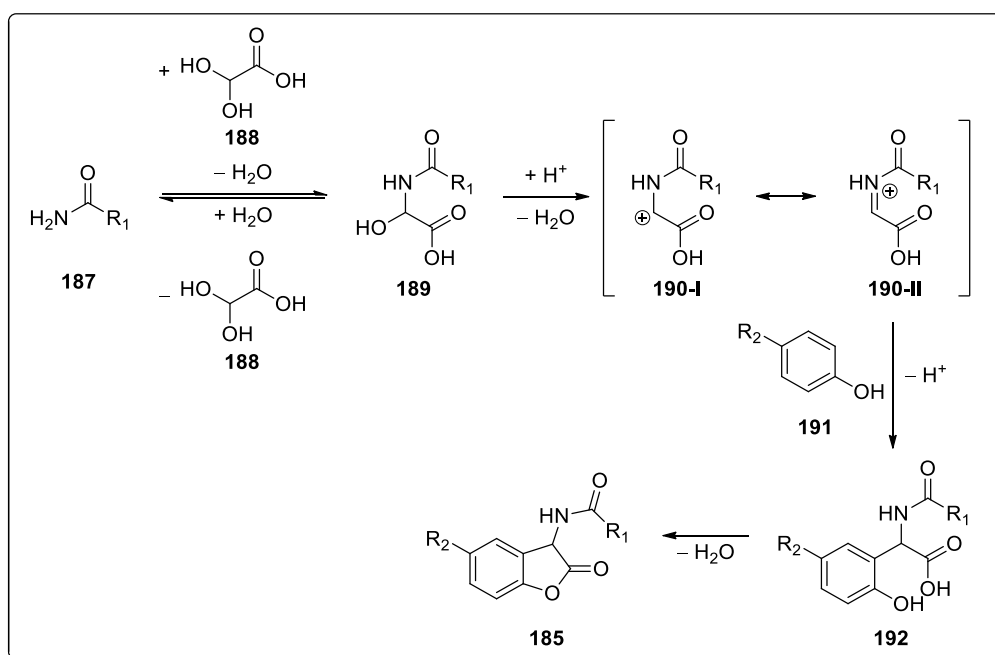
The formation of an emitting state of the carbonyl product during thermal decomposition involves the breaking the O–O bond as the initial and rate-determining step.^[272–274] For the unsubstituted 1,2-dioxetane, both experimental and theoretical investigations have determined the activation energy required for the initial ring opening to be approximately 23.0 and 23.5 kcal mol⁻¹, respectively.^[275] Apart from the considerable energy barrier for O–O bond cleavage, thermal decompositions of 1,2-dioxetanes usually exhibit low quantum yields.^[276,277] Taking into account the influence of effective spin-orbit coupling (SOC) according to the *El-Sayed's* rule^[278,279] and the phenomenon of "entropic trapping"^[275], excited triplet states are more populated than excited singlet states, which explains the poor emission efficiency.

Though *Kopecky* and *Mumford* achieved the first successful thermal synthesis of trimethyl-1,2-dioxetane (**175**)^[280,281], the preferred method became the [2+2] cycloaddition of electron rich olefins with singlet oxygen. Applying this photooxygenation method *Wieringa et al.* published the synthesis of *bis*-adamantylideneoxetane (**176**), the first dioxetane completely stable at room temperature (Scheme 41).^[282] This important discovery enabled various syntheses and modifications of spiroadamantyl-substituted dioxetanes that had the stability required for applications in analytical fields such as immunoassays and enzyme activity studies. The first studies on the enzymatic or chemical activation of 1,2-dioxetanes with adamantane groups such as AMPPD (**177**) and AMPGD (**178**) were carried out by *Schaap*^[218] and *Bronstein*^[216,217] and further research was done in particular by *Shabat's* group.^[283–285] During deprotection, a phenolate is formed, which represents the HEI and initiates the cleavage of the weak O–O bond and leads to the decomposition of the dioxetane. The electronically excited carbonyl species obtained emits light either by direct CL or by transferring its energy to a fluorophore. A CIEEL mechanism is assumed for these reactions.

2.7.3.4 2-Coumaranones^[137]

2-Coumaranones represent the youngest CL system. The initial research of their chemiluminescence began the late 1970s when *Lofthouse et al.* investigated the luminescence properties of 3-alkoxycarbonyl substituted 2-coumaranones.^[219] Later, *Matuszczak et al.* continued the research, expanding the scope of substitution patterns for these compounds and also establishing enzyme activity studies with horse radish peroxidase (HRP).^[286–289] In 2019 *Krieg et al.* published the first synthesis of urea-coumaranones and discussed their luminescence properties (Scheme 42).^[290]

is singlet excited. After the emission of light, the emitter relaxes back to its ground state. According to the literature, if the substructure contains a carbamate group, the phenolate performs a nucleophilic attack on the carbonyl carbon, producing the corresponding alkoxide and the cyclised product **186**. This process has not been studied for coumaranones with a urea substructure. In addition, the peroxide anion can take an alternative pathway via a dark reaction as a side reaction. This pathway involves a nucleophilic attack on the amide carbonyl carbon leading to the formation of a spirodioxazolidinone **185-VII**. Subsequently after eliminating the sidechain of R_1 , compound **185-VIII** decarboxylates and forms the transition state **185-IX** that ultimately leads to the same end product **186**.



Scheme 44: Mechanism of the *Tscherniak-Einhorn* reaction forming the 2-coumaranone **185**, starting from an amide compound **187**, GAM (**188**) and a phenol compound (**191**).

Through optimisations a one-pot *Tscherniak-Einhorn* reaction became the method of choice for the synthesis of 2-coumaranone derivatives, using an amide compound **187**, glyoxylic acid monohydrate (GAM, **188**) and TFA or acetic acid containing 10% sulfuric acid as solvent and catalyst (Scheme 44).^[290,295] After a defined amount of time a *para*-substituted phenol compound **191** is added to give the desired coumaranone **185** in good yields. In the first step, condensation takes place between the amide **187** and GAM (**188**), forming compound **189**. Acid catalysis eliminates a second equivalent of water to give the iminium ion **190-II**. The cationic species is nucleophilically attacked by the phenolic compound **192**, resulting in the orthoamidoalkylated compound **192**. In a final step, ring closure leads to the desired product.

3. Task and motivation

Though the chemistry of protecting and releasing defined functional groups within a substrate has already been optimised and fine-tuned over the past decades, an analytical measurement is always required and desirable to trace the efficiency of those processes. Especially a quick and easily detectable deprotection of a functional group is desirable for planning ahead for further syntheses. Considering the aforementioned PPGs, that can also be designed as orthogonal protective groups, the substrate is released via the usage of light either by direct absorption or by photocatalytic methods in order to release the protected molecule. The reverse principle is the release of a protected molecule accompanied by the emission of light, i.e., chemiluminescent protecting groups (CLPG, Figure 10).

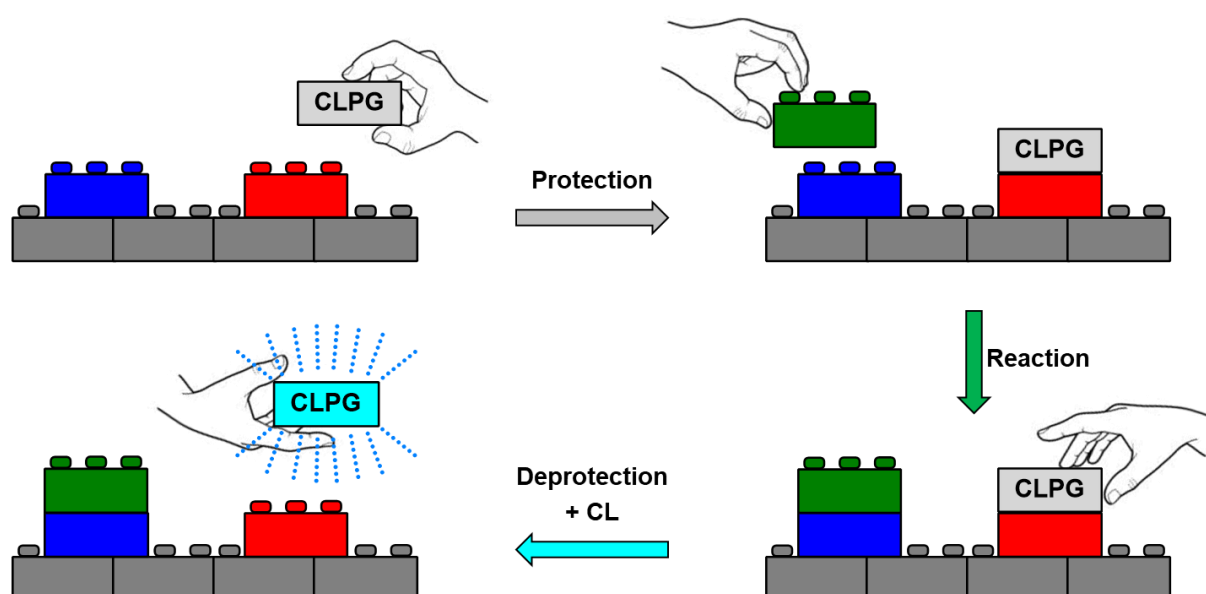
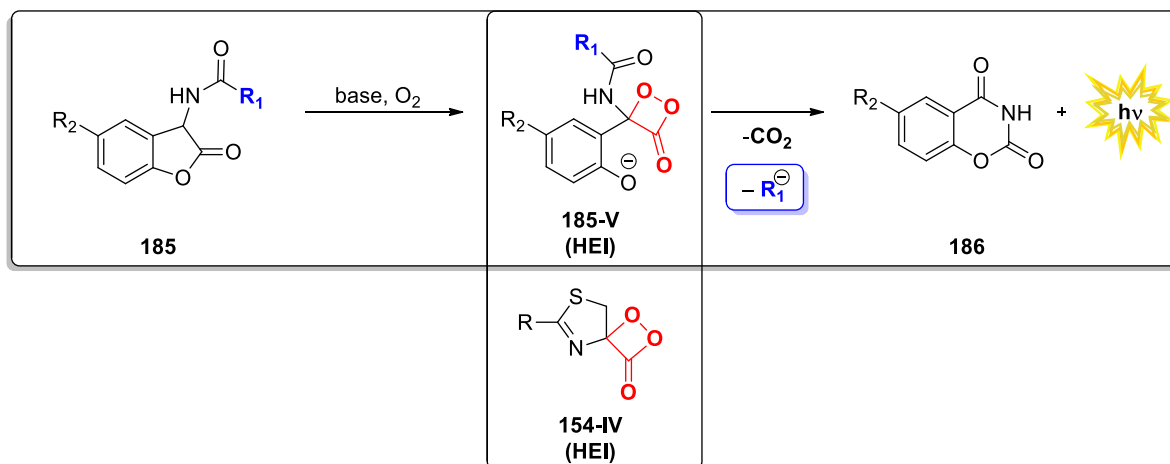


Figure 10: Simplified scheme for the concept and application of a CLPG. One functional group is protected and therefore inhibited for the subsequent reaction. Afterwards the PG is removed again and shows a fluorescence via CL, indicating that the PG was successfully removed.

In general, chemiluminescent systems or compounds, such as oxalate diesters, adamantanedioxetanes, luminol and coumaranones, can be regarded a PG, considering the requirement of a high energy intermediate (HEI), which decomposes and may release smaller molecules. Thus, the emission of light can be interpreted as a signal indicating the successful cleavage of the CLPG. Coumaranones represent a versatile class of potent chemiluminescent compounds, due to their basic scaffold, which allows many variations. The CL mechanism shows also similar characteristics when compared to BL reactions, which involve a 1,2-dioxetanone as well. With the addition of a non-nucleophilic base (e.g., DBU), it can react with molecular oxygen and generates a dioxetanone as the crucial HEI. After CO_2 is

eliminated, an excited species is obtained, which emits a photon. Finally, a ring enlargement occurs and the protected molecule (“payload”) is released again.



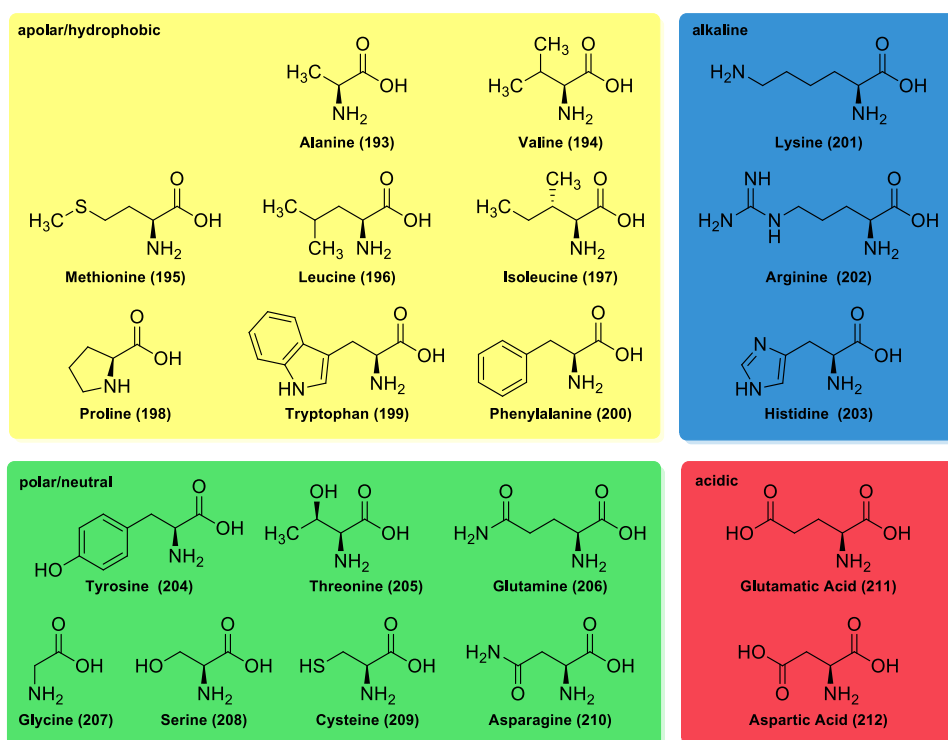
Scheme 45: Illustration of the decomposition of a coumaranone in a basic environment. The HEI **185-V** of the coumaranone CL reaction is similar to the HEI of the firefly BL **154-IV**.

Considering the demands for good and effective PGs, additional ones for the concept of CLPGs must be considered: I) a bright chemiluminescence in the visible range that ends with the completion of deprotection, and II) the CLPG itself should not exhibit any interfering absorption or fluorescence properties until the start of deprotection. In this present work, therefore, the synthesis of the protected substrates as well as the additional requirements imposed by the CLPGs are examined in detail, discussed and checked for their validity. Thus, the range, efficiency and limitation of coumaranones as potential CLPGs is demonstrated.

4. Results and discussion

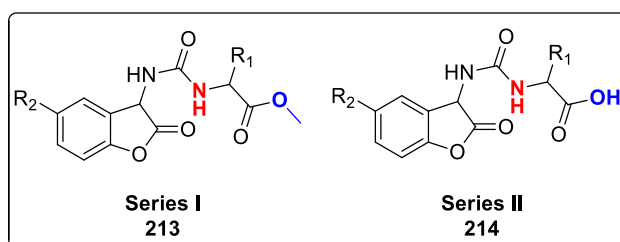
4.1 Protection and deprotection of amines

Based on the latest results published in 2019^[290], the protection of amines by coumaranones was further investigated to gain a better understanding of this new topic. Proteinogenic amino acids were chosen as the starting material for an application-based option (Scheme 46).



Scheme 46: Overview of 20 proteinogenic amino acids, sorted according to the properties of their side chain. Selenocysteine is excluded.

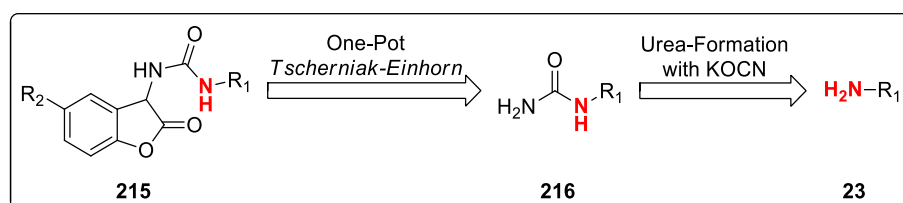
Overall, two new series of urea-coumaranones were designed (Scheme 47). For the first one, the amino acids were additionally protected as methyl esters, in order to circumvent possible side reactions during the planned synthesis route. The other series was directly converted to the urea derivatives. If the synthesis of coumaranones proved to be successful in both cases, the major differences between these two compound classes could be analysed.



Scheme 47: Basic scaffold of the first and second series of coumaranones with a urea substructure.

4.1.1 General protection protocol of amines

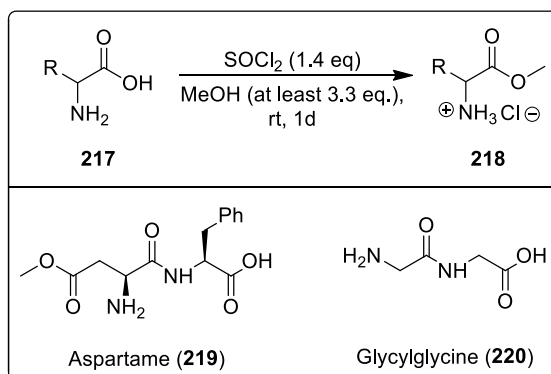
For the protection of amines with coumaranones, a two-step procedure was used (Scheme 48). First, amine **23** is converted to the corresponding urea derivative **216** by addition of potassium cyanate. Then a one-pot *Tscherniak-Einhorn* reaction is carried out to give the desired urea-coumaranone **215**.



Scheme 48: Retrosynthesis of the protection of amines.

4.1.1.1 Syntheses of amino acid methyl esters

The first series of urea-coumaranones includes the methyl ester derivatives of proteinogenic amino acids and the dipeptides aspartame (**219**) and glycylglycine (**220**). The esterification was performed according to the synthesis instructions by *Molinaro et al.*^[296] (Scheme 49).



Scheme 49: (Top) Illustration of the synthesis of amino acid methyl ester hydrochlorides; (Bottom) Structure of aspartame (**219**) and glycylglycine (**220**).

Since the esterification of amino acids has been optimised over the last decades and the obtained yields are often quantitative these compounds will not be mentioned within the experimental section. The substrates used for this reaction are summarised in Table 3. Of all proteinogenic amino acids (excluding selenocysteine) the products of the esterification of glutamine and asparagine showed two new signals in the area of 3.60 – 3.70 ppm with an integral of three protons. This led to the assumption that the amide group was also converted

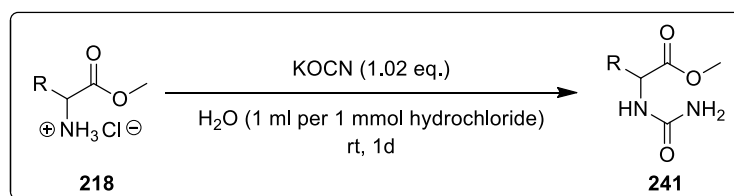
to a methyl ester. Purification via column chromatography as well as a test reaction to obtain the corresponding urea compound, proved that instead of glutamine and asparagine methyl ester the dimethyl esters of aspartic and glutamic acid were obtained.

Table 3: Proteinogenic amino acids and dipeptides used for the methyl esterification according to the adapted synthesis protocol of *Molinaro et al.* Every methyl ester was obtained in a quantitative yield. The compound names highlighted in bold represent dipeptides.

Entry	Methyl ester of	Entry	Methyl ester of
221	Glycin	231	Histidine
222	Alanine	232	Phenylalanine
223	Valine	233	Proline
224	Isoleucine	234	Tryptophan
225	Leucine	235	Tyrosine
226	Methionine	236	Serine
227	Aspartic acid	237	Arginine
228	Glutamic acid	238	Lysine
229	Theronine	239	Glycylglycine
230	Cysteine	240	Aspartame

4.1.1.2 Syntheses of ureido carboxylic acids and methyl esters

The preparation of the urea compounds, which are the starting material for the *Tscherniak-Einhorn* reaction, was done in two different ways depending on the substrate. For the amino acid methyl ester hydrochlorides, the synthesis protocol of *I. Nicolas et al.*^[297] was followed with minor adaptations (Scheme 50).



Scheme 50: Illustration of the synthesis of ureido carboxylic acid methyl esters.

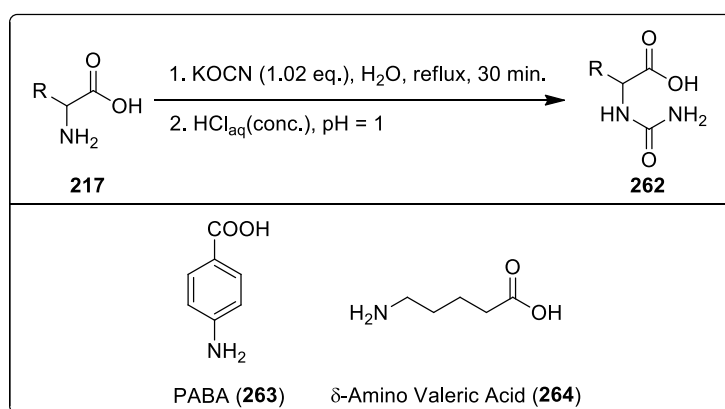
Instead of stirring the solution for one hour the duration was extended to 1 day, which led to better yields in many cases. Additionally, the amount of water was changed from 170 eq. to 1 ml per 1 mmol of amino acid methyl ester hydrochloride. The starting material was always highly soluble in small amounts of water, which then sometimes enabled the precipitation of the urea products. In opposite to that other urea compounds had a high solubility in water, which was counteracted by removing excessive water at reduced pressure or saturating the aqueous phase with salt before extraction. The yields are summarised in Table 4. All urea

derivates of the amino acid methyl esters were successfully prepared except in the case of cysteine, arginine and lysine. Though $^1\text{H-NMR}$ spectra of the latter two revealed that the urea product was formed, a lot of starting material remained and the urea product could not be extracted efficiently. Basic work up of the aqueous phase as well as different purification methods did not result in a better yield and the product itself had a poor solubility in organic solvents. Therefore, no further attempts were made to obtain the coumaranones of these amino acids. The achieved yields varied among the respective amino acids from 95% for the histidine urea **252** to the lowest yield with 13% for the proline urea **254**.

Table 4: Proteinogenic amino acids and dipeptides used for the synthesis of ureido carboxylic acid methyl esters according to the adapted synthesis protocol of *I. Nicolas et al.*^[297] Cysteine could not be converted to the corresponding urea compound. Lysine and Arginine formed the desired products but it was not possible to obtain it in a good yield and high purity.

Entry	Urea of	Yield [%]	Entry	Urea of	Yield [%]
242	Glycine-OMe	69	252	Histidine-OMe	95
243	Alanine-OMe	91	253	Phenylalanine-OMe	71
244	Valine-OMe	71	254	Proline-OMe	17
245	Isoleucine-OMe	84	255	Tryptophan-OMe	87
246	Leucine-OMe	90	256	Tyrosine-OMe	48
247	Methionine-OMe	92	257	Serine-OMe	36
248	Aspartic acid-(OMe) ₂	72	258	Arginine-OMe	n.a.
249	Glutamic acid-(OMe) ₂	46	259	Lysine-OMe	n.a.
250	Theronine-OMe	56	260	Glycylglycine-OMe	21
251	Cysteine-OMe	0	261	Aspartame-OMe	70

For the second series of urea-coumaranones the carboxylic acid of the amino acids was not protected and the synthesis protocol of *A. N. Kravchenko et al.*^[298,299] was followed with minor adaptations (Scheme 51).



Scheme 51: (Top) Illustration of the synthesis of ureido carboxylic acids; (Bottom) Structure of PABA (**263**) and δ -amino valeric acid (**264**).

Instead of adding KOCN in portions to a refluxing solution of the amino acid in water, it was already added to the suspension of the amino acid in water prior to the reaction. The reaction mixture was always refluxed for 30 instead of 20 minutes regardless if the substrate was an amino acid or a dipeptide. Besides proteinogenic amino acids, PABA (**263**) and δ -amino valeric acid (**264**) were also used for this reaction in order to increase the amount of possible urea substrates for the subsequent synthesis of the coumaranones.

While the many amino acids did all precipitate after the acidification it was not possible to obtain any urea derivative in the case of acidic (aspartic (**271**) and glutamic acid (**272**)), alkaline amino acids (lysine (**282**), arginine (**281**), histidine (**275**)) or dipeptides (aspartame (**286**), glycylglycine (**285**)) with this method. The products showed high solubility in water and could not be extracted or obtained in a good yield and high purity, regardless of the work up procedures. In the case of the polar amino acids, the synthesis protocol could be optimised by using EtOH instead of water as solvent and refluxing the solution for 4 hours, which led to better yields. The urea derivatives of tyrosine (**279**), glutamine (**283**) and asparagine (**284**) could be verified via NMR or HR-MS. However, it was only possible to obtain a few milligrams of product. In table 5 the yields of the ureido carboxylic acids are summarised and compared to the ones of the ureido carboxylic acids methyl esters.

Table 5: Proteinogenic and non-proteinogenic amino acids and dipeptides used for the synthesis of ureido carboxylic acids according to the adapted synthesis protocol of *A. N. Kravchenko et al.*^[298,299] The yield percentage in brackets represents the yield of the ureido carboxylic acid methyl ester derivative. The urea derivatives of tyrosine, glutamine and asparagine could be verified but the yield remained very low. The methyl ester of PABA and δ -amino valeric acid have not been synthesised.

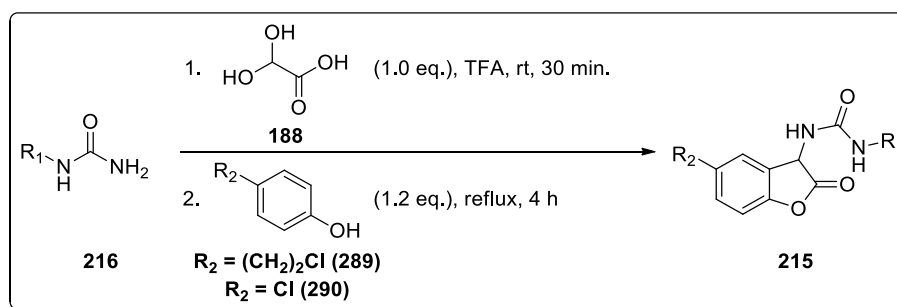
Entry	Urea of	Yield [%]	Entry	Urea of	Yield [%]
265	Glycine	28 (69)	277	Proline	8 (17)
266	Alanine	50 (91)	278	Tryptophan	84 (87)
267	Valine	62 (71)	279	Tyrosine	n.a. (48)
268	Isoleucine	85 (84)	280	Serine	79 (36)
269	Leucine	76 (90)	281	Arginine	0 (n.a.)
270	Methionine	86 (92)	282	Lysine	0 (n.a.)
271	Aspartic acid	0 (72)	283	Glutamine	n.a. (0)
272	Glutamic acid	0 (46)	284	Asparagine	n.a. (0)
273	Theronine	49 (56)	285	Glycylglycine	0 (21)
274	Cysteine	45 (0)	286	Aspartame	n.a. (70)
275	Histidine	0 (95)	287	PABA	82
276	Phenylalanine	85 (71)	288	δ -Amino valeric acid	72

In total, 14 amino acids could be converted to the corresponding urea compounds, while it was possible to obtain 15 proteinogenic amino acids and two dipeptides as ureido carboxylic acid methyl esters. As it can be seen in table 5 many yields strongly deviate from the ones of

the methyl esters derivatives. In most cases the yield of the ureido carboxylic acid is lower than that of the methyl ester derivative. The largest reduction in yield, excluding reactions with no yield at all, is for glycine (**265**) and alanine (**266**), with a difference of 41%. In contrast to this the ureido carboxylic acid derivatives of phenylalanine (**276**) and serine (**280**) could be obtained in a higher yield with a positive difference of 14% and 43% respectively.

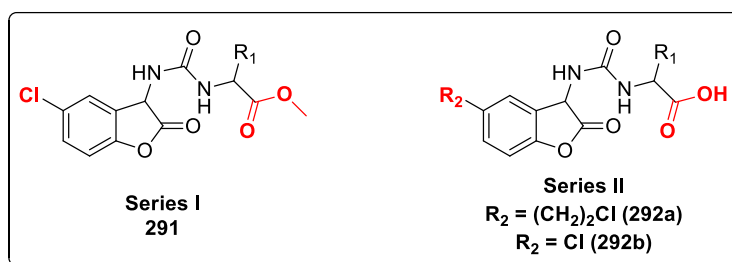
4.1.1.3 Tscherniak-Einhorn reaction with urea compounds

The coumaranones with a urea substructure were synthesised according to an adapted synthesis protocol of *R. Krieg et al.*^[290] Instead of stirring the solution at room temperature for longer time periods, the reaction had to be refluxed in order to be successful (Scheme 52). This also shortened the reaction time to 4-8 hours, while longer reflux times led to a reduction in yield and caused the almost complete hydrolysis of the ester group. Trifluoroacetic acid was not removed under reduced pressure, but the solution was poured on an excess amount of ice water and the crude product was filtrated and dried. If no products precipitated, they were extracted with EtOAc or DCM. Every compound was purified via column chromatography using mixtures of DCM/MeOH, additionally with one percent of acetic acid in the case of the ureido carboxylic acid derivatives, as eluent.



Scheme 52: Illustration of the synthesis of coumaranones with a urea substructure according to the adapted synthesis protocol of *R. Krieg et al.*^[290]

In general *para*-chloro phenol (**290**) was the preferred phenol compound for the first series of coumaranones with ureido carboxylic acid methyl ester sidechains, but *para*-chloroethyl phenol (**289**) was mainly used as phenol compound for the second series of coumaranones with an ureido carboxylic acid sidechain (Scheme 53). The original intention with the latter was to enable substitution reactions on the benzofuran backbone with silica nanoparticles. This project however was not further investigated as all reactions failed.



Scheme 53: Basic scaffold of the first and second series of coumaranones with a urea substructure. Series 1 was synthesised with ureido carboxylic acid methyl esters and *para*-chloro phenol to give the coumaranone derivative **291** and series 2 with ureido carboxylic acids and mainly *para*-chloroethyl phenol but also *para*-chloro phenol to yield the coumaranone derivatives **292a** and **292b**.

Table 6 summarises the yields of all coumaranones with a urea sidechain. Overall, it was possible to obtain 23 different derivatives, whereby the yield of the coumaranones with an ureido carboxylic acid sidechain (with the exception of leucine and aspartic and glutamic acid) is always higher compared to the methyl esters. According to literature the substitution of the phenol compound can have a major influence on the yield, especially regarding the comparison of *para*-fluoro/chloro/bromo derivatives. Since *para*-chloro phenol (**290**) as well as *para*-chloroethyl phenol (**289**) were used for the coumaranone syntheses of both the ureido carboxylic acid and methyl ester derivatives of alanine, it can be stated that in this case the yield is also influenced by the different phenol compounds. Additionally, it could be proven that in general the carboxylic acid group of the urea compound is tolerated during the *Tscherniak-Einhorn* reaction and shows a positive effect on the synthesis, considering the low yields in most cases given by the reactions with protected carboxylic acids. None of the alkaline amino acids as well as tryptophan, proline, cysteine, glutamine, asparagine and glycylglycine could be protected by coumaranones. The synthesis of the precursors of the former were already problematic. With regard to tryptophan (and also the alkaline amino acids), the synthesis of coumaranones could be hindered because of the additional aliphatic/aromatic amine or guanidine groups, which cause undesirable side reactions due to their nucleophilic potential. In the work of *R. Krieg et al.*^[290] it was possible to synthesise a pyrrolidine-coumaranone derivative, suggesting that the unsuccessful synthesis of proline-coumaranones could be a result of steric hindrance of the additional carboxylic acid bound to the cyclic system. The synthesis of the tyrosine-coumaranone was successful and could be verified via NMR, but it was not possible to obtain this compound in a good yield and high purity despite multiple optimisation and purification attempts. However, it proves that the *para* substituted phenol rest of this amino acid does not enable a competitive reaction during the one-pot synthesis.

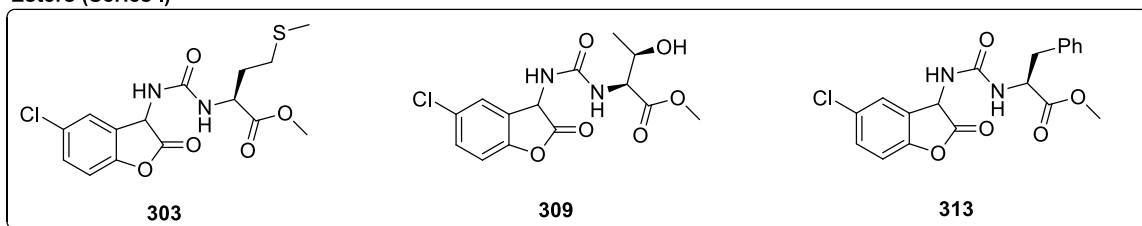
Table 6: Urea derivatives of proteinogenic and non-proteinogenic amino acids and dipeptides used for the synthesis of coumaranones according to the adapted synthesis protocol of *R. Krieg et al.*^[290] The yield percentage in brackets represents the yield of the coumaranones with ureido carboxylic acid sidechains. *Para*-chloroethyl phenol (**289**) and *para*-chloro phenol (**290**) were both used for the synthesis of the unprotected alanine (bold, italics) coumaranone **296a** and **296b** respectively. For the synthesis of the unprotected phenylalanine (bold) coumaranone **314** only *para*-chloro phenol (**290**) was used as precursor.

Entry	Coumaranone of	Yield [%]	Entry	Coumaranone of	Yield [%]
293 (294)	Glycine	6 (23)	315	Proline	0
295 (296a/b)	<i>Alanine</i>	12 (38/23)	316	Tryptophan	0
297 (298)	Valine	24 (35)	317	Tyrosine	n.a.
299 (300)	Isoleucine	27 (46)	318 (319)	Serine	0 (5)
301 (302)	Leucine	24 (16)	320	Arginine	-
303 (304)	Methionine	38 (22)	321	Lysine	-
305 (306)	Aspartic acid	8 (0)	322	Glutamine	-
307 (308)	Glutamic acid	16 (0)	323	Asparagine	-
309 (310)	Theronine	19 (30)	324	Glycylglycine	0
311	Cysteine	-	325 (326)	Aspartame	23 (-)
312	Histidine	0	327	PABA	(39)
313 (314)	Phenylalanine	23 (73)	328	δ -Amino valeric acid	(13)

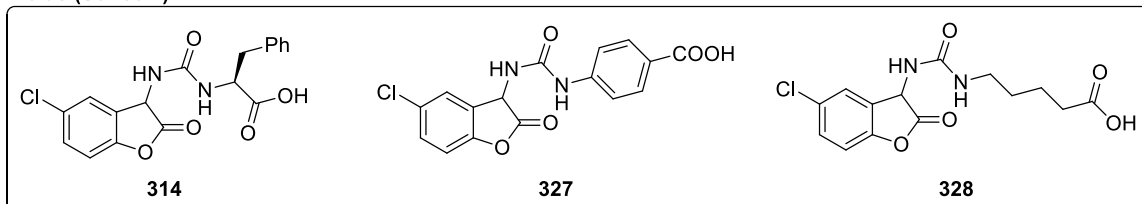
4.1.2 Investigations of urea-coumaranones via NMR^[300]

Of the 23 available urea-coumaranones the following six were chosen for further investigations, with 3 derivatives of series I and II respectively (Scheme 54).

Esters (Series I)



Acids (Series II)



Scheme 54: Overview of the urea-coumaranones whose decomposition reaction in an alkaline solution with oxygen were investigated via proton NMR. (Top) Urea-coumaranones of series I; (Bottom) Urea-coumaranones of series II.

The different sidechains of the proteinogenic amino acids as well as the aromatic scaffold (in the case of **327**) and varying positions of the functional groups of the non-proteinogenic ones could show to which degree the oxidation process is influenced by these different sidechains. Especially the comparison between **313** and **314** might show if the protection of the carboxylic acid leads to different results, while the hydroxy-group of **309** may act as a nucleophilic group when in an alkaline solution.

In order to follow the progress of the reaction and to determine the time required for the complete decomposition of the coumaranone-PG compound, proton NMR spectra were measured at regular intervals during the reaction. The following protocol was used for all coumaranones discussed in this Thesis: 20 mg of the substrate was dissolved in 0.7 ml of DMSO- d_6 and 2 equivalents of DBU were added. As soon as the addition was finished and the solution was homogenised, a proton NMR spectrum was immediately measured. Between each measurement, the solution was saturated with oxygen.

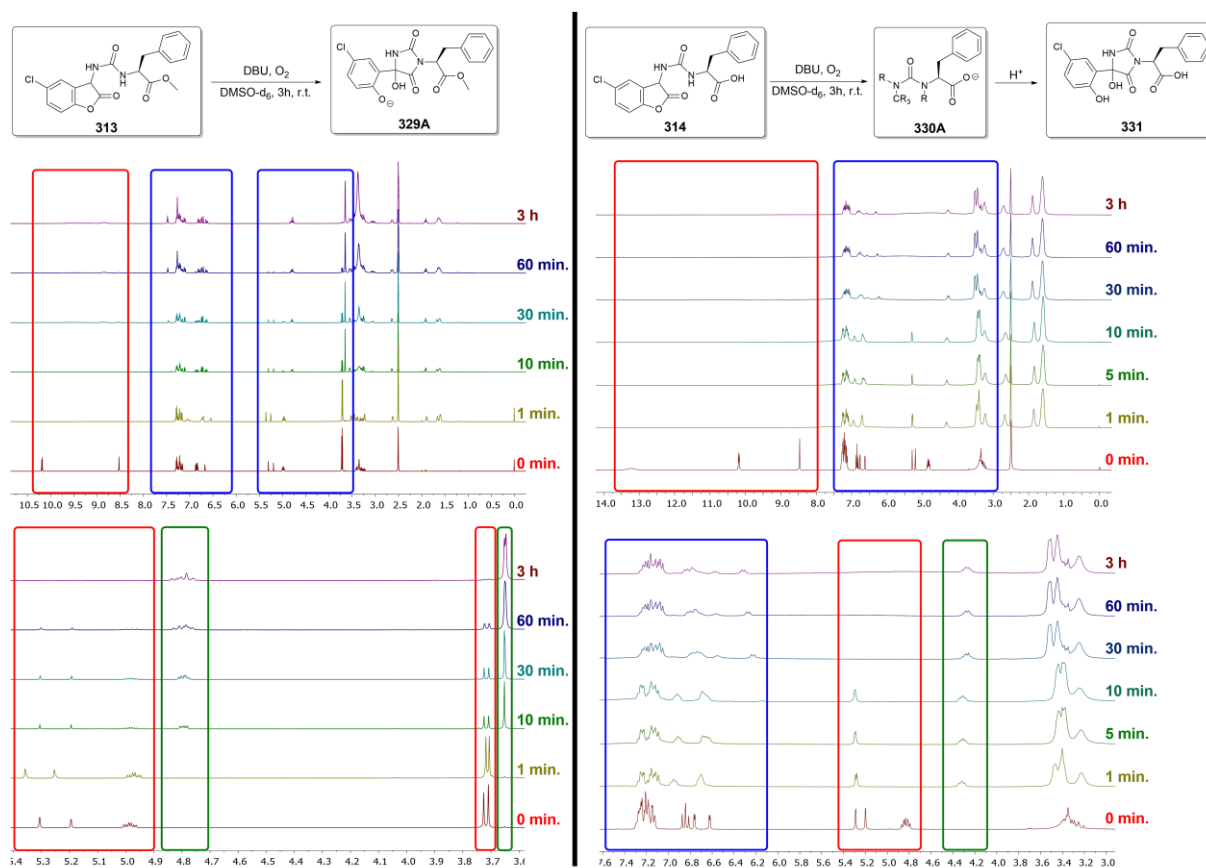
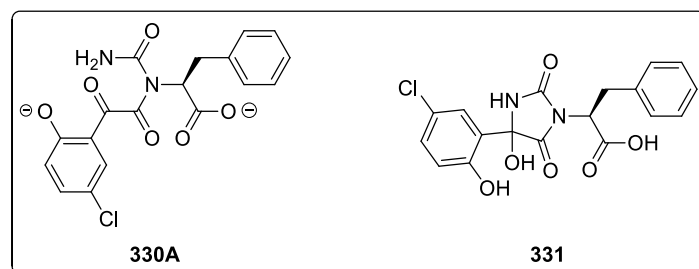


Figure 11: NMR measurements of the decomposition of urea-coumaranones **313** and **314** with associated reaction equations. The image above shows the entire NMR spectra during the reaction; below is a section of a selected area where significant changes occur. (Left) phenylalanine-coumaranone (**313**); (Right); phenylalanine-ester-coumaranone (**314**). Blue boxes = change in signal intensity and occurrence of new signals; red boxes = reduction/disappearance of signals; green boxes = appearance of new signals.

The first measurements were done with compounds **313** and **314**. During the whole experiment only a weak flash of light could be observed after the addition of DBU. When comparing both urea-coumaranones, a significant change could already be seen after the addition of DBU. Both NH protons in the chemical shift range of 8 to 10 ppm have vanished. Throughout the entire experiment a visible alteration in the region of the aromatic protons (6.5 to 7.5 ppm) can be seen. However, the most important change occurs at 5.25 ppm, representing the α -acidic proton of the benzofuranone moiety, which was expected to exhibit a doublet but instead appears as a doublet of doublets. Coalescence experiments confirmed the presence of rotamers for both substrates. According to literature, DBU α -deprotonates in order to obtain the anionic species which reacts with oxygen. By the end of the reaction, the corresponding carbon atom undergoes oxidation to form a carbonyl group. While this signal completely disappears after 30 minutes for compound **314**, the ester derivative **313** is significantly slower oxidised. Since both experiments still show the presence of rotamers and no proton or carbon signals from phenylalanine (**220**) are detected, it was assumed that the amino acid remained bound to the initial coumaranone. Therefore, additional decomposition experiments in a larger scale were carried out to determine the precise structure of the unknown compounds formed under the basic conditions. The obtained products were extracted, multiple times washed with water to remove excess DBU, and characterised via 2D-NMR for a complete structure elucidation (see Experimental section for details). The spectra of time-interval measurements were compared to those of the products obtained after extraction, since the aqueous work-up may induce side reactions. The ^{13}C -spectrum of the decomposition experiment of **313**, revealed that all nineteen carbon atoms were still present, with most peaks splitting into two signals, again indicating the presence of rotamers. Furthermore, the analysis of 2D-NMR spectra showed a new and unique signal of a quaternary carbon atom with a chemical shift of 81.8 ppm. This suggests that instead of undergoing decomposition (including CO_2 loss), a rearrangement occurred. Subsequent 2D-NMR and ESI experiments confirmed the hydantoin structure of compound **329** as the primary product, providing evidence of α -carbon oxidation. The formation of a five-membered ring must result from a nucleophilic attack of the urea moiety on the lactone carbonyl-carbon atom.

The decomposition experiment of **314** gave different results. No products could be extracted from the alkaline solution and the ^{13}C -NMR of the crude product (excluding the signals of DBU) showed that many NMR peaks were split into two signals, again indicating the existence of rotamers. However, no quaternary carbon was found in the 80–100 ppm range,

suggesting that, unlike in the case of **313**, the main product is not a hydantoin. Due to the contamination with DBU and other byproducts, the analysis of the 2D-spectra only allowed the elucidation of fragment **330A**. After protonation of the aqueous phase with two equivalents of hydrochloric acid, a product (compound **331**) could be extracted, whose structure was fully resolved and represents the unprotected acid hydantoin derivative of **329**. Because of the pH dependency it is assumed that **314** generates an open-chained carboxylate derivative as the primary product in an alkaline environment (Scheme 55).



Scheme 55: Assumed structure of an open-chained oxidation product **330A** of the urea-coumaranone **314** in an alkaline solution. Protonation yields the confirmed hydantoin **331**.

The decomposition experiment of urea-coumaranones **303** (Figure 12) and **328** (Figure 13) provided further insight and showed similar results with the corresponding hydantoin derivatives **332** and **334** as the main products of oxidation and without clearly visible CL. Although not structurally similar, it again shows that the decomposition of the methyl ester derivative takes more time than that of the unprotected acid.

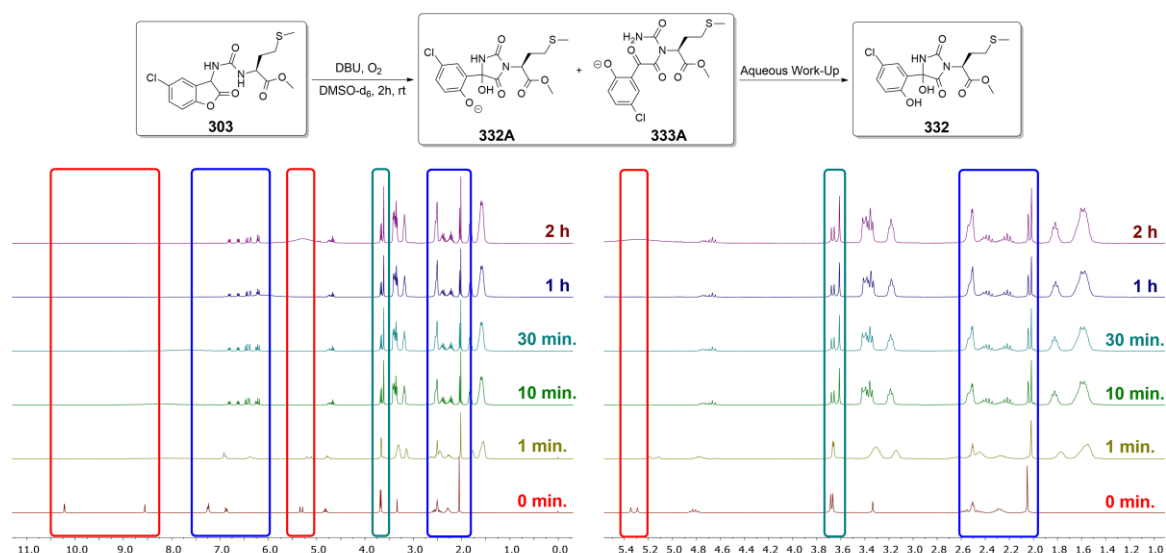


Figure 12: NMR measurements of the decomposition of urea-coumaranone **303** with associated reaction equation. The image on the left shows the entire NMR spectra during the reaction; on the right is a section of a selected area where significant changes occur. Blue boxes = change in signal intensity and occurrence of new signals; red boxes = reduction/disappearance of signals.

The decomposition experiment of **303** can be compared with those of **313** and **314**. The signals of the NH protons in the range of 8.5 to 10.5 ppm disappear after the addition of DBU, and the signals in the aromatic range of 6.0 to 7.5 ppm show changes over time. In addition, a new singlet is seen next to the ester signal at 3.66 ppm, possibly representing another ester group and thus indicating the formation of a second structurally similar byproduct. Without extraction or purification, ^1H -, ^{13}C - and 2D-spectra were recorded, allowing complete structural elucidation of hydantoin **332A** and oxoacetylphenolate **333A** (ratio 1.2:1) and verifying the hypothetical oxoacetylphenolate of **314**, which can also be assumed for urea-coumaranone **313**. After aqueous work-up however, only the hydantoin derivative was obtained.

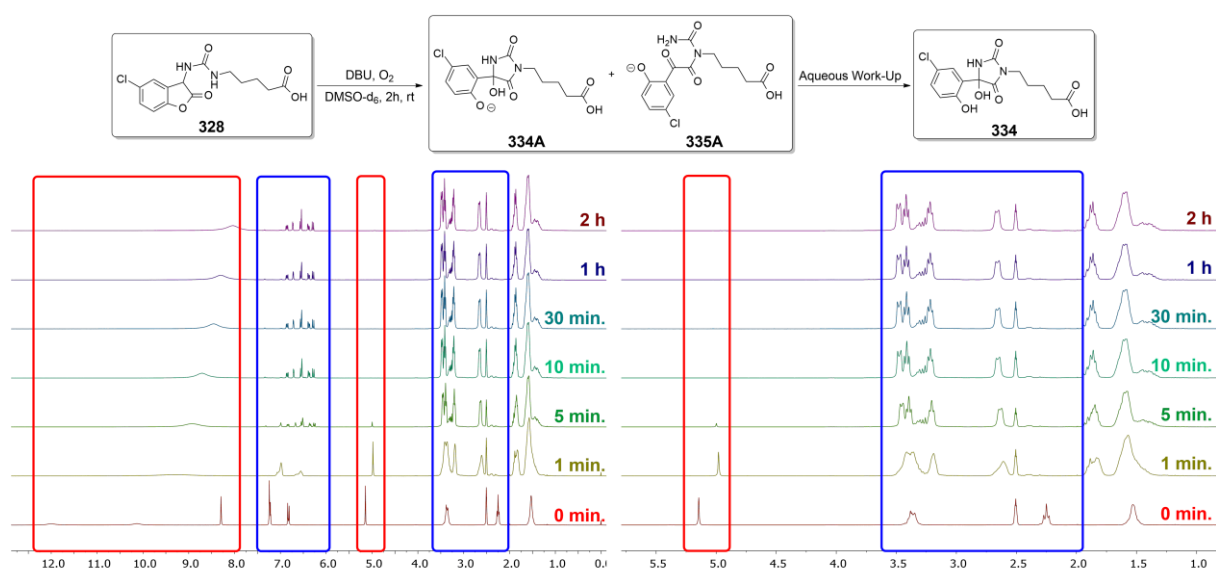


Figure 13: NMR measurements of the decomposition of urea-coumaranone **328** with associated reaction equation. The image on the left shows the entire NMR spectra during the reaction; on the right is a section of a selected area where significant changes occur. Blue boxes = change in signal intensity and occurrence of new signals; red boxes = reduction/disappearance of signals.

The same results were obtained in the decomposition experiment of urea-coumaranone **328**, which also shows an equilibrium between the hydantoin **334A** and the oxoacetyl phenolate **335A** in the ratio 1:1.1. Since the hydantoin form could not be detected in the experiment with urea-coumaranone **314**, this shows that the longer alkyl chain of **328** influences the equilibrium. Due to the different ratios favouring either the hydantoin or the open chain products, both NMR spectra of **303** and **328** were measured again after two days to determine a further shift in equilibrium. The ratio remained the same for the experiment of **303**, while that of **328** showed a slight shift towards the oxoacetyl anion **335A**, resulting in a new ratio of 1:1.3.

Although no complete structure elucidation was possible for hydantoin **336A** and the open-chain derivative **337A**, both could be determined as main products of the oxidation of threonine-coumaranone **309** (Figure 14). In addition to these two compounds, other signals are visible that indicate the presence of further byproducts. However, when worked up in aqueous solution, all signals of **336A** and **337A** disappeared and a new main product was obtained whose exact structure could not be resolved.

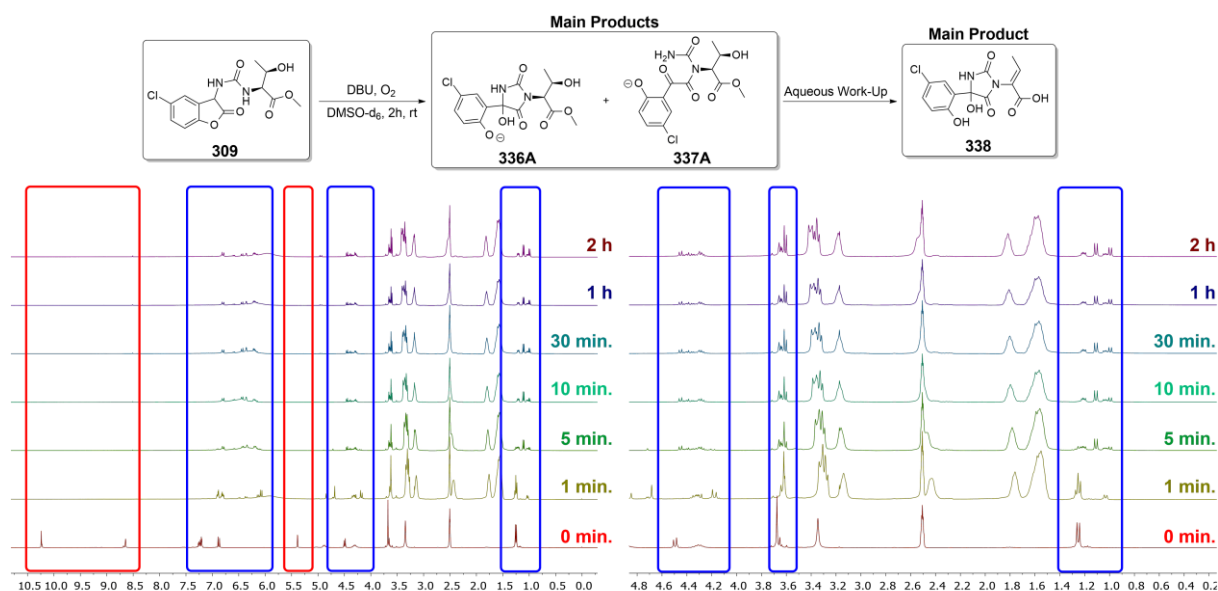


Figure 14: NMR measurements of the decomposition of urea-coumaranone **309** with associated reaction equation. The image on the left shows the entire NMR spectra during the reaction; on the right is a section of a selected area where significant changes occur. Blue boxes = change in signal intensity and occurrence of new signals; red boxes = reduction/disappearance of signals.

2D NMR showed 11 carbon signals. Coumaranone **309** has a total of 14 carbon atoms, suggesting that two carbon atoms are missing, considering that the CH₃ group of the original methyl ester group was hydrolysed. In addition to a 4-chlorophenolate fragment that is still present and clearly visible, a urea component can also be suspected based on the significant ¹³C signal at 154.9 ppm, which is a typical shift for the carbonyl group. ¹H-NMR and HMBC show that the CH₃ group of the threonine side chain at 1.75 ppm has a cross peak with a quaternary carbon atom at 131.3 ppm and a CH group with a chemical shift of 106.8 ppm. The COSY spectrum also verifies the direct vicinity of the strongly deshielded CH fragment with the CH₃ group. These results indicate the formation of an olefin under water loss, which would give a Michael-system. Therefore, hydantoin **338** can be proposed as the major product obtained after aqueous work-up of the decomposition experiment of urea-coumaranone **309**. However, due to several failed purification attempts to obtain better spectra and the missing ¹³C signals, hydantoin **338** could not be fully elucidated.

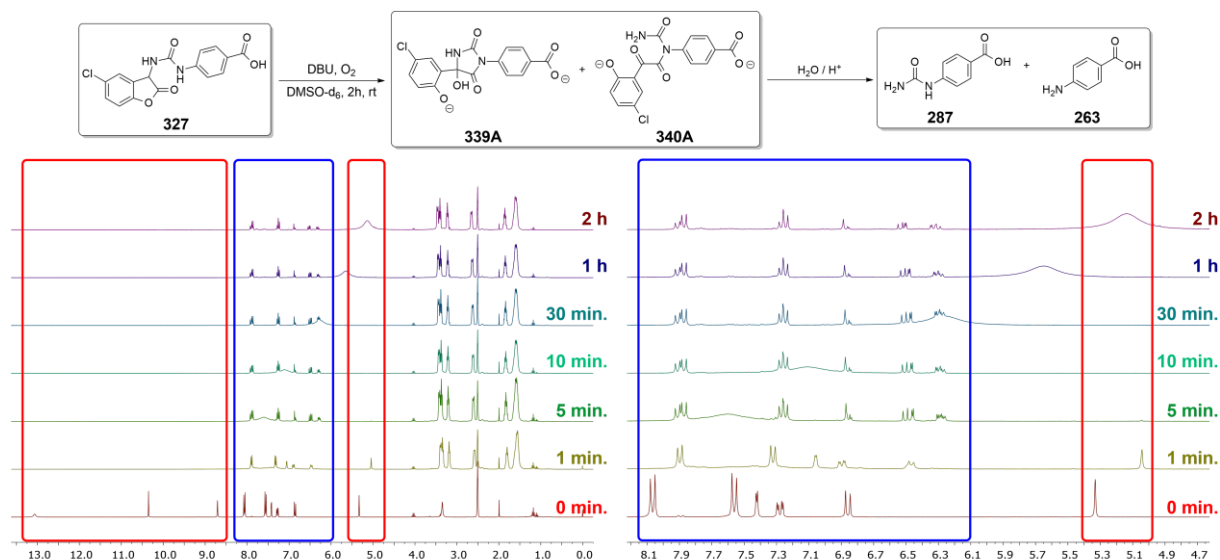


Figure 15: NMR measurements of the decomposition of urea-coumaranone **327** with associated reaction equation. The image on the left shows the entire NMR spectra during the reaction; on the right is a section of a selected area where significant changes occur. Blue boxes = change in signal intensity and occurrence of new signals; red boxes = reduction/disappearance of signals.

Though the oxidation of coumaranone-protected PABA **327** has the same equilibrium as the above derivatives, the acidic work-up of this experiment yielded the urea derivative of PABA (**287**) as the major product and completely deprotected PABA (**263**) as the minor product (Figure 15).

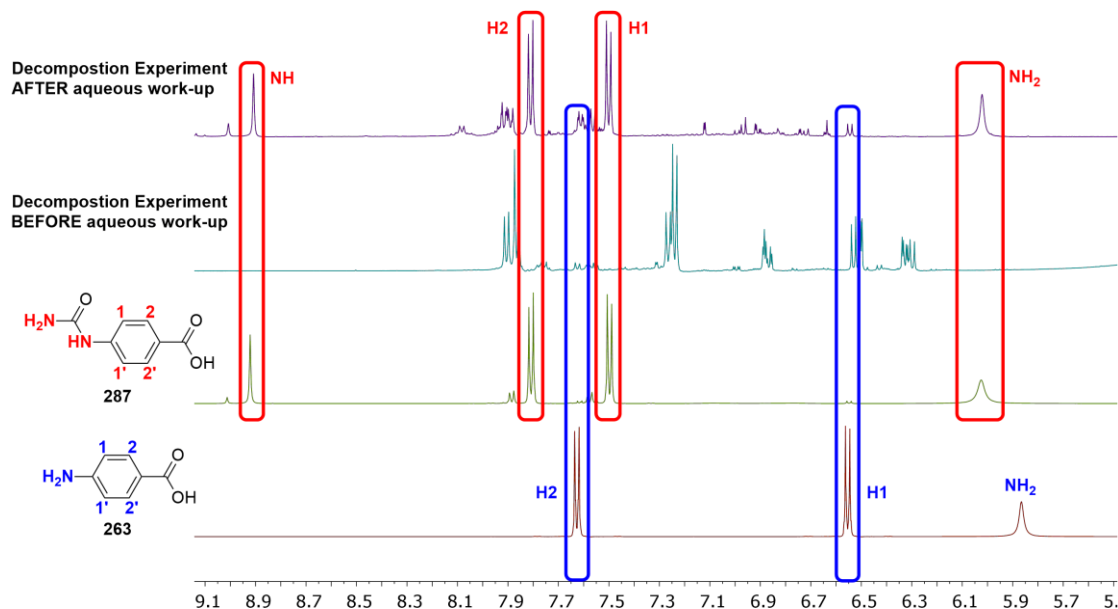
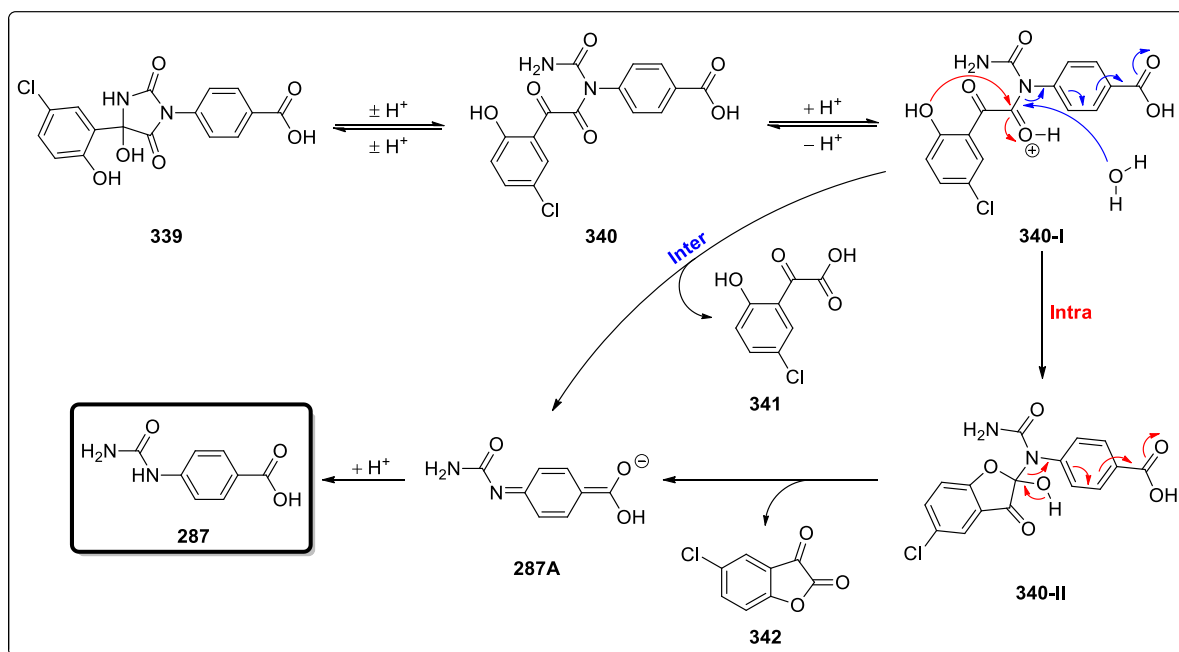


Figure 16: Comparison of the ^1H NMR spectra of the decomposition experiment of urea-coumaranone **327** before and after work-up with those of ureido-PABA (**287**) and PABA (**263**). All spectra were recorded in DMSO-d_6 . The blue boxes encircle the significant signals of PABA, while the red ones encircle those of the corresponding urea derivative.

The direct comparison of the $^1\text{H-NMR}$ spectra of the two obtained products with the corresponding decomposition experiment before and after the work-up procedure verify that the addition of water and HCl is necessary for the release of the substrates. The ^1H -, ^{13}C - and 2D-NMR spectra of the alkaline solution with DBU only show the signals of the hydantoin **339A** and the open-chain derivative **340A** (Figure 16). While it could be argued that traces of PABA are visible in the $^1\text{H-NMR}$ of the decomposition experiment before the aqueous work-up, the corresponding COSY does not show any cross peaks between the specific signals at 6.53 ppm and 7.62 ppm.

According to literature, hydantoin s are mainly hydrolysed in an alkaline solution, requiring high temperatures and long reaction times. Apart from that there are also examples which can be cleaved in acidic media, but still require harsh reaction conditions.^[301] In general, the decomposition experiments of coumaranone protected proteinogenic amino acids yield the corresponding hydantoin s after aqueous work-up with or without minor protonation. Hence the PABA hydantoin derivative (**339**) appears to enable further decomposition in lightly acidic aqueous media, due to the aromatic sidechain of the imide protected nitrogen allowing the stabilisation of charges. A proposed mechanism for the further decomposition to obtain PABA urea (**287**) is illustrated in Scheme 56.



Scheme 56: Proposed mechanism for the decomposition of hydantoin **339**. The hydrolysis yields either 2-(5-chloro-2-hydroxyphenyl)-2-oxoacetic acid (**341**) or 5-chlorobenzofuran-2,3-dione (**342**) and PABA urea **287**.

The $^1\text{H-NMR}$ after aqueous work-up shows a product ratio of 11:1 for the PABA urea (**287**). Since the urea-coumaranones investigated so far (with the exception of the threonine

derivative **309**) always give the hydantoin product after aqueous work-up, the mechanism starts from the derivative **339**. Due to the aromatic amine, which can additionally shift electron density to the neighbouring carbonyl groups, an acid-catalysed equilibrium between **339** and **340** can be assumed. After protonation of the amide carbonyl group, an intramolecular nucleophilic attack of the phenol group can be considered (**340-I**), although intermolecular hydrolysis with water is also possible. After decomposition of the benzofuranone derivative **340-II**, the mesomerically stabilised anion of PABA urea (**287A**) is formed and subsequently protonated. The two suspected byproducts **341** or **342** could not be detected in the NMR spectra, which could be explained by the water solubility of 2-(3-chlorophenyl)-2-oxoacetic acid (**341**) and the hydrolysis susceptibility of 5-chlorobenzofuran-2,3-dione (**342**). With regard to the formation of completely deprotected PABA (**263**), a complete hydrolysis of hydantoin **339** can be assumed. Due to the low yield, the equilibrium seems to be mainly on the side of the open-chain derivative **340**, which is not a suitable substrate for the release of PABA.

4.1.3 CL of urea-coumaranones^[300]

For the characterisation of the photophysical properties of the previously investigated urea-coumaranones and their reaction products emission and excitation experiments were conducted. The following protocol was used for all coumaranones discussed in this Thesis: Each compound was initially measured at a concentration of $c = 10^{-2}$ mol/l in acetonitrile. 50 equivalents of DBU were added to 1 ml of the coumaranone stock solution in a cuvette. After rapid and thorough mixing, the luminescence was then continuously monitored by several scans. The cuvette itself was not sealed during all measurements to prevent oxygen depletion.

The first experiments and comparisons were done with the phenylalanine coumaranone derivatives **313** and **314**. Figure 17 displays the emission and excitation spectra of **313**. The CL emission peaks at 436 nm, but diminishes rapidly within the first two scans and fades away after the twelfth measurement (Figure 17a). This is in agreement with the results by *Krieg et al.*^[290], who described the CL of urea-coumaranones as brief yet intense when compared to carbamate-coumaranone derivatives. Following the CL experiment, subsequent emission scans revealed the presence of an absorbing species that fluoresces at a maximum wavelength of 435 nm. This photoluminescence can be attributed to the oxoacetyl phenolate **343A**. Hence, a second CL experiment was carried out, during which the sample is also

excited with a wavelength of 370 nm. Initially, CL decreases, but after 50 scans, photoluminescence gradually begins to increase over time. The emission also shows a slight red-shift with a peak at 436 nm (Figure 17b). In the third spectroscopic experiment, multiple excitation scans were performed to monitor changes in the absorption of the previously observed fluorescent species. Over the course of 100 scans, an absorbing species with a maximum at 402 nm became evident. This species gradually diminished, giving way to a new species with a maximum at 396 nm (Figure 17c).

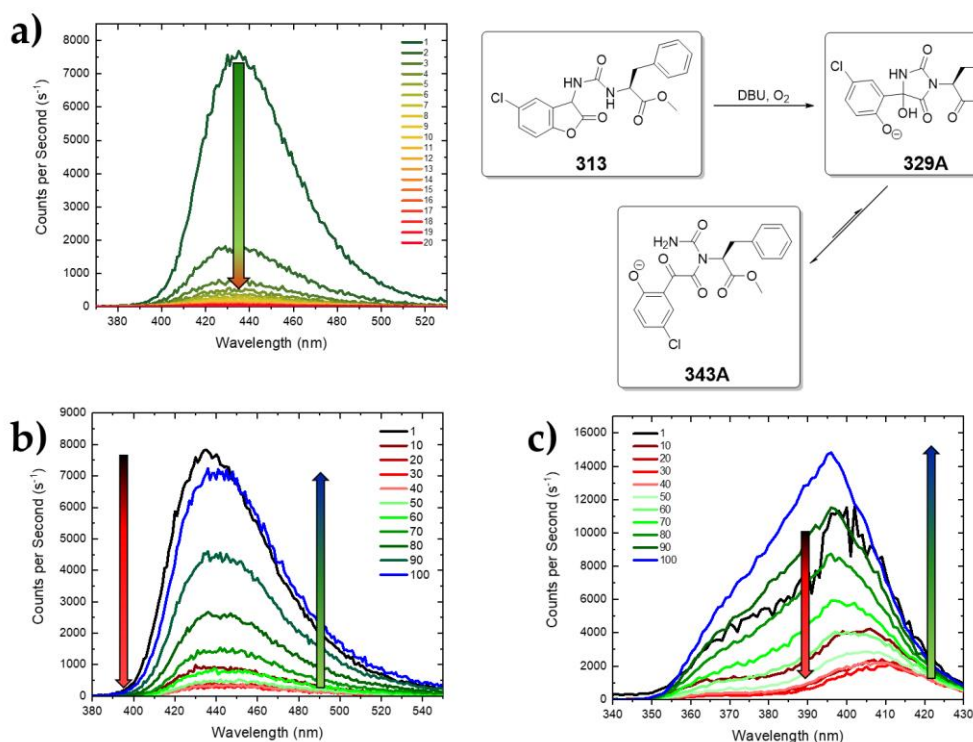


Figure 17: Emission and excitation spectra of **313** in acetonitrile (every scan took 45 s) with associated reaction equation: (a) emission scans of CL (i.e., without external excitation, Slit: 10), the arrow indicates the decrease in the CL; (b) emission scans during CL reaction (external excitation $\lambda_{\text{Ex}} = 370$ nm, Slit: 1.0). The first scan was performed after addition of DBU. The left red arrow indicates the decrease in CL after 40 scans. Starting from the 50th scan, the right green arrow indicates the increase in photoluminescence; (c) excitation scans during CL reaction ($\lambda_{\text{Em}} = 430$ nm, Slit: 1.0). The first scan was performed after addition of DBU. The left red arrow indicates the decrease in an absorbing species after 40 scans. Starting from the 50th scan, the right green arrow indicates the increase in absorption of a new species.

The same three spectroscopic experiments were performed for compound **314** (Figure 18). While the quick decrease of the CL ($\lambda_{\text{max}} = 436$ nm) is comparable to that of **313** (Figure 18a) the results of the emission and excitation experiments exhibit significant differences. Both, the absorbing and emitting species initially displayed an increase, followed by a minor decrease within 100 scans, eventually reaching equilibrium. The emission maximum remains at 435/436 nm (Figure 18b), while the absorption maximum shifts from 381 nm to 376 nm

(Figure 18c). These experiments demonstrate the remarkable fluorescence properties of **330A**, which is rapidly generated and even overlaps its own CL.

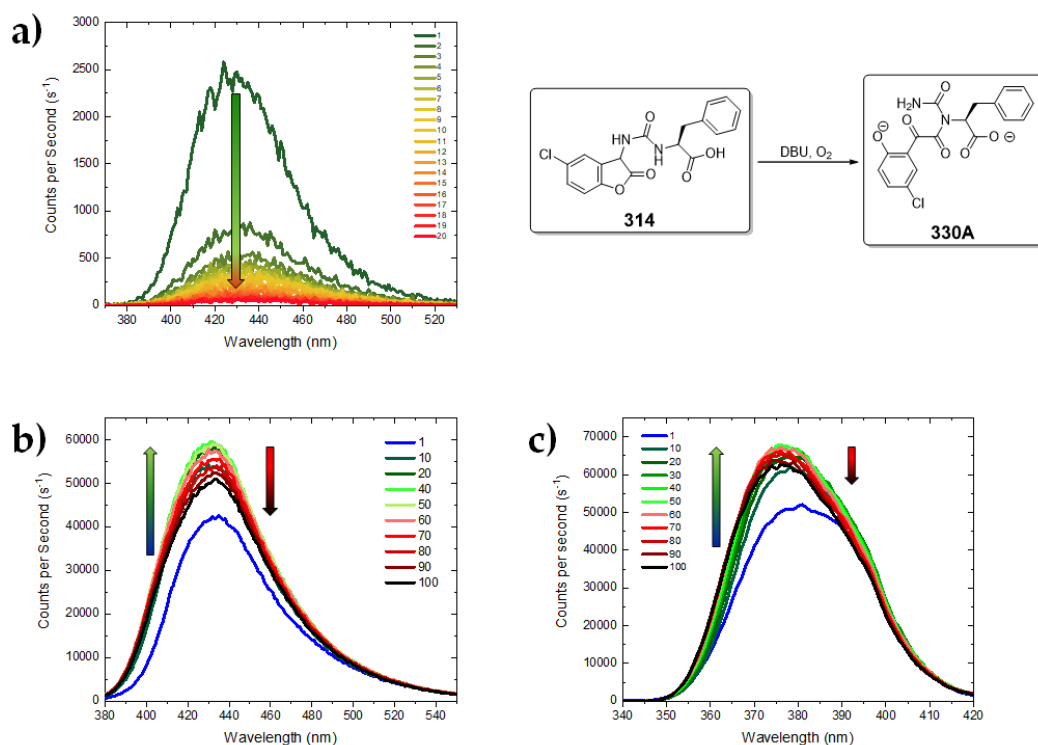


Figure 18: Emission and excitation spectra of **314** in acetonitrile (every scan took 45 s) with associated reaction equation: (a) emission scans of CL (i.e., without external excitation, Slit: 10), the arrow indicates the decrease in the CL; (b) emission scans during CL reaction (external excitation $\lambda_{\text{Ex}} = 370$ nm, Slit: 1.0). The first scan was performed after addition of DBU. The left green arrow indicates the initial CL (scan 1) and the increase in photoluminescence after 40 scans. Starting from the 50th scan, the right red arrow indicates the small decrease in photoluminescence; (c) excitation scans during CL reaction ($\lambda_{\text{Em}} = 430$ nm, Slit: 1.0). The first scan was performed after addition of DBU. The left green arrow indicates the increase in an absorbing species after 40 scans. Starting from the 50th, scan the right red arrow indicates a minor decrease in absorption.

The first CL scan of methionine-coumaranone **303** shows a high intensity at 423 nm, but strongly decreases thereafter and a red shift towards 440 nm occurs (Figure 19a). The CL was visible to the human eye for a few seconds with a strong flash of light, which is consistent with the luminescence measurements, although the CL was detectable with the instrument for more than 30 minutes. Due to the established equilibrium of oxidised urea-coumaranones, which could be determined by the NMR experiments and the results of luminescence spectra of the phenylalanine-coumaranones **313** and **314** only one emission and excitation scan was performed to investigate the photophysical properties of the open-chain derivative **333A**. After the CL was finished the sample exhibited an absorption maximum at 380 nm (Figure 19c), which resulted in a potent photoluminescence at 440 nm (Figure 19b). When compared to the phenylalanine methyl ester coumaranone **313** it can be seen the photoluminescence is much stronger in regard to the photons counted per second and the smaller slit of the scanner.

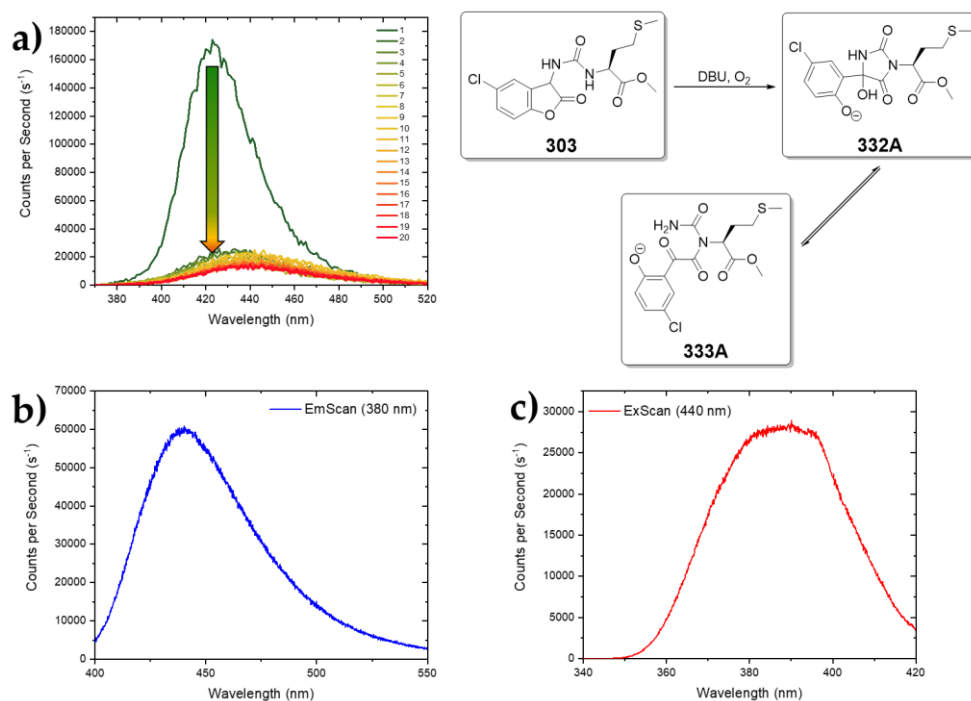


Figure 19: Emission and excitation spectra of **303** in acetonitrile (every scan took 45 s) with associated reaction equation: (a) emission scans of CL (i.e., without external excitation, Slit: 0.1), the arrow indicates the decrease in the CL; (b) emission scan of **303** after CL was finished (external excitation $\lambda_{\text{Ex}} = 380$ nm, Slit: 0.8); (c) excitation scan of **303** after CL was finished ($\lambda_{\text{Em}} = 440$ nm, Slit: 0.8).

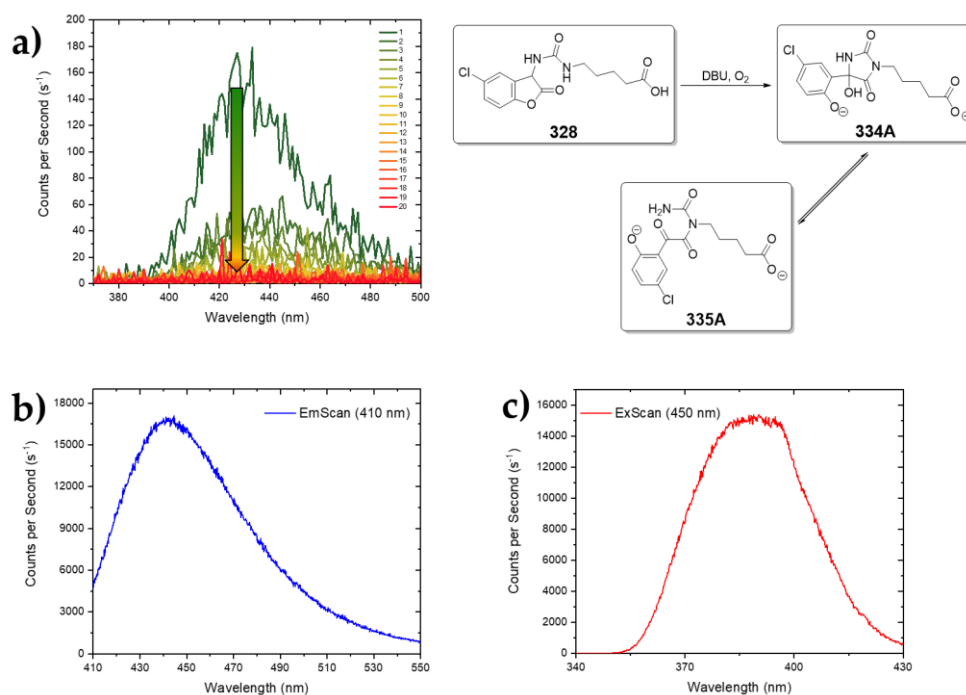


Figure 20: Emission and excitation spectra of **328** in acetonitrile (every scan took 45 s) with associated reaction equation: (a) emission scans of CL (i.e., without external excitation, Slit: 10), the arrow indicates the decrease in the CL; (b) emission scan of **328** after CL was finished (external excitation $\lambda_{\text{Ex}} = 410$ nm, Slit: 0.7); (c) excitation scan of **328** after CL was finished ($\lambda_{\text{Em}} = 450$ nm, Slit: 0.7).

Of all six urea-coumaranones that were chosen for these experiments the coumaranone protected δ -aminovaleric acid **328** had the weakest CL (Figure 20a). The first scan already shows a very low CL intensity with a maximum at 433 nm, which quickly reaches zero after a few measurements. In accordance with the previous results subsequent emission and excitation scans revealed the photoluminescence of **333A** with a maximum at 445 nm (Figure 20b) with a corresponding absorption at 395 nm (Figure 20c).

While additional byproducts were detected in the NMR experiment of **309**, the luminescence spectra did not show any new absorbing/fluorescent species besides **337A**. The CL again remains very weak and decays rapidly with a maximum at 430 nm (Figure 21a). Subsequently, an emission and excitation scan showed photoluminescence with a maximum at 455 nm (Figure 21b) and an absorption maximum at 395 nm (Figure 21c).

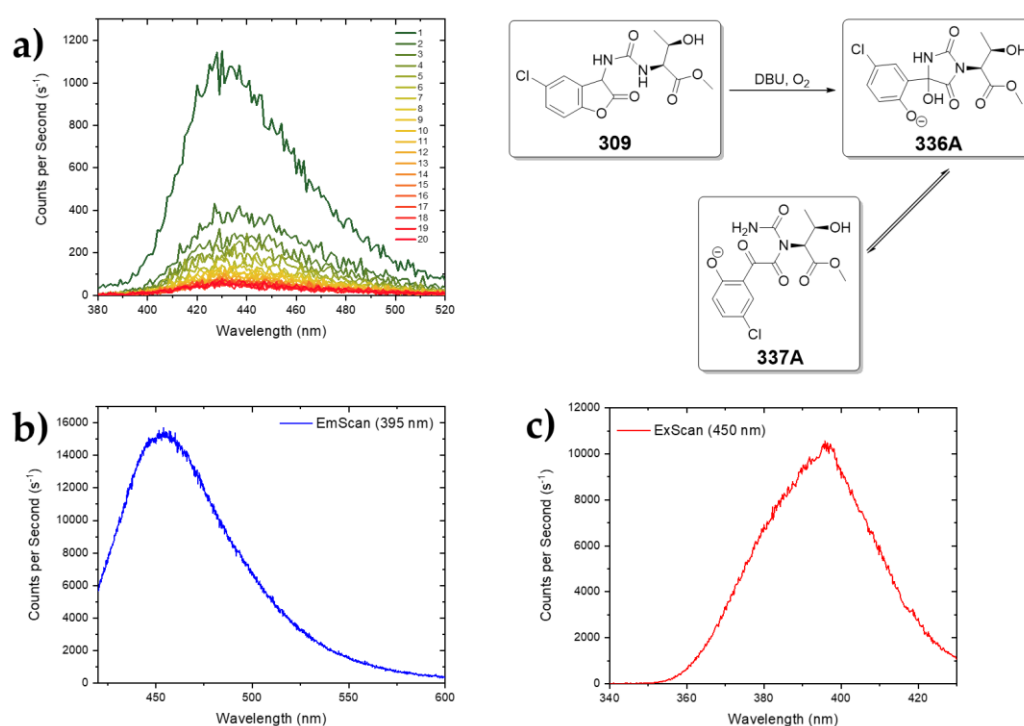


Figure 21: Emission and excitation spectra of **309** in acetonitrile (every scan took 45 s) with associated reaction equation: (a) emission scans of CL (i.e., without external excitation, Slit: 10), the arrow indicates the decrease in the CL; (b) emission scan of **309** after CL was finished (external excitation $\lambda_{\text{Ex}} = 395$ nm, Slit: 0.8); (c) excitation scan of **309** after CL was finished ($\lambda_{\text{Em}} = 450$ nm, Slit: 0.8).

In the case of the urea-coumaranone **327** the CL intensity ($\lambda_{\text{max}} = 440$ nm) decreases in more steady manner when compared to the other derivatives, but remains overall weak and cannot be detected anymore after 20 scans (Figure 22a). The photophysical properties of **340A** do not deviate from the other corresponding derivatives as it has an absorption maximum at 390 nm (Figure 22c) and shows a fluorescence peak at 450 nm (Figure 22b).

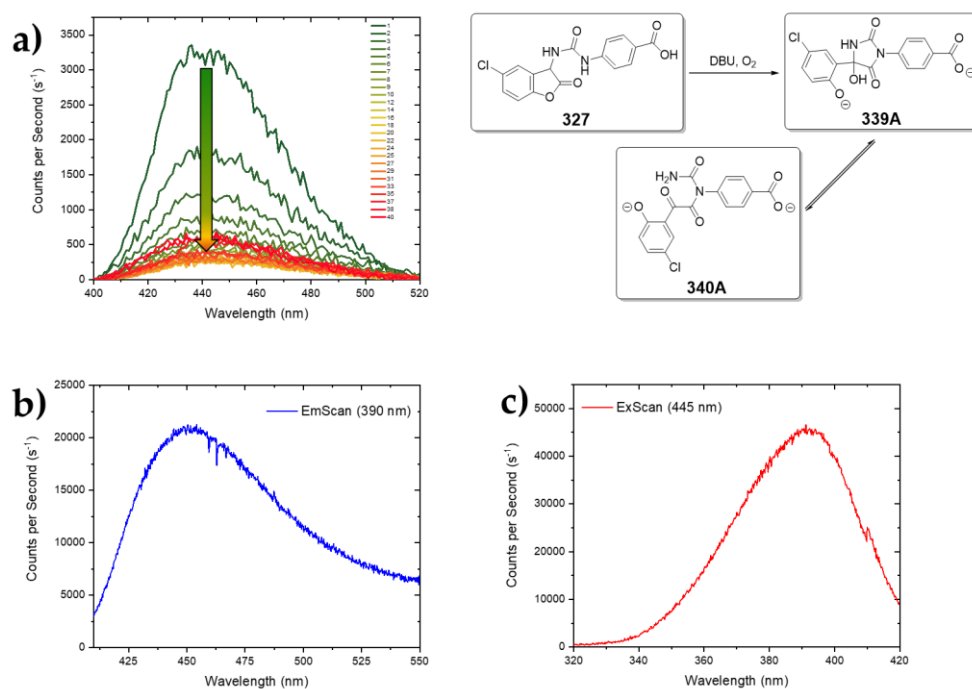
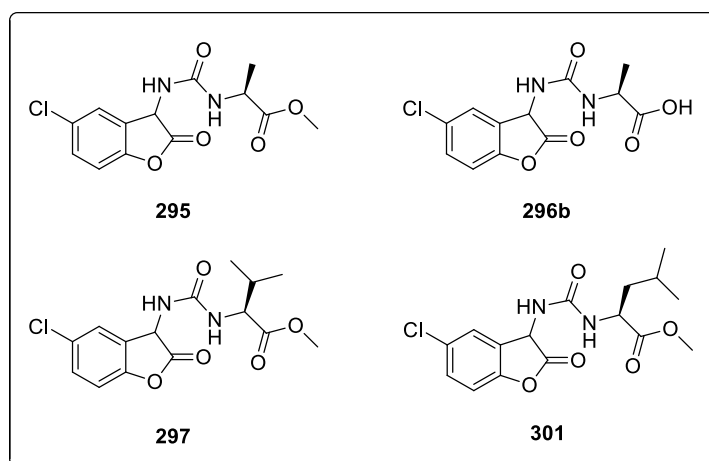


Figure 22: Emission and excitation spectra of **327** in acetonitrile (every scan took 45 s) with associated reaction equation: (a) emission scans of CL (i.e., without external excitation, Slit: 10), the arrow indicates the decrease in the CL; (b) emission scan of **327** after CL was finished (external excitation $\lambda_{\text{Ex}} = 390 \text{ nm}$, Slit: 3); (c) excitation scan of **327** after CL was finished ($\lambda_{\text{Em}} = 445 \text{ nm}$, Slit: 3).

Besides these urea-coumaranones more derivatives were investigated in regards of their CL and the absorption and fluorescence properties of the expected products (Figure 19). The corresponding spectra of **295**, **296b**, **297** and **301** can be found in Chapter 7.



Scheme 57: Illustration of urea-coumaranones, whose CL properties were also investigated.

The results from every luminescence experiment are summarised in Table 7. Overall, it can be stated that the sidechain of the amino acid moieties does not greatly influence the photophysical properties. It is noteworthy however that the CL of derivative **297** and **303**

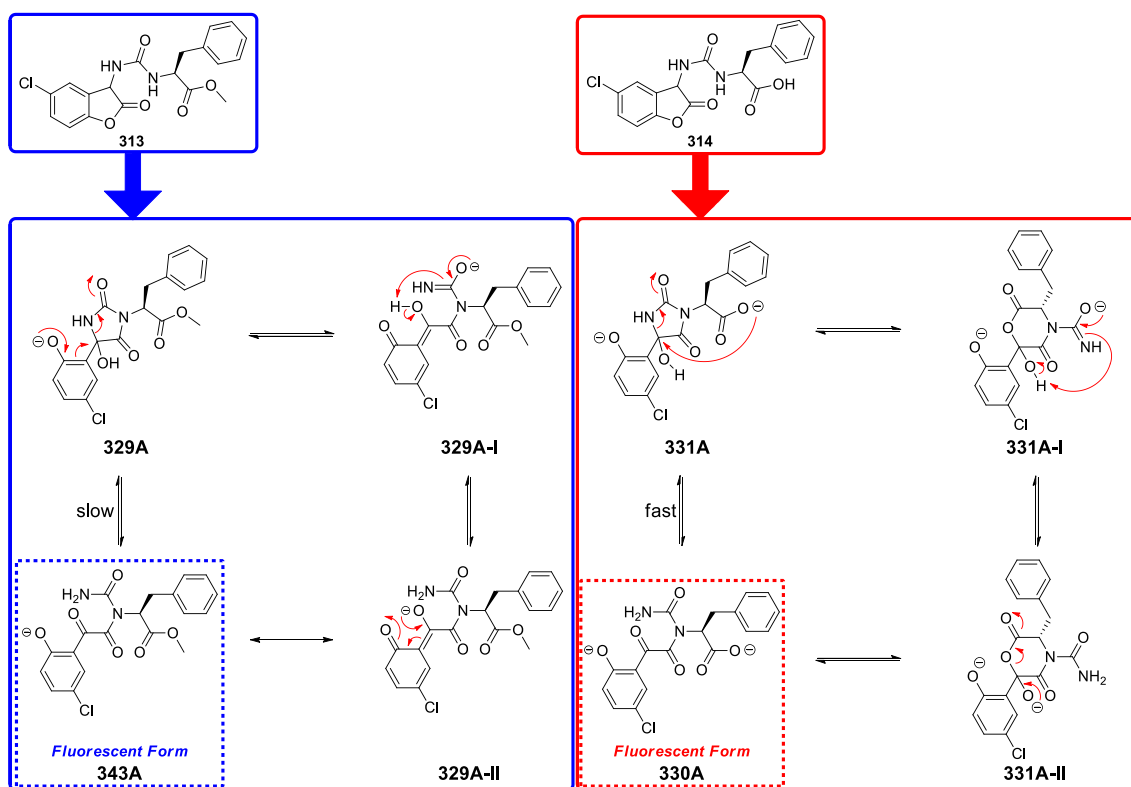
could be detected for over 30 minutes, though its intensity was very low and not visible for the human eye.

Table 7: Summary of the photophysical properties of urea-coumaranones. The first 6 entries represent the previously discussed derivatives. The absorption and fluorescence maxima refer to the oxidised byproducts of the respective coumaranone.

Entry	CL λ_{\max} [nm]	CL Intensity/Duration	Absorption λ_{\max} [nm]	Fluorescence λ_{\max} [nm]
303	440	Visible \rightarrow weak / < 30 min.	380	440
309	430	Very weak / 3 min.	395	455
313	436	Shortly visible / 14 min.	396	436
314	436	Weak / 4 min.	381	435/436
327	440	Weak / 7 min.	390	450
328	433	Very weak / > 1 min.	395	445
295	430	Weak / 12 min.	385	445
296b	430	Very weak / 45 sec.	381	442
297	432	Weak / < 30 min.	384	437
301	438	Very weak / 3 min.	385	435

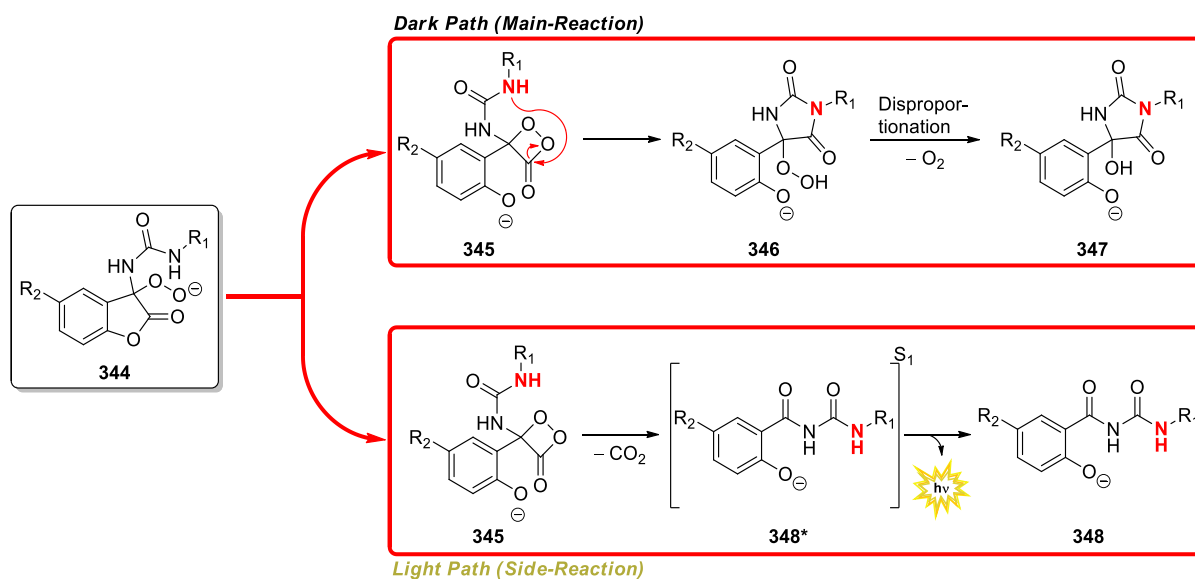
4.1.4 Conclusions on the chemistry of urea-coumaranones^[300]

Considering the results of the NMR and luminescence experiments, it is apparent from the excitation spectra that all urea-coumaranones generate a potent fluorescent species after the oxidation with molecular oxygen in an alkaline solution. The emission maxima do not greatly differ from each other with the largest difference being 20 nm between derivative **301** and **309**. Regarding the luminescence-experiment of **313**, the initial stages of the excitation experiments show no photoluminescence, with steady and gradual increase after 36 minutes. This suggests the occurrence of a slow equilibrium between **329A** and the open-chained oxoacetyl phenolate species **338A**, with a shift towards the latter after approximately 30 minutes. Additionally, the hydantoin form could not be detected in the experiment with urea-coumaranone **314**, while in the case of **328** and **327** both tautomers could be seen. This suggests that the deprotonated carboxylic acid has an influence on the equilibrium but is dependent on the distance from the hydantoin ring. A proposed mechanism and comparison for the formation of the fluorescent oxoacetyl phenolate of methylesters and unprotected acids is illustrated in Scheme 58. Through tautomerisation, the phenolate directs electron density towards the urea moiety's carbonyl oxygen, causing ring opening (**329A-I**). Subsequent deprotonation (**329A-II**) and rearomatisation result in the generation of an oxoacetyl phenolate **343A**, which is responsible for the observed fluorescence.



Scheme 58: Proposal for the equilibrium between hydantoin and fluorescent species. Illustrated with compound **313** (left) and **314** (right). The rate of the tautomerisation processes differs due to the ester/free carboxylic acid. The fluorescent form is highlighted by a dashed box.

In stark contrast, compound **314** gives the carboxylate **331A** in an alkaline environment and triggers ring expansion via a nucleophilic attack. This leads to a redistribution of electron density towards the carbonyl group of the urea moiety (**331A-I**). Subsequent deprotonation of the alcohol (**331A-II**) leads to the formation of the oxoacetylphenolate (**330A**). Therefore, the formation of the fluorescent species occurs at an accelerated rate due to the induced ring expansion by the carboxylate (resulting in a five- to six-membered ring). This mechanism can in general be assumed for all urea-coumaranones. Potential nucleophilic groups such as carboxylates can shift the equilibrium towards the fluorescent form (Scheme 58, dashed boxes), while alkoxides (in the case of **309**) cause the formation of new products besides the expected hydantoin and the open-chain derivative. Also, the CL itself remains faint and barely visible because of the preferred hydantoin formation, which circumvents decarboxylation and subsequent light emission. In view of the decomposition mechanism a nucleophilic attack of the urea moiety on 1,2-dioxetanone can be considered, which yields 5-hydroperoxy hydantoin **345** and eventually leads to the corresponding 5-hydroxy hydantoin **346** (Scheme 59).



Scheme 59: Proposal for the general mechanism of urea-coumaranones.

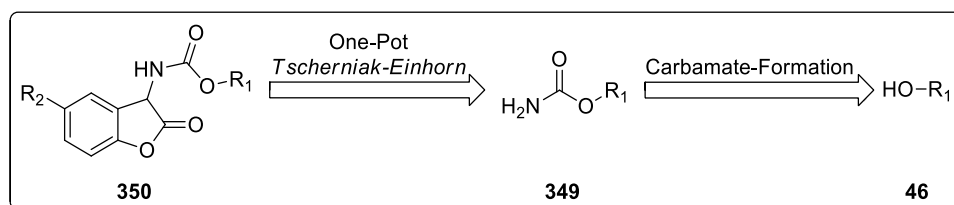
In summary urea-coumaranones do not fulfil the requirements of CLPGs but instead can be described as fluorescent protection groups (FPGs) as the fluorescent properties of the products in an alkaline environment are more potent than the CL. According to literature, however, there is still the option of cleaving the hydantoin PG either enzymatically or chemically with refluxing solutions of NaOH or acids and thus releasing the amino acid.^[301]

4.2 Protection and deprotection of alcohols

Carbamate coumaranones were the first substrates investigated by *Lofthouse*^[219] and *Matuszczak*^[286–289] with regard to their CL properties. Therefore, there is already a wide range of literature known compounds, including natural and pharmacologically relevant alcohols that have been used for the synthesis of coumaranones. However, as research has mainly focused on the CL and the oxidation mechanism, the release efficiency of the protected alcohols has not been thoroughly investigated. For these reasons, the following chapter discusses a selected range of vitamins, steroids and other pharmaceutically relevant compounds chosen for protection with coumaranones and the corresponding release from the CLPG.

4.2.1 General protection protocol of alcohols

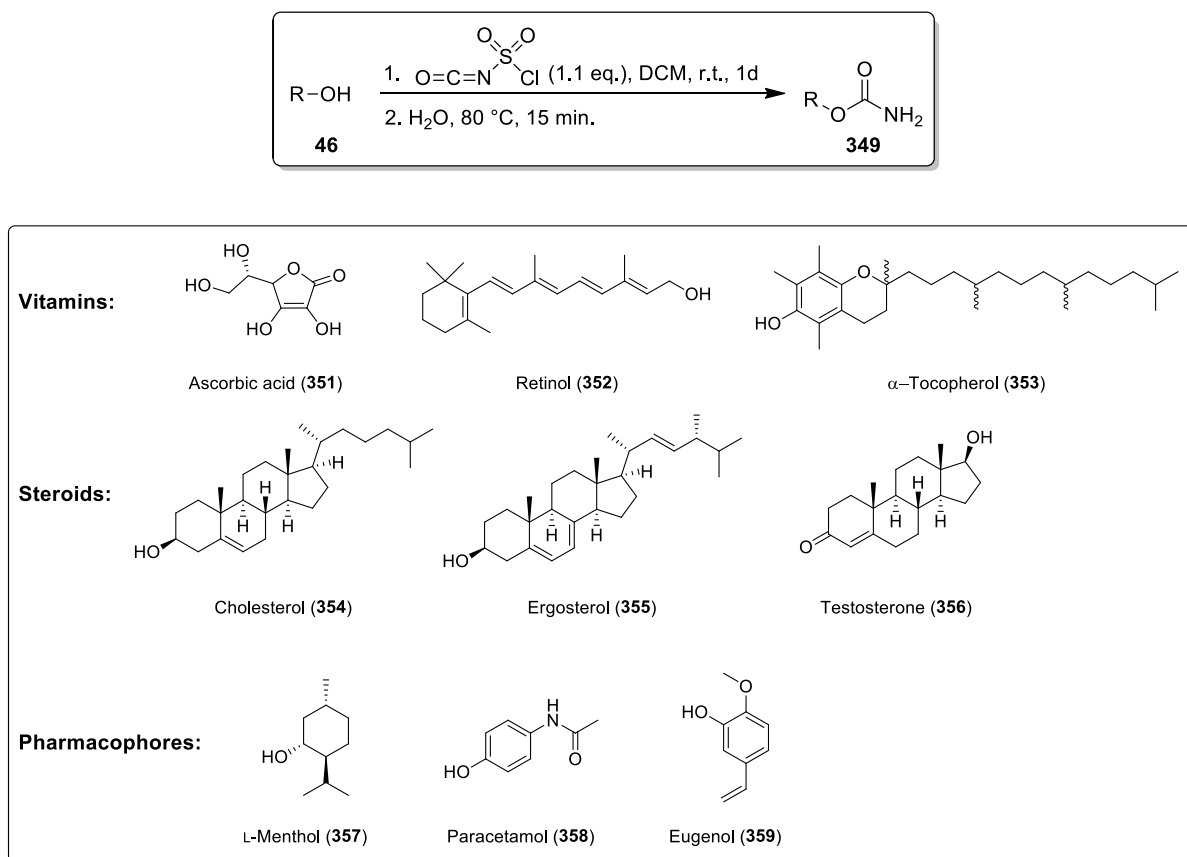
Similar to the protection of amines, a two-step procedure was used for the synthesis of coumaranones with a carbamate side chain (Scheme 60). The alcohol **46** is converted to the corresponding carbamate derivative **349**. Subsequently, a one-pot *Tscherniak-Einhorn* reaction is again carried out to obtain the carbamate coumaranone **350**.



Scheme 60: Retrosynthesis of the protection of alcohols.

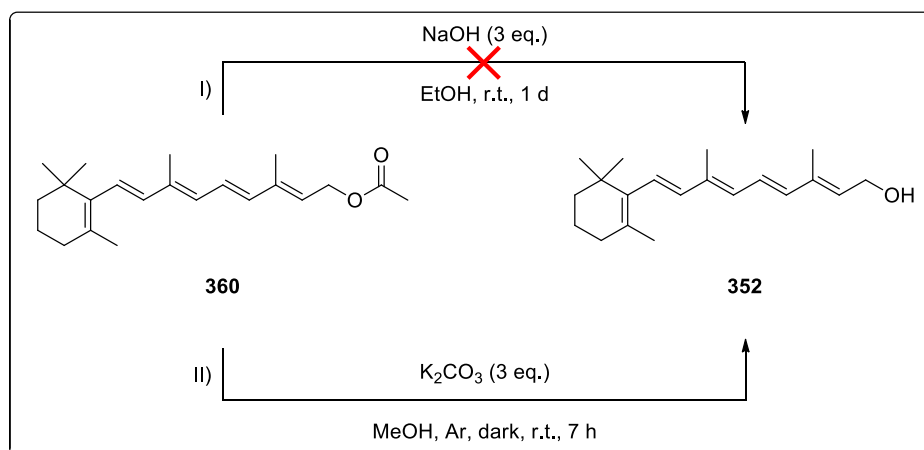
4.2.1.1 Syntheses of carbamates

The synthesis of the carbamate substrates was performed according to an adapted synthesis protocol of *R. Graf et al.*^[302] using chlorosulfonyl isocyanate (CSI) in DCM (Scheme 61). The vitamins L-ascorbic acid (**351**), retinol (**352**) and α -(\pm)-tocopherol (**353**), the steroids cholesterol (**354**), ergosterol (**355**) and testosterone (**356**) and the pharmacological relevant substrates L-menthol (**357**), paracetamol (**358**) and eugenol (**359**) were investigated.



Scheme 61: (Top) General synthesis of carbamates; (Bottom) Substrates used for synthesis of carbamates.

Besides the synthesis of the carbamates of L-menthol and paracetamol, which were already known to literature and could be easily reproduced, most reactions were successful, with the exception of those with L-ascorbic acid, ergosterol and retinol. Because of the multiple hydroxy groups present in the ascorbic acid molecule, a mixture of products was expected. Instead, no formation of any possible carbamate was detected. To obtain retinol (352), the commercially available retinyl acetate (360) needed to be saponified first, which was done via two different routes: I) NaOH in EtOH under ambient conditions II) Na₂CO₃ in dry MeOH under inert conditions and the exclusion of light^[303] (Scheme 62). Method I gave a mixture containing the product but also considerable amounts of impurities, which are caused by oxidation of retinol under the chosen conditions, due to its high sensitivity towards oxygen and UV-A/UV-B irradiation. Conducting the reaction with method II resulted in a high yield of retinol, which was immediately used for the subsequent reaction without further purification. The reaction was additionally carried out under inert conditions in a flask wrapped in aluminium foil, but was unsuccessful. Considering the structural similarities and the identical position of the hydroxy group, it remains unclear why the carbamate formation of ergosterol could not be realised, while that of cholesterol was possible.



Scheme 62: Synthesis of retinol (**352**) by saponification of retinyl acetate (**360**). Method I) NaOH in EtOH at room temperature was unsuccessful; Method II) K₂CO₃ in MeOH under inert conditions and exclusion of light led to the successful cleavage of the ester.

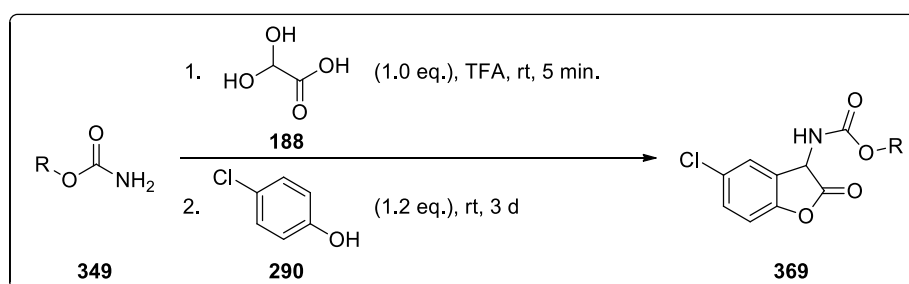
The yields of the syntheses are summarised in Table 8. α -Tocopherol has the highest yield with 91%. Every other reaction resulted in yields above 80% with the exception of the carbamate of testosterone **366** and paracetamol **368**.

Table 8: Vitamins, steroids and pharmacophores with hydroxy groups used for the synthesis of carbamates according to the adapted synthesis protocol of *R. Graf et al.*^[302]

Entry	Carbamate of	Yield [%]	Entry	Carbamate of	Yield [%]
361	Ascorbic acid	0	365	Eugenol	82
362	Retinol	0	366	Testosterone	64
363	α -Tocopherol	91	367	L-Menthol	88
364	Cholesterol	83	368	Paracetamol	72

4.2.1.2 Tscherniak-Einhorn reaction with carbamates

2-Coumaranones bearing a carbamate substructure were synthesised according to the procedure of *Schramm*.^[295] with minor adaptations (Scheme 63).



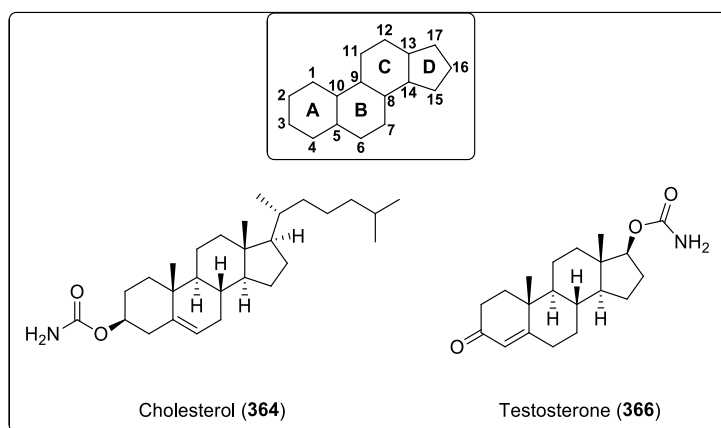
Scheme 63: Illustration of the synthesis of coumaranones with a carbamate substructure according to the adapted synthesis protocol of *S. Schramm*.^[295]

Similar to the reaction with urea substrates, the synthesis is carried out in a one-pot reaction. The preferred acid was TFA, since using acetic acid/sulfuric acid (9:1) as well as formic acid resulted in very low yields. The stirring time of the carbamate and the glyoxylic acid in TFA was reduced to 5 minutes and after the addition of the phenol compound the reaction was stirred at room temperature for three days. Refluxing the solution was also possible, but resulted in an increased yield of byproducts. The results of these syntheses are summarised in Table 9.

Table 9: Carbamate derivatives used for the synthesis of coumaranones according to the adapted synthesis protocol of *S. Schramm*^[295] and the corresponding yields.

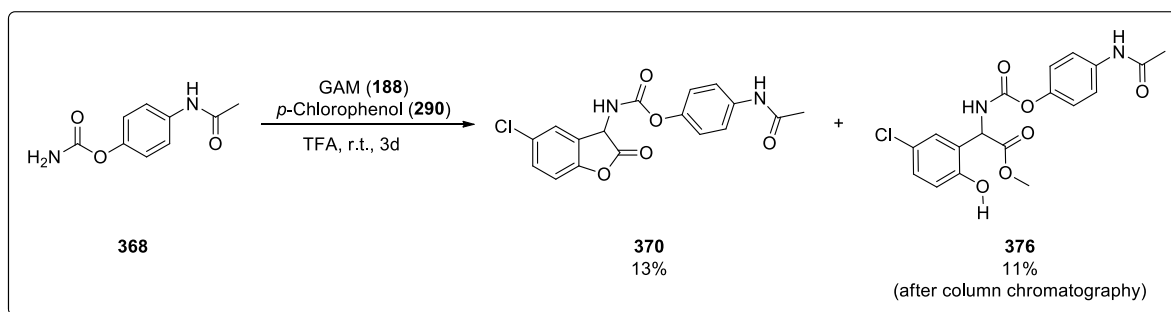
Entry	Coumaranone of	Yield [%]
370	Paracetamol	13
371	L-Menthol	25
372	Testosterone	54
373	α -Tocopherol	43
374	Cholesterol	0
375	Eugenol	0

The best yields were obtained with the 2-coumaranones of testosterone **372** and α -tocopherol **373** with 54% and 43% respectively. When comparing the reactions of the steroid carbamates **372** and **374**, the position of the carbamate moiety within the sterane structure appears to influence the outcome of the reaction (Scheme 64). While the testosterone coumaranone **372** could be successfully synthesised the reaction with the cholesteryl carbamate **364** failed. Also, of the two carbamate derivatives of the aromatic pharmacophores **365** (paracetamol) and **368** (eugenol), only the reaction of the latter gave the desired coumaranone **370**.



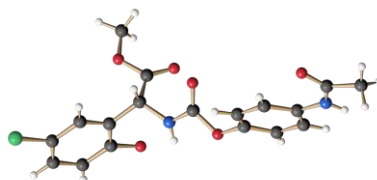
Scheme 64: (Top) General structure of the sterane-scaffold including the numeration of the carbon atoms; (Bottom) Structure of the carbamates of cholesterol (**364**) and testosterone (**366**). Only the coumaranone synthesis with testosterone carbamate **366** as precursor was successful.

Considering the yields of the literature known 5-fluorocoumaranones of paracetamol (36%) and L-menthol (36%) the use of 4-chlorophenol led to different results. The highest possible yield for the 5-chlorocoumaranone derivative of L-menthol is 25%, while that of paracetamol amounted to 13% and was accompanied by an uncondensed phenol byproduct with a yield of 11% (Scheme 65). The formation of uncondensed acid and ester compounds is already mentioned in previous publications.



Scheme 65: Synthesis of coumaranone **370** and the uncondensed byproduct **376** via the *Tscherniak-Einhorn* reaction.

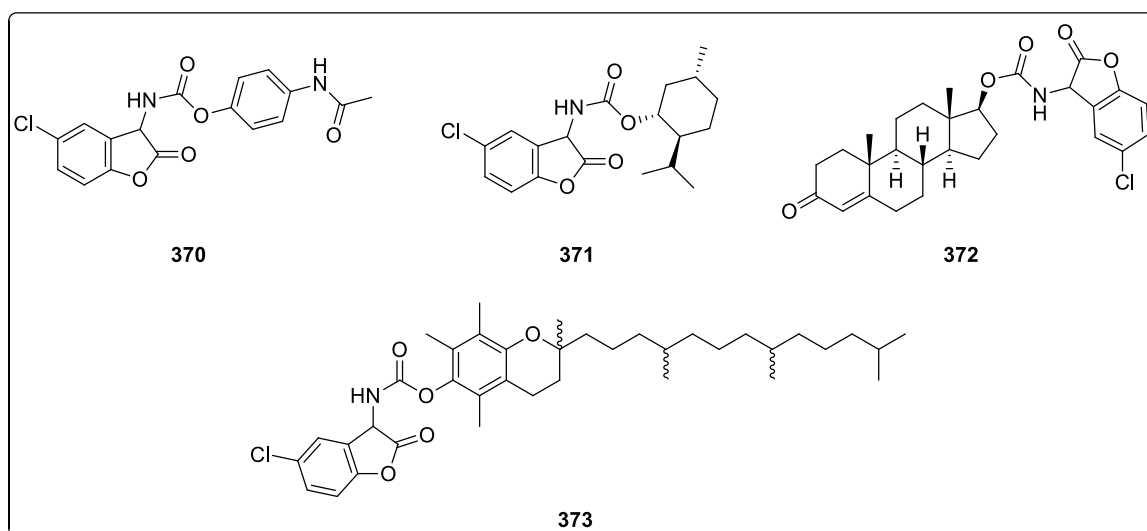
Due to the usage of methanol during column chromatography, the former carboxylic acid of byproduct **376** must have undergone esterification. This compound could also be analysed and verified by X-ray crystal structure determination (Scheme 66).



Scheme 66: Crystal structure of the uncondensed product **376**.

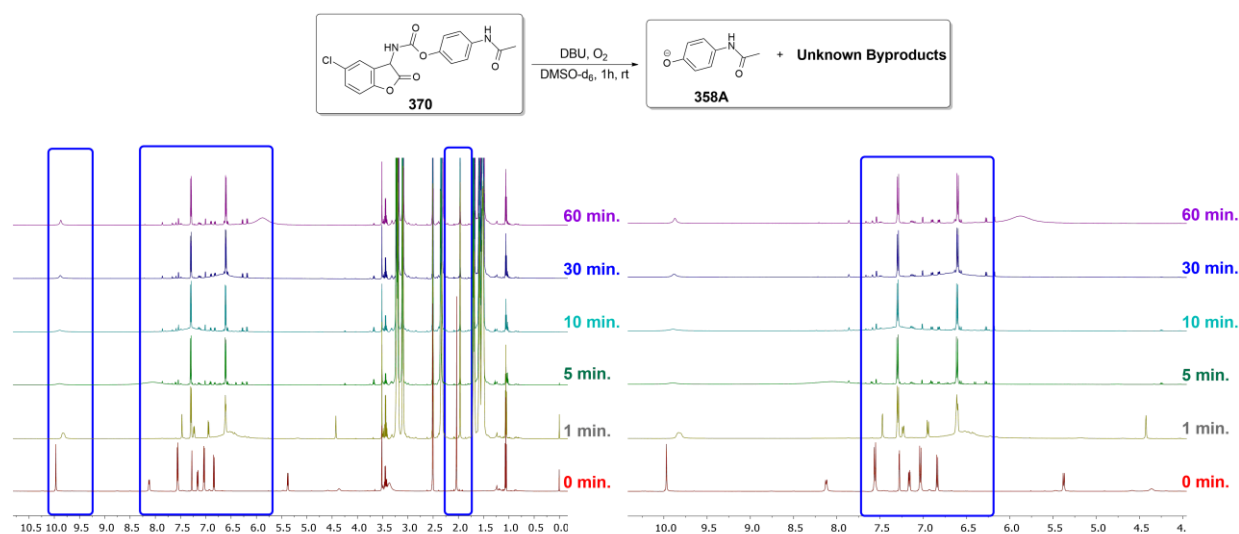
4.2.2 Investigations of carbamate-coumaranones via NMR^[300]

The decomposition of all four synthesised carbamate coumaranones was investigated (Scheme 67). Special attention was paid to the possible differences between the oxidation of coumaranones with aromatic and aliphatic carbamate side chains, since different results were already observed with urea coumaranones. In addition, testosterone and α -tocopherol are large molecules that can influence the deprotonation/oxidation rate and thus the CL properties.



Scheme 67: Overview of the carbamate-coumaranones whose decomposition reaction in an alkaline solution with oxygen were investigated via proton NMR.

The first experiment was performed with coumaranone-protected paracetamol **370**. While the previously discussed urea-coumaranone derivatives did not release the corresponding amino acids, paracetamol **358A** was effectively separated from coumaranone **370**, accompanied by a brief but intense chemiluminescence (CL), as shown in Figure 23. Within one minute, the bright blue emission rapidly decreased and became imperceptible to the human eye. In the NMR experiment, an increase of the aromatic signals of paracetamol **358A** at 6.60 and 7.29 ppm was observed immediately after the addition of DBU. The CH₃ group of the acetyl moiety at 2.01 ppm shifts slightly towards 1.97 ppm. Overall, the complete cleavage of the CLPG was observed within less than 5 minutes.



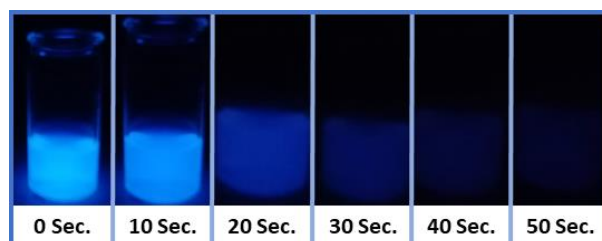


Figure 23: NMR measurements of the decomposition experiments with the paracetamol-coumaranone (**370**) with associated reaction equation. (Top, left) Complete NMR-spectrum. (Top, right) Enlarged extract of the aromatic area from 4.5 – 10 ppm. Blue boxes = change in signal intensity and occurrence of new signals. (Bottom) Decay of the CL of coumaranone **370**. 10 mg of **370** were dissolved in MeCN and a few drops of DBU were added. Within 50 seconds, the intensity of the initially strong and bright emission decreases and is no longer visible thereafter.

An important observation was the appearance of new signals in the aromatic region (other than those of paracetamol) during the decomposition process. Despite the appearance of several new aromatic signals from various byproducts, no compounds other than **358A** were identifiable in the 2D-NMR spectra after the decomposition experiment was completed.

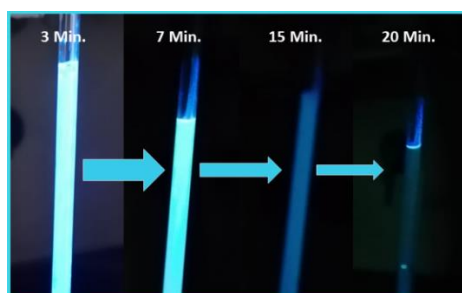
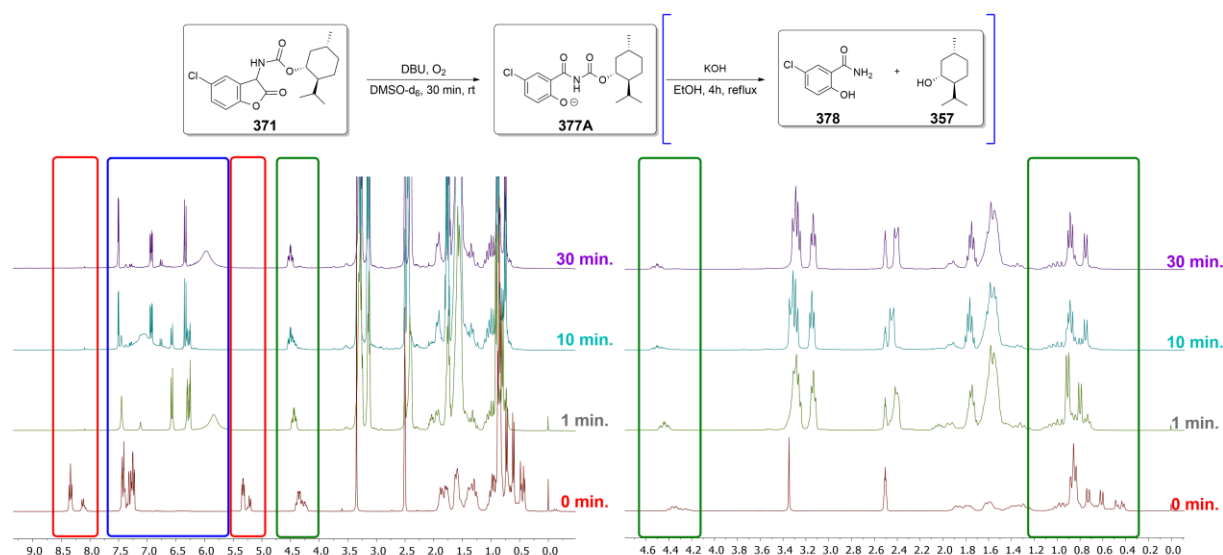


Figure 24: NMR measurements of the CL-decomposition experiment with the L-menthol-coumaranone (**371**) with associated reaction equation. The reaction in the blue brackets was performed after the decomposition experiment. (Top, left) Complete NMR-spectrum. (Top, right) Enlarged extract of the area from 0.0 – 4.6 ppm. Blue boxes = change in signal intensity and occurrence of new signals; red boxes = reduction/disappearance of signals; green boxes = appearance/shift of new signals. (Bottom) Photos of the CL of **371** during saturation with oxygen.

The oxidation of L-menthol coumaranone **371** showed differences compared to **370**. Due to the longer decomposition process, a more intense and longer lasting CL was observed accordingly as soon as the sample was saturated with oxygen in the NMR tube, as shown in Figure 24. After 20 minutes, the CL remained weak and finally faded a few minutes later, which is consistent with the NMR results. While after one minute the proton signals of the CH group in α -position at 5.30 ppm and of the NH proton at 8.25 ppm had already disappeared, the aromatic region (6.0 – 7.5 ppm) and the range of 0.4 – 1.2 ppm still showed visible changes. This indicates a stepwise progression of the entire oxidation process. The signal of the CH group next to the oxygen atom in the menthol molecule (4.34 ppm) showed a slight shift to higher ppm values after the oxidation process, which did not correspond to the signal of free L-menthol. Without purification, 2D-NMR spectra were recorded, which allowed the structural elucidation of the decarboxylated compound **377A**, which is also the species responsible for CL of coumaranones described in the literature. To cleave the PG, the substrate was again decarboxylated with KOH in boiling ethanol to give L-menthol (**357**) and 5-chlorosalicylamide (**378**).

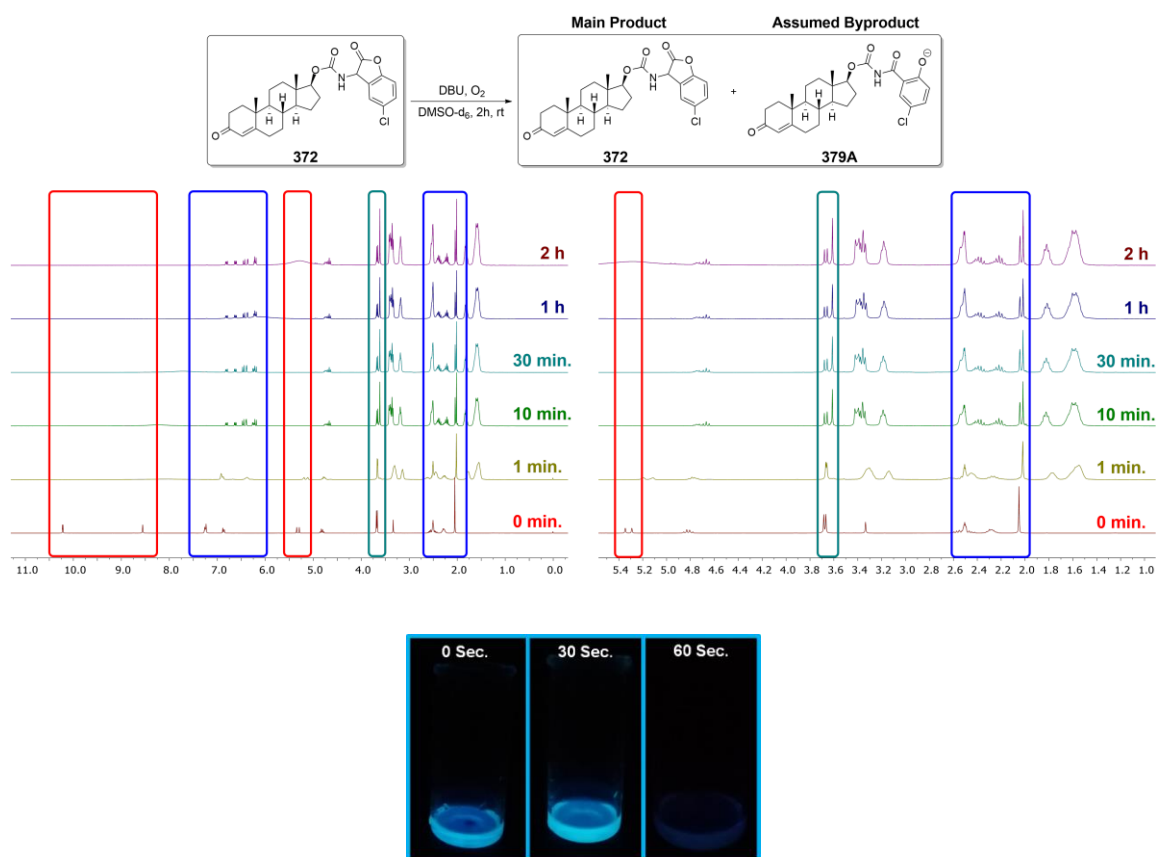
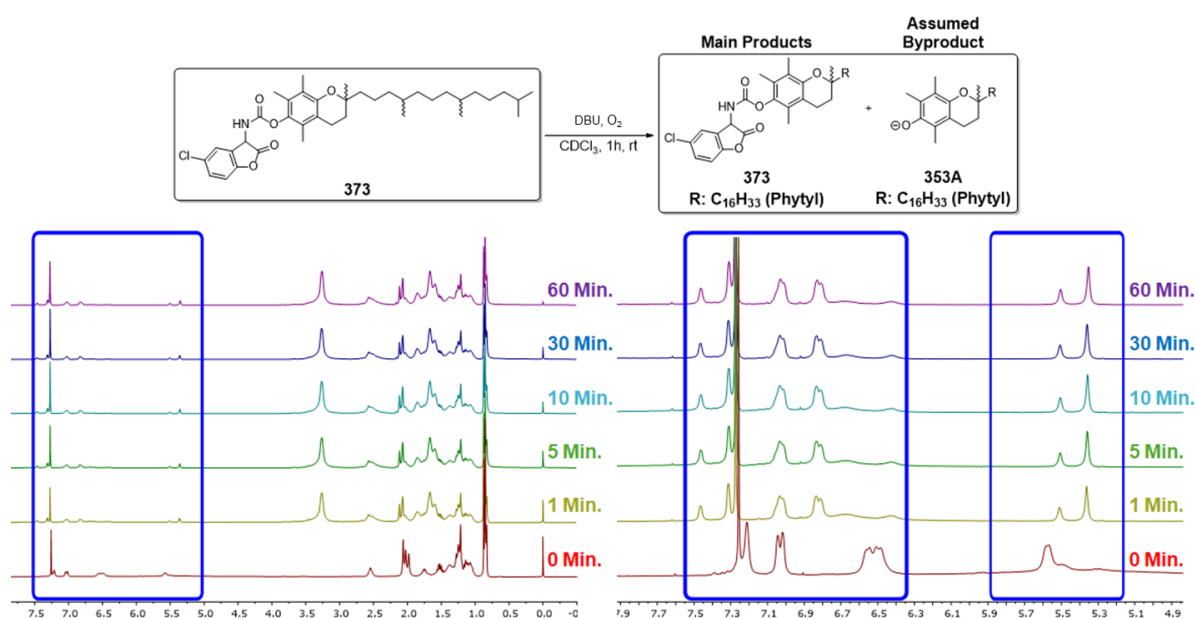


Figure 25: NMR measurements of the CL-decomposition experiment with the testosterone-coumaranone (**372**) with associated reaction equation. (Top, left) Complete NMR-spectrum. (Top, right) Enlarged extract of the area from 4.4 – 7.7 ppm. Blue boxes = change in signal intensity and occurrence of new signals. (Bottom) Decay of the CL of coumaranone **372**. 10 mg of **372** were dissolved in MeCN and a few drops of DBU were added. The blue CL lasted for 60 seconds.

Addition of DBU to testosterone coumaranone **372** results in a blue and visible CL that remains bright for 30 seconds and then decays rapidly within another 30 seconds (Figure 25). $^1\text{H-NMR}$ spectra show the shift of signals in the range of 4.4 – 5.7 ppm and 6.7 – 7.7 ppm after the addition of DBU was completed, but no further changes can be observed thereafter. While the CH group in α -position to the lactone moiety of the coumaranone-PG (5.43 ppm, doublet) vanishes, a new signal appears at 4.88 ppm with a triplet multiplicity. The same observation can be made with the CH signal of testosterone (4.41 ppm, triplet), which is adjacent to the carbamate unit. After one minute, the signal separates into two triplet signals at 4.38 and 4.47 ppm, respectively. Since no further changes could be seen within one hour, 2D spectra were recorded. Apart from the mentioned signal shift of the CH groups, the comparison of the obtained HMBC and COSY spectra with those of the starting material shows the same cross peaks and thus confirms that coumaranone **372** is still intact. Considering the results of carbamate-coumaranones **370** and **371** and the brief but bright CL of **372** it can be assumed that a small amount underwent decarboxylation and generated compound **379A**. Since both DBU and coumaranone **372** are large molecules with high steric demands, it was attempted to decarboxylate the carbamate sidechain of the coumaranone-PG in order to release testosterone. Using the same experimental procedure as for the decarboxylation of **377A**, three equivalents of KOH were added to coumaranone **372** and refluxed in ethanol for 4 hours, but the reaction did not occur. Similar results were obtained from the NMR-measurements of coumaranone **373** (Figure 26). The CL remained overall weak but was visible over a time period of 5 minutes. After the addition of DBU a shift of signals can be seen in the area from 5.3 to 7.5 ppm.



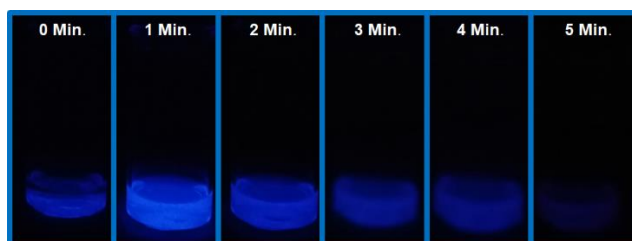


Figure 26: NMR measurements of the CL-decomposition experiment with the α -tocopherol-coumaranone (**373**) with associated reaction equation. (Top, left) Complete NMR-spectrum. (Top, right) Enlarged extract of the area from 5.1 – 7.7 ppm. Blue boxes = change in signal intensity and occurrence of new signals. (Bottom) Decay of the CL of coumaranone **373**. 5 mg of **373** were dissolved in MeCN and a few drops of DBU were added. The blue CL lasted for 5 minutes.

Also in this case, the sample was saturated with oxygen for one hour but did not show any further changes, so that again 2D spectra were recorded. Although no cross peaks can be seen between the protons of the methyl-substituted chromane system and the carbamate carbon atom due to the larger distances ($> ^4J$), HMBC confirms the complete coumaranone scaffold. Due to the aromatic ring, which can stabilise a negative charge, and the visible CL, which implies a partial decarboxylation of **373**, it is possible that a small amount of anionic α -tocopherol (**353A**) was released, as in the case of paracetamol derivative **370**.

4.2.3 CL of carbamate-coumaranones^[300]

The characterisation of the photophysical properties of the carbamate coumaranones followed the same experimental procedure as for the urea coumaranones, with the coumaranone **370** being dissolved in DMF instead of MeCN and the stock solution of **373** having to be further diluted to a concentration of $c = 10^{-3}$ mol/l due to poor solubility.

Since the NMR experiments of **370** clearly showed the release of paracetamol, other photophysical properties were expected. The CL of **370** is clearly visible to the human eye and very intense, but disappears within one minute, which is confirmed by the initial emission scans showing a maximum at 406 nm after one scan. After that, no further emission can be detected (Figure 27a). Several emission scans with an excitation wavelength of 495 nm showed increasing and strong photoluminescence with a maximum at 558 nm. However, while the CL decreased after one scan, the formation of the fluorescent species takes much longer and reaches equilibrium only after 19 minutes (Figure 27b). In agreement with these results, the excitation scans (Figure 27c, $\lambda_{Em} = 555$ nm) show a very strong absorption at 449 nm, shifting slightly towards 452 nm after the first scan. During the decay of the first absorbing species, a new slight increase in absorption is observed after the second scan with a

maximum at 505 nm. Since several aromatic byproducts were seen in the NMR experiments of **370**, it remains unknown which one causes the observed absorption and fluorescence.

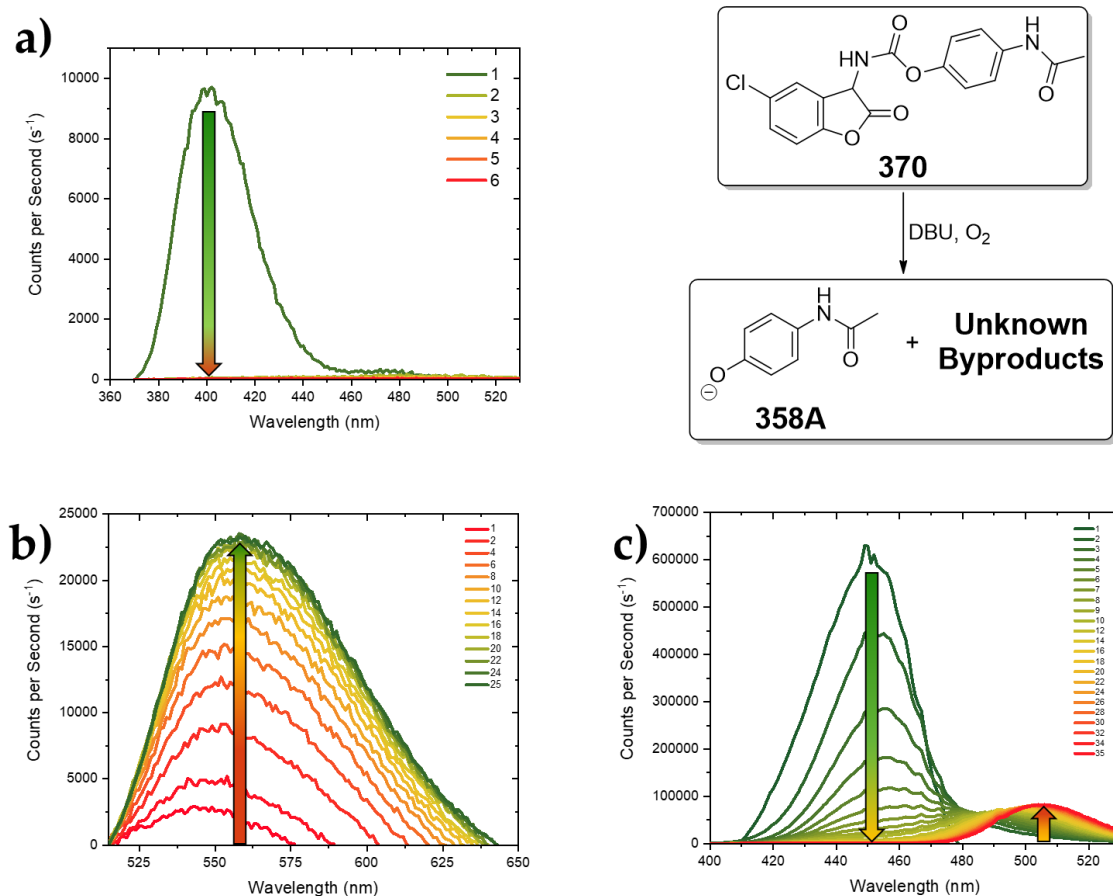


Figure 27: Emission and excitation spectra of **370** in DMF (every scan took 45 s): (a) emission scans of CL (i.e., without external excitation, Slit: 5.0), the arrow indicates the decrease in the CL; (b) emission scans during CL reaction (external excitation $\lambda_{\text{Ex}} = 495$ nm, Slit: 1.5). The first scan was performed after addition of DBU. The arrow indicates the increase in a fluorescent species within 25 scans; (c) excitation scans during CL reaction ($\lambda_{\text{Em}} = 555$ nm, Slit: 1.5). The first scan was performed after addition of DBU. The left green arrow indicates the decrease in an absorbing species after 20 scans. Starting from the 22nd scan, the right orange/red arrow indicates a minor increase in absorption at higher wavelengths.

The CL of **371** is initially very strong and bright and persists for about 21 minutes before fading (Figure 28a). After the 8th scan, the maximum shifts from 426 nm to 440 nm. Based on previous NMR experiments, it is known that compound **377** is formed during the CL reaction in an alkaline solution. Therefore, only one emission and excitation scan were performed to investigate the photophysical properties of this product. After completion of the CL reaction, a broad photoluminescence with a maximum at 463 nm could be detected (Figure 28b, $\lambda_{\text{Ex}} = 420$ nm). An excitation scan with $\lambda_{\text{Em}} = 470$ nm showed the corresponding absorption maximum at 415 nm (Figure 28c).

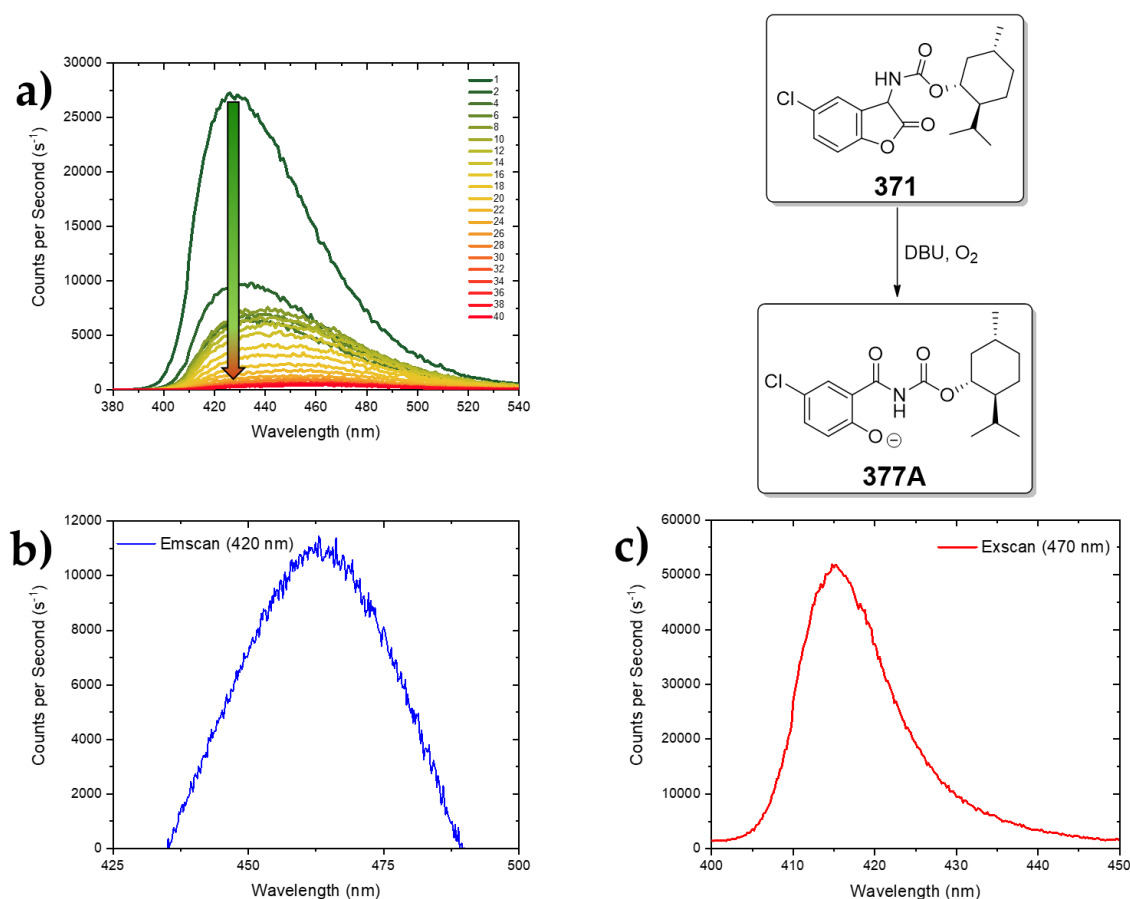


Figure 28: Emission and excitation spectra of **371** in acetonitrile (every scan took 45 s): (a) emission scans of CL (i.e., without external excitation, Slit: 0.1), the arrow indicates the decrease in the CL; (b) emission scan of **371** after CL was finished (external excitation $\lambda_{\text{Ex}} = 420$ nm, Slit: 0.5); (c) excitation scan of **371** after CL was finished ($\lambda_{\text{Em}} = 470$ nm, Slit: 1.0).

Both carbamate coumaranones **372** and **373** showed a short and visible blue CL when oxidised in alkaline solution with DBU, suggesting that a defined amount of these compounds was decarboxylated. However, NMR experiments showed in both cases that the starting material remained as the main product after the reaction and no clear signs of byproducts could be detected.

The luminescence experiments of **372** are presented in Figure 29. The CL of **372** could be perceived with the human eye for one minute, but was detectable with the detector of the spectrometer for 4 minutes with a maximum at 462 nm (Figure 29a). Since the coumaranone remains intact but shows slight signals shift in certain areas of the ¹H-NMR one emission and excitation scan were performed after CL was finished. The emission scan shows a photoluminescence with a maximum at 483 nm (Figure 29b, $\lambda_{\text{Ex}} = 420$ nm), while a broad absorption from 350 to 450 nm with a maximum at 420 nm could be detected during the corresponding excitation scan with $\lambda_{\text{Em}} = 480$ nm (Figure 29c). Due to an instrument error a straight line appears at 410 nm. Since both maxima could be compared with the results of the

decarboxylated menthol-coumaranone **377A**, the proposed decomposition product of testosterone-coumaranone **379A** can be assumed to be the fluorophore. The structure itself however, could not be detected in NMR and thus remains a hypothesis.

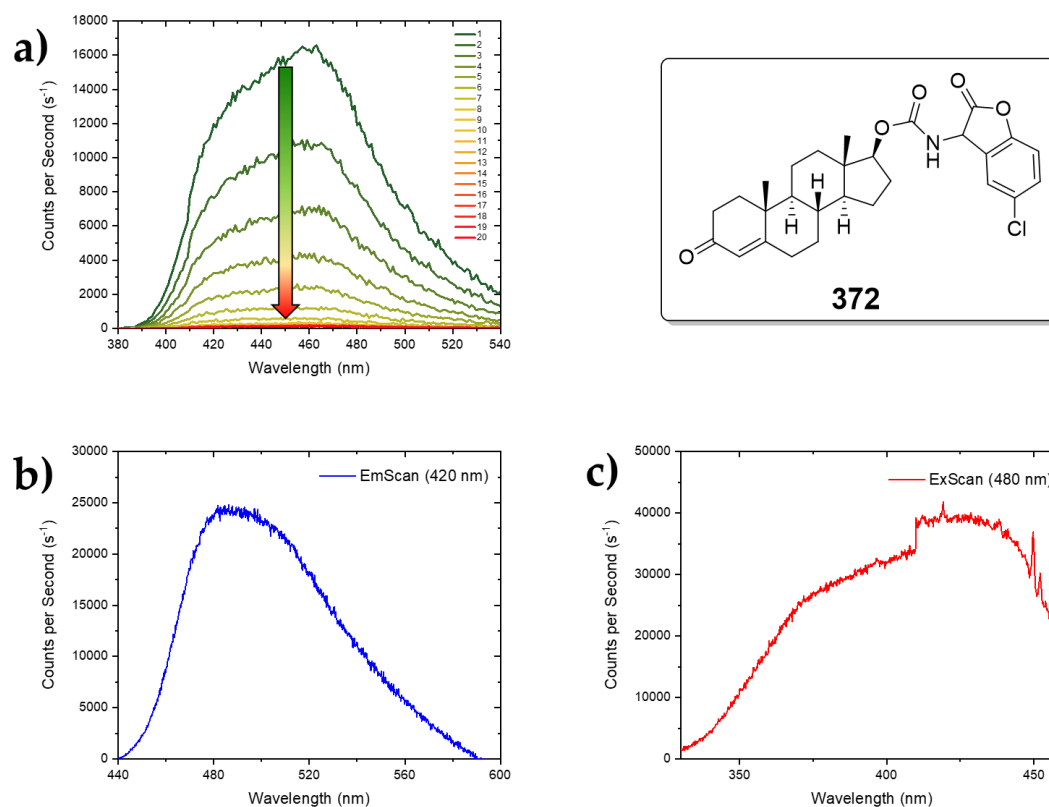


Figure 29: Emission and excitation spectra of **372** in acetonitrile (every scan took 45 s): (a) emission scans of CL (i.e., without external excitation, Slit: 1.0), the arrow indicates the decrease in the CL; (b) emission scan of **372** after CL was finished (external excitation $\lambda_{\text{Ex}} = 420$ nm, Slit: 0.4); (c) excitation scan of **372** after CL was finished ($\lambda_{\text{Em}} = 480$ nm, Slit: 0.4).

Within 7 scans (5 minutes), the CL of **373** ($\lambda_{\text{max}} = 436$ nm) completely decays, which is consistent with the period when the CL is also visible (Figure 30a). The emission scan revealed a fluorescent species with a maximum at 416 nm (Figure 30b, $\lambda_{\text{Ex}} = 360$ nm). The subsequent excitation scan with $\lambda_{\text{Em}} = 425$ nm showed a corresponding absorption at 359 nm (Figure 30c). Since coumaranones themselves do not exhibit fluorescent properties and absorb mainly light in the UV-B range, the alkaline solution seems to alter the photophysical properties of **373**. While CL indicates an oxidation process, most of the starting material is unaffected by the reaction. Therefore, the products obtained after oxidation can be considered as a potential fluorophore, but remain unknown.

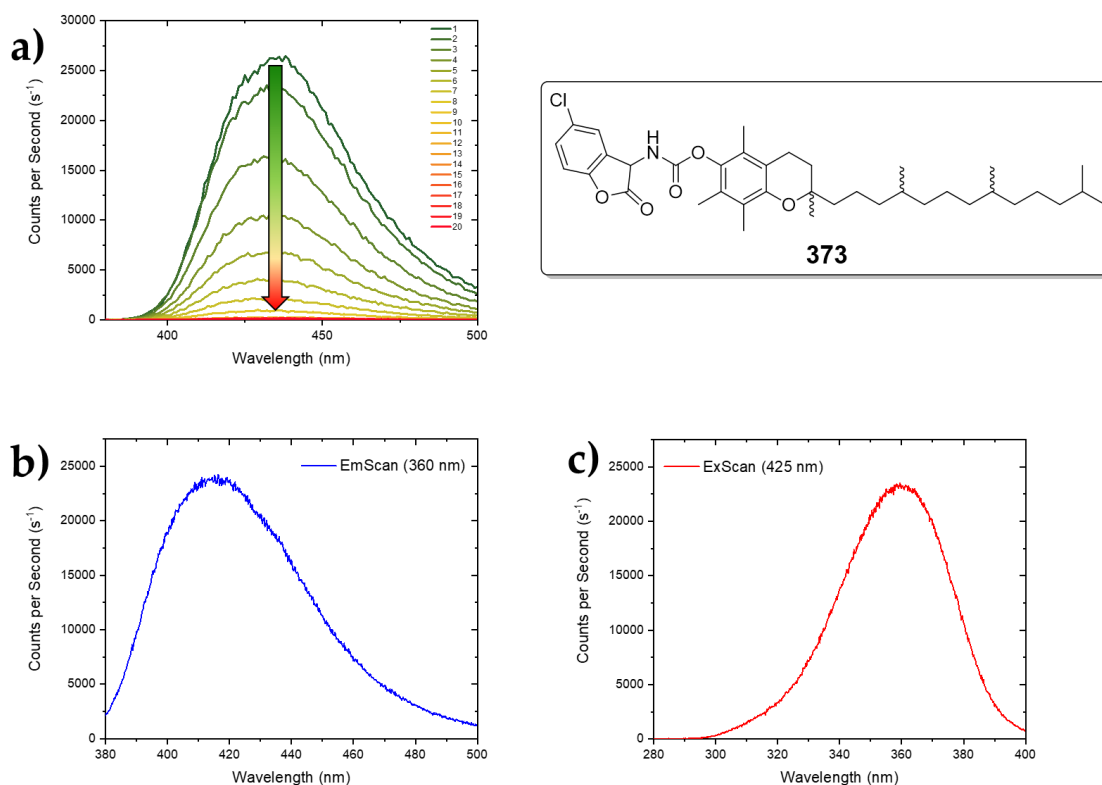


Figure 30: Emission and excitation spectra of **373** in acetonitrile (every scan took 45 s): (a) emission scans of CL (i.e., without external excitation, Slit: 1.0), the arrow indicates the decrease in the CL; (b) emission scan of **373** after CL was finished (external excitation $\lambda_{\text{Ex}} = 360$ nm, Slit: 0.5); (c) excitation scan of **373** after CL was finished ($\lambda_{\text{Em}} = 425$ nm, Slit: 0.5).

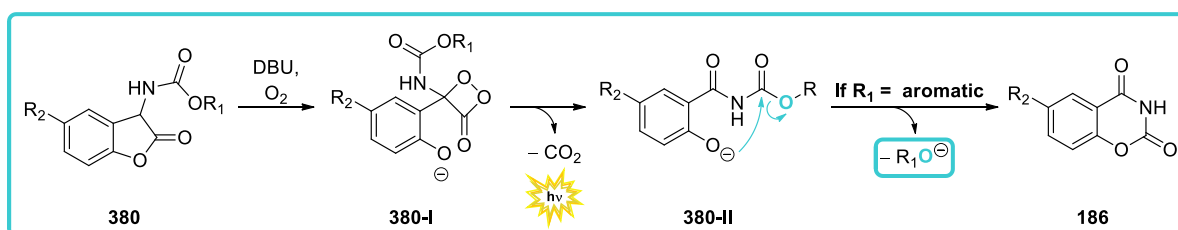
The results of the luminescence experiments are summarised in table 10. All carbamate-coumaranones are able to show a clearly visible CL, with that of the L-menthol derivative **372** having the longest duration. With the exception of the paracetamol coumaranone (**370**), which was measured in DMF and therefore cannot be compared with the other results, the emission wavelength of the CL of **372** differs by 22 to 26 nm compared to the respective maxima of **371** and **373**. Besides the similar absorption and fluorescence maxima of **377A** (which is derived from **371**) and the oxidised product of **372**, the unknown fluorescence product of **373** shows clear differences to the other measurements.

Table 10: Summary of the photophysical properties of urea-coumaranones. The absorption and fluorescence maxima refer to the unknown oxidised products of the respective coumaranone.

Entry	CL λ_{max} [nm]	CL Intensity/Duration	Absorption λ_{max} [nm]	Fluorescence λ_{max} [nm]
370	406	Bright / 1 min.	449	558
371	426/440	Very Bright / 21 min.	415	463
372	462	Bright / 1 - 4 min.	420	483
373	436	Weak but visible / 5 min.	359	416

4.2.4 Conclusions on the chemistry of carbamate-coumaranones^[300]

The deprotection of aromatic and aliphatic alcohols shows large differences compared to the results of urea-coumaranones. NMR and luminescence studies on carbamate-coumaranones show that the CLPG concept is strongly dependent on the properties and size of the nucleofuge (Scheme 68). While the phenolate of paracetamol (**358A**) is quickly released in the CL reaction of **370** with DBU, the L-menthol coumaranone (**371**) also shows a strong CL but is not cleaved from the PG unless additional decarboxylation with KOH is performed. Therefore, coumaranones that protect aliphatic alcohols can be considered as a "two-step" PG.



Scheme 68: Proposal for the general mechanism of carbamate-coumaranones. Structure **186** could not be verified by NMR.

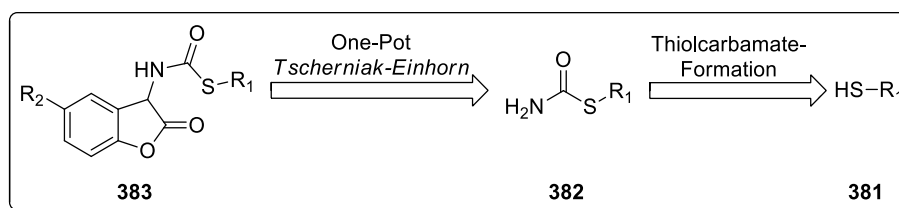
Deprotection of α -tocopherol (**353**) and testosterone (**358**) was unsuccessful, although CL was observed for a short period when DBU was added to the respective coumaranones. This indicates that both substrates are oxidised, but most of the starting material does not interact with the base, which can be justified by the steric requirements of DBU and the corresponding coumaranones **372** and **373**. The steric requirements of the latter appear to be of greater importance, as decarboxylation/oxidation of **372** with KOH in boiling ethanol did not result in the release of testosterone. Despite the different results in the oxidation reactions, each carbamate-coumaranone had a clearly visible CL. In the case of derivatives **370** and **371**, the duration correlates with the progress of the oxidation process. The nucleofuges themselves also play an important role, as paracetamol was released, while L-menthol remains bound to the decarboxylated benzoylcarbamate **377A**. This suggests that the phenolate formed during decarboxylation requires stabilised leaving groups for subsequent ring formation, making it a selective nucleophilic group for the concept of CLPGs. Therefore, coumaranones are a viable choice for the protection of aromatic alcohols, which, however, must not have too high steric demands.

4.3 Protection and deprotection of thiols

The biological and medical importance of molecules containing a thiol group can be demonstrated by various examples. For example, the proteinogenic amino acid cysteine (**209**) is easily oxidised and forms disulfide bridges with other cysteine residues, which are responsible for stabilising the protein structure. Both thiols and cysteine are also components of numerous cofactors that are essential for many bio-synthetic processes. In the case of the tripeptide glutathione, the cysteine residue exhibits strong antioxidant properties and protects cellular components from reactive oxygen species. The main medical applications are the use of thiols to treat metal poisoning through chelation therapy and hypertension through the prescription of ACE inhibitors. Therefore, to further increase the range of possible substrates, which can be bonded to a coumaranone, the synthesis of simple thiol carbamates was investigated for the first time.

4.3.1 General protection protocol of thiols

Since the protection of thiols with coumaranone PGs has not yet been explored, the same synthesis strategy was used as in the case of alcohols. The thiols were first converted to the corresponding thiolcarbamate derivative **382**, and then a one-pot *Tscherniak-Einhorn* reaction was carried out to give the coumaranone-protected thiol **383** (Scheme 69).

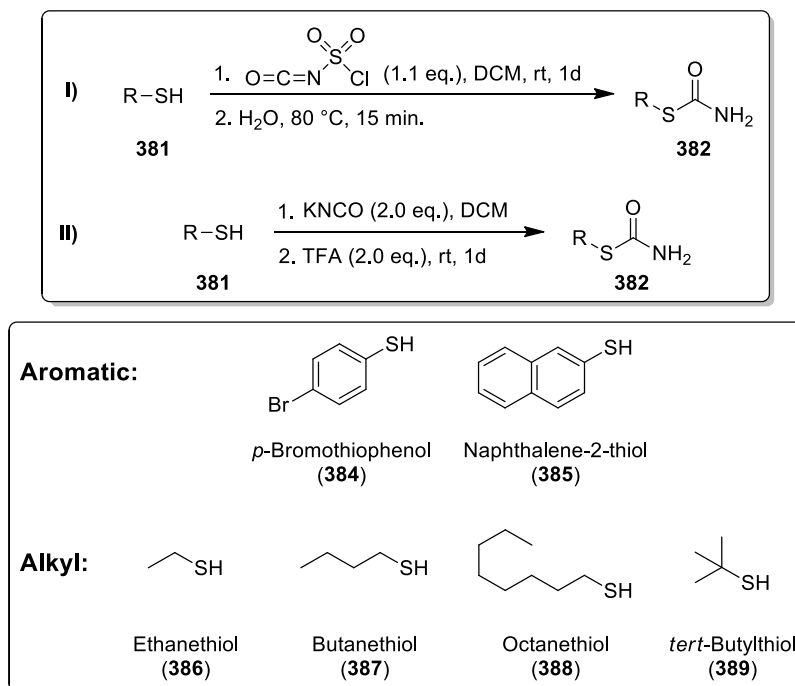


Scheme 69: Retrosynthesis of the protection of thiols.

4.3.1.1 Syntheses of thiolcarbamates

Analogous to the synthesis of carbamates the adapted synthesis protocol of *R. Graf et al*^[302] was followed. However only aromatic thiols could be converted to the thiolcarbamates with this method. In the case of aliphatic thiols, the synthesis protocol of *B. Loev and F. Kormendy*^[304] was adapted and used instead (Scheme 70). This procedure was developed for the synthesis of carbamates with primary, secondary and tertiary alcohols as starting material.

The nucleophilic substrate is stirred with either sodium or potassium cyanate, trifluoroacetic acid in benzene or DCM as solvent. The latter was used because of its lower toxicity.



Scheme 70: (Top) Illustration of the synthesis of thiolcarbamates. method I) is according to the adapted synthesis protocol of *R. Graf*^[302] and method II) according to *B. Loev and F. Kormendy*^[304]. (Bottom) Substrates used for synthesis of thiolcarbamates.

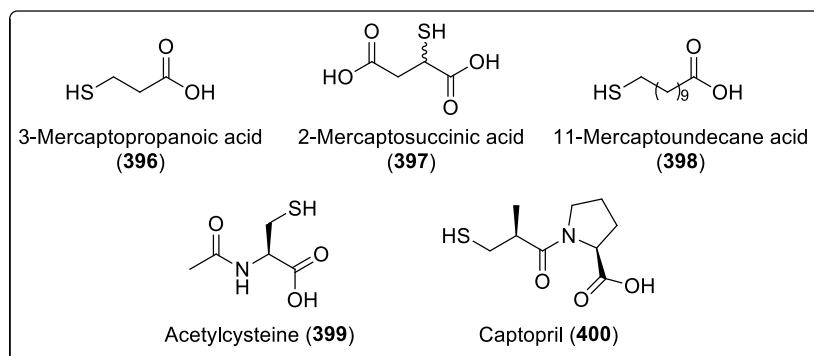
It was possible to synthesise two aromatic and four aliphatic thiolcarbamates with the respective synthesis options. The yields are summarised in Table 11. Every aromatic thiolcarbamate could be obtained with a yield above 50%, with *p*-bromothiophenol having the highest one. In the case of the aliphatic thiols the length of the carbon chain correlates with a better yield of the product, while the lower yield of *tert*-butylthiol (389) can be explained with its steric demands.

Table 11: Obtained aromatic and aliphatic thiolcarbamates according to procedure I and II.

Entry	Method	Thiolcarbamate of	Yield [%]
390	I	<i>p</i> -Bromothiophenol	83
391	I	Naphthalene-2-thiol	67
392	II	Ethanethiol	35
393	II	Butanethiol	55
394	II	Octanethiol	69
395	II	<i>tert</i> -Butylthiol	41

Further investigations were done in order to see if different functional groups are tolerated during these reactions. Thus, similar to the results with amino acids, mercapto acids (396 –

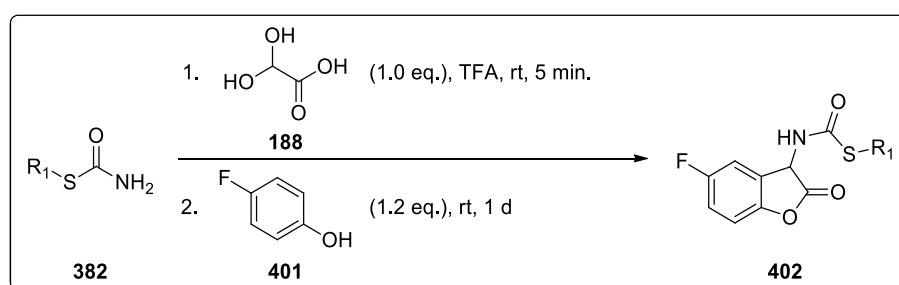
398), acetylcysteine (**399**) and captopril (**400**) were used for both reactions to obtain the corresponding thiolcarbamates (Scheme 71). However, all experiments remained unsuccessful, which indicates that carboxylic acids and amide group, regardless of the length of the carbon chain, are not tolerated in these reactions. Esterification of these substrates via multiple synthesis routes gave poor yields, so that no further attempts were performed, considering that the intended simple coumaranone synthesis, representing a PG, becomes a less favourable and reasonable choice.



Scheme 71: Illustration of the mercapto acids, which could not be converted to the corresponding thiolcarbamates.

4.3.1.2 *Tscherniak-Einhorn* reaction with thiolcarbamates

Since 2-coumaranones with a thiolcarbamate substructure represent a new compound class, until now unknown to literature, the optimal reaction parameters were thoroughly investigated with the synthesis protocol of *Schramm et al.*^[295] as a basis (Scheme 71).



Scheme 72: Illustration of the synthesis of coumaranones with a thiolcarbamate substructure according to the adapted synthesis protocol of *S. Schramm et al.*^[295]

Again, the best acid for this reaction was TFA, while a mixture of acetic acid/sulfuric acid (9:1) or formic acid gave lower or no yields. In many cases the reaction time, after the addition of the phenol compound, could be reduced to one day. Refluxing the reaction also

worked but was not as efficient and if stirred for longer time periods, an accumulation of byproducts was observed. Experiments with different *para*-substituted phenol compounds showed that the use of *para*-fluorophenol (**401**) gave the best results, which is why it was used for all syntheses.

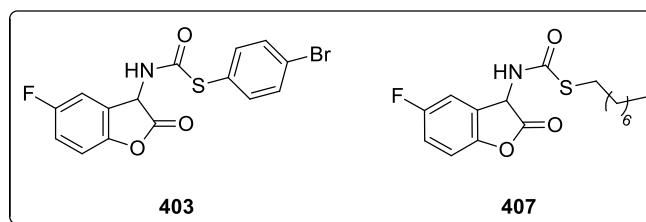
Table 12: Thiolcarbamate derivatives used for the synthesis of coumaranones according to the adapted synthesis protocol of *S. Schramm et al.*^[295] and the corresponding yields.

Entry	Coumaranone of	Yield [%]
403	<i>p</i> -Bromothiophenol	20
404	Naphthalene-2-thiol	12
405	Ethanethiol	8
406	Butanethiol	4
407	Octanethiol	17
408	<i>tert</i> -Butylthiol	0

NMR examination of the crude products revealed that, similar to the synthesis of some carbamate coumaranones, a small amount of an uncondensed byproduct was produced. However, after column chromatography, the yield of each coumaranone was greatly reduced, suggesting that the compound might decompose during the process. Therefore, different work-up and purification procedures and, for certain substrates, longer reaction times should be investigated to optimise the yield. Apart from the failed synthesis with the thiol carbamate of *tert*-butylthiol (**395**), all other coumaranones could be synthesised, with derivative **403** having the highest yield of 20% (Table 12).

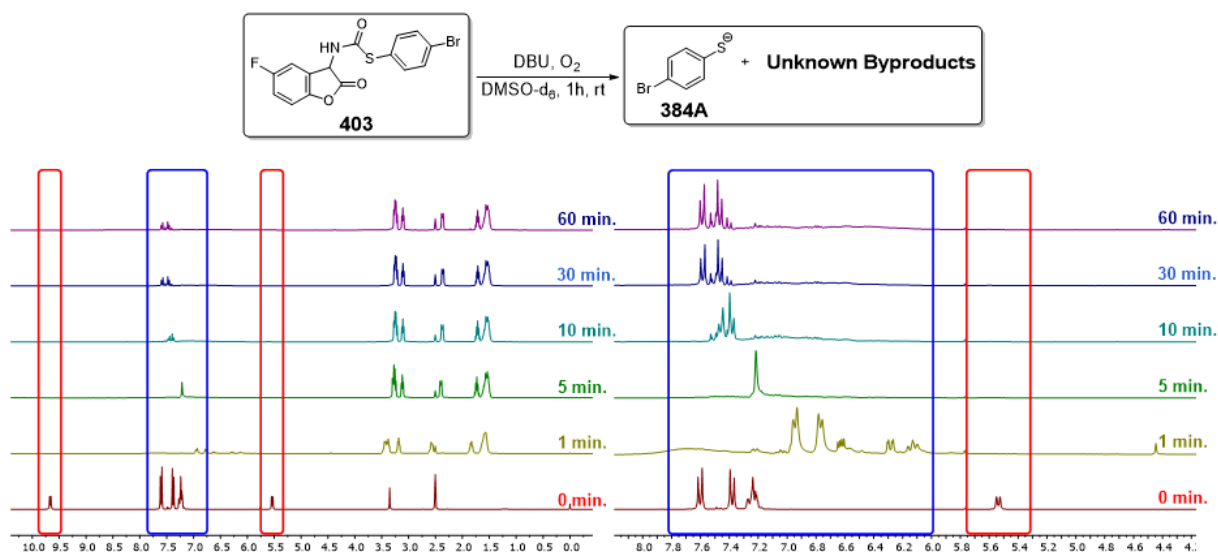
4.3.2 Investigations of thiolcarbamate-coumaranones via NMR

Of the five synthesised thiocarbamate-coumaranones, the *p*-bromothiophenol **403** and octanethiol derivative **407** were chosen for NMR investigations (Scheme 73). While the release of the first is easily detectable due to its significant aromatic signals (similar to paracetamol), the second is best extracted after the oxidation process, as the ^1H -signals of DBU overlay those of octanethiol (and all other aliphatic thiols as well).



Scheme 73: Overview of the thiolcarbamate-coumaranones whose decomposition reaction in an alkaline solution with oxygen were investigated via proton NMR.

The decomposition of thiolcarbamate-coumaranone **403** is shown in Figure 31. After the addition of DBU, the signals of the α -CH group at 5.54 ppm and the NH group at 9.67 ppm disappear and changes occur in the aromatic range from 6.0 to 7.8 ppm. In this case, the reaction leads to a CL with green instead of blue light, indicating a red-shift compared to the previously discussed coumaranones. The initially blue and then green emission fades after more than 10 minutes. Within the same period, the two signals of *p*-bromothiophenol (**384A**) show a clearly visible increase at 7.47 and 7.59 ppm. After 30 minutes, no further change in the signals is observed and the complete deprotection of **384** could be verified. The exact structure of the byproduct however, could not be elucidated.



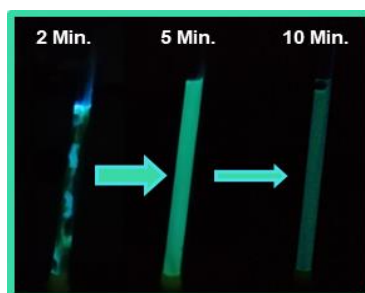


Figure 31: NMR measurements of the CL-decomposition experiment with the *p*-bromothiophenol-coumaranone (**403**) with associated reaction equation. (Top, left) Complete NMR-spectrum. (Top, right) Enlarged extract of the area from 4.4 – 8.0 ppm. Blue boxes = change in signal intensity and occurrence of new signals; red boxes = reduction/disappearance of signals. (Bottom) Photos of the CL of **403** during saturation with oxygen.

The results of the NMR investigations of **407** also prove the successful deprotection of octanthiol (**388A**) (Figure 32). While again the signals of the α -CH- and NH-group disappear after the addition of DBU, the preferential formation of a specific aromatic byproduct in the range of 7.0 to 7.5 ppm is observed after 5 minutes.

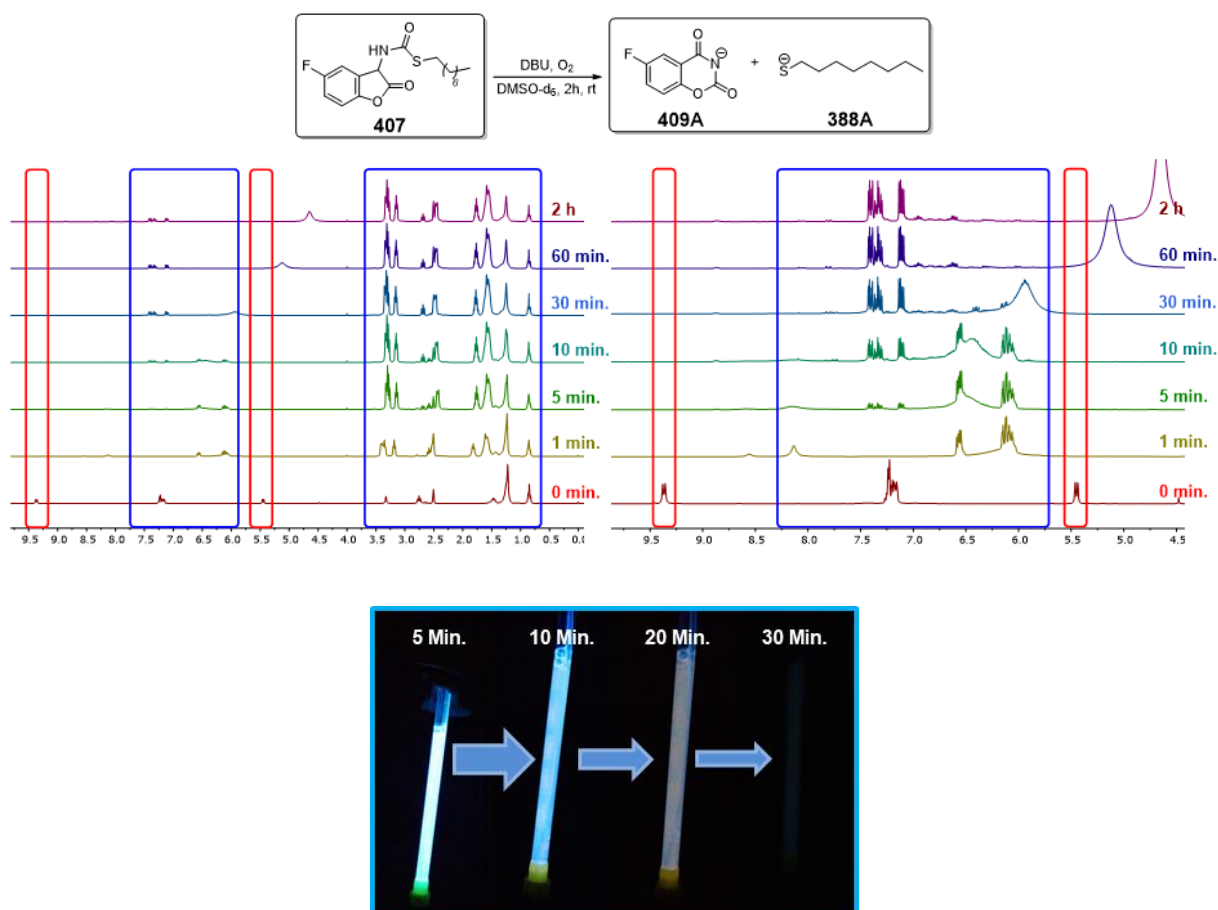


Figure 32: NMR measurements of the CL-decomposition experiment with the octanthiol-coumaranone (**407**) with associated reaction equation. (Top, left) Complete NMR-spectrum. (Top, right) Enlarged extract of the area from 4.5 – 9.5 ppm. Blue boxes = change in signal intensity and occurrence of new signals; red boxes = reduction/disappearance of signals. (Bottom) Photos of the CL of **407** during saturation with oxygen.

The CL of **407** differs from that of **403** by its much longer duration of 30 minutes and its light blue colour. After the CL has completely decayed, no change is visible in the $^1\text{H-NMR}$ either. Subsequent 2D spectra allowed the identification of completely deprotected octanethiol (**388A**) and compound **409A** as the primary aromatic byproduct of the decomposition. In summary, the complete removal of CLPG could be demonstrated in both experiments.

4.3.3 CL of thiolcarbamate-coumaranones

Luminescence experiments were conducted with all five thiolcarbamate-coumaranones. As the results of the NMR experiments indicate that the corresponding thiol is always cleaved from the coumaranone CLPG, a clearly visible CL as well as similar decomposition patterns were expected.

The luminescence spectra of **403** are presented in Figure 33. The first scan of the CL has an emission maximum at 435 nm which then shifts towards 455 nm and shows a major intensity loss after the 10th scan (Figure 33a). This is all in agreement with the observations from the NMR experiment. When the sample was excited at 410 nm afterwards a fluorescent species could be detected with an emission maximum at 468 nm (Figure 33b). The excitation scan (Figure 33c, $\lambda_{\text{Em}} = 465 \text{ nm}$) shows a strong absorption with $\lambda_{\text{max}} = 411 \text{ nm}$. Similar results were obtained from the luminescence spectra of **404** (Figure 34). The CL has an emission maximum between 450 to 455 nm and appears overall weaker to the visible eye but also in regard to the lower counts per second values (Figure 34a). This suggests that a larger aromatic system, which also increases the ability to stabilise negative charges, is released more quickly, reducing the overall CL, as the emitting species decays very fast in solution. The fluorescent species of this reaction exhibits similar properties to that of **403**. The emission maximum is detected at 467 nm (Figure 34b, $\lambda_{\text{Em}} = 415 \text{ nm}$), while the corresponding excitation scan reveals an absorption with a maximum at 409 nm (Figure 34c).

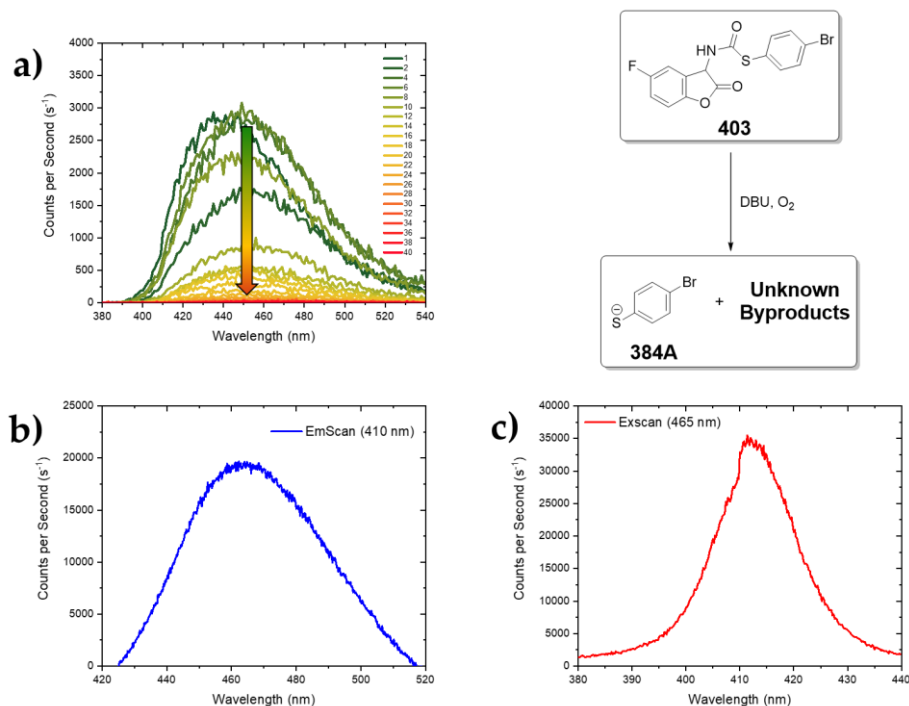


Figure 33: Emission and excitation spectra of **403** in acetonitrile (every scan took 45 s): (a) emission scans of CL (i.e., without external excitation, Slit: 0.4), the arrow indicates the decrease in the CL; (b) emission scan of **403** after CL was finished (external excitation $\lambda_{\text{Ex}} = 410$ nm, Slit: 0.7); (c) excitation scan of **403** after CL was finished ($\lambda_{\text{Em}} = 465$ nm, Slit: 0.7).

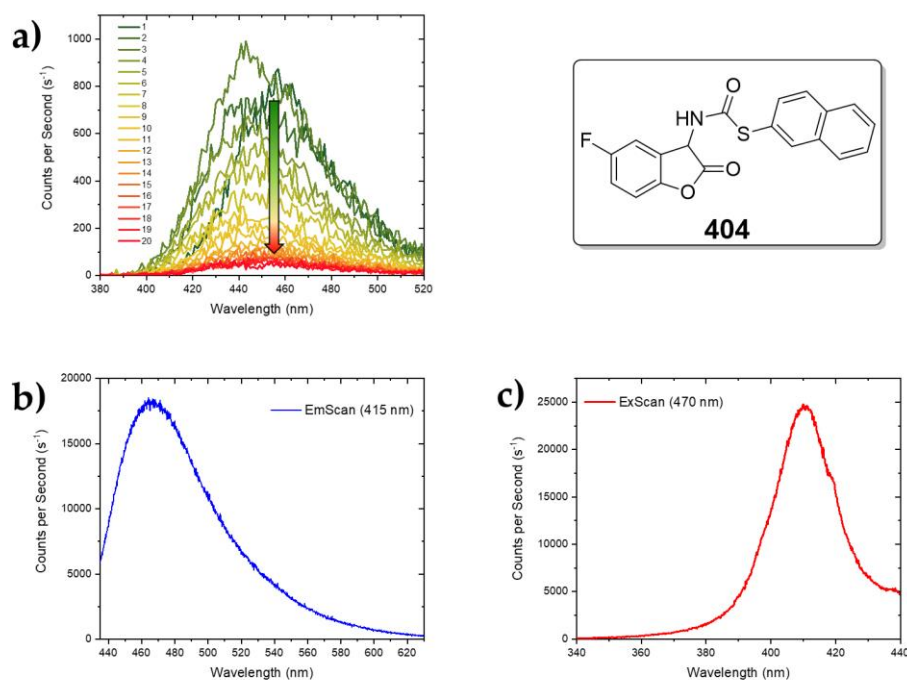


Figure 34: Emission and excitation spectra of **404** in acetonitrile (every scan took 45 s): (a) emission scans of CL (i.e., without external excitation, Slit: 0.2), the arrow indicates the decrease in the CL; (b) emission scan of **404** after CL was finished (external excitation $\lambda_{\text{Ex}} = 415$ nm, Slit: 1.0); (c) excitation scan of **403** after CL was finished ($\lambda_{\text{Em}} = 470$ nm, Slit: 1.0).

Direct comparison of the three protected aliphatic thiol derivatives **405** to **407** shows that the duration of CL decreases as the alkyl side chain becomes longer. While the CL of **405** was detectable for 36 scans/27 minutes (Figure 35a), that of **406** already has a much shorter duration with 7 scans/5 minutes (Figure 36a) and the CL of **407** fades after 5 scans/4 minutes (Figure 37a). The duration of the latter differs greatly from that of the NMR experiment. Therefore, an additional large-scale experiment was conducted, which confirmed the shortened duration of about 4 minutes (Figure 37, bottom). This difference could thus be explained by the generally insufficient oxygen concentration in the NMR sample solution. Apart from these discrepancies, the CL maxima of all three compounds are in the range of 443 to 446 nm. Furthermore, the emission and excitation scans of all three derivatives after CL decay show that the fluorescent byproducts have similar photophysical properties. The emission of **406** and **407** show emission maxima at 450 (Figure 36b) and 452 nm (Figure 37b) respectively, with the excitation scans revealing a corresponding absorption at 415 (Figure 36c) and 407 nm (Figure 37c). After oxidation of **405**, the scans show a fluorescent species emitting at 443 nm (Figure 35b) and absorbing at 387 nm (Figure 35c), which could mean that a different byproduct is formed in this reaction due to the lower absorption maximum.

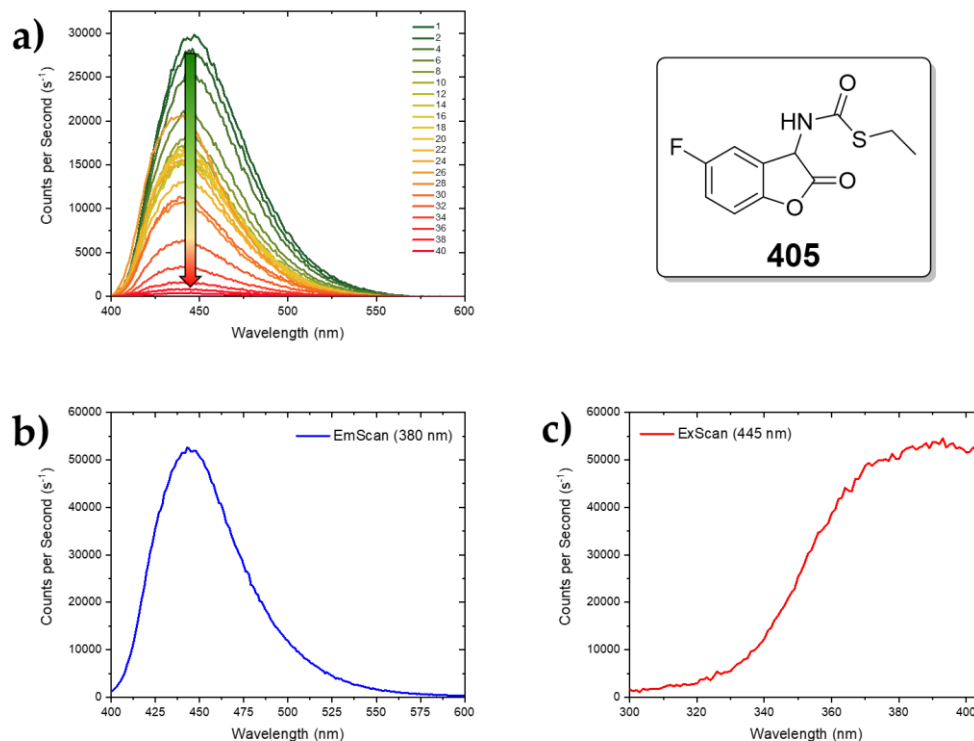


Figure 35: Emission and excitation spectra of **405** in acetonitrile (every scan took 45 s): (a) emission scans of CL (i.e., without external excitation, Slit: 0.8), the arrow indicates the decrease in the CL; (b) emission scan of **405** after CL was finished (external excitation $\lambda_{\text{Ex}} = 380$ nm, Slit: 1.3); (c) excitation scan of **405** after CL was finished ($\lambda_{\text{Em}} = 445$ nm, Slit: 1.2).

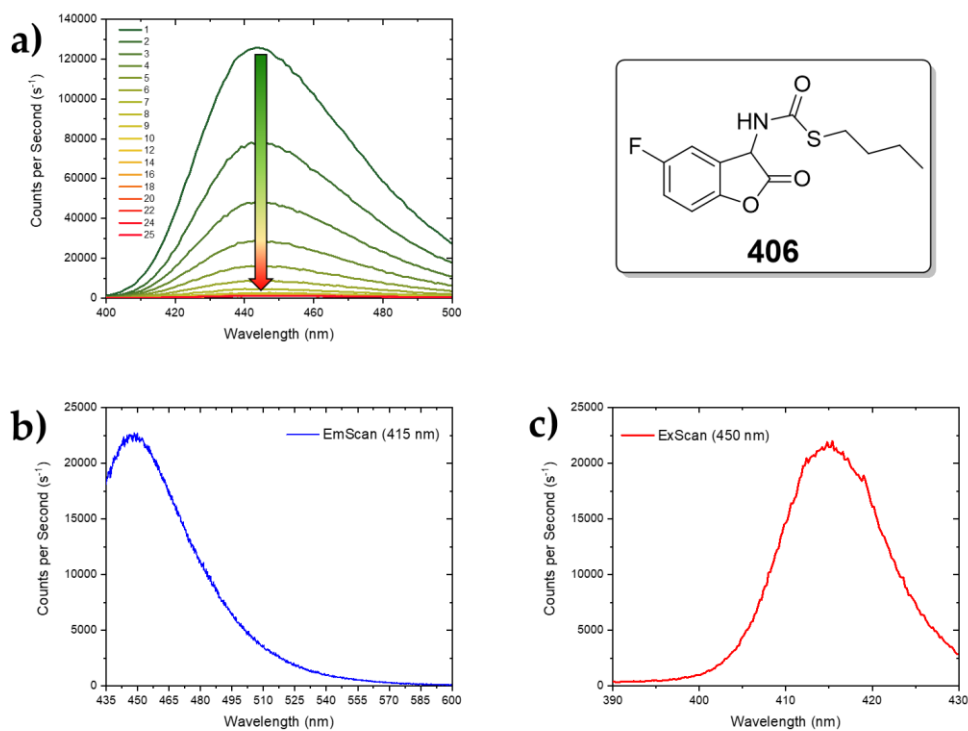
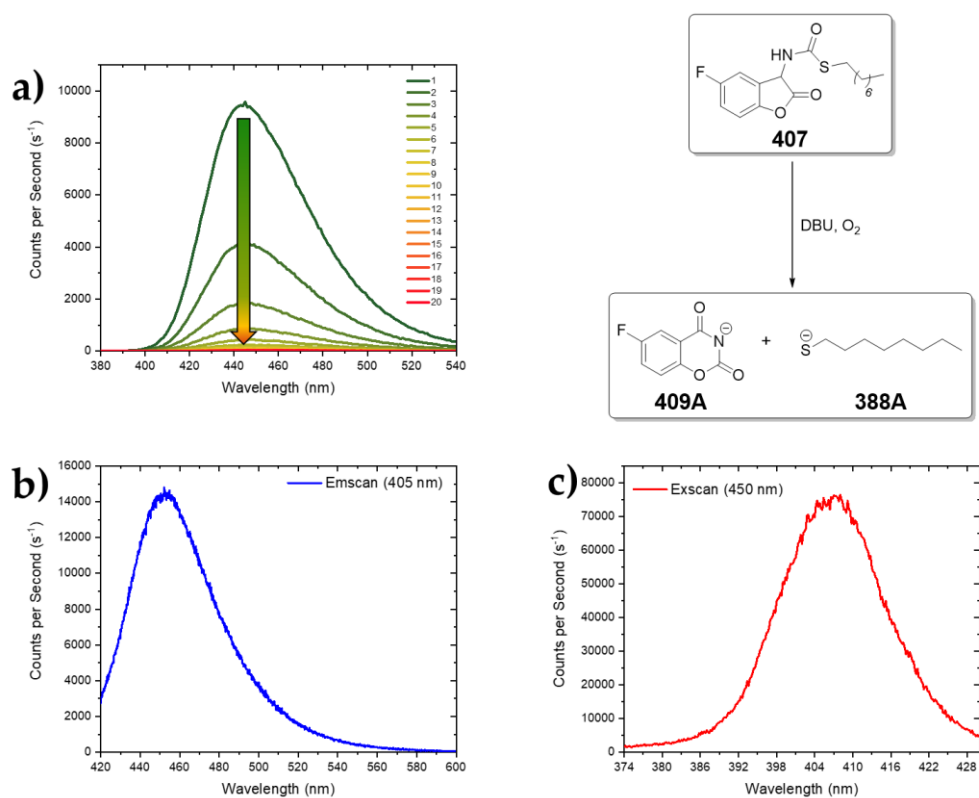


Figure 36: Emission and excitation spectra of **406** in acetonitrile (every scan took 45 s): (a) emission scans of CL (i.e., without external excitation, Slit: 0.2), the arrow indicates the decrease in the CL; (b) emission scan of **406** after CL was finished (external excitation $\lambda_{\text{Ex}} = 415$ nm, Slit: 0.5); (c) excitation scan of **406** after CL was finished ($\lambda_{\text{Em}} = 450$ nm, Slit: 0.5).



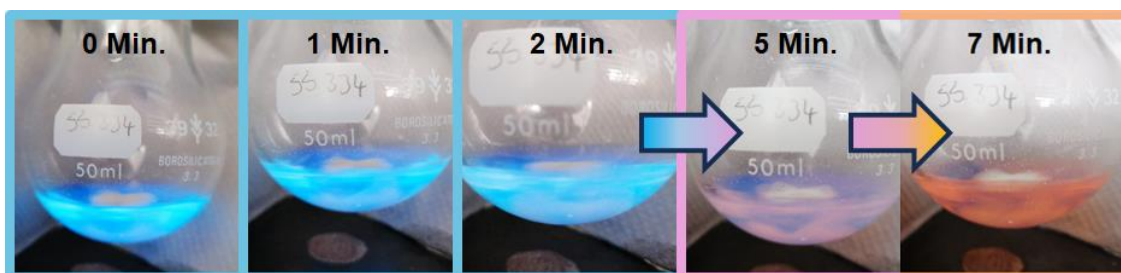


Figure 37: (Top) Emission and excitation spectra of **407** in acetonitrile (every scan took 45 s): (a) emission scans of CL (i.e., without external excitation, Slit: 0.2), the arrow indicates the decrease in the CL; (b) emission scan of **407** after CL was finished (external excitation $\lambda_{\text{Ex}} = 405 \text{ nm}$, Slit: 0.5); (c) excitation scan of **407** after CL was finished ($\lambda_{\text{Em}} = 450 \text{ nm}$, Slit: 0.5). (Bottom) Photos of the CL of coumaranone **407** in a round-bottom flask. 50 mg were dissolved in 10 ml MeCN and 2 equivalents of DBU were added. The solution was colourless before the addition of DBU. The light blue CL is clearly visible in an illuminated room. After 5 minutes, the solution turns pink due to the decreasing blue CL and the solution slowly becoming orange. After 7 minutes, only the latter colour remains, while the CL is no longer visible.

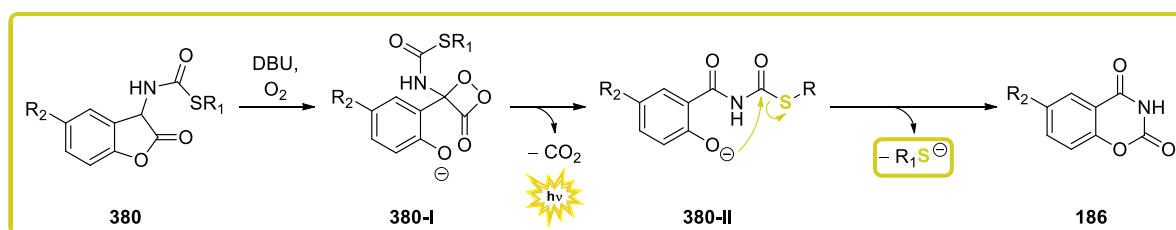
The results of the luminescence experiments are summarised in Table 13. Each derivative shows a strong and bright CL between 443 and 455 nm with varying duration depending on either the length of the alkyl side chain or the complexity of the conjugated aromatic system. The generated fluorescent species show similar photophysical properties, with that of **405** showing the greatest variation, considering the absorption and fluorescence maxima at 387 nm and 443 nm respectively.

Table 13: Summary of the photophysical properties of thiolcarbamate-coumaranones. The absorption and fluorescence maxima refer to the oxidised byproducts of the respective coumaranone.

Entry	CL λ_{max} [nm]	CL Intensity/Duration	Absorption λ_{max} [nm]	Fluorescence λ_{max} [nm]
403	435/453	Bright / 5 min.	411	468
404	450 – 455	Bright / 4 min.	409	467
405	443	Very Bright / 30 min.	387	443
406	444	Very Bright / 5 min.	415	450
407	446	Very Bright / 4 min.	407	452

4.3.4 Conclusions on the chemistry of thiolcarbamate-coumaranones

While the carbamate-coumaranones already showed positive results and allowed the release of aromatic but not aliphatic alcohols, the deprotection of both classes of thiols was successfully demonstrated. The first studies were conducted with the protection and deprotection of simple thiols, all of which were suitable examples of the concept of CLPGs. Comparing the results of the NMR studies, aromatic thiols are released much faster than aliphatic ones, which is similar to the deprotection of alcohols, although aliphatic ones only decarboxylate and are still bound to the PG. This means that a longer deprotection time correlates with a longer CL duration, since after decarboxylation the emitting species is obtained. The faster the phenolate attacks the carbonyl group, the shorter the CL as the concentration of the emitter quickly decreases. The degradation of all investigated thiolcarbamate-coumaranones also appears to be comparable to each other, as the photophysical properties of the detected fluorescent species do not show major differences, with the exception of absorption maximum of the fluorescent species of **405**.

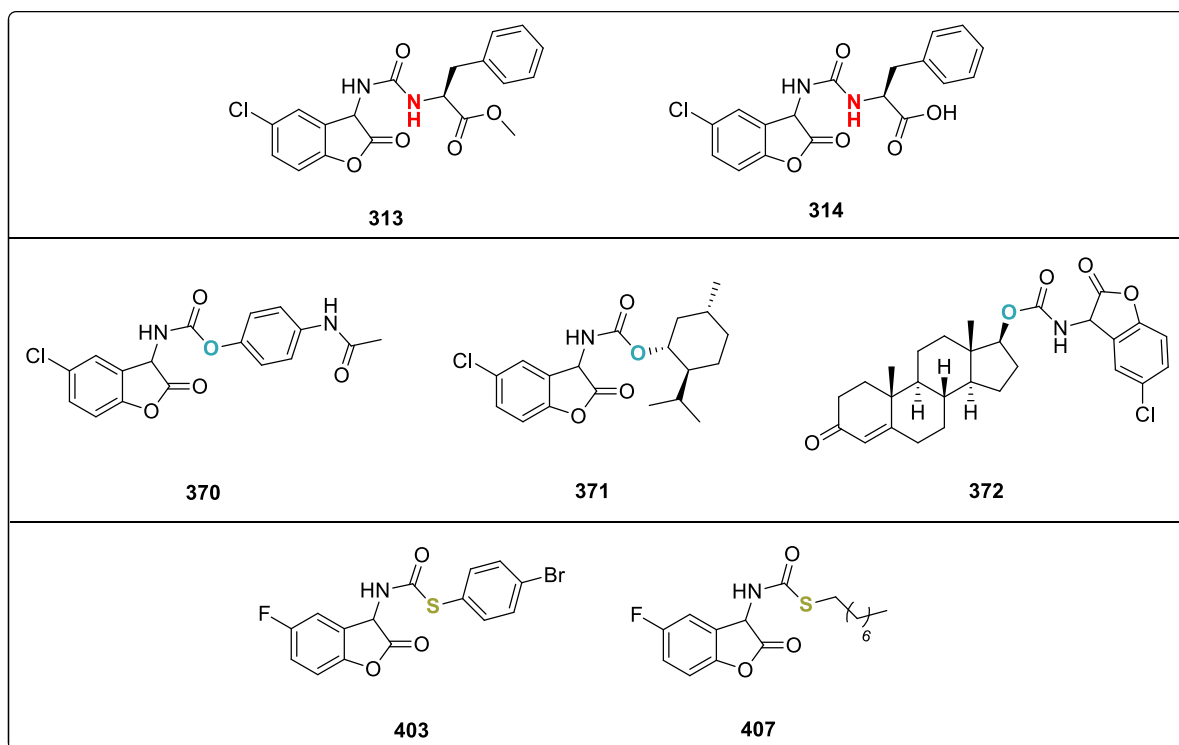


Scheme 74: Proposal for the general mechanism of thiolcarbamate-coumaranones.

Overall, the thiolcarbamate-coumaranones represent a promising and potent class with a bright blue/greenish CL and, according to these studies, allow efficient and fast release of the protected thiols. In addition, further insights were gained into the relationship between the duration and emission maximum of the CL and the size and charge stabilisation properties of the potential nucleofuge (Scheme 74).

4.4 Decomposition with HRP and urease

In addition to oxidation of coumaranones in alkaline solution with DBU or other strong non-nucleophilic bases, *Matuszczak* has shown that enzymatically triggered CL can be achieved with HRP.^[289] Therefore, a selection of coumaranones from all three different types was chosen for the study of decomposition and associated CL with HRP in order to compare the results with those of oxidations with DBU (Scheme 75).

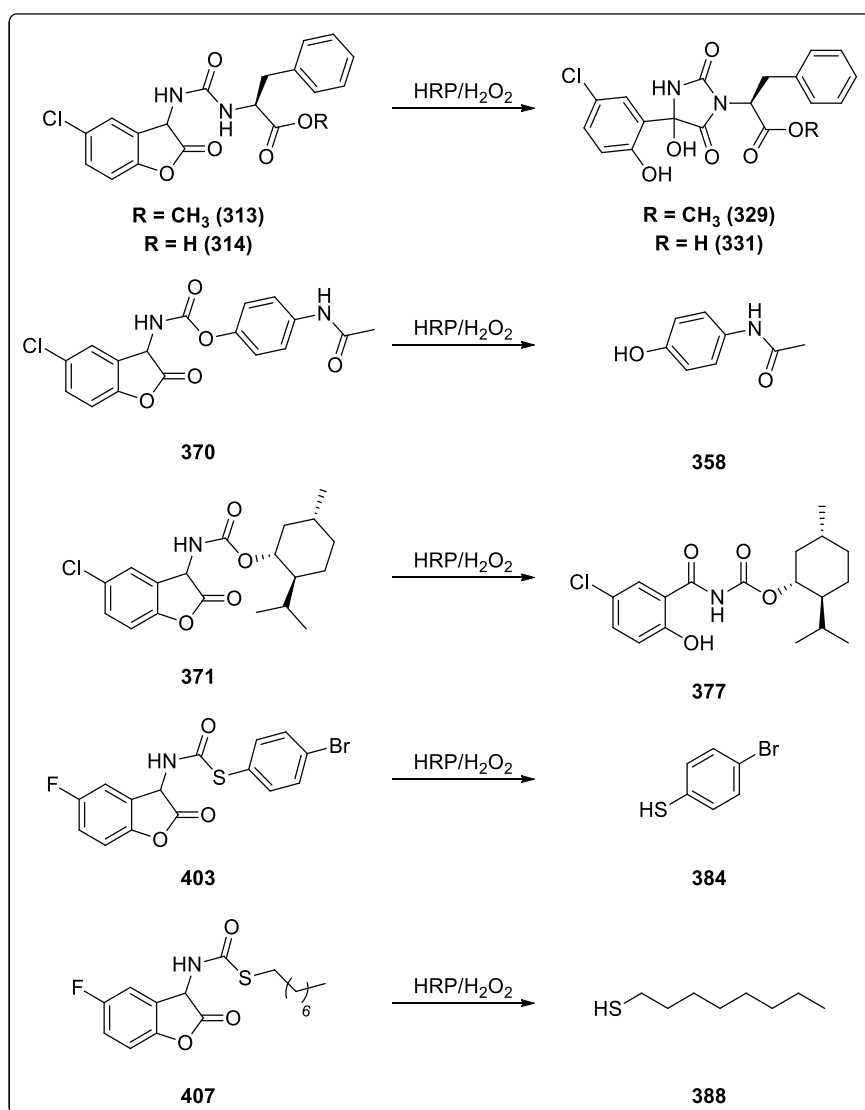


Scheme 75: Overview of the coumaranones whose decomposition reaction and CL with HRP was investigated. Since *p*-aminobenzoic acid (**263**) acts as an inhibitor for HRP its coumaranone derivative has not been used for these experiments.

HRP is the peroxidase of horseradish and catalyses the reduction of various peroxides (but mainly hydrogen peroxide) to produce water and an oxidised species. This process is enabled through a haem-group with a Fe(III) centre.^[305] In terms of substrate selectivity, several compounds have been described as viable options for oxidation with HRP, which has been exploited to produce visible colour changes, fluorescent species and CL with luminol.^[306] Besides these remarkable advantages, HRP became an overall useful enzyme for immunoassays due to its high stability, lower cost than other potential options and high conversion rate within a short time.^[307,308]

The procedure by *Matuszczak*^[289] has been modified to a synthesis protocol for large-scale experiments (see experimental section for details). The coumaranone was dissolved in a mixture of MeCN/water (1:1), a sodium phosphate buffer (pH = 7.8, 1 M) and an EDTA

solution (10^{-1} M). Subsequently, a HRP solution and H_2O_2 were added. In control reactions, the enzyme and H_2O_2 were omitted. None of the reactions showed a clearly visible CL, however, the progress of the reaction was evident from the fact that the clear solution turned red/brown. Although TLC indicated that the reaction was generally complete after one or two days, the reaction was always stirred for three days to ensure complete oxidation of the coumaranone. The reaction was then worked up without any purification methods and analysed by NMR. The results of all enzyme-catalysed reactions are in agreement with those of the reactions with DBU (Scheme 76).

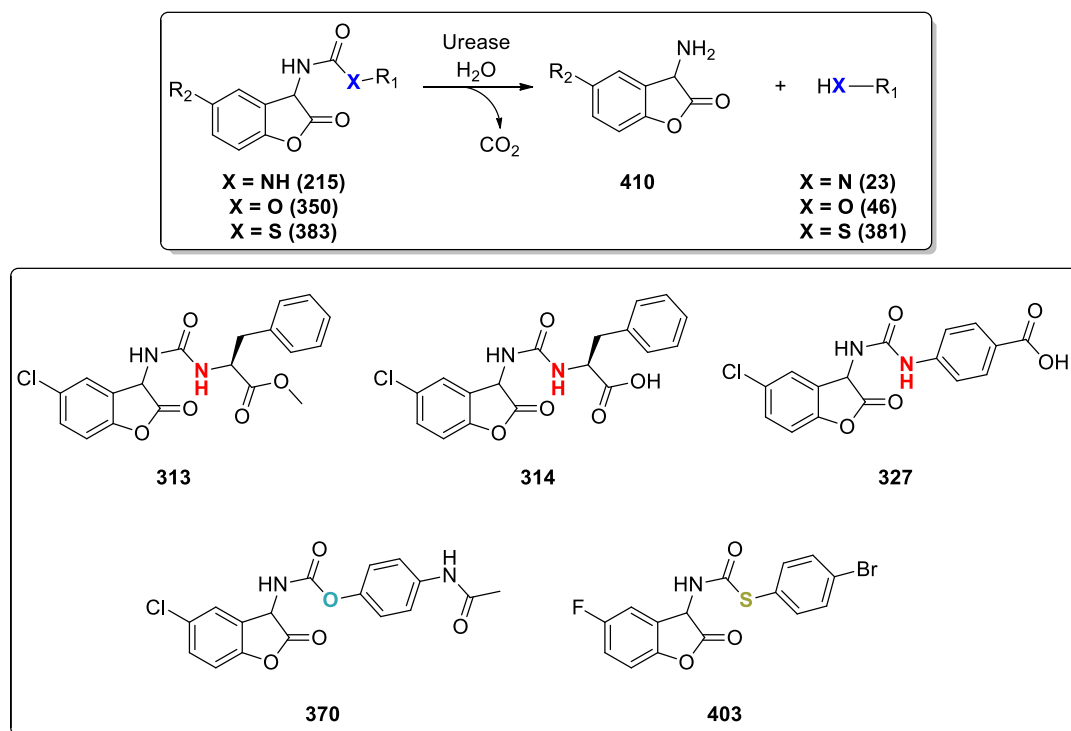


Scheme 76: Reaction equations of the coumaranones which were oxidised with HRP. After aqueous workup of the HRP catalysed reaction of **407** the ^1H -spectrum verified the release of **388** but was also contaminated with starting material and other byproducts.

In the case of the urea-coumaranones **313** and **314** and the carbamate-coumaranone **371**, the hydantoin derivatives **329** and **331** and the decarboxylated species **377** were obtained, while the

oxidation of the testosterone derivative **372** was again unsuccessful. The reactions with the paracetamol (**370**) and the thiol carbamate derivative **403** led to the quantitative release of the corresponding aromatic substrates, while the ^1H -spectrum of the reaction with **407** still showed the presence of starting material and other byproducts after three days.

Besides HRP, further experiments were carried out with urease (Scheme 77). The literature^[292,295] mentions that the decomposition of carbamate-coumaranones with urease was investigated, but no exact procedures or results regarding decomposition and CL were reported. Therefore, a standard protocol similar to the one used with HRP was applied. Here, a modified sodium phosphate buffer (pH = 7.0, 0.75 M) and no EDTA solution were used. Urease was dissolved in 5 ml of the diluted buffer solution (pH = 7.0, 0.02 M) to give a concentration of 200 units/ml. The coumaranone was dissolved in a mixture of MeCN/water (1:1) and stirred for three days after addition of all stock solutions.

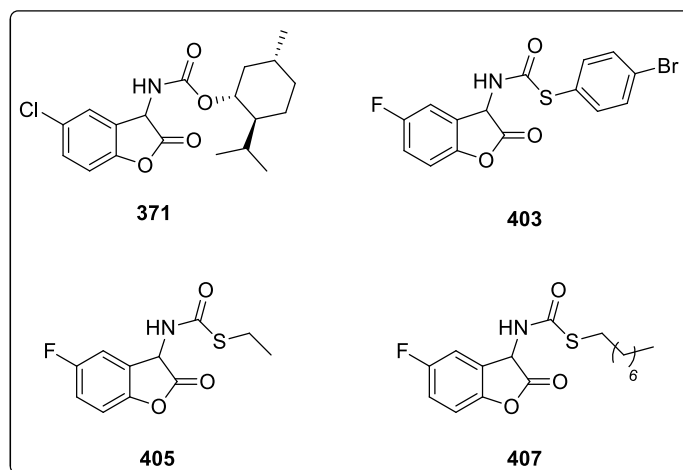


Scheme 77: (Top) Proposed reaction equation the decomposition of coumaranones with urease. (Bottom) Overview of substrates which were used for the urease experiments.

However, each reaction was unsuccessful as only starting material was reisolated after stirring for three days. Therefore, it could not be proven in this work that urease can cleave urea-, carbamate- or thiocarbamate-coumaranones under the above-mentioned conditions or generally induces CL.

4.4.1 CL with HRP

Luminescence experiments with HRP were performed according to a modified protocol of *Matuszczak*^[289]. The reaction was triggered by injecting subsequently the coumaranone stock solution (0.5 ml, 10^{-3} M in MeCN) and H_2O_2 (0.5 ml, 10^{-3} M) to the mixture consisting of phosphate buffer I (0.5 ml, pH = 7.8, 1 M), EDTA (0.5 ml, 10^{-3} M), and HRP working solution (0.5 ml, 49.5 units/ml in 10^{-3} M phosphate buffer). HRP and/or H_2O_2 were omitted from control measurements. As already shown with DBU, urea coumaranones and the paracetamol-derivative (**370**) do not show a long-lasting CL, which in the case of the former is also barely visible. Therefore, only a small selection of coumaranones was chosen whose CL is bright and has a duration that allows it to be followed over several scans (Scheme 78).



Scheme 78: Overview of substrates which were used for the HRP triggered luminescence experiments.

Before each measurement, an emission and excitation scan were performed for the mixture of phosphate buffer, EDTA and HRP solution, which showed no significant absorption or fluorescence. According to the literature, the photophysical properties of HRP are strongly dependent on the oxidation state of its haem group, temperature and pH. HRP emits a weak fluorescence^[309] with a maximum at 338 nm when excited at $\lambda_{\text{Ex}} = 297$ nm at pH = 3.0, which is caused by a tryptophan residue.^[310] A decrease in pH or an increase in temperature leads to higher fluorescence intensities as the protein starts to denature and thus reduces the quenching effect of the neighbouring haem group. The latter shows a strong *Soret*-peak at 403 nm and a second maximum at 500 nm with additional smaller absorption peaks at 540 and 638 nm.^[305] The absorbance values vary when the Fe-centre of the haem group is oxidised, but show no major differences to the spectrum of the native enzyme.^[305,310,311] These results from the literature were taken into account for each luminescence experiment.

The HRP-induced CL of **371** is much weaker compared to the DBU experiment, which showed an intense CL that lasted for 21 minutes (Figure 28a and 38a). The first scan reaches only 1400 counts per second with a maximum at 439 nm. After a sharp decrease after the second scan, the CL decreases more evenly and is barely detectable after 20 scans. The emission and excitation scan revealed a photoluminescence with a maximum at 437 nm (Figure 38b, $\lambda_{\text{Ex}} = 360$ nm) with a corresponding absorption maximum at 356 nm (Figure 38c, $\lambda_{\text{Em}} = 445$ nm), which can be attributed to phenolate **377A**. The shoulder at 320 nm is caused by the *Raman*-band of water.

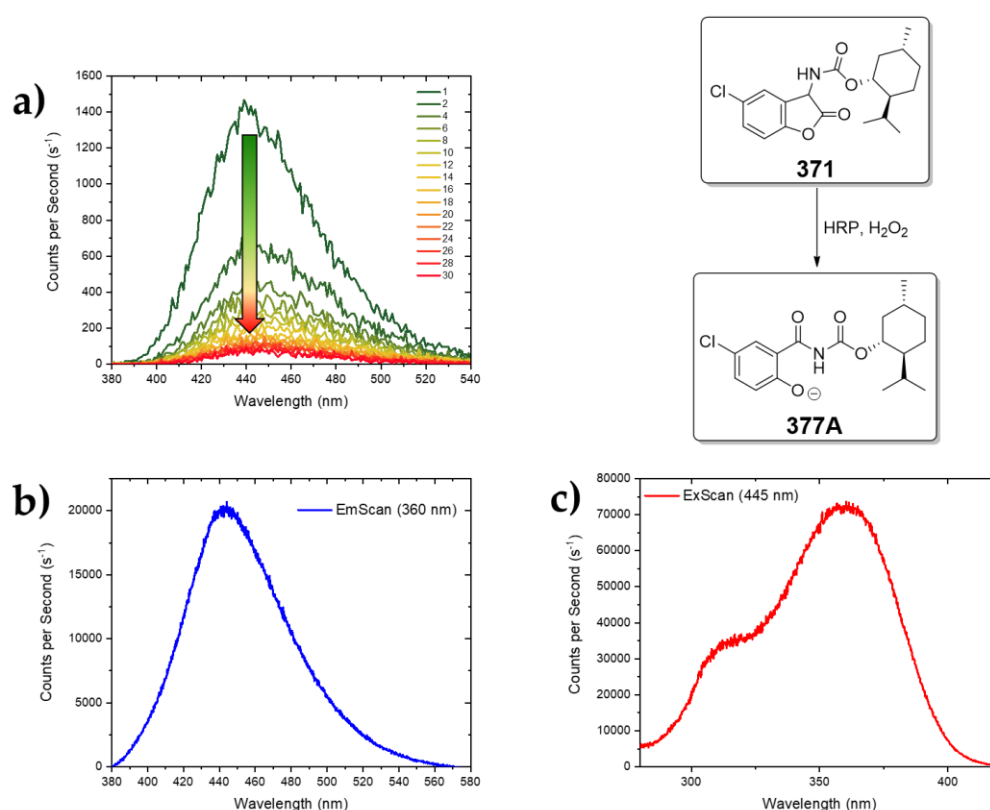


Figure 38: Emission and excitation spectra of **371** with HRP in water/acetonitrile (every scan took 45 s): (a) emission scans of CL (i.e., without external excitation, Slit: 4.0), the arrow indicates the decrease in the CL; (b) emission scan of **371** after CL was finished (external excitation $\lambda_{\text{Ex}} = 360$ nm, Slit: 0.7); (c) excitation scan of **371** after CL was finished ($\lambda_{\text{Em}} = 445$ nm, Slit: 0.7).

Figure 39 presents the luminescence spectra of the decomposition of **403** with HRP. The CL has a maximum at 464 nm and remains overall very weak but decreases in small intervals and reaches 0 counts per second after 20 scans (Figure 39a). After CL was finished excitation of the sample at 360 nm revealed a fluorescent species with an emission maximum at 428 nm (Figure 39b). Excluding the *Raman*-band of water the excitation scan (Figure 39c, $\lambda_{\text{Em}} = 445$ nm) shows an absorption maximum with $\lambda_{\text{max}} = 341$ nm.

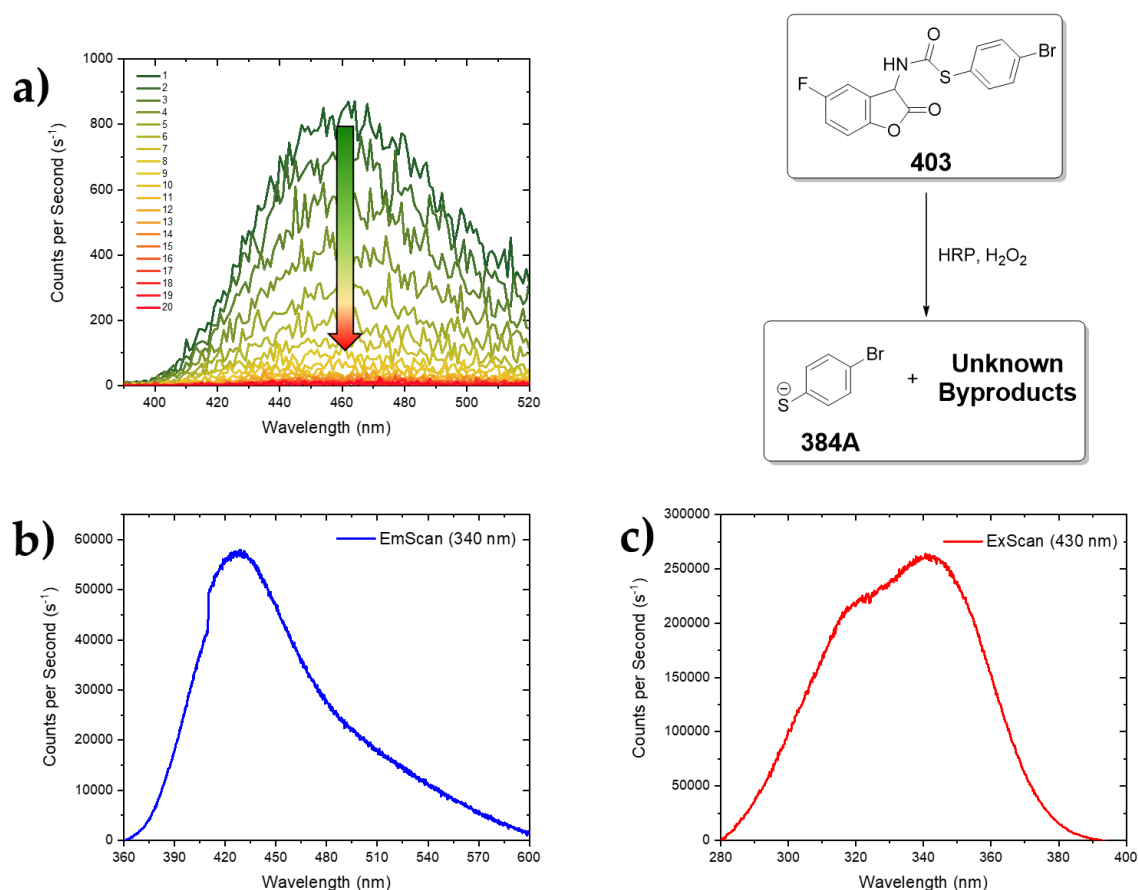


Figure 39: Emission and excitation spectra of **403** with HRP in water/acetonitrile (every scan took 45 s): (a) emission scans of CL (i.e., without external excitation, Slit: 10), the arrow indicates the decrease in the CL; (b) emission scan of **403** after CL was finished (external excitation $\lambda_{\text{Ex}} = 340$ nm, Slit: 1.0); (c) excitation scan of **403** after CL was finished ($\lambda_{\text{Em}} = 430$ nm, Slit: 1.5).

While the DBU-initiated CL of the aliphatic thiol derivatives **405** and **407** was detectable for 27 minutes (Figure 35a) and 4 minutes (Figure 37a), respectively, the HRP-induced CL is much weaker in both cases and fades within a few scans. In the case of **407**, the CL is barely detectable overall. The subsequent emission and excitation scans of both derivatives show similar results with respect to the photophysical properties of the fluorescent byproducts. In both cases, the emission maxima are detected at 424 nm for **405** (Figure 40b, $\lambda_{\text{Ex}} = 310$ nm) and 426 nm for **407** (Figure 41b, $\lambda_{\text{Ex}} = 310$ nm). The excitation scans of **405** and **407** with $\lambda_{\text{Em}} = 420$ nm show a correspondingly strong absorption at 308 nm (Figure 40c) and a sharper but weaker absorption at 307 nm (Figure 41c). This also indicates that HRP has a similar effect to DBU with regard to the oxidation and decomposition process of coumaranones, as the photophysical properties of the fluorescent byproducts were also comparable in the case of the DBU experiments.

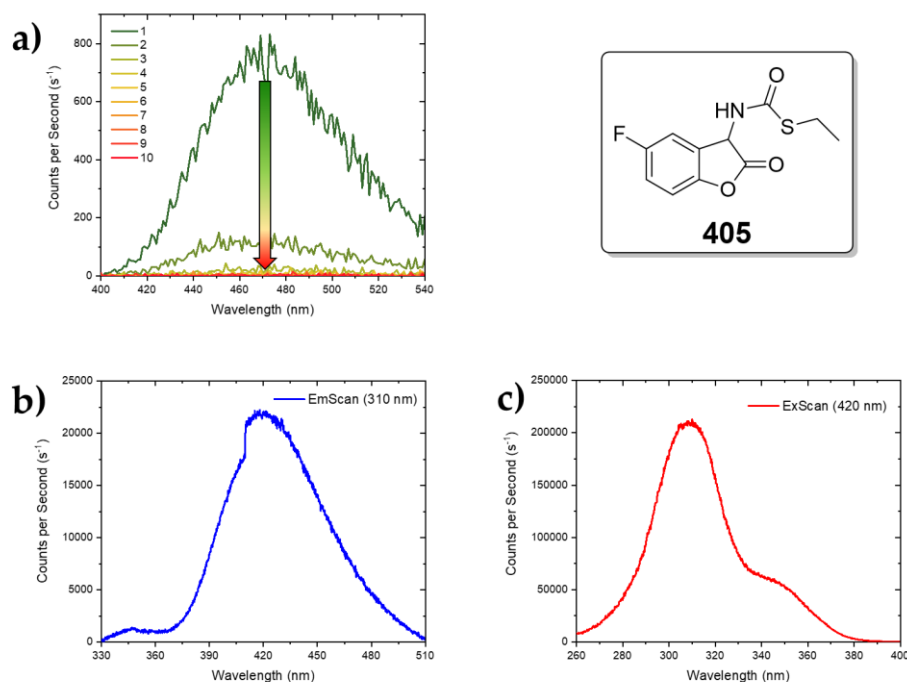


Figure 40: Emission and excitation spectra of **405** with HRP in water/acetonitrile (every scan took 45 s): (a) emission scans of CL (i.e., without external excitation, Slit: 10), the arrow indicates the decrease in the CL; (b) emission scan of **405** after CL was finished (external excitation $\lambda_{\text{Ex}} = 310$ nm, Slit: 1.0); (c) excitation scan of **405** after CL was finished ($\lambda_{\text{Em}} = 420$ nm, Slit: 0.9).

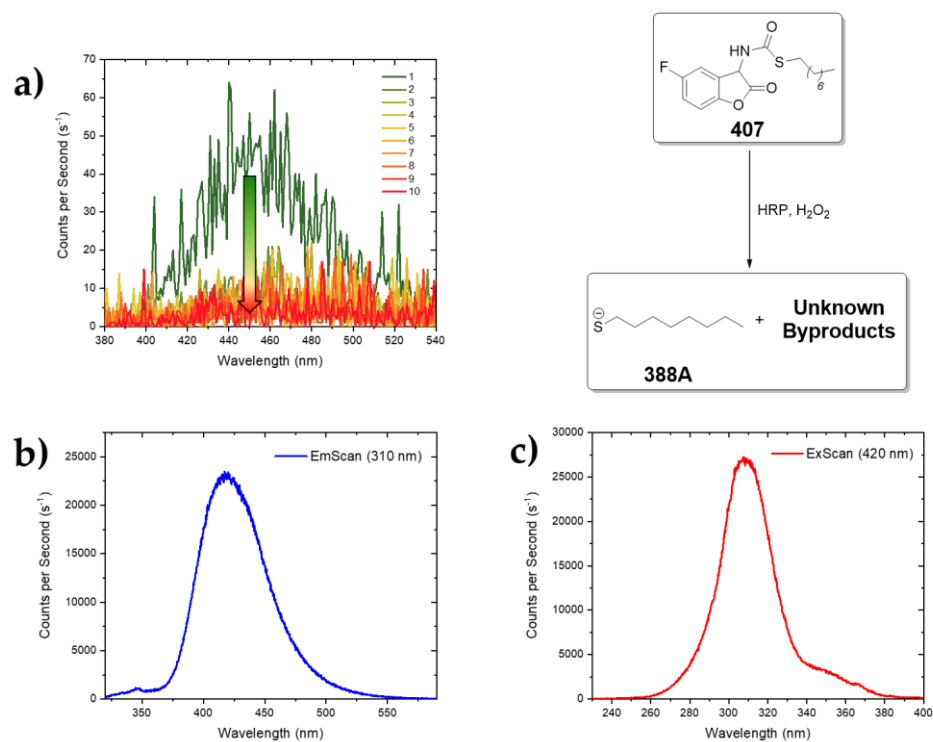


Figure 41: Emission and excitation spectra of **407** with HRP in water/acetonitrile (every scan took 45 s): (a) emission scans of CL (i.e., without external excitation, Slit: 10), the arrow indicates the decrease in the CL; (b) emission scan of **407** after CL was finished (external excitation $\lambda_{\text{Ex}} = 310$ nm, Slit: 1.0); (c) excitation scan of **407** after CL was finished ($\lambda_{\text{Em}} = 420$ nm, Slit: 1.0).

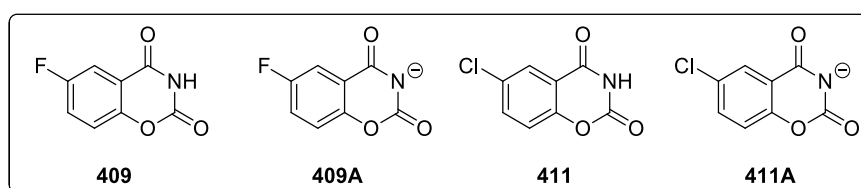
Table 14 compares the results of the luminescence experiments with HRP and DBU. Apart from the different solvents and concentrations of the stock solutions, it can be stated that HRP is not suitable for triggering clearly visible CL, as even substrates with a bright and long-lasting CL (when initiated by DBU) were hardly detectable. Although the photophysical properties of the fluorescent species produced are not directly comparable due to the different solvents, they further demonstrate the similarities between oxidation with DBU and HRP, particularly in the case of the oxidation of **405** and **407** which, similar to the DBU experiments, show comparable absorbance and emission values for their fluorescent byproducts.

Table 14: Summary of the results of the HRP-induced CL reactions of selected coumaranones. The absorption and fluorescence maxima refer to the oxidised byproducts of the respective coumaranone. The DBU experiments were recorded in MeCN with stock solutions having a concentration of 10^{-2} mol/l; HRP experiments in a mixture of water and MeCN with stock solutions having a concentration of 10^{-3} mol/l

Entry	Trigger via	CL λ_{\max} [nm]	Absorption λ_{\max} [nm]	Fluorescence λ_{\max} [nm]
371	DBU	426/440	415	463
371	HRP	439	356	437
403	DBU	435/453	411	468
403	HRP	464	341	428
405	DBU	443	387	443
405	HRP	469	308	424
407	DBU	446	407	452
407	HRP	440	307	426

4.5 Theoretical calculations on the photophysical properties of 409A

Compound **409A** could be unambiguously detected after the decomposition of coumaranone **407** as the terminal product of the CL mechanism. [292–295] This compound could thus represent the fluorescent species of this reaction. The fluorescent species produced after the oxidation of other thiolcarbamate- and carbamate-coumaranones gave different results. Despite *Schramm's* [295] findings that this compound does not represent an emitter, additional theoretical calculations were performed by *M.Sc. Robert Herzhoff* for two different derivatives in their protonated and deprotonated states to obtain comparable values (Scheme 79).



Scheme 79: Benzoxazinedione derivatives in their protonated and deprotonated states, which were used for theoretical calculations.

The applied calculation method first starts with a geometry optimisation in the ground state in order to obtain a suitable input structure for the subsequently performed geometry optimisation in the excited state. To obtain $E_{ex}(r_{ex})$, a one-point calculation was performed in the excited state with the equilibrium geometry of the excited state and the equilibrium solution. For $E_{gs}(r_{ex})$, a one-point calculation was performed in the ground state with the equilibrium geometry of the excited state and the equilibrium solution of the excited state. This procedure takes into account that the light emission is so fast that the molecules themselves and the surrounding solvation molecules do not have time to geometrically adapt to the different electronic state, which is consistent with the Franck-Condon principle. All calculations were performed using *Gaussian 16* [312] and the B3LYP [313] functional together with the 6-31+G(d,p) basis set. [314] Input structures were sketched using Avogadro. [315] The PCM (polarisable continuum model) method was used for the solvents. [316] For each substrate, the absorption ($S_0 \rightarrow S_1$) and emission ($S_1 \rightarrow S_0$) including the oscillator strength in acetonitrile, DMF, DMSO and water were calculated. Table 15 summarises the results of the calculation for all four compounds. Interestingly, both the $S_0 \rightarrow S_1$ and $S_1 \rightarrow S_0$ transitions are forbidden for the two deprotonated species **409A** and **411A**, since the oscillator strength is equal to 0, so that both species can be excluded as potential emitters. On the other hand, the absorption and emission processes of **409** and **411** are allowed but have a low probability.

Table 15: Obtained values of the theoretical calculations of the absorption, emission and oscillator strength of **409**, **409A**, **410** and **410A** in acetonitrile, DMF, DMSO and water. The values in bold indicate that the absorption and emission processes are allowed. The absorption and emission values are compared to the obtained maxima after the CL reaction of **407**.

Entry	Solvent	Absorption ($S_0 \rightarrow S_1$) in [nm] and [eV]	Emission ($S_1 \rightarrow S_0$) in [nm] and [eV]	Oscillator Strength of ($S_0 \rightarrow S_1$) and ($S_1 \rightarrow S_0$)
409	MeCN	286.205895 / 4.33193	345.533871 / 3.58814	0.0578 / 0.1494
	DMF	286.941808 / 4.32082	345.21926 / 3.59141	0.0577 / 0.1496
	DMSO	286.864794 / 4.32198	345.675488 / 3.58667	0.0577 / 0.1507
	Water	286.196646 / 4.33207	346.701091 / 3.57606	0.0577 / 0.1525
409A	MeCN	267.317498 / 4.63802	399.66343 / 3.10217	0.0000 / 0.0001
	DMF	269.350101 / 4.60302	402.087227 / 3.08347	0.0000 / 0.0001
	DMSO	268.405467 / 4.61922	399.417509 / 3.10408	0.0000 / 0.0001
	Water	265.388036 / 4.67174	400.716189 / 3.09402	0.0000 / 0.0001
411	MeCN	294.477502 / 4.21025	366.186688 / 3.38451	0.0425 / 0.1186
	DMF	295.813149 / 4.19124	365.570165 / 3.39148	0.0425 / 0.1188
	DMSO	295.617775 / 4.19401	366.323014 / 3.38451	0.0425 / 0.1197
	Water	294.318118 / 4.21253	368.101249 / 3.36816	0.0425 / 0.1213
411A	MeCN	266.928445 / 4.64478	399.673737 / 3.10209	0.0000 / 0.0001
	DMF	268.895032 / 4.61081	397.272498 / 3.12084	0.0000 / 0.0001
	DMSO	267.964006 / 4.62683	397.096906 / 3.12222	0.0000 / 0.0001
	Water	265.014771 / 4.67832	398.113158 / 3.11425	0.0000 / 0.0001
Entry	Solvent	Absorption λ_{max} [nm]	Fluorescence λ_{max} [nm]	
407	MeCN	407	452	

Direct comparison of the theoretical absorption and emission values of **409** and **411** with the experimental data after decomposition of the thiolcarbamate-coumaranones **407** show no agreement. Additional calculations were performed for the oscillator strength of the absorption for the first 10 excited states (Table 16). It is noteworthy that the oscillator strength of the $S_0 \rightarrow S_6$ transition of **409** represents the most probable process ranging between 0.411 and 0.415 while the $S_0 \rightarrow S_4$ transition of **411** has even higher values with 0.697 – 0.705. This suggests that the substitution of the halide has a major influence on the overall photophysical properties. In contrast, the $GS \rightarrow S_2$ and S_3 transitions are most likely for the two deprotonated species **409A** and **411A**, but have significantly lower values for the oscillator strength. However, this suggests that the deprotonated species can also be excited and can therefore be regarded as potential emitters. These further findings on the photophysical properties of all four compounds indicate, that the protonated compounds are capable of effective absorption and fluorescence, while it is also possible to excite the deprotonated species to higher excited states $> S_1$. The emission from a higher excited state however is not reasonable as the $GS \rightarrow S_1$ absorption of all four compounds is already in the UV range. Moreover, it can be assumed that the concentration of the protonated species can

only be very low due to the generally low pK_s -values of phthalimides and the fact that the decomposition takes place in an alkaline environment with either 2 or 50 equivalents of DBU. Thus, it would be possible that species **409A** and **411A** can react further via several pathways (nucleophilic attack, redox reactions), producing different fluorescent species via several pathways depending on the potential nucleofuge, or that several fragmentation reactions take place and are responsible for the formation of different fluorescent species. Thus, it could be additionally confirmed by the theoretical calculations that benzoxazinediones can be excluded as possible fluorescent species.

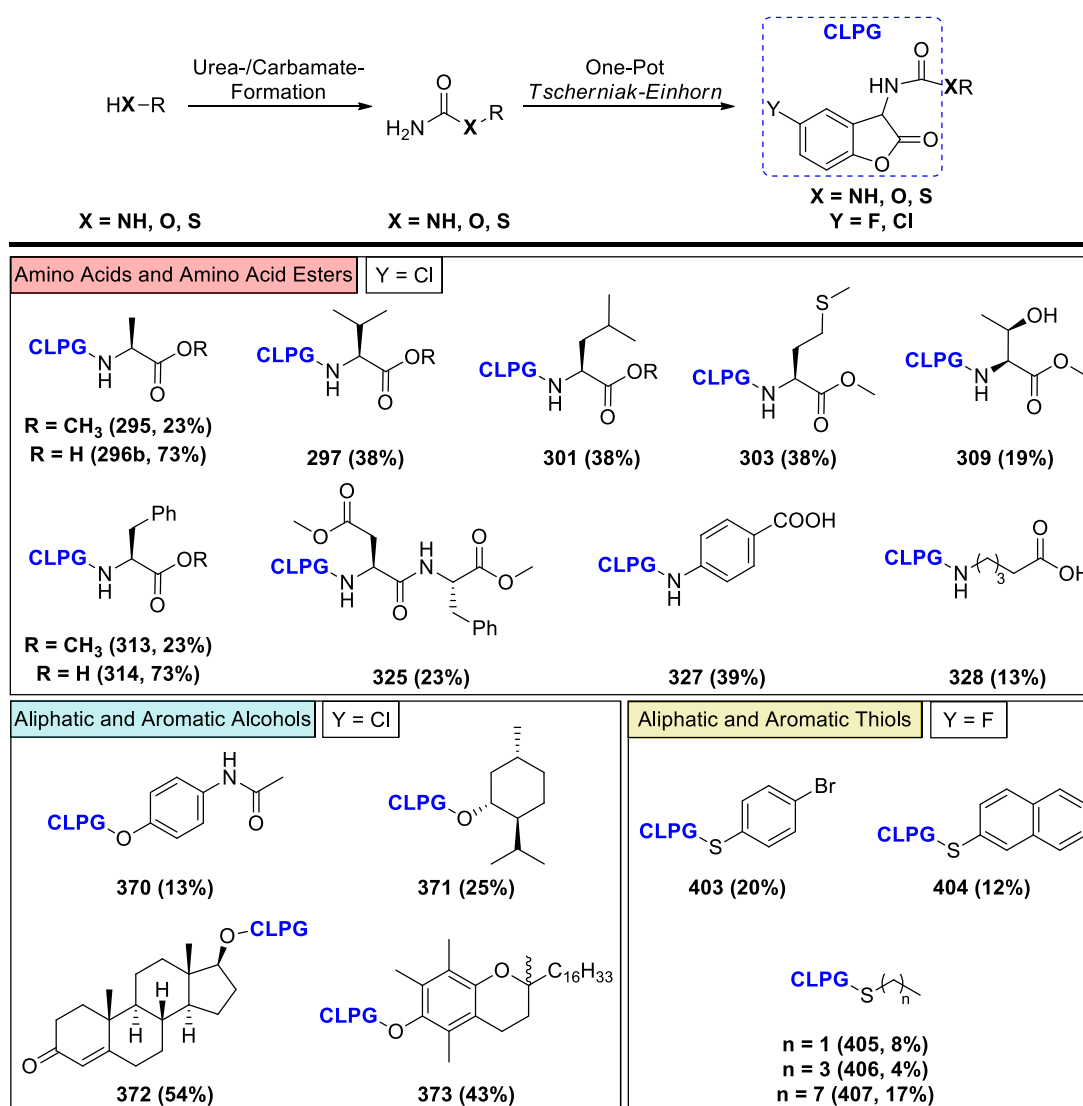
Table 16: Obtained values of the theoretical calculations for the oscillator strength of the absorption for the first ten excited states of **409**, **409A**, **410** and **410A** in acetonitrile, DMF, DMSO and water. The values in bold indicate the most probable transitions of **409** and **410** ($GS \rightarrow S_x$).

Excited State	409				409A			
	DMF	MeCN	DMSO	Water	DMF	MeCN	DMSO	Water
S ₁	0.0577	0.0578	0.0577	0.0577	0	0	0	0
S ₂	0.0001	0.0001	0.0001	0.0001	0.0745	0.0756	0.0749	0.0759
S ₃	0.0814	0.0805	0.0815	0.0809	0.0688	0.0692	0.0689	0.0698
S ₄	0.0769	0.0719	0.0774	0.0742	0.0004	0.0004	0.0004	0.0004
S ₅	0	0	0	0	0	0	0	0
S ₆	0.1468	0.1515	0.1473	0.1521	0.0003	0.0005	0.0003	0.022
S ₇	0.4132	0.4148	0.4118	0.4105	0.0158	0.0194	0.0176	0.0004
S ₈	0	0	0	0	0.0042	0.0019	0.0031	0.0011
S ₉	0.0004	0.0004	0.0004	0.0004	0	0	0	0
S ₁₀	0.1547	0.1546	0.1552	0.1559	0.0001	0.0001	0.0001	0.0001

Excited State	411				411A			
	DMF	MeCN	DMSO	Water	DMF	MeCN	DMSO	Water
S ₁	0.0425	0.0425	0.0425	0.0425	0	0	0	0
S ₂	0.0001	0.0001	0.0001	0.0001	0.0604	0.0605	0.0603	0.0603
S ₃	0.0258	0.0255	0.0259	0.0259	0.0564	0.0572	0.0567	0.058
S ₄	0.7046	0.6982	0.7036	0.6971	0.0003	0.0003	0.0003	0.0004
S ₅	0.0002	0.0051	0.0002	0.0045	0.0003	0.0003	0.0003	0.0003
S ₆	0.0027	0.0002	0.0027	0.0002	0.0041	0.0057	0.0045	0.0077
S ₇	0.096	0.1062	0.0974	0.1072	0	0	0	0.0098
S ₈	0	0	0	0	0.0131	0.0118	0.0127	0
S ₉	0	0	0	0	0	0	0	0
S ₁₀	0.0253	0.0233	0.025	0.0232	0.0002	0.0002	0.0002	0.0002

5. Summary and outlook

The original intention of this Thesis was the investigation of 2-coumaranones for the release of biologically relevant compounds in order to optimise therapies that require drugs which cause significant side effects. Hence, the 2-coumaranone was to be bound to nanoparticles to enable efficient transport through body tissue. In addition, the light of the CL reaction could have been used by means of damaging the growth of malignant cells (for example in the case of cancer). In this work, the concept of CLPGs with 2-coumaranones as a potential PG for the protection and deprotection of amines (especially proteinogenic amino acids), alcohols (including pharmaceutically relevant compounds) and simple aromatic and aliphatic thiols, whose coumaranone derivatives were synthesised for the first time, was investigated (Scheme 80).



Scheme 80: (Top) Standard synthesis procedure for the protection of amines, alcohols and thiols with coumaranones. (Bottom) Overview of selected compounds for each substrate class with the respective yields.

For substrate protection a two-step process has been established. First, the respective amine, alcohol and thiol was converted to the corresponding urea-, carbamate- or thiocarbamate derivative using potassium cyanate or CSI as electrophilic agent. Subsequently, a one-pot *Tscherniak-Einhorn* reaction was carried out to give the desired coumaranone. A total of 32 coumaranones were synthesised unknown to the literature. In order to trace the duration and efficiency of the release of the protected substrates, the decomposition of the CLPG was triggered by DBU and analysed via NMR (Figure 42a). The duration of CL (Figure 42b) as well as fluorescent species after the oxidation have been investigated via emission and excitation spectra (Figure 42c and d).

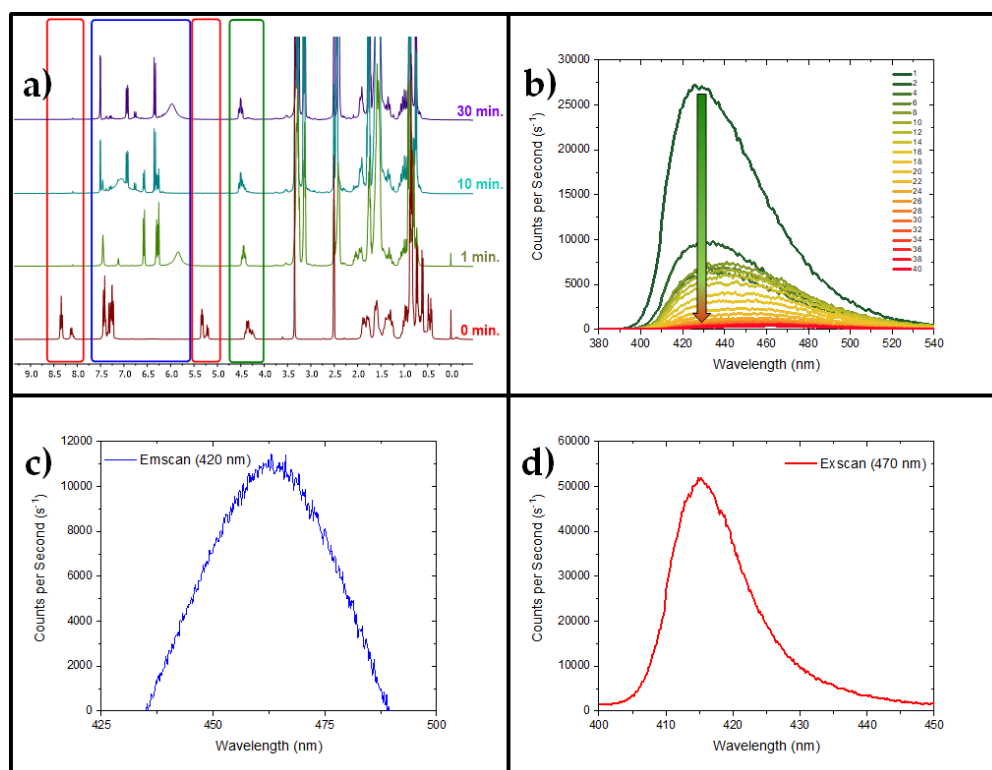
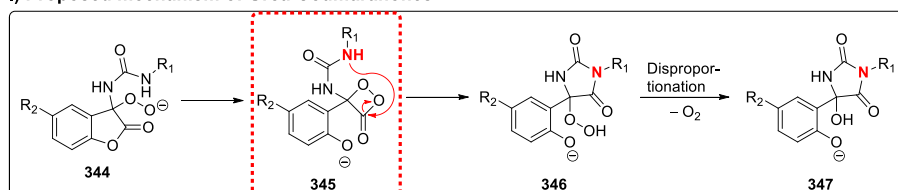


Figure 42: Selected examples of a time-dependent NMR (a), CL (b), emission (c) and excitation (d) spectrum. The spectra belong to the measurements of the CLPG protected L-menthol (**371**).

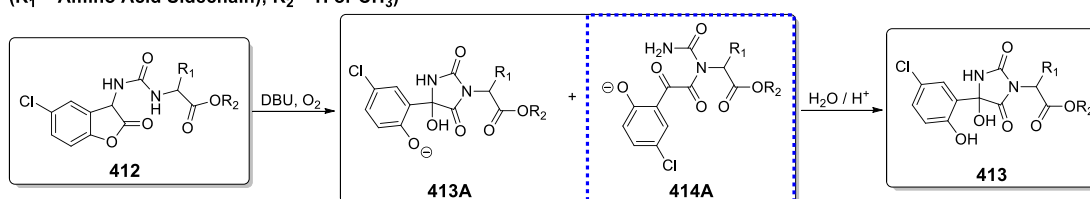
Overall, the results show that the CLPG concept strongly depends on the charge stabilisation of the potential nucleofuge and the heteroatom attached to the amide side chain of the benzofuranone. None of the urea-coumaranones released the corresponding amino acids due to the low leaving group potential. The very weak and flash-like CL can be explained by the preference of a nucleophilic attack of the urea moiety on the critical 1,2-dioxetanone intermediate **345** (Scheme 81, I). This leads to the formation of a hydantoin **413A** or an open-chain carboxylate species **414A**, with both structures having a certain equilibrium depending on the derivative (Scheme 81, II). Luminescence experiments additionally indicated that the

analysed urea-coumaranones generated a similar fluorescent species due to the comparable absorption and emission values. This is assumed to be caused by the open-chain derivative (Scheme 81, blue dashed box). Amino acid esters show a time-delayed photoluminescence compared to their unprotected counterparts, which reveal fluorescence immediately after the addition of DBU. Thus, the protection of the carboxylic acid, but also the side chain of the amino acids, clearly influences the equilibrium for the formation of the fluorescent species. However, when acidifying, the equilibrium was always completely shifted towards the hydantoin structure **413** which could also be extracted being stable at room temperature. A different result was obtained after hydrolysis of the oxidised urea-coumaranone derivative **327**. Instead of the expected hydantoin, the urea-protected PABA compound (**287**) was obtained as the main product and completely deprotected PABA (**263**) as a byproduct (Scheme 81, III). In view of the fact that the amine group is directly bound to an aromatic ring, this seems to allow further decomposition in slightly acidic aqueous media, which is due to better stabilisation of the charges.

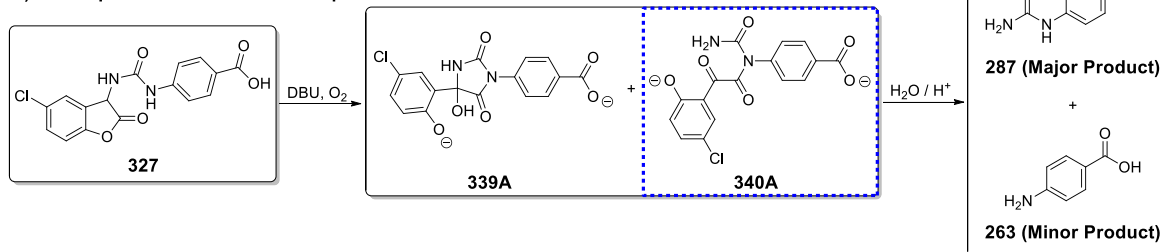
I) Proposed mechanism of Urea-Coumaranones



II) General decomposition of Coumaranone-protected Amino Acids (R_1 = Amino Acid Sidechain; R_2 = H or CH_3)

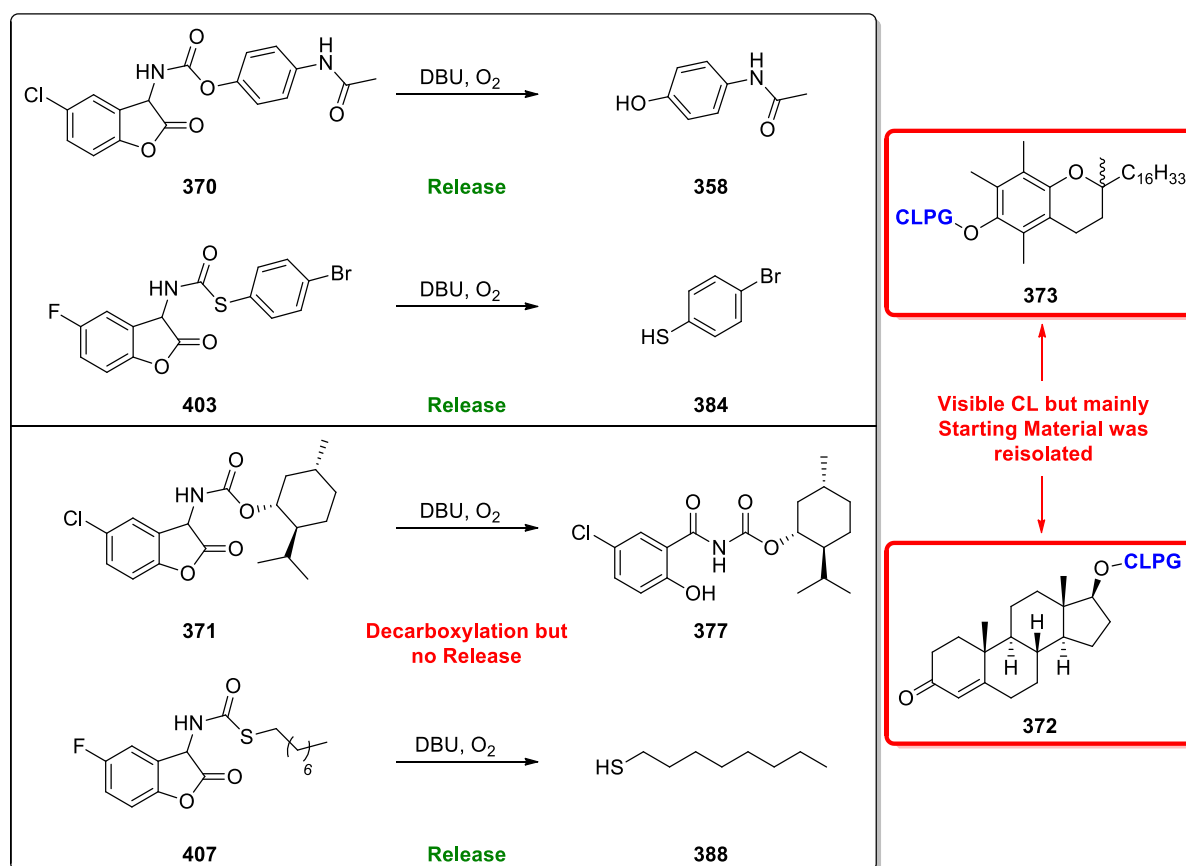


III) Decomposition of Coumaranone-protected PABA



Scheme 81: I) Proposal for the general mechanism of urea-coumaranones. The assumed nucleophilic attack of the urea-group on the dioxetanone moiety is highlighted in a red dashed box. II) General decomposition of coumaranone-protected amino acids and esters. Compound **414A** (blue dashed box) represents the assumed fluorescent species, which could be detected after the oxidation process of the coumaranone. III) Decomposition of coumaranone-protected PABA (**327**). Similar to the other investigated urea-coumaranones the hydantoin **339A** and open-chain derivative **340A** could be determined in an alkaline solution. After acidic workup urea-protected PABA (**287**) and fully deprotected PABA (**263**) were obtained.

Based on these results, urea-coumaranones can be considered as fluorescent protecting groups (FPGs) instead of CLPGs. The proposed reaction mechanism does not lead to the release of the amino acids and the identified products show a strong and visible photoluminescence in the alkaline solution. While aromatic alcohols and thiols are released quickly, which is also accompanied by a shorter CL duration due to the rapid decomposition, aliphatic derivatives are completely cleaved from the PG only in the case of thiols (Scheme 82).

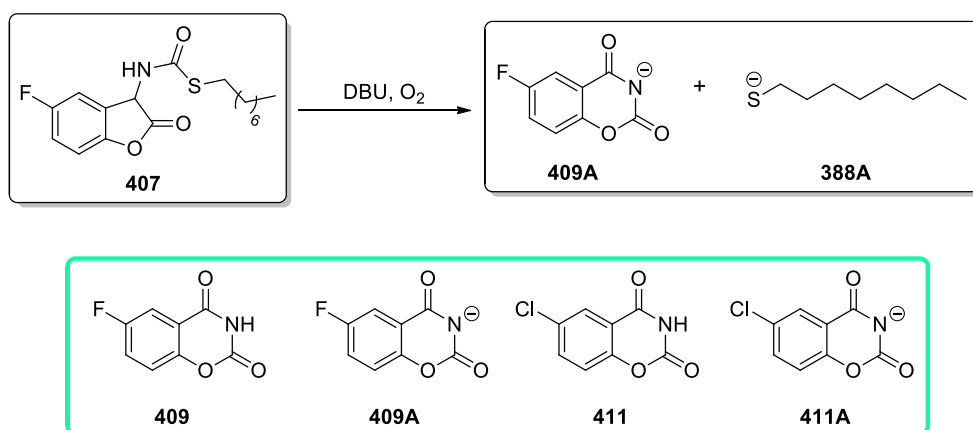


Scheme 82: Coumaranone oxidation by oxygen in an alkaline solution with DBU. (Upper Half) While the release of aromatic alcohols and thiols was successful, larger molecules such as protected α -tocopherol (**373**) could not be cleaved from its CLPG. (Bottom Half) Aliphatic thiols (in e.g., **388**) are quantitatively released from the 2-coumaranone PG while the deprotection L-menthol yielded compound **377** instead. Similar to **373** the CLPG-protected testosterone (**372**) remained intact and could not be deprotected efficiently.

As shown with the coumaranone-protected L-menthol **371**, only the decarboxylated derivative **377** could be obtained, which is also the emitting species of the CL reaction of coumaranones. Therefore, the long and bright CL of this specific derivative can be explained by the accumulation of this fluorophore. Performing an additional decarboxylation of **377** with KOH allowed the complete removal of the PG in a two-step process, which, however, takes place under very harsh conditions. Although a briefly visible CL was observed after the addition of DBU to the testosterone (**372**) and α -tocopherol (**373**) coumaranones, suggesting that a

decarboxylation reaction must have occurred, the NMR spectra showed that much of the starting material was not oxidised and deprotection was unsuccessful. This could be explained by the steric requirements of the coumaranones themselves. The size of DBU seems to be of less importance considering that decarboxylation/oxidation of **372** with KOH in boiling ethanol also failed to release testosterone. In addition to the different results between the release of alcohols and thiols, each coumaranone derivative had a clearly visible CL, whose duration correlated with the progress of the reaction.

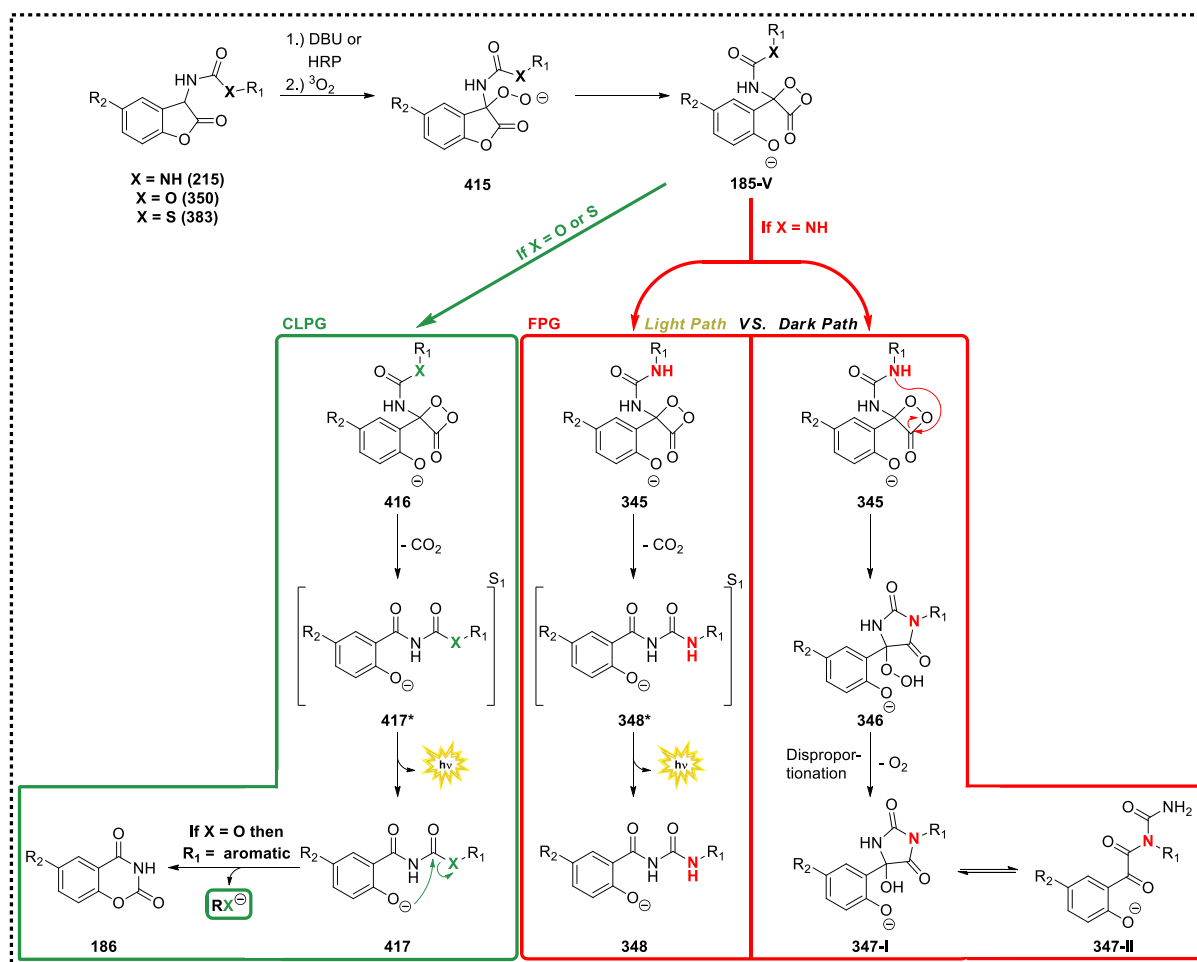
Besides DBU, the enzymatically triggered degradation of coumaranones with HRP and urease was also investigated. While the reactions with urease were all unsuccessful, the products obtained after the reactions with HRP are in agreement with the degradation reactions with DBU. However, the CL intensity is drastically reduced and could not be observed even for substrates with very bright emissions. Instead, the reaction progress could be traced by the colour change of the solution. Based on the luminescence spectra, HRP could be a useful tool for fluorescence immunoassays, especially with regard to coumaranone-protected amino acids. Since a benzoxazinedione derivative is the generally expected end product after the release of the protected substrate and could also be elucidated in the reaction of thiolcarbamate-coumaranone **407**, it was assumed to be the fluorescent species of this reaction (Scheme 83).^[294]



Scheme 83: (Top) Decomposition of coumaranone **407** with oxygen and DBU. The release of **388A** and the byproduct of the benzoxazinedione **409A** could be verified by NMR as (Bottom) Benzoxazinedione derivatives in their protonated and deprotonated states, which were used for theoretical calculations.

Although *Schramm*^[295] already ruled out the possibility that this compound was a potential emitter, additional theoretical calculations on the photophysical properties of this compound were carried out by *M.Sc. Robert Herzhoff*. The values obtained showed that benzoxazinedione (Scheme 83, in e.g. **409** and **411**) should be protonated in order to exhibit efficient fluorescence. Furthermore, the calculated wavelengths of the absorption and

emission maxima for the $GS \rightarrow S_1$ and $S_1 \rightarrow GS$ transitions do not match those of the fluorescent species detected after the oxidation of thiolcarbamate-coumaranone **407**. Therefore, either a further decomposition of **409A** or different fragmentation reactions occur that deviate from the general mechanism in the literature and thus could explain the formation of different fluorescent species.



Scheme 84: Mechanistic comparison of urea-, carbamate- and thiolcarbamate-coumaranones.

In summary, 2-coumaranones represent a potential substance group as CLPGs for phenolic compounds and aromatic as well as aliphatic thiols, since both requirements, namely I) a bright CL in the visible range ending with the completion of deprotection and II) no interfering absorption or fluorescence properties until the start of deprotection, are fulfilled (Scheme 84). The PG itself can be cleaved in alkaline solutions with non-nucleophilic bases, but also enzymatically with HRP, although in the latter case the CL is not very intense or not visible at all. In addition, the phenolate formed during decarboxylation requires stabilised leaving groups that must not have too high steric requirements, which makes it a selective nucleophilic group. With regard to urea-coumaranones the suggested equilibrium between the hydantoin **347-I** and open-chain structure **347-II** was determined. The latter presumably

enables a strong and visible photoluminescence, which can also be delayed in time with certain structural features of the substrate. We have termed this remarkable property FPG, which could be a potential tool for the visualisation of biologically relevant amine compounds and imaging for medical applications.

„One sometimes finds what one is not looking for.”

Sir Alexander Fleming, 1881 - 1955.

6. Experimental section

6.1 General experimental requirements

6.1.1 Analysing methods

Nuclear magnetic resonance (NMR) spectroscopy

^1H - and ^{13}C -NMR spectra were recorded at 300, 500 or 600 MHz and 75, 125 or 150 MHz respectively. The measurements were performed on a *Bruker Avance II+ 600*, *Bruker Avance III 500*, *Bruker Avance III 499* and on a *Bruker Avance II 300*. The chemical shifts δ are reported in ppm downfield of the internal standard of TMS [δ (^1H -NMR) = 0.00 ppm, δ (^{13}C -NMR) = 0.00 ppm].

CDCl_3 [δ (^1H -NMR) = 7.24 ppm, δ (^{13}C -NMR) = 77.2 ppm], DMSO-d_6 [δ (^1H -NMR) = 2.50 ppm, δ (^{13}C -NMR) = 39.5 ppm] and MeOD-d_3 [δ (^1H -NMR) = 3.31 ppm, δ (^{13}C -NMR) = 49.0 ppm] were used as solvents. H,H couplings are represented with *J* (italic) and given in Hz, while H,C interactions in the HMBC spectrum are described with *J* (not italic). The fine structure is designated using the following abbreviations: s (singlet), d (doublet), t (triplet), q (quartet), quin (quintet), sxt (sextet), br (broad), ψ (pseudo) and m (multiplet).

The spectra were evaluated using *MestReNova*. The atom numbering illustrated in the figures does not correspond to the rules of IUPAC. Besides the one-dimensional ^1H -NMR and ^{13}C -APT-experiments, 2D-spectra (H,C-HMBC, H,C-HSQC, H,H-COSY, H,H-NOESY) were additionally measured for a suitable structure determination. All relevant data for each compound is summarised in a clear spread sheet. COSY and NOESY interactions of each molecule are represented by respective arrows.

Luminescence spectroscopy

The chemiluminescence spectra were measured using a FLS980 Photoluminescence Spectrometer (*Edinburgh Instruments*) with a photomultiplier tube-detector and a xenon lamp. Quartz cells with a diameter of 1 cm were used for the measurements. Every stock solution was prepared with a concentration of 10^{-2} mol/l in acetonitrile or DMF.

For enzyme experiments with horse radish peroxidase the following stock solutions were prepared:^[289]

Phosphate buffer I (pH 7.8, 1 M): 6.8 g KH_2PO_4 were dissolved in water, 8 M NaOH was added until pH 7.8, solution was filled up 50 ml.

Phosphate buffer II (pH 7.8, 10^{-3} M): dilution of 0.05 ml phosphate buffer I and water to a final volume of 50 ml.

EDTA solution (pH 7.0, 10^{-3} M): 18.6 mg of EDTA disodium salt dihydrate were dissolved in water, 1 M NaOH was added until pH 7.0, solution was filled up 50 ml.

HRP solution (1100 units/mg): 2.27 mg of horseradish peroxidase were dissolved in 50 ml of phosphate buffer II with a final concentration of 0.045 mg/ml \Rightarrow 49.9 units/ml.

H₂O₂-solution (10^{-3} M): 5.2 μ l of a 30% (w/v) H₂O₂-solution were diluted with water with a final volume of 50 ml.

Decomposition was triggered by injecting subsequently the benzofuranone stock solution (0.5 ml, 10^{-3} M) and H₂O₂ (0.5 ml, 10^{-3} M) to the mixture consisting of phosphate buffer I (0.5 ml, 1 M), EDTA (0.5 ml, 10^{-3} M) and the HRP working solution (0.5 ml, 0.045 mg/ml, 49.5 units/ml). For control measurements HRP and H₂O₂ were omitted.

Melting points

Melting points of solid compounds were determined with a MP50 Melting Point System (*Mettler Toledo*). The given temperatures refer to the moment, where the sample begins to melt.

Infrared-spectroscopy (IR)

Infrared-spectra were measured using a Nicolet 380 FT-IR, a Nicolet iS20 FTIR (*Thermo Fischer Scientific*) and a UATR Two Instrument (*Perkin Elmer*). The wave numbers are categorised from 4000 to 800 cm^{-1} . The signals are listed with the following abbreviations: w (weak), m (medium), s (strong), vs (very strong) and br (broad).

Mass spectrometry and high-resolution mass spectrometry (HR-MS)

High resolution mass spectra were measured with a MAT 900 S (*Finnigan*) and with a LTQ Orbitrap XL (*Thermo Fischer Scientific*) via electron spray ionisation (ESI).

X-Ray structure analysis

Crystal structure analyses were performed on a *Nonius KappaCCD*-Circle diffractometer. The structure was resolved using *SHELXS-97* and *SHELXL-97*.

Column chromatography

Flash chromatography was performed on silica gel (*Macherey-Nagel* Kieselgel 60 Å, particle size 0.035-0.070 mm). The silica gel was equilibrated with the corresponding mixture of different solvents and concentrated with compressed air. The diameter and height of the glass tube were adjusted for the actual load. The rates of the solvents are represented in volume fractions.

Thin layer chromatography (TLC)

Analytical thin layer chromatography (TLC) was performed on *Macherey-Nagel* ALUGRAM® Xtra SIL G/UV₂₅₄ plates. Different solvent mixtures with varying ratios were used to determine the R_f -values. The mixtures itself are represented in volume fractions. The separated substances were visualised via irradiation with a UV-lamp (254 nm and 366 nm).

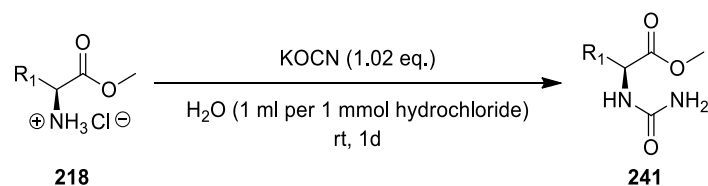
Chemicals and solvents

The applied reagents and solvents were purchased from commercial sources (*Alfa Aesar*, *Fischer Scientific*, *Carbolution*, *Arcos Organics* and *TCI*). The degree of purity of the compounds amounted to at least 95% and were used without any further treatment. DCM was refluxed over calcium hydride and THF over sodium and benzophenone, as an indicator, under argon atmosphere and freshly distilled prior to use.

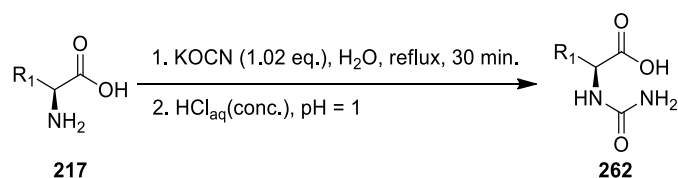
Removal of solvents

Large amounts of solvents were constrained under reduced pressure with a rotary evaporator (*Heidolph*, *VWR*) and a water bath temperature of 40 °C. Solvent residues were removed in an oil pump vacuum.

6.2 General procedures

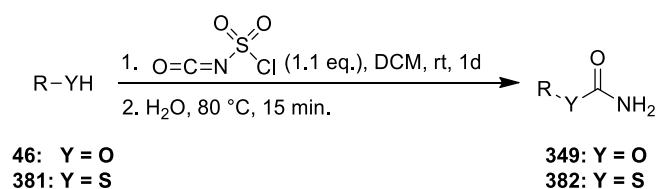


Synthesis of ureido carboxylic acid methyl esters (GP-I): The synthesis protocol of *I. Nicolas et al.*^[297] was followed with minor adaptations. The amino acid methyl ester hydrochloride (1.00 eq.) was dissolved in water (1 ml per 1 mmol amino acid methyl ester hydrochloride) and KOCN (1.02 eq.) was added. The solution was stirred for one day at room temperature. If the product precipitated it was filtered off, washed with water and dried in vacuum over night over P₂O₅ in a desiccator. If no precipitation occurred the solution was extracted three times with EtOAc (1.5 times the volume of the aqueous phase). In the case of very polar substrates, the aqueous phase was additionally saturated with sodium chloride. The combined organic phases were dried over Na₂SO₄, filtered off and the solvent was removed at reduced pressure.

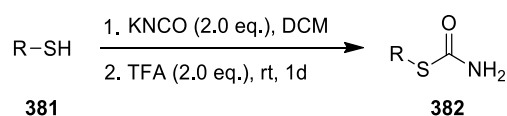


Synthesis of ureido carboxylic acids (GP-IIa): The synthesis protocol of *A. N. Kravchenko et al.*^[299] was followed with minor adaptations. The amino acid (1.00 eq.) and KOCN (1.02 eq.) were suspended in H₂O (5-6 ml per 1 g amino acid) and refluxed for 30 minutes. The reaction solution was acidified with HCl (conc.) to pH 1 and the resulting precipitate was filtered off, washed with H₂O and dried overnight in vacuo over P₂O₅ in a desiccator.

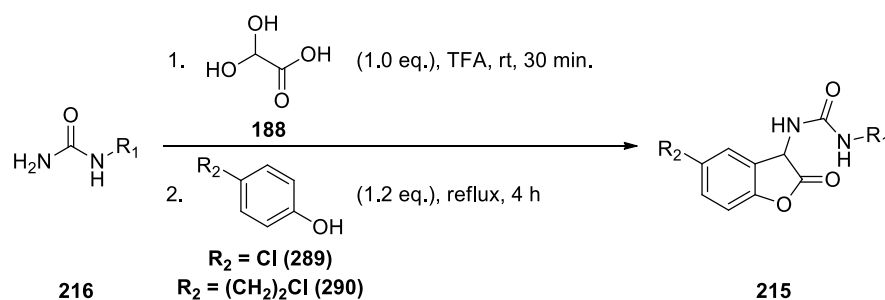
Special procedure for polar amino acids (GP-IIb): To a solution of amino acid (1.00 eq.) in EtOH (50 mL per 1 g amino acid), KOCN (1.02 eq.) was added. The solution was refluxed for 4 h. Afterwards, the reaction mixture was cooled down and the solvent was removed under reduced pressure. The product was washed with cold MeOH and dried in vacuum over P₂O₅.



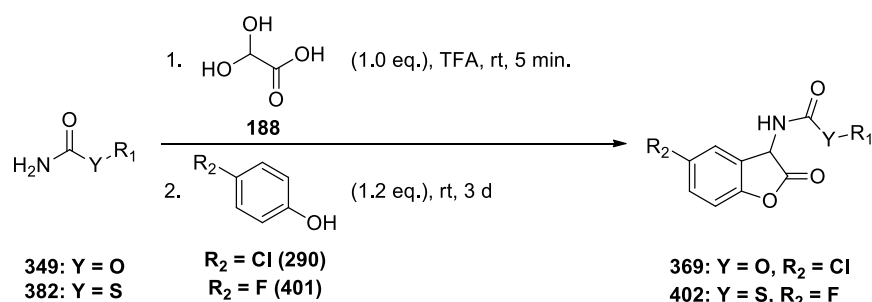
Synthesis of (thiol)carbamates (GP-III): The synthesis protocol of *R. Graf*^[302] was followed with minor adaptations. CSI (1.1 eq.) was added dropwise at room temperature to a solution of the corresponding alcohol/thiol (1.0 eq.) dissolved in DCM (7.6 ml per 1 mmol of the alcohol/thiol). The solution must not be allowed to reach 40 °C during the addition. Afterwards the solution is stirred at room temperature for 24 h. The solvent is removed at reduced pressure and ice is added to the residue (5 g per 1 mmol of the alcohol/thiol). The reaction mixture is stirred intensively at room temperature until the ice has completely melted. Hereafter the aqueous suspension/solution is heated to 80 °C for 15 minutes and then again cooled down to room temperature. The resulting precipitate is filtered off, washed with water and finally dried overnight in vacuo over P₂O₅ in a desiccator.



Synthesis of alkyl thiolcarbamates (GP-IV): The synthesis protocol of *B. Loev and M. F. Kormendy*^[304] was followed with minor adaptations. The corresponding alcohol/thiol (1.0 eq.) and KOCN (2.0 eq.) are suspended in DCM (1.8 mL per 1 mmol of the thiol) and stirred at room temperature. Subsequently trifluoroacetic acid (2.0 eq.) was added dropwise. The suspension was stirred overnight at room temperature. The reaction is then quenched with water (at least 4.0 eq.). The organic phase is separated and dried over Na₂SO₄, filtered off, and the solvent is removed at reduced pressure. If necessary, the aqueous phase was extracted 2-3 times with DCM or EtOAc (1.5 times the volume of the aqueous phase). The combined organic phases were washed with brine (the same volume of the solution), dried over MgSO₄, filtered off and the solvent was removed at reduced pressure.



Synthesis of 2-coumaranones with urea-substructures (GP-V): The synthesis protocol of *R. Krieg et al.*^[290] was followed with minor adaptations. Glyoxylic acid monohydrate (1.00 eq.) and the respective urea compound (1.00 eq.) were dissolved in trifluoroacetic acid (1.6 mL per 1 mmol urea compound). After 30 minutes the phenol compound (1.20 eq.) was added, and the solution was refluxed for 4 h. After cooling down to room temperature, the reaction was poured into a beaker with ice water (at least 4 times the volume of the reaction mixture) and the precipitated solid was filtered off, washed with water and dried overnight in vacuo over P_2O_5 in a desiccator. If no precipitation occurred the solution was extracted three times with EtOAc or DCM (1.5 times the volume of the aqueous phase). The combined organic phases were dried over Na_2SO_4 , filtered off and the solvent was removed at reduced pressure. The raw product was purified by column chromatography on silica gel with $(\text{CH}_2\text{Cl}_2/\text{MeOH})$, $(\text{CH}_2\text{Cl}_2/\text{MeOH} + 1\% \text{ AcOH})$ or $(\text{Toluene}/\text{MeOH} + 1\% \text{ AcOH})$.



Synthesis of 2-coumaranones with (thiol)carbamate-substructures (GP-VI): The synthesis protocol of *S. Schramm*^[295] was followed with minor adaptations. Glyoxylic acid monohydrate (1.00 eq.) and the respective (thiol)carbamate compound (1.00 eq.) were dissolved in trifluoroacetic acid (1.6 mL per 1 mmol (thiol)carbamate compound). After 5 minutes the phenol compound (1.20 eq.) was added, and the solution was stirred at room temperature for 1-3 days. After that the reaction was poured into a beaker with ice water (at least 4 times the volume of the reaction mixture) and the precipitated solid was filtered off, washed with water and dried overnight in vacuo over P_2O_5 in a desiccator. If no precipitation

occurred the solution was extracted three times with EtOAc or DCM (1.5 times the volume of the aqueous phase). The combined organic phases were dried over Na_2SO_4 , filtered off and the solvent was removed at reduced pressure. The raw product was purified by column chromatography on silica gel with ($\text{CH}_2\text{Cl}_2/\text{MeOH}$), ($\text{CH}_2\text{Cl}_2/\text{MeOH} + 1\% \text{ AcOH}$), (Toluene/MeOH), (Toluene /MeOH + 1% AcOH) or (*c*-Hex/Toluene 1:1 + 1% AcOH).

Decomposition experiments (small scale + large scale) (GP-VII): To follow the rate of decomposition, the coumaranone (1.00 eq.) was dissolved in DMSO-d_6 (0.7 ml) in an NMR tube and DBU (2.00 eq.) was added. At the beginning of the addition, a small flash or a long-lasting emission of blue/blue-greenish light was seen and the colour of the solution changed slowly with time. A $^1\text{H-NMR}$ was recorded before the addition of DBU. Then, after addition of the base, a $^1\text{H-NMR}$ spectrum was measured again at specific time intervals. Between measurements, the sample was saturated with oxygen. The reaction was continued until complete oxidation.

At the same time the coumaranone (1.00 eq.) was dissolved in MeCN (20 ml per 1 mmol of coumaranone) and DBU (2.00 eq.) was added. At the begin of the addition a small flash or a long-lasting emission of blue/blue-greenish light could be seen and the colour of the solution slowly changes over the time. After 4 hours the solvent was removed under reduced pressure and 10 ml of water were added to the crude product. The aqueous phase was extracted three times with EtOAc (15 ml per extraction) and the combined organic layers were washed four times with water and subsequently dried over Na_2SO_4 . Finally, the solvent was removed under reduced pressure and the obtained product was analysed via NMR-spectroscopy.

Decomposition experiments with horse radish peroxidase (HRP) (GP-VIII): The coumaranone (1.00 eq.) was dissolved in MeCN/water (1:1, 0.25 ml per mg substrate). Subsequently phosphate buffer solution I (10.0 eq., 1 M) and EDTA solution (1.0 eq., 10^{-1} M) were added. The reaction was initiated with the simultaneous addition of HRP solution (2 units per mg substrate) and H_2O_2 (1.0 eq.). The colour of the solution slowly changed over the time. After 3 days most of the solvent was removed under reduced pressure and the aqueous phase was extracted three times with EtOAc (15 ml per extraction) and the combined organic layers were washed three times with water and subsequently dried over Na_2SO_4 .

Finally, the solvent was removed under reduced pressure and the obtained product was analysed via NMR-spectroscopy.

For large scale enzyme experiments with horse radish peroxidase the following stock solutions were prepared:^[289]

Phosphate buffer I (pH 7.8, 1 M): 6.8 g KH_2PO_4 were dissolved in water, 8 M NaOH was added until pH 7.8, solution was filled up 50 ml.

Phosphate buffer II (pH 7.8, 10^{-3} M): dilution of 0.05 ml phosphate buffer I and water to a final volume of 50 ml.

EDTA solution (pH 7.0, 10^{-1} M): 1.86 g of EDTA disodium salt dihydrate were dissolved in water, 1 M NaOH was added until pH 7.0, solution was filled up 50 ml.

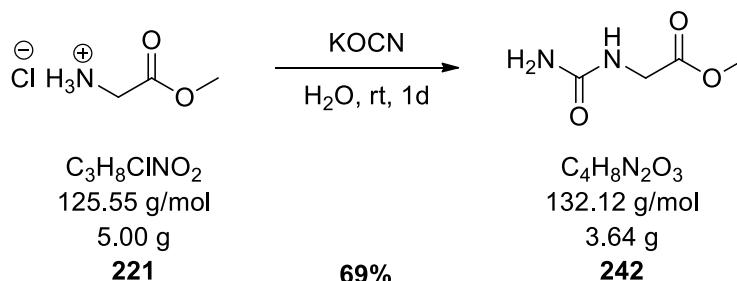
HRP solution (1100 units/mg): 2.27 mg of horseradish peroxidase were dissolved in 50 ml of phosphate buffer II with a final concentration of 0.045 mg/ml \Rightarrow 49.9 units/ml.

6.3 Experimental section

6.3.1 Synthesis of urea derivatives

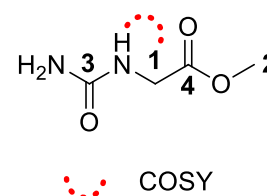
6.3.1.1 Ureido carboxylic acid methyl esters

6.3.1.1.1 Synthesis of methyl 2-ureidoacetate (**242**)



Prepared according to *GP-I* using glycine methyl ester hydrochloride **221** (5.00 g, 39.8 mmol, 1.00 eq.) and KOCN (3.30 g, 40.7 mmol, 1.02 eq.) in 40 ml of water. Urea **242** was obtained as a colourless solid in a yield of 69%.

Yield: 3.64 g (27.6 mmol, 69%).



Appearance: Colourless solid.

Table 17: 1D and 2D-NMR data of methyl 2-ureidoacetate (**242**) in DMSO- d_6 , at 298 K and 400 MHz for ^1H and 100 MHz for ^{13}C .

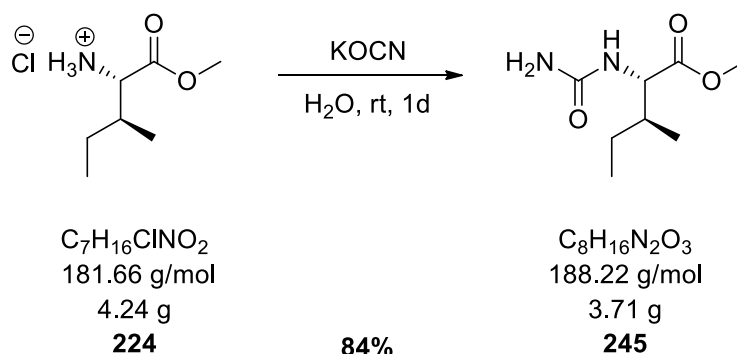
No.	δ_{H} [ppm], J in [Hz]	δ_{C} [ppm], mult.	HMBC ($^{\circ}\text{J}$)
1	3.74 (2H, d, $J = 6.0$ Hz)	41.3, CH_2	$\text{C1} \rightarrow \text{H2} (^4\text{J}), \text{NH} (^2\text{J}), \text{NH}_2 (^4\text{J})$
2	3.61 (3H, s)	51.5, CH_3	-
3	-	158.7, C_q	$\text{C3} \rightarrow \text{H1} (^3\text{J}), \text{NH} (^2\text{J})$
4	-	171.1, C_q	$\text{C4} \rightarrow \text{H1} (^2\text{J}), \text{H2} (^3\text{J})$
NH	6.45 (1H, t, $J = 5.6$ Hz)		-
NH_2	5.76 (2H, s)		-

IR: $\tilde{\nu}$ [cm^{-1}] = 3458 (w), 3364 (w), 2962 (w), 1774 (w), 1734 (s), 1678 (m), 1653 (s), 1624 (w), 1603 (s), 1543 (s), 1439 (s), 1417 (w), 1390 (s), 1282 (w), 1232 (s), 1180 (m), 1126 (w), 1090 (w), 1070 (w), 1030 (w), 987 (w), 968 (w), 935 (w), 908 (w), 901 (w), 887 (w), 870 (w), 850 (w), 818 (w), 812 (w).

MP: 197 °C.

HR-MS (ESI): Theor. $[\text{M}+\text{H}]^+$: 133.06076, found: 133.06081.

Theor. $[\text{M}+\text{Na}]^+$: 155.04271, found: 155.04270.

6.3.1.1.4 Synthesis of (2*S*,3*S*)-methyl 3-methyl-2-ureidopentanoate (**245**)

Prepared according to *GP-I* using L-isoleucine methyl ester hydrochloride **224** (4.24 g, 23.3 mmol, 1.00 eq.) and KOCN (1.93 g, 25.8 mmol, 1.02 eq.) in 23 ml of water. **245** was obtained as a colourless solid in a yield of 84%.

Yield: 3.71 g (19.7 mmol, 84%).

Appearance: Colourless solid.

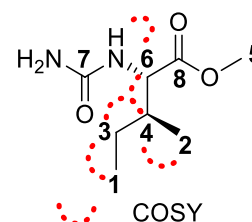


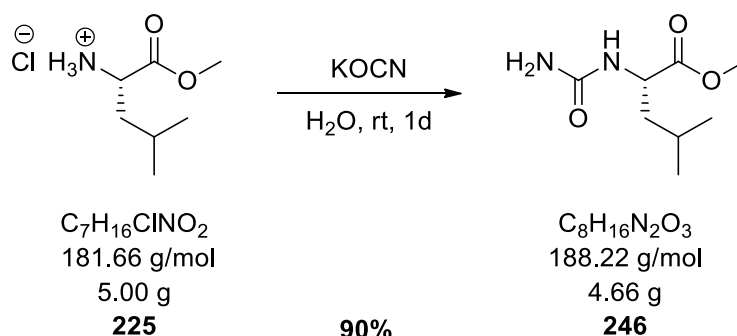
Table 20: 1D and 2D-NMR data of (2*S*,3*S*)-methyl 3-methyl-2-ureidopentanoate (**245**) in DMSO- d_6 , at 298 K and 500 MHz for ^1H and 125 MHz for ^{13}C .

No.	δ_{H} [ppm], J in [Hz]	δ_{C} [ppm], mult.	HMBC ($^{\circ}\text{J}$)
1	0.85 (3H, m)	11.3, CH ₃	C1→H2(^4J), H3(^2J), H4(^3J)
2	0.83 (3H, m)	15.5, CH ₃	C2→H3(^3J), H4(^2J), H6(^3J)
3	1.13 (1H, m); 1.36 (1H, dqd, $J = 14.9, 7.5, 4.7$ Hz)	24.7, CH ₂	C3→H1(^2J), H2(^3J), H4(^2J), H6(^3J)
4	1.70 (1H, ddq, $J = 13.5, 9.0, 6.7$ Hz)	37.1, CH	C4→H1(^3J), H2(^2J), H3(^2J), H6(^2J), NH(^3J)
5	3.62 (3H, s)	51.4, CH ₃	-
6	4.10 (1H, dd, $J = 8.8, 5.7$ Hz)	56.6, CH	C6→H2(^3J), H3(^3J), H4(^2J), H5(^4J), NH(^2J), NH ₂ (^4J)
7	-	158.2, C _q	C7→H6(^3J), NH(^2J)
8	-	173.2, C _q	C8→H4(^3J), H5(^3J), H6(^2J), NH(^3J)
NH	6.29 (1H, d, $J = 8.8$ Hz)	-	-
NH ₂	5.58 (2H, s)	-	-

IR: $\tilde{\nu}$ [cm^{-1}] = 3676 (w), 3460 (m), 3362 (m), 3267 (w), 3215 (w), 3085 (w), 2988 (m), 2971 (s), 2960 (s), 2933 (m), 2902 (m), 2885 (m), 2361 (w), 2114 (w), 1919 (w), 1722 (s), 1679 (m), 1651 (s), 1621 (m), 1591 (s), 1564 (s), 1462 (m), 1437 (s), 1407 (m), 1385 (m), 1366 (s), 1339 (s), 1308 (m), 1281 (m), 1259 (s), 1200 (s), 1170 (s), 1140 (m), 1104 (m), 1076 (s), 1066 (s), 1057 (s), 1028 (m), 993 (m), 845 (w).

MP: 101 °C.

HR-MS (ESI): Theor.[M+H]⁺: 189.12336, found: 189.12345.
Theor.[M+Na]⁺: 211.10531, found: 211.10531.

6.3.1.1.5 Synthesis of (*S*)-methyl 4-methyl-2-ureidopentanoate (**225**)

Prepared according to *GP-I* using L-leucine methyl ester hydrochloride **225** (5.00 g, 27.5 mmol, 1.00 eq.) and KOCN (2.30 g, 28.1 mmol, 1.02 eq.) in 28 ml of water. **246** was obtained as a colourless solid in a yield of 90%.

Yield: 4.66 g (24.8 mmol, 90%).

Appearance: Colourless solid.

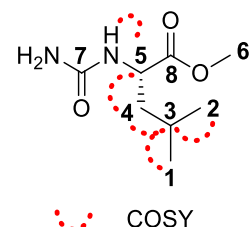


Table 21: 1D and 2D-NMR data of (*S*)-methyl 4-methyl-2-ureidopentanoate (**246**) in DMSO- d_6 , at 298 K and 500 MHz for ^1H and 125 MHz for ^{13}C .

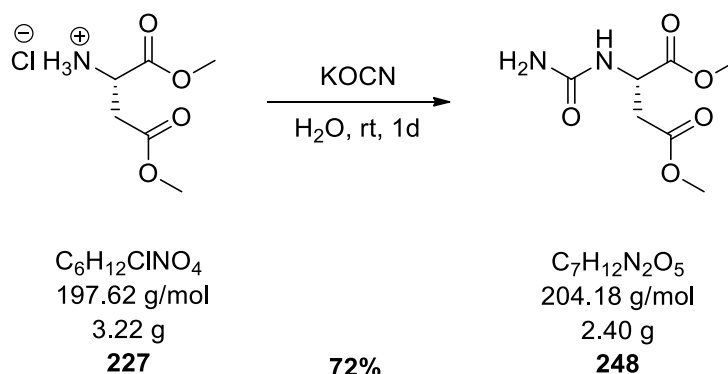
No.	δ_{H} [ppm], J in [Hz]	δ_{C} [ppm], mult.	HMBC ($^{\circ}\text{J}$)
1	0.86 (3H, d, $J = 6.6$ Hz)	21.5, CH ₃	C1→H2(³ J), H3(² J), H4(³ J)
2	0.89 (3H, d, $J = 6.7$ Hz)	22.7, CH ₃	C2→H1(³ J), H3(² J), H4(³ J)
3	1.62 (1H, sep, $J = 6.7$ Hz)	24.3, CH	C3→H1(² J), H2(² J), H4(² J), H5(³ J)
4	1.43 (2H, m)	40.8, CH ₂	C4→H1(³ J), H2(³ J), H3(² J), H5(² J), NH(³ J)
5	4.10 (1H, ψq , $J = 8.0$ Hz)	50.8, CH	C5→H3(³ J), H4(² J), H6(⁴ J), NH(² J), NH ₂ (⁴ J)
6	3.61 (3H, s)	51.6, CH ₃	-
7	-	158.2, C _q	C7→H5(³ J), NH(² J)
8	-	174.3, C _q	C8→H4(³ J), H5(² J), H6(³ J), NH(³ J)
NH	6.30 (1H, d, $J = 8.3$ Hz)	-	-
NH ₂	5.56 (2H, s)	-	-

IR: $\tilde{\nu}$ [cm^{-1}] = 3676 (w), 3451 (w), 3306 (m), 3214 (w), 2964 (m), 2910 (m), 2873 (m), 2112 (w), 1981 (w), 1739 (s), 1732 (s), 1662 (s), 1607 (m), 1549 (s), 1471 (m), 1435 (m), 1371 (s), 1305 (w), 1271 (m), 1239 (s), 1226 (s), 1168 (s), 1123 (m), 1079 (m), 1066 (m), 1057 (m), 1028 (m), 1005 (m), 984 (m), 955 (w), 924 (w), 901 (w), 857 (w), 827 (w).

MP: 80 °C.

HR-MS (ESI): Theor.[M+H]⁺: 189.12336, found: 189.12353.

Theor.[M+Na]⁺: 211.10513, found: 211.10532.

6.3.1.1.7 Synthesis of (*S*)-dimethyl 2-ureidosuccinate (**248**)

Prepared according to *GP-I* using L-aspartic acid dimethyl ester hydrochloride **227** (3.22 g, 16.3 mmol, 1.00 eq.) and KOCN (1.35 g, 16.6 mmol, 1.02 eq.) in 16 ml of water. **248** was obtained as a colourless solid in a yield of 72%.

Yield: 2.40 g (11.8 mmol, 72%).

Appearance: Colourless solid.

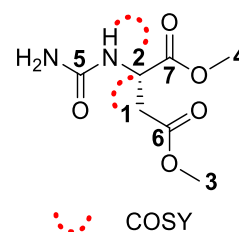


Table 23: 1D and 2D-NMR data of (*S*)-dimethyl 2-ureidosuccinate (**248**) in DMSO- d_6 , at 298 K and 500 MHz for ^1H and 125 MHz for ^{13}C .

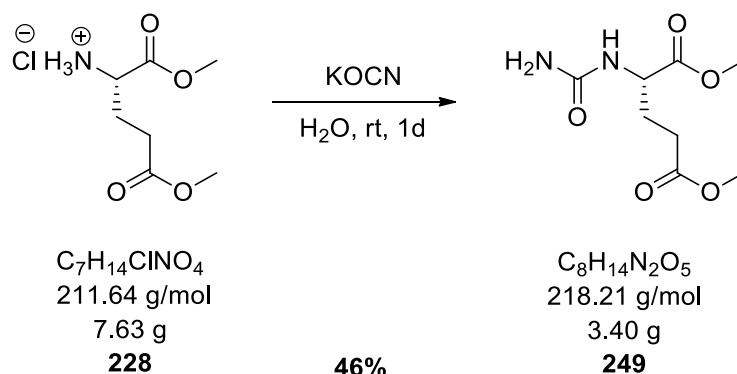
No.	δ_{H} [ppm], J in [Hz]	δ_{C} [ppm], mult.	HMBC ($^{\times}J$)
1	2.75 (2H, m)	36.7, CH_2	$\text{C1} \rightarrow \text{H2}({}^2J)$, $\text{H3}({}^4J)$, $\text{NH}({}^3J)$
2	4.51 (1H, ψ dt, $J = 8.5, 5.8$ Hz)	49.0, CH	$\text{C2} \rightarrow \text{H1}({}^2J)$, $\text{H4}({}^4J)$, $\text{NH}({}^2J)$, $\text{NH}_2({}^4J)$
3	3.61 (3H, s)	51.6, CH_3	-
4	3.62 (3H, s)	52.1, CH_3	-
5	-	157.9, C_q	$\text{C5} \rightarrow \text{H2}({}^3J)$, $\text{NH}({}^2J)$
6	-	171.0, C_q	$\text{C6} \rightarrow \text{H1}({}^2J)$, $\text{H2}({}^3J)$, $\text{H3}({}^3J)$
7	-	172.2, C_q	$\text{C7} \rightarrow \text{H1}({}^3J)$, $\text{H2}({}^2J)$, $\text{H4}({}^3J)$, $\text{NH}({}^3J)$
NH	6.42 (1H, d, $J = 8.5$ Hz)	-	-
NH_2	5.73 (2H, s)	-	-

IR: $\tilde{\nu}$ [cm^{-1}] = 3672 (w), 3463 (m), 3361 (w), 3304 (w), 2959 (w), 2933 (w), 1956 (w), 1730 (s), 1721 (s), 1683 (m), 1651 (s), 1607 (m), 1582 (m), 1537 (s), 1439 (m), 1427 (m), 1402 (m), 1374 (m), 1327 (w), 1290 (w), 1214 (s), 1174 (s), 1162 (s), 1110 (w), 1061 (m), 1022 (w), 997 (m), 966 (w), 956 (w), 881 (w), 853 (m).

MP: 106 °C.

HR-MS (ESI): Theor.[$\text{M}+\text{H}$] $^+$: 205.08189, found: 205.08216.

Theor.[$\text{M}+\text{Na}$] $^+$: 227.06384, found: 227.06398.

6.3.1.1.8 Synthesis of (*S*)-dimethyl 2-ureidopentanedioate (**249**)

Prepared according to *GP-I* using L-glutamic acid dimethyl ester hydrochloride **228** (7.63 g, 36.1 mmol, 1.00 eq.) and KOCN (2.98 g, 36.8 mmol, 1.02 eq.) in 36 ml of water. **249** was obtained as a colourless solid in a yield of 43%.

Yield: 3.40 g (15.6 mmol, 43%).

Appearance: Colourless solid.

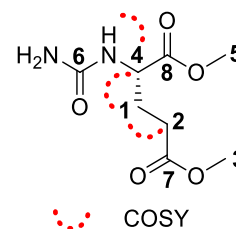


Table 24: 1D and 2D-NMR data of (*S*)-dimethyl 2-ureidopentanedioate (**249**) in DMSO-*d*₆, at 298 K and 500 MHz for ¹H and 125 MHz for ¹³C.

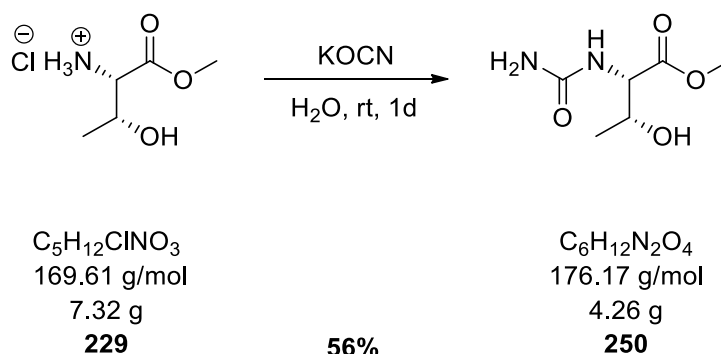
No.	δ_{H} [ppm] (<i>J</i> in Hz)	δ_{C} [ppm], mult.	HMBC ($^{\times}J$)
1	1.78 (1H, dtd, <i>J</i> = 14.5, 8.3, 6.5 Hz); 1.94 (1H, dtd, <i>J</i> = 13.6, 7.6, 5.5 Hz)	27.0, CH ₂	C1→H2(² J), H4(² J), NH(³ J)
2	2.35 (2H, m)	29.6, CH ₂	C2→H1(² J), H3(⁴ J), H4(³ J)
3	3.59 (3H, s)	51.4, CH ₃	-
4	4.15 (1H, td, <i>J</i> = 8.5, 5.4 Hz)	51.6, CH	C4→H1(² J), H2(³ J), H5(⁴ J), NH(² J), NH ₂ (⁴ J)
5	3.62 (3H, s)	51.8, CH ₃	-
6	-	158.2, C _q	C6→H4(³ J), NH(² J)
7	-	172.7, C _q	C7→H1(³ J), H2(² J), H3(³ J)
8	-	173.3, C _q	C8→H1(³ J), H4(² J), H5(³ J), NH(³ J)
NH	6.39 (1H, d, <i>J</i> = 8.2 Hz)	-	-
NH ₂	5.61 (2H, s)	-	-

IR: $\tilde{\nu}$ [cm⁻¹] = 3407 (m), 3315 (m), 3272 (w), 3229 (m), 2957 (w), 2095 (w), 1999 (w), 1872 (w), 1833 (w), 1737 (m), 1717 (s), 1688 (s), 1646 (m), 1620 (s), 1539 (s), 1456 (m), 1434 (s), 1393 (m), 1383 (m), 1329 (m), 1299 (m), 1287 (m), 1247 (s), 1199 (s), 1179 (s), 1150 (s), 1104 (m), 1066 (m), 1019 (s), 984 (m), 950 (w), 892 (w), 857 (w).

MP: 90 °C.

HR-MS (ESI): Theor.[M+H]⁺: 219.09754, found: 219.09787.

Theor.[M+Na]⁺: 241.07949, found: 241.07961.

6.3.1.1.9 Synthesis of (2*S*,3*R*)-methyl 3-hydroxy-2-ureidobutanoate (**250**)

Prepared according to *GP-I* using L-threonine methyl ester hydrochloride **229** (7.32 g, 43.2 mmol, 1.00 eq.) and KOCN (3.57 g, 44.0 mmol, 1.02 eq.) in 43 ml of water. **250** was obtained as a colourless solid in a yield of 56%.

Yield: 4.26 g (24.2 mmol, 56%).

Appearance: Colourless solid.

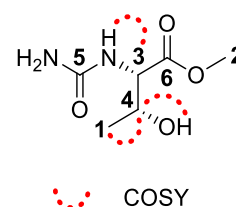


Table 25: 1D and 2D-NMR data of (2*S*,3*R*)-methyl 3-hydroxy-2-ureidobutanoate (**250**) in DMSO-*d*₆, at 298 K and 499 MHz for ¹H and 125 MHz for ¹³C.

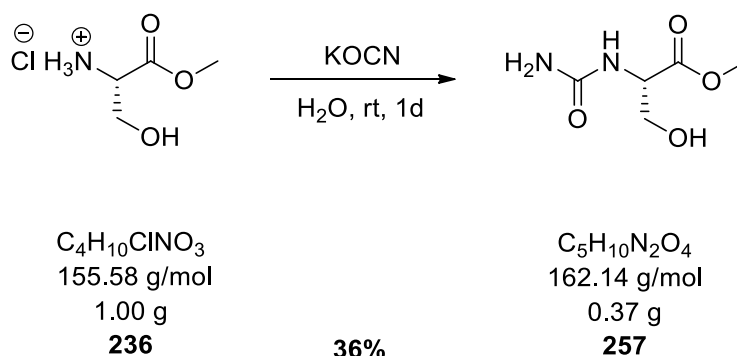
No.	δ_{H} [ppm] (<i>J</i> in Hz)	δ_{C} [ppm], mult.	HMBC (² J)
1	1.06 (3H, d, <i>J</i> = 6.3 Hz)	20.4, CH ₃	C1→H4(² J), OH(³ J)
2	3.62 (3H, s)	51.6, CH ₃	-
3	4.08 (1H, m)	58.1, CH	C3→H1(³ J), NH(² J), NH ₂ (⁴ J), OH(³ J)
4	4.09 (1H, m)	66.5, CH	C4→H1(² J), H3(² J), NH(³ J), OH(² J)
5	-	158.7, C _q	C5→H3(³ J), NH(² J)
6	-	172.5, C _q	C6→H3(² J), H4(³ J), H2(³ J)
NH	6.13 (1H, d, <i>J</i> = 8.7 Hz)	-	-
NH ₂	5.76 (2H, s)	-	-
OH	5.00 (1H, d, <i>J</i> = 4.6 Hz)	-	-

IR: $\tilde{\nu}$ [cm⁻¹] = 3488 (br), 3453 (br), 3332 (br), 3079 (w), 2981 (w), 2955 (w), 2923 (w), 2360 (s), 2341 (s), 1730 (s), 1719 (s), 1682 (w), 1652 (vs), 1590 (s), 1559 (vs), 1507 (w), 1437 (m), 1370 (m), 1343 (w), 1326 (w), 1288 (m), 1249 (m), 1218 (s), 1176 (s), 1134 (w), 1111 (m), 1089 (m), 1054 (w), 1026 (w), 997 (m), 959 (w), 905 (w), 870 (w), 860 (w), 826 (w).

MP: 145 °C.

HR-MS (ESI): Theor.[M+H]⁺: 177.08698, found: 177.08712.

Theor.[M+Na]⁺: 199.06892, found: 199.06897.

6.3.1.1.10 Synthesis of (*S*)-methyl 3-hydroxy-2-ureidopropanoate (**257**)

Prepared according to *GP-I* using L-serine methyl ester hydrochloride **236** (1.00 g, 6.43 mmol, 1.00 eq.) and KOCN (0.53 g, 6.56 mmol, 1.02 eq.) in 7 ml of water. **257** was obtained as a colourless solid in a yield of 35%.

Yield: 0.37 g (2.28 mmol, 35%).

Appearance: Colourless solid.

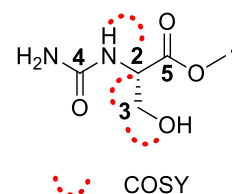


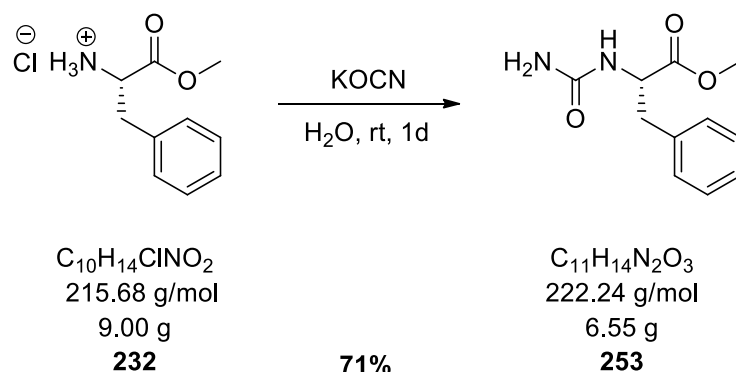
Table 26: 1D and 2D-NMR data of (*S*)-methyl 3-hydroxy-2-ureidopropanoate (**258**) in DMSO- d_6 , at 298 K and 400 MHz for ^1H and 100 MHz for ^{13}C .

No.	δ_{H} [ppm], J in [Hz]	δ_{C} [ppm], mult.	HMBC ($^{\circ}\text{J}$)
1	3.62 (3H, s)	51.7, CH_3	-
2	4.19 (1H, m)	54.8, CH	$\text{C}2 \rightarrow \text{H}3(^2\text{J}), \text{OH}(^3\text{J}), \text{NH}(^2\text{J}), \text{NH}_2(^4\text{J})$
3	3.54 (1H, m); 3.71 (1H, m)	62.1, CH_2	$\text{C}3 \rightarrow \text{H}2(^2\text{J}), \text{OH}(^2\text{J}), \text{NH}(^3\text{J})$
4	-	158.2, C_q	$\text{C}4 \rightarrow \text{H}2(^3\text{J}), \text{NH}(^2\text{J})$
5	-	172.3, C_q	$\text{C}5 \rightarrow \text{H}1(^3\text{J}), \text{H}2(^2\text{J})$
OH	5.09 (1H, t, $J = 5.3$ Hz)	-	-
NH	6.30 (1H, d, $J = 8.5$ Hz)	-	-
NH_2	5.74 (2H, s)	-	-

IR: $\tilde{\nu}$ [cm^{-1}] = 3445 (w), 3202 (br), 3013 (w), 2957 (w), 2051 (w), 1731 (m), 1716 (m), 1648 (m), 1553 (m), 1402 (s), 1223 (w), 1169 (w), 1048 (vs), 973 (m), 872 (w), 804 (w).

MP: Decomposition above 200 °C.

HR-MS (ESI): Theor. $[\text{M}+\text{H}]^+$: 163.07133, found: 163.07146.
Theor. $[\text{M}+\text{Na}]^+$: 185.05327, found: 185.05352.

6.3.1.1.11 Synthesis of (*S*)-methyl 3-phenyl-2-ureidopropanoate (**253**)

Prepared according to *GP-I* using L-phenylalanine methyl ester hydrochloride **232** (9.00 g, 41.7 mmol, 1.00 eq.) and KOCN (3.45 g, 42.6 mmol, 1.02 eq.) in 42 ml of water. **253** was obtained as a light beige coloured solid in a yield of 71%.

Yield: 6.55 g (29.5 mmol, 71%).

Appearance: Light beige coloured solid.

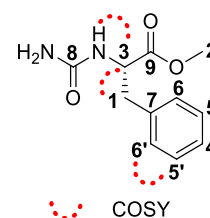
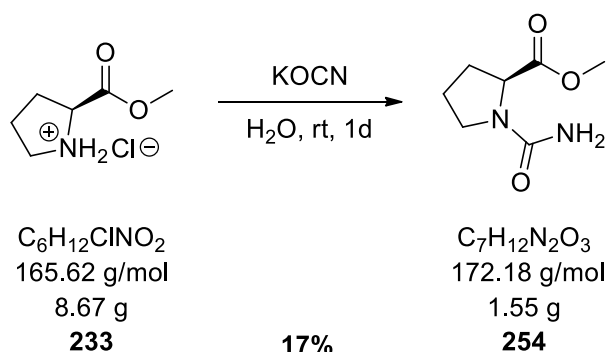


Table 27: 1D and 2D-NMR data of (*S*)-methyl 3-phenyl-2-ureidopropanoate (**253**) in DMSO- d_6 , at 298 K and 500 MHz for ^1H and 125 MHz for ^{13}C .

No.	δ_{H} [ppm], J in [Hz]	δ_{C} [ppm], mult.	HMBC ($^{\times}J$)
1	2.87 (1H, dd, 13.7, $J = 8.1$ Hz); 2.96 (1H, dd, 13.7, $J = 5.5$ Hz)	37.6, CH_2	$\text{C1} \rightarrow \text{H3} (^2J)$, $\text{H6} (^3J)$, $\text{NH} (^3J)$
2	3.59 (3H, s)	51.7, CH_3	-
3	4.38 (1H, ψ td, $J = 8.1, 5.5$ Hz)	53.9, CH	$\text{C3} \rightarrow \text{H1} (^2J)$, $\text{NH} (^2J)$, $\text{NH}_2 (^4J)$
4	7.22 (1H, m)	126.5, CH_{arom}	$\text{C4} \rightarrow \text{H6} (^3J)$
5	7.29 (2H, m)	128.3, $2 \times \text{CH}_{\text{arom}}$	$\text{C5} \rightarrow \text{H5} (^3J)$
6	7.17 (2H, m)	129.1, $2 \times \text{CH}_{\text{arom}}$	$\text{C6} \rightarrow \text{H4} (^3J)$, $\text{H6} (^3J)$
7	-	137.2, C_{q}	$\text{C7} \rightarrow \text{H1} (^2J)$, $\text{H3} (^3J)$, $\text{H5} (^3J)$
8	-	158.0, C_{q}	$\text{C8} \rightarrow \text{H3} (^3J)$, $\text{NH} (^2J)$
9	-	173.1, C_{q}	$\text{C9} \rightarrow \text{H1} (^3J)$, $\text{H2} (^3J)$, $\text{H3} (^2J)$, $\text{NH} (^3J)$
NH	6.33 (1H, d, $J = 8.2$ Hz)	-	-
NH_2	5.65 (2H, s)	-	-

IR: $\tilde{\nu}$ [cm^{-1}] = 3676 (w), 3482 (w), 3359 (m), 3280 (w), 2988 (m), 2902 (m), 2286 (w), 2051 (w), 1981 (w), 1741 (s), 1673 (m), 1642 (s), 1607 (s), 1569 (s), 1489 (m), 1459 (m), 1432 (s), 1382 (s), 1357 (m), 1346 (m), 1279 (s), 1232 (m), 1217 (m), 1194 (s), 1175 (s), 1075 (s), 1057 (s), 1029 (s), 1010 (m), 988 (m), 930 (m), 870 (w), 817 (w).

MP: 100 °C.

6.3.1.1.12 Synthesis of (*S*)-methyl 1-carbamoylpyrrolidine-2-carboxylate (**254**)

Prepared according to *GP-I* using L-proline methyl ester hydrochloride **233** (8.67 g, 52.3 mmol, 1.00 eq.) and KOCN (4.33 g, 53.4 mmol, 1.02 eq.) in 52 ml of water. **254** was obtained as a colourless solid in a yield of 17%.

Yield: 1.55 g (9.00 mmol, 17%).

Appearance: Colourless solid.

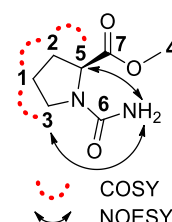


Table 28: 1D and 2D-NMR data of (*S*)-methyl 1-carbamoylpyrrolidine-2-carboxylate (**254**) in DMSO- d_6 , at 298 K and 500 MHz for ^1H and 125 MHz for ^{13}C .

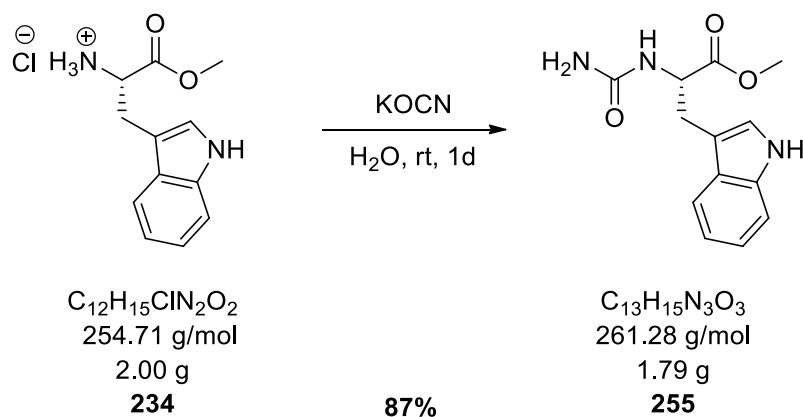
No.	δ_{H} [ppm], J in [Hz]	δ_{C} [ppm], mult.	HMBC ($^{\circ}J$)
1	1.87 (2H, m)	24.2, CH ₂	C1→H2(² J), H3(² J), H5(³ J)
2	1.79 (1H, m); 2.11 (1H, ψ dq, J = 12.2, 8.4 Hz, 1H)	29.4, CH ₂	C2→H1(² J), H3(³ J), H5(³ J)
3	3.26 (1H, ψ dt, J = 9.5, 7.2 Hz); 3.33 (1H, m)	46.0, CH ₂	C3→H1(² J), H2(³ J), H5(³ J)
4	3.59 (3H, s)	51.6, CH ₃	-
5	4.21 (1H, dd, J = 8.8, 3.5 Hz)	58.3, CH	C5→H1(³ J), H2(² J), H3(³ J)
6	-	157.0, C _q	C6→H3(³ J), H5(³ J), NH(² J)
7	-	173.6, C _q	C7→H2(³ J), H4(³ J), H5(² J)
NH	5.86 (2H, s)	-	-

IR: $\tilde{\nu}$ [cm⁻¹] = 3418 (w), 3360 (w), 3287 (w), 3201 (w), 3134 (w), 2985 (w), 2958 (w), 2891 (w), 1733 (s), 1660 (s), 1609 (vs), 1447 (s), 1435 (vs), 1372 (m), 1355 (m), 1325 (w), 1293 (m), 1273 (m), 1248 (w), 1220 (m), 1197 (s), 1169 (s), 1146 (m), 1117 (m), 1082 (m), 1032 (w), 1016 (w), 997 (w), 978 (w), 927 (w), 910 (w), 876 (w), 861 (w), 836 (w).

MP: 140 °C.

HR-MS (ESI): Theor.[M+H]⁺: 173.09206, found: 173.09223.

Theor.[M+Na]⁺: 195.07401, found: 195.07422.

6.3.1.1.13 Synthesis of (*S*)-methyl 3-(1*H*-indol-3-yl)-2-ureidopropanoate (**255**)

Prepared according to *GP-I* using L-tryptophan methyl ester hydrochloride **234** (2.00 g, 7.85 mmol, 1.00 eq.) and KOCN (0.65 g, 8.01 mmol, 1.02 eq.) in 8 ml of water. **255** was obtained as a light beige coloured solid in a yield of 87%.

Yield: 1.79 g (6.85 mmol, 87%).

Appearance: Light beige coloured solid.

IR: $\tilde{\nu}$ [cm^{-1}] = 3676 (w), 3484 (w), 3357 (w), 3280 (w), 3103 (w), 2988 (m), 2973 (m), 2901 (m), 2051 (w), 1981 (w), 1742 (s), 1673 (w), 1641 (m), 1607 (m), 1570 (s), 1489 (w), 1457 (m), 1431 (s), 1394 (m), 1381 (s), 1356 (m), 1345 (m), 1278 (s), 1232 (m), 1217 (m), 1193 (s), 1174 (m), 1075 (s), 1067 (s), 1057 (s), 1029 (s), 1010 (m), 989 (m), 929 (w), 880 (w), 870 (w), 817 (w).

MP: 170 °C.

HR-MS (ESI): Theor. $[\text{M}+\text{Na}]^+$: 284.10056, found: 284.10080.

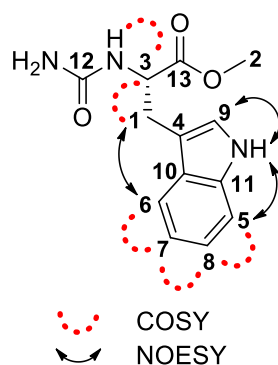
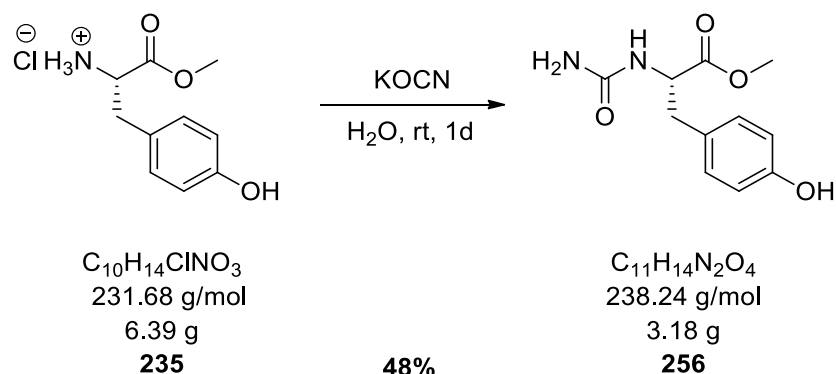


Table 29: 1D and 2D-NMR data of (*S*)-methyl 3-(1*H*-indol-3-yl)-2-ureidopropanoate (255) in DMSO-*d*₆, at 298 K and 500 MHz for ¹H and 125 MHz for ¹³C.

No.	δ_{H} [ppm], J in [Hz]	δ_{C} [ppm], mult.	HMBC ($^{\times}J$)
1	3.03 (1H, dd, $J = 14.6, 7.0$ Hz); 3.08 (1H, dd, $J = 14.6, 5.6$ Hz)	27.9, CH ₂	C1→H3(² J), H9(³ J), NH(³ J)
2	3.57 (3H, s)	51.6, CH ₃	-
3	4.44 (1H, m)	53.3, CH	C3→H1(² J), H2(⁴ J), H9(⁴ J), NH(² J), NH ₂ (⁴ J)
4	-	109.3, C _q	C4→H1(² J), H3(³ J), H6(³ J), H7(⁴ J), H9(² J), NH _{arom} (³ J)
5	7.34 (1H, d, $J = 8.0$ Hz)	111.4, CH _{arom}	C5→H6(⁴ J), H7(³ J)
6	7.46 (1H, d, $J = 7.9$ Hz)	118.1, CH _{arom}	C6→H8(³ J)
7	6.99 (1H, m)	118.4, CH _{arom}	C7→H5(³ J)
8	7.06 (1H, m)	121.0, CH _{arom}	C8→H6(³ J), H7(² J)
9	7.11 (1H, d, $J = 2.3$ Hz)	123.7, CH _{arom}	C9→H1(³ J), NH _{arom} (² J)
10	-	127.2, C _q	C10→H1(³ J), H5(³ J), H6(² J), H7(³ J), H9(³ J), NH _{arom} (³ J)
11	-	136.1, C _q	C11→H6(³ J), H9(³ J), H8(³ J), NH _{arom} (² J)
12	-	158.0, C _q	C12→H3(³ J), NH(² J)
13	-	173.4, C _q	C13→H1(³ J), H2(³ J), H3(² J), NH(³ J)
NH	6.24 (1H, d, $J = 8.0$ Hz)	-	-
NH ₂	5.65 (2H, s)	-	-
NH _{arom}	10.89 (1H, s)	-	-

6.3.1.1.14 Synthesis of (*S*)-methyl 3-(4-hydroxyphenyl)-2-ureidopropanoate (**256**)

Prepared according to *GP-I* using L-tyrosine methyl ester hydrochloride **235** (6.39 g, 27.6 mmol, 1.00 eq.) and KOCN (2.28 g, 28.1 mmol, 1.02 eq.) in 28 ml of water. **256** was obtained as a colourless solid in a yield of 49%.

Yield: 3.18 g (13.4 mmol, 49%).

Appearance: Colourless solid.

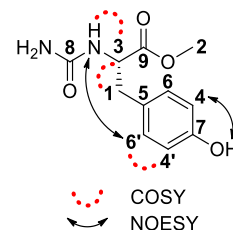
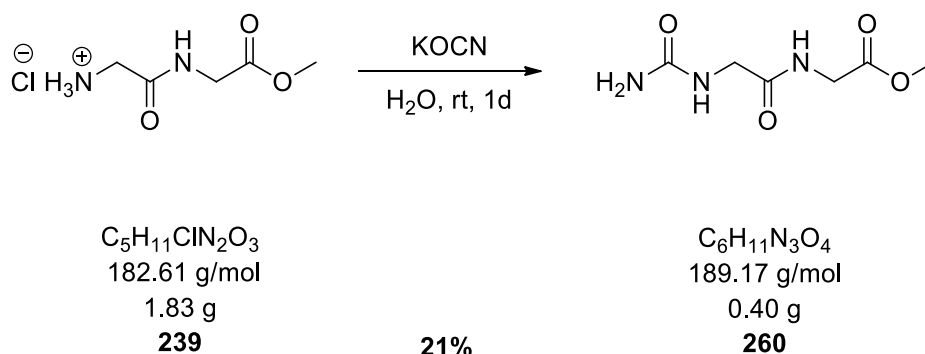


Table 30: 1D and 2D-NMR data of (*S*)-methyl 3-(4-hydroxyphenyl)-2-ureidopropanoate (**256**) in DMSO- d_6 , at 298 K and 500 MHz for ^1H and 125 MHz for ^{13}C .

No.	δ_{H} [ppm], J in [Hz]	δ_{C} [ppm], mult.	HMBC ($^{\times}J$)
1	2.75 (1H, dd, $J = 13.8, 7.7$ Hz); 2.82 (1H, dd, $J = 13.8, 5.7$ Hz)	36.9, CH ₂	C1→H3(² J), H6(³ J), NH(³ J)
2	3.58 (3H, s)	51.6, CH ₃	-
3	4.30 (1H, td, $J = 7.9, 5.6$ Hz)	54.1, CH	C3→H1(² J), H2(⁴ J), H6(⁴ J), NH(² J), NH ₂ (⁴ J)
4	6.67 (2H, d, $J = 8.5$ Hz)	115.1, 2xCH _{arom}	C4→H4(³ J), H6(² J), OH(³ J)
5	-	127.0, C _q	C5→H1(² J), H3(³ J), H4(³ J)
6	6.94 (2H, d, $J = 8.5$ Hz)	130.1, 2xCH _{arom}	C6→H1(³ J), H4(² J), H6(³ J)
7	-	156.0, C _q	C7→H4(² J), H6(³ J), OH(² J)
8	-	158.0, C _q	C8→H3(³ J), NH(² J)
9	-	173.2, C _q	C9→H1(³ J), H2(³ J), H3(² J)
NH	6.20 (1H, d, $J = 8.2$ Hz)	-	-
NH ₂	5.86 (2H, s)	-	-
OH	9.23 (1H, s)	-	-

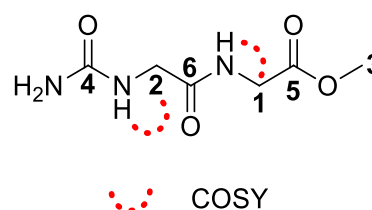
IR: $\tilde{\nu}$ [cm⁻¹] = 3489 (w), 3376 (w), 3317 (w), 3089 (w), 2817 (w), 1732 (s), 1648 (s), 1610 (w), 1597 (w), 1556 (m), 1515 (m), 1446 (m), 1381 (w), 1331 (w), 1293 (m), 1252 (s), 1206 (w), 1178 (w), 1141 (w), 1101 (w), 1043 (w), 1008 (m), 964 (w), 923 (w), 891 (w), 863 (w), 834 (m), 826 (m).

MP: 138 °C.

6.3.1.1.15 Synthesis of methyl 2-(2-ureidoacetamido)acetate (**260**)

Prepared according to *GP-I* using glycylglycine methyl ester hydrochloride **239** (1.83 g, 10.0 mmol, 1.00 eq.) and KOCN (0.83 g, 10.2 mmol, 1.02 eq.) in 10 ml of water. **260** was obtained as a colourless solid in a yield of 21%.

Yield: 0.40 g (2.11 mmol, 21%).



Appearance: Colourless solid.

Table 31: 1D and 2D-NMR data of methyl 2-(2-ureidoacetamido)acetate (**260**) in DMSO- d_6 , at 298 K and 500 MHz for ^1H and 125 MHz for ^{13}C .

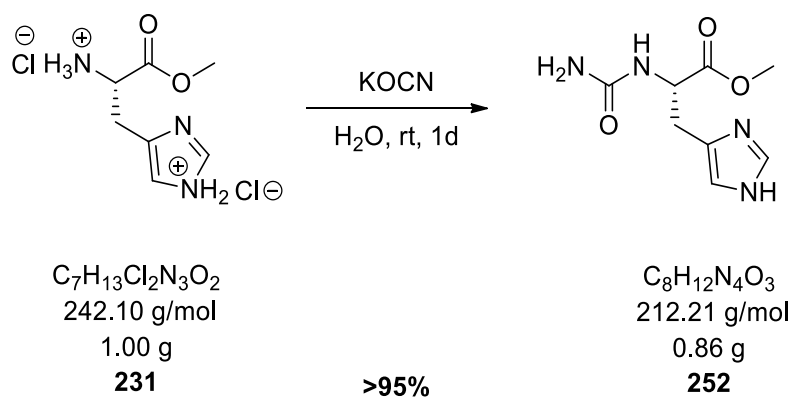
No.	δ_{H} [ppm], J in [Hz]	δ_{C} [ppm], mult.	HMBC ($^{\circ}\text{J}$)
1	3.85 (2H, d, $J = 5.9$ Hz)	40.5, CH_2	$\text{C1} \rightarrow \text{NH}_{\text{amide}}(^2\text{J})$
2	3.65 (2H, d, $J = 5.7$ Hz)	42.6, CH_2	$\text{C2} \rightarrow \text{NH}(^2\text{J}), \text{NH}_2(^4\text{J})$
3	3.63 (3H, s)	51.7, CH_3	-
4	-	158.6, C_q	$\text{C4} \rightarrow \text{H2}(^3\text{J}), \text{NH}(^2\text{J})$
5	-	170.3, C_q	$\text{C5} \rightarrow \text{H1}(^2\text{J}), \text{H3}(^3\text{J})$
6	-	170.7, C_q	$\text{C6} \rightarrow \text{NH}_{\text{amide}}(^2\text{J})$
NH	6.23 (1H, t, $J = 5.3$ Hz)	-	-
NH_2	5.67 (2H, s)	-	-
NH_{amide}	8.24 (1H, t, $J = 5.7$ Hz)	-	-

IR: $\tilde{\nu}$ [cm^{-1}] = 3676 (w), 3467 (w), 3274 (w), 2988 (w), 2901 (w), 2360 (w), 1736 (m), 1701 (w), 1648 (vs), 1560 (m), 1437 (w), 1414 (w), 1369 (m), 1294 (w), 1266 (w), 1207 (s), 1175 (m), 1066 (m), 1038 (m), 1005 (w), 976 (m), 888 (w).

MP: 150 °C.

HR-MS (ESI): Theor.[$\text{M}+\text{H}$] $^+$: 190.08223, found: 190.08238.

Theor.[$\text{M}+\text{Na}$] $^+$: 212.06417, found: 212.06409.

6.3.1.1.16 Synthesis of (*S*)-methyl 3-(1*H*-imidazol-4-yl)-2-ureidopropanoate (**252**)

Prepared according to *GP-I* using L-histidine methyl ester dihydrochloride **231** (1.00 g, 4.13 mmol, 1.00 eq.) and KOCN (0.34 g, 4.21 mmol, 1.02 eq.) in 5 ml of water. **252** was obtained as a colourless solid in a quantitative yield.

Yield: 0.86 g (4.05 mmol, >95%).

Appearance: Colourless solid.

IR: $\tilde{\nu}$ [cm^{-1}] = 3676 (w), 3389 (w), 3323 (w), 3149 (w), 2988 (m), 2901 (m), 2360 (w), 1728 (s), 1654 (s), 1620 (w), 1551 (s), 1497 (w), 1441 (w), 1394 (w), 1361 (w), 1337 (w), 1312 (w), 1283 (w), 1255 (w), 1241 (m), 1183 (w), 1163 (w), 1066 (m), 1053 (s), 954 (w), 901 (w), 869 (w), 811 (m).

MP: 160 °C.

HR-MS (ESI): Theor.[M+H]⁺: 213.09821, found: 213.09823.

Theor.[M+Na]⁺: 235.08016, found: 235.08033.

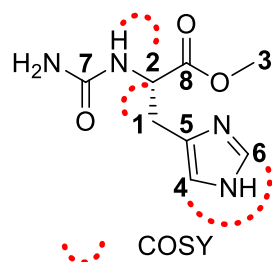
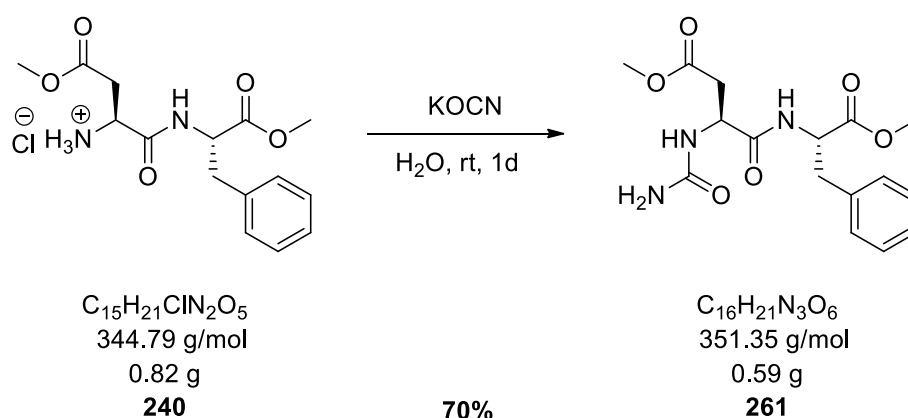


Table 32: 1D and 2D-NMR data of (*S*)-methyl 3-(1*H*-imidazol-4-yl)-2-ureidopropanoate (252) in DMSO-*d*₆, at 298 K and 500 MHz for ¹H and 125 MHz for ¹³C.

No.	δ_{H} [ppm], J in [Hz]	δ_{C} [ppm], mult.	HMBC ($^{\times}J$)
1	2.98 (1H, dd, $J = 15.0, 8.8$ Hz); 3.09 (1H, dd, $J = 15.1, 5.3$ Hz)	27.1, CH ₂	C1→H2(² J), H4(³ J), NH(³ J)
2	4.47 (1H, td, $J = 8.5, 5.3$ Hz)	51.8, CH	C2→H1(² J), H4(⁴ J), NH(² J), NH ₂ (⁴ J)
3	3.63 (3H, s)	52.0, CH ₃	-
4	7.38 (1H, s)	116.9, CH _{arom}	C4→H1(³ J), H6(³ J)
5	-	129.5, C _q	C5→H1(² J), H2(³ J), H4(² J), H6(³ J)
6	8.94 (1H, d, $J = 1.3$ Hz)	133.6, CH _{arom}	C6→H4(³ J)
7	-	158.0, C _q	C7→H2(³ J), NH(² J)
8	-	172.3, C _q	C8→H1(³ J), H2(² J), H3(³ J), NH(³ J)
NH	6.71 (1H, d, $J = 8.1$ Hz)	-	-
NH ₂	5.75 (2H, s)	-	-

Note: The signal of carbon atom C6 is not visible in the ¹³C-NMR and was determined via the correlations within the HSQC and HMBC spectra.

6.3.1.1.17 Synthesis of (*S*)-methyl 4-(((*S*)-1-methoxy-1-oxo-3-phenylpropan-2-yl)amino)-4-oxo-3-ureidobutanoate (**261**)



Prepared according to *GP-I* using aspartame methyl ester hydrochloride **240** (0.82 g, 2.40 mmol, 1.00 eq.) and KOCN (0.20 g, 2.42 mmol, 1.02 eq.) in 4 ml of water. **261** was obtained as a colourless solid in a quantitative yield.

Yield: 0.59 g (1.69 mmol, 70%).

Appearance: Colourless solid.

IR: $\tilde{\nu}$ [cm^{-1}] = 3414 (w), 3374 (w), 3339 (w), 3284 (w), 3219 (w), 3027 (w), 2950 (w), 2359 (w), 2342 (w), 1749 (s), 1740 (s), 1731 (s), 1652 (vs), 1622 (w), 1549 (m), 1530 (m), 1496 (w), 1456 (w), 1439 (w), 1424 (w), 1396 (w), 1376 (w), 1366 (w), 1349 (w), 1310 (w), 1288 (w), 1268 (w), 1217 (w), 1203 (w), 1175 (w), 1159 (m), 1128 (w), 1078 (w), 1037 (w), 1030 (w), 1011 (w), 995 (w), 984 (w), 945 (w), 903 (w), 889 (w), 855 (w), 822 (w).

MP: 150 °C

HR-MS (ESI): Theor. $[\text{M}+\text{H}]^+$: 352.15031, found: 352.15054.

Theor. $[\text{M}+\text{Na}]^+$: 374.13225, found: 374.13223.

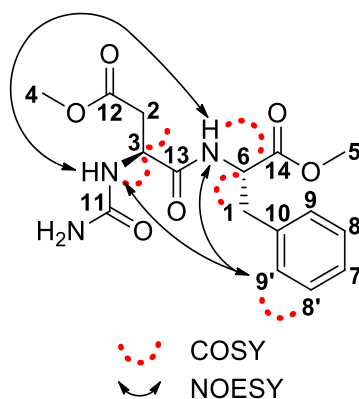
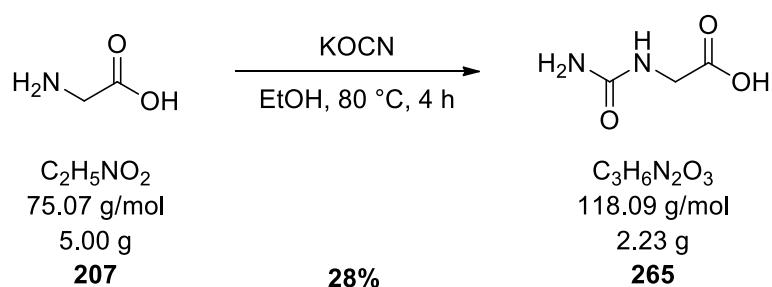


Table 33: 1D and 2D-NMR data of (*S*)-methyl 4-(((*S*)-1-methoxy-1-oxo-3-phenylpropan-2-yl)amino)-4-oxo-3-ureidobutanoate (261) in DMSO- d_6 , at 298 K and 500 MHz for ^1H and 125 MHz for ^{13}C .

No.	δ_{H} [ppm], J in [Hz]	δ_{C} [ppm], mult.	HMBC ($^{\times}J$)
1	2.94 (1H, dd, $J = 13.8, 8.3$ Hz); 3.01 (1H, dd, $J = 13.8, 5.7$ Hz)	36.6, CH_2	$\text{C1} \rightarrow \text{H6} (^2J), \text{H8} (^4J), \text{H9} (^3J), \text{NH}_{\text{amide}} (^3J)$
2	2.49 (1H, m); 2.60 (1H, dd, $J = 15.7, 5.6$ Hz)	36.9, CH_2	$\text{C2} \rightarrow \text{H3} (^2J), \text{NH} (^3J)$
3	4.47 (1H, m)	49.6, CH	$\text{C3} \rightarrow \text{H2} (^2J), \text{NH} (^2J), \text{NH}_2 (^4J)$
4	3.57 (3H, s)	51.4, CH_3	-
5	3.58 (3H, s)	51.9, CH_3	-
6	4.47 (1H, m)	53.6, CH	$\text{C6} \rightarrow \text{H1} (^2J), \text{NH}_{\text{amide}} (^2J)$
7	7.21 (1H, m)	126.6, CH_{arom}	$\text{C7} \rightarrow \text{H8} (^2J), \text{H9} (^3J)$
8	7.28 (2H, m)	128.3, $2 \times \text{CH}_{\text{arom}}$	$\text{C8} \rightarrow \text{H8} (^3J)$
9	7.20 (2H, m)	129.1, $2 \times \text{CH}_{\text{arom}}$	$\text{C9} \rightarrow \text{H1} (^3J), \text{H7} (^3J), \text{H9} (^3J)$
10	-	137.0, C_q	$\text{C10} \rightarrow \text{H1} (^2J), \text{H6} (^3J), \text{H8} (^3J)$
11	-	158.1, C_q	$\text{C11} \rightarrow \text{H3} (^3J), \text{NH} (^2J)$
12	-	170.7, C_q	$\text{C12} \rightarrow \text{H2} (^2J), \text{H3} (^3J), \text{H4} (^3J)$
13	-	171.3, C_q	$\text{C13} \rightarrow \text{H2} (^3J), \text{H3} (^2J), \text{NH} (^3J), \text{NH}_{\text{amide}} (^2J)$
14	-	171.6, C_q	$\text{C14} \rightarrow \text{H1} (^3J), \text{H5} (^3J), \text{H6} (^2J)$
NH	6.30 (1H, d, $J = 8.6$ Hz)	-	-
NH_2	5.72 (2H, s)	-	-
NH_{amide}	8.26 (1H, d, $J = 7.7$ Hz)	-	-

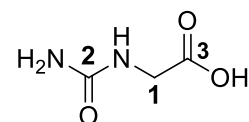
6.3.1.2 Ureido carboxylic acids

6.3.1.2.1 Synthesis of 2-ureidoacetic acid (265)



Prepared according to *GP-IIIb* using glycine **207** (5.00 g, 66.6 mmol, 1.00 eq.) and KOCN (5.51 g, 67.9 mmol, 1.02 eq.) in 250 ml of EtOH. **265** was obtained as a colourless solid in a yield of 28%.

Yield: 2.23 g (18.9 mmol, 28%).



Appearance: Colourless solid.

Table 34: 1D and 2D-NMR data of 2-ureidoacetic acid (265) in DMSO- d_6 , at 298 K and 500 MHz for ^1H and 125 MHz for ^{13}C .

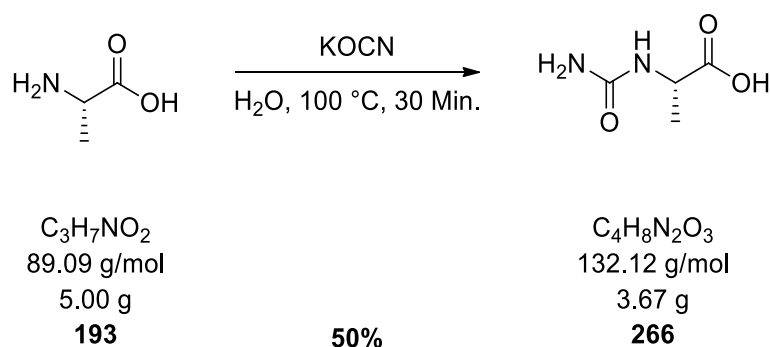
No.	δ_{H} [ppm], J in [Hz]	δ_{C} [ppm], mult.	HMBC ($^{\circ}\text{J}$)
1	3.24 (2H, d, $J = 4.1$ Hz)	30.6, CH_2	-
2	-	158.4, C_q	$\text{C}2 \rightarrow \text{H}1$ (^3J)
3	-	not detectable	not detectable
NH	5.71 (1H, br)	-	-
NH_2	5.44 (2H, s)	-	-

Note: With the exception of D_2O it was not possible to completely dissolve the product in any deuterated solvent. Since the spectrum with D_2O showed no visible product signals, the spectrum with $\text{DMSO-}d_6$ as solvent was used for analysis. The solubility and signal intensity of the product were very low.

IR: $\tilde{\nu}$ [cm^{-1}] = 3478 (w), 3273 (w), 3168 (w), 2930 (w), 2857 (w), 2364 (w), 2342 (w), 1652 (s), 1634 (s), 1617 (m), 1577 (m), 1538 (s), 1458 (w), 1412 (vs), 1358 (w), 1278 (m), 1236 (w), 1170 (w), 1137 (w), 1089 (m), 1019 (m), 994 (w), 967 (w), 936 (w), 916 (w), 895 (w), 875 (w), 855 (w), 844 (w), 824 (w), 814 (w).

MP: 240 $^\circ\text{C}$.

HR-MS (ESI): Theor. $[\text{M}+\text{H}]^+$: 117.03056, found: 117.03092.

6.3.1.2.2 Synthesis of (*S*)-2-ureidopropanoic acid (**266**)

Prepared according to *GP-IIa* using L-alanine **193** (5.00 g, 56.1 mmol, 1.00 eq.) and KOCN (4.64 g, 57.2 mmol, 1.02 eq.) in 25 ml of water. **266** was obtained as a colourless solid in a yield of 50%.

Yield: 3.67 g (27.8 mmol, 50%).

Appearance: Colourless solid.

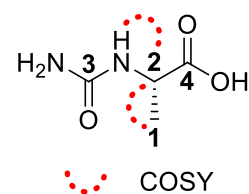


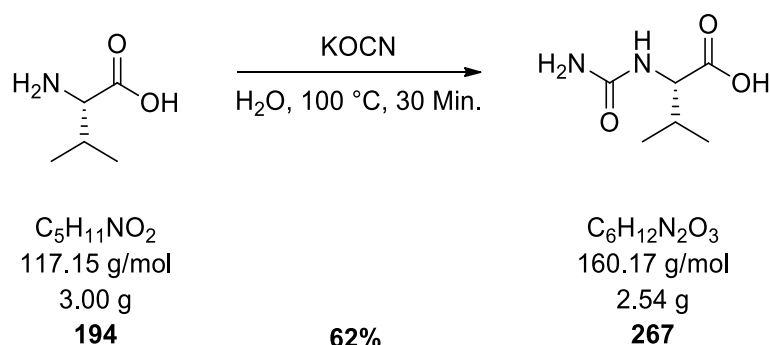
Table 35: 1D and 2D-NMR data of (*S*)-2-ureidopropanoic acid (**266**) in DMSO- d_6 , at 298 K and 500 MHz for ^1H and 125 MHz for ^{13}C .

No.	δ_{H} [ppm], J in [Hz]	δ_{C} [ppm], mult.	HMBC ($^{\circ}\text{J}$)
1	1.22 (3H, d, $J = 7.2$ Hz).	18.4, CH_3	$\text{C1} \rightarrow \text{H2} (^2\text{J}), \text{NH} (^3\text{J})$
2	4.05 (1H, quin, $J = 7.3$ Hz)	48.0, CH	$\text{C2} \rightarrow \text{H1} (^2\text{J}), \text{NH} (^2\text{J})$
3	-	158.2, C_q	$\text{C3} \rightarrow \text{H2} (^3\text{J}), \text{NH} (^2\text{J})$
4	-	175.3, C_q	$\text{C4} \rightarrow \text{H1} (^3\text{J}), \text{H2} (^2\text{J}), \text{NH} (^3\text{J})$
NH	6.24 (1H, d, $J = 7.7$ Hz)	-	-
NH_2	5.59 (2H, s)	-	-
COOH	12.48 (1H, s)	-	-

IR: $\tilde{\nu}$ [cm^{-1}] = 3455 (m), 3310 (m), 2360 (w), 1922 (br), 1681 (m), 1631 (m), 1573 (vs), 1408 (m), 1379 (w), 1302 (s), 1186 (s), 1120 (w), 1066 (m), 1008 (s), 934 (w), 846 (m).

MP: 192 $^\circ\text{C}$.

HR-MS (ESI): Theor. $[\text{M}+\text{H}]^+$: 133.06076, found: 133.06075.
Theor. $[\text{M}+\text{Na}]^+$: 155.04271, found: 155.04272.

6.3.1.2.3 Synthesis of (*S*)-3-methyl-2-ureidobutanoic acid (**267**)

Prepared according to *GP-IIa* using L-valine **194** (3.00 g, 25.6 mmol, 1.00 eq.) and KOCN (2.12 g, 26.1 mmol, 1.02 eq.) in 18 ml of water. **267** was obtained as a colourless solid in a yield of 62%.

Yield: 2.54 g (15.9 mmol, 62%).

Appearance: Colourless solid.

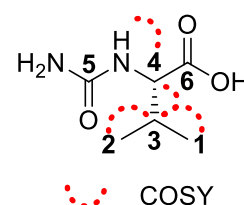


Table 36: 1D and 2D-NMR data of (*S*)-3-methyl-2-ureidobutanoic acid (**267**) in DMSO- d_6 , at 298 K and 500 MHz for ^1H and 125 MHz for ^{13}C .

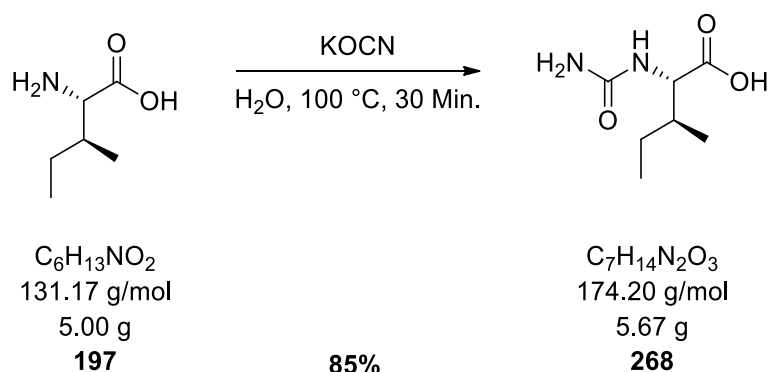
No.	δ_{H} [ppm], J in [Hz]	δ_{C} [ppm], mult.	HMBC ($^{\circ}\text{J}$)
1	0.83 (3H, d, $J = 6.8$ Hz).	17.7, CH_3	$\text{C1} \rightarrow \text{H2} (^3\text{J}), \text{H3} (^2\text{J}), \text{H4} (^3\text{J})$
2	0.87 (3H, d, $J = 6.8$ Hz)	19.2, CH_3	$\text{C2} \rightarrow \text{H1} (^3\text{J}), \text{H3} (^2\text{J}), \text{H4} (^3\text{J})$
3	2.00 (1H, pd, $J = 6.9, 5.0$ Hz)	30.3, CH	$\text{C3} \rightarrow \text{H1} (^2\text{J}), \text{H2} (^2\text{J}), \text{H4} (^2\text{J}), \text{NH} (^3\text{J})$
4	4.00 (1H, dd, $J = 9.0, 5.0$ Hz)	57.3, CH	$\text{C4} \rightarrow \text{H1} (^3\text{J}), \text{H2} (^3\text{J}), \text{NH} (^2\text{J})$
5	-	158.6, C_q	$\text{C5} \rightarrow \text{H4} (^3\text{J}), \text{NH} (^2\text{J})$
6	-	174.2, C_q	$\text{C6} \rightarrow \text{H3} (^3\text{J}), \text{H4} (^2\text{J}), \text{NH} (^3\text{J})$
NH	6.16 (1H, d, $J = 9.0$ Hz)	-	-
NH_2	5.60 (2H, s)	-	-
COOH	12.49 (1H, s)	-	-

IR: $\tilde{\nu}$ [cm^{-1}] = 3684 (m), 3675 (m), 3450 (w), 3293 (w), 2988 (s), 2972 (s), 2901 (s), 1923 (br), 1683 (m), 1682 (m), 1559 (m), 1451 (w), 1469 (w), 1406 (m), 1394 (m), 1387 (m), 1308 (w), 1288 (w), 1250 (w), 1242 (w), 1230 (w), 1176 (w), 1164 (w), 1075 (vs), 1066 (vs), 1057 (vs), 1028 (s), 898 (w), 880 (w).

MP: 213 °C.

HR-MS (ESI): Theor. $[\text{M}+\text{H}]^+$: 161.09207, found: 161.09212.

Theor. $[\text{M}+\text{Na}]^+$: 183.07401, found: 183.07416.

6.3.1.2.4 Synthesis of (2*S*,3*S*)-3-methyl-2-ureidopentanoic acid (**268**)

Prepared according to *GP-IIa* using L-isoleucine **197** (5.00 g, 38.1 mmol, 1.00 eq.) and KOCN (3.16 g, 38.9 mmol, 1.02 eq.) in 25 ml of water. **268** was obtained as a colourless solid in a yield of 85%.

Yield: 5.67 g (32.5 mmol, 85%).

Appearance: Colourless solid.

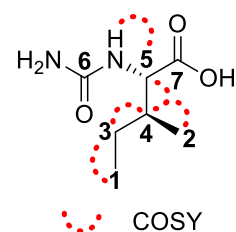


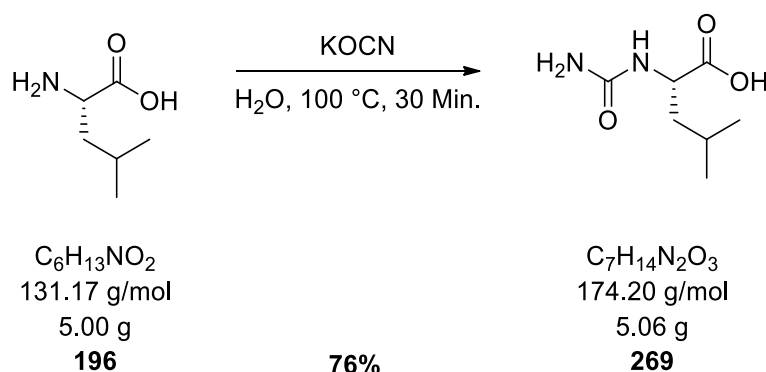
Table 37: 1D and 2D-NMR data of (2*S*,3*S*)-3-methyl-2-ureidopentanoic acid (**268**) in DMSO- d_6 , at 298 K and 500 MHz for ^1H and 125 MHz for ^{13}C .

No.	δ_{H} [ppm], J in [Hz]	δ_{C} [ppm], mult.	HMBC ($^{\times}J$)
1	0.85 (3H, m).	11.5, CH ₃	C1→H3(2J), H4(3J)
2	0.84 (3H, m)	15.7, CH ₃	C2→H3(3J), H4(2J), H5(3J)
3	1.12 (1H, m); 1.37 (1H, dqd, $J = 14.8, 7.5, 4.6$ Hz)	24.6, CH ₂	C3→H1(2J), H2(3J), H4(2J), H5(3J)
4	1.71 (1H, ddq, $J = 15.3, 7.2, 4.8$ Hz)	37.1, CH	C4→H1(3J), H2(2J), H3(2J), H5(2J), NH(3J)
5	4.04 (1H, dd, $J = 9.0, 5.3$ Hz)	56.6, CH	C5→H2(3J), H3(3J), H4(2J), NH(2J), NH ₂ (4J)
6	-	158.4, C _q	C6→H5(3J), NH(2J)
7	-	174.2, C _q	C7→H4(3J), H5(2J), NH(3J)
NH	6.16 (1H, d, $J = 9.0$ Hz)	-	-
NH ₂	5.58 (2H, s)	-	-
COOH	12.47 (1H, s)	-	-

IR: $\tilde{\nu}$ [cm⁻¹] = 3685 (m), 3676 (m), 3448 (w), 3293 (w), 2988 (s), 2972 (s), 2901 (s), 1923 (br), 1683 (m), 1634 (m), 1558 (m), 1454 (w), 1405 (w), 1394 (m), 1383 (m), 1308 (m), 1288 (m), 1241 (w), 1229 (w), 1169 (w), 1075 (vs), 1066 (vs), 1057 (vs), 1028 (s), 946 (w), 899 (w).

MP: 207 °C.

HR-MS (ESI): Theor.[M-H]⁻: 173.09316, found: 173.09362.

6.3.1.2.5 Synthesis of (S)-4-methyl-2-ureidopentanoic acid (**269**)

Prepared according to *GP-IIa* using L-leucine **196** (5.00 g, 38.1 mmol, 1.00 eq.) and KOCN (3.15 g, 38.9 mmol, 1.02 eq.) in 25 ml of water. **269** was obtained as a colourless solid in a yield of 76%.

Yield: 5.06 g (29.0 mmol, 76%).

Appearance: Colourless solid.

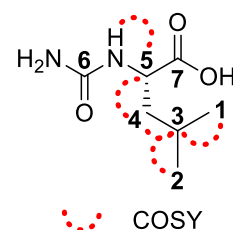


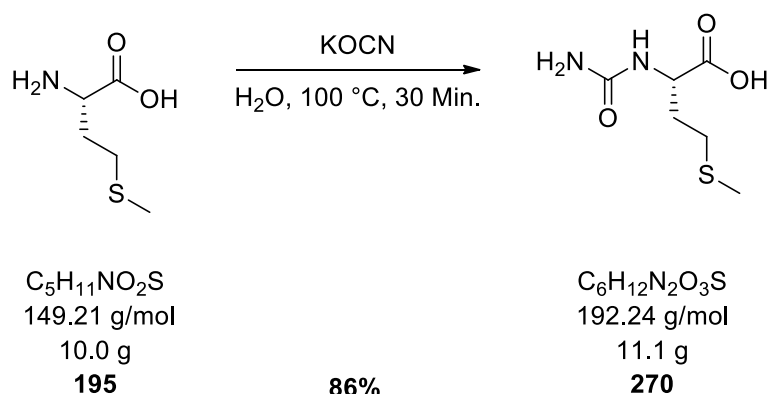
Table 38: 1D and 2D-NMR data of (S)-4-methyl-2-ureidopentanoic acid (**269**) in DMSO- d_6 , at 298 K and 500 MHz for ^1H and 125 MHz for ^{13}C .

No.	δ_{H} [ppm], J in [Hz]	δ_{C} [ppm], mult.	HMBC ($^{\circ}\text{J}$)
1	0.86 (3H, d, $J = 6.6$ Hz)	21.6, CH_3	$\text{C1} \rightarrow \text{H2} (^3\text{J}), \text{H3} (^2\text{J}), \text{H4} (^3\text{J})$
2	0.89 (3H, d, $J = 6.7$ Hz)	22.9, CH_3	$\text{C2} \rightarrow \text{H1} (^3\text{J}), \text{H3} (^2\text{J}), \text{H4} (^3\text{J})$
3	1.64 (1H, ddq, $J = 12.9, 8.2, 6.5$ Hz)	24.3, CH	$\text{C3} \rightarrow \text{H1} (^2\text{J}), \text{H2} (^2\text{J}), \text{H4} (^2\text{J}), \text{H5} (^3\text{J})$
4	1.43 (2H, m)	41.1, CH_2	$\text{C4} \rightarrow \text{H1} (^3\text{J}), \text{H2} (^3\text{J}), \text{H3} (^2\text{J}), \text{H5} (^2\text{J}), \text{NH} (^3\text{J})$
5	4.07 (1H, td, $J = 9.2, 5.3$ Hz)	50.7, CH	$\text{C5} \rightarrow \text{H3} (^3\text{J}), \text{H4} (^2\text{J}), \text{NH} (^2\text{J}), \text{NH}_2 (^4\text{J})$
6	-	158.4, C_q	$\text{C6} \rightarrow \text{H5} (^3\text{J}), \text{NH} (^2\text{J})$
7	-	175.3, C_q	$\text{C7} \rightarrow \text{H4} (^3\text{J}), \text{H5} (^2\text{J}), \text{NH} (^3\text{J})$
NH	6.17 (1H, d, $J = 8.5$ Hz)	-	-
NH_2	5.54 (2H, s)	-	-
COOH	12.41 (1H, s)	-	-

IR: $\tilde{\nu}$ [cm^{-1}] = 3684 (w), 3678 (m), 3458 (m), 3305 (m), 2988 (vs), 2972 (vs), 2901 (s), 1924 (br), 1684 (m), 1634 (m), 1570 (m), 1472 (w), 1451 (w), 1407 (m), 1394 (m), 1385 (m), 1317 (m), 1302 (m), 1260 (m), 1242 (w), 1228 (m), 1175 (m), 1075 (vs), 1066 (vs), 1057 (vs), 1028 (s), 922 (w), 892 (w), 880 (w), 866 (w), 827 (w).

MP: 206 $^\circ\text{C}$.

HR-MS (ESI): Theor. $[\text{M}-\text{H}]^-$: 173.09316, found: 173.09364.

6.3.1.2.6 Synthesis of (*S*)-4-(methylthio)-2-ureidobutanoic acid (**270**)

Prepared according to *GP-IIa* using L-methionine **195** (10.0 g, 67.0 mmol, 1.00 eq.) and KOCN (5.54 g, 68.3 mmol, 1.02 eq.) in 50 ml of water. **270** was obtained as a colourless solid in a yield of 86%.

Yield: 11.1 g (57.7 mmol, 86%).

Appearance: Colourless solid.

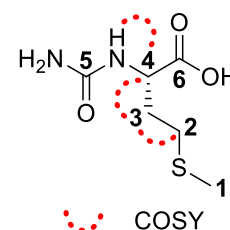


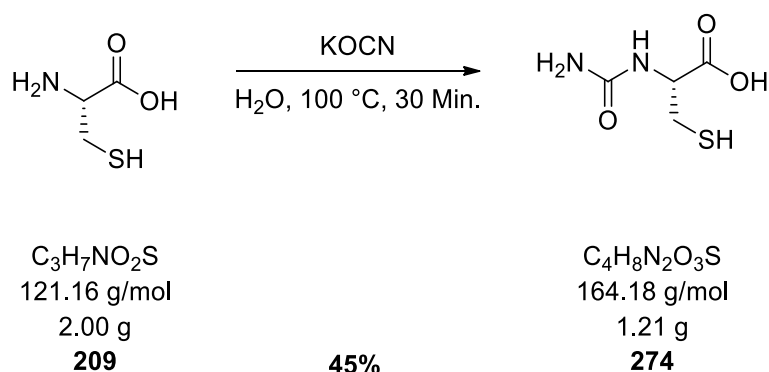
Table 39: 1D and 2D-NMR data of (*S*)-4-(methylthio)-2-ureidobutanoic acid (**270**) in DMSO- d_6 , at 298 K and 500 MHz for ^1H and 125 MHz for ^{13}C .

No.	δ_{H} [ppm], J in [Hz]	δ_{C} [ppm], mult.	HMBC ($^{\circ}\text{J}$)
1	2.04 (3H, s)	14.6, CH ₃	C1→H2(^3J)
2	2.46 (2H, t, $J = 7.6$ Hz)	29.6, CH ₂	C2→H1(^3J), H3(^2J), H4(^3J)
3	1.77 (1H, m); 1.92 (1H, m)	31.8, CH ₂	C3→H2(^2J), H4(^2J), NH(^3J)
4	4.16 (1H, td, $J = 8.4, 4.7$ Hz)	51.5, CH	C4→H2(^3J), H3(^2J), NH(^3J), NH ₂ (^4J)
5	-	158.4, C _q	C5→H4(^3J), NH(^2J)
6	-	174.4, C _q	C6→H3(^3J), H4(^2J), NH(^3J)
NH	6.29 (1H, d, $J = 8.3$ Hz)	-	-
NH ₂	5.59 (2H, s)	-	-
COOH	12.57 (1H, s)	-	-

IR: $\tilde{\nu}$ [cm^{-1}] = 3458 (m), 3285 (m), 2952 (w), 2921 (w), 2367 (br), 1920 (br), 1684 (s), 1628 (s), 1553 (s), 1447 (w), 1406 (w), 1334 (w), 1305 (s), 1293 (s), 1203 (m), 1193 (m), 1139 (w), 1105 (w), 1012 (w), 993 (w), 982 (w), 972 (w), 957 (w), 937 (w), 902(w), 885 (w), 867 (w), 859 (w), 825 (w), 809 (w).

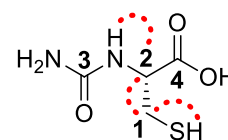
MP: 165 °C.

HR-MS (ESI): Theor.[M-H]⁻: 191.04958, found: 191.04989.

6.3.1.2.7 Synthesis of (*R*)-3-mercapto-2-ureidopropanoic acid (**274**)

Prepared according to *GP-IIIa* using L-cysteine **209** (2.00 g, 16.5 mmol, 1.00 eq.) and KOCN (1.37 g, 16.8 mmol, 1.02 eq.) in 10 ml of water. **274** was obtained as a colourless solid in a yield of 45%.

Yield: 1.21 g (7.37 mmol, 45%).



COSY

Appearance: Colourless solid.

Table 40: 1D and 2D-NMR data of (*R*)-3-mercapto-2-ureidopropanoic acid (**274**) in DMSO-*d*₆, at 298 K and 499 MHz for ¹H and 125 MHz for ¹³C.

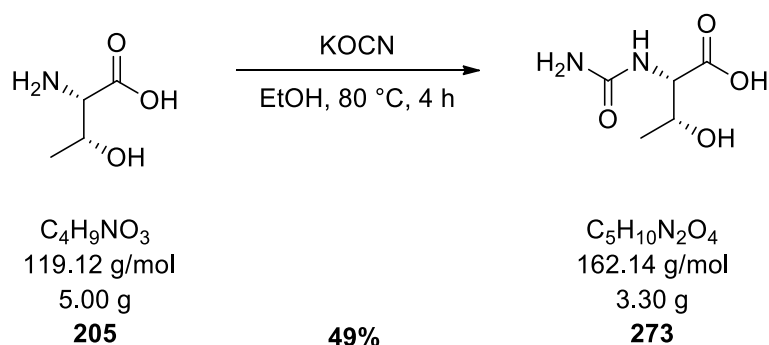
No.	δ_{H} [ppm], <i>J</i> in [Hz]	δ_{C} [ppm], mult.	HMBC ($^{\times}$ J)
1	2.81 (2H, m)	26.8, CH ₂	C1→H2(² J), NH(³ J), SH(² J)
2	4.34 (1H, dt, <i>J</i> = 7.9, 5.1 Hz)	54.2, CH	C2→H1(² J), NH(² J), NH ₂ (⁴ J), SH(³ J)
3	-	158.0, C _q	C3→H2(³ J), NH(² J)
4	-	172.5, C _q	C4→H1(³ J), H2(² J), NH(³ J)
NH	6.35 (1H, d, <i>J</i> = 8.0 Hz)	-	-
NH ₂	5.74 (2H, s)	-	-
SH	2.19 (1H, t, <i>J</i> = 8.3 Hz)	-	-
COOH	12.83 (1H, s)	-	-

IR: $\tilde{\nu}$ [cm⁻¹] = 3441 (m), 3337 (m), 3243 (w), 3008 (w), 2908 (w), 2727 (w), 2548 (m), 2442 (w), 2360 (m), 2342 (m), 1895 (br), 1683 (s), 1635 (s), 1538 (vs), 1456 (s), 1423 (m), 1398 (m), 1314 (m), 1297 (w), 1248 (vs), 1239 (vs), 1205 (m), 1160 (w), 1112 (w), 1051 (w), 1020 (s), 935 (w), 910 (w), 866 (w), 855 (w), 831 (w).

MP: 177 °C.

HR-MS (ESI): Theor.[M+H]⁺: 165.03283, found: 165.03296.

Theor.[M+Na]⁺: 187.01478, found: 187.01498.

6.3.1.2.8 Synthesis of (2*S*,3*R*)-3-hydroxy-2-ureidobutanoic acid (**273**)

Prepared according to *GP-IIIb* using L-threonine **205** (5.00 g, 42.0 mmol, 1.00 eq.) and KOCN (3.47 g, 42.8 mmol, 1.02 eq.) in 250 ml of EtOH. **273** was obtained as a colourless solid in a yield of 49%.

Yield: 3.30 g (20.4 mmol, 49%).

Appearance: Colourless solid.

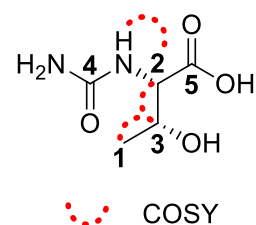


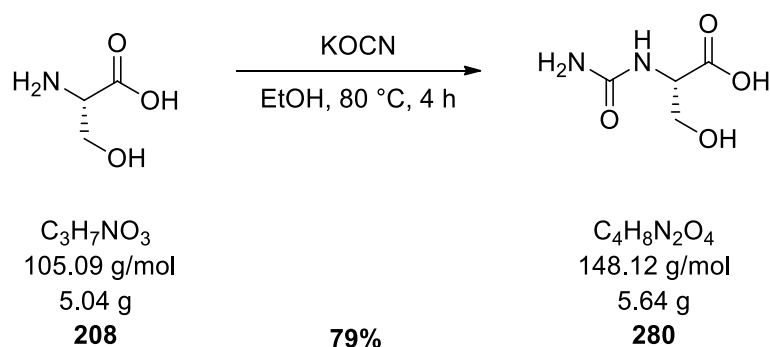
Table 41: 1D and 2D-NMR data of (2*S*,3*R*)-3-hydroxy-2-ureidobutanoic acid (**273**) in DMSO-*d*₆, at 298 K and 400 MHz for ¹H and 100 MHz for ¹³C.

No.	δ_{H} [ppm], <i>J</i> in [Hz]	δ_{C} [ppm], mult.	HMBC ($^{\circ}\text{J}$)
1	0.87 (3H, d, <i>J</i> = 6.3 Hz)	18.6, CH ₃	C1→H2(³ J), H3(² J)
2	3.66 (1H, dd, <i>J</i> = 5.6, 4.6 Hz)	57.5, CH	C2→H1(³ J), H3(² J), NH(² J)
3	3.76 (1H, qd, <i>J</i> = 6.2, 4.6 Hz)	66.7, CH	C3→H1(² J), H2(² J), NH(³ J)
4	-	158.4, C _q	C4→H2(³ J), NH(² J)
5	-	173.2, C _q	C5→H2(² J), H3(³ J), NH(³ J)
NH	5.96 (1H, d, <i>J</i> = 5.6 Hz)	-	-
NH ₂	5.54 (2H, s)	-	-

IR: $\tilde{\nu}$ [cm⁻¹] = 3379 (br), 3205 (br), 2971 (w), 2928 (w), 2360 (w), 2343 (w), 1644 (s), 1587 (vs), 1558 (s), 1475 (w), 1449 (m), 1393 (s), 1339 (w), 1282 (m), 1243 (w), 1189 (w), 1119 (s), 1092 (w), 1066 (w), 1040 (w), 989 (w), 931 (w), 872 (m), 833 (w), 803 (w).

MP: 173 °C.

HR-MS (ESI): Theor.[M-H]⁻: 161.05678, found: 161.05720.

6.3.1.2.9 Synthesis of (*S*)-3-hydroxy-2-ureidopropanoic acid (**280**)

Prepared according to *GP-IIb* using L-serine **208** (5.04 g, 48.0 mmol, 1.00 eq.) and KOCN (3.97 g, 49.0 mmol, 1.02 eq.) in 250 ml of EtOH. **280** was obtained as a colourless solid in a yield of 79%.

Yield: 5.64 g (38.1 mmol, 79%).

Appearance: Colourless solid.

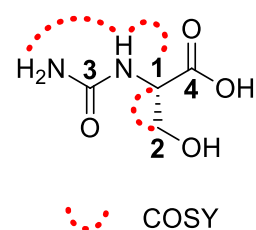


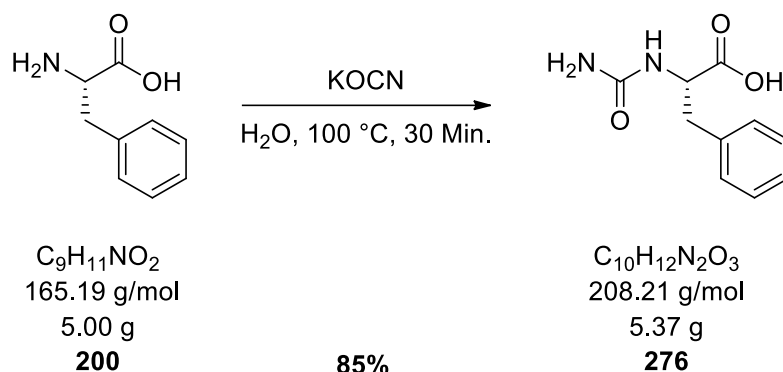
Table 42: 1D and 2D-NMR data of (*S*)-3-hydroxy-2-ureidopropanoic acid (**280**) in DMSO- d_6 , at 298 K and 500 MHz for ^1H and 125 MHz for ^{13}C .

No.	δ_{H} [ppm], J in [Hz]	δ_{C} [ppm], mult.	HMBC ($^{\circ}\text{J}$)
1	3.51 (1H, m)	55.1, CH	C1 \rightarrow H2(^2J)
2	3.24 (1H, m); 3.49 (1H, m)	64.7, CH ₂	C2 \rightarrow H1(^2J)
3	-	159.1, C _q	-
4	-	173.2, C _q	C4 \rightarrow H1(^2J), H2(^3J)
NH	6.04 (1H, br)	-	-
NH ₂	5.67 (2H, s)	-	-

IR: $\tilde{\nu}$ [cm^{-1}] = 3391 (m), 3217 (br), 3059 (w), 2981 (w), 2941 (w), 2359 (w), 2344 (w), 1627 (s), 1585 (vs), 1553 (vs), 1449 (w), 1418 (s), 1368 (m), 1356 (w), 1301 (vs), 1275 (w), 1247 (m), 1169 (w), 1101 (s), 1039 (m), 1000 (w), 945 (w), 919 (w), 891 (w), 870 (w), 829 (w).

MP: 183 $^\circ\text{C}$.

HR-MS (ESI): Theor.[M-H]⁻: 147.04113, found: 147.04149.

6.3.1.2.10 Synthesis of (*S*)-3-phenyl-2-ureidopropanoic acid (**276**)

Prepared according to *GP-IIa* using L-phenylalanine **200** (5.00 g, 30.3 mmol, 1.00 eq.) and KOCN (2.51 g, 30.9 mmol, 1.02 eq.) in 30 ml of water. **276** was obtained as a colourless solid in a yield of 85%.

Yield: 5.37 g (25.8 mmol, 85%).

Appearance: Colourless solid.

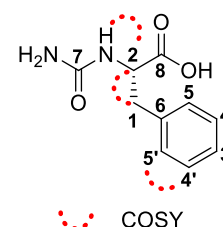


Table 43: 1D and 2D-NMR data of (*S*)-3-phenyl-2-ureidopropanoic acid (**276**) in DMSO- d_6 , at 298 K and 500 MHz for ^1H and 125 MHz for ^{13}C .

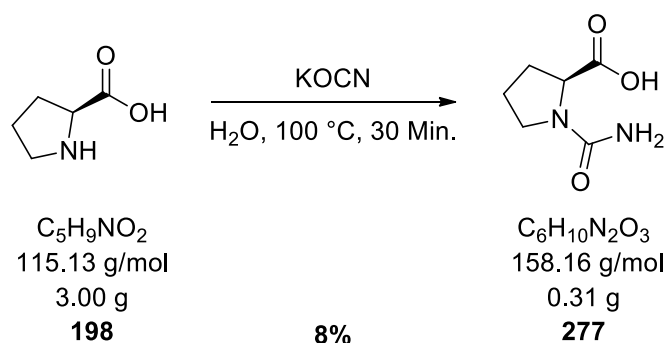
No.	δ_{H} [ppm], J in [Hz]	δ_{C} [ppm], mult.	HMBC ($^{\circ}\text{J}$)
1	2.85 (1H, dd, $J = 13.8, 7.9$ Hz); 2.99 (1H, dd, $J = 13.7, 5.2$ Hz);	37.6, CH_2	$\text{C1} \rightarrow \text{H2} (^2\text{J}), \text{H5} (^3\text{J}), \text{NH} (^3\text{J})$
2	4.33 (1H, td, $J = 8.0, 5.1$ Hz)	53.7, CH	$\text{C2} \rightarrow \text{H1} (^2\text{J}), \text{NH} (^2\text{J}), \text{NH}_2 (^4\text{J})$
3	7.21 (1H, m)	126.4, CH_{arom}	$\text{C3} \rightarrow \text{H5} (^3\text{J})$
4	7.28 (2H, m)	128.2, $2 \times \text{CH}_{\text{arom}}$	$\text{C4} \rightarrow \text{H4} (^3\text{J})$
5	7.19 (2H, m)	129.3, $2 \times \text{CH}_{\text{arom}}$	$\text{C5} \rightarrow \text{H1} (^3\text{J}), \text{H3} (^3\text{J}), \text{H5} (^3\text{J})$
6	-	137.6, C_{q}	$\text{C6} \rightarrow \text{H1} (^2\text{J}), \text{H2} (^3\text{J}), \text{H3} (^4\text{J}), \text{H4} (^3\text{J})$
7	-	158.2, C_{q}	$\text{C7} \rightarrow \text{H2} (^3\text{J}), \text{NH} (^2\text{J})$
8	-	174.0, C_{q}	$\text{C8} \rightarrow \text{H1} (^3\text{J}), \text{H2} (^2\text{J}), \text{NH} (^3\text{J})$
NH	6.16 (1H, s, $J = 8.3$ Hz)	-	-
NH_2	5.62 (2H, s)	-	-
COOH	12.64 (1H, s)	-	-

IR: $\tilde{\nu}$ [cm^{-1}] = 3450 (br), 3301 (br), 2361 (m), 2344 (m), 1910 (br), 1684 (s), 1636 (s), 1561 (vs), 1498 (w), 1456 (w), 1435 (w), 1403 (m), 1302 (s), 1258 (s), 1211 (w), 1159 (m), 1104 (w), 1079 (w), 1029 (w), 1015 (w), 1000 (w), 977 (w), 937 (w), 912 (w), 869 (w), 839 (m).

MP: 188 °C.

HR-MS (ESI): Theor. $[\text{M}+\text{H}]^+$: 209.09206, found: 209.09226.

Theor. $[\text{M}+\text{Na}]^+$: 231.07401, found: 231.07415.

6.3.1.2.11 Synthesis of (*S*)-1-carbamoylpyrrolidine-2-carboxylic acid (**277**)

Prepared according to *GP-IIa* using L-proline **198** (3.00 g, 26.1 mmol, 1.00 eq.) and KOCN (2.16 g, 26.6 mmol, 1.02 eq.) in 15 ml of water. **277** was obtained as a colourless solid in a yield of 8%.

Yield: 0.31 g (1.96 mmol, 8%).

Appearance: Colourless solid.

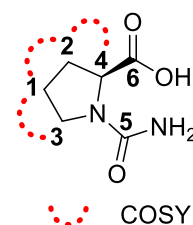


Table 44: 1D and 2D-NMR data of (*S*)-1-carbamoylpyrrolidine-2-carboxylic acid (**277**) in DMSO- d_6 , at 298 K and 500 MHz for ^1H and 125 MHz for ^{13}C .

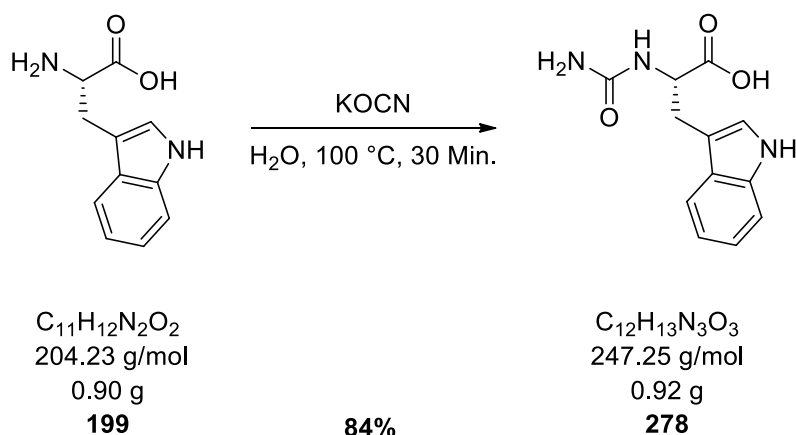
No.	δ_{H} [ppm], J in [Hz]	δ_{C} [ppm], mult.	HMBC ($^{\times}J$)
1	1.85 (2H, m)	24.2, CH ₂	C1→H2(² J), H3(² J), H4(³ J)
2	1.85 (1H, m); 2.08 (1H, m)	29.3, CH ₂	C2→H1(² J), H3(³ J), H4(² J)
3	3.25 (1H, m); 3.32 (1H, m)	46.1, CH ₂	C3→H1(² J), H2(³ J), H4(³ J)
4	4.15 (1H, dd, $J = 8.4, 2.6$ Hz)	58.4, CH	C4→H1(³ J), H2(² J), H3(³ J)
5	-	157.4, C _q	C5→H4(³ J)
6	-	174.5, C _q	C6→H1(⁴ J), H2(³ J), H4(² J)
NH ₂	5.89 (2H, s)	-	-
COOH	12.42 (1H, s)	-	-

IR: $\tilde{\nu}$ [cm⁻¹] = 3687 (m), 3675 (m), 3413 (br), 3225 (br), 2988 (s), 2972 (s), 2901 (s), 1917 (w), 1747 (w), 1683 (w), 1651 (m), 1521 (m), 1456 (w), 1406 (w), 1394 (w), 1384 (w), 1356 (w), 1315 (w), 1302 (w), 1250 (w), 1242 (w), 1230 (w), 1200 (w), 1148 (w), 1077 (vs), 1066 (vs), 1056 (vs), 1028 (s), 892 (w), 879 (w), 825 (w).

MP: 210 °C.

HR-MS (ESI): Theor.[M+H]⁺: 159.07641, found: 159.07641.

Theor.[M+Na]⁺: 181.05836, found: 181.05848.

6.3.1.2.12 Synthesis of (S)-3-(1H-indol-3-yl)-2-ureidopropanoic acid (**278**)

Prepared according to *GP-IIa* using L-tryptophan **199** (0.90 g, 4.41 mmol, 1.00 eq.) and KOCN (0.36 g, 4.49 mmol, 1.02 eq.) in 5 ml of water. **278** was obtained as a colourless solid in a yield of 84%.

Yield: 0.92 g (3.72 mmol, 84%).

Appearance: Colourless solid.

IR: $\tilde{\nu}$ [cm^{-1}] = 3421 (m), 3393 (m), 3382 (m), 3227 (br), 1889 (br), 1699 (w), 1645 (s), 1540 (s), 1456 (w), 1429 (w), 1402 (w), 1359 (w), 1341 (w), 1290 (w), 1251 (m), 1233 (w), 1218 (w), 1196 (w), 1164 (w), 1096 (w), 1062 (w), 1011 (w), 993 (br), 931 (w), 884 (w), 832 (w).

MP: 190 °C.

HR-MS (ESI): Theor. $[\text{M}+\text{H}]^+$: 248.10296, found: 248.10305.
 Theor. $[\text{M}+\text{Na}]^+$: 270.08491, found: 270.08504.

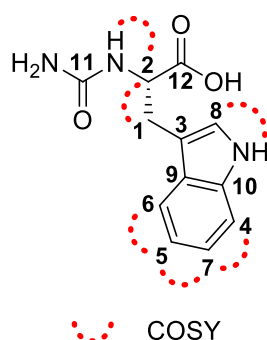
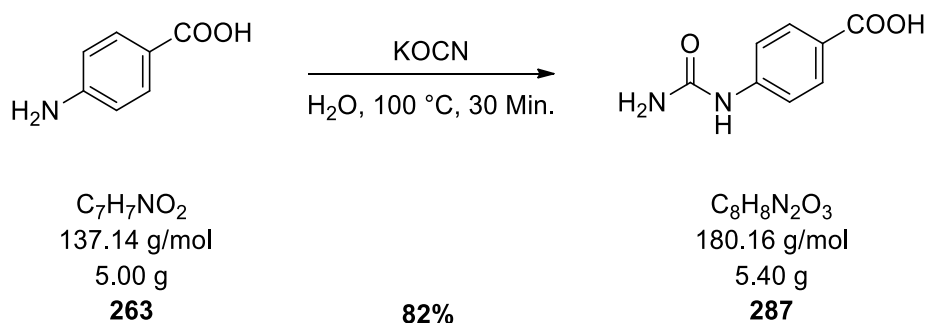


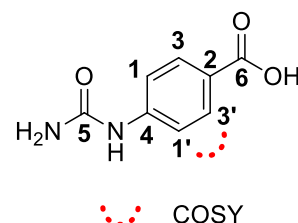
Table 45: 1D and 2D-NMR data of (*S*)-3-(1*H*-indol-3-yl)-2-ureidopropanoic acid (278) in DMSO-*d*₆, at 298 K and 500 MHz for ¹H and 125 MHz for ¹³C.

No.	δ_{H} [ppm], J in [Hz]	δ_{C} [ppm], mult.	HMBC ($^{\circ}\text{J}$)
1	3.02 (1H, dd, $J = 14.6, 7.0$ Hz); 3.11 (1H, dd, $J = 14.6, 5.2$ Hz)	27.9, CH ₂	C1→H2(² J), H8(³ J), NH(³ J)
2	4.39 (1H, td, $J = 7.3, 5.4$ Hz)	53.2, CH	C2→H1(² J), NH(² J), NH ₂ (⁴ J)
3	-	109.7, C _q	C3→H1(² J), H2(³ J), H6(³ J), H8(² J), NH _{arom} (³ J)
4	7.33 (1H, d, $J = 8.2$ Hz)	111.3, CH _{arom}	C4→H5(³ J)
5	6.97 (1H, m)	118.37, CH _{arom}	C5→H4(³ J)
6	7.52 (1H, d, $J = 7.9$ Hz)	118.41, CH _{arom}	C6→H7(³ J)
7	7.06 (1H, m)	120.9, CH _{arom}	C7→H5(² J), H6(³ J)
8	7.10 (1H, d, $J = 2.3$ Hz)	123.6, CH _{arom}	C8→H1(³ J), NH _{arom} (² J)
9	-	127.5, C _q	C9→H1(³ J), H4(³ J), H5(³ J), H6(² J), H8(³ J), NH _{arom} (³ J)
10	-	136.1, C _q	C10→H6(³ J), H7(³ J), H8(³ J), NH _{arom} (² J)
11	-	158.2, C _q	C11→H2(³ J), NH(² J)
12	-	174.4, C _q	C12→H1(³ J), H2(² J), NH(³ J)
NH	6.13 (1H, d, $J = 8.0$ Hz)	-	-
NH ₂	5.63 (2H, s)	-	-
NH _{arom}	10.86 (1H, s)	-	-
COOH	12.54 (1H, s)	-	-

6.3.1.2.13 Synthesis of 4-ureidobenzoic acid (**287**)

Prepared according to *GP-IIa* using PABA **263** (5.00 g, 36.5 mmol, 1.00 eq.) and KOCN (3.02 g, 37.2 mmol, 1.02 eq.) in 25 ml of water. **287** was obtained as a colourless solid in a yield of 82%.

Yield: 5.40 g (30.0 mmol, 82%).



Appearance: Colourless solid.

Table 46: 1D and 2D-NMR data of 4-ureidobenzoic acid (**287**) in DMSO- d_6 , at 298 K and 499 MHz for ^1H and 125 MHz for ^{13}C .

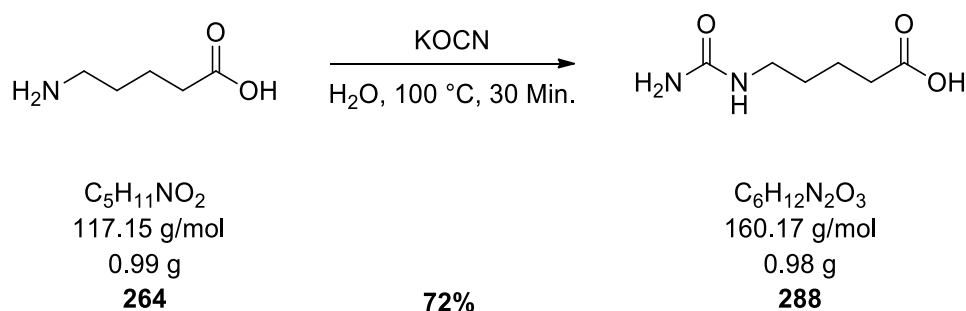
No.	δ_{H} [ppm], J in [Hz]	δ_{C} [ppm], mult.	HMBC ($^{\circ}\text{J}$)
1	7.50 (2H, d, $J = 8.8$ Hz)	116.8, $2\times\text{CH}_{\text{arom}}$	$\text{C1}\rightarrow\text{H1}({}^3\text{J})$, $\text{H3}({}^2\text{J})$, $\text{NH}({}^3\text{J})$
2	-	122.9, C_{q}	$\text{C2}\rightarrow\text{H1}({}^3\text{J})$
3	7.81 (2H, d, $J = 8.8$ Hz)	130.5, $2\times\text{CH}_{\text{arom}}$	$\text{C3}\rightarrow\text{H3}({}^3\text{J})$
4	-	144.9, C_{q}	$\text{C4}\rightarrow\text{H3}({}^3\text{J})$, $\text{NH}({}^2\text{J})$
5	-	155.7, C_{q}	$\text{C5}\rightarrow\text{NH}({}^2\text{J})$
6	-	167.2, C_{q}	$\text{C6}\rightarrow\text{H3}({}^3\text{J})$
NH	8.92 (1H, s)	-	-
NH ₂	6.03 (2H, br)	-	-
COOH	12.49 (1H, br)	-	-

IR: $\tilde{\nu}$ [cm^{-1}] = 3435 (w), 3322 (br), 3208 (w), 2988 (w), 2839 (w), 2673 (w), 2560 (w), 1678 (vs), 1657 (vs), 1622 (m), 1589 (s), 1542 (vs), 1426 (m), 1412 (w), 1355 (w), 1320 (s), 1295 (s), 1259 (s), 1177 (s), 1131 (m), 1114 (m), 1020 (w), 981 (w), 929 (br), 877 (w), 853 (w), 832 (w), 805 (w).

MP: Above 300 °C.

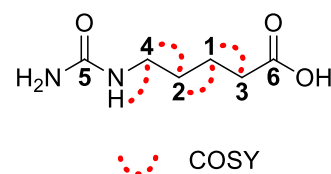
HR-MS (ESI): Theor.[$\text{M}+\text{H}$] $^+$: 181.06076, found: 181.06094.

Theor.[$\text{M}+\text{Na}$] $^+$: 203.04271, found: 203.04288.

6.3.1.2.14 Synthesis of 5-ureidopentanoic acid (**288**)

Prepared according to *GP-IIa* using δ -amino valeric acid **264** (0.99 g, 8.50 mmol, 1.00 eq.) and KOCN (0.70 g, 8.67 mmol, 1.02 eq.) in 5 ml of water. **288** was obtained as a colourless solid in a yield of 72%.

Yield: 0.98 g (6.12 mmol, 72%).



Appearance: Colourless solid.

Table 47: 1D and 2D-NMR data of 5-ureidopentanoic acid (**288**) in DMSO- d_6 , at 298 K and 500 MHz for ^1H and 125 MHz for ^{13}C .

No.	δ_{H} [ppm], J in [Hz]	δ_{C} [ppm], mult.	HMBC ($^{\times}J$)
1	1.47 (2H, m)	22.0, CH ₂	C1→H2(² J), H3(² J), H4(³ J)
2	1.36 (2H, m)	29.5, CH ₂	C2→H1(² J), H3(³ J), H4(² J)
3	2.20 (2H, t, $J = 7.4$ Hz)	33.4, CH ₂	C3→H1(² J), H2(³ J)
4	2.94 (2H, q, $J = 6.7$ Hz)	38.8, CH ₂	C4→H1(³ J), H2(² J), NH(² J)
5	-	158.8, C _q	C5→H4(³ J), NH(² J)
6	-	174.6, C _q	C6→H1(³ J), H3(² J)
NH	5.94 (1H, t, $J = 5.6$ Hz)	-	-
NH ₂	5.39 (2H, s)	-	-
COOH	12.04 (1H, s)	-	-

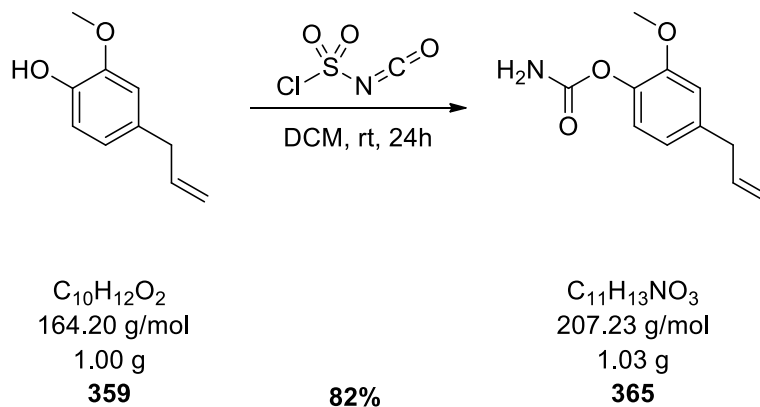
IR: $\tilde{\nu}$ [cm⁻¹] = 3438 (m), 3218 (br), 2954 (w), 2875 (w), 2463 (w), 1927 (br), 1674 (vs), 1644 (m), 1589 (br), 1515 (w), 1475 (w), 1445 (w), 1413 (w), 1383 (w), 1363 (w), 1313 (m), 1287 (s), 1238 (w), 1157 (w), 1087 (w), 1017 (m), 924 (w), 896 (w).

MP: 175 °C.

HR-MS (ESI): Theor.[M+H]⁺: 159.07751, found: 159.07782.

6.3.2 Carbamate and *S*-organyl thiocarbamate syntheses

6.3.2.1 Carbamates

6.3.2.1.1 Synthesis of 4-allyl-2-methoxyphenyl carbamate (**365**)

Prepared according to *GP-III* using eugenol **359** (0.93 g, 6.09 mmol, 1.0 eq.) and CSI (0.58 ml, 6.70 mmol, 1.1 eq.) in 46 ml of DCM. **365** was obtained as a beige, shimmering solid in a yield of 82%.

Yield: 1.03 g (4.97 mmol, 82%).

Appearance: Beige, shimmering solid.

IR: $\tilde{\nu}$ [cm^{-1}] = 3414 (br), 3341 (w), 3274 (w), 3206 (w), 2967 (w), 2359 (w), 1704 (vs), 1640 (w), 1617 (m), 1510 (m), 1467 (w), 1452 (w), 1421 (w), 1379 (s), 1273 (m), 1210 (s), 1188 (w), 1149 (m), 1123 (m), 1037 (m), 985 (m), 949 (w), 924 (w), 899 (w), 854 (w), 842 (w).

MP: 137 °C.

HR-MS (ESI): Theor. $[\text{M}+\text{H}]^+$: 208.09681, found: 208.09648.

Theor. $[\text{M}+\text{Na}]^+$: 230.07876, found: 230.07839.

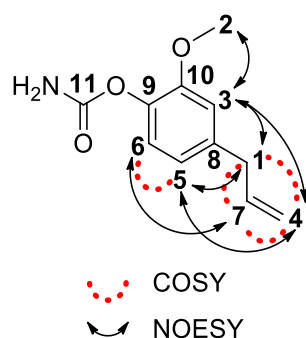
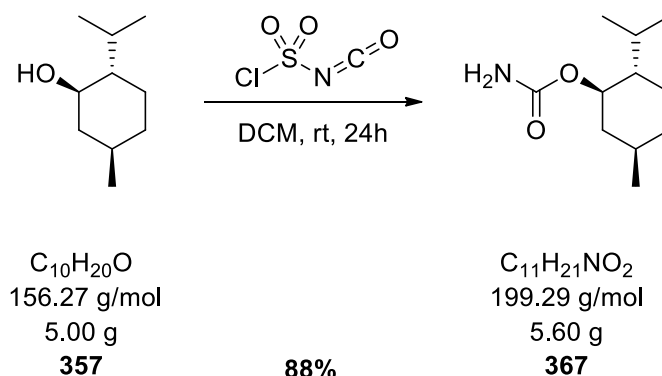


Table 48: 1D and 2D-NMR data of 4-allyl-2-methoxyphenyl carbamate (365) in DMSO- d_6 , at 298 K and 400 MHz for ^1H and 100 MHz for ^{13}C .

No.	δ_{H} [ppm], J in [Hz]	δ_{C} [ppm], mult.	HMBC ($^{\circ}\text{J}$)
1	3.34 (2H, d, $J = 6.8$ Hz)	39.2, CH_2	$\text{C1} \rightarrow \text{H3} (^3\text{J}), \text{H4} (^3\text{J}), \text{H5} (^3\text{J}), \text{H7} (^2\text{J})$
2	3.74 (3H, s)	55.5, CH_3	-
3	6.89 (1H, d, $J = 1.9$ Hz)	112.8, CH_{arom}	$\text{C3} \rightarrow \text{H1} (^3\text{J}), \text{H5} (^3\text{J}), \text{H6} (^4\text{J})$
4	5.05 (1H, m); 5.11 (1H, dq, $J = 17.0, 1.6$ Hz)	115.8, $\text{CH}_2, \text{alkene}$	$\text{C4} \rightarrow \text{H1} (^3\text{J})$
5	6.71 (1H, dd, $J = 8.0, 2.0$ Hz)	120.0, CH_{arom}	$\text{C5} \rightarrow \text{H1} (^3\text{J}), \text{H3} (^3\text{J}), \text{H6} (^2\text{J})$
6	6.93 (1H, d, $J = 8.0$ Hz)	123.1, CH_{arom}	$\text{C6} \rightarrow \text{H3} (^4\text{J})$
7	5.97 (1H, ddt, $J = 16.9, 10.0, 6.8$ Hz)	137.5, $\text{CH}_{\text{alkene}}$	$\text{C7} \rightarrow \text{H1} (^2\text{J}), \text{H4} (^2\text{J})$
8	-	137.7, C_q	$\text{C8} \rightarrow \text{H1} (^2\text{J}), \text{H6} (^3\text{J})$
9	-	138.1, C_q	$\text{C9} \rightarrow \text{H3} (^3\text{J}), \text{H5} (^3\text{J})$
10	-	151.4, C_q	$\text{C10} \rightarrow \text{H2} (^3\text{J}), \text{H3} (^2\text{J}), \text{H5} (^4\text{J}), \text{H6} (^3\text{J})$
11	-	154.5, C_q	-
NH_2	6.70-7.00 (2H, br)	-	-

6.3.2.1.2 Synthesis of (1*R*,2*S*,5*R*)-2-isopropyl-5-methylcyclohexyl carbamate (**367**)

Prepared according to *GP-III* using L-menthol **357** (5.00 g, 32.0 mmol, 1.0 eq.) and CDI (3.06 ml, 35.2 mmol, 1.1 eq.) in 243 ml of DCM. **367** was obtained as a colourless solid in a yield of 88%.

Yield: 5.60 g (28.1 mmol, 88%).

Appearance: Colourless solid.

IR: $\tilde{\nu}$ [cm^{-1}] = 3441 (m), 3324 (w), 3259 (w), 3206 (w), 2953 (w), 2927 (w), 2870 (w), 2852 (w), 2360 (w), 2341 (w), 1682 (vs), 1611 (m), 1457 (w), 1406 (s), 1373 (w), 1340 (m), 1320 (w), 1241 (w), 1184 (w), 1108 (w), 1083 (w), 1061 (m), 1048 (vs), 1006 (w), 982 (w), 951 (w), 915 (w), 877 (w), 841 (w), 828 (w), 821 (w).

MP: 168 °C.

HR-MS (ESI): Theor. $[\text{M}+\text{H}]^+$: 200.16450, found: 200.16470.

Theor. $[\text{M}+\text{Na}]^+$: 222.14645, found: 222.14660.

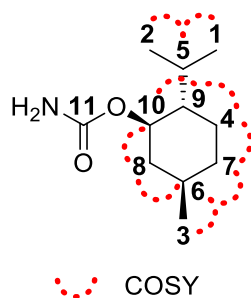
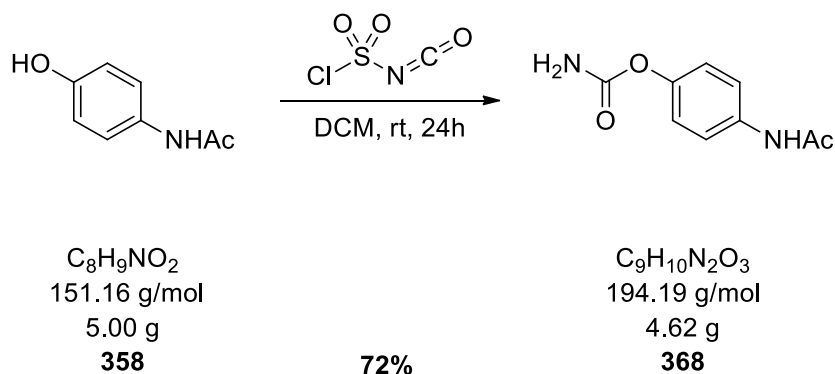


Table 49: 1D and 2D-NMR data of (1*R*,2*S*,5*R*)-2-isopropyl-5-methylcyclohexyl carbamate (XX) in DMSO-*d*₆, at 298 K and 499 MHz for ¹H and 125 MHz for ¹³C.

No.	δ_H [ppm], <i>J</i> in [Hz]	δ_C [ppm], mult.	HMBC (nJ)
1	0.74 (3H, d, <i>J</i> = 7.0 Hz)	16.3, CH ₃	C1→H2(³ J), H5(² J), H9(³ J)
2	0.86 (3H, d, <i>J</i> = 7.1 Hz)	20.6, CH ₃	C2→H1(³ J), H5(² J), H9(³ J)
3	0.87 (3H, d, <i>J</i> = 6.7 Hz)	22.0, CH ₃	C3→H8(³ J)
4	1.01 (1H, qd, <i>J</i> = 13.5, 12.8, 3.8 Hz); 1.62 (1H, m)	23.1, CH ₂	C4→H1(⁴ J), H5(³ J), H9(² J)
5	1.90 (1H, m)	25.7, CH	C5→H1(² J), H2(² J), H9(² J), H10(³ J)
6	1.41 (1H, m)	30.9, CH	C6→H3(² J), H7(² J), H8(² J)
7	0.82(1H, m); 1.61 (1H, m)	33.9, CH ₂	C7→H3(³ J), H4(² J), H8(³ J)
8	0.91 (1H, m); 1.89 (1H, m)	41.3, CH ₂	C8→H3(³ J), H7(³ J), H10(² J)
9	1.25 (1H, m)	46.9, CH	C9→H1(³ J), H2(³ J), H4(² J), H5(² J), H10(² J)
10	4.36 (1H, td, <i>J</i> = 10.9, 4.3 Hz)	72.3, CH	C10→H4(³ J), H8(² J), H9(² J)
11	-	156.6, C _q	C11→H10(³ J)
NH ₂	6.37 (2H, br)	-	-

6.3.2.1.3 Synthesis of 4-acetamidophenyl carbamate (368)



Prepared according to *GP-III* using paracetamol **358** (5.00 g, 33.1 mmol, 1.0 eq.) and CSI (3.16 ml, 36.4 mmol, 1.1 eq.) in 251 ml of DCM. **368** was obtained as a colourless solid in a yield of 72%.

Yield: 4.62 g (23.8 mmol, 72%).

Appearance: Colourless solid.

IR: $\tilde{\nu}$ [cm^{-1}] = 3359 (w), 3318 (br), 3262 (w), 3207 (w), 3072 (w), 3049 (w), 1722 (s), 1665 (vs), 1624 (w), 1605 (w), 1532 (s), 1510 (s), 1454 (w), 1405 (w), 1363 (s), 1310 (m), 1264 (w), 1242 (w), 1230 (w), 1208 (vs), 1171 (w), 1115 (m), 1036 (w), 1019 (w), 988 (s), 965 (w), 955 (w), 937 (w), 912 (w), 853 (m), 827 (w).

MP: 196 °C.

HR-MS (ESI): Theor. $[\text{M}+\text{H}]^+$: 195.07641, found: 195.07652.

Theor. $[\text{M}+\text{Na}]^+$: 217.05836, found: 217.05846.

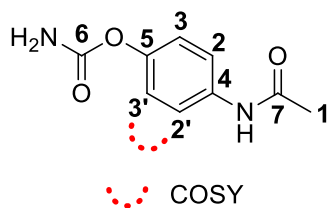
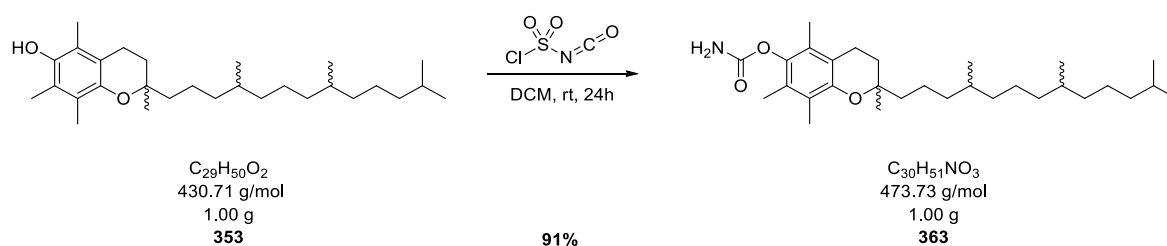


Table 50: 1D and 2D-NMR data of 4-acetamidophenyl carbamate (368) in DMSO-d₆, at 298 K and 500 MHz for ¹H and 125 MHz for ¹³C.

No.	δ_{H} [ppm], J in [Hz]	δ_{C} [ppm], mult.	HMBC ($^{\circ}J$)
1	2.03 (3H, s)	23.9, CH ₃	-
2	7.54 (2H, d, $J = 8.9$ Hz)	119.7, 2xCH _{arom}	C2→H2(³ J), H3(² J), NH _{Ac} (³ J)
3	7.00 (2H, d, $J = 8.9$ Hz)	122.1, 2xCH _{arom}	C3→H2(² J), H3(³ J)
4	-	136.2, C _q	C4→H1(⁴ J), H2(² J), H3(³ J), NH _{Ac} (² J)
5	-	146.3, C _q	C5→H2(³ J), H3(² J)
6	-	155.0, C _q	C6→H3(⁴ J)
7	-	168.1, C _q	C7→H1(² J), NH _{Ac} (² J)
NH ₂	6.83+7.12 (2H, s)	-	-
NH _{Ac}	9.93 (1H, s)	-	-

6.3.2.1.4 Synthesis of 2,5,7,8-tetramethyl-2-(4,8,12-trimethyltridecyl)chroman-6-yl carbamate (**363**)



Prepared according to **GP-III** using (\pm)- α -tocopherol **353** (1.00 g, 2.31 mmol, 1.00 eq.) and chlorosulfonyl isocyanate (0.22 ml, 2.53 mmol, 1.10 eq.) in 17.5 ml of DCM. The crude product was additionally column chromatographically purified on silica gel with *c*-Hex/EtOAc (5:1). **363** was obtained as a yellow oil in a yield of 91%.

Yield: 1.00 g (2.11 mmol, 91%).

Appearance: Yellow oil.

R_f-Value: 0.32 (SiO₂, *c*-Hex/EtOAc 4:1).

IR: $\tilde{\nu}$ [cm⁻¹] = 3334 (br), 2950 (m), 2926 (s), 2868 (m), 2358 (w), 1716 (s), 1654 (w), 1601 (w), 1581 (w), 1497 (m), 1461 (s), 1423 (m), 1377 (s), 1365 (s), 1280 (m), 1243 (s), 1168 (m), 1109 (m), 1088 (s), 996 (w), 968 (w), 926 (w), 878 (w), 818 (m).

HR-MS (ESI): Theor.[M+H]⁺: 474.39417, found: 474.39401.

Theor.[M+Na]⁺: 496.37611, found: 496.37541.

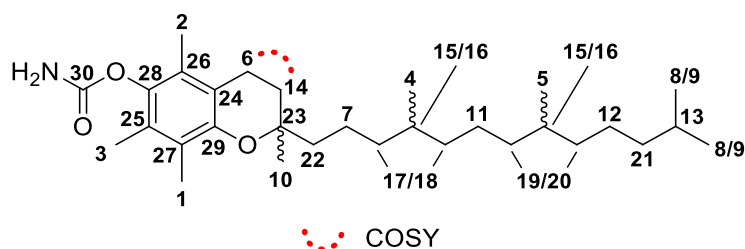
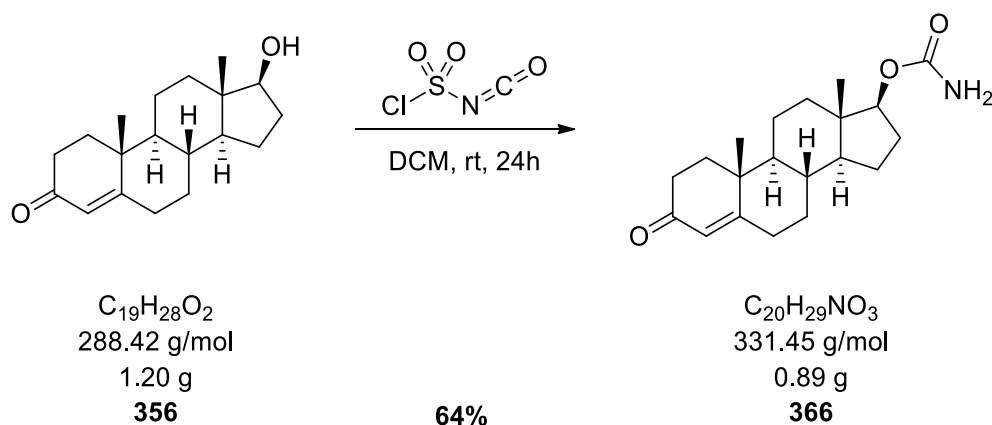


Table S1: 1D and 2D-NMR data of 2,5,7,8-tetramethyl-2-(4,8,12-trimethyltridecyl)chroman-6-yl carbamate (363) in DMSO-d₆, at 298 K and 500 MHz for ¹H and 125 MHz for ¹³C.

No.	δ_H [ppm], J in [Hz]	δ_C [ppm], mult.	HMBC (nJ)
1	2.10 (3H, s)	11.91+11.92, CH ₃	-
2	2.05 (3H, s)	12.0, CH ₃	-
3	2.09 (3H, s)	12.9, CH ₃	-
4	0.85+0.87 (3H, s)	19.73+19.76+19.79, CH ₃	C4→H17/18(³ J)
5	0.86 (3H, s)	19.82+19.89, CH ₃	C5→19/20(³ J)
6	2.60 (2H, t, $J = 6.8$ Hz)	20.7, CH ₂	C6→H14(² J)
7	1.38 (1H, m); 1.44 (2H, m)	21.16+21.18, CH ₂	C7→H22(² J)
8	0.88 (3H, s)	22.8, CH ₃	C8→H13(² J)
9	0.87 (3H, s)	22.9, CH ₃	C9→H13(² J)
10	1.24 (3H, s)	24.1, CH ₃	C10→H14(³ J)
11	1.26 (2H, m)	24.58+24.59, CH ₂	C11→17/18(^{2/4} J)
12	1.26 (2H, m)	24.94+24.96, CH ₂	C12→H13(³ J), H21(² J)
13	1.53 (1H, m)	28.1, CH	C13→H8(³ J), H9(³ J), H21(³ J)
14	1.70-1.85 (2H, dt, $J = 13.3, 6.5$ Hz)	31.10+31.15, CH ₂	C14→H6(² J), H10(³ J)
15	1.40 (1H, m)	32.83-32.86, CH	n.a.
16	1.37 (1H, m)	32.91+32.93, CH	n.a.
17	1.07 (2H, m)	37.43+37.53, CH ₂	n.a.
18	1.07 (2H, m)	37.49+37.51+37.55, CH ₂	n.a.
19	1.26 (2H, m)	37.58+37.60, CH ₂	n.a.
20	1.26 (2H, m)	37.67+37.69, CH ₂	n.a.
21	1.14 (2H, m)	39.5, CH ₂	C21→H9(³ J), H13(² J)
22	1.55 (2H, m)	40.3, CH ₂	C22→H10(³ J), H14(³ J)
23	-	75.2, C _q	C23→H6(³ J), H10(² J), H14(² J), H22(² J)
24	-	117.5, C _q	C24→H2(³ J), H1(⁴ J), H6(² J), H14(³ J)
25	-	123.2, C _q	C25→H1(³ J), H2(⁴ J), H3(² J)
26	-	125.8, C _q	C26→H2(² J), H3(⁴ J), H6(³ J)
27	-	127.5, C _q	C27→H1(² J), H3(³ J)
28	-	140.2, C _q	C28→H2(³ J), H3(³ J), H6(⁴ J)
29	-	149.7, C _q	C29→H1(³ J), H6(³ J)
30	-	156.5, C _q	-
NH ₂	5.23-5.44 (2H, br)	-	-

Note: Functional groups and the position within the molecule were identified. The clear assignment of C8/C9, C15/C16, C17/C18 and C19/C20 was not possible due to the similarity of the carbon and hydrogen signals and the associated signal overlap.

6.3.2.1.5 Synthesis of (8*R*,9*S*,10*R*,13*S*,14*S*,17*S*)-10,13-dimethyl-3-oxo-2,3,6,7,8,9,10,11,12,13,14,15,16,17-tetradecahydro-1*H*-cyclopenta[*a*]phenanthren-17-yl carbamate (**366**)



Prepared according to **GP-III** using testosterone **356** (1.20 g, 4.16 mmol, 1.0 eq.) and CSI (0.40 ml, 4.58 mmol, 1.1 eq.) in 32 ml of DCM. The crude product was additionally column chromatographically purified on silica gel with *n*-Hex/EtOAc (2:1→1:1). **366** was obtained as a colourless solid in a yield of 65%.

Yield: 0.89 g (2.69 mmol, 65%).

Appearance: Colourless solid.

R_f-Value: 0.22 (SiO₂, *n*-Hex/EtOAc 4:1).

IR: $\tilde{\nu}$ [cm⁻¹] = 3494 (w), 3372 (br), 2982 (w), 2939 (w), 2912 (w), 2051 (w), 1736 (vs), 1694 (vs), 1662 (vs), 1595 (vs), 1454 (w), 1434 (w), 1393 (m), 1379 (m), 1336 (s), 1324 (s), 1292 (w), 1272 (w), 1231 (m), 1192 (w), 1131 (w), 1118 (w), 1097 (w), 1072 (vs), 1061 (s), 1040 (w), 1026 (m), 999 (w), 960 (w), 940 (w), 870 (m), 861 (m), 835 (w).

MP: 155 °C.

HR-MS (ESI): Theor.[M+H]⁺: 332.22202, found: 332.22223.

Theor.[M+Na]⁺: 354.20396, found: 354.20405.

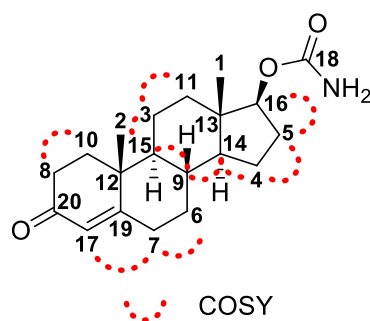
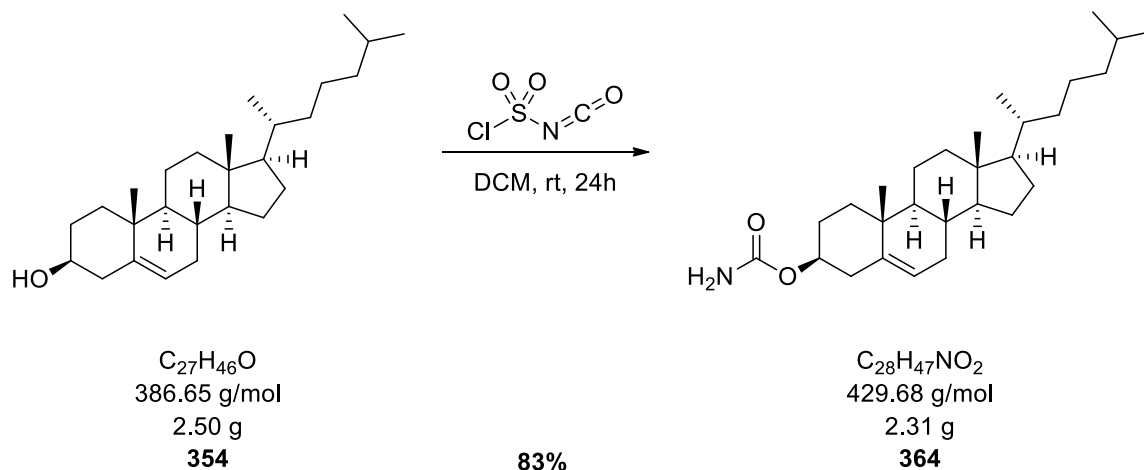


Table 52: 1D and 2D-NMR data of (8*R*,9*S*,10*R*,13*S*,14*S*,17*S*)-10,13-dimethyl-3-oxo-2,3,6,7,8,9,10,11,12,13,14,15,16,17-tetradecahydro-1*H*-cyclopenta[*a*]phenanthren-17-yl carbamate (366) in CDCl₃, at 298 K and 499 MHz for ¹H and 125 MHz for ¹³C.

No.	δ_H [ppm], <i>J</i> in [Hz]	δ_C [ppm], mult.	HMBC ($^{\circ}J$)
1	0.82 (3H, s)	12.1, CH ₃	C1→H11(³ J), H14(³ J), H16(³ J)
2	1.18 (3H, s)	17.5, CH ₃	C2→H10(³ J), H15(³ J)
3	1.40 (1H, m); 1.58 (1H, m)	20.7, CH ₂	C3→H11(² J), H15(² J)
4	1.33 (1H, m); 1.65 (1H, m)	23.5, CH ₂	C4→H5(² J), H9(³ J), H14(² J)
5	1.55 (1H, m); 2.17 (1H, m)	27.6, CH ₂	C5→H4(² J), H16(² J)
6	1.02 (1H, m); 1.84 (1H, m)	31.6, CH ₂	C6→H7(² J), H9(² J), H14(³ J)
7	2.29 (1H, m); 2.38 (1H, m)	32.9, CH ₂	C7→H6(² J), H17(³ J)
8	2.35 (1H, m); 2.41 (1H, m)	34.1, CH ₂	C8→H10(² J), H17(³ J)
9	1.56 (1H, m)	35.6, CH	C9→H4(³ J), H6(² J), H14(² J), H15(² J)
10	1.70 (1H, m); 2.02 (1H, m)	35.8, CH ₂	C10→H2(³ J), H8(² J)
11	1.21 (1H, m); 1.82 (1H, m)	36.7, CH ₂	C11→H1(³ J), H14(³ J), H16(³ J)
12	-	38.8, C _q	C12→H2(² J), H17(³ J)
13	-	42.5, C _q	C13→H1(² J), H5(³ J), H11(² J), H14(² J)
14	1.04 (1H, m)	50.3, CH	C14→H1(³ J), H4(² J)
15	0.94 (1H, td, <i>J</i> = 12.2, 4.1 Hz)	53.8, CH	C15→H2(³ J), H3(² J), H10(³ J), H11(³ J), H14(³ J)
16	4.54 (1H, t, <i>J</i> = 8.5 Hz)	83.2, CH	C16→H1(³ J), H5(² J), H11(³ J), H14(³ J)
17	5.72 (1H, s)	124.1, CH _{alkene}	C17→H7(³ J)
18	-	157.1, C _q	C18→H16(³ J)
19	-	171.1, C _{q, alkene}	C19→H2(³ J), H7(² J)
20	-	199.6, C _q	C20→H8(² J)
NH ₂	4.61 (2H, br)	-	-

6.3.2.1.6 Synthesis of (3*S*,8*S*,9*S*,10*R*,13*R*,14*S*,17*R*)-10,13-dimethyl-17-((*R*)-6-methylheptan-2-yl)-2,3,4,7,8,9,10,11,12,13,14,15,16,17-tetradecahydro-1*H*-cyclopenta[*a*]phenanthren-3-yl carbamate (364**)**



Prepared according to *GP-III* using cholesterol **354** (2.50 g, 6.47 mmol, 1.0 eq.) and CSI (0.62 ml, 7.14 mmol, 1.1 eq.) in 50 ml of DCM. **364** was obtained as a colourless solid in a yield of 83%.

Yield: 2.31 g (5.38 mmol, 83%).

Appearance: Colourless solid.

IR: $\tilde{\nu}$ [cm^{-1}] = 3483 (w), 3326 (w), 3275 (w), 3172 (w), 2941 (m), 2903 (w), 2867 (w), 2360 (w), 2341 (w), 1725 (m), 1707 (vs), 1691 (m), 1602 (w), 1558 (w), 1540 (w), 1507 (w), 1467 (w), 1440 (w), 1409 (m), 1376 (mw), 1364 (m), 1351 (m), 1334 (m), 1314 (w), 1257 (w), 1197 (w), 1134 (w), 1060 (s), 1026 (w), 993 (w), 961 (w), 941 (w), 923 (w), 881 (w), 842 (w), 802 (w).

MP: 213 °C.

HR-MS (ESI): Theor. $[\text{M}+\text{Na}]^+$: 452.34990, found: 452.34999.

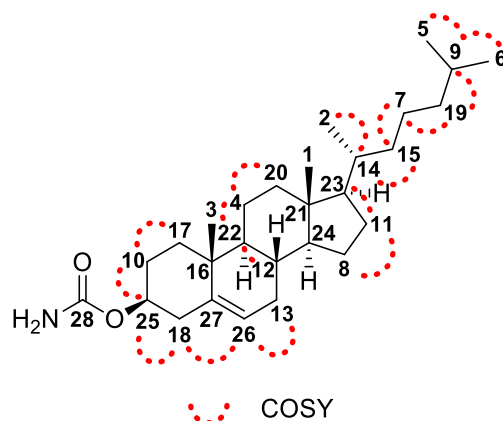
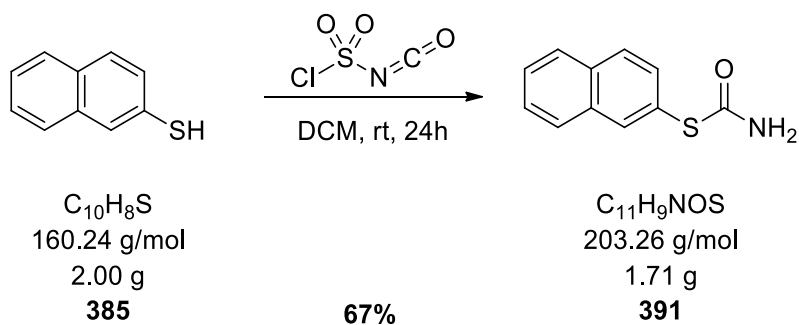


Table 53: 1D and 2D-NMR data of (3*S*,8*S*,9*S*,10*R*,13*R*,14*S*,17*R*)-10,13-dimethyl-17-((*R*)-6-methylheptan-2-yl)-2,3,4,7,8,9,10,11,12,13,14,15,16,17-tetradecahydro-1*H*-cyclopenta[*a*]phenanthren-3-yl carbamate (364) in CDCl₃, at 298 K and 500 MHz for ¹H and 125 MHz for ¹³C.

No.	δ_{H} [ppm], J in [Hz]	δ_{C} [ppm], mult.	HMBC ($^{\circ}$ J)
1	0.67 (3H, s)	12.0, CH ₃	C1→H20(³ J), H23(³ J), H24(³ J)
2	0.91 (3H, d, $J = 6.6$ Hz)	18.9, CH ₃	C2→H14(² J), H15(³ J)
3	1.01 (3H, s)	19.5, CH ₃	C3→H17(³ J), H22(³ J)
4	1.43 (1H, m); 1.48 (1H, m)	21.2, CH ₂	C4→H20(² J), H22(² J)
5	0.86 (3H, d, $J = 6.6$ Hz)	22.7, CH ₃	C5→H6(³ J), H9(² J)
6	0.86 (3H, d, $J = 6.6$ Hz)	23.0, CH ₃	C6→H5(³ J), H9(² J)
7	1.13 (1H, m); 1.33 (1H, m)	24.0, CH ₂	C7→H9(³ J), H15(² J), H19(² J)
8	1.05 (1H, m); 1.57 (1H, m)	24.4, CH ₂	C8→H24(² J)
9	1.51 (1H, m)	28.15, CH	C9→H5(² J), H6(² J)
10	1.56 (1H, m); 1.89 (1H, m)	28.16, CH ₂	C10→H17(² J), H18(³ J)
11	1.24 (1H, m); 1.82 (1H, m)	28.4, CH ₂	C11→H23(² J)
12	1.43 (1H, m)	32.00, CH	C12→H4(³ J), H24(² J), H26(³ J)
13	1.51 (1H, m); 1.96 (1H, m)	32.03, CH ₂	C13→H12(² J), H24(³ J), H26(² J)
14	1.37 (1H, m)	35.9, CH	C14→H2(² J)
15	0.98 (1H, m); 1.32 (1H, m)	36.3, CH ₂	C15→H7(² J)
16	-	36.7, C _q	C16→H3(² J), H10(³ J), H18(³ J), H26(³ J)
17	1.12 (1H, m); 1.85 (1H, m)	37.1, CH ₂	C17→H3(³ J), H10(² J), H25(³ J)
18	2.29 (1H, m); 2.36 (1H, m)	38.5, CH ₂	C18→H25(² J), H26(³ J)
19	1.12 (1H, m)	39.7, CH ₂	C19→H5(³ J), H6(³ J), H9(² J)
20	1.17 (1H, m); 1.99 (2H, m)	39.9, CH ₂	C20→H1(³ J), H4(² J)
21	-	42.5, C _q	C21→H1(² J), H11(³ J), H23(² J)
22	0.94 (1H, m)	50.2, CH	C22→H3(³ J), H12(² J), H13(³ J), H20(³ J)
23	1.08 (1H, m)	56.3, CH	C23→H1(³ J), H2(³ J), H11(² J)
24	0.98 (1H, m)	56.8, CH	C24→H1(³ J), H12(² J), H23(³ J)
25	4.48 (1H, tt, $J = 11.5, 4.8$ Hz)	74.87, CH	C25→H10(² J), H18(² J)
26	5.37 (1H, m)	122.8, CH _{alkene}	C26→H13(² J), H18(³ J)
27	-	139.8, C _q	C27→H3(³ J), H13(³ J), H18(² J)
28	-	156.7, C _q	C28→H25(³ J)
NH ₂	4.67 (2H, br)	-	-

6.3.2.2. Synthesis of *S*-naphthalen-2-yl carbamothioate (**391**)

Prepared according to *GP-III* using naphthalene-2-thiol **385** (2.00 g, 12.5 mmol, 1.0 eq.) and CSI (1.20 ml, 13.8 mmol, 1.1 eq.) in 95 ml of DCM. **391** was obtained as a colourless solid in a yield of 67%.

Yield: 1.71 g (8.40 mmol, 67%).

Appearance: Beige solid.

IR: $\tilde{\nu}$ [cm^{-1}] = 3409 (m), 3316 (m), 3296 (m), 3172 (w), 3047 (w), 2112 (w), 1941 (w), 1916 (w), 1860 (w), 1794 (w), 1772 (w), 1646 (s), 1608 (s), 1575 (m), 1497 (w), 1455 (w), 1362 (w), 1343 (w), 1312 (s), 1267 (m), 1237 (m), 1194 (m), 1153 (m), 1132 (m), 1111 (m), 1080 (w), 1070 (w), 1016 (w), 975 (w), 945 (m), 888 (w), 856 (m), 823 (s).

MP: 173 °C.

HR-MS (ESI): Theor. $[\text{M}+\text{H}]^+$: 204.04776, found: 204.04777.

Theor. $[\text{M}+\text{Na}]^+$: 226.02970, found: 226.02967.

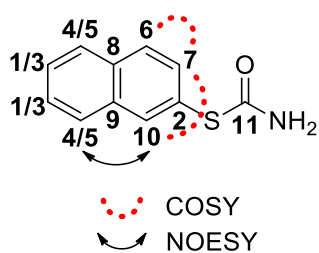
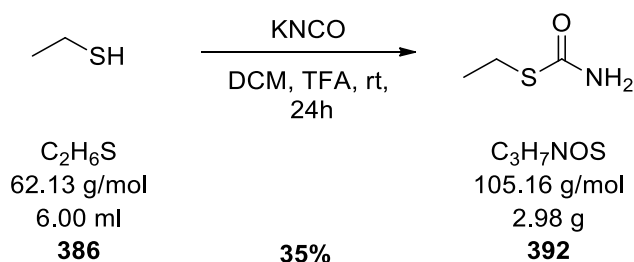


Table 55: 1D and 2D-NMR data of *S*-naphthalen-2-yl carbamothioate (391) in DMSO- d_6 , at 298 K and 600 MHz for ^1H and 150 MHz for ^{13}C .

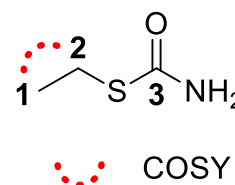
No.	δ_{H} [ppm], J in [Hz]	δ_{C} [ppm], mult.	HMBC ($^{\circ}\text{J}$)
1	7.57 (1H, m)	126.6, CH_{arom}	$\text{C1} \rightarrow \text{H3} (^3\text{J}), \text{H6} (^3\text{J})$
2	-	126.7, C_{q}	$\text{C2} \rightarrow \text{H6} (^3\text{J})$
3	7.57 (1H, m)	127.0, CH_{arom}	$\text{C3} \rightarrow \text{H1} (^3\text{J})$
4	7.95 (1H, m)	127.6, CH_{arom}	$\text{C4} \rightarrow \text{H10} (^3\text{J})$
5	7.95 (1H, m)	127.7, CH_{arom}	$\text{C5} \rightarrow \text{H1/3} (^2\text{J}), \text{H4} (^3\text{J})$
6	7.93 (1H, d, $J = 8.6$ Hz)	128.1, CH_{arom}	-
7	7.52 (1H, dd, $J = 8.5, 1.8$ Hz)	132.0, CH_{arom}	$\text{C7} \rightarrow \text{H10} (^3\text{J})$
8	-	132.5, C_{q}	$\text{C8} \rightarrow \text{H7} (^3\text{J}), \text{H10} (^3\text{J})$
9	-	133.0, C_{q}	$\text{C9} \rightarrow \text{H4} (^2\text{J}), \text{H6} (^3\text{J})$
10	8.08 (1H, d, $J = 1.4$ Hz)	134.3, CH_{arom}	$\text{C10} \rightarrow \text{H4} (^3\text{J}), \text{H7} (^3\text{J})$
11	-	165.1, C_{q}	-
NH_2	7.65-7.82 (2H, br)	-	-

Note: C1/C3 and C4/C5 could not be assigned.

6.3.2.2.3 Synthesis of *S*-ethyl carbamothioate (**392**)

Prepared according to **GP-IV** using ethanethiol **386** (6.00 ml, 83.2 mmol, 1.0 eq.), KOCN (13.5 g, 166 mmol, 2.0 eq.) and TFA (12.7 ml, 166 mmol, 2.0 eq.) in 150 ml of DCM. **392** was obtained as a colourless solid in a yield of 34%.

Yield: 2.98 g (28.3 mmol, 34%).



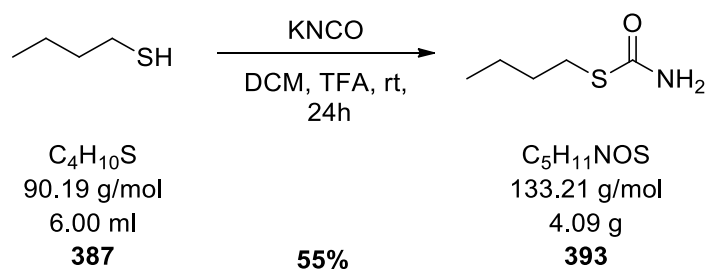
Appearance: Colourless solid.

Table 56: 1D and 2D-NMR data of *S*-ethyl carbamothioate (**392**) in DMSO- d_6 , at 298 K and 500 MHz for ^1H and 125 MHz for ^{13}C .

No.	δ_{H} [ppm], J in [Hz]	δ_{C} [ppm], mult.	HMBC ($^{\circ}\text{J}$)
1	1.17 (3H, t, $J = 7.3$ Hz)	16.0, CH_3	$\text{C1} \rightarrow \text{H2} (^2\text{J})$
2	2.72 (2H, q, $J = 7.3$ Hz)	23.1, CH_2	$\text{C2} \rightarrow \text{H1} (^2\text{J})$
3	-	167.0, C_q	$\text{C3} \rightarrow \text{H2} (^3\text{J})$
NH_2	7.44 (1H, br)	-	-

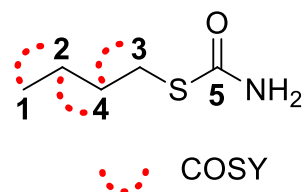
IR: $\tilde{\nu}$ [cm^{-1}] = 3676 (w), 3369 (m), 3284 (m), 3213 (m), 3177 (m), 2985 (w), 2970 (w), 2932 (w), 2871 (w), 2763 (w), 2083 (w), 1638 (s), 1610 (s), 1447 (w), 1440 (w), 1413 (w), 1377 (w), 1299 (s), 1252 (s), 1112 (m), 1057 (w), 977 (w).

MP: 107 °C.

6.3.2.2.4 Synthesis of *S*-butyl carbamothioate (**393**)

Prepared according to *GP-IV* using butane-1-thiol **387** (6.00 ml, 55.9 mmol, 1.0 eq.), KOCN (9.08 g, 112 mmol, 2.0 eq.) and TFA (8.63 ml, 112 mmol, 2.0 eq.) in 100 ml of DCM. **393** was obtained as a colourless solid in a yield of 55%.

Yield: 4.09 g (30.7 mmol, 55%).



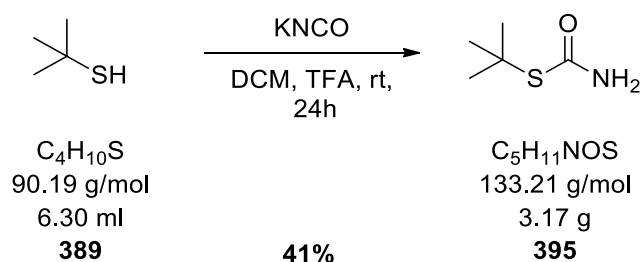
Appearance: Colourless solid.

Table 57: 1D and 2D-NMR data of *S*-butyl carbamothioate (**393**) in DMSO- d_6 , at 298 K and 500 MHz for ^1H and 125 MHz for ^{13}C .

No.	δ_{H} [ppm], J in [Hz]	δ_{C} [ppm], mult.	HMBC ($^{\circ}J$)
1	0.87 (3H, t, $J = 7.3$ Hz)	13.5, CH ₃	C1→H2(2J), H3(4J), H4(3J)
2	1.33 (2H, sxt, $J = 7.3$ Hz)	21.3, CH ₂	C2→H1(2J), H3(3J), H4(2J)
3	2.73 (2H, t, $J = 7.2$ Hz)	28.4, CH ₂	C3→H2(3J), H4(2J)
4	1.48 (2H, quin, $J = 7.5$ Hz)	32.3, CH ₂	C4→H1(3J), H2(2J), H3(2J)
5	-	167.1, C _q	C5→H3(3J)
NH ₂	7.43 (2H, br)	-	-

IR: $\tilde{\nu}$ [cm⁻¹] = 3661 (w), 3379 (m), 3286 (m), 3216 (m), 3180 (m), 2957 (m), 2929 (m), 2873 (w), 2860 (w), 2764 (w), 1643 (s), 1616 (s), 1464 (w), 1438 (w), 1409 (w), 1377 (w), 1313 (s), 1293 (s), 1269 (s), 1225 (m), 1202 (m), 1113 (m), 1077 (w), 1050 (w), 911 (w), 875 (w).

MP: 100 °C.

6.3.2.2.5 Synthesis of *S*-*tert*-butyl carbamothioate (395)

Prepared according to *GP-IV* using 2-methylpropane-2-thiol **389** (6.30 ml, 58.0 mmol, 1.0 eq.), KOCN (9.41 g, 116 mmol, 2.0 eq.) and TFA (8.94 ml, 116 mmol, 2.0 eq.) in 104 ml of DCM. **395** was obtained as a colourless solid in a yield of 41%.

Yield: 3.17 g (23.8 mmol, 41%).

Appearance: Colourless solid.

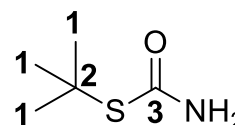
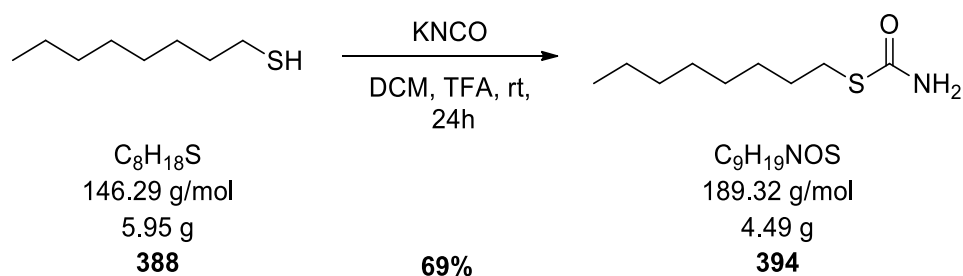


Table 58: 1D and 2D-NMR data of *S*-*tert*-butyl carbamothioate (395) in DMSO-*d*₆, at 298 K and 500 MHz for ¹H and 125 MHz for ¹³C.

No.	δ_{H} [ppm], <i>J</i> in [Hz]	δ_{C} [ppm], mult.	HMBC ($^{\circ}\text{J}$)
1	1.41 (9H, s)	30.4, 3xCH ₃	-
2	-	45.7, C _q	C2→H1 (^2J)
3	-	167.6, C _q	-
NH ₂	7.23 (2H, br)	-	-

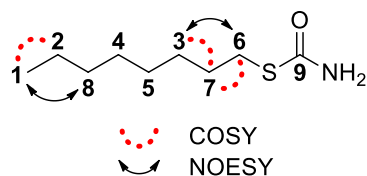
IR: $\tilde{\nu}$ [cm⁻¹] = 3662 (w), 3413 (m), 3334 (w), 3287 (w), 3199 (m), 3175 (m), 2989 (w), 2967 (m), 2923 (w), 2868 (w), 2388 (w), 1739 (w), 1683 (w), 1629 (s), 1598 (s), 1476 (w), 1449 (m), 1389 (w), 1363 (m), 1290 (s), 1156 (vs), 1116 (m), 1028 (w), 933 (w), 811 (w).

MP: 88 °C.

6.3.2.2.6 Synthesis of *S*-octyl carbamothioate (**394**)

Prepared according to *GP-IV* using octane-1-thiol **388** (5.95 ml, 34.2 mmol, 1.0 eq.), KOCN (5.54 g, 68.4 mmol, 2.0 eq.) and TFA (5.27 ml, 68.4 mmol, 2.0 eq.) in 62 ml of DCM. **394** was obtained as a colourless solid in a yield of 69%.

Yield: 4.49 g (23.7 mmol, 69%).



Appearance: Colourless solid.

Table 59: 1D and 2D-NMR data of *S*-octyl carbamothioate (**394**) in DMSO- d_6 , at 298 K and 500 MHz for ^1H and 125 MHz for ^{13}C .

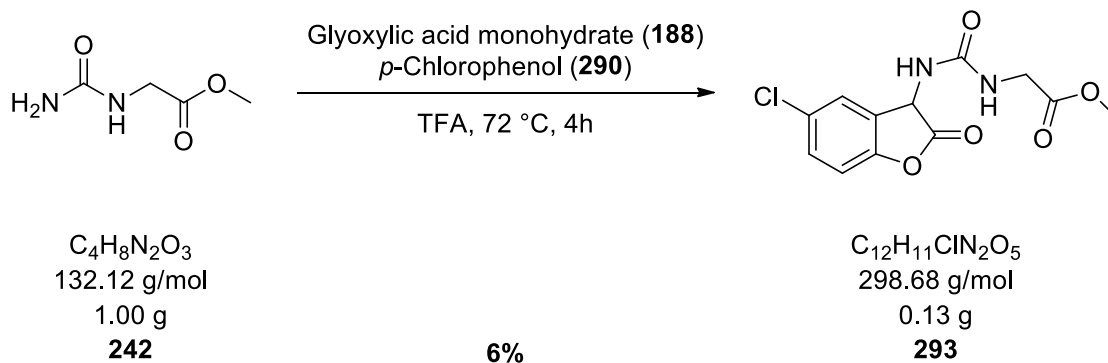
No.	δ_{H} [ppm], J in [Hz]	δ_{C} [ppm], mult.	HMBC ($^{\circ}\text{J}$)
1	0.85 (3H, t, $J = 7.1$ Hz)	13.8, CH_3	$\text{C1} \rightarrow \text{H2} (^2\text{J}), \text{H8} (^3\text{J})$
2	1.27 (2H, m)	22.0, CH_2	$\text{C2} \rightarrow \text{H1} (^2\text{J}), \text{H8} (^2\text{J})$
3	1.31 (2H, m)	28.0, CH_2	$\text{C3} \rightarrow \text{H6} (^3\text{J})$
4	1.26 (2H, m)	28.4, CH_2	$\text{C4} \rightarrow \text{H2} (^3\text{J})$
5	1.26 (2H, m)	28.5, CH_2	$\text{C5} \rightarrow \text{H3} (^2\text{J})$
6	2.73 (2H, t, $J = 7.2$ Hz)	28.7, CH_2	$\text{C6} \rightarrow \text{H7} (^2\text{J})$
7	1.49 (2H, quin, $J = 7.3$ Hz)	30.1, CH_2	$\text{C7} \rightarrow \text{H6} (^2\text{J})$
8	1.25 (2H, m)	31.1, CH_2	$\text{C8} \rightarrow \text{H1} (^3\text{J}), \text{H2} (^2\text{J})$
9	-	167.0, C_q	$\text{C9} \rightarrow \text{H6} (^3\text{J})$
NH_2	7.38 (2H, br)	-	-

IR: $\tilde{\nu}$ [cm^{-1}] = 3381 (m), 3287 (w), 3214 (m), 3180 (m), 2957 (m), 2918 (s), 2873 (w), 2850 (m), 2767 (w), 1645 (vs), 1617 (s), 1463 (w), 1406 (w), 1323 (m), 1297 (s), 1276 (s), 1239 (m), 1200 (m), 1115 (m), 958 (w), 891 (w), 849 (w).

MP: 100 °C.

6.3.3 Protection of Substrates with Coumaranones

6.3.3.1 2-Coumaranones with urea substructures

6.3.3.1.1 Synthesis of methyl 2-(3-(5-chloro-2-oxo-2,3-dihydrobenzofuran-3-yl)ureido)acetate (**293**)

Prepared according to *GP-V* using methyl 2-ureidoacetate **242** (1.00 g, 7.57 mmol, 1.0 eq.), glyoxylic acid monohydrate **188** (0.70 g, 7.57 mmol, 1.0 eq.), *p*-chlorophenol **290** (1.17 g, 9.08 mmol, 1.2 eq.) in 12 ml of TFA. **293** was obtained as a colourless solid in a yield of 6%.

Yield: 0.13 g (0.44 mmol, 6%).

Appearance: Colourless solid.

R_f-Value: 0.30 (SiO₂, DCM/MeOH 50:1).

IR: $\tilde{\nu}$ [cm⁻¹] = 3256 (br), 3192 (w), 2956 (w), 2326 (w), 1759 (w), 1741 (w), 1693 (vs), 1647 (w), 1601 (w), 1543 (w), 1504 (w), 1471 (w), 1440 (w), 1423 (w), 1404 (w), 1376 (w), 1336 (m), 1279 (w), 1228 (br), 1200 (w), 1186 (w), 1149 (w), 1126 (w), 1093 (w), 1078 (w), 1068 (w), 1045 (w), 993 (w), 935 (w), 912 (w), 864 (w), 837 (w), 824 (w).

MP: 190 °C.

HR-MS (ESI): Theor.[M+H]⁺: 299.04292, found: 299.04344.

Theor.[M+Na]⁺: 321.02487, found: 321.02527.

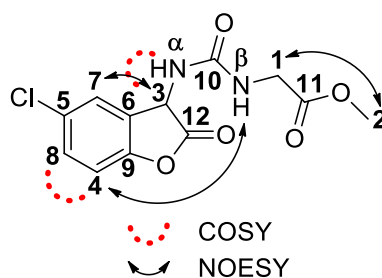
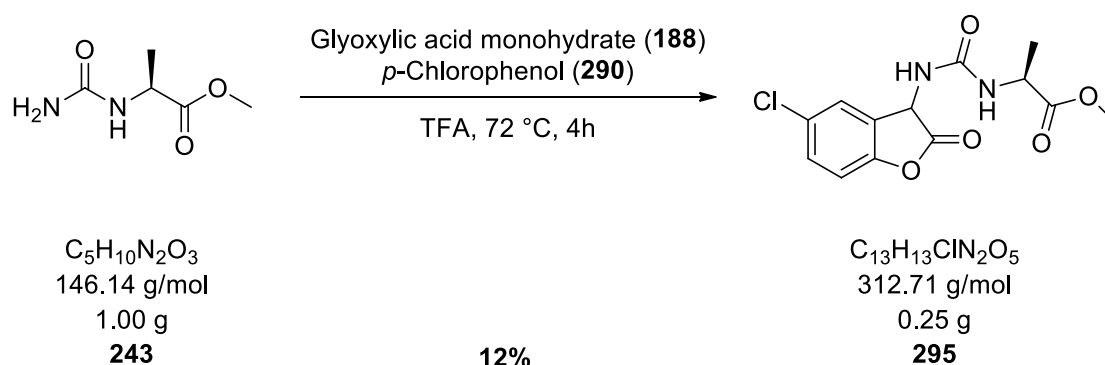


Table 60: 1D and 2D-NMR data of methyl 2-(3-(5-chloro-2-oxo-2,3-dihydrobenzofuran-3-yl)ureido)acetate (293) in DMSO-d₆, at 298 K and 500 MHz for ¹H and 125 MHz for ¹³C.

No.	δ _H [ppm], <i>J</i> in [Hz]	δ _C [ppm], mult.	HMBC ([×] <i>J</i>)
1	4.23 (2H, d, <i>J</i> = 1.9 Hz)	39.1, CH ₂	C1→NH _α (⁴ <i>J</i>)
2	3.70 (3H, s)	52.4, CH ₃	-
3	5.38 (1H, d, <i>J</i> = 0.9 Hz)	56.0, CH	C3→H4(⁴ <i>J</i>), H7(³ <i>J</i>), NH _α (² <i>J</i>)
4	6.86 (1H, m)	117.3, CH _{arom}	C4→H8(² <i>J</i>), NH _β (⁷ <i>J</i>)
5	-	122.4, C _q	C5→H4(³ <i>J</i>), H7(² <i>J</i>)
6	-	123.8, C _q	C6→H3(² <i>J</i>), H4(³ <i>J</i>), NH _β (⁵ <i>J</i>)
7	7.23 (1H, m)	129.1, CH _{arom}	C7→H3(³ <i>J</i>), H8(³ <i>J</i>)
8	7.24 (1H, m)	129.5, CH _{arom}	C8→H7(³ <i>J</i>)
9	-	154.8, C _q	C9→H3(³ <i>J</i>), H4(² <i>J</i>), H7(³ <i>J</i>), H8(³ <i>J</i>), NH _β (⁶ <i>J</i>)
10	-	156.0, C _q	C10→H1(³ <i>J</i>), H3(³ <i>J</i>), NH _α (² <i>J</i>)
11	-	168.1, C _q	C11→H1(² <i>J</i>), H2(³ <i>J</i>)
12	-	172.4, C _q	C12→H1(⁶ <i>J</i>), H3(² <i>J</i>), NH _α (³ <i>J</i>)
NH _α	8.60 (1H, d, <i>J</i> = 1.2 Hz)	-	-
NH _β	10.20 (1H, s)	-	-

6.3.3.1.2 Synthesis of (2*S*)-methyl 2-(3-(5-chloro-2-oxo-2,3-dihydrobenzofuran-3-yl)ureido)propanoate (**295**)



Prepared according to **GP-V** using (*S*)-methyl 2-ureidopropanoate **243** (1.00 g, 6.84 mmol, 1.0 eq.), glyoxylic acid monohydrate **188** (0.63 g, 6.84 mmol, 1.0 eq.), *p*-chlorophenol **290** (1.06 g, 8.21 mmol, 1.2 eq.) in 11 ml of TFA. **295** was obtained as a colourless solid in a yield of 12%.

Yield: 0.25 g (0.80 mmol, 12%).

Appearance: Colourless solid.

R_f-Value: 0.23 (SiO₂, DCM/MeOH 60:1).

IR: $\tilde{\nu}$ [cm⁻¹] = 3287 (br), 3001 (w), 2953 (w), 2051 (w), 1765 (m), 1745 (s), 1697 (vs), 1601 (m), 1496 (m), 1431 (s), 1379 (w), 1318 (w), 1305 (w), 1280 (m), 1234 (m), 1224 (m), 1205 (w), 1181 (m), 1154 (m), 1117 (s), 1081 (w), 1060 (w), 1016 (w), 972 (m), 948 (w), 904 (w), 881 (w), 859 (w), 840 (w), 828 (s), 821 (s).

MP: 191 °C.

HR-MS (ESI): Theor.[M+H]⁺: 313.05857, found: 313.05905.

Theor.[M+Na]⁺: 335.04052, found: 335.04094.

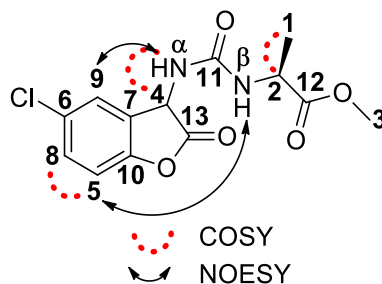
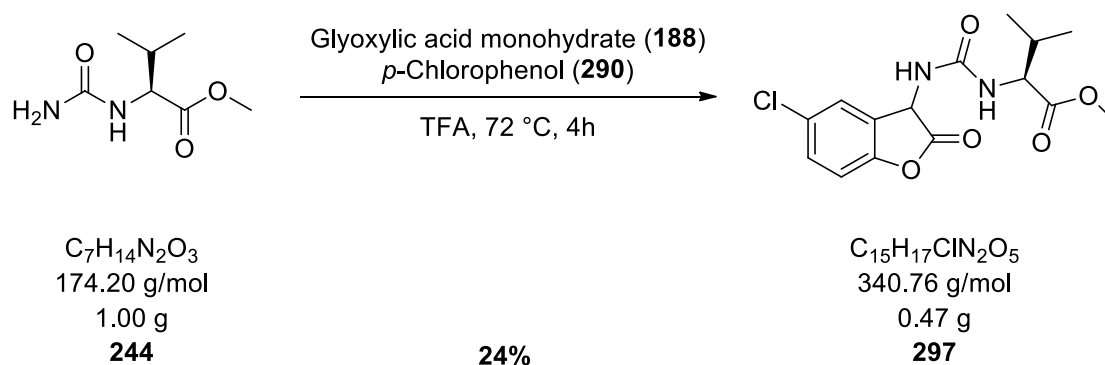


Table 61: 1D and 2D-NMR data of (2*S*)-methyl 2-(3-(5-chloro-2-oxo-2,3-dihydrobenzofuran-3-yl)ureido)propanoate (295) in DMSO-*d*₆, at 298 K and 500 MHz for ¹H and 125 MHz for ¹³C.

No.	δ_H [ppm], <i>J</i> in [Hz]	δ_C [ppm], mult.	HMBC (^{\times} <i>J</i>)
1	1.45 (3H, d, <i>J</i> = 7.1 Hz)	14.1+14.3, CH ₃	C1→H2(² <i>J</i>)
2	4.74+4.78 (1H, q, <i>J</i> = 7.2 Hz)	46.9+47.1, CH	C2→H1(² <i>J</i>),
3	3.65+3.67 (3H, s)	52.34+52.43, CH ₃	-
4	5.24-5.28 (1H, s)	56.40+56.47, CH	C4→H5(⁴ <i>J</i>), H9(³ <i>J</i>), NH _α (² <i>J</i>)
5	6.84-6.85 (1H, m)	117.3, CH _{arom}	C5→H8(² <i>J</i>), NH _β (⁷ <i>J</i>)
6	-	122.24+122.25, C _q	C6→H5(³ <i>J</i>), H8(² <i>J</i>), H9(² <i>J</i>)
7	-	123.86+123.94, C _q	C7→H4(² <i>J</i>), H5(³ <i>J</i>), NH _β (⁵ <i>J</i>)
8	7.23 (1H, m)	129.5, CH _{arom}	C8→H9(³ <i>J</i>)
9	7.23 (1H, m)	129.68+129.74, CH _{arom}	C9→H4(³ <i>J</i>), H8(³ <i>J</i>), NH _α (⁴ <i>J</i>), NH _β (⁶ <i>J</i>)
10	-	154.84+154.88, C _q	C10→H4(³ <i>J</i>), H5(² <i>J</i>), H8(³ <i>J</i>), H9(³ <i>J</i>), NH _β (⁶ <i>J</i>)
11	-	155.8+155.9, C _q	C11→H2(³ <i>J</i>), H4(³ <i>J</i>), NH _α (² <i>J</i>)
12	-	170.03+170.07, C _q	C12→H1(³ <i>J</i>), H2(² <i>J</i>), H3(³ <i>J</i>)
13	-	172.05+172.09, C _q	C13→H2(⁶ <i>J</i>), H4(² <i>J</i>), NH _α (³ <i>J</i>)
NH _α	8.50+8.51 (1H, s)	-	-
NH _β	10.19+10.21 (1H, s)	-	-

Note: The ¹H- and ¹³C-NMR-spectra show a mixture of rotamers.

6.3.3.1.3 Synthesis of (2*S*)-methyl 2-(3-(5-chloro-2-oxo-2,3-dihydrobenzofuran-3-yl)ureido)-3-methylbutanoate (**297**)



Prepared according to *GP-V* using (*S*)-methyl 3-methyl-2-ureidobutanoate **244** (1.00 g, 5.74 mmol, 1.0 eq.), glyoxylic acid monohydrate **188** (0.53 g, 5.74 mmol, 1.0 eq.), *p*-chlorophenol **290** (0.89 g, 6.89 mmol, 1.2 eq.) in 9 ml of TFA. **297** was obtained as a colourless solid in a yield of 24%.

Yield: 0.47 g (1.38 mmol, 24%).

Appearance: Colourless solid.

R_f-Value: 0.56 (SiO₂, DCM/MeOH 20:1).

IR: $\tilde{\nu}$ [cm⁻¹] = 3325 (br), 2966 (w), 1776 (m), 1704 (vs), 1600 (w), 1552 (w), 1500 (m), 1427 (s), 1280 (s), 1215 (m), 1175 (m), 1116 (m), 1011 (w), 941 (w), 911 (w), 891 (w), 857 (w), 816 (m).

MP: 121 °C.

HR-MS (ESI): Theor.[M+H]⁺: 341.08987, found: 341.09031.

Theor.[M+Na]⁺: 363.07182, found: 363.07224.

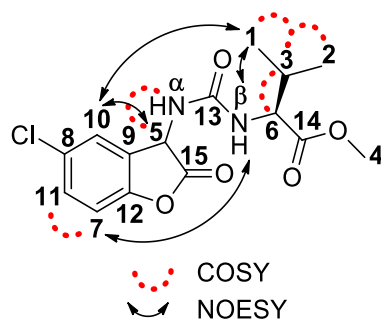
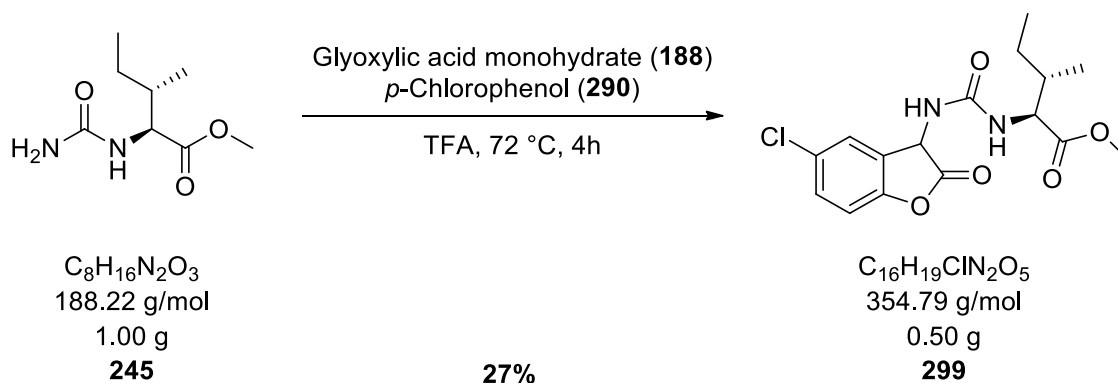


Table 62: 1D and 2D-NMR data of (2S)-methyl 2-(3-(5-chloro-2-oxo-2,3-dihydrobenzofuran-3-yl)ureido)-3-methylbutanoate (297) in DMSO-d₆, at 298 K and 500 MHz for ¹H and 125 MHz for ¹³C.

No.	δ_{H} [ppm], J in [Hz]	δ_{C} [ppm], mult.	HMBC ($^{\circ}J$)
1	0.89 (3H, d, $J = 6.8$ Hz)	18.92+18.94, CH ₃	C1→H2(³ J), H3(² J), H6(³ J)
2	1.03 (3H, d, $J = 6.8$ Hz)	20.50+20.58, CH ₃	C2→H1(³ J), H3(² J), H6(³ J)
3	2.52 (1H, m)	27.9+28.1, CH	C3→H1(² J), H2(² J), H6(² J)
4	3.63 (3H, s)	52.01+52.10, CH ₃	-
5	5.32 (1H, d, $J = 0.8$ Hz)	56.12+56.42, CH	C5→H7(⁴ J), H10(³ J), NH _{α} (² J)
6	4.33 (1H, d, $J = 6.5$ Hz)	56.97+57.06, CH	C6→H1(³ J), H2(³ J), H3(² J)
7	6.86 (1H, d, $J = 8.7$ Hz)	117.24+117.27, CH _{arom}	C7→H10(⁴ J), NH _{β} (⁷ J)
8	-	122.19+122.22, C _q	C8→H7(³ J), H10(² J), H11(² J)
9	-	123.6+123.7, C _q	C9→H5(² J), H7(³ J), NH _{β} (⁵ J)
10	7.19 (1H, d, $J = 2.7$ Hz)	129.35+129.67, CH _{arom}	C10→H5(³ J), H11(³ J)
11	7.24+7.25 (1H, dd, $J = 8.7, 2.7$ Hz)	129.52+129.55, CH _{arom}	C11→H10(³ J)
12	-	154.82+154.86, C _q	C12→H7(² J), H10(³ J), H11(³ J), NH _{β} (⁶ J)
13	-	156.20+156.29, C _q	C13→H5(³ J), H6(³ J), NH _{α} (² J)
14	-	168.8+168.9, C _q	C14→H3(³ J), H4(³ J), H6(² J)
15	-	172.33+172.44, C _q	C15→H5(² J), H6(⁶ J), NH _{α} (³ J)
NH _{α}	8.53+8.55 (1H, s)		
NH _{β}	10.2+10.22 (1H, s)	-	-

Note: The ¹H- and ¹³C-NMR-spectra show a mixture of rotamers.

6.3.3.1.4 Synthesis of (2*S*,3*S*)-methyl 2-(3-(5-chloro-2-oxo-2,3-dihydrobenzofuran-3-yl)ureido)-3-methylpentanoate (**299**)



Prepared according to **GP-V** using (2*S*,3*S*)-methyl 3-methyl-2-ureidopentanoate **245** (1.00 g, 5.31 mmol, 1.0 eq.), glyoxylic acid monohydrate **188** (0.49 g, 5.32 mmol, 1.0 eq.), *p*-chlorophenol **290** (0.82 g, 6.37 mmol, 1.2 eq.) in 9 ml of TFA. **299** was obtained as a colourless solid in a yield of 27%.

Yield: 0.50 g (1.41 mmol, 27%).

Appearance: Colourless solid.

R_f-Value: 0.07 (SiO₂, DCM/MeOH 50:1).

IR: $\tilde{\nu}$ [cm⁻¹] = 3309 (br), 2963 (w), 2329 (w), 1868 (w), 1844 (w), 1772 (w), 1702 (vs), 1653 (w), 1647 (w), 1635 (w), 1616 (w), 1576 (w), 1558 (w), 1541 (w), 1522 (w), 1508 (m), 1498 (m), 1489 (w), 1473 (w), 1430 (s), 1387 (w), 1362 (w), 1339 (w), 1279 (m), 1204 (w), 1116 (m), 1020 (w), 1003 (w), 949 (w), 909 (w), 888 (w), 878 (w), 856 (w), 837 (w), 828 (w), 816 (m).

MP: 157 °C.

HR-MS (ESI): Theor.[M+H]⁺: 355.10552, found: 355.10600.

Theor.[M+Na]⁺: 377.08747, found: 377.08790.

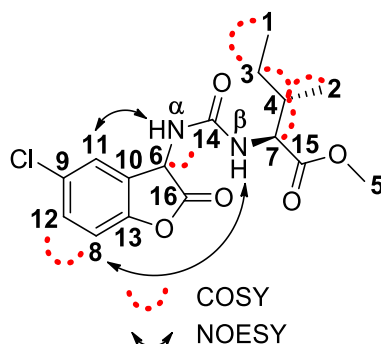
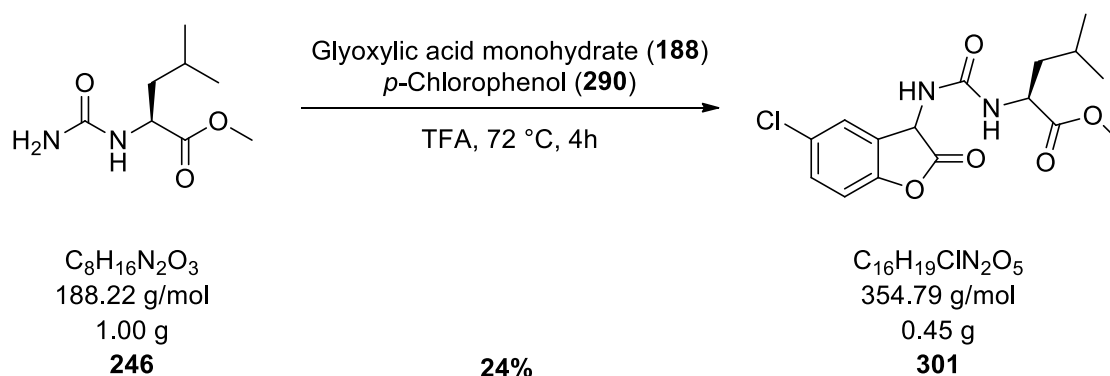


Table 63: 1D and 2D-NMR data of (2S,3S)-methyl 2-(3-(5-chloro-2-oxo-2,3-dihydrobenzofuran-3-yl)ureido)-3-methylpentanoate (299) in DMSO- d_6 , at 298 K and 500 MHz for ^1H and 125 MHz for ^{13}C .

No.	δ_{H} [ppm], J in [Hz]	δ_{C} [ppm], mult.	HMBC ($^{\circ}\text{J}$)
1	0.83 (3H, t, $J = 7.4$ Hz)	10.8+10.9, CH_3	$\text{C1} \rightarrow \text{H3} (^2\text{J}), \text{H4} (^3\text{J}),$
2	1.00 (3H, d, $J = 6.7$ Hz)	16.41+16.44, CH_3	$\text{C2} \rightarrow \text{H3} (^3\text{J}), \text{H4} (^2\text{J}), \text{H7} (^3\text{J})$
3	1.03-1.09 (1H, m); 1.52 (1H, ddq, $J = 14.3, 10.8, 7.3$ Hz)	24.8+24.9, CH_2	$\text{C3} \rightarrow \text{H1} (^2\text{J}), \text{H2} (^3\text{J}), \text{H4} (^2\text{J}), \text{H7} (^3\text{J})$
4	2.26-2.37 (1H, m)	33.7+34.0, CH	$\text{C4} \rightarrow \text{H1} (^3\text{J}), \text{H2} (^2\text{J}), \text{H3} (^2\text{J}), \text{H7} (^2\text{J})$
5	3.62+3.64 (3H, s)	52.02+52.10, CH_3	-
6	5.28+5.33 (1H, d, $J = 0.8$ Hz)	56.03+56.35, CH	$\text{C6} \rightarrow \text{H11} (^3\text{J}), \text{NH}_\alpha (^2\text{J})$
7	4.37+4.39 (1H, d, $J = 8.0$ Hz)	56.30+56.41, CH	$\text{C7} \rightarrow \text{H2} (^3\text{J}), \text{H4} (^2\text{J})$
8	6.86+6.88 (1H, d, $J = 8.7$ Hz)	117.26+117.29, CH_{arom}	$\text{C8} \rightarrow \text{NH}_\beta (^7\text{J})$
9	-	122.20+122.22, C_q	$\text{C9} \rightarrow \text{H8} (^3\text{J}), \text{H11} (^2\text{J}), \text{H12} (^2\text{J})$
10	-	123.66+123.74, C_q	$\text{C10} \rightarrow \text{H6} (^2\text{J}), \text{H8} (^3\text{J}), \text{NH}_\beta (^5\text{J})$
11	7.15+7.20 (1H, d, $J = 2.7$ Hz)	129.33+129.62, CH_{arom}	$\text{C11} \rightarrow \text{H6} (^3\text{J})$
12	7.24+7.25 (1H, dd, $J = 8.6, 2.4$ Hz)	129.51+129.54, CH_{arom}	$\text{C12} \rightarrow \text{H11} (^3\text{J})$
13	-	154.83+154.86, C_q	$\text{C13} \rightarrow \text{H6} (^3\text{J}), \text{H8} (^2\text{J}), \text{H11} (^3\text{J}), \text{H12} (^3\text{J}), \text{NH}_\beta (^6\text{J})$
14	-	156.19+159.28, C_q	$\text{C14} \rightarrow \text{H6} (^3\text{J}), \text{H7} (^3\text{J}), \text{NH}_\alpha (^2\text{J})$
15	-	168.85+168.97, C_q	$\text{C15} \rightarrow \text{H5} (^3\text{J}), \text{H7} (^2\text{J})$
16	-	172.32+172.41, C_q	$\text{C16} \rightarrow \text{H6} (^2\text{J}), \text{H7} (^6\text{J}), \text{NH}_\alpha (^3\text{J})$
NH_α	8.53+8.55 (1H, s)	-	-
NH_β	10.17+10.19 (1H, d, $J = 8.0$ Hz)	-	-

Note: The ^1H - and ^{13}C -NMR-spectra show a mixture of rotamers.

6.3.3.1.5 Synthesis of (2*S*)-methyl 2-(3-(5-chloro-2-oxo-2,3-dihydrobenzofuran-3-yl)ureido)-4-methylpentanoate (**301**)



Prepared according to *GP-V* using (*S*)-methyl 4-methyl-2-ureidopentanoate **246** (1.00 g, 5.31 mmol, 1.0 eq.), glyoxylic acid monohydrate **188** (0.49 g, 5.32 mmol, 1.0 eq.), *p*-chlorophenol **290** (0.82 g, 6.38 mmol, 1.2 eq.) in 9 ml of TFA. **301** was obtained as a colourless solid in a yield of 24%.

Yield: 0.45 g (1.27 mmol, 24%).

Appearance: Colourless solid.

R_f-Value: 0.33 (SiO₂, DCM/MeOH 60:1).

IR: $\tilde{\nu}$ [cm⁻¹] = 3309 (br), 2959 (w), 2872 (w), 2083 (w), 1776 (m), 1699 (vs), 1599 (w), 1498 (m), 1424 (s), 1389 (w), 1368 (w), 1318 (w), 1276 (m), 1217 (m), 1173 (w), 1135 (w), 1115 (w), 1026 (w), 989 (w), 955 (w), 888 (w), 818 (m).

MP: 80 °C.

HR-MS (ESI): Theor.[M+H]⁺: 355.10552, found: 355.10601.

Theor.[M+Na]⁺: 377.08747, found: 377.08800.

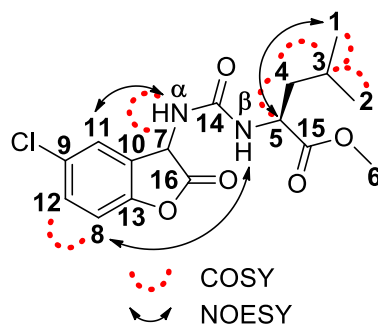
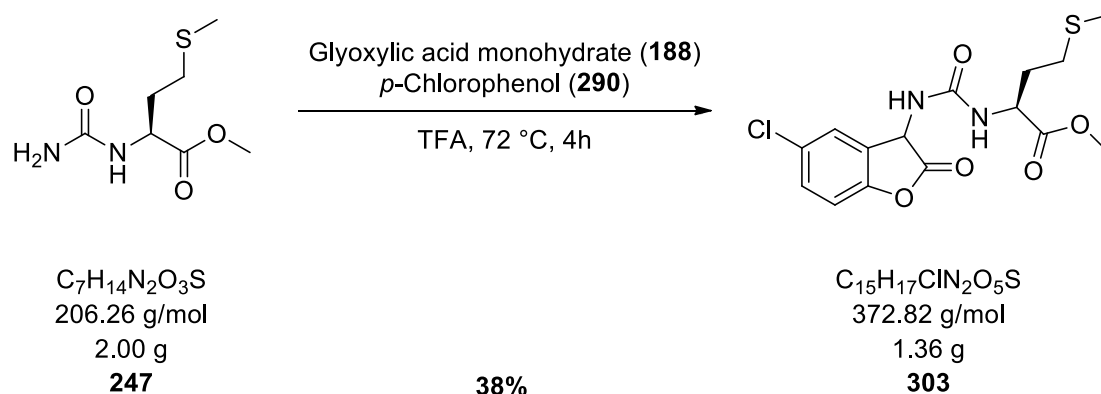


Table 64: 1D and 2D-NMR data of (2*S*)-methyl 2-(3-(5-chloro-2-oxo-2,3-dihydrobenzofuran-3-yl)ureido)-4-methylpentanoate (301) in DMSO- d_6 , at 298 K and 500 MHz for ^1H and 125 MHz for ^{13}C .

No.	δ_{H} [ppm], J in [Hz]	δ_{C} [ppm], mult.	HMBC ($^{\circ}\text{J}$)
1	0.87-0.89 (3H, d, $J = 6.5$ Hz)	20.9, CH_3	$\text{C1} \rightarrow \text{H2} (^3\text{J}), \text{H3} (^2\text{J}), \text{H4} (^3\text{J})$
2	0.90-0.91 (3H, d, $J = 6.5$ Hz)	23.18+23.19, CH_3	$\text{C2} \rightarrow \text{H1} (^3\text{J}), \text{H3} (^2\text{J}), \text{H4} (^3\text{J})$
3	1.54-1.64 (1H, m)	24.0+24.1, CH	$\text{C3} \rightarrow \text{H1} (^2\text{J}), \text{H2} (^2\text{J}), \text{H4} (^2\text{J}), \text{H5} (^3\text{J})$
4	1.72-1.79 (1H, m); 2.03-2.13 (1H, m)	36.5+36.6, CH_2	$\text{C4} \rightarrow \text{H1} (^3\text{J}), \text{H2} (^3\text{J}), \text{H3} (^2\text{J}), \text{H5} (^2\text{J})$
5	4.65+4.67 (1H, dd, $J = 11.1, 4.5$ Hz)	50.04-50.15, CH	$\text{C5} \rightarrow \text{H2} (^4\text{J}), \text{H4} (^2\text{J}), \text{NH}_{\alpha} (^4\text{J})$
6	3.65+3.67 (3H, s)	52.4+52.5, CH_3	-
7	5.30+5.36 (1H, d, $J = 1.1$ Hz)	56.0+56.1, CH	$\text{C7} \rightarrow \text{H8} (^4\text{J}), \text{H11} (^3\text{J}), \text{NH}_{\alpha} (^2\text{J})$
8	6.87+6.88 (1H, d, $J = 8.6$ Hz)	117.25+117.33, CH_{arom}	$\text{C8} \rightarrow \text{NH}_{\beta} (^7\text{J})$
9	-	122.3, C_q	$\text{C9} \rightarrow \text{H8} (^3\text{J}), \text{H11} (^2\text{J}), \text{H12} (^2\text{J})$
10	-	123.68+123.72, C_q	$\text{C10} \rightarrow \text{H7} (^2\text{J}), \text{H8} (^3\text{J}), \text{NH}_{\beta} (^2\text{J})$
11	7.18+7.21 (1H, d, $J = 2.7$ Hz)	129.3, CH_{arom}	$\text{C11} \rightarrow \text{H7} (^3\text{J}), \text{H12} (^3\text{J})$
12	7.23+7.26 (1H, dd, $J = 8.7, 2.7$ Hz)	129.5, CH_{arom}	$\text{C12} \rightarrow \text{H11} (^3\text{J})$
13	-	154.8+154.9, C_q	$\text{C13} \rightarrow \text{H7} (^3\text{J}), \text{H8} (^2\text{J}), \text{H11} (^3\text{J}), \text{H12} (^3\text{J}),$ $\text{NH}_{\beta} (^6\text{J})$
14	-	156.0+156.1, C_q	$\text{C14} \rightarrow \text{H5} (^3\text{J}), \text{H7} (^3\text{J}), \text{NH}_{\alpha} (^2\text{J})$
15	-	169.87+169.92, C_q	$\text{C15} \rightarrow \text{H4} (^3\text{J}), \text{H5} (^2\text{J}), \text{H6} (^3\text{J})$
16	-	172.32+172.37, C_q	$\text{C16} \rightarrow \text{H5} (^6\text{J}), \text{H7} (^2\text{J}), \text{NH}_{\alpha} (^3\text{J})$
NH_{α}	8.55 (1H, s)	-	-
NH_{β}	10.16 (1H, d, $J = 3.8$ Hz)	-	-

Note: The ^1H - and ^{13}C -NMR-spectra show a mixture of rotamers.

6.3.3.1.6 Synthesis of (2*S*)-methyl 2-(3-(5-chloro-2-oxo-2,3-dihydrobenzofuran-3-yl)ureido)-4-(methylthio)butanoate (**303**)



Prepared according to **GP-V** using (*S*)-methyl 4-(methylthio)-2-ureidobutanoate **247** (2.00 g, 9.70 mmol, 1.0 eq.), glyoxylic acid monohydrate **188** (0.89 g, 9.67 mmol, 1.0 eq.), *p*-chlorophenol **290** (1.49 g, 11.6 mmol, 1.2 eq.) in 16 ml of TFA. **303** was obtained as a pale-yellow solid in a yield of 38%.

Yield: 1.36 g (3.65 mmol, 38%).

Appearance: Pale-yellow solid.

R_f-Value: 0.36 (SiO₂, DCM/MeOH 40:1).

IR: $\tilde{\nu}$ [cm⁻¹] = 3324 (m), 2955 (w), 2920 (w), 2875 (w), 1776 (w), 1705 (vs), 1648 (w), 1636 (w), 1601 (w), 1536 (w), 1499 (w), 1430 (s), 1362 (w), 1278 (m), 1245 (w), 1199 (w), 1176 (w), 1119 (w), 1094 (w), 1053 (w), 987 (w), 966 (w), 958 (w), 938 (w), 907 (w), 894 (w), 818 (w), 808 (w).

MP: 226 °C.

HR-MS (ESI): Theor.[M+H]⁺: 373.06194, found: 373.06239.

Theor.[M+Na]⁺: 395.04389, found: 395.04416.

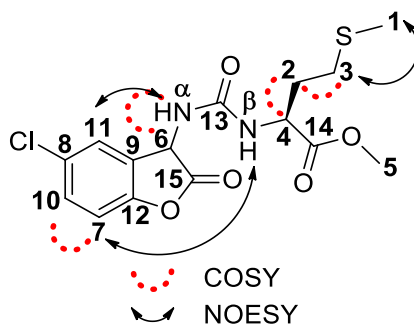
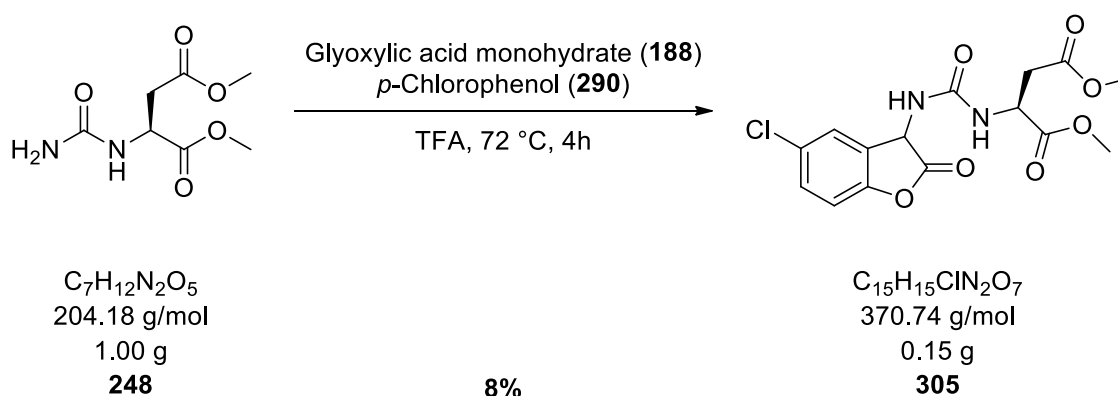


Table 65: 1D and 2D-NMR data of (2*S*)-methyl 2-(3-(5-chloro-2-oxo-2,3-dihydrobenzofuran-3-yl)ureido)-4-(methylthio)butanoate (303) in DMSO-*d*₆, at 298 K and 500 MHz for ¹H and 125 MHz for ¹³C.

No.	δ_{H} [ppm], J in [Hz]	δ_{C} [ppm], mult.	HMBC ($^{\circ}$ J)
1	2.05 (3H, s)	14.45+14.46, CH ₃	C1→H3(³ J)
2	2.27 (2H, m)	27.4+27.7, CH ₂	C2→H3(² J), H4(² J)
3	2.46 (1H, m); 2.56 (1H, m)	29.55+29.63, CH ₂	C3→H1(³ J), H2(² J)
4	4.81 (1H, m)	50.5+50.7, CH	C4→H2(² J), H3(³ J)
5	3.66+3.68 (3H, s)	52.50+52.6, CH ₃	-
6	5.28+5.34 (1H, d, $J = 1.1$ Hz)	56.3+56.4, CH	C6→H7(⁴ J), H11(³ J), NH _{α} (² J)
7	6.85-6.87+6.86-6.88 (1H, d, $J = 8.9$ Hz)	117.25+117.30, CH _{arom}	C7→NH _{β} (⁷ J)
8	-	122.26+122.27, C _q	C8→H10(² J), H11(² J), H7(³ J)
9	-	123.63+123.65, C _q	C9→H6(² J), H7(³ J), NH _{β} (⁵ J)
10	7.24 (1H, m)	129.55+129.57, CH _{arom}	C10→H11(³ J)
11	7.24 (1H, m)	129.7+129.9, CH _{arom}	C11→H6(³ J), H10(³ J)
12	-	154.77+154.84, C _q	C12→H6(³ J), H7(² J), H10(³ J), H11(³ J), NH _{β} (⁶ J)
13	-	155.9+156.0, C _q	C13→H4(³ J), H6(³ J), NH _{α} (² J)
14	-	169.4+169.5, C _q	C14→H2(³ J), H4(² J), H5(³ J)
15	-	172.38+172.40, C _q	C15→H4(⁶ J), H6(² J), NH _{α} (³ J)
NH _{α}	8.55 (1H, s)	-	-
NH _{β}	10.22 (1H, d, $J = 4.9$ Hz)	-	-

Note: The ¹H- and ¹³C-NMR-spectra show a mixture of rotamers.

6.3.3.1.7 Synthesis of (2*S*)-dimethyl 2-(3-(5-chloro-2-oxo-2,3-dihydrobenzofuran-3-yl)ureido)succinate (**305**)



Prepared according to **GP-V** using (*S*)-dimethyl 2-ureidosuccinate **248** (1.00 g, 4.90 mmol, 1.0 eq.), glyoxylic acid monohydrate **188** (0.44 g, 4.90 mmol, 1.0 eq.), *p*-chlorophenol **390** (0.76 g, 5.88 mmol, 1.2 eq.) in 8 ml of TFA. **305** was obtained as a colourless solid in a yield of 8%.

Yield: 0.15 g (0.40 mmol, 8%).

Appearance: Colourless solid.

R_f-Value: 0.50 (SiO₂, DCM/MeOH 50:1).

IR: $\tilde{\nu}$ [cm⁻¹] = 3326 (br), 2956 (w), 2329 (w), 1773 (w), 1708 (vs), 1647 (w), 1636 (w), 1602 (w), 1558 (w), 1541 (w), 1498 (w), 1435 (s), 1373 (w), 1279 (m), 1233 (w), 1174 (m), 1118 (w), 1004 (m), 951 (w), 904 (w), 817 (m).

MP: 95 °C.

HR-MS (ESI): Theor.[M+H]⁺: 371.06405, found: 371.06458.

Theor.[M+Na]⁺: 393.04599, found: 393.04631.

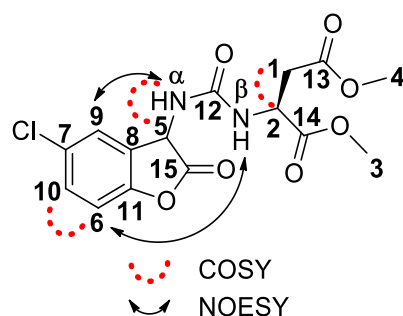
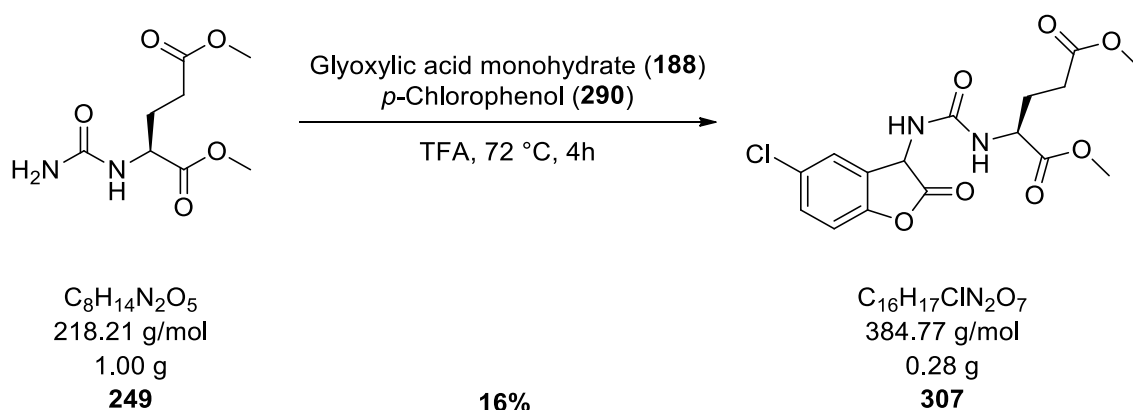


Table 66: 1D and 2D-NMR data of (2*S*)-dimethyl 2-(3-(5-chloro-2-oxo-2,3-dihydrobenzofuran-3-yl)ureido)succinate (305) in DMSO-*d*₆, at 298 K and 500 MHz for ¹H and 125 MHz for ¹³C.

No.	δ_H [ppm], <i>J</i> in [Hz]	δ_C [ppm], mult.	HMBC (nJ)
1	3.13+3.18 (1H, dd, <i>J</i> = 16.6, 8.0 Hz); 2.83+2.86 (1H, ψ t, <i>J</i> = 16.6, 6.8 Hz)	33.0+33.2, CH ₂	C1→H2(² J)
2	5.02-5.07 (1H, ψ dd, <i>J</i> = 8.0, 6.4 Hz)	47.7+47.8, CH	C2→H1(² J)
3	3.63+3.64 (3H, s)	51.8, CH ₃	-
4	3.67+3.68 (3H, s)	52.8+52.9, CH ₃	-
5	5.30+5.33 (1H, d, <i>J</i> = 1.0 Hz)	56.0+56.1, CH	C5→H6(⁴ J), H9(³ J), NH _{α} (² J)
6	6.85-6.86+6.85-6.87 (1H, d, <i>J</i> = 8.7 Hz)	117.28+117.32, CH _{arom}	C6→NH _{β} (⁷ J)
7	-	122.34+122.35, C _q	C7→H6(³ J), H9(² J), H10(² J)
8	-	123.62+123.63, C _q	C8→H5(² J), H6(³ J), NH _{β} (⁵ J)
9	7.18-7.20+7.19-7.21 (1H, d, <i>J</i> = 2.7 Hz)	129.28+129.32, CH _{arom}	C9→H5(³ J), H10(³ J)
10	7.25 (1H, dd, <i>J</i> = 8.6, 2.7 Hz)	129.6, CH _{arom}	C10→H9(³ J)
11	-	154.75+154.78, C _q	C11→H5(³ J), H9(³ J), H10(³ J), NH _{β} (⁶ J)
12	-	155.5, C _q	C12→H2(³ J), H5(³ J), NH _{α} (² J)
13	-	168.68+168.74, C _q	C13→H1(² J), H2(³ J), H4(³ J)
14	-	170.13+170.15, C _q	C14→H1(³ J), H2(² J), H3(³ J)
15	-	171.9+172.0, C _q	C15→H2(⁶ J), H5(² J), NH _{α} (³ J)
NH _{α}	8.62+8.63 (1H, d, <i>J</i> = 1.2 Hz)	-	-
NH _{β}	10.21 (1H, d, <i>J</i> = 3.8 Hz)	-	-

Note: The ¹H- and ¹³C-NMR-spectra show a mixture of rotamers.

6.3.3.1.8 Synthesis of (2*S*)-dimethyl 2-(3-(5-chloro-2-oxo-2,3-dihydrobenzofuran-3-yl)ureido)pentanedioate (**307**)



Prepared according to **GP-V** using (*S*)-dimethyl 2-ureidopentanedioate **249** (1.00 g, 4.58 mmol, 1.0 eq.), glyoxylic acid monohydrate **188** (0.42 g, 4.58 mmol, 1.0 eq.), *p*-chlorophenol **290** (0.71 g, 5.50 mmol, 1.2 eq.) in 7 ml of TFA. **307** was obtained as a colourless solid in a yield of 16%.

Yield: 0.28 g (0.73 mmol, 16%).

Appearance: Colourless solid.

R_f-Value: 0.23 (SiO₂, DCM/MeOH 80:1).

IR: $\tilde{\nu}$ [cm⁻¹] = 3318 (br), 2955 (w), 2924 (w), 2852 (w), 2080 (w), 1778 (w), 1699 (vs), 1600 (w), 1497 (m), 1424 (s), 1362 (w), 1326 (w), 1275 (m), 1202 (w), 1173 (m), 1137 (w), 1118 (w), 1094 (w), 1001 (w), 985 (w), 907 (w), 858 (w), 819 (m).

MP: 71 °C.

HR-MS (ESI): Theor.[M+H]⁺: 385.07970, found: 385.08033.

Theor.[M+Na]⁺: 407.06164, found: 407.06205.

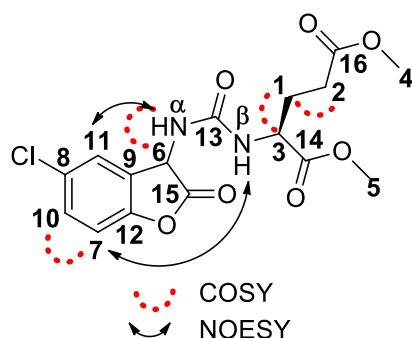
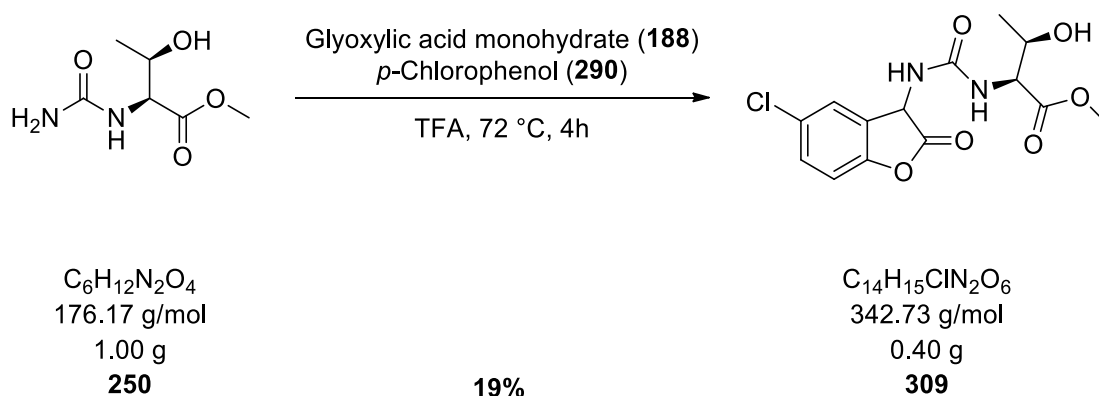


Table 67: 1D and 2D-NMR data of (2S)-dimethyl 2-(3-(5-chloro-2-oxo-2,3-dihydrobenzofuran-3-yl)ureido)pentanedioate (307) in DMSO- d_6 , at 298 K and 500 MHz for ^1H and 125 MHz for ^{13}C .

No.	δ_{H} [ppm], J in [Hz]	δ_{C} [ppm], mult.	HMBC ($^{\circ}\text{J}$)
1	2.14-2.23 (1H, m); 2.28-2.37 (1H, m)	23.3+23.5, CH_2	$\text{C1} \rightarrow \text{H2} (^2\text{J}), \text{H3} (^2\text{J})$
2	2.37-2.45 (2H, m)	29.54+29.59, CH_2	$\text{C2} \rightarrow \text{H1} (^2\text{J}), \text{H3} (^3\text{J})$
3	4.65-4.68+4.69-4.72 (1H, dd, $J = 10.4, 4.5$ Hz)	50.81+50.84, CH	$\text{C3} \rightarrow \text{H1} (^2\text{J}), \text{H2} (^3\text{J})$
4	3.59+3.60 (3H, s)	51.4, CH_3	-
5	3.66+3.68 (3H, s)	52.46+52.54, CH_3	-
6	5.28-5.34 (1H, s)	56.3+56.5, CH	$\text{C6} \rightarrow \text{H7} (^4\text{J}), \text{H11} (^3\text{J}), \text{NH}_{\alpha} (^2\text{J})$
7	6.87 (1H, d, $J = 9.0$ Hz)	117.26+117.32, CH_{arom}	$\text{C7} \rightarrow \text{NH}_{\beta} (^7\text{J})$
8	-	122.28+122.30, C_q	$\text{C8} \rightarrow \text{H7} (^3\text{J}), \text{H10} (^2\text{J}), \text{H11} (^2\text{J})$
9	-	123.60+123.64, C_q	$\text{C9} \rightarrow \text{H6} (^2\text{J}), \text{H7} (^3\text{J}), \text{NH}_{\beta} (^5\text{J})$
10	7.21+7.24 (1H, d, $J = 2.6$ Hz)	129.54+129.93, CH_{arom}	$\text{C10} \rightarrow \text{H6} (^5\text{J}), \text{H11} (^3\text{J})$
11	7.25 (1H, m)	129.57+129.59, CH_{arom}	-
12	-	154.8+154.9, C_q	$\text{C12} \rightarrow \text{H6} (^3\text{J}), \text{H7} (^2\text{J}), \text{H10} (^3\text{J}), \text{H11} (^3\text{J}),$ $\text{NH}_{\beta} (^6\text{J})$
13	-	155.9+156.0, C_q	$\text{C13} \rightarrow \text{H3} (^3\text{J}), \text{H6} (^3\text{J}), \text{NH}_{\alpha} (^2\text{J})$
14	-	169.2+169.3, C_q	$\text{C14} \rightarrow \text{H3} (^2\text{J}), \text{H5} (^3\text{J})$
15	-	172.35+172.40, C_q	$\text{C15} \rightarrow \text{H3} (^6\text{J}), \text{H6} (^2\text{J}), \text{NH}_{\alpha} (^3\text{J})$
16	-	172.65+172.72, C_q	$\text{C16} \rightarrow \text{H1} (^3\text{J}), \text{H2} (^3\text{J}), \text{H3} (^4\text{J}), \text{H4} (^3\text{J})$
NH_{α}	8.56 (1H, s)	-	-
NH_{β}	10.23+10.24 (1H, s)	-	-

Note: The ^1H - and ^{13}C -NMR-spectra show a mixture of rotamers.

6.3.3.1.9 Synthesis of (2*S*,3*R*)-methyl 2-(3-(5-chloro-2-oxo-2,3-dihydrobenzofuran-3-yl)ureido)-3-hydroxybutanoate (**309**)



Prepared according to **GP-V** using (2*S*,3*R*)-methyl 3-hydroxy-2-ureidobutanoate **250** (1.00 g, 5.68 mmol, 1.0 eq.), glyoxylic acid monohydrate **188** (0.53 g, 5.68 mmol, 1.0 eq.), *p*-chlorophenol **290** (0.88 g, 6.82 mmol, 1.2 eq.) in 10 ml of TFA. **309** was obtained as a colourless solid in a yield of 19%.

Yield: 0.40 g (1.17 mmol, 19%).

Appearance: Colourless solid.

R_f-Value: 0.21 (SiO₂, DCM/MeOH 60:1).

IR: $\tilde{\nu}$ [cm⁻¹] = 3231 (br), 2955 (w), 2104 (w), 1746 (w), 1690 (vs), 1600 (m), 1497 (m), 1423 (s), 1382 (w), 1362 (w), 1277 (s), 1224 (w), 1175 (m), 1116 (w); 1076 (w), 1026 (w), 945 (w), 900 (w), 885 (w), 864 (w), 819 (w).

MP: 195 °C.

HR-MS (ESI): Theor.[M+H]⁺: 343.06914, found: 343.06964.

Theor.[M+Na]⁺: 365.05108, found: 365.05162.

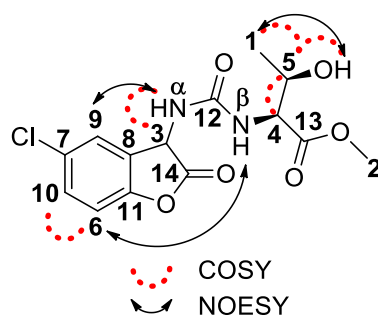
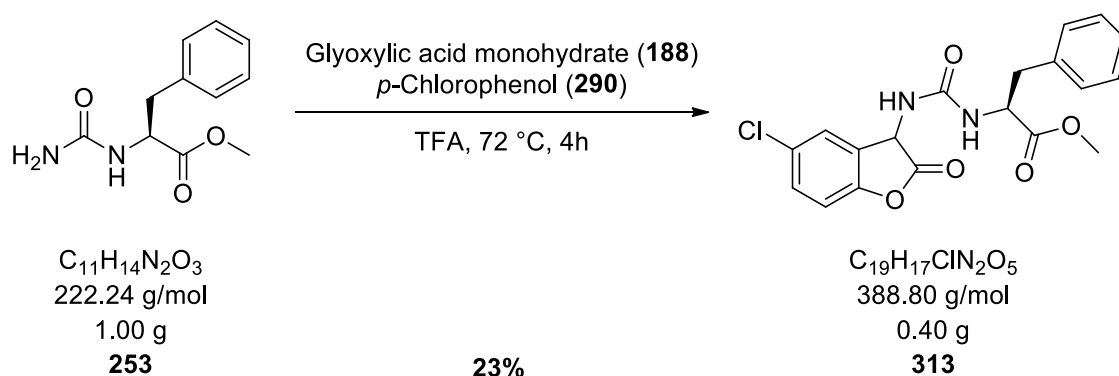


Table 68: 1D and 2D-NMR data of (2*S*,3*R*)-methyl 2-(3-(5-chloro-2-oxo-2,3-dihydrobenzofuran-3-yl)ureido)-3-hydroxybutanoate (309) in DMSO- d_6 , at 298 K and 500 MHz for ^1H and 125 MHz for ^{13}C .

No.	δ_{H} [ppm], J in [Hz]	δ_{C} [ppm], mult.	HMBC ($^{\circ}\text{J}$)
1	1.24 (3H, d, $J = 6.3$ Hz)	21.31+21.34, CH_3	C1→H4(^3J)
2	3.65+3.67 (3H, s)	52.2+52.3, CH_3	-
3	5.38+5.39 (1H, d, $J = 1.1$ Hz)	55.4+55.6, CH	C3→H9(^3J), NH_{α} (^2J)
4	4.47-4.49+4.48-4.49 (1H, d, $J = 7.4$ Hz)	58.2+58.3, CH	C4→H1(^3J)
5	4.26-4.35 (1H, m)	63.6+63.8, CH	C5→H1(^2J), H4(^2J)
6	6.86+6.88 (1H, d, $J = 8.7$ Hz)	117.2+117.3, CH_{arom}	C6→ NH_{β} (^7J)
7	-	122.39+122.42, C_{q}	C7→H6(^3J), H9(^2J), H10(^2J),
8	-	123.81+123.83, C_{q}	C8→H3(^2J), H6(^3J), NH_{β} (^5J)
9	7.19+7.20 (1H, d, $J = 2.7$ Hz)	128.88+128.93, CH_{arom}	C9→H3(^3J), H10(^3J)
10	7.23-7.25 (1H, dd, $J = 8.6, 2.7$ Hz)	129.5, CH_{arom}	C10→H9(^3J)
11	-	154.7+154.8, C_{q}	C11→H3(^3J), H6(^2J), H9(^3J), H10(^3J), NH_{β} (^6J)
12	-	156.5+156.6, C_{q}	C12→H3(^3J), H4(^3J), NH_{α} (^2J)
13	-	168.2, C_{q}	C13→H2(^3J), H4(^2J)
14	-	172.7+172.9, C_{q}	C14→H3(^2J), H4(^6J), NH_{α} (^3J)
OH	4.88+5.03 (1H, d, $J = 7.0$ Hz)	-	-
NH_{α}	8.64+8.68 (1H, s)	-	-
NH_{β}	10.22+10.23 (1H, s)	-	-

Note: The ^1H - and ^{13}C -NMR-spectra show a mixture of rotamers.

6.3.3.1.10 Synthesis of (2*S*)-methyl 2-(3-(5-chloro-2-oxo-2,3-dihydrobenzofuran-3-yl)ureido)-3-phenylpropanoate (**313**)



Prepared according to *GP-V* using (*S*)-methyl 3-phenyl-2-ureidopropanoate **253** (1.00 g, 4.50 mmol, 1.0 eq.), glyoxylic acid monohydrate **188** (0.42 g, 4.50 mmol, 1.0 eq.), *p*-chlorophenol **290** (0.69 g, 5.40 mmol, 1.2 eq.) in 7 ml of TFA. **313** was obtained as a colourless solid in a yield of 23%.

Yield: 0.40 g (1.03 mmol, 23%).

Appearance: Colourless solid.

R_f-Value: 0.35 (SiO₂, DCM/MeOH 20:1).

IR: $\tilde{\nu}$ [cm⁻¹] = 3325 (w), 2955 (w), 2330 (w), 1773 (w), 1705 (s), 1647 (w), 1635 (w), 1597 (w), 1556 (w), 1541 (w), 1497 (w), 1454 (w), 1430 (m), 1363 (w), 1326 (w), 1279 (m), 1249 (w), 1204 (w), 1175 (w), 1118 (w), 1032 (w), 996 (w), 967 (w), 960 (w), 950 (w), 907 (w), 879 (w), 816 (w).

MP: 206 °C.

HR-MS (ESI): Theor.[M+H]⁺: 398.08987, found: 397.08991.

Theor.[M+Na]⁺: 411.07182, found: 411.07179.

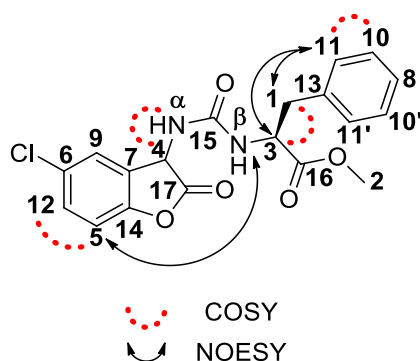
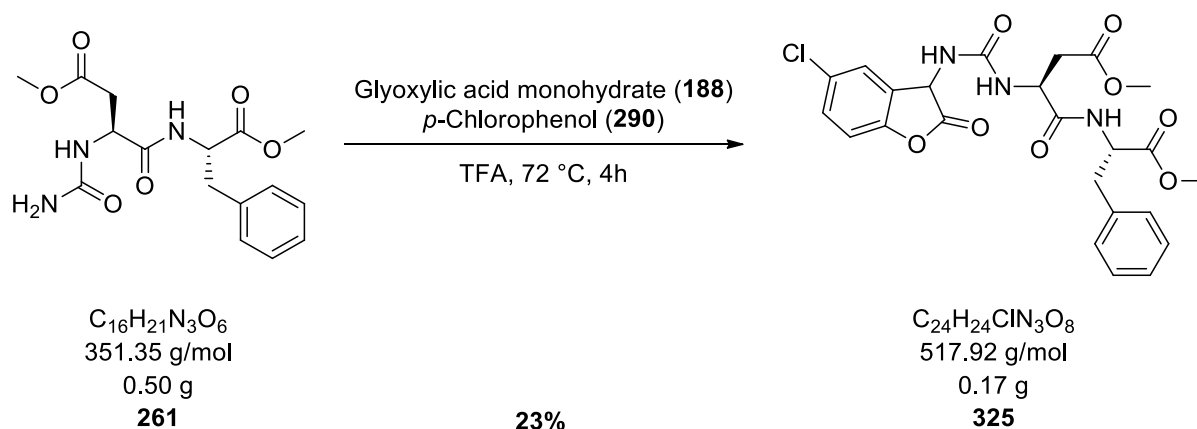


Table 69: 1D and 2D-NMR data of (2*S*)-methyl 2-(3-(5-chloro-2-oxo-2,3-dihydrobenzofuran-3-yl)ureido)-3-phenylpropanoate (313) in DMSO- d_6 , at 298 K and 500 MHz for ^1H and 125 MHz for ^{13}C .

No.	δ_{H} [ppm], J in [Hz]	δ_{C} [ppm], mult.	HMBC ($^{\circ}\text{J}$)
1	3.21-3.32 (1H, m) 3.38+3.40 (1H, m)	33.45+33.41, CH_2	$\text{C1} \rightarrow \text{H3} (^2\text{J})$, $\text{H11} (^3\text{J})$
2	3.70+3.72 (3H, s)	52.62+52.56, CH_3	-
3	4.95-5.00 (1H, m)	52.66, CH	$\text{C3} \rightarrow \text{H1} (^2\text{J})$,
4	5.19+5.30 (1H, d, $J = 1.1$ Hz)	54.5+54.4, CH	$\text{C4} \rightarrow \text{H5} (^4\text{J})$, $\text{H9} (^3\text{J})$, $\text{NH}_{\alpha} (^2\text{J})$
5	6.84+6.86 (1H, d, $J = 8.7$ Hz)	117.3+117.1, CH_{arom}	$\text{C5} \rightarrow \text{NH}_{\beta} (^7\text{J})$
6		122.45+122.42, C_q	$\text{C6} \rightarrow \text{H5} (^3\text{J})$, $\text{H9} (^2\text{J})$, $\text{H12} (^2\text{J})$
7		123.51+123.50, C_q	$\text{C7} \rightarrow \text{H4} (^2\text{J})$, $\text{H5} (^3\text{J})$, $\text{NH}_{\beta} (^5\text{J})$
8	7.23 (1H, m)	126.8+126.7, CH_{arom}	$\text{C8} \rightarrow \text{H11} (^3\text{J})$
9	6.67+6.82 (1H, d, $J = 2.7$ Hz)	127.8+127.6, CH_{arom}	$\text{C9} \rightarrow \text{H4} (^3\text{J})$, $\text{H12} (^3\text{J})$
10	7.27 (2H, m)	128.36+128.35, $2 \times \text{CH}_{\text{arom}}$	$\text{C10} \rightarrow \text{H10} (^3\text{J})$
11	7.16+7.21 (2H, m)	128.97+128.93, $2 \times \text{CH}_{\text{arom}}$	$\text{C11} \rightarrow \text{H1} (^3\text{J})$, $\text{H11} (^3\text{J})$
12	7.21 (1H, m)	129.45+129.42, CH_{arom}	$\text{C12} \rightarrow \text{H9} (^3\text{J})$
13	-	136.92+136.89, C_q	$\text{C13} \rightarrow \text{H1} (^2\text{J})$, $\text{H10} (^3\text{J})$
14	-	154.64+154.63, C_q	$\text{C14} \rightarrow \text{H9} (^3\text{J})$, $\text{H12} (^3\text{J})$, $\text{NH}_{\beta} (^6\text{J})$
15	-	155.9+155.7, C_q	$\text{C15} \rightarrow \text{H3} (^3\text{J})$, $\text{H4} (^3\text{J})$, $\text{NH}_{\alpha} (^2\text{J})$
16	-	169.14+169.07, C_q	$\text{C16} \rightarrow \text{H1} (^3\text{J})$, $\text{H2} (^3\text{J})$, $\text{H3} (^2\text{J})$
17	-	171.9+171.8, C_q	$\text{C17} \rightarrow \text{H3} (^6\text{J})$, $\text{H4} (^2\text{J})$, $\text{NH}_{\alpha} (^3\text{J})$
NH_{α}	8.52 (1H, s)		
NH_{β}	10.17+10.18 (1H, s)		

Note: The ^1H - and ^{13}C -NMR-spectra show a mixture of rotamers.

6.3.3.1.11 Synthesis of (3*S*)-methyl 3-(3-(5-chloro-2-oxo-2,3-dihydrobenzofuran-3-yl)ureido)-4-(((*S*)-1-methoxy-1-oxo-3-phenylpropan-2-yl)amino)-4-oxobutanoate (**325**)



Prepared according to **GP-V** using (*S*)-methyl 4-(((*S*)-1-methoxy-1-oxo-3-phenylpropan-2-yl)amino)-4-oxo-3-ureidobutanoate **261** (0.50 g, 1.42 mmol, 1.0 eq.), glyoxylic acid monohydrate **188** (0.13 g, 1.42 mmol, 1.0 eq.), *p*-chlorophenol **290** (0.22 g, 1.70 mmol, 1.2 eq.) in 3 ml of TFA. **325** was obtained as a colourless solid in a yield of 23%.

Yield: 0.17 g (0.33 mmol, 23%).

Appearance: Colourless solid.

R_f-Value: 0.40 (SiO₂, DCM/MeOH 40:1).

IR: $\tilde{\nu}$ [cm⁻¹] = 3325 (br), 2953 (w), 2924 (w), 2853 (w), 1779 (w), 1715 (vs), 1681 (m), 1603 (w), 1532 (w), 1497 (m), 1426 (s), 1371 (w), 1278 (m), 1221 (m), 1203 (w), 1177 (m), 1014 (w), 944 (w), 903 (w), 820 (m).

MP: 147 °C.

HR-MS (ESI): Theor.[M+H]⁺: 518.13246, found: 518.13259.

Theor.[M+Na]⁺: 540.11441, found: 540.11427.

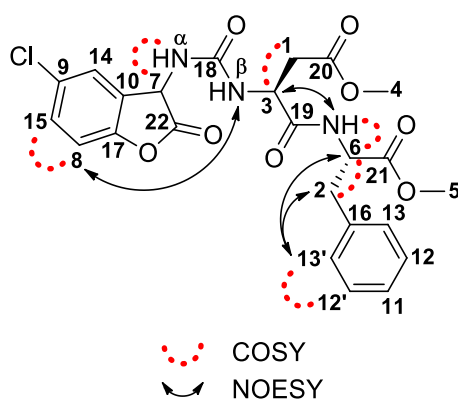
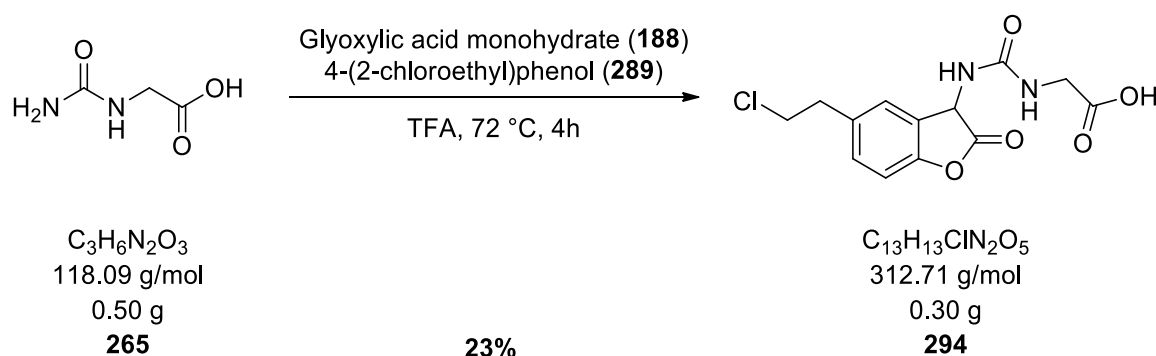


Table 70: 1D and 2D-NMR data of (3*S*)-methyl 3-(3-(5-chloro-2-oxo-2,3-dihydrobenzofuran-3-yl)ureido)-4-(((*S*)-1-methoxy-1-oxo-3-phenylpropan-2-yl)amino)-4-oxobutanoate (325) in DMSO-*d*₆, at 298 K and 500 MHz for ¹H and 125 MHz for ¹³C.

No.	δ_{H} [ppm], J in [Hz]	δ_{C} [ppm], mult.	HMBC ($^{\circ}J$)
1	2.69-2.77 (dd, $J = 16.4, 6.7$ Hz); 3.02-3.13 (1H, dd, $J = 16.4, 7.8$ Hz)	32.7+33.1, CH ₂	C1→H3(² J)
2	2.88-3.01 (1H, m); 2.98 (1H, m)	36.3+36.4, CH ₂	C2→H6(² J), H13(³ J), NH _{amide} (³ J)
3	4.85-4.90 (1H, m)	48.6+49.2, CH	C3→H1(² J)
4	3.59-3.60 (3H, s)	51.60+51.62, CH ₃	-
5	3.58-3.59 (3H, s)	51.90+51.93, CH ₃	-
6	4.38-4.45 (1H, ψ dtd, $J = 11.1, 8.5, 6.1$ Hz)	54.2+54.3, CH	C6→H2(² J), NH _{amide} (² J)
7	5.15+5.28 (1H, d, $J = 1.1$ Hz)	55.7+56.3, CH	C7→H8(⁴ J), H14(³ J), NH _{α} (² J)
8	6.85 (1H, d, $J = 8.7$ Hz)	117.17+117.22, CH _{arom}	-
9	-	122.5+122.6, C _q	C9→H8(³ J), H14(² J), H15(² J)
10	-	123.94+123.95, C _q	C10→H7(² J), H8(³ J)
11	7.19 (1H, m)	126.49+126.51, CH _{arom}	C11→H13(³ J)
12	7.26 (2H, m)	128.24, 2xCH _{arom}	C12→H12(³ J)
13	7.18 (2H, m)	129.0+129.1, 2xCH _{arom}	C13→H2(³ J), H11(³ J)
14	7.25+7.38 (1H, d, $J = 2.7$ Hz)	129.41+129.58, CH _{arom}	C14→H7(³ J), H15(³ J)
15	7.24 (1H, m)	129.46, CH _{arom}	C15→H14(³ J)
16	-	137.16+137.19, C _q	C16→H2(² J), H6(³ J), H12(³ J)
17	-	154.68+154.72, C _q	C17→H7(³ J), H8(² J), H14(³ J), H15(³ J)
18	-	155.7+156.0, C _q	C18→H3(³ J), H7(³ J), NH _{α} (² J)
19	-	167.5+167.6, C _q	C19→H1(³ J), H3(² J), H6(³ J), NH _{amide} (² J)
20	-	170.6+170.7, C _q	C20→H1(² J), H3(³ J), H4(³ J)
21	-	171.8+171.9, C _q	C21→H2(³ J), H5(³ J), H6(² J)
22	-	172.1+172.3, C _q	C22→H7(² J), NH _{α} (³ J)
NH _{amide}	8.65+8.66 (1H, d, $J = 6.0$ Hz)	-	-
NH _{α}	8.47+8.53 (1H, d, $J = 1.2$ Hz)	-	-
NH _{β}	10.19+10.22 (1H, s)	-	-

Note: The ¹H- and ¹³C-NMR-spectra show a mixture of rotamers.

6.3.3.1.12 Synthesis of 2-(3-(5-(2-chloroethyl)-2-oxo-2,3-dihydrobenzofuran-3-yl)ureido)acetic acid (**294**)



Prepared according to *GP-V* using 2-ureidoacetic acid **265** (0.50 g, 4.23 mmol, 1.0 eq.), glyoxylic acid monohydrate **188** (0.39 g, 4.23 mmol, 1.0 eq.), 4-(2-chloroethyl)phenol **289** (0.80 g, 5.08 mmol, 1.2 eq.) in 5 ml of TFA (1.8 ml per 1 mmol of the alcohol/thiol). **294** was obtained as a light-yellow solid in a yield of 23%.

Yield: 0.30 g (0.96 mmol, 23%).

Appearance: Light-yellow solid.

R_f-Value: 0.52 (SiO₂, DCM/MeOH 20:1 + 1% AcOH).

IR: $\tilde{\nu}$ [cm⁻¹] = 3296 (br), 2926 (w), 2331 (w), 1775 (m), 1706 (vs), 1616 (w), 1513 (m), 1456 (m), 1439 (m), 1392 (w), 1331 (w), 1280 (w), 1240 (m), 1207 (w), 1157 (m), 1110 (w), 1074 (w), 926 (m), 851 (w), 823 (w).

MP: Decomposition above 216 °C.

HR-MS (ESI): Theor.[M+H]⁺: 313.05857, found: 313.05886.

Theor.[M+Na]⁺: 335.04052, found: 335.04081.

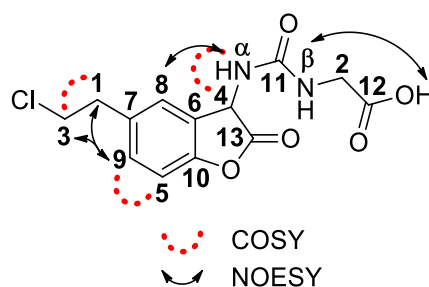
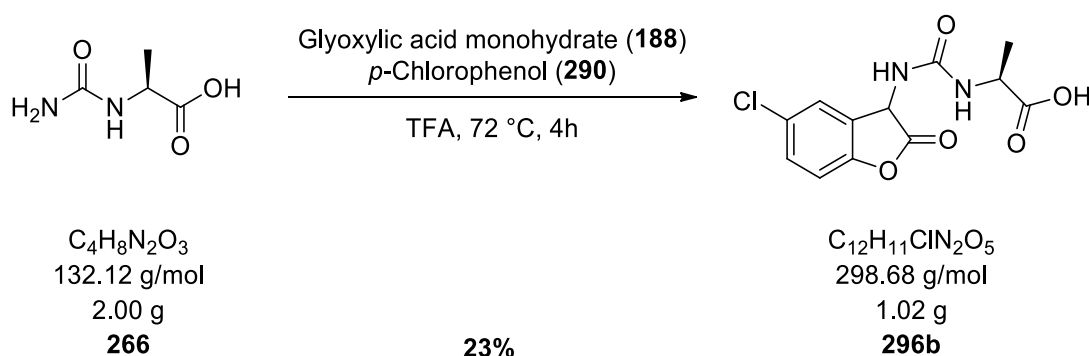


Table 71: 1D and 2D-NMR data of 2-(3-(5-(2-chloroethyl)-2-oxo-2,3-dihydrobenzofuran-3-yl)ureido)acetic acid (294) in DMSO- d_6 , at 298 K and 500 MHz for ^1H and 125 MHz for ^{13}C .

No.	δ_{H} [ppm], J in [Hz]	δ_{C} [ppm], mult.	HMBC ($^{\times}J$)
1	2.90 (2H, td, $J = 7.2, 3.4$ Hz)	37.5, CH_2	$\text{C1} \rightarrow \text{H3} (^2J), \text{H9} (^3J)$
2	4.09 (2H, s)	39.1, CH_2	-
3	3.75 (2H, t, $J = 7.2$ Hz)	45.4, CH_2	$\text{C3} \rightarrow \text{H1} (^2J)$
4	5.30 (1H, d, $J = 1.0$ Hz)	56.3, CH	$\text{C4} \rightarrow \text{H8} (^3J), \text{NH}_{\alpha} (^2J)$
5	6.77 (1H, d, $J = 8.1$ Hz)	115.5, CH_{arom}	$\text{C5} \rightarrow \text{NH}_{\beta} (^7J)$
6	-	121.8, C_q	$\text{C6} \rightarrow \text{H4} (^2J), \text{H5} (^3J), \text{H9} (^4J), \text{NH}_{\beta} (^5J)$
7	-	128.6, C_q	$\text{C7} \rightarrow \text{H1} (^2J), \text{H3} (^3J), \text{H5} (^3J)$
8	7.11 (1H, m)	129.8, CH_{arom}	$\text{C8} \rightarrow \text{H4} (^3J), \text{H9} (^3J)$
9	7.10 (1H, m)	130.2, CH_{arom}	$\text{C9} \rightarrow \text{H1} (^3J), \text{H8} (^3J)$
10	-	154.5, C_q	$\text{C10} \rightarrow \text{H4} (^3J), \text{H5} (^2J), \text{H8} (^3J), \text{H9} (^3J), \text{NH}_{\beta} (^6J)$
11	-	156.3, C_q	$\text{C11} \rightarrow \text{H2} (^3J), \text{H4} (^3J), \text{NH}_{\alpha} (^2J)$
12	-	169.0, C_q	$\text{C12} \rightarrow \text{H2} (^2J)$
13	-	172.9, C_q	$\text{C13} \rightarrow \text{H2} (^6J), \text{H4} (^2J), \text{NH}_{\alpha} (^3J)$
NH_{α}	8.50 (1H, d, $J = 1.1$ Hz)	-	-
NH_{β}	9.76 (1H, s)	-	-
COOH	13.07 (1H, s)	-	-

6.3.3.1.13 Synthesis of (2*S*)-2-(3-(5-chloro-2-oxo-2,3-dihydrobenzofuran-3-yl)ureido)propanoic acid (**296b**)



Prepared according to *GP-V* using (*S*)-2-ureidopropanoic acid **266** (2.00 g, 15.1 mmol, 1.0 eq.), glyoxylic acid monohydrate **188** (1.39 g, 15.1 mmol, 1.0 eq.), *p*-chlorophenol **290** (2.33 g, 18.1 mmol, 1.2 eq.) in 24 ml of TFA. In this case no column chromatography was done, since the product was already pure. **296b** was obtained as a colourless solid in a yield of 24%.

Yield: 1.02 g (3.42 mmol, 23%).

Appearance: Colourless solid.

IR: $\tilde{\nu}$ [cm^{-1}] = 3304 (w), 3149 (br), 1759 (m), 1745 (w), 1686 (vs), 1599 (w), 1499 (w), 1455 (m), 1445 (m), 1427 (m), 1392 (w), 1362 (w), 1290 (m), 1261 (w), 1232 (m), 1185 (m), 1114 (w), 1073 (w), 1013 (w), 989 (w), 908 (w), 893 (w), 854 (w), 825 (m).

MP: Change of colour: 248 °C; Melting at 254 °C.

HR-MS (ESI): Theor. $[\text{M}+\text{Na}]^+$: 321.02487, found: 321.02498.

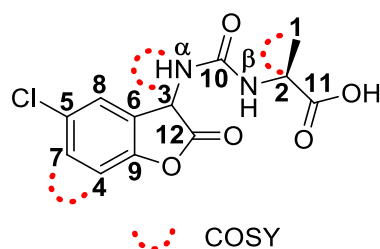
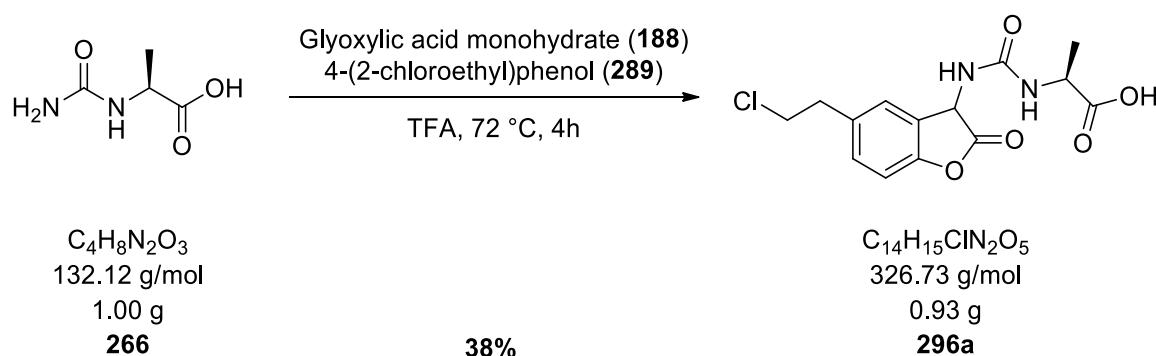


Table 72: 1D and 2D-NMR data of (2*S*)-2-(3-(5-chloro-2-oxo-2,3-dihydrobenzofuran-3-yl)ureido)propanoic acid (296b) in DMSO-*d*₆, at 298 K and 500 MHz for ¹H and 125 MHz for ¹³C.

No.	δ_{H} [ppm], J in [Hz]	δ_{C} [ppm], mult.	HMBC ($^{\circ}J$)
1	1.45 (3H, d, $J = 7.2$ Hz)	14.5, CH ₃	C1→H2(² J)
2	4.62 (1H, q, $J = 7.3$ Hz)	47.7, CH	C2→H1(² J)
3	5.24 (1H, d, $J = 1.1$ Hz)	56.6, CH	C3→H4(⁴ J), H8(³ J), NH _α (² J)
4	6.84-6.86 (1H, m)	117.7, CH _{arom}	C4→H7(² J), NH _β (⁷ J)
5	-	122.7, C _q	C5→H4(³ J), H7(² J), H8(² J)
6	-	124.4, C _q	C6→H3(² J), H4(³ J), NH _β (⁵ J)
7	7.23 (1H, m)	129.9, CH _{arom}	C7→H8(³ J)
8	7.24 (1H, m)	130.1, CH _{arom}	C8→H3(³ J), H7(³ J)
9	-	155.3, C _q	C9→H3(³ J), H4(² J), H7(³ J), H8(³ J), NH _β (⁶ J)
10	-	156.7, C _q	C10→H2(³ J), H3(³ J), NH _α (² J)
11	-	171.6, C _q	C11→H1(³ J), H2(² J)
12	-	172.6, C _q	C12→H2(⁶ J), H3(² J), NH _α (³ J)
NH _α	8.47 (1H, d, $J = 1.2$ Hz)	-	-
NH _β	10.18 (1H, s)	-	-

6.3.3.1.14 Synthesis of (2S)-2-(3-(5-(2-chloroethyl)-2-oxo-2,3-dihydrobenzofuran-3-yl)ureido)propanoic acid (296a)



Prepared according to *GP-V* using (*S*)-2-ureidopropanoic acid **266** (1.00 g, 7.57 mmol, 1.0 eq.), glyoxylic acid monohydrate **188** (0.70 g, 7.57 mmol, 1.0 eq.), 4-(2-chloroethyl)phenol **289** (1.42 g, 9.08 mmol, 1.2 eq.) in 12 ml of TFA. **296a** was obtained as a colourless solid in a yield of 38%.

Yield: 0.93 g (2.85 mmol, 38%).

Appearance: Colourless solid.

R_f-Value: 0.07 (SiO₂, DCM/MeOH 25:1 + 1% AcOH).

IR: $\tilde{\nu}$ [cm⁻¹] = 3684 (w), 3670 (br), 2988 (s), 2972 (s), 2901 (s), 1702 (s), 1514 (w), 1438 (m), 1407 (m), 1394 (m), 1394 (w), 1382 (w), 1250 (m), 1242 (m), 1230 (m), 1153 (w), 1076 (vs), 1066 (vs), 1057 (vs), 1028 (m), 892 (w), 880 (w), 822 (w).

MP: Change of colour: 104 °C; Melting at 145 °C.

HR-MS (ESI): Theor.[M+H]⁺: 327.07422, found: 372.07437.

Theor.[M+Na]⁺: 349.05617, found: 349.05646.

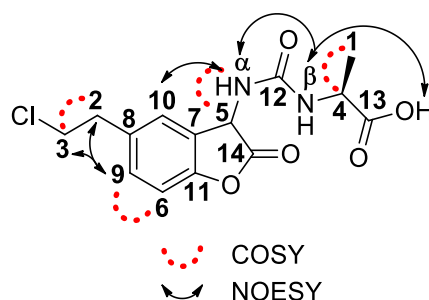
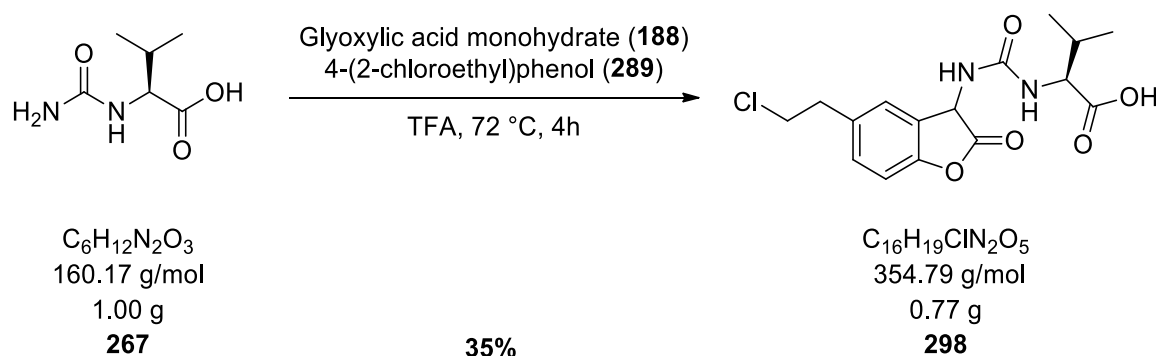


Table 73: 1D and 2D-NMR data of (2*S*)-2-(3-(5-(2-chloroethyl)-2-oxo-2,3-dihydrobenzofuran-3-yl)ureido)propanoic acid (296a) in DMSO-*d*₆, at 298 K and 500 MHz for ¹H and 125 MHz for ¹³C.

No.	δ_{H} [ppm], J in [Hz]	δ_{C} [ppm], mult.	HMBC ($^{\times}J$)
1	1.43+1.45 (3H, d, $J = 7.2$ Hz)	14.1+14.4, CH ₃	C1→H4(² J)
2	2.90 (2H, t, $J = 7.2$ Hz)	37.42+37.45, CH ₂	C2→H3(² J), H10(³ J)
3	3.75 (2H, t, $J = 7.2$ Hz)	45.5, CH ₂	C3→H2(² J)
4	4.60+4.63 (1H, q, $J = 7.2$ Hz)	46.9+47.2, CH	C4→H1(² J)
5	5.14+5.20 (1H, d, $J = 1.0$ Hz)	56.67+56.70, CH	C5→H6(⁴ J), H10(³ J), NH _α (² J)
6	6.77 (1H, d, $J = 8.0$ Hz)	115.48+115.52, CH _{arom}	C6→NH _β (⁷ J)
7		121.9+122.0, C _q	C7→H5(² J), H6(³ J), H10(² J), NH _β (⁵ J)
8		128.46+128.48, C _q	C8→H2(² J), H3(³ J), H6(³ J)
9	7.08 (1H, m)	130.2, CH _{arom}	C9→H2(³ J), H10(³ J)
10	7.09 (1H, m)	130.3+130.4, CH _{arom}	C10→H5(³ J), H9(³ J)
11		154.57+154.58, C _q	C11→H5(³ J), H6(² J), H9(³ J), H10(³ J), NH _β (⁶ J)
12		156.1+156.3, C _q	C12→H4(³ J), H5(³ J), NH _α (² J)
13		171.18, C _q	C13→H1(³ J), H4(² J)
14		172.6+172.7, C _q	C14→H4(⁶ J), H5(² J), NH _α (³ J)
NH _α	8.39+8.42 (1H, d, $J = 1.1$ Hz)	-	-
NH _β	9.74+9.76 (1H, s)	-	-
COOH	12.90 (1H, s)	-	-

Note: The ¹H- and ¹³C-NMR-spectra show a mixture of rotamers.

6.3.3.1.15 Synthesis of (2S)-2-(3-(5-(2-chloroethyl)-2-oxo-2,3-dihydrobenzofuran-3-yl)ureido)-3-methylbutanoic acid (**298**)



Prepared according to **GP-V** using (S)-3-methyl-2-ureidobutanoic acid **267** (1.00 g, 6.24 mmol, 1.0 eq.), glyoxylic acid monohydrate **188** (0.57 g, 6.24 mmol, 1.0 eq.), 4-(2-chloroethyl)phenol **289** (1.17 g, 7.49 mmol, 1.2 eq.) in 10 ml of TFA. **298** was obtained as a yellow solid in a yield of 35%.

Yield: 0.77 g (2.17 mmol, 35%).

Appearance: Yellow solid.

R_f-Value: 0.09 (SiO₂, DCM/MeOH 20:1 + 1% AcOH).

IR: $\tilde{\nu}$ [cm⁻¹] = 3662 (w), 3649 (w), 3294 (br), 2988 (s), 2971 (s), 2901 (s), 1770 (w), 1704 (vs), 1615 (w), 1514 (m), 1434 (s), 1394 (w), 1375 (w), 1277 (m), 1224 (m), 1154 (w), 1105 (w), 1075 (m), 1066 (m), 1056 (m), 1028 (w), 983 (w), 902 (w), 867 (w), 821 (w).

MP: 71 °C.

HR-MS (ESI): Theor.[M+H]⁺: 355.10552, found: 355.10541.

Theor.[M+Na]⁺: 377.08747, found: 377.08742.

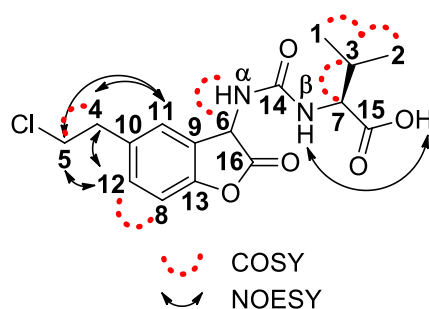
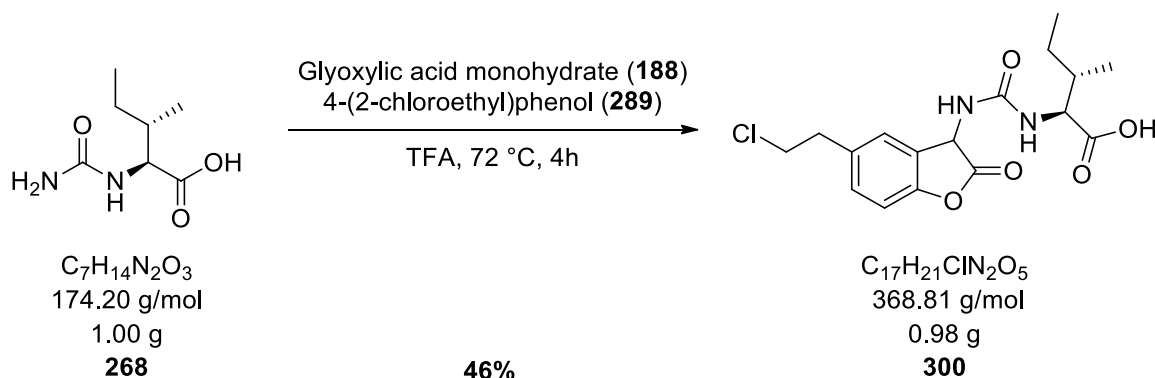


Table 74: 1D and 2D-NMR data of (2*S*)-2-(3-(5-(2-chloroethyl)-2-oxo-2,3-dihydrobenzofuran-3-yl)ureido)-3-methylbutanoic acid (298) in DMSO- d_6 , at 298 K and 500 MHz for ^1H and 125 MHz for ^{13}C .

No.	δ_{H} [ppm], J in [Hz]	δ_{C} [ppm], mult.	HMBC ($^{\circ}\text{J}$)
1	0.87+0.88 (3H, d, $J = 6.8$ Hz)	19.26+19.29, CH_3	$\text{C1} \rightarrow \text{H2} (^3\text{J}), \text{H3} (^2\text{J}), \text{H7} (^3\text{J})$
2	1.04+1.05 (3H, d, $J = 6.7$ Hz)	20.8+21.0, CH_3	$\text{C2} \rightarrow \text{H1} (^3\text{J}), \text{H3} (^2\text{J}), \text{H7} (^3\text{J})$
3	2.49 (1H, m)	27.7+27.9, CH	$\text{C3} \rightarrow \text{H1} (^2\text{J}), \text{H2} (^2\text{J}), \text{H7} (^2\text{J})$
4	2.89+2.90 (2H, t, $J = 7.2$ Hz)	37.4+37.5, CH_2	$\text{C4} \rightarrow \text{H5} (^2\text{J}), \text{H11} (^3\text{J}), \text{H12} (^3\text{J})$
5	3.73+3.74 (2H, t, $J = 7.1$ Hz)	45.5, CH_2	$\text{C5} \rightarrow \text{H4} (^2\text{J})$
6	5.20+5.29 (1H, d, $J = 1.1$ Hz)	56.1+56.5, CH	$\text{C6} \rightarrow \text{H11} (^3\text{J}), \text{NH}_{\alpha} (^2\text{J})$
7	4.19 (1H, d, $J = 7.9$ Hz)	57.1+57.3, CH	$\text{C7} \rightarrow \text{H1} (^3\text{J}), \text{H2} (^3\text{J})$
8	6.79 (1H, d, $J = 8.2$ Hz)	115.5+115.6, CH_{arom}	$\text{C8} \rightarrow \text{NH}_{\beta} (^7\text{J})$
9	-	121.6+121.7, C_{q}	$\text{C9} \rightarrow \text{H6} (^2\text{J}), \text{H8} (^3\text{J}), \text{NH}_{\beta} (^5\text{J})$
10	-	128.4+128.5, C_{q}	$\text{C10} \rightarrow \text{H4} (^2\text{J}), \text{H5} (^3\text{J}), \text{H8} (^3\text{J})$
11	7.02+7.05j (1H, d, $J = 2.3$ Hz)	129.7+130.1, CH_{arom}	$\text{C11} \rightarrow \text{H6} (^3\text{J}), \text{H12} (^3\text{J})$
12	7.09 (1H, ψdt , $J = 8.3, 2.3$ Hz)	130.1+130.2, CH_{arom}	$\text{C12} \rightarrow \text{H4} (^3\text{J}), \text{H11} (^3\text{J})$
13	-	154.5+154.6, C_{q}	$\text{C13} \rightarrow \text{H6} (^3\text{J}), \text{H8} (^2\text{J}), \text{H11} (^3\text{J}), \text{H12} (^3\text{J}), \text{NH}_{\beta} (^6\text{J})$
14	-	156.5, 156.7, C_{q}	$\text{C14} \rightarrow \text{H6} (^3\text{J}), \text{H7} (^3\text{J}), \text{NH}_{\alpha} (^2\text{J})$
15	-	169.97+167.00, C_{q}	$\text{C15} \rightarrow \text{H7} (^2\text{J})$
16	-	172.7+172.9, C_{q}	$\text{C16} \rightarrow \text{H6} (^2\text{J}), \text{H7} (^6\text{J}), \text{NH}_{\alpha} (^3\text{J})$
NH_{α}	8.44+8.46 (1H, dd, $J = 1.2$ Hz)	-	-
NH_{β}	9.78+9.79 (1H, s)	-	-
COOH	12.83 (1H, s)	-	-

Note: The ^1H - and ^{13}C -NMR-spectra show a mixture of rotamers.

6.3.3.1.16 Synthesis of (2*S*,3*S*)-2-(3-(5-(2-chloroethyl)-2-oxo-2,3-dihydrobenzofuran-3-yl)ureido)-3-methylpentanoic acid (**300**)



Prepared according to **GP-V** using (2*S*,3*S*)-3-methyl-2-ureidopentanoic acid **268** (1.00 g, 5.74 mmol, 1.0 eq.), glyoxylic acid monohydrate **188** (0.53 g, 5.74 mmol, 1.0 eq.), 4-(2-chloroethyl)phenol **289** (1.08 g, 6.89 mmol, 1.2 eq.) in 9 ml of TFA. **300** was obtained as a yellow solid in a yield of 30%.

Yield: 0.98 g (2.66 mmol, 46%).

Appearance: Yellow solid.

R_f-Value: 0.33 (SiO₂, DCM/MeOH 30:1 + 1% AcOH).

IR: $\tilde{\nu}$ [cm⁻¹] = 3684 (w), 3675 (br), 2988 (vs), 2972 (vs), 2901 (s), 1772 (w), 1705 (m), 1616 (w), 1514 (w), 1407 (m), 1394 (m), 1382 (m), 1250 (m), 1242 (m), 1229 (m), 1075 (vs), 1066 (vs), 1057 (vs), 1028 (s), 892 (w), 880 (w), 870 (w), 822 (w).

MP: 82 °C.

HR-MS (ESI): Theor.[M+H]⁺: 369.12117, found: 369.12149.

Theor.[M+Na]⁺: 391.10312, found: 391.10336.

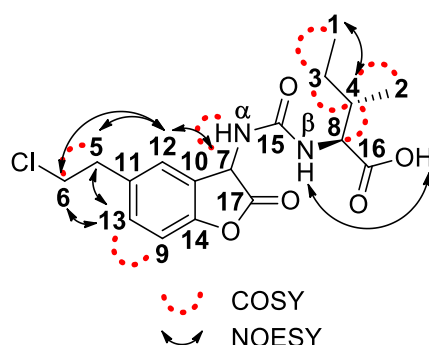
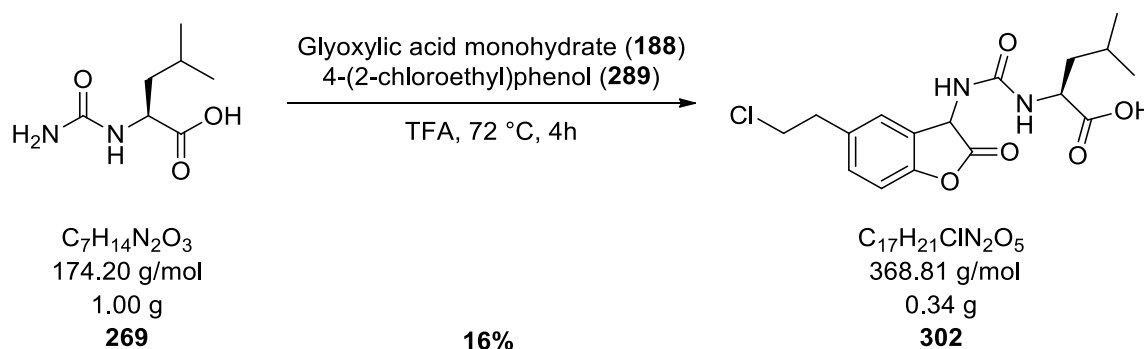


Table 75: 1D and 2D-NMR data of (2*S*,3*S*)-2-(3-(5-(2-chloroethyl)-2-oxo-2,3-dihydrobenzofuran-3-yl)ureido)-3-methylpentanoic acid (300) in DMSO-*d*₆, at 298 K and 500 MHz for ¹H and 125 MHz for ¹³C.

No.	δ_{H} [ppm], <i>J</i> in [Hz]	δ_{C} [ppm], mult.	HMBC ($^{\circ}$ J)
1	0.81+0.82 (3H, t, <i>J</i> = 7.5 Hz)	10.8+10.9, CH ₃	C1→H2(⁴ J), H3(² J), H4(³ J)
2	1.02+1.02 (3H, d, <i>J</i> = 6.8 Hz)	16.7+16.8, CH ₃	C2→H1(⁴ J), H3(³ J), H4(² J), H8(³ J)
3	1.06 (1H, m); 1.48-1.58 (1H, m)	25.05+25.11, CH ₂	C3→H1(² J), H2(³ J), H4(² J)
4	2.24-2.37 (1H, m)	33.5+33.9, CH	C4→H1(³ J), H2(² J), H8(² J)
5	2.89+2.90 (2H, t, <i>J</i> = 7.0 Hz)	37.4+37.5, CH ₂	C5→H6(² J), H12(³ J), H13(³ J)
6	3.74+3.74 (2H, t, <i>J</i> = 7.1 Hz)	45.54+45.55, CH ₂	C6→H5(² J)
7	5.20+5.29 (1H, d, <i>J</i> = 1.1 Hz)	56.0+56.3, CH	C7→H12(³ J), NH _α (² J)
8	4.25+4.26 (1H, d, <i>J</i> = 7.9 Hz)	56.4+56.7, CH	C8→H2(³ J), H3(³ J), H4(² J)
9	6.79 (1H, d, <i>J</i> = 8.2 Hz)	115.5+115.6, CH _{arom}	C9→H13(² J), NH _β (⁷ J)
10	-	121.7+121.8, C _q	C10→H7(² J), H9(³ J), NH _β (⁵ J)
11	-	128.45+128.49, C _q	C11→H5(² J), H6(³ J), H9(³ J)
12	7.01+7.03 (1H, d, <i>J</i> = 2.2 Hz)	129.6+130.0, CH _{arom}	C12→H7(³ J), H13(³ J)
13	7.09 (1H, ψ dt, <i>J</i> = 8.2, 2.0 Hz)	130.1+130.2, CH _{arom}	C13→H5(³ J), H12(³ J)
14	-	154.5+154.6, C _q	C14→H7(³ J), H9(² J), H12(³ J), H13(³ J), NH _β (⁶ J)
15	-	156.5+156.7, C _q	C15→H7(³ J), H8(³ J), NH _α (² J)
16	-	170.06+170.11, C _q	C16→H8(² J)
17	-	172.7+172.9, C _q	C17→H7(² J), H8(⁶ J), NH _α (³ J)
NH _α	8.45+8.47 (1H, d, <i>J</i> = 1.1 Hz)	-	-
NH _β	9.76+9.77 (1H, s)	-	-
COOH	12.84 (1H, s)	-	-

Note: The ¹H- and ¹³C-NMR-spectra show a mixture of rotamers.

6.3.3.1.17 Synthesis of (2*S*)-2-(3-(5-(2-chloroethyl)-2-oxo-2,3-dihydrobenzofuran-3-yl)ureido)-4-methylpentanoic acid (**302**)



Prepared according to *GP-V* using (*S*)-4-methyl-2-ureidopentanoic acid **269** (1.00 g, 5.74 mmol, 1.0 eq.), glyoxylic acid monohydrate **188** (0.53 g, 5.68 mmol, 1.0 eq.), 4-(2-chloroethyl)phenol **289** (1.08 g, 6.90 mmol, 1.2 eq.) in 9 ml of TFA. **302** was obtained as a colourless solid in a yield of 16%.

Yield: 0.34 g (0.92 mmol, 16%).

Appearance: Colourless solid.

R_f-Value: 0.24 (SiO₂, DCM/MeOH 20:1 + 1% AcOH).

IR: $\tilde{\nu}$ [cm⁻¹] = 3662 (br), 3294 (br), 2968 (m), 2901 (w), 2364 (w), 1704 (vs), 1615 (w), 1558 (w), 1514 (w), 1435 (s), 1394 (w), 1370 (w), 1273 (m), 1221 (w), 1200 (w), 1135 (w), 1109 (w), 1066 (m), 1057 (m), 984 (w), 901 (w), 825 (w).

MP: Change of colour: 122 °C; Melting at 178 °C.

HR-MS (ESI): Theor.[M+H]⁺: 369.12117, found: 369.12150.

Theor.[M+Na]⁺: 391.10312, found: 391.10340.

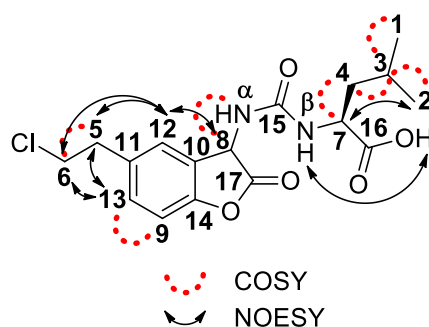
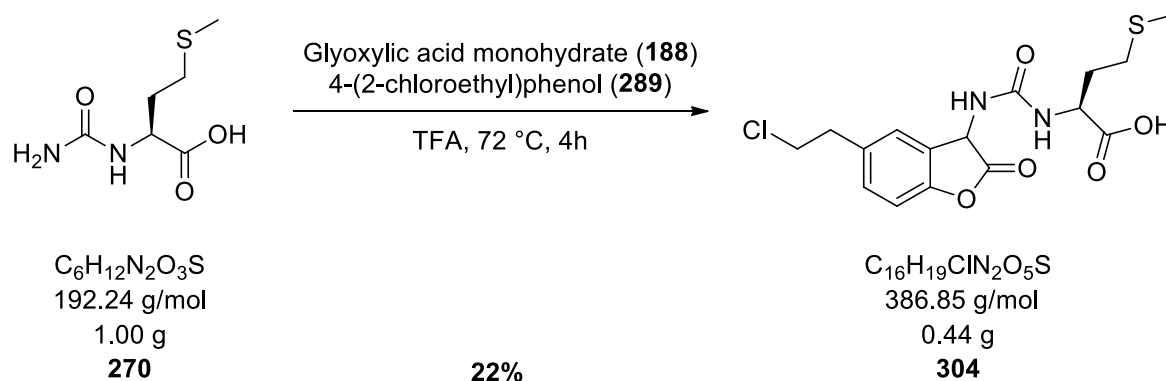


Table 76: 1D and 2D-NMR data of (2*S*)-2-(3-(5-(2-chloroethyl)-2-oxo-2,3-dihydrobenzofuran-3-yl)ureido)-4-methylpentanoic acid (302) in DMSO-*d*₆, at 298 K and 500 MHz for ¹H and 125 MHz for ¹³C.

No.	δ_H [ppm], <i>J</i> in [Hz]	δ_C [ppm], mult.	HMBC ($^{\circ}J$)
1	0.86+0.90 (3H, d, <i>J</i> = 6.6 Hz)	20.88+20.91, CH ₃	C1→H2(³ J), H4(³ J)
2	0.88 (3H, d, <i>J</i> = 6.7 Hz)	23.3, CH ₃	C2→H1(³ J)
3	1.58 (1H, m)	24.2+24.3, CH	C3→H1(² J), H2(² J), H4(² J), H7(³ J)
4	1.69-1.76 (1H, m); 2.06-2.17 (1H, m)	36.4+36.6, CH ₂	C4→H1(³ J), H2(³ J), H7(² J)
5	2.88 (2H, t, <i>J</i> = 7.1 Hz)	37.4+37.5, CH ₂	C5→H6(² J), H12(³ J), H13(³ J)
6	3.74 (2H, t, <i>J</i> = 7.1 Hz)	45.5, CH ₂	C6→H5(² J)
7	4.51+4.54 (1H, dd, <i>J</i> = 11.3, 4.3 Hz)	50.0+50.3, CH	C7→H4(² J)
8	5.20+5.28 (1H, s)	56.0+56.2, CH	C8→H9(⁴ J), H12(³ J), NH _α (² J)
9	6.80 (1H, d, <i>J</i> = 8.2 Hz)	115.5+115.6, CH _{arom}	C9→H13(² J), NH _β (⁷ J)
10	-	121.7+121.8, C _q	C10→H9(³ J), H8(² J), NH _β (³ J)
11	-	128.48+128.49, C _q	C11→H5(² J), H6(³ J), H9(³ J)
12	7.04 (1H, ψ t, <i>J</i> = 2.4 Hz)	129.7+129.9, CH _{arom}	C12→H5(³ J), H8(³ J), H13(³ J)
13	7.09 (1H, dd, <i>J</i> = 8.2, 1.5 Hz)	130.12+130.14, CH _{arom}	C13→H5(³ J), H12(³ J)
14	-	154.5+154.6, C _q	C14→H8(³ J), H9(² J), H12(³ J), H13(³ J), NH _β (⁶ J)
15	-	156.3+156.5, C _q	C15→H7(³ J), H8(³ J), NH _α (² J)
16	-	171.08+171.09, C _q	C16→H7(² J)
17	-	172.8+172.9, C _q	C17→H7(⁶ J), H8(² J), NH _α (³ J)
NH _α	8.44+8.47 (1H, s)	-	-
NH _β	9.73 (1H, s)	-	-
COOH	12.99 (1H, s)	-	-

Note: The ¹H- and ¹³C-NMR-spectra show a mixture of rotamers.

6.3.3.1.18 Synthesis of (2*S*)-2-(3-(5-(2-chloroethyl)-2-oxo-2,3-dihydrobenzofuran-3-yl)ureido)-4-(methylthio)butanoic acid (**304**)



Prepared according to **GP-V** using (*S*)-4-(methylthio)-2-ureidobutanoic acid **270** (1.00 g, 5.20 mmol, 1.0 eq.), glyoxylic acid monohydrate **188** (0.48 g, 5.20 mmol, 1.0 eq.), 4-(2-chloroethyl)phenol **289** (0.98 g, 6.24 mmol, 1.2 eq.) in 8 ml of TFA. **304** was obtained as a colourless solid in a yield of 22%.

Yield: 0.44 g (1.14 mmol, 22%).

Appearance: Colourless solid.

R_f-Value: 0.18 (SiO₂, DCM/MeOH 70:1 + 1% AcOH).

IR: $\tilde{\nu}$ [cm⁻¹] = 3288 (br), 2918 (w), 2051 (w), 1980 (w), 1767 (w), 1699 (vs), 1614 (w), 1513 (m), 1432 (s), 1357 (w), 1276 (m), 1201 (w), 1135 (w), 1120 (w), 1076 (w), 1036 (w), 922 (w), 823 (m).

MP: 78 °C.

HR-MS (ESI): Theor.[M+H]⁺: 387.07759, found: 387.07775.

Theor.[M+Na]⁺: 409.05954, found: 409.05960.

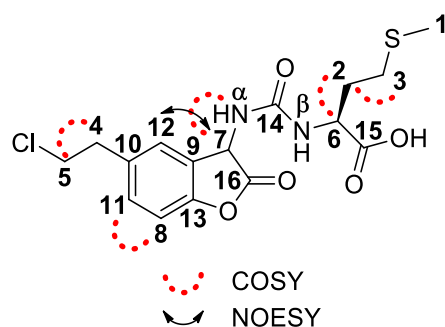
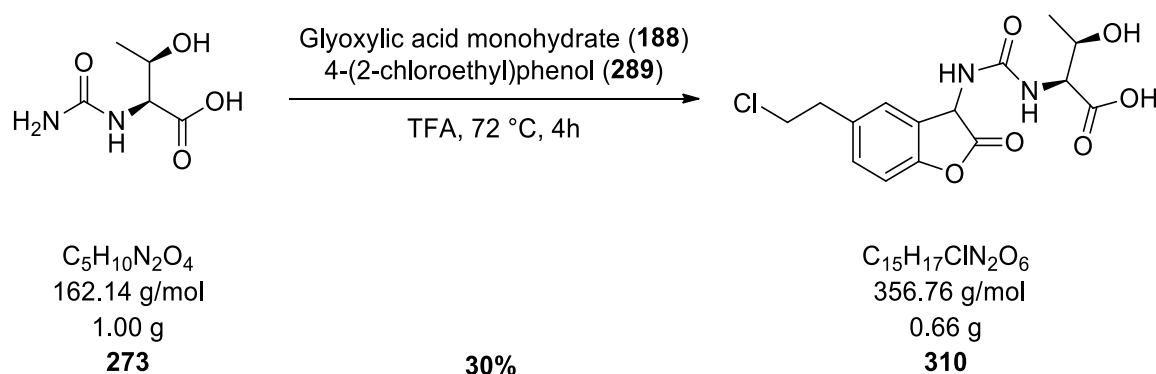


Table 77: 1D and 2D-NMR data of (2S)-2-(3-(5-(2-chloroethyl)-2-oxo-2,3-dihydrobenzofuran-3-yl)ureido)-4-(methylthio)butanoic acid (304) in DMSO- d_6 , at 298 K and 500 MHz for ^1H and 125 MHz for ^{13}C .

No.	δ_{H} [ppm], J in [Hz]	δ_{C} [ppm], mult.	HMBC ($^{\circ}\text{J}$)
1	2.05 (3H, s)	14.46, CH_3	-
2	2.24 (1H, m); 2.29 (1H, m)	27.3+27.6, CH_2	$\text{C}2 \rightarrow \text{H}3(^2\text{J}), \text{H}6(^2\text{J})$
3	2.45 (1H, m), 2.55 (1H, m)	29.85+29.91, CH_2	$\text{C}3 \rightarrow \text{H}1(^3\text{J}), \text{H}2(^2\text{J}), \text{H}6(^3\text{J})$
4	2.90 (2H, t, $J = 7.2$ Hz)	37.4+37.5, CH_2	$\text{C}4 \rightarrow \text{H}5(^2\text{J}), \text{H}11(^3\text{J}), \text{H}12(^3\text{J})$
5	3.75 (2H, t, $J = 7.2$ Hz)	45.5, CH_2	$\text{C}5 \rightarrow \text{H}4(^2\text{J})$
6	4.68 (1H, m)	50.6+50.9, CH	$\text{C}6 \rightarrow \text{H}2(^2\text{J}), \text{H}3(^3\text{J})$
7	5.18+5.25 (1H, d, $J = 1.1$ Hz)	56.7+56.8, CH	$\text{C}7 \rightarrow \text{H}8(^4\text{J}), \text{H}12(^3\text{J}), \text{NH}_{\alpha}(^2\text{J})$
8	6.79+6.79 (1H, d, $J = 8.1$ Hz)	115.5+115.6, CH_{arom}	$\text{C}8 \rightarrow \text{H}11(^2\text{J}), \text{NH}_{\beta}(^7\text{J})$
9	-	121.6+121.7, C_{q}	$\text{C}9 \rightarrow \text{H}8(^3\text{J}), \text{NH}_{\beta}(^5\text{J})$
10	-	128.47+128.50, C_{q}	$\text{C}10 \rightarrow \text{H}4(^2\text{J}), \text{H}5(^3\text{J}), \text{H}8(^3\text{J})$
11	7.10 (1H, m)	130.19+130.21, CH_{arom}	$\text{C}11 \rightarrow \text{H}12(^3\text{J})$
12	7.09 (1H, m)	130.4+130.6, CH_{arom}	$\text{C}12 \rightarrow \text{H}7(^3\text{J}), \text{H}11(^3\text{J})$
13	-	154.5+154.6, C_{q}	$\text{C}13 \rightarrow \text{H}7(^3\text{J}), \text{H}8(^2\text{J}), \text{H}11(^3\text{J}), \text{H}12(^3\text{J}), \text{NH}_{\beta}(^6\text{J})$
14	-	156.2+156.4, C_{q}	$\text{C}14 \rightarrow \text{H}6(^3\text{J}), \text{H}7(^3\text{J}), \text{NH}_{\alpha}(^2\text{J})$
15	-	170.60+170.3, C_{q}	$\text{C}15 \rightarrow \text{H}6(^2\text{J}), \text{H}2(^3\text{J})$
16	-	172.9+173.0, C_{q}	$\text{C}16 \rightarrow \text{H}6(^6\text{J}), \text{H}7(^2\text{J}), \text{NH}_{\alpha}(^3\text{J})$
NH_{α}	8.44+8.46 (1H, d, $J = 1.2$ Hz)	-	-
NH_{β}	9.78+9.79 (1H, s)	-	-
COOH	13.08 (1H, s)	-	-

Note: The ^1H - and ^{13}C -NMR-spectra show a mixture of rotamers.

6.3.3.1.19 Synthesis of (2*S*,3*R*)-2-(3-(5-(2-chloroethyl)-2-oxo-2,3-dihydrobenzofuran-3-yl)ureido)-3-hydroxybutanoic acid (**310**)



Prepared according to **GP-V** using (2*S*,3*R*)-3-hydroxy-2-ureidobutanoic acid **273** (1.00 g, 6.17 mmol, 1.0 eq.), glyoxylic acid monohydrate **188** (0.57 g, 6.17 mmol, 1.0 eq.), 4-(2-chloroethyl)phenol **289** (1.16 g, 7.40 mmol, 1.2 eq.) in 10 ml of TFA. **310** was obtained as a colourless solid in a yield of 30%.

Yield: 0.66 g (1.85 mmol, 30%).

Appearance: Colourless solid.

R_f-Value: 0.29 (SiO₂, DCM/MeOH 10:1 + 1% AcOH).

IR: $\tilde{\nu}$ [cm⁻¹] = 3310 (br), 2930 (w), 1703 (vs), 1616 (w), 1513 (m), 1431 (s), 1360 (w), 1277 (m), 1217 (w), 1110 (w), 1084 (w), 1026 (w), 960 (w), 910 (w), 869 (w), 849 (w), 822 (w).

MP: 108 °C.

HR-MS (ESI): Theor.[M+H]⁺: 357.08479, found: 357.08515.

Theor.[M+Na]⁺: 379.06673, found: 379.06717.

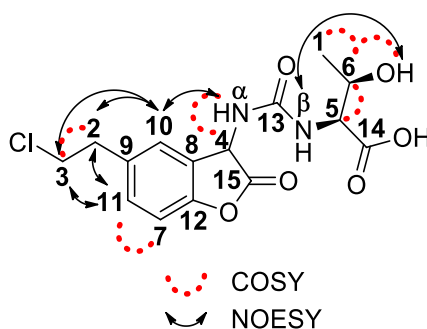
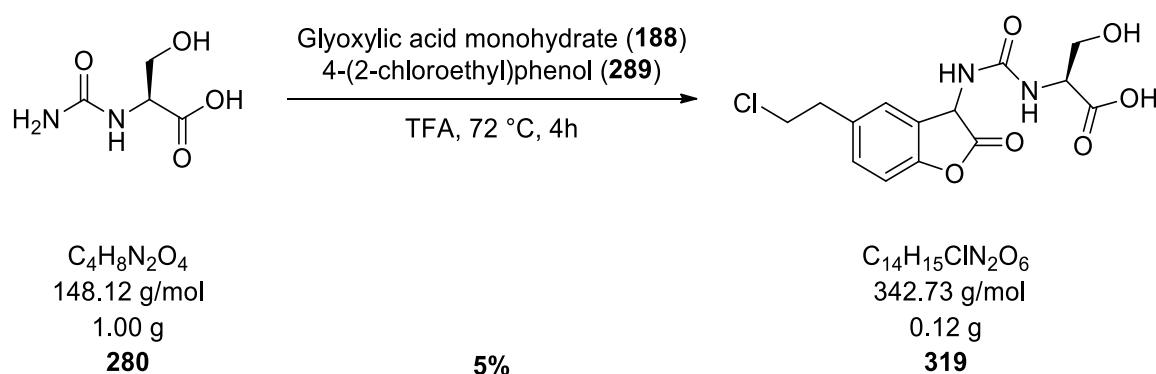


Table 78: 1D and 2D-NMR data of (2*S*,3*R*)-2-(3-(5-(2-chloroethyl)-2-oxo-2,3-dihydrobenzofuran-3-yl)ureido)-3-hydroxybutanoic acid (310) in DMSO-*d*₆, at 298 K and 500 MHz for ¹H and 125 MHz for ¹³C.

No.	δ_{H} [ppm], J in [Hz]	δ_{C} [ppm], mult.	HMBC ($^{\circ}$ J)
1	1.23+1.23 (3H, d, $J = 6.3$ Hz)	21.4+21.5, CH ₃	C1→H5(³ J)
2	2.84-2.94 (2H, m)	37.50+37.52, CH ₂	C2→H3(² J), H10(³ J), H11(³ J)
3	3.72-3.75 (2H, m)	45.43+45.44, CH ₂	C3→H2(² J)
4	5.34+5.36 (1H, d, $J = 1.1$ Hz)	55.85+55.88, CH	C4→H7(⁴ J), H10(³ J), NH _{α} (² J)
5	4.42 (1H, ψ t, $J = 7.1$ Hz)	58.6+58.9, CH	C5→H1(³ J)
6	4.32 (1H, m)	64.1+64.2, CH	C6→H1(² J), H5(² J)
7	6.79+6.80 (1H, d, $J = 8.4$ Hz)	115.4+115.5, CH _{arom}	C7→NH _{β} (⁷ J)
8	-	121.8, C _q	C8→H4(² J), H7(³ J), NH _{β} (⁵ J)
9	-	128.59+128.60, C _q	C9→H2(² J), H3(³ J), H7(³ J)
10	7.08 (1H, m)	129.65+129.70, CH _{arom}	C10→H4(³ J), H11(³ J)
11	7.10 (1H, m)	130.2, CH _{arom}	C11→H10(³ J)
12	-	154.4+154.5, C _q	C12→H4(³ J), H7(² J), H10(³ J), H11(³ J), NH _{β} (⁶ J)
13	-	156.8+157.1, C _q	C13→H4(³ J), H5(³ J), NH _{α} (² J)
14	-	169.2+169.3, C _q	C14→H5(² J)
15	-	173.38+173.83, C _q	C15→H4(² J), H5(⁶ J), NH _{α} (³ J)
OH	4.82+5.01 (1H, br)	-	-
NH _{α}	8.62+8.63 (1H, d, $J = 1.2$ Hz)	-	-
NH _{β}	9.81+9.83 (1H, s)	-	-
COOH	12.77 (1H, s)	-	-

Note: The ¹H- and ¹³C-NMR-spectra show a mixture of rotamers.

6.3.3.1.20 Synthesis of (2S)-2-(3-(5-(2-chloroethyl)-2-oxo-2,3-dihydrobenzofuran-3-yl)ureido)-3-hydroxypropanoic acid (**319**)



Prepared according to **GP-V** using (*S*)-3-hydroxy-2-ureidopropanoic acid **280** (1.00 g, 6.75 mmol, 1.0 eq.), glyoxylic acid monohydrate **188** (0.62 g, 6.75 mmol, 1.0 eq.), 4-(2-chloroethyl)phenol **289** (1.27 g, 8.10 mmol, 1.2 eq.) in 11 ml of TFA. **319** was obtained as a colourless solid in a yield of 6%.

Yield: 0.13 g (0.35 mmol, 5%).

Appearance: Colourless solid.

R_f-Value: 0.37 (SiO₂, DCM/MeOH 12:1 + 1% AcOH).

IR: $\tilde{\nu}$ [cm⁻¹] = 3331 (br), 2925 (w), 2366 (w), 1704 (vs), 1614 (w), 1559 (w), 1513 (m), 1438 (s), 1359 (w), 1271 (m), 1207 (m), 1121 (w), 1092 (w), 1052 (w), 926 (w), 906 (w), 870 (w), 833 (w), 806 (w).

MP: 80 °C.

HR-MS (ESI): Theor.[M+H]⁺: 343.06914, found: 343.06953.

Theor.[M+Na]⁺: 365.05108, found: 365.05153.

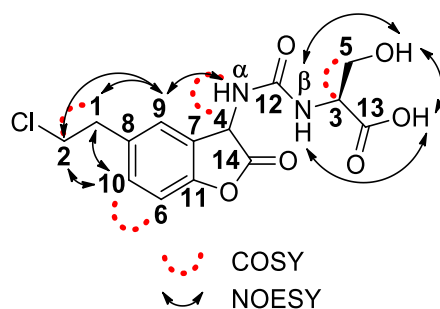
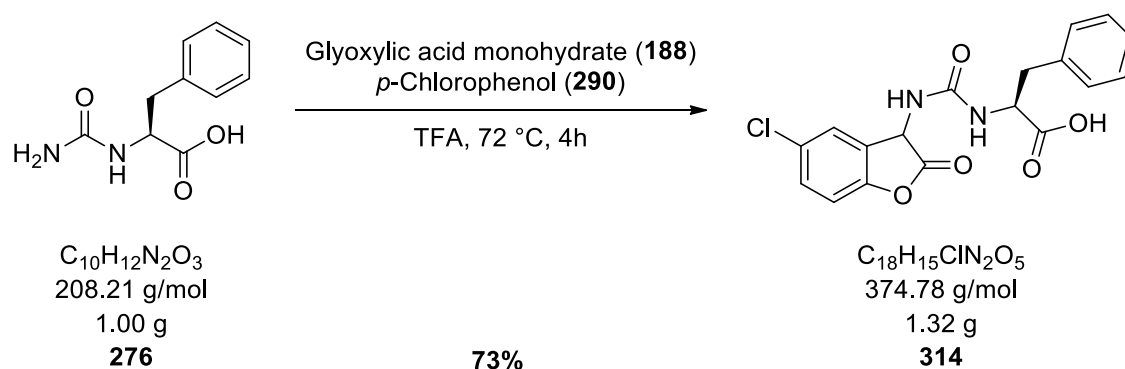


Table 79: 1D and 2D-NMR data of (2*S*)-2-(3-(5-(2-chloroethyl)-2-oxo-2,3-dihydrobenzofuran-3-yl)ureido)-3-hydroxypropanoic acid (319) in DMSO-*d*₆, at 298 K and 500 MHz for ¹H and 125 MHz for ¹³C.

No.	δ_{H} [ppm], J in [Hz]	δ_{C} [ppm], mult.	HMBC ($^{\circ}J$)
1	2.88 (2H, m)	37.5+37.6, CH ₂	C1→H2(² J), H9(³ J), H10(³ J)
2	3.72 (2H, m)	45.4, CH ₂	C2→H1(² J)
3	4.58 (1H, m)	54.41+54.41, CH	C3→H5(² J)
4	5.30+5.34 (1H, d, $J = 0.9$ Hz)	54.8+55.3, CH	C4→H9(³ J), NH _{α} (² J)
5	3.94 (2H, m)	57.8+58.0, CH ₂	C5→H3(² J)
6	6.80 (1H, d, $J = 8.1$ Hz)	115.4+115.5, CH _{arom}	C6→H10(² J), NH _{β} (⁷ J)
7	-	122.06+122.12, C _q	C7→H4(² J), H6(³ J), NH _{β} (⁵ J)
8	-	128.6+128.7, C _q	C8→H1(² J), H2(³ J), H6(³ J)
9	7.05 (1H, m)	128.9+129.1, CH _{arom}	C9→H4(³ J), H10(³ J)
10	7.08 (1H, m)	129.99+130.02, CH _{arom}	C10→H9(³ J)
11	-	154.42+154.43, C _q	C11→H4(³ J), H6(² J), H9(³ J), H10(³ J), NH _{β} (⁶ J)
12	-	156.5+156.6, C _q	C12→H3(³ J), H4(³ J), NH _{α} (² J)
13	-	169.21+169.24, C _q	C13→H3(² J)
14	-	173.04+173.11, C _q	C14→H3(⁶ J), H4(² J), NH _{α} (³ J)
OH	4.88+4.93 (1H, br)	-	-
NH _{α}	8.49+8.52 (1H, s)	-	-
NH _{β}	9.78 (1H, s)	-	-
COOH	13.08 (1H, br)	-	-

Note: The ¹H- and ¹³C-NMR-spectra show a mixture of rotamers.

6.3.3.1.21 Synthesis of (2*S*)-2-(3-(5-chloro-2-oxo-2,3-dihydrobenzofuran-3-yl)ureido)-3-phenylpropanoic acid (**314**)



Prepared according to **GP-V** using (*S*)-3-phenyl-2-ureidopropanoic acid **276** (1.00 g, 4.80 mmol, 1.0 eq.), glyoxylic acid monohydrate **188** (0.44 g, 4.80 mmol, 1.0 eq.), *p*-chlorophenol **290** (0.74 g, 5.76 mmol, 1.2 eq.) in 8 ml of TFA. **314** was obtained as a colourless solid in a yield of 73%.

Yield: 1.32 g (3.52 mmol, 73%).

Appearance: Colourless solid.

R_f-Value: 0.25 (SiO₂, DCM/MeOH 20:1 + 1% AcOH).

IR: $\tilde{\nu}$ [cm⁻¹] = 3854 (w), 3650 (w), 3620 (w), 3600 (w), 3315 (br), 2363 (w), 1772 (w), 1737 (w), 1716 (m), 1694 (vs), 1599 (w), 1559 (w), 1497 (m), 1438 (m), 1426 (m), 1359 (w), 1281 (m), 1203 (m), 1143 (w), 1121 (w), 1017 (w), 959 (w), 932 (s), 906 (w), 821 (m).

MP: Decomposition above 190 °C.

HR-MS (ESI): Theor.[M+H]⁺: 375.07422, found: 375.07423.

Theor.[M+Na]⁺: 397.05617, found: 397.05614.

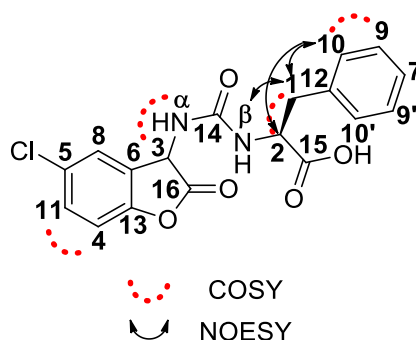
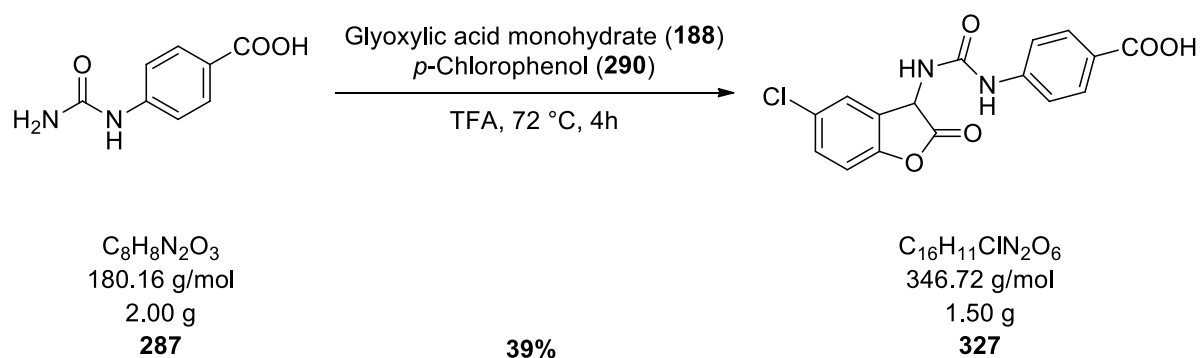


Table 80: 1D and 2D-NMR data of (2S)-2-(3-(5-chloro-2-oxo-2,3-dihydrobenzofuran-3-yl)ureido)-3-phenylpropanoic acid (314) in DMSO-d₆, at 298 K and 500 MHz for ¹H and 125 MHz for ¹³C.

No.	δ_H [ppm], J in [Hz]	δ_C [ppm], mult.	HMBC ($^{\circ}J$)
1	3.26+3.36 (2H, m)	33.3+33.4, CH ₂	C1→H2(² J), H10(³ J)
2	4.83+4.84 (1H, ψ t, $J = 10.9$ Hz)	52.92+52.98, CH	C2→H1(² J)
3	5.21+5.30 (1H, s)	54.01+54.04, CH	C3→H4(⁴ J), H8(³ J), NH _{α} (² J)
4	6.84+6.87 (1H, d, $J = 8.7$ Hz)	117.0+117.2, CH _{arom}	C4→NH _{β} (⁷ J)
5	-	122.42+122.47, C _q	C5→H8(² J), H4(³ J), H11(² J)
6	-	123.59+123.60, C _q	C6→H3(² J), H4(³ J), NH _{β} (⁵ J)
7	7.22 (1H, m)	126.6+126.7, CH _{arom}	C7→H10(³ J)
8	6.63+6.77 (1H, d, $J = 2.5$ Hz)	127.3+127.4, CH _{arom}	C8→H3(³ J), H11(³ J)
9	7.27 (2H, m)	128.28+128.31, 2xCH _{arom}	C9→H9(³ J)
10	7.15 +7.21 (2H, m)	128.81+128.86, 2xCH _{arom}	C10→H1(³ J), H10(³ J)
11	7.13+7.19 (1H, m)	129.30+129.33, CH _{arom}	C11→H8(³ J)
12		137.34+137.36, C _q	C12→H1(² J), H2(³ J), H9(³ J)
13		154.6, C _q	C13→H3(³ J), H4(² J), H8(³ J), H11(³ J), NH _{β} (⁶ J)
14	-	155.96+156.07, C _q	C14→H2(³ J), H3(³ J), NH _{α} (² J)
15	-	170.1, C _q	C15→H1(³ J), H2(² J)
16	-	171.87+171.95, C _q	C16→H2(⁶ J), H3(² J), NH _{α} (³ J)
NH _{α}	8.48 (1H, s)	-	-
NH _{β}	10.19+10.21 (1H, s)	-	-
COOH	13.24 (1H, br)	-	-

Note: The ¹H- and ¹³C-NMR-spectra show a mixture of rotamers.

6.3.3.1.22 Synthesis of 4-(3-(5-chloro-2-oxo-2,3-dihydrobenzofuran-3-yl)ureido)benzoic acid (**327**)



Prepared according to *GP-V* using 4-ureidobenzoic acid **287** (2.00 g, 11.1 mmol, 1.0 eq.), glyoxylic acid monohydrate **188** (1.02 g, 11.1 mmol, 1.0 eq.), *p*-chlorophenol **290** (1.71 g, 13.3 mmol, 1.2 eq.) in 18 ml of TFA. **327** was obtained as a light beige solid in a yield of 43%.

Yield: 1.50 g (4.33 mmol, 39%).

Appearance: Light beige solid.

R_f-Value: 0.19 (SiO₂, DCM/MeOH 25:1 + 1% AcOH).

IR: $\tilde{\nu}$ [cm⁻¹] = 3220 (br), 2981 (w), 2891 (w), 2814 (w), 2360 (w), 2341 (w), 1780 (w), 1716 (vs), 1693 (s), 1654 (w), 1636 (w), 1604 (m), 1559 (w), 1540 (w), 1507 (m), 1472 (w), 1418 (s), 1375 (w), 1305 (w), 1272 (s), 1221 (w), 1163 (m), 1115 (m), 1041 (w), 1016 (w), 972 (w), 899 (w), 884 (w), 862 (w), 825 (w).

MP: Decomposition above 250 °C.

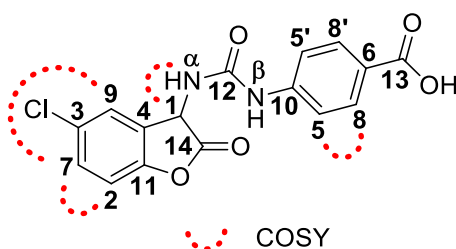
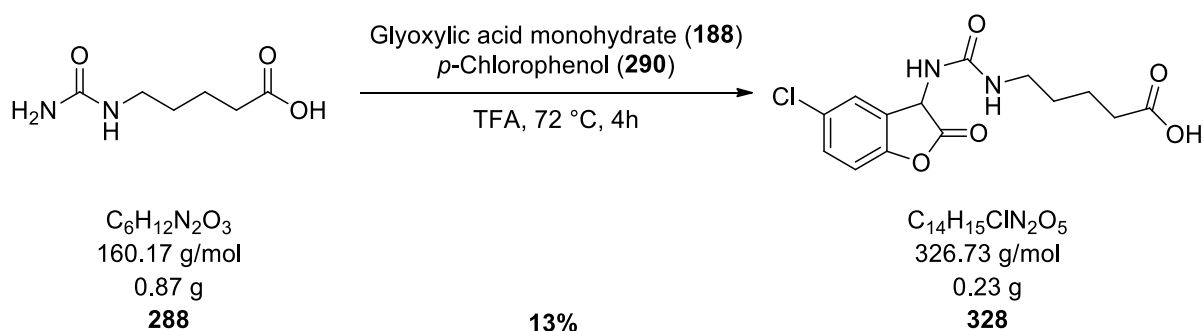


Table 81: 1D and 2D-NMR data of 4-(3-(5-chloro-2-oxo-2,3-dihydrobenzofuran-3-yl)ureido)benzoic acid (327) in DMSO-d₆, at 298 K and 500 MHz for ¹H and 125 MHz for ¹³C.

No.	δ_H [ppm], J in [Hz]	δ_C [ppm], mult.	HMBC (nJ)
1	5.33 (1H, d, $J = 1.0$ Hz)	57.5, CH	C1→H2(4J), H9(3J), NH $_{\alpha}$ (2J)
2	6.86 (1H, d, $J = 8.6$ Hz)	117.3, CH _{arom}	C2→NH $_{\beta}$ (7J)
3	-	122.3, C _q	C3→H2(3J), H7(2J), H9(2J)
4	-	124.0, C _q	C4→H1(2J), H2(3J), NH $_{\beta}$ (5J)
5	7.56 (2H, d, $J = 8.8$ Hz)	126.1, 2xCH _{arom}	C5→H5(3J)
6	-	129.6, C _q	C6→H5(3J)
7	7.28 (1H, dd, $J = 8.6, 2.7$ Hz)	129.7, CH _{arom}	C7→H9(3J)
8	8.06 (2H, d, $J = 8.8$ Hz)	129.8, 2xCH _{arom}	C8→H8(3J)
9	7.42 (1H, d, $J = 2.7$ Hz)	130.8, CH _{arom}	C9→H1(3J), H7(3J)
10	-	136.5, C _q	C10→H5(2J), H8(3J)
11	-	154.9, C _q	C11→H1(3J), H2(2J), H7(3J), H9(3J), NH $_{\beta}$ (6J)
12	-	155.4, C _q	C12→H1(3J), NH $_{\alpha}$ (2J)
13	-	166.8, C _q	C13→H8(3J)
14	-	171.9, C _q	C14→H1(2J), NH $_{\alpha}$ (3J)
NH $_{\alpha}$	8.71 (1H, d, $J = 1.1$ Hz)	-	-
NH $_{\beta}$	10.35 (1H, s)	-	-
COOH	13.07 (1H, br)	-	-

6.3.3.1.23 Synthesis of 5-(3-(5-chloro-2-oxo-2,3-dihydrobenzofuran-3-yl)ureido)pentanoic acid (**328**)



Prepared according to **GP-V** using 5-ureidopentanoic acid **288** (0.87 g, 5.43 mmol, 1.0 eq.), glyoxylic acid monohydrate **188** (0.50 g, 5.43 mmol, 1.0 eq.), *p*-chlorophenol **290** (0.84 g, 6.52 mmol, 1.2 eq.) in 9 ml of TFA. **328** was obtained as a colourless solid in a yield of 13%.

Yield: 0.23 g (0.70 mmol, 13%).

Appearance: Colourless solid.

R_f-Value: 0.45 (SiO₂, Toluene/MeOH 3:1 + 1% AcOH).

IR: $\tilde{\nu}$ [cm⁻¹] = 3249 (w), 3171 (w), 2946 (w), 1760 (w), 1734 (w), 1695 (vs), 1678 (vs), 1611 (w), 1599 (w), 1505 (w), 1469 (w), 1433 (m), 1384 (w), 1353 (w), 1318 (w), 1278 (m), 1266 (m), 1236 (w), 1187 (w), 1134 (w), 1101 (w), 1076 (w), 1002 (w), 946 (w), 927 (w), 912 (w), 888 (w), 851 (w), 820 (w).

MP: 175 °C.

HR-MS (ESI): Theor. [M+Na]⁺: 349.05617, found: 349.05583.

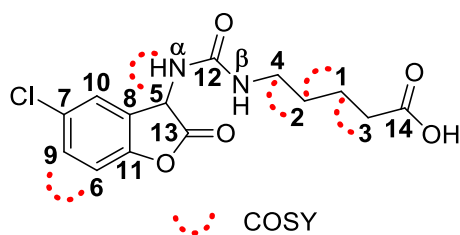
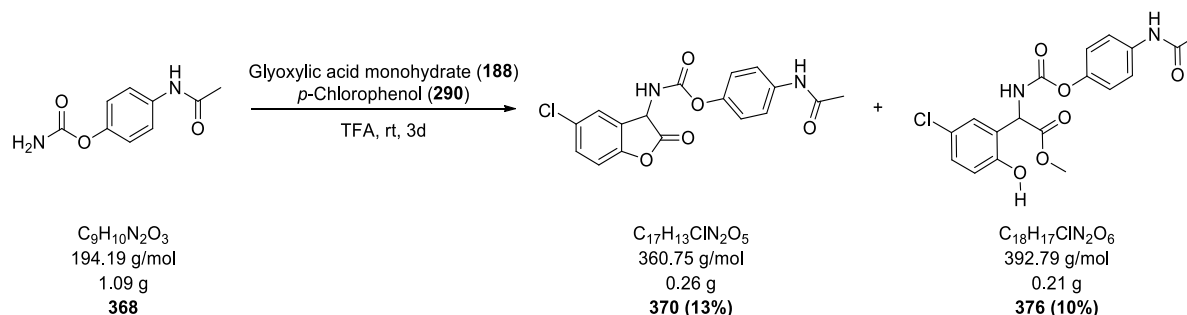


Table 82: 1D and 2D-NMR data of 5-(3-(5-chloro-2-oxo-2,3-dihydrobenzofuran-3-yl)ureido)pentanoic acid (328) in DMSO-d₆, at 298 K and 500 MHz for ¹H and 125 MHz for ¹³C.

No.	δ_{H} [ppm], J in [Hz]	δ_{C} [ppm], mult.	HMBC ($^{\circ}\text{J}$)
1	1.51 (2H, m)	21.7, CH ₂	C1→H2(² J), H3(² J), H4(³ J)
2	1.54 (2H, m)	27.0, CH ₂	C2→H1(² J), H3(³ J), H4(² J)
3	2.25 (2H, t, $J = 6.9$ Hz)	33.1, CH ₂	C3→H1(² J), H2(³ J)
4	3.37 (2H, m)	37.5, CH ₂	C4→H1(³ J), H2(² J)
5	5.14 (1H, d, $J = 1.0$ Hz)	57.0, CH	C5→H6(⁴ J), H10(³ J), NH _{α} (² J)
6	6.82 (1H, m)	117.2, CH _{arom}	C6→H10(⁴ J)
7	-	122.2, C _q	C7→H6(³ J), H9(² J), H10(² J)
8	-	124.1, C _q	C8→H5(² J), H6(³ J), H10(² J)
9	7.23 (1H, m)	129.4, CH _{arom}	C9→H10(³ J)
10	7.24 (1H, m)	130.1, CH _{arom}	C10→H5(³ J), H9(³ J)
11	-	154.9, C _q	C11→H5(³ J), H6(² J), H9(³ J), H10(³ J)
12	-	157.1, C _q	C12→H4(³ J), H5(³ J), NH _{α} (² J)
13	-	172.9, C _q	C13→H4(⁶ J), H5(² J), NH _{α} (³ J)
14	-	174.3, C _q	C14→H1(³ J), H3(² J)
NH _{α}	8.30 (1H, d, $J = 1.1$ Hz)	-	-
NH _{β}	10.12 (1H, s)	-	-
COOH	12.02 (1H, br)	-	-

6.3.3.2 2-Coumaranones with carbamate substructures

6.3.3.2.1 Synthesis of 4-acetamidophenyl (5-chloro-2-oxo-2,3-dihydrobenzofuran-3-yl)carbamate (**370**) and methyl 2-(((4-acetamidophenoxy)carbonyl)amino)-2-(5-chloro-2-hydroxyphenyl)acetate (**376**)



Prepared according to *GP-VI* using 4-acetamidophenyl carbamate **370** (1.09 g, 5.61 mmol, 1.0 eq.), glyoxylic acid monohydrate **188** (0.52 g, 5.61 mmol, 1.0 eq.), *p*-chlorophenol **290** (0.87 g, 6.73 mmol, 1.2 eq.) in 10 ml of TFA. **370** and **376** were both obtained as colourless solids in a yield of 13% and 10% respectively.

Yield: 0.26 g (0.72 mmol, **370**, 13%); 0.21 g (0.53 mmol, **376**, 10%)

Appearance: Colourless solid.

Analytical Data for XX

R_f-Value: 0.06 (SiO₂, DCM/MeOH 10:1 + 1% AcOH).

IR: $\tilde{\nu}$ [cm⁻¹] = 3303 (br), 2923 (w), 2854 (w), 2360 (w), 2343 (w), 1717 (m), 1667 (w), 1609 (w), 1540 (w), 1496 (s), 1409 (w), 1372 (w), 1320 (w), 1278 (w), 1203 (vs), 1111 (w), 1028 (m), 1018 (m), 992 (w), 971 (w), 940 (w), 925 (w), 917 (w), 845 (w), 821 (m).

MP: Change of colour: 148 °C; Melting at 175 °C.

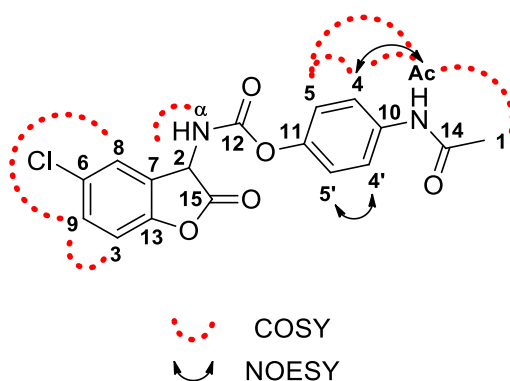


Table 83: 1D and 2D-NMR data of 4-acetamidophenyl (5-chloro-2-oxo-2,3-dihydrobenzofuran-3-yl)carbamate (370) in DMSO- d_6 , at 298 K and 500 MHz for ^1H and 125 MHz for ^{13}C .

No.	δ_{H} [ppm], J in [Hz]	δ_{C} [ppm], mult.	HMBC ($^{\times}J$)
1	2.03 (3H, s)	23.9, CH_3	-
2	5.37 (1H, d, $J = 8.2$ Hz)	53.0, CH	$\text{C}2 \rightarrow \text{H}3(^4J)$, $\text{H}8(^3J)$, $\text{NH}_{\alpha}(^2J)$
3	6.84 (1H, d, $J = 8.7$ Hz)	117.5, CH_{arom}	$\text{C}3 \rightarrow \text{H}8(^4J)$
4	7.56 (2H, d, $J = 8.9$ Hz)	119.8, $2 \times \text{CH}_{\text{arom}}$	$\text{C}4 \rightarrow \text{H}4(^3J)$, $\text{H}5(^2J)$, $\text{NH}_{\text{Ac}}(^3J)$
5	7.03 (2H, d, $J = 9.0$ Hz)	121.9, $2 \times \text{CH}_{\text{arom}}$	$\text{C}5 \rightarrow \text{H}4(^2J)$, $\text{H}5(^3J)$
6	-	122.2, C_{q}	$\text{C}6 \rightarrow \text{H}3(^3J)$, $\text{H}8(^2J)$, $\text{H}9(^2J)$
7	-	126.7, C_{q}	$\text{C}7 \rightarrow \text{H}2(^2J)$, $\text{H}3(^3J)$
8	7.27 (1H, d, $J = 2.7$ Hz)	127.1, CH_{arom}	$\text{C}8 \rightarrow \text{H}9(^3J)$
9	7.16 (1H, dd, $J = 8.7, 2.7$ Hz)	128.3, CH_{arom}	$\text{C}9 \rightarrow \text{H}8(^3J)$
10	-	136.4, C_{q}	$\text{C}10 \rightarrow \text{H}4(^2J)$, $\text{H}5(^3J)$, $\text{NH}_{\text{Ac}}(^2J)$
11	-	146.2, C_{q}	$\text{C}11 \rightarrow \text{H}4(^3J)$, $\text{H}5(^2J)$
12	-	154.2, C_{q}	$\text{C}12 \rightarrow \text{H}2(^3J)$, $\text{NH}_{\alpha}(^2J)$
13	-	154.4, C_{q}	$\text{C}13 \rightarrow \text{H}3(^2J)$, $\text{H}8(^3J)$, $\text{H}9(^3J)$
14	-	168.2, C_{q}	$\text{C}14 \rightarrow \text{H}1(^2J)$, $\text{NH}_{\text{Ac}}(^2J)$
15	-	171.71, C_{q}	$\text{C}15 \rightarrow \text{H}2(^2J)$
NH_{α}	8.11 (1H, d, $J = 8.2$ Hz)	-	-
NH_{Ac}	9.97 (1H, s)	-	-

Analytical Data for XX

R_f-Value: 0.15 (SiO_2 , DCM/MeOH 10:1 + 1% AcOH).

IR: $\tilde{\nu}$ [cm^{-1}] = 3306 (br), 3079 (w), 2954 (w), 2850 (w), 2362 (w), 2340 (w), 1721 (m), 1667 (m), 1609 (w), 1538 (m), 1497 (s), 1424 (w), 1408 (w), 1371 (w), 1315 (m), 1279 (m), 1203 (vs), 1137 (w), 1119 (w), 1027 (m), 1017 (m), 967 (w), 845 (w), 821 (m).

MP: 195 °C.

HR-MS (ESI): Theor. $[\text{M}+\text{H}]^+$: 393.08479, found: 393.08517.

Theor. $[\text{M}+\text{Na}]^+$: 415.06673, found: 415.06694.

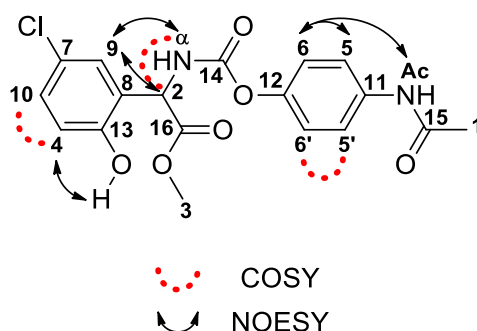
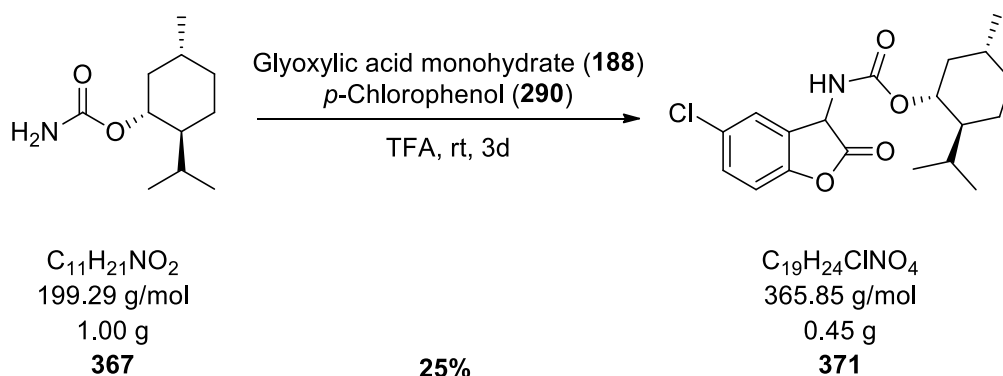


Table 84: 1D and 2D-NMR data of methyl 2-(((4-acetamidophenoxy)carbonyl)amino)-2-(5-chloro-2-hydroxyphenyl)acetate (376) in DMSO- d_6 , at 298 K and 500 MHz for ^1H and 125 MHz for ^{13}C .

No.	δ_{H} [ppm], J in [Hz]	δ_{C} [ppm], mult.	HMBC ($^{\times}\text{J}$)
1	2.03 (3H, s)	23.91, CH_3	-
2	5.59 (1H, d, $J = 8.5$ Hz)	51.82, CH	$\text{C}2 \rightarrow \text{H}4(^4\text{J}), \text{H}9(^3\text{J}), \text{NH}_{\alpha}(^2\text{J})$
3	3.65 (3H, s)	52.43, CH_3	-
4	6.88 (1H, d, $J = 8.7$ Hz)	116.98, CH	$\text{C}4 \rightarrow \text{OH}(^3\text{J})$
5	7.56 (2H, d, $J = 9.0$ Hz)	119.77, $2\text{xCH}_{\text{arom}}$	$\text{C}5 \rightarrow \text{H}5(^3\text{J}), \text{NH}_{\text{Ac}}(^3\text{J})$
6	7.03 (2H, d, $J = 8.9$ Hz)	121.84, $2\text{xCH}_{\text{arom}}$	$\text{C}6 \rightarrow \text{H}6(^3\text{J})$
7	-	122.41, C_{q}	$\text{C}7 \rightarrow \text{H}4(^3\text{J}), \text{H}9(^2\text{J}), \text{H}10(^2\text{J})$
8	-	124.80, C_{q}	$\text{C}8 \rightarrow \text{H}2(^2\text{J}), \text{H}4(^3\text{J}), \text{OH}(^3\text{J}), \text{NH}_{\alpha}(^3\text{J})$
9	7.30 (1H, d, $J = 2.6$ Hz)	128.24, CH_{arom}	$\text{C}9 \rightarrow \text{H}2(^3\text{J}), \text{H}10(^3\text{J})$
10	7.21 (1H, dd, $J = 8.7, 2.7$ Hz)	129.08, CH_{arom}	$\text{C}10 \rightarrow \text{H}9(^3\text{J})$
11	-	136.49, C_{q}	$\text{C}11 \rightarrow \text{H}5(^2\text{J}), \text{H}6(^3\text{J}), \text{NH}_{\text{Ac}}(^2\text{J})$
12	-	146.03, C_{q}	$\text{C}12 \rightarrow \text{H}5(^3\text{J}), \text{H}6(^2\text{J})$
13	-	153.79, C_{q}	$\text{C}13 \rightarrow \text{H}2(^3\text{J}), \text{H}4(^2\text{J}), \text{H}9(^3\text{J}), \text{H}10(^3\text{J}), \text{OH}(^2\text{J})$
14	-	154.45, C_{q}	$\text{C}14 \rightarrow \text{H}2(^3\text{J}), \text{NH}_{\alpha}(^2\text{J})$
15	-	168.17, C_{q}	$\text{C}15 \rightarrow \text{H}1(^2\text{J}), \text{NH}_{\text{Ac}}(^2\text{J})$
16	-	170.87, C_{q}	$\text{C}16 \rightarrow \text{H}2(^2\text{J}), \text{H}3(^3\text{J})$
NH_{α}	8.50 (d, $J = 8.5$ Hz, 1H)	-	-
NH_{Ac}	9.96 (s, 1H)	-	-
OH	10.22 (s, 1H)	-	-

6.3.3.2 Synthesis of (1*R*,2*S*,5*R*)-2-isopropyl-5-methylcyclohexyl (5-chloro-2-oxo-2,3-dihydrobenzofuran-3-yl)carbamate (**371**)



Prepared according to *GP-VI* using L-menthol carbamate **367** (1.00 g, 5.02 mmol, 1.0 eq.), glyoxylic acid monohydrate **188** (0.46 g, 5.02 mmol, 1.0 eq.), *p*-chlorophenol **290** (0.77 g, 6.02 mmol, 1.2 eq.) in 8 ml of TFA. **371** was obtained as a colourless solid in a yield of 25%.

Yield: 0.45 g (1.23 mmol, 25%).

Appearance: Colourless solid.

R_f-Value: 0.27 (SiO₂, Toluene/MeOH 100:1 + 1% AcOH).

IR: $\tilde{\nu}$ [cm⁻¹] = 3366 (br), 2955 (w), 2871 (w), 2843 (w), 2360 (w), 2340 (w), 1832 (s), 1686 (vs), 1653 (w), 1616 (w), 1558 (w), 1529 (s), 1472 (s), 1458 (w), 1432 (w), 1388 (w), 1369 (w), 1332 (w), 1299 (w), 1285 (w), 1275 (w), 1263 (m), 1221 (w), 1200 (w), 1183 (w), 1157 (w), 1070 (s), 1016 (m), 1003 (w), 988 (w), 975 (w), 925 (w), 912 (w), 888 (w), 857 (w), 832 (m).

MP: 172 °C.

HR-MS (ESI): Theor.[M+Na]⁺: 388.12860, found: 388.12883.

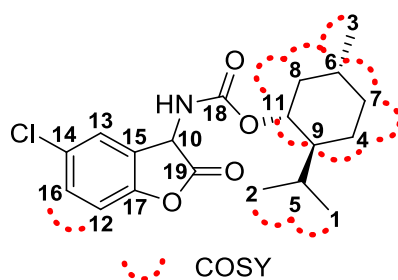
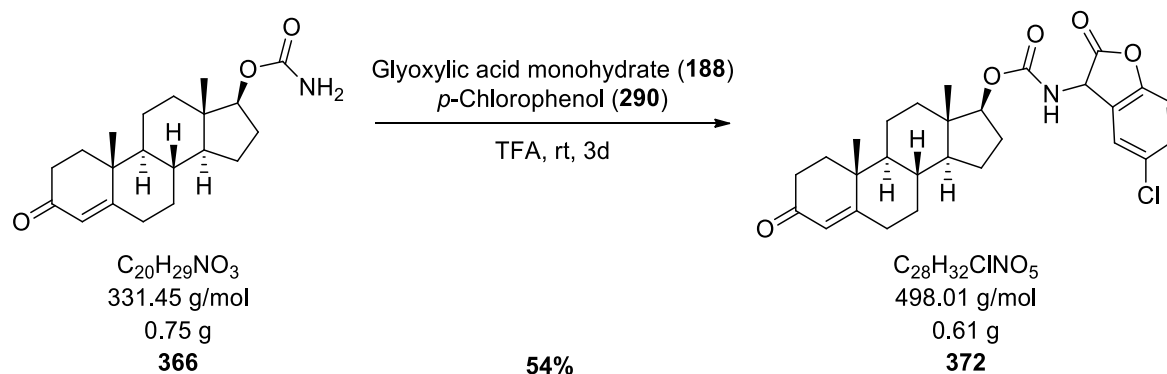


Table 85: 1D and 2D-NMR data of (1*R*,2*S*,5*R*)-2-isopropyl-5-methylcyclohexyl (5-chloro-2-oxo-2,3-dihydrobenzofuran-3-yl)carbamate (371) in CDCl₃, at 298 K and 500 MHz for ¹H and 125 MHz for ¹³C.

No.	δ_H [ppm], J in [Hz]	δ_C [ppm], mult.	HMBC (nJ)
1	0.74-0.80 (3H, d, $J = 6.9$ Hz)	16.5, CH ₃	C1→H2(³ J)
2	0.90 (3H, m)	20.85+20.88, CH ₃	C2→H1(³ J)
3	0.89 (3H, m)	22.0, CH ₃	C3→H8(³ J)
4	1.04 (1H, m); 1.67 (1H, m)	23.7, CH ₂	-
5	1.89 (1H, m)	26.5, CH	C5→H1(² J), H2(² J)
6	1.43 (1H, m)	31.5, CH	C6→H3(² J), H7(² J), H8(² J)
7	0.84 (1H, m); 1.65 (1H, m)	34.3, CH ₂	C7→H3(³ J), H8(³ J)
8	0.98 (1H, m); 1.99 (1H, m)	41.2, CH ₂	C8→H3(³ J)
9	1.33 (1H, m)	47.4+47.5, CH	C9→H1(³ J), H2(³ J)
10	5.20-5.60 (1H, br)	52.4+52.8, CH	C10→H12(⁴ J), H13(³ J)
11	4.53 (1H, m)	76.9, CH	C11→H8(² J), H9(² J)
12	7.05 (1H, d, $J = 8.3$ Hz)	112.3+112.4, CH _{arom}	C12→H13(⁴ J)
13	7.34 (1H, m)	124.85+124.94, CH _{arom}	C13→H16(³ J)
14	-	126.6, C _q	C14→H12(³ J)
15	-	130.10+130.12, C _q	C15→H12(³ J), H16(⁴ J)
16	7.33 (1H, m)	130.4, CH _{arom}	C16→H13(³ J)
17	-	152.19+152.24, C _q	C17→H12(² J), H13(³ J), H16(³ J)
18	-	155.9, C _q	C18→H10(³ J)
19	-	172.9+173.0, C _q	C19→H10(² J)

Note: The ¹H- and ¹³C-NMR-spectra show a mixture of rotamers.

6.3.3.2.3 Synthesis of (8*R*,9*S*,10*R*,13*S*,14*S*,17*S*)-10,13-dimethyl-3-oxo-2,3,6,7,8,9,10,11,12,13,14,15,16,17-tetradecahydro-1*H*-cyclopenta[*a*]phenanthren-17-yl (5-chloro-2-oxo-2,3-dihydrobenzofuran-3-yl)carbamate (372)



Prepared according to **GP-VI** using testosterone carbamate **366** (0.75 g, 2.26 mmol, 1.0 eq.), glyoxylic acid monohydrate **188** (0.21 g, 2.26 mmol, 1.0 eq.), *p*-chlorophenol **290** (0.35 g, 2.71 mmol, 1.2 eq.) in 4 ml of TFA. **372** was obtained as a colourless solid in a yield of 54%.

Yield: 0.61 g (1.22 mmol, 54%).

Appearance: Colourless solid.

R_f-Value: 0.27 (SiO₂, Toluene/MeOH 4:1 + 1% AcOH).

IR: $\tilde{\nu}$ [cm⁻¹] = 3247 (br), 2942 (br), 2876 (w), 2854 (w), 2573 (w), 1720 (s), 1694 (s), 1673 (s), 1657 (s), 1644 (s), 1499 (s), 1449 (w), 1423 (s), 1376 (w), 1331 (m), 1278 (s), 1232 (vs), 1115 (m), 1056 (s), 999 (w), 981 (w), 959 (w), 942 (w), 916 (w), 893 (w), 871 (w), 819 (w).

MP: 172 °C.

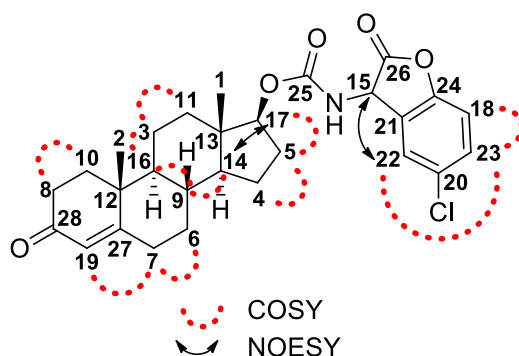
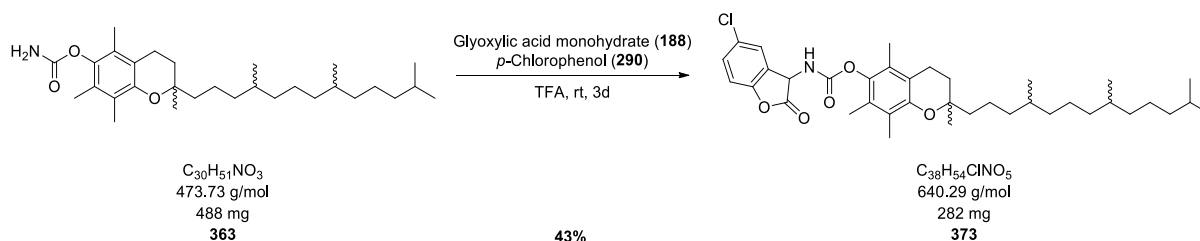


Table 86: 1D and 2D-NMR data of (8*R*,9*S*,10*R*,13*S*,14*S*,17*S*)-10,13-dimethyl-3-oxo-2,3,6,7,8,9,10,11,12,13,14,15,16,17-tetradecahydro-1*H*-cyclopenta[*a*]phenanthren-17-yl (5-chloro-2-oxo-2,3-dihydrobenzofuran-3-yl)carbamate (372) in MeOD-*d*₄, at 298 K and 500 MHz for ¹H and 125 MHz for ¹³C.

No.	δ_{H} [ppm], <i>J</i> in [Hz]	δ_{C} [ppm], mult.	HMBC ($^{\circ}\text{J}$)
1	0.88 (3H, m)	12.39+12.42, CH ₃	C1→H11(³ J), H14(³ J), H17(³ J)
2	1.23 (3H, m)	17.70+17.71, CH ₃	C2→H10(³ J), H16(³ J), H19(⁴ J)
3	1.45 (1H, m); 1.58 (1H, m)	21.64+21.65, CH ₂	C3→H16(² J)
4	1.38 (1H, m); 1.66 (1H, m)	24.3, CH ₂	C4→H14(² J)
5	1.59 (1H, m); 2.12 (1H, m)	28.54+28.57, CH ₂	C5→H4(² J), H17(² J)
6	1.03 (1H, m); 1.88 (1H, m)	32.8, CH ₂	C6→H7(² J), H9(² J)
7	2.29 (1H, m); 2.48 (1H, m)	33.8, CH ₂	C7→H6(² J), H19(³ J)
8	2.30 (1H, m); 2.45 (1H, m)	34.7, CH ₂	C8→H19(³ J)
9	1.64 (1H, m)	36.6, CH	C9→H6(² J), H14(² J)
10	1.70 (1H, m); 2.06 (1H, m)	36.7, CH ₂	C10→H2(³ J), H8(² J)
11	1.19 (1H, m); 1.77-1.88 (1H, m)	37.82, CH ₂	C11→H1(³ J), H17(³ J)
12	-	39.97+39.98, C _q	C12→H2(² J), H7(³ J), H8(³ J), H19(³ J)
13	-	43.7, C _q	C13→H1(² J), H14(² J), H17(² J)
14	1.08 (1H, m)	51.46+51.43, CH	C14→H1(³ J), H4(² J), H6(³ J)
15	5.46 (1H, s)	54.7, CH	C15→H18(⁴ J), H22(³ J)
16	0.96 (1H, m)	55.2, CH	C16→H2(³ J)
17	4.51 (1H, m)	84.62+84.64, CH	C17→H1(³ J), H4(³ J), H14(³ J)
18	6.79 (1H, d, <i>J</i> = 8.6 Hz)	117.7, CH _{arom}	C18→H22(⁴ J)
19	5.70 (1H, s)	124.2, CH _{alkene}	C19→H7(³ J), H8(³ J)
20	-	125.0, C _q	C20→H18(³ J), H22(² J), H23(² J)
21	-	127.1, C _q	C21→H15(² J), H18(³ J)
22	7.22 (1H, d, <i>J</i> = 2.5 Hz)	130.05, CH _{arom}	C22→H15(³ J), H23(³ J)
23	7.12 (1H, m)	130.09, CH _{arom}	C23→H22(³ J)
24	-	155.25+155.26, C _q	C24→H18(² J), H22(³ J), H23(³ J)
25	-	158.4, C _q	C25→H15(³ J), H17(³ J)
26	-	174.0, C _q	C26→H15(² J)
27	-	175.0, C _q	C27→H2(³ J), H6(³ J), H7(² J)
28	-	202.3, C _q	C28→H7(⁴ J), H8(² J), H10(³ J)

6.3.3.2.4 Synthesis of 2,5,7,8-tetramethyl-2-(4,8,12-trimethyltridecyl)chroman-6-yl (5-chloro-2-oxo-2,3-dihydrobenzofuran-3-yl)carbamate (**373**)



Prepared according to **GP-VI** using tocopherol carbamate **363** (488 mg, 1.03 mmol, 1.0 eq.), glyoxylic acid monohydrate **188** (94.8 mg, 1.03 mmol, 1.0 eq.), *p*-chlorophenol **290** (159 mg, 1.24 mmol, 1.2 eq.) in 2 ml of TFA. **373** was obtained as a colourless solid in a yield of 43%.

Yield: 282 mg (0.44 mmol, 43%).

Appearance: Colourless solid.

R_f-Value: 0.17 (SiO₂, Toluene/MeOH 15:1 + 1% AcOH).

IR: $\tilde{\nu}$ [cm⁻¹] = 3307 (br), 2926 (m), 2866 (w), 2845 (w), 1705 (vs), 1636 (w), 1606 (w), 1576 (w), 1559 (w), 1540 (w), 1497 (s), 1457 (s), 1423 (s), 1376 (s), 1366 (s), 1336 (m), 1279 (m), 1226 (vs), 1169 (s), 1110 (m), 1088 (m), 1030 (w), 1023 (w), 994 (w), 976 (w), 940 (w), 914 (w), 877 (w), 817 (s).

MP: 115 °C.

HR-MS (ESI): Theor. [M+Na]⁺: 662.35827, found: 662.35880.

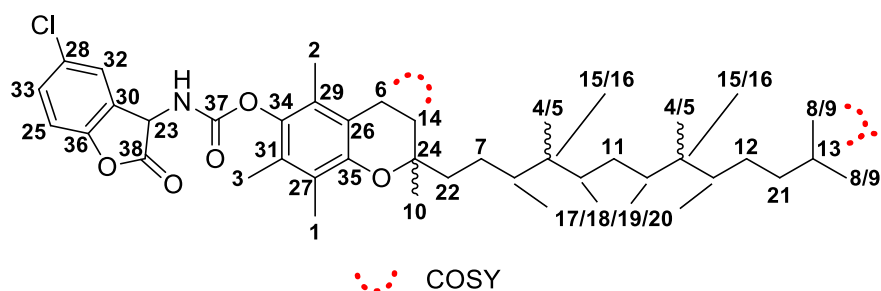
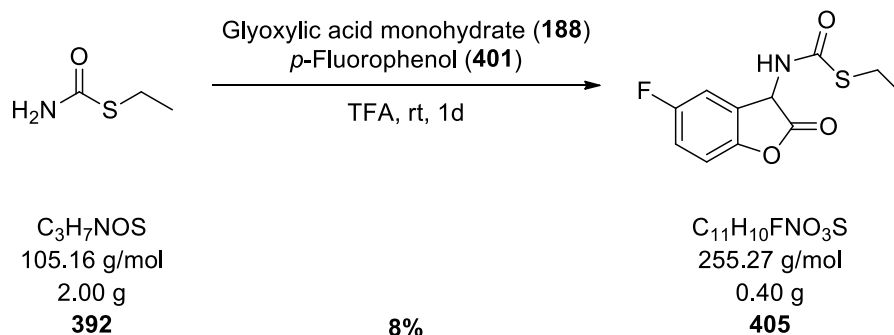


Table 87: 1D and 2D-NMR data of 2,5,7,8-tetramethyl-2-(4,8,12-trimethyltridecyl)chroman-6-yl (5-chloro-2-oxo-2,3-dihydrobenzofuran-3-yl)carbamate (373) in DMSO- d_6 , at 298 K and 500 MHz for ^1H and 125 MHz for ^{13}C .

No.	δ_{H} [ppm], J in [Hz]	δ_{C} [ppm], mult.	No.	δ_{H} [ppm], J in [Hz]	δ_{C} [ppm], mult.
1	2.00 (3H, s)	11.5, CH ₃	20	1.23 (2H, m)	36.93+36.90+36.84 CH ₂
2	1.93 (3H, s)	11.8, CH ₃	21	1.11 (2H, m)	38.8, CH ₂
3	1.95 (3H, s)	12.6, CH ₃	22	1.50 (2H, m)	39.4, CH ₂
4	0.82 (3H, s)	19.59+19.46, CH ₃	23	5.46 (1H, d, $J = 8.7$ Hz)	52.1, CH
5	0.82 (3H, s)	19.61+19.55+19.52, CH ₃	24	-	74.6, C _q
6	2.53 (2H, m)	19.9, CH ₂	25	6.86 (1H, d, $J = 8.6$ Hz)	116.9, CH _{arom}
7	1.37-1.41 (2H, m)	20.36+20.40, CH ₂	26	-	117.0, C _q
8	0.84 (3H, s)	22.45, CH ₃	27	-	121.5, C _q
9	0.84 (3H, s)	22.54, CH ₃	28	-	122.3, C _q
10	1.18 (3H, s)	23.53, CH ₃	29	-	125.7, C _q
11	1.20-1.23 (2H, m)	23.74+23.72+23.70, CH ₂	30	-	125.8, C _q
12	1.20-1.23 (2H, m)	24.18+24.17+24.16 CH ₂	31	-	127.2, C _q
13	1.49 (1H, m)	27.4, CH	32	7.33 (1H, d, $J = 2.7$ Hz)	128.0, CH _{arom}
14	1.74 (2H, m)	30.75+30.68, CH ₂	33	7.18 (1H, dd, $J = 8.6,$ 2.7 Hz)	128.6, CH _{arom}
15	1.36 (1H, m)	32.00+31.98+31.96 CH	34	-	140.4, C _q
16	1.36 (1H, m)	32.07+32.03, CH	35	-	148.3, C _q
17	1.21 (2H, m)	36.70+36.56, CH ₂	36	-	153.9, C _q
18	1.05 (2H, m)	36.73+36.63, CH ₂	37	-	154.6, C _q
19	1.05 (2H, m)	36.78, CH ₂	38	-	171.8, C _q
			NH	8.22 (1H, d, $J = 8.7$ Hz)	-

Note: C4/C5, C8/C9, C15/C16, C17/C18 and C19/C20 could not be assigned.

6.3.3.3 2-Coumaranones with thiolcarbamate substructures

6.3.3.3.1 Synthesis of *S*-ethyl (5-fluoro-2-oxo-2,3-dihydrobenzofuran-3-yl)carbamothioate (**405**)

Prepared according to **GP-VI** using *S*-ethyl carbamothioate **392** (2.00 g, 19.0 mmol, 1.0 eq.), glyoxylic acid monohydrate **188** (1.75 g, 19.0 mmol, 1.0 eq.), *p*-fluorophenol **401** (2.56 g, 22.8 mmol, 1.2 eq.) in 30 ml of TFA. **405** was obtained as a colourless solid in a yield of 8%.

Yield: 0.40 g (1.58 mmol, 8%).

Appearance: Colourless solid.

R_f-Value: 0.13 (SiO₂, *c*-Hex/Toluene 1:1 + 1% AcOH).

IR: $\tilde{\nu}$ [cm⁻¹] = 3348 (br), 3076 (w), 2976 (w), 2912 (w), 2359 (w), 2341 (w), 1799 (s), 1646 (vs), 1505 (s), 1479 (s), 1457 (w), 1446 (w), 1383 (w), 1321 (m), 1268 (m), 1253 (w), 1233 (w), 1203 (s), 1195 (s), 1119 (s), 1076 (vs), 1047 (w), 955 (w), 947 (w), 899 (m), 885 (m), 822 (s).

MP: 183 °C.

HR-MS (EI): Theor. [M+H]⁺: 255.0359, found: 255.0361.

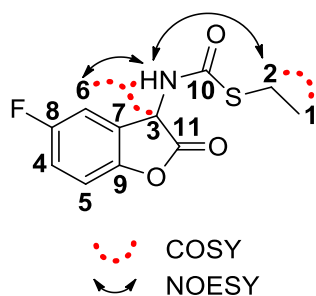
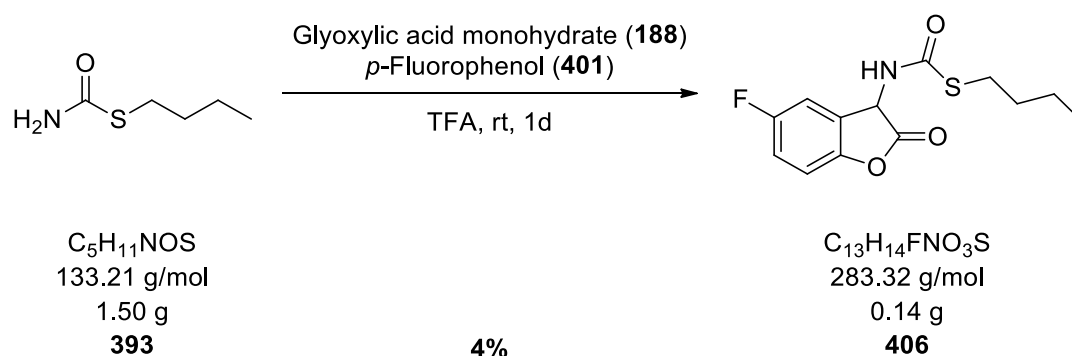


Table 88: 1D and 2D-NMR data of *S*-ethyl (5-fluoro-2-oxo-2,3-dihydrobenzofuran-3-yl)carbamothioate (405) in DMSO- d_6 , at 298 K and 499 MHz for ^1H and 125 MHz for ^{13}C .

No.	δ_{H} [ppm], J in [Hz]	δ_{C} [ppm], mult.	HMBC ($^{\times}J$)
1	1.14 (3H, t, $J = 7.3$ Hz)	15.5, CH_3	$\text{C1} \rightarrow \text{H2} (^2J)$
2	2.76 (2H, m)	23.4, CH_2	$\text{C2} \rightarrow \text{H1} (^2J)$
3	5.46 (1H, d, $J = 7.2$ Hz)	52.29+52.30, CH	$\text{C3} \rightarrow \text{H6} (^3J)$, $\text{NH} (^2J)$
4	7.19 (1H, m)	111.3+111.5, CH_{arom}	$\text{C4} \rightarrow \text{H6} (^3J)$
5	7.25 (1H, m)	111.7+111.8, CH_{arom}	$\text{C5} \rightarrow \text{H3} (^4J)$, $\text{H6} (^4J)$
6	7.21 (1H, m)	116.0+115.8, CH_{arom}	$\text{C6} \rightarrow \text{H3} (^3J)$, $\text{H4} (^3J)$
7	-	127.56+127.63, C_{q}	$\text{C7} \rightarrow \text{H3} (^2J)$, $\text{H5} (^3J)$, $\text{NH} (^3J)$
8	-	149.42+149.44, C_{q}	$\text{C8} \rightarrow \text{H3} (^4J)$, $\text{H4} (^2J)$
9	-	157.9+159.8, C_{q}	$\text{C9} \rightarrow \text{H3} (^3J)$, $\text{H5} (^2J)$, $\text{H6} (^3J)$
10	-	167.0, C_{q}	$\text{C10} \rightarrow \text{H2} (^3J)$, $\text{H3} (^3J)$, $\text{NH} (^2J)$
11	-	173.0, C_{q}	$\text{C11} \rightarrow \text{H3} (^2J)$, $\text{NH} (^3J)$
NH	9.37 (1H, d, $J = 7.4$ Hz)	-	-

6.3.3.2 Synthesis of *S*-butyl (5-fluoro-2-oxo-2,3-dihydrobenzofuran-3-yl)carbamothioate (**406**)



Prepared according to *GP-VI* using *S*-butyl carbamothioate **393** (1.50 g, 11.3 mmol, 1.0 eq.), glyoxylic acid monohydrate **188** (1.04 g, 11.3 mmol, 1.0 eq.), *p*-fluorophenol **401** (1.51 g, 13.5 mmol, 1.2 eq.) in 18 ml of TFA. **406** was obtained as a colourless solid in a yield of 4%.

Yield: 0.14 g (0.49 mmol, 4%).

Appearance: Colourless solid.

R_f-Value: 0.13 (SiO₂, *c*-Hex/Toluene 1:1 + 1% AcOH).

IR: $\tilde{\nu}$ [cm⁻¹] = 3346 (br), 3076 (w), 2960 (w), 2930 (w), 2873 (w), 2358 (w), 1797 (s), 1649 (vs), 1507 (s), 1480 (s), 1447 (w), 1379 (w), 1324 (m), 1268 (m), 1254 (w), 1236 (w), 1203 (s), 1194 (s), 1121 (vs), 1078 (vs), 1053 (w), 956 (w), 947 (w), 918 (w), 902 (w), 887 (s), 821 (s).

MP: 162 °C.

HR-MS (ESI): Theor. [M+Na]⁺: 306.05706, found: 306.05694.

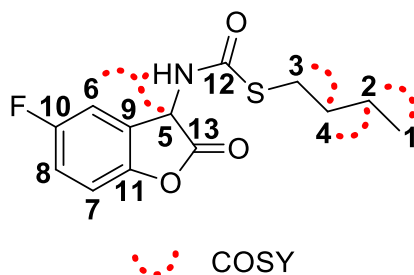
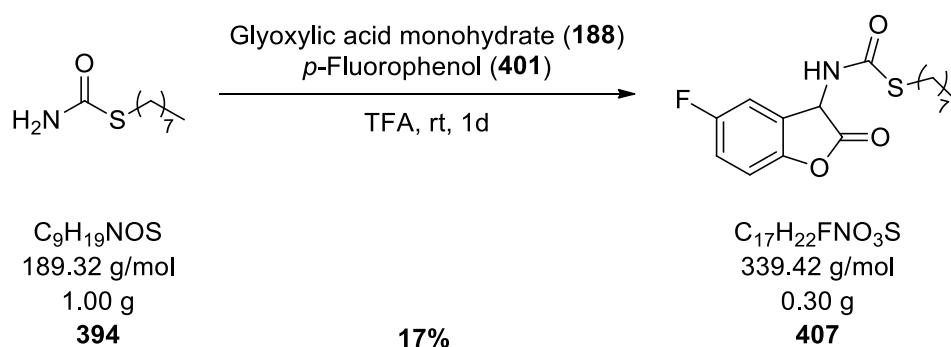


Table 89: 1D and 2D-NMR data of *S*-butyl (5-fluoro-2-oxo-2,3-dihydrobenzofuran-3-yl)carbamothioate (406) in DMSO- d_6 , at 298 K and 500 MHz for ^1H and 125 MHz for ^{13}C .

No.	δ_{H} [ppm], J in [Hz]	δ_{C} [ppm], mult.	HMBC ($^{\times}\text{J}$)
1	0.84 (3H, t, $J = 7.4$ Hz)	13.4, CH_3	$\text{C1} \rightarrow \text{H2} (^2\text{J}), \text{H4} (^3\text{J})$
2	1.29 (2H, sxt, $J = 7.3$ Hz)	21.2, CH_2	$\text{C2} \rightarrow \text{H1} (^2\text{J}), \text{H3} (^3\text{J}), \text{H4} (^2\text{J})$
3	2.76 (2H, m)	28.6, CH_2	$\text{C3} \rightarrow \text{H2} (^3\text{J}), \text{H4} (^2\text{J})$
4	1.45 (2H, quin, $J = 7.3$ Hz)	31.9, CH_2	$\text{C4} \rightarrow \text{H1} (^3\text{J}), \text{H2} (^2\text{J}), \text{H3} (^2\text{J})$
5	5.45 (1H, d, $J = 7.2$ Hz)	52.3, CH	$\text{C5} \rightarrow \text{H6} (^3\text{J}), \text{NH} (^2\text{J})$
6	7.18 (1H, m)	111.3+111.5, CH_{arom}	$\text{C6} \rightarrow \text{H5} (^3\text{J}), \text{H8} (^3\text{J})$
7	7.25 (1H, m)	111.7+111.8, CH_{arom}	$\text{C7} \rightarrow \text{H5} (^4\text{J})$
8	7.21 (1H, m)	115.8+116.0, CH_{arom}	$\text{C8} \rightarrow \text{H6} (^3\text{J})$
9	-	127.55+127.63, C_{q}	$\text{C9} \rightarrow \text{H5} (^2\text{J}), \text{H7} (^3\text{J}), \text{NH} (^3\text{J})$
10	-	149.42+149.43, C_{q}	$\text{C10} \rightarrow \text{H5} (^4\text{J}), \text{H6} (^2\text{J}), \text{H8} (^2\text{J})$
11	-	157.9+159.8, C_{q}	$\text{C11} \rightarrow \text{H5} (^3\text{J}), \text{H7} (^2\text{J}), \text{H8} (^3\text{J})$
12	-	167.0, C_{q}	$\text{C12} \rightarrow \text{H3} (^3\text{J}), \text{H5} (^3\text{J}), \text{NH} (^2\text{J})$
13	-	173.0, C_{q}	$\text{C13} \rightarrow \text{H5} (^2\text{J}), \text{NH} (^3\text{J})$
NH	9.38 (1H, d, $J = 7.4$ Hz)	-	-

6.3.3.3 Synthesis of *S*-octyl (5-fluoro-2-oxo-2,3-dihydrobenzofuran-3-yl)carbamothioate (**407**)



Prepared according to **GP-VI** using *S*-octyl carbamothioate **394** (1.00 g, 5.28 mmol, 1.0 eq.), glyoxylic acid monohydrate **188** (0.49 g, 5.28 mmol, 1.0 eq.), *p*-fluorophenol **401** (0.71 g, 6.34 mmol, 1.2 eq.) in 9 ml of TFA. **407** was obtained as a colourless solid in a yield of 17%.

Yield: 0.30 g (0.88 mmol, 17%).

Appearance: Colourless solid.

R_f-Value: 0.13 (SiO₂, *c*-Hex/Toluene 1:1 + 1% AcOH).

IR: $\tilde{\nu}$ [cm⁻¹] = 3342 (m), 3072 (w), 2951 (w), 2921 (br), 2852 (w), 2363 (w), 1799 (s), 1708 (w), 1651 (vs), 1506 (m), 1482 (s), 1467 (m), 1448 (w), 1437 (w), 1381 (w), 1321 (w), 1268 (w), 1254 (s), 1232 (w), 1205 (s), 1194 (s), 1120 (s), 1077 (s), 1006 (w), 955 (w), 946 (w), 900 (w), 886 (w), 824 (m).

MP: 133 °C.

HR-MS (ESI): Theor.[M+H]⁺: 340.13771, found: 340.13754.

Theor.[M+Na]⁺: 362.11966, found: 362.11962.

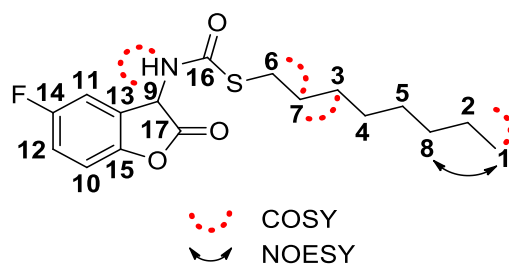
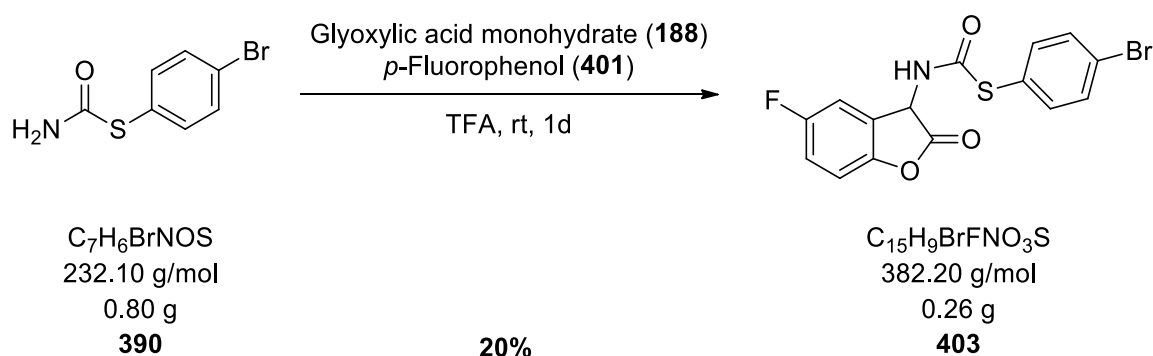


Table 90: 1D and 2D-NMR data of *S*-octyl (5-fluoro-2-oxo-2,3-dihydrobenzofuran-3-yl)carbamothioate (407) in DMSO- d_6 , at 298 K and 500 MHz for ^1H and 125 MHz for ^{13}C .

No.	δ_{H} [ppm], J in [Hz]	δ_{C} [ppm], mult.	HMBC ($^{\circ}\text{J}$)
1	0.85 (3H, t, $J = 7.0$ Hz)	13.9, CH_3	$\text{C1} \rightarrow \text{H2} (^2\text{J})$
2	1.24 (2H, m)	22.1, CH_2	$\text{C2} \rightarrow \text{H1} (^2\text{J}), \text{H8} (^2\text{J})$
3	1.25 (2H, m)	28.0, CH_2	$\text{C3} \rightarrow \text{H6} (^3\text{J})$
4	1.22 (2H, m)	28.4, CH_2	$\text{C4} \rightarrow \text{H3} (^2\text{J}), \text{H7} (^3\text{J})$
5	1.23 (2H, m)	28.6, CH_2	-
6	2.75 (2H, m)	28.9, CH_2	$\text{C6} \rightarrow \text{H7} (^2\text{J})$
7	1.46 (2H, quin, $J = 7.3$ Hz)	29.9, CH_2	$\text{C7} \rightarrow \text{H6} (^2\text{J})$
8	1.21 (2H, m)	31.2, CH_2	$\text{C8} \rightarrow \text{H1} (^3\text{J}), \text{H2} (^2\text{J})$
9	5.44 (1H, d, $J = 7.1$ Hz)	52.3, CH	$\text{C9} \rightarrow \text{H11} (^3\text{J}), \text{NH} (^2\text{J})$
10	7.17 (1H, m)	111.25+111.45, CH_{arom}	$\text{C10} \rightarrow \text{H9} (^4\text{J}), \text{H12} (^2\text{J})$
11	7.24 (1H, m)	111.73+111.79, CH_{arom}	$\text{C11} \rightarrow \text{H9} (^3\text{J}), \text{H12} (^3\text{J})$
12	7.21 (1H, m)	115.8+116.0, CH_{arom}	$\text{C12} \rightarrow \text{H10} (^2\text{J})$
13	-	127.56+127.63, C_q	$\text{C13} \rightarrow \text{H9} (^2\text{J}), \text{H11} (^2\text{J}), \text{NH} (^3\text{J})$
14	-	149.42+149.43, C_q	$\text{C14} \rightarrow \text{H9} (^4\text{J}), \text{H12} (^2\text{J}), \text{H11} (^2\text{J}), \text{H10} (^2\text{J})$
15	-	159.8+157.9, C_q	$\text{C15} \rightarrow \text{H9} (^3\text{J}), \text{H11} (^3\text{J})$
16	-	167.1, C_q	$\text{C16} \rightarrow \text{H6} (^3\text{J}), \text{H9} (^3\text{J}), \text{NH} (^2\text{J})$
17	-	173.0, C_q	$\text{C17} \rightarrow \text{H9} (^2\text{J}), \text{NH} (^3\text{J})$
NH	9.37 (1H, d, $J = 7.3$ Hz)	-	-

6.3.3.4 Synthesis of *S*-(4-bromophenyl) (5-fluoro-2-oxo-2,3-dihydrobenzofuran-3-yl)carbamothioate (**403**)



Prepared according to *GP-VI* using *S*-(4-bromophenyl) carbamothioate **390** (0.80 g, 3.45 mmol, 1.0 eq.), glyoxylic acid monohydrate **188** (0.32 g, 3.45 mmol, 1.0 eq.), *p*-fluorophenol **401** (0.46 g, 4.14 mmol, 1.2 eq.) in 6 ml of TFA. **403** was obtained as a colourless solid in a yield of 20%.

Yield: 0.26 g (0.68 mmol, 20%).

Appearance: Colourless solid.

R_f-Value: 0.10 (SiO₂, *c*-Hex/Toluene 1:1 + 1% AcOH).

IR: $\tilde{\nu}$ [cm⁻¹] = 3327 (br), 3087 (w), 2931 (w), 2359 (w), 1814 (s), 1652 (s), 1610 (w), 1563 (w), 1500 (s), 1485 (s), 1477 (s), 1448 (w), 1386 (w), 1323 (w), 1273 (w), 1263 (w), 1250 (w), 1235 (w), 1209 (m), 1191 (w), 1129 (s), 1118 (s), 1089 (vs), 1076 (vs), 1052 (w), 1009 (w), 958 (w), 939 (w), 898 (w), 865 (w), 834 (m), 824 (vs).

MP: 191 °C.

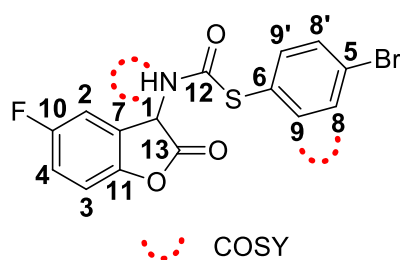
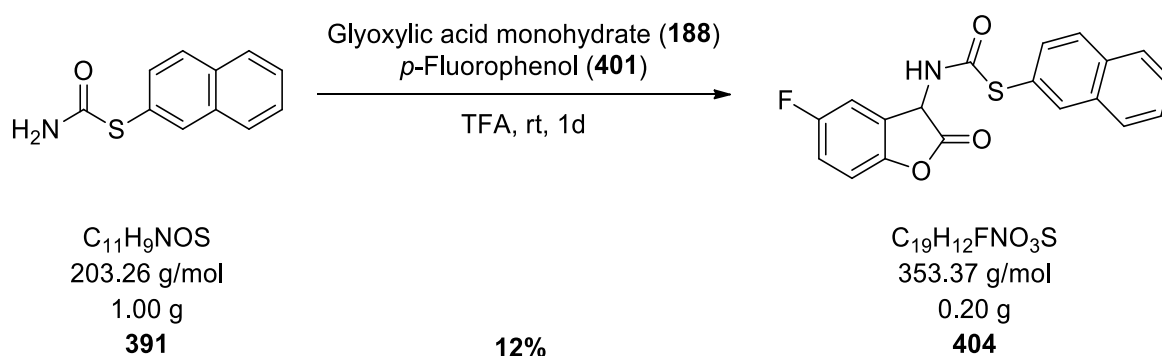


Table 91: 1D and 2D-NMR data of *S*-(4-bromophenyl) (5-fluoro-2-oxo-2,3-dihydrobenzofuran-3-yl)carbamothioate (403) in DMSO- d_6 , at 298 K and 500 MHz for ^1H and 125 MHz for ^{13}C .

No.	δ_{H} [ppm], J in [Hz]	δ_{C} [ppm], mult.	HMBC ($^{\times}\text{J}$)
1	5.54 (1H, d, $J = 7.3$ Hz)	52.5, CH	C1 \rightarrow H2(^3J), NH(^2J)
2	7.25 (1H, m)	111.46+111.67, CH _{arom}	C2 \rightarrow H4(^3J)
3	7.22 (1H, m)	111.78+111.84, CH _{arom}	-
4	7.21 (1H, m)	116.0+116.2, CH _{arom}	C4 \rightarrow H2(^3J)
5	-	123.1, C _q	C5 \rightarrow H8(^2J), H9(^3J)
6	-	126.9, C _q	C6 \rightarrow H8(^3J), H9(^2J)
7	-	127.1+127.2, C _q	C7 \rightarrow H1(^2J), H2(^2J), NH(^3J)
8	7.60 (2H, d, $J = 8.5$ Hz)	132.1, 2xCH _{arom}	C8 \rightarrow H8(^3J)
9	7.38 (2H, d, $J = 8.5$ Hz)	136.9, 2xCH _{arom}	C9 \rightarrow H9(^3J)
10	-	149.41+149.43, C _q	C10 \rightarrow H1(^4J), H2(^2J), H3(^3J), H4(^2J)
11	-	157.9+159.8, C _q	C11 \rightarrow H2(^3J), H4(^3J)
12	-	164.6, C _q	C12 \rightarrow H1(^3J), H9(^4J), NH(^2J)
13	-	172.8, C _q	C13 \rightarrow H1(^2J), NH(^3J)
NH	9.64 (1H, d, $J = 7.4$ Hz)	-	-

6.3.3.5 Synthesis of *S*-naphthalen-2-yl (5-fluoro-2-oxo-2,3-dihydrobenzofuran-3-yl)carbamothioate (**404**)



Prepared according to *GP-VI* using *S*-naphthalen-2-yl carbamothioate **391** (1.00 g, 4.91 mmol, 1.0 eq.), glyoxylic acid monohydrate **188** (0.45 g, 4.91 mmol, 1.0 eq.), *p*-fluorophenol **401** (0.66 g, 5.90 mmol, 1.2 eq.) in 8 ml of TFA. **404** was obtained as a brownish solid in a yield of 12%.

Yield: 0.20 g (0.57 mmol, 12%).

Appearance: Colourless solid.

R_f-Value: 0.10 (SiO₂, *c*-Hex/Toluene 1:1 + 1% AcOH).

IR: $\tilde{\nu}$ [cm⁻¹] = 3326 (br), 3059 (w), 2934 (w), 2361 (w), 2341 (w), 1816 (s), 1716 (w), 1700 (w), 1648 (vs), 1612 (w), 1586 (w), 1559 (w), 1480 (vs), 1449 (w), 1366 (w), 1341 (w), 1318 (m), 1274 (w), 1253 (w), 1233 (w), 1209 (s), 1190 (m), 1131 (s), 1119 (s), 1079 (s), 1066 (s), 1052 (w), 1019 (w), 980 (w), 939 (m), 893 (m), 873 (w), 859 (w), 849 (s), 830 (s), 818 (s), 800 (w).

MP: 175 °C.

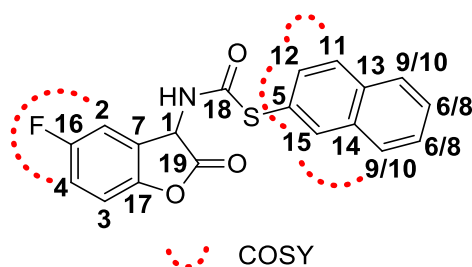


Table 92: 1D and 2D-NMR data of *S*-naphthalen-2-yl (5-fluoro-2-oxo-2,3-dihydrobenzofuran-3-yl)carbamothioate (391) in DMSO- d_6 , at 298 K and 500 MHz for ^1H and 125 MHz for ^{13}C .

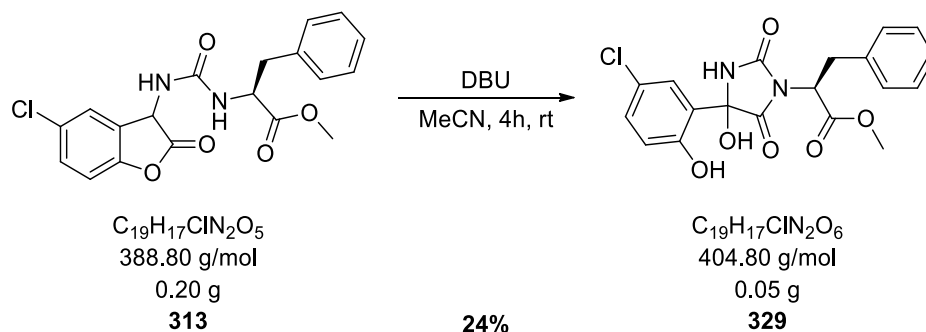
No.	δ_{H} [ppm], J in [Hz]	δ_{C} [ppm], mult.	HMBC ($^{\circ}\text{J}$)
1	5.55 (1H, d, $J = 7.4$ Hz)	52.5, CH	C1 \rightarrow H2(^3J), NH(^2J)
2	7.27 (1H, m)	111.5+111.6, CH _{arom}	C2 \rightarrow H4(^3J)
3	7.21 (1H, m)	111.76+111.81, CH _{arom}	-
4	7.20 (1H, m)	116.0+116.1, CH _{arom}	C4 \rightarrow H2(^3J)
5	-	124.7, C _q	C5 \rightarrow H11(^3J)
6	7.56 (1H, m)	126.7, CH _{arom}	-
7	-	127.26, C _q	C7 \rightarrow H3(^3J)
8	7.58 (1H, m)	127.32, CH _{arom}	-
9	7.95 (1H, m)	127.6, CH _{arom}	-
10	7.95 (1H, m)	127.8, CH _{arom}	-
11	7.93 (1H, m)	128.5, CH _{arom}	C11 \rightarrow H9/10(^3J)
12	7.48 (1H, dd, $J = 8.5, 1.8$ Hz)	131.7, CH _{arom}	C12 \rightarrow H11(^2J), H15(^3J)
13	-	132.8, C _q	C13 \rightarrow H9/H10(^3J), H12(^3J), H15(^3J)
14	-	133.0, C _q	C14 \rightarrow H9/H10(^3J), H15(^2J)
15	8.10 (1H, d, $J = 1.4$ Hz)	134.7, CH _{arom}	C15 \rightarrow H12(^3J)
16	-	149.41+149.42, C _q	C16 \rightarrow H2(^2J), H3(^3J), H4(^2J)
17	-	158.1+159.7, C _q	C17 \rightarrow H2(^3J), H3(^2J)
18	-	165.3, C _q	C18 \rightarrow H1(^3J), NH(^2J)
19	-	172.8, C _q	C19 \rightarrow H1(^2J), NH(^3J)
NH	9.59 (1H, d, $J = 7.5$ Hz)	-	-

Note: C6/C8 and C9/C10 could not be assigned.

6.3.4 Decomposition experiments

6.3.4.1 Decomposition of urea-coumaranones

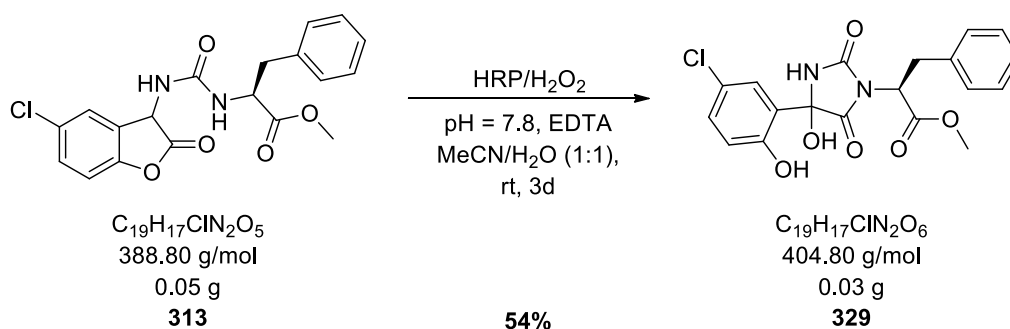
6.3.4.1.1A Decomposition of 313 with DBU



Prepared according to **GP-VII**. Small scale experiment: Urea-coumaranone **313** (0.02 g, 0.05 mmol, 1.0 eq.) and DBU (15.0 μ l, 0.10 mmol, 2.0 eq.) in 0.70 ml of DMSO- d_6 . Large scale experiment: Urea-coumaranone **313** (0.20 g, 0.51 mmol, 1.0 eq.) and DBU (0.15 ml, 1.03 mmol, 2.0 eq.) in 10.0 ml of MeCN. **329** was obtained as a brownish solid in a yield of 24%.

Yield (Large scale): 0.05 g (0.12 mmol, 24%).

6.3.4.1.1B Decomposition of 313 with HRP



Prepared according to **GP-VIII** using urea-coumaranone **313** (0.05 g, 0.13 mmol, 1.0 eq.), phosphate buffer solution I (1.3 ml, 1.30 mmol, 10 eq), EDTA solution (1.3 ml, 0.13 mmol, 1.0 eq.), H_2O_2 (13 μ l, 0.13 mmol, 1.0 eq.) and HRP solution (2.0 ml, 100 units) in 12.5 ml of MeCN/ H_2O (1:1). **329** was obtained as a brownish solid in a yield of 57%. The results of the NMR-spectra are in agreement with those of decomposition experiment **6.3.4.1.1A**.

Yield: 0.03 g (0.07 mmol, 54%).

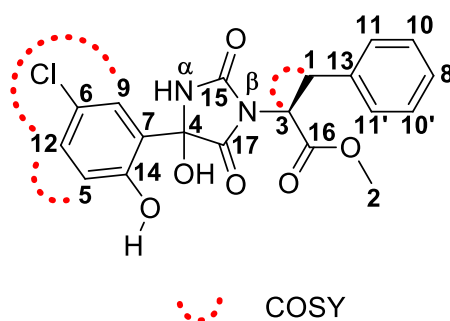


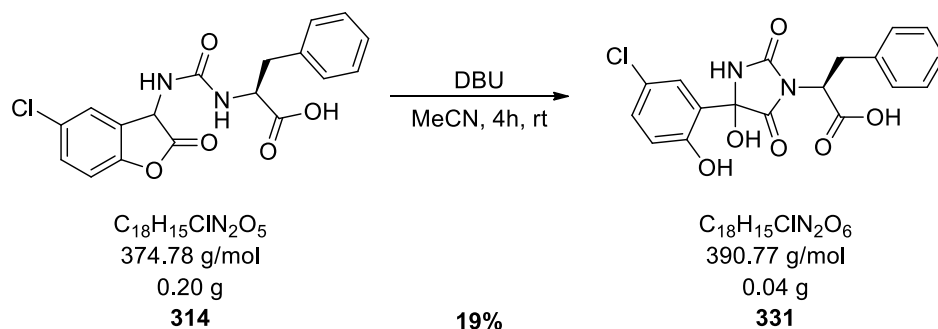
Table 93: 1D and 2D-NMR data of (2S)-methyl 2-(4-(5-chloro-2-hydroxyphenyl)-4-hydroxy-2,5-dioxoimidazolidin-1-yl)-3-phenylpropanoate (329) in DMSO-*d*₆, at 298 K and 499 MHz for ¹H and 126 MHz for ¹³C.

No.	δ_{H} [ppm], <i>J</i> in [Hz]	δ_{C} , δ_{N} [ppm], mult.	HMBC ($^{\circ}\text{J}$)
1	3.04 (1H, dd, <i>J</i> = 14.2, 1.6 Hz) +3.45 (1H, dd, <i>J</i> = 14.2, 7.2 Hz)	33.38+33.61, CH ₂	C1→H3(² J), H11(³ J)
2	3.64 (3H, s)	52.30+52.32, CH ₃	-
3	4.78 (1H, dd, <i>J</i> = 7.8, 1.8 Hz)	52.7, CH	C3→H1(² J),
4	-	81.76+81.92, C _q	C4→H5(⁴ J), H9(³ J), NH _α (² J)
5	6.80 (1H, d, <i>J</i> = 8.6 Hz)	117.1, CH _{arom}	-
6	-	122.0, C _q	C6→H5(³ J), H9(² J), H12(² J)
7	-	126.25+126.33, C _q	C7→H5(³ J)
8	7.20 (1H, m)	126.5, CH _{arom}	C8→H11(³ J)
9	7.49 (1H, d, <i>J</i> = 2.6 Hz)	127.37, CH _{arom}	C9→H12(³ J)
10	7.27 (2H, m)	128.31+128.34, 2xCH _{arom}	C10→H10(³ J)
11	7.25 (2H, m)	129.02+129.07, 2xCH _{arom}	C11→H1(³ J), H8(³ J), H11(³ J)
12	7.24 (1H, m)	129.5, CH _{arom}	C12→H9(³ J)
13	-	137.7, C _q	C13→H1(² J), H10(³ J)
14	-	153.48+153.54, C _q	C14→H5(² J), H9(³ J), H12(³ J)
15	-	154.93+154.97, C _q	C15→H3(³ J), NH _α (² J)
16	-	168.92+169.04, C _q	C16→H1(³ J), H2(³ J), H3(² J)
17	-	172.16+172.29, C _q	C17→H3(³ J), NH _α (³ J)
NH _α	8.86+8.83 (1H, s)	112.6, NH	-
N _β	-	147.8, NR ₃	N _β →H1(³ J), H3(² J), NH _α (³ J)
Ph-OH	10.13 (1H, br)	-	-

Note: The ¹H- and ¹³C-NMR-spectra show a mixture of rotamers.

MS (ESI): m/z (%) 427.0668 [M+Na⁺] (27), 409.556 [M+Na⁺-H₂O] (100).

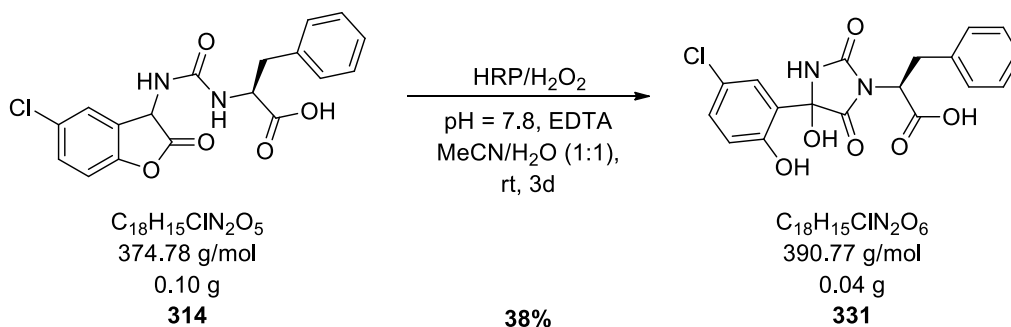
6.3.4.1.2A Decomposition of 314 with DBU



Prepared according to *GP-VII*. Small scale experiment: Urea-coumaranone **314** (0.02 g, 0.05 mmol, 1.0 eq.) and DBU (16.4 μ l, 0.11 mmol, 2.0 eq.) in 0.70 ml of DMSO- d_6 . Large scale experiment: Urea-coumaranone **314** (0.20 g, 0.53 mmol, 1.0 eq.) and DBU (0.16 ml, 1.07 mmol, 2.0 eq.) in 10.0 ml of MeCN. Before extraction, the aqueous phase was acidified with 0.1 ml of a 2 M HCl solution. **331** was obtained as a brownish solid in a yield of 19%.

Yield (Large scale): 0.04 g (0.10 mmol, 19%).

6.3.4.1.2B Decomposition of 314 with HRP



Prepared according to *GP-VIII* using urea-coumaranone **314** (0.10 g, 0.27 mmol, 1.0 eq.), phosphate buffer solution I (2.7 ml, 2.70 mmol, 10 eq), EDTA solution (2.7 ml, 0.27 mmol, 1.0 eq.), H₂O₂ (28 μ l, 0.27 mmol, 1.0 eq.) and HRP solution (4.0 ml, 200 units) in 25 ml of MeCN/H₂O (1:1). Before extraction, the aqueous phase was acidified with 0.3 ml of a 2 M HCl solution. **331** was obtained as a brownish, orange solid in a yield of 38%. The results of the NMR-spectra are in agreement with those of decomposition experiment **6.3.4.1.2A**.

Yield: 0.04 g (0.10 mmol, 38%).

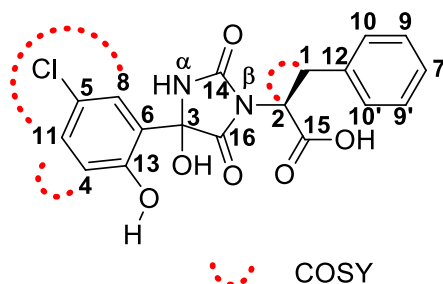
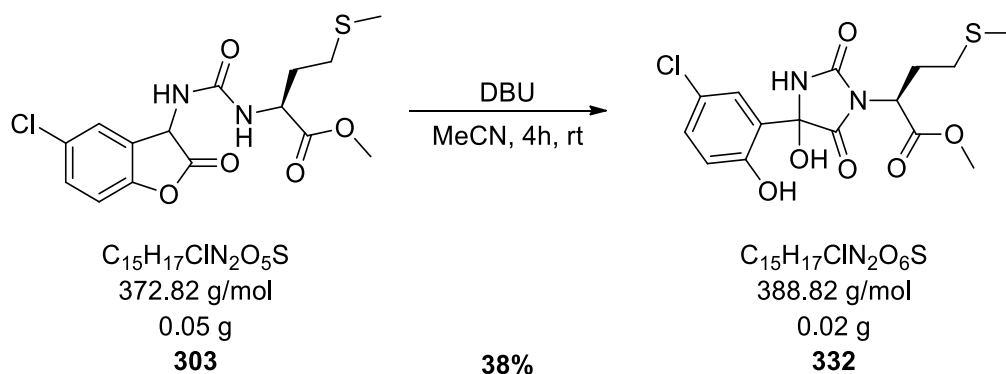


Table 94: 1D and 2D-NMR data of (2S)-2-(4-(5-chloro-2-hydroxyphenyl)-4-hydroxy-2,5-dioximidazolidin-1-yl)-3-phenylpropanoic acid (331) in DMSO-d₆, at 298 K and 499 MHz for ¹H and 126 MHz for ¹³C.

No.	δ_H [ppm], J in [Hz]	δ_C [ppm], mult.	HMBC (3J)
1	3.02 (½ H, dd, $J = 14.2, 6.6$ Hz)/3.18 (½ H dd, $J = 14.2, 10.8$ Hz) + 3.44 (1H, dd, $J = 14.2, 5.6$ Hz)	33.79+34.63, CH ₂	C1→H2(² J), H10(³ J)
2	4.67 (½ H, m)+5.01 (½ H, dd, $J = 10.8, 5.2$ Hz)	52.92/53.00+53.76, CH	C2→H1(² J)
3	-	81.72+82.17, C _q	C3→H4(⁴ J), H8(³ J), NH _α (² J)
4	6.80 (1H, d, $J = 8.6$ Hz)	117.2, CH _{arom}	-
5	-	122.0, C _q	C5→H4(³ J), H8(² J), H11(² J)
6	-	126.26+126.37, C _q	C6→H4(³ J), Ph-OH(³ J)
7	7.20 (1H, m)	126.32, CH _{arom}	C7→H10(³ J)
8	7.46 (1H, d, $J = 2.7$ Hz)	126.8+127.37/127.39, CH _{arom}	C8→H11(³ J)
9	7.19 (1H, m)+7.26 (1H, m)	128.27/128.30+128.47, 2xCH _{arom}	C9→H9(³ J)
10	7.19 (1H, m)+7.25 (1H, m)	128.8+128.95/128.99, 2xCH _{arom}	C10→H1(³ J), H7(³ J), H10(³ J)
11	7.23 (1H, m)	129.4, CH _{arom}	C11→H8(³ J)
12	-	137.0+138.30/138.31, C _q	C12→H1(² J), H2(³ J), H9(³ J)
13	-	153.39+153.58/153.66, C _q	C13→H4(² J), H8(³ J), H11(³ J)
14	-	155.11+155.15, C _q	C14→H2(³ J), NH _α (² J)
15	-	169.14+169.94/169.96, C _q	C15→H1(³ J), H2(² J)
16	-	172.23+172.34, C _q	C16→H2(³ J), NH _α (³ J)
NH _α	8.78+8.83 (1H, s)	-	-
Ph-OH	10.14+10.16(1H, br)	-	-
COOH	12.95 (1H, br)	-	-

Note: The ¹H- and ¹³C-NMR-spectra show a mixture of rotamers.

6.3.4.1.3 Decomposition of **303** with DBU

Prepared according to *GP-VII*. Small scale experiment: Urea-coumaranone **303** (0.02 g, 0.05 mmol, 1.0 eq.) and DBU (16.4 μ l, 0.11 mmol, 2.0 eq.) in 0.70 ml of DMSO- d_6 . Large scale experiment: Urea-coumaranone **303** (0.05 g, 0.13 mmol, 1.0 eq.) and DBU (0.04 ml, 0.27 mmol, 2.0 eq.) in 3.00 ml of MeCN. **332** was obtained as a slightly brownish solid in a yield of 40%.

Yield (Large scale): 20.0 mg (0.05 mmol, 38%).

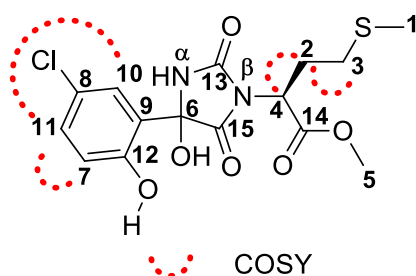


Table 95: 1D and 2D-NMR data of (2*S*)-methyl 2-(4-(5-chloro-2-hydroxyphenyl)-4-hydroxy-2,5-dioximidazolidin-1-yl)-4-(methylthio)butanoate (332) in DMSO- d_6 , at 298 K and 499 MHz for ^1H and 126 MHz for ^{13}C .

No.	δ_{H} [ppm], J in [Hz]	δ_{C} [ppm], mult.	HMBC ($^{\circ}\text{J}$)
1	2.05 (3H, s)	14.35+14.40, CH_3	$\text{C1} \rightarrow \text{H3} (^3\text{J})$
2	2.20+2.28 (2H, m)	28.1, CH_2	$\text{C2} \rightarrow \text{H3} (^2\text{J}), \text{H4} (^2\text{J})$
3	2.49+2.59 (2H, m)	29.5+29.6, CH_2	$\text{C3} \rightarrow \text{H1} (^3\text{J}), \text{H2} (^2\text{J}), \text{H4} (^3\text{J})$
4	4.78 (1H, m)	50.1+50.2, CH	$\text{C4} \rightarrow \text{H2} (^2\text{J}), \text{H3} (^3\text{J})$
5	3.66 (3H, s)	52.4, CH_3	-
6	-	81.4+81.6, C_q	$\text{C6} \rightarrow \text{H7} (^4\text{J}), \text{H10} (^3\text{J}), \text{NH}_\alpha (^2\text{J})$
7	6.80+6.82 (1H, d, $J = 8.6$ Hz)	117.0, CH_{arom}	-
8	-	122.0+122.1, C_q	$\text{C8} \rightarrow \text{H7} (^3\text{J}), \text{H10} (^2\text{J}), \text{H11} (^2\text{J})$
9	-	126.2+126.3, C_q	$\text{C9} \rightarrow \text{H7} (^3\text{J})$
10	7.56 (1H, ψt , $J = 3.1$ Hz)	127.47+127.54, CH_{arom}	$\text{C10} \rightarrow \text{H11} (^3\text{J})$
11	7.25 (1H, dd, $J = 8.6, 2.7$ Hz)	129.5, CH_{arom}	$\text{C11} \rightarrow \text{H10} (^3\text{J})$
12	-	153.4+153.5, C_q	$\text{C12} \rightarrow \text{H7} (^2\text{J}), \text{H10} (^3\text{J}), \text{H11} (^3\text{J})$
13	-	155.15+155.17, C_q	$\text{C13} \rightarrow \text{H4} (^3\text{J}), \text{NH}_\alpha (^2\text{J})$
14	-	169.36+169.40, C_q	$\text{C14} \rightarrow \text{H2} (^3\text{J}), \text{H4} (^2\text{J}), \text{H5} (^3\text{J})$
15	-	172.5+172.6, C_q	$\text{C15} \rightarrow \text{H4} (^3\text{J}), \text{NH}_\alpha (^3\text{J})$
NH_α	8.84+8.87 (1H, s)	-	-
Ph-OH	10.17 (1H, s)	-	-

Note: The ^1H - and ^{13}C -NMR-spectra show a mixture of rotamers.

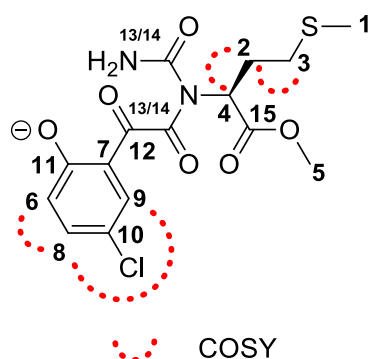
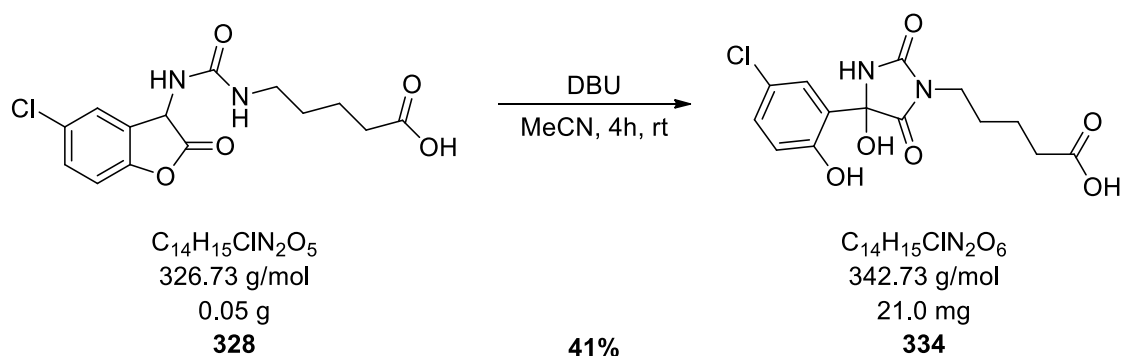


Table 96: 1D and 2D-NMR data of (S)-4-chloro-2-(2-(1-(1-methoxy-4-(methylthio)-1-oxobutan-2-yl)ureido)-2-oxoacetyl)phenolate (333A) in DMSO-d₆, at 298 K and 499 MHz for ¹H and 126 MHz for ¹³C.

No.	δ_{H} [ppm], J in [Hz]	δ_{C} [ppm], mult.	HMBC ($^{\circ}J$)
1	2.01 (3H, s)	14.60, CH ₃	C1→H3(³ J)
2	2.20 (2H, m)	28.2, CH ₂	C2→H3(² J), H4(² J)
3	2.39 (2H, m)	29.9, CH ₂	C3→H1(³ J), H2(² J), H4(³ J)
4	4.66 (1H, t, $J = 7.4$ Hz)	50.01, CH	C4→H2(² J), H3(³ J)
5	3.61 (3H, s)	52.3, CH ₃	-
6	6.44 (1H, d, $J = 8.2$ Hz)	112.8, CH _{arom}	C6→H8(² J)
7	-	113.0, C _q	C7→H8(⁴ J)
8	6.20-6.22 (1H, m)	113.2, CH _{arom}	C8→H9(³ J)
9	6.36 (1H, d, $J = 2.5$ Hz)	113.7, CH _{arom}	C9→H8(³ J)
10	-	120.7, C _q	C10→H6(³ J), H8(² J), H9(² J)
11	-	148.2, C _q	C11→H6(² J), H8(³ J), H9(³ J)
12	-	153.5, C _q	C12→H6(⁴ J), H9(³ J)
13	-	163.7, C _q	C13→H4(³ J)
14	-	166.9, C _q	C14→H4(³ J)
15	-	170.2, C _q	C15→H2(³ J), H4(² J), H5(³ J)

Note: The ¹H- and ¹³C-NMR-spectra are from the small scale experiment and were not purified. Contamination by DBU and hydantoin **332A** can be seen. The carbon atoms 13 and 14 could not be distinguished and therefore could not be clearly assigned.

6.3.4.1.4 Decomposition of 328 with DBU



Prepared according to *GP-VII*. Small scale experiment: Urea-coumaranone **328** (0.02 g, 0.06 mmol, 1.0 eq.) and DBU (17.9 μ l, 0.12 mmol, 2.0 eq.) in 0.70 ml of DMSO- d_6 . Large scale experiment: Urea-coumaranone **328** (0.05 g, 0.15 mmol, 1.0 eq.) and DBU (0.05 ml, 0.31 mmol, 2.0 eq.) in 3.00 ml of MeCN. Before extraction, the aqueous phase was acidified with 0.08 ml of a 2 M HCl solution. **334** was obtained as a brownish solid in a yield of 40%.

Yield (Large scale): 21.0 mg (0.06 mmol, 41%).

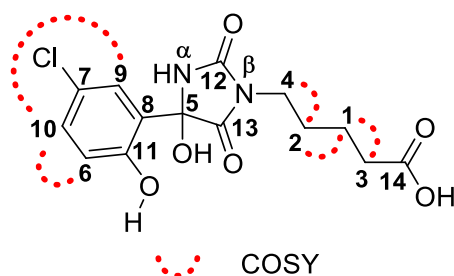


Table 97: 1D and 2D-NMR data of 5-(4-(5-chloro-2-hydroxyphenyl)-4-hydroxy-2,5-dioxoimidazolidin-1-yl)pentanoic acid (334) in DMSO- d_6 , at 298 K and 499 MHz for ^1H and 126 MHz for ^{13}C .

No.	δ_{H} [ppm], J in [Hz]	δ_{C} [ppm], mult.	HMBC ($^{\circ}\text{J}$)
1	1.55+1.49 (2H, m)	21.6+21.7, CH_2	$\text{C1} \rightarrow \text{H2} (^2\text{J}), \text{H3} (^2\text{J}), \text{H4} (^3\text{J})$
2	1.55 (2H, m)	27.1+27.0, CH_2	$\text{C2} \rightarrow \text{H1} (^2\text{J}), \text{H3} (^3\text{J}), \text{H4} (^2\text{J})$
3	2.22+2.26 (2H, t, $J = 6.6$ Hz)	33.1+33.2, CH_2	$\text{C3} \rightarrow \text{H2} (^3\text{J})$
4	3.36 (1H, m) + 3.43 (1H, t, $J = 6.6$ Hz)	37.3+37.8, CH_2	$\text{C4} \rightarrow \text{H1} (^3\text{J}), \text{H2} (^2\text{J})$
5	-	81.5, C_q	$\text{C5} \rightarrow \text{H6} (^4\text{J}), \text{H9} (^3\text{J}), \text{NH}_\alpha (^2\text{J})$
6	6.76 (1H, d, $J = 8.7$ Hz)	117.0, CH_{arom}	$\text{C6} \rightarrow \text{Ph-OH} (^3\text{J})$
7	-	122.0, C_q	$\text{C7} \rightarrow \text{H6} (^3\text{J}), \text{H9} (^2\text{J}), \text{H10} (^2\text{J})$
8	-	126.7, C_q	$\text{C8} \rightarrow \text{H6} (^3\text{J}), \text{Ph-OH} (^3\text{J})$
9	7.55 (1H, d, $J = 2.7$ Hz)	127.4, CH_{arom}	$\text{C9} \rightarrow \text{H10} (^3\text{J})$
10	7.22 (1H, dd, $J = 8.6, 2.7$ Hz)	129.2, CH_{arom}	$\text{C10} \rightarrow \text{H9} (^3\text{J})$
11	-	153.4, C_q	$\text{C11} \rightarrow \text{H6} (^2\text{J}), \text{H9} (^3\text{J}), \text{H10} (^3\text{J}),$ $\text{Ph-OH} (^2\text{J})$
12	-	156.2, C_q	$\text{C12} \rightarrow \text{H4} (^3\text{J}), \text{NH}_\alpha (^2\text{J})$
13	-	173.4, C_q	$\text{C13} \rightarrow \text{H4} (^3\text{J}), \text{NH}_\alpha (^3\text{J})$
14	-	174.26+174.34, C_q	$\text{C14} \rightarrow \text{H1} (^3\text{J}), \text{H3} (^2\text{J})$
NH_α	8.63 (1H, s)	-	-
Ph-OH	10.12 (1H, s)	-	-
COOH	11.97 (1H, s)	-	-

Note: The ^1H - and ^{13}C -NMR-spectra show a mixture of rotamers and are contaminated by DBU.

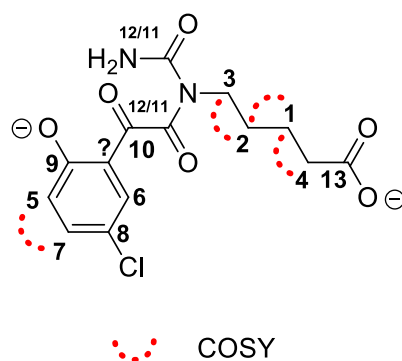
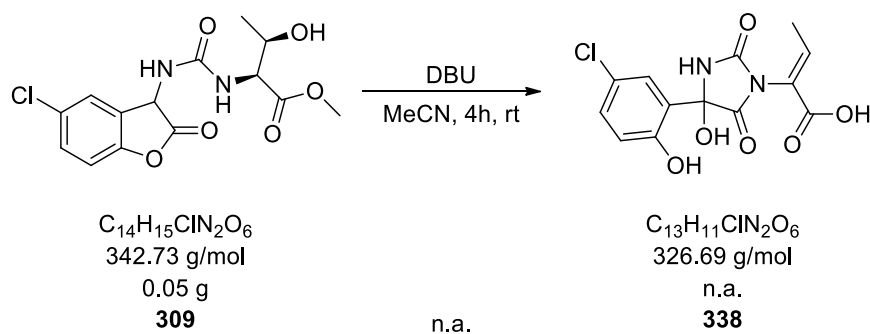


Table 98: 1D and 2D-NMR data of (S)-4-chloro-2-(2-(1-(1-methoxy-4-(methylthio)-1-oxobutan-2-yl)ureido)-2-oxoacetyl)phenolate (335A) in DMSO-d₆, at 298 K and 499 MHz for ¹H and 126 MHz for ¹³C.

No.	δ_{H} [ppm], J in [Hz]	δ_{C} [ppm], mult.	HMBC ($^{\circ}J$)
1	1.30-1.36 (2H, m)	23.7, CH ₂	C1→H2(² J), H3(³ J), H4(² J)
2	1.38-1.44 (2H, m)	28.6, CH ₂	C2→H1(² J), H4(³ J)
3	3.25 (2H, t, $J = 6.9$ Hz)	37.3, CH ₂	C3→H1(³ J)
4	1.89 (2H, m)	37.7, CH ₂	C4→H1(² J)
5	6.54 (1H, m)	115.1, CH _{arom}	C5→H7(² J)
6	6.55 (1H, m)	115.3, CH _{arom}	-
7	6.38 (1H, dd, $J = 8.2, 2.6$ Hz)	115.7, CH _{arom}	C7→H6(³ J)
8	-	121.1, C _q	C8→H5(³ J), H6(² J), H7(² J)
9	-	147.0, C _q	C9→H6(³ J), H7(³ J)
10	-	150.6, C _q	C10→H5(⁴ J), H6(³ J)
11	-	164.0, C _q	C11→H3(³ J)
12	-	168.0, C _q	C12→H3(³ J)
13	-	176.7, C _q	C13→H1(³ J), H4(² J)

Note: The ¹H- and ¹³C-NMR-spectra are from the small scale experiment and were not purified. Contamination by DBU and hydantoin **334A** can be seen. Out of 14 carbon atoms only 13 could be found. The carbon atoms 11 and 12 could not be distinguished and therefore could not be clearly assigned.

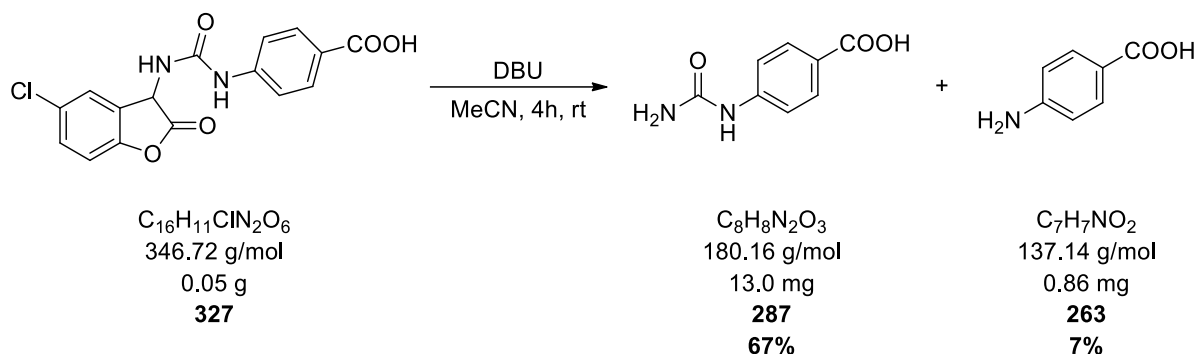
6.3.4.1.5 Decomposition of **309** with DBU

Prepared according to *GP-VII*. Small scale experiment: Urea-coumaranone **309** (0.02 g, 0.06 mmol, 1.0 eq.) and DBU (18.0 μl , 0.12 mmol, 2.0 eq.) in 0.70 ml of DMSO- d_6 . Large scale experiment: Urea-coumaranone **309** (0.05 g, 0.15 mmol, 1.0 eq.) and DBU (0.05 ml, 0.30 mmol, 2.0 eq.) in 3.00 ml of MeCN. Compound **338** is assumed to be the main product after the aqueous work-up.

Yield (Large scale): n.a. due to various impurities.

Note: Product **338** could not be completely elucidated.

6.3.4.1.6 Decomposition of 327 with DBU



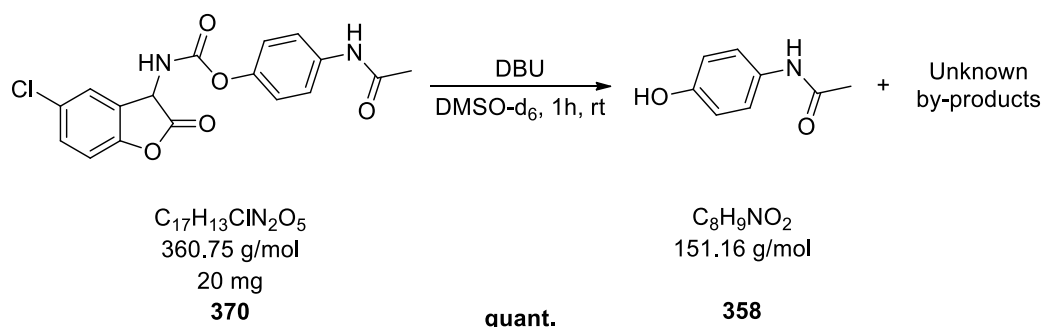
Prepared according to *GP-VII*. Small scale experiment: Urea-coumaranone **327** (0.02 g, 0.06 mmol, 1.0 eq.) and DBU (18.0 μ l, 0.12 mmol, 2.0 eq.) in 0.70 ml of DMSO- d_6 . Large scale experiment: Urea-coumaranone **327** (0.05 g, 0.15 mmol, 1.0 eq.) and DBU (0.05 ml, 0.30 mmol, 2.0 eq.) in 3.00 ml of MeCN. Before extraction, the aqueous phase was acidified with 0.07 ml of a 2 M HCl solution. Both **287** and **263** were obtained as a grey solid in a yield of 67% and 7% respectively.

Yield of 287 (Large scale): 17.0 mg (0.09 mmol, 67%); major product.

Yield of 263 (Large scale): 0.86 mg (6.30 μ mol, 7%), minor product.

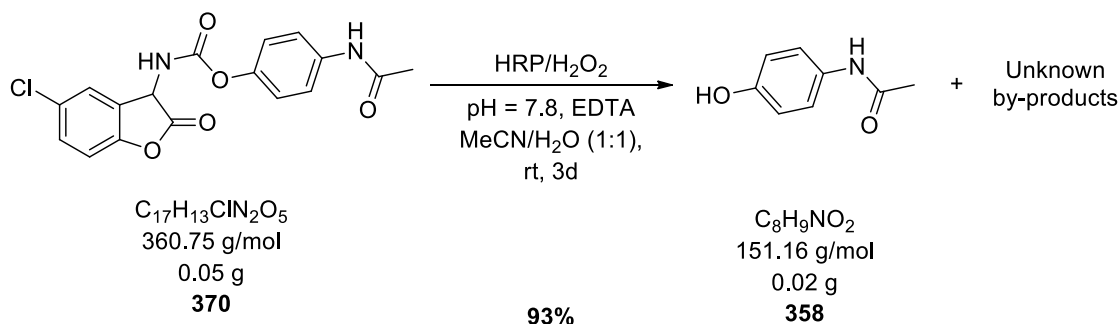
Note: Yields were calculated according to the 1H -NMR after the aqueous workup.

6.3.4.2 Decomposition of carbamate-coumaranones

6.3.4.2.1A Decomposition of **370** with DBU

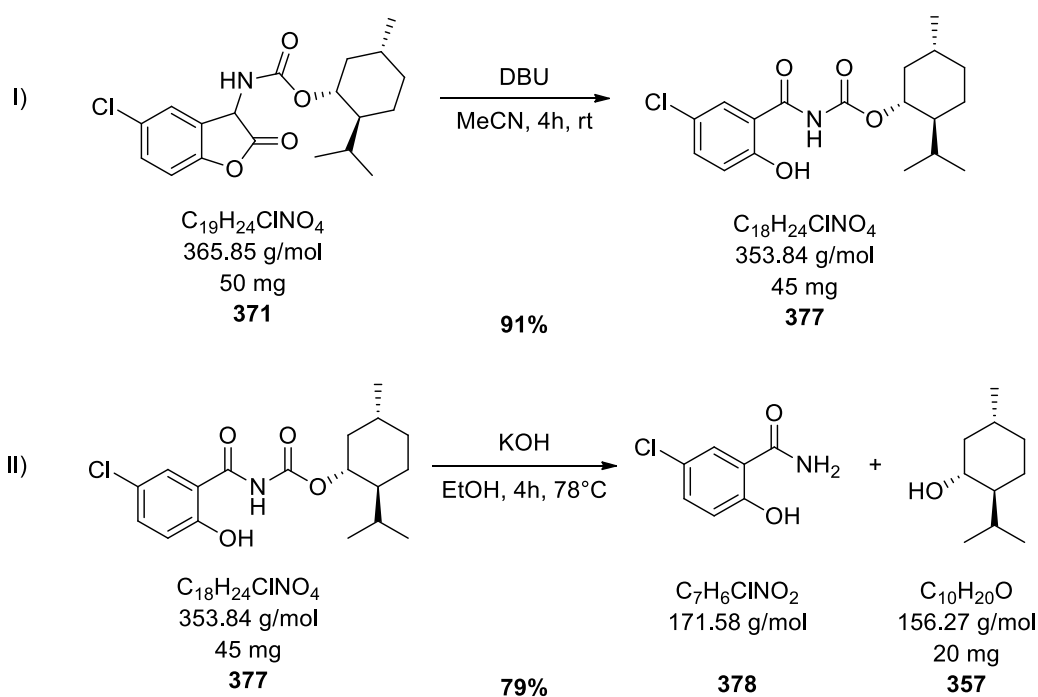
Prepared according to *GP-VII*. Only a small scale experiment was done using carbamate-coumaranone **370** (20 mg, 0.06 mmol, 1.0 eq.) and DBU (17.9 μ l, 0.12 mmol, 2.0 eq.) in 0.70 ml of DMSO- d_6 . During the experiment a short but strong emission of blue light could be seen over a time period of one minute. **358** was deprotected in a quantitative yield.

Yield (Small scale): Quantitative.

6.3.4.2.1B Decomposition of **370** with HRP

Prepared according to *GP-VIII* using carbamate-coumaranone **370** (0.05 g, 0.14 mmol, 1.0 eq.), phosphate buffer solution I (1.4 ml, 1.40 mmol, 10 eq), EDTA solution (1.4 ml, 0.14 mmol, 1.0 eq.), H_2O_2 (14 μ l, 0.14 mmol, 1.0 eq.) and HRP solution (2.0 ml, 100 units) in 12.5 ml of MeCN/ H_2O (1:1). **358** was obtained as a colourless solid in a yield of 95%. The results of the NMR-spectra are in agreement with those of decomposition experiment **6.3.4.2.1A**.

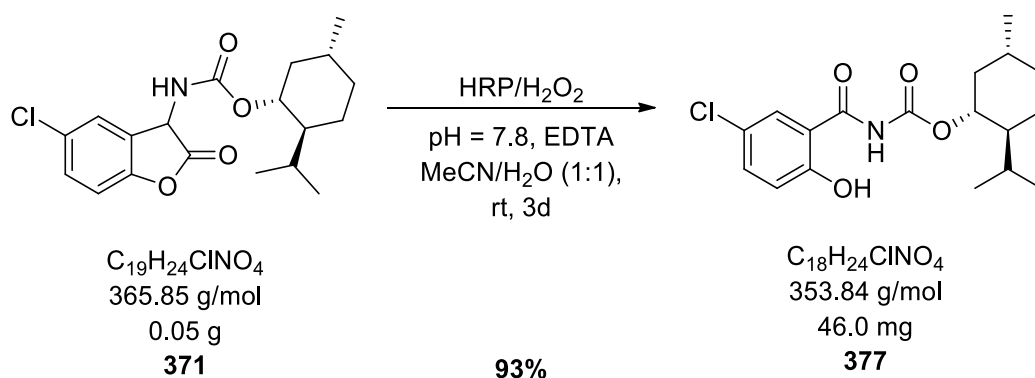
Yield: 0.02 g (0.13 mmol, 93%).

6.3.4.2.2A Decomposition of **371** with DBU

Step I) was done according to **GP-VII**. Small scale experiment: Carbamate-coumaranone **371** (0.02 g, 0.06 mmol, 1.0 eq.) and DBU (18.0 μ l, 0.12 mmol, 2.0 eq.) in 0.70 ml of DMSO- d_6 . Large scale experiment: Carbamate-coumaranone **371** (0.05 g, 0.14 mmol, 1.0 eq.) and DBU (0.05 ml, 0.31 mmol, 2.0 eq.) in 2.40 ml of MeCN. During both experiments a strong emission of blue light could be seen over a time period of 20 minutes. **377** was obtained as a green solid in a yield of 91%.

Step II) was done by dissolving compound **377** in 5 ml EtOH. KOH (24.0 mg, 0.42 mmol, 3.0 eq.) was added and the solution was refluxed for 4 hours. After that the solvent was removed under reduced pressure and 10 ml of water were added to the crude product. The aqueous phase was extracted three times with ethylacetate (15 ml per extraction) and the combined organic layers were washed with brine and subsequently dried over sodium sulfate. Finally, the solvent was removed under reduced pressure to give 0.02 g (0.11 mmol, 79%) of L-menthol **357** with minor impurities of **378**.

Yield (After step II): 0.02 g (0.11 mmol, 79%).

6.3.4.2B Decomposition of **371** with HRP

Prepared according to *GP-VIII* using carbamate-coumaranone **371** (0.05 g, 0.14 mmol, 1.0 eq.), phosphate buffer solution I (1.4 ml, 1.40 mmol, 10 eq), EDTA solution (1.4 ml, 0.14 mmol, 1.0 eq.), H₂O₂ (14 μ l, 0.14 mmol, 1.0 eq.) and HRP solution (2.0 ml, 100 units) in 12.5 ml of MeCN/H₂O (1:1). **377** was obtained as a slightly green solid in a yield of 93%. The results of the NMR-spectra are in agreement with those of decomposition experiment **6.3.4.2.A**.

Yield: 46.0 mg (0.13 mmol, 93%).

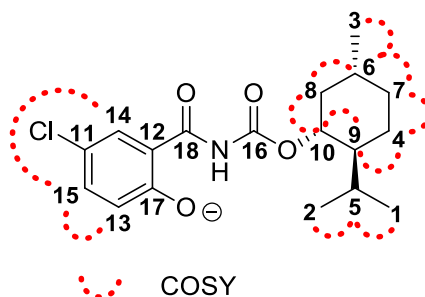


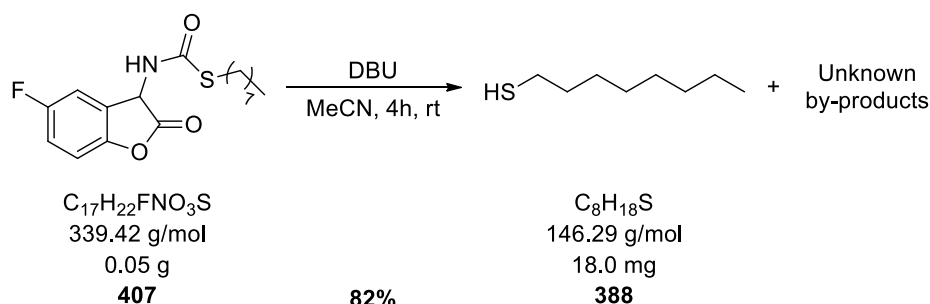
Table 99: 1D and 2D-NMR data of 4-chloro-2-((((1R,2S,5R)-2-isopropyl-5-methylcyclohexyl)oxy)carbonyl)carbamoylphenolate (377A) in DMSO-d₆, at 298 K and 500 MHz for ¹H and 125 MHz for ¹³C.

No.	δ_{H} [ppm], J in [Hz]	δ_{C} , δ_{N} [ppm], mult.	HMBC ($^{\circ}\text{J}$)
1	0.75 (3H, d, $J = 7.0$ Hz)	16.3, CH ₃	C1→H2(³ J), H5(² J)
2	0.87 (3H, m)	20.5, CH ₃	C2→H1(³ J), H5(² J)
3	0.89 (3H, m)	22.0, CH ₃	C3→H8(³ J)
4	1.04 (1H, m); 1.62 (1H, m)	23.1, CH ₂	C4→H9(² J)
5	1.90 (1H, m)	25.8, CH	C5→H1(² J), H2(² J), H10(³ J)
6	1.45 (1H, m)	30.9, CH	C6→H3(² J), H8(² J)
7	0.84 (1H, m); 1.65 (1H, m)	33.8, CH ₂	C7→H3(³ J), H8(³ J)
8	0.98 (1H, m); 1.92 (1H, m)	40.9, CH ₂	C8→H3(³ J), H10(² J)
9	1.34 (1H, m)	46.6, CH	C9→H1(³ J), H2(³ J), H4(² J), H5(² J), H7(³ J), H8(³ J), H10(² J)
10	4.50 (1H, td, $J = 10.9, 4.3$ Hz)	72.9, CH	C10→H4(³ J), H8(² J), H9(² J)
11	-	112.5, C _q	C11→H13(³ J), H14(² J), H15(² J)
12	-	117.6, C _q	C12→H13(³ J)
13	6.34 (1H, d, $J = 8.9$ Hz)	124.0, CH _{arom}	-
14	7.50 (1H, d, $J = 3.1$ Hz)	128.2, CH _{arom}	C14→H15(³ J)
15	6.92 (1H, dd, $J = 9.0, 3.1$ Hz)	132.5, CH _{arom}	C15→H14(³ J)
16	-	151.8, C _q	C16→H10(³ J)
17	-	165.9, C _q	C17→H13(² J), H14(³ J)
18	-	170.8, C _q	C18→H13(⁴ J), H14(³ J), H15(³ J)
NH	15.91 (1H, s)	139.9, NH	-

Note: The NMR-spectra are contaminated with DBU.

6.3.4.3 Decomposition of thiolcarbamate-coumaranones

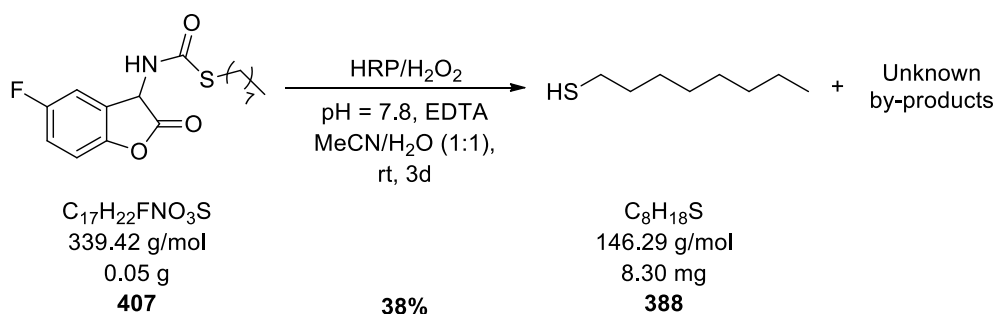
6.3.4.3.1A Decomposition of 407 with DBU



Prepared according to *GP-VII*. Small scale experiment: Thiolcarbamate-coumaranone **407** (0.02 g, 0.06 mmol, 1.0 eq.) and DBU (17.6 μ l, 0.12 mmol, 2.0 eq.) in 0.70 ml of DMSO- d_6 . Large scale experiment: Thiolcarbamate-coumaranone **407** (0.05 g, 0.15 mmol, 1.0 eq.) and DBU (0.04 ml, 0.29 mmol, 2.0 eq.) in 10.0 ml of MeCN. During both experiments a strong emission of light blue light could be seen over a time period of 20 minutes. **388** was deprotected in a yield of 82%.

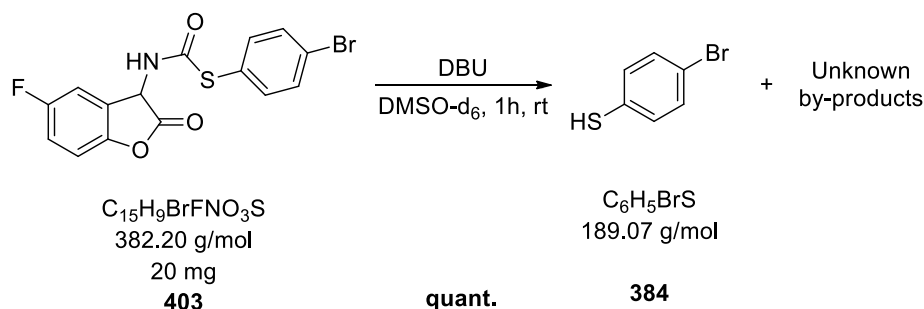
Yield (Large scale): 18.0 mg (0.12 mmol, 82%).

6.3.4.3.1B Decomposition of 407 with HRP



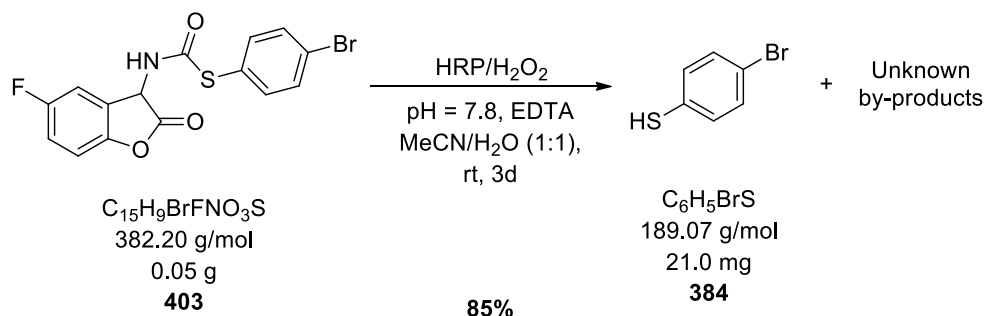
Prepared according to *GP-VIII* using thiolcarbamate-coumaranone **407** (0.05 g, 0.15 mmol, 1.0 eq.), phosphate buffer solution I (2.0 ml, 2.00 mmol, 10 eq), EDTA solution (2.0 ml, 0.20 mmol, 1.0 eq.), H_2O_2 (20 μ l, 0.20 mmol, 1.0 eq.) and HRP solution (2.0 ml, 100 units) in 12.5 ml of MeCN/ H_2O (1:1). **388** was obtained as a grey-white oil, in a yield of 38%. The results of the NMR-spectra are in agreement with those of decomposition experiment

Yield: 25.0 mg (0.06 mmol, 38%).

6.3.4.3.2A Decomposition of **403** with DBU

Prepared according to *GP-VII*. Only a small scale experiment was done using thiolcarbamate-coumaranone **403** (0.02 g, 0.05 mmol, 1.0 eq.) and DBU (14.9 μl , 0.10 mmol, 2.0 eq.) in 0.70 ml of DMSO- d_6 . During the experiment a strong emission of mint green light could be seen over a time period of 10 minutes. **384** was deprotected in a quantitative yield.

Yield (Small scale): Quantitative.

6.3.4.3.2B Decomposition of **403** with HRP

Prepared according to *GP-VIII* using thiolcarbamate -coumaranone **403** (0.05 g, 0.13 mmol, 1.0 eq.), phosphate buffer solution I (1.3 ml, 1.30 mmol, 10 eq), EDTA solution (1.3 ml, 0.13 mmol, 1.0 eq.), H_2O_2 (28 μl , 0.27 mmol, 1.0 eq.) and HRP solution (2.0 ml, 100 units) in 12.5 ml of MeCN/ H_2O (1:1). **384** was obtained as a colourless solid in a yield of 38%. The results of the NMR-spectra are in agreement with those of decomposition experiment **6.3.4.3.2A**.

Yield: 21.0 g (0.11 mmol, 85%).

7. Analytical data and spectra

7.1 NMR spectra of selected compounds

7.1.1 Urea, carbamate and thiol carbamate precursors

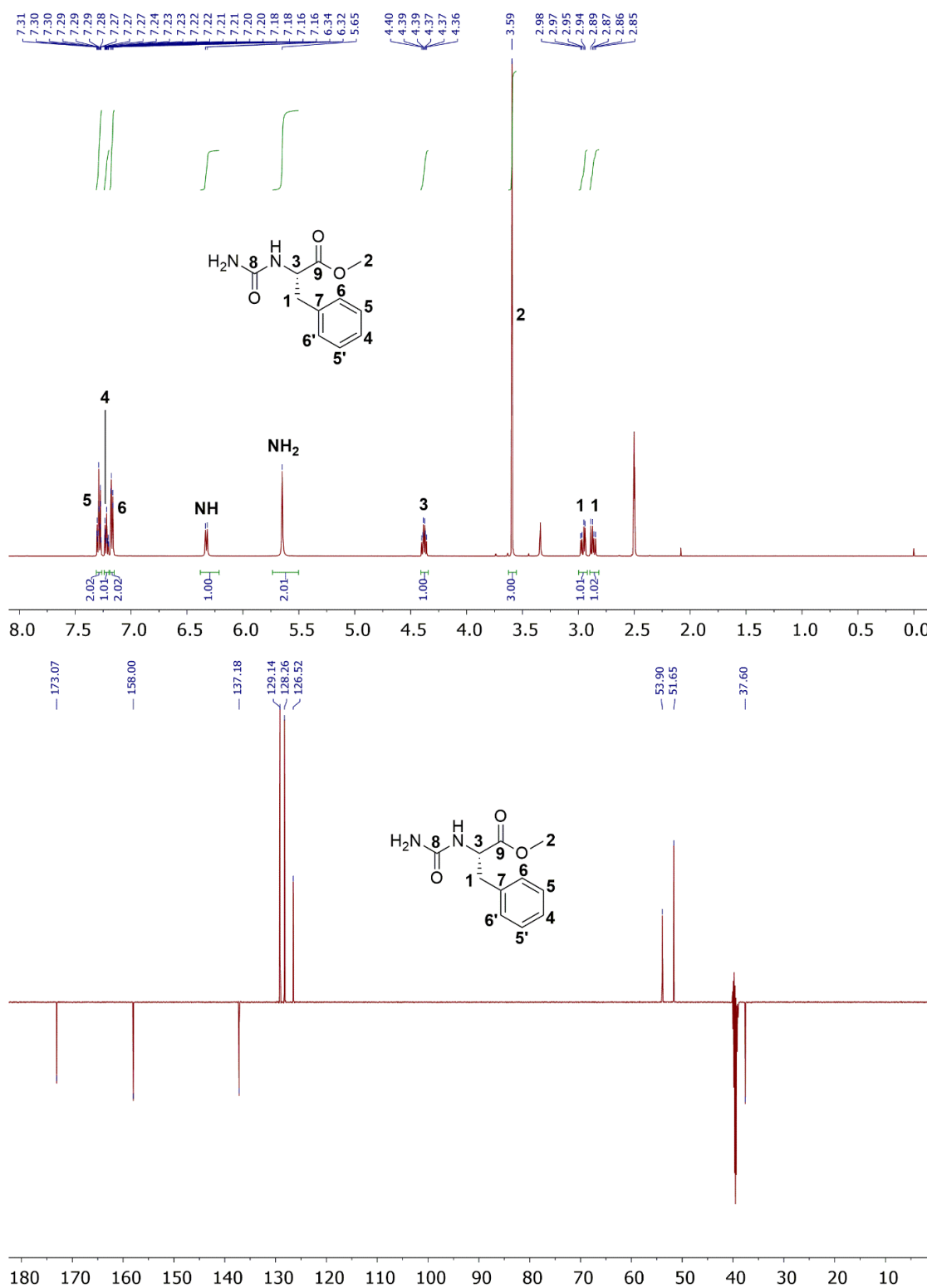


Figure 43: ^1H - and ^{13}C -NMR-spectrum of (S)-methyl 3-phenyl-2-ureidopropanoate (253) in DMSO- d_6 .

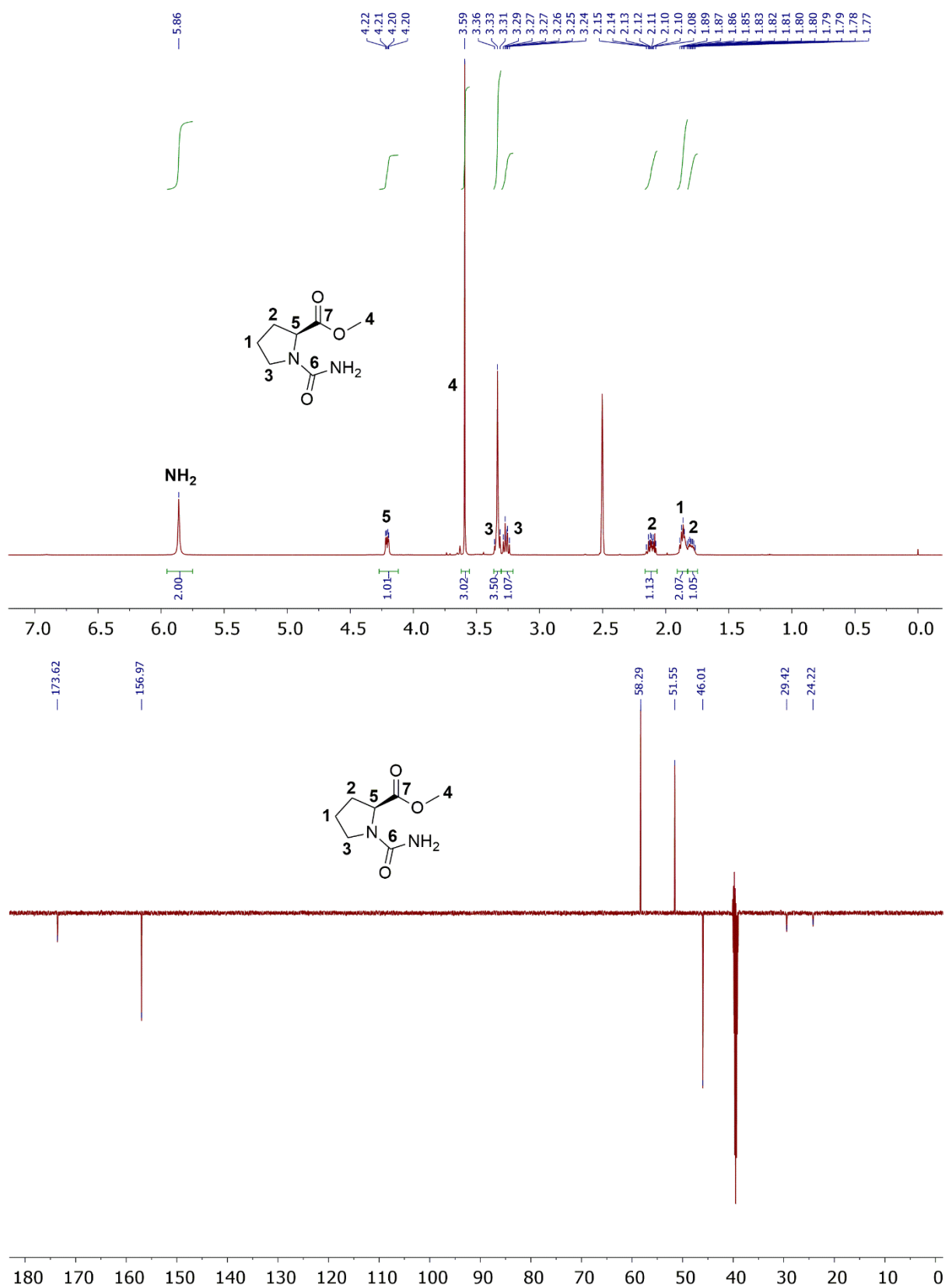


Figure 44: ¹H- and ¹³C-NMR-spectrum of (*S*)-methyl 1-carbamoylpyrrolidine-2-carboxylate (**254**) in DMSO-d₆.

7. Analytical data and spectra

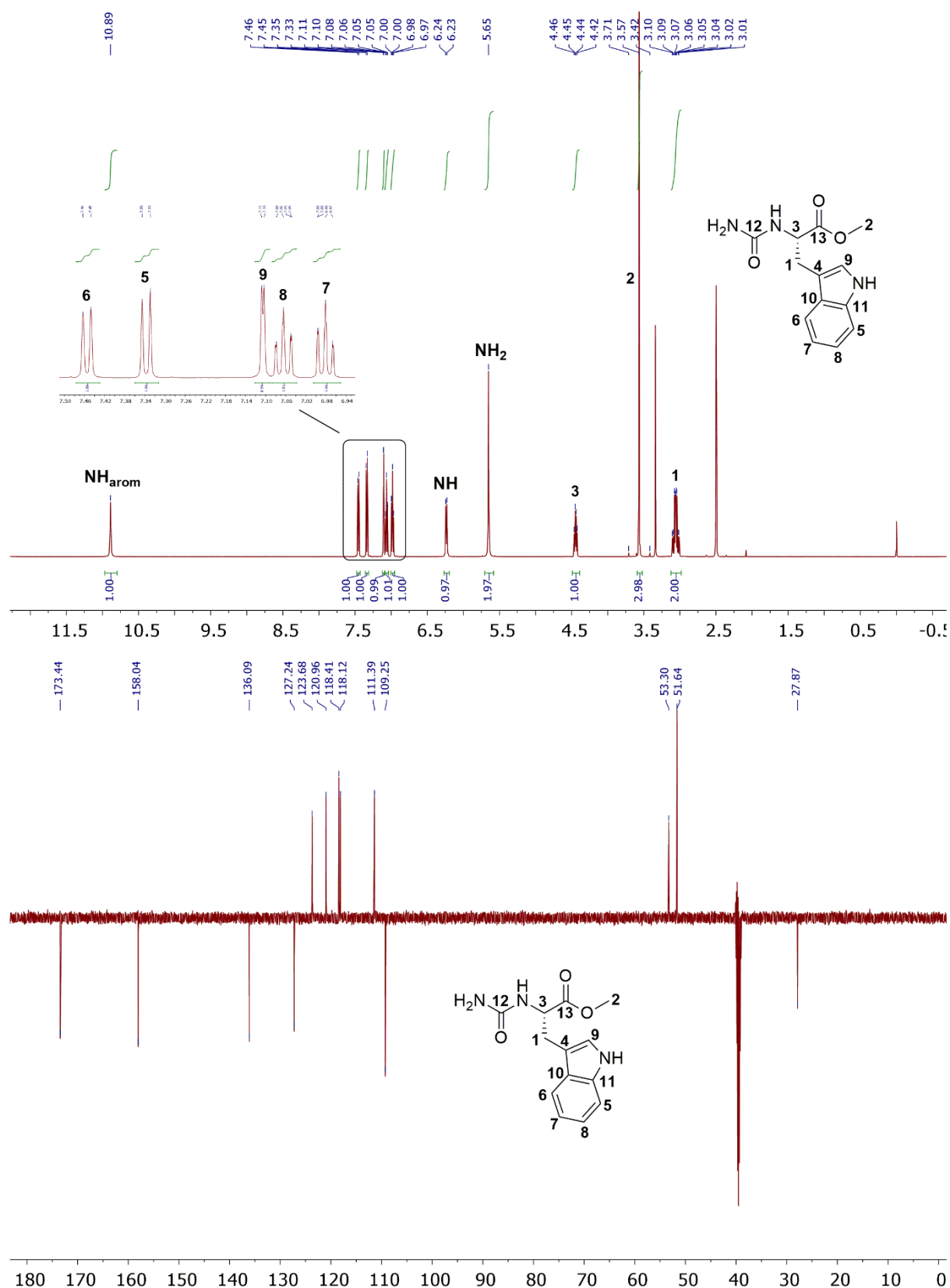


Figure 45: ¹H- and ¹³C-NMR-spectrum of (S)-methyl 3-(1H-indol-3-yl)-2-ureidopropanoate (255) in DMSO-d₆.

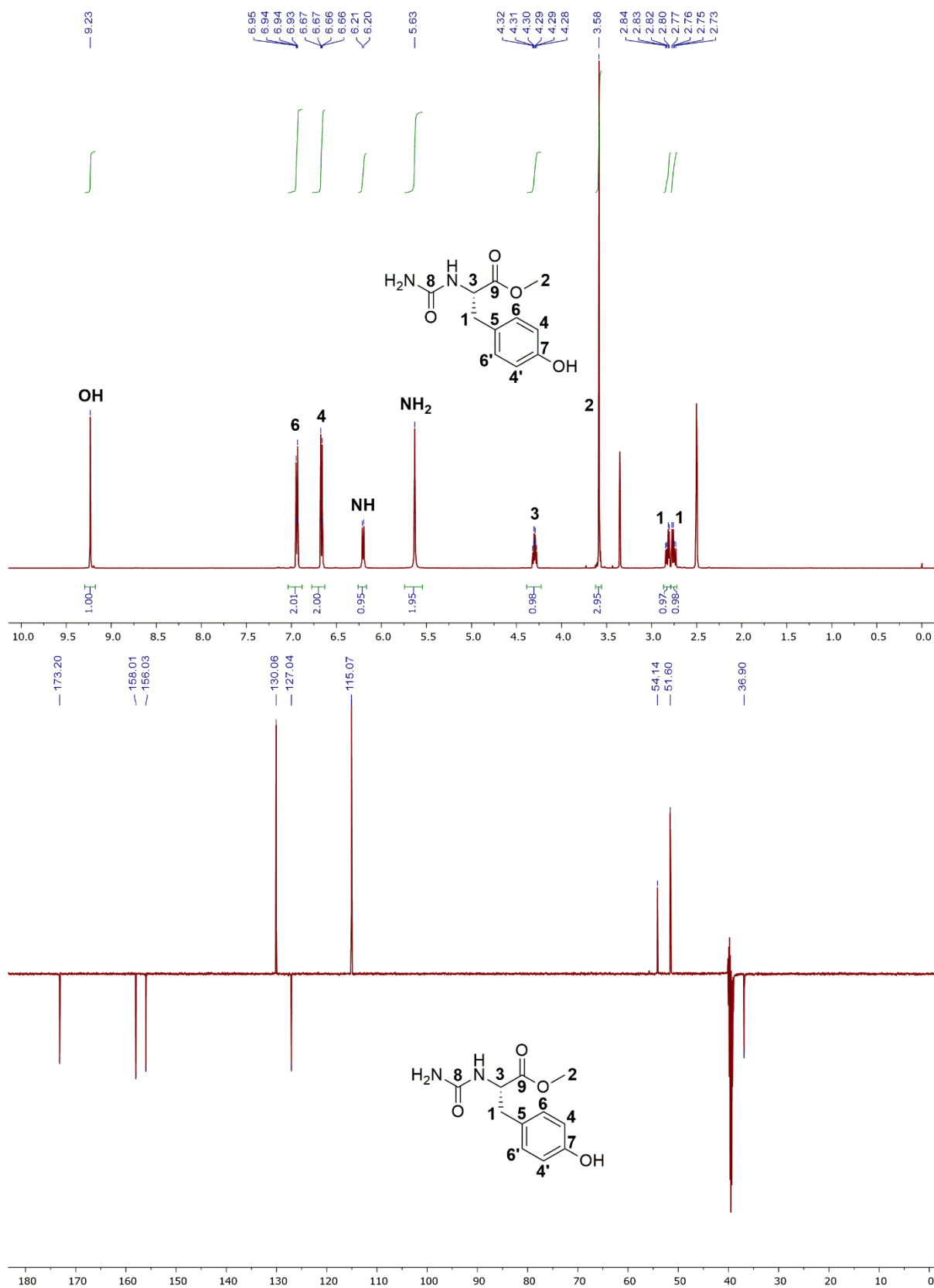


Figure 46: ^1H - and ^{13}C -NMR-spectrum of (S)-methyl 3-(4-hydroxyphenyl)-2-ureidopropanoate (256) in DMSO- d_6 .

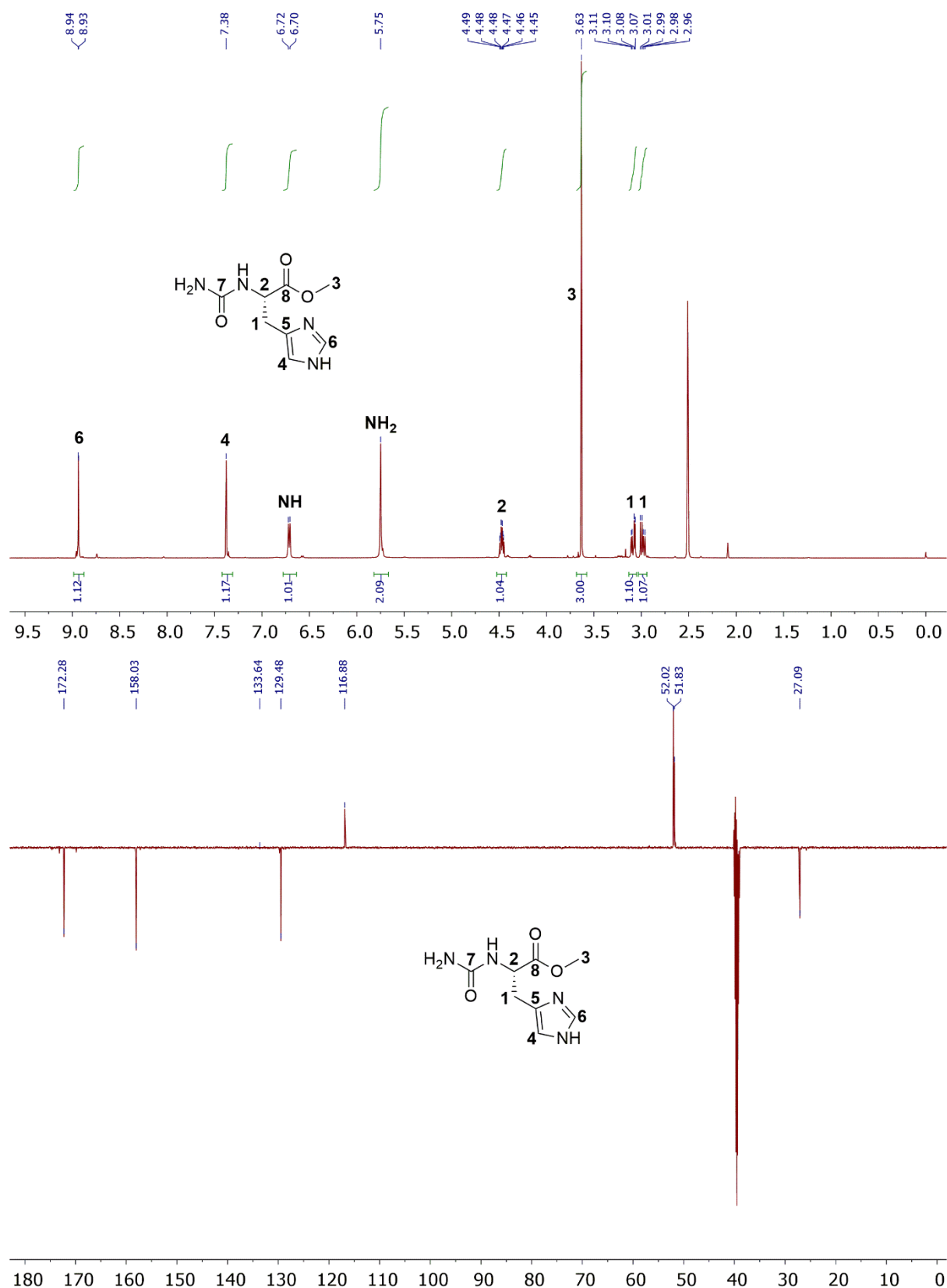


Figure 47: ^1H - and ^{13}C -NMR-spectrum of (S)-methyl 3-(1H-imidazol-4-yl)-2-ureidopropanoate (**252**) in DMSO-d_6 .

7. Analytical data and spectra

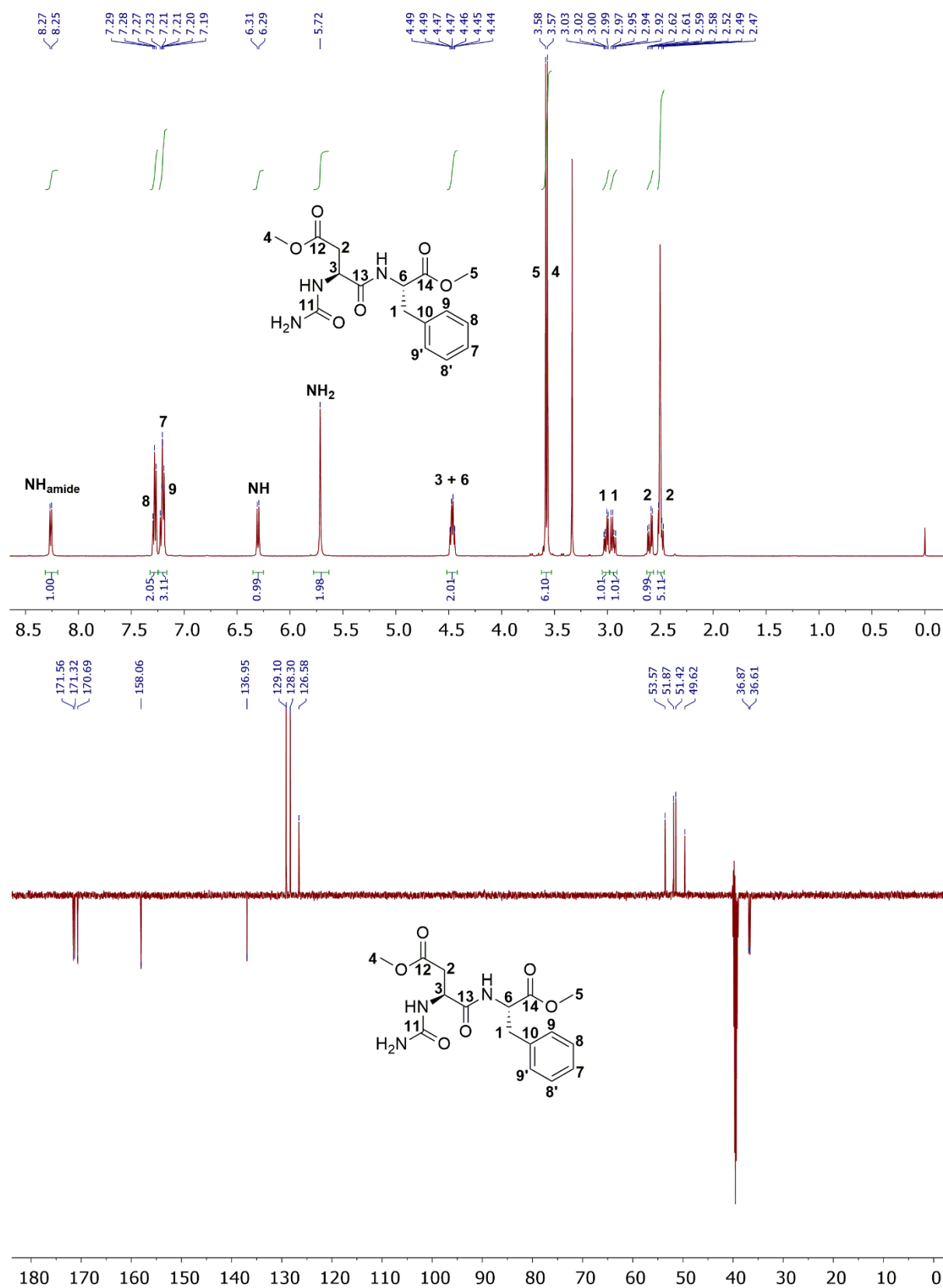


Figure 48: ^1H - and ^{13}C -NMR-spectrum of (S)-methyl 4-(((S)-1-methoxy-1-oxo-3-phenylpropan-2-yl)amino)-4-oxo-3-ureidobutanoate (**261**) in $\text{DMSO-}d_6$.

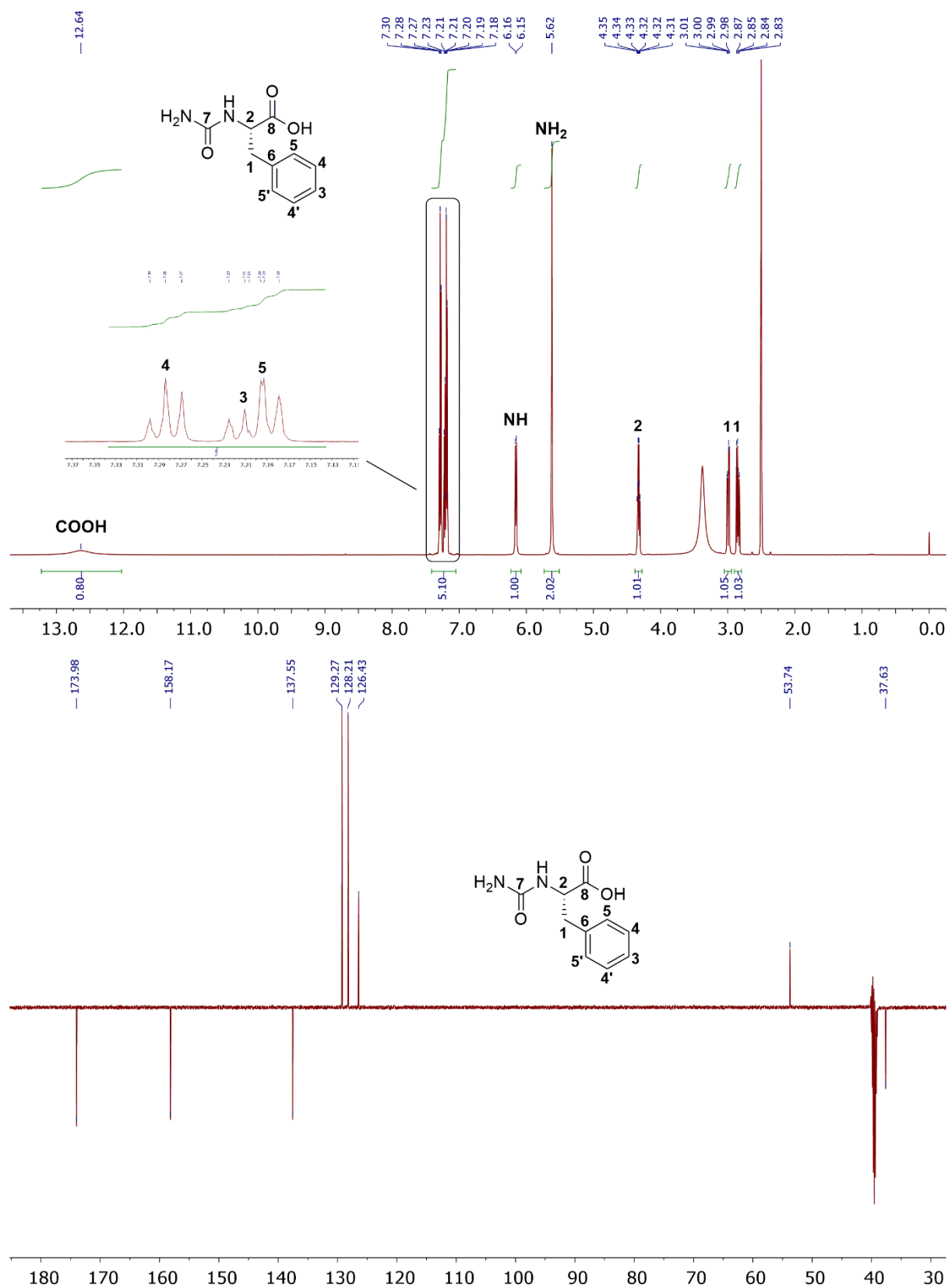


Figure 49: ^1H - and ^{13}C -NMR-spectrum of *(S)*-3-phenyl-2-ureidopropanoic acid (**276**) in DMSO-d_6 .

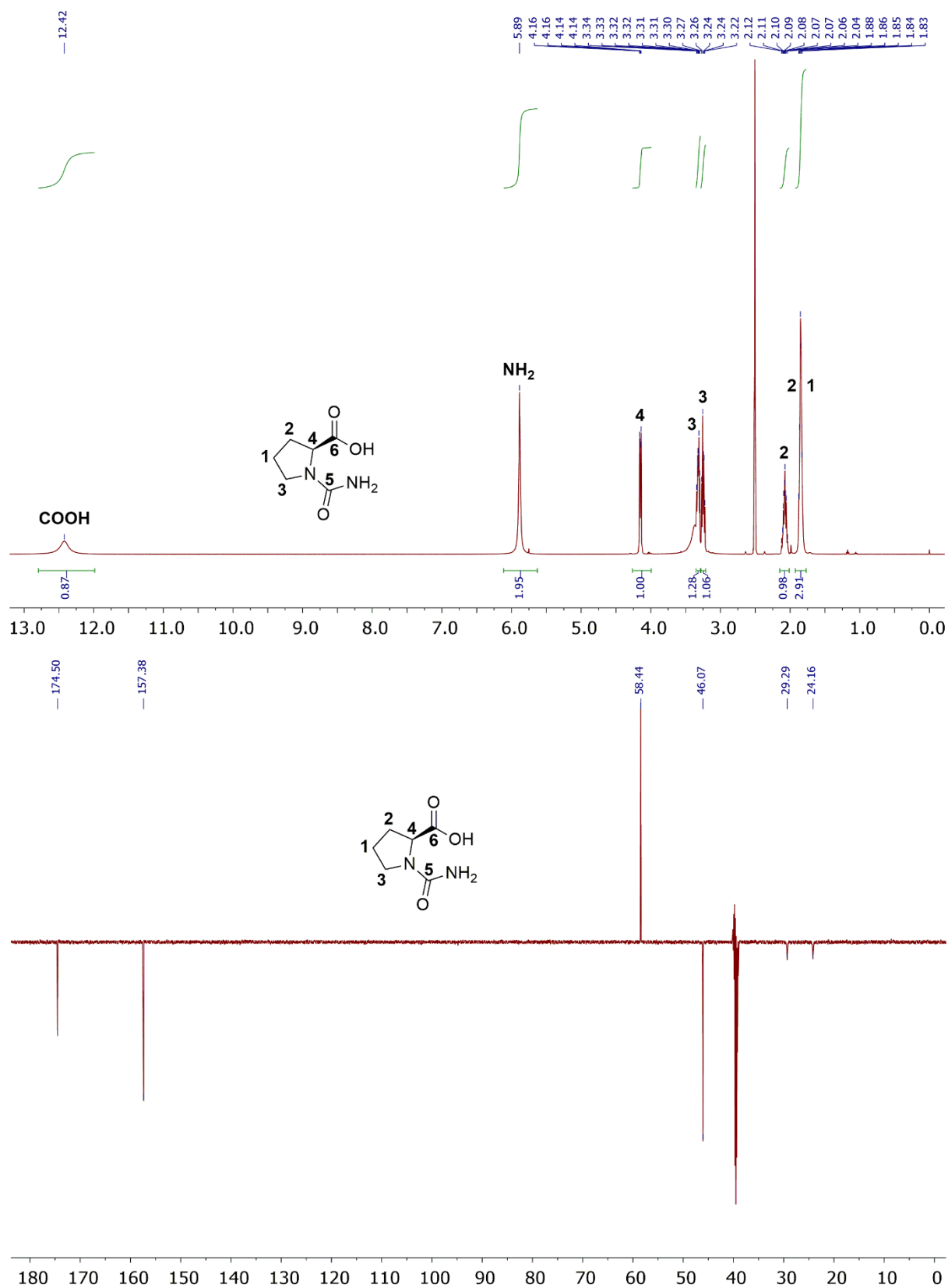


Figure 50: ^1H - and ^{13}C -NMR-spectrum of (S)-1-carbamoylpyrrolidine-2-carboxylic acid (277) in DMSO-d_6 .

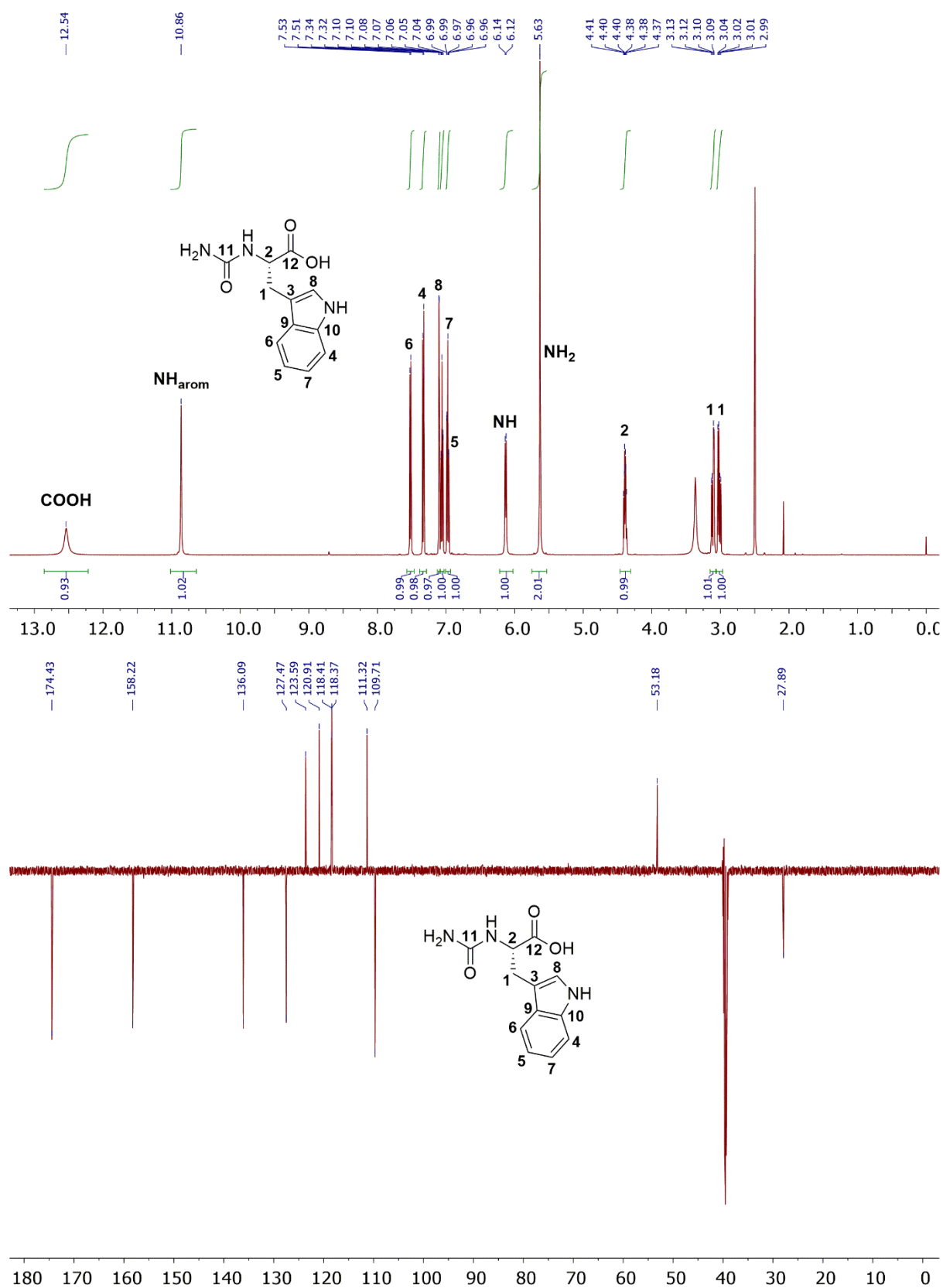


Figure 51: ¹H- and ¹³C-NMR-spectrum of (S)-3-(1H-indol-3-yl)-2-ureidopropanoic acid (**278**) in DMSO-d₆.

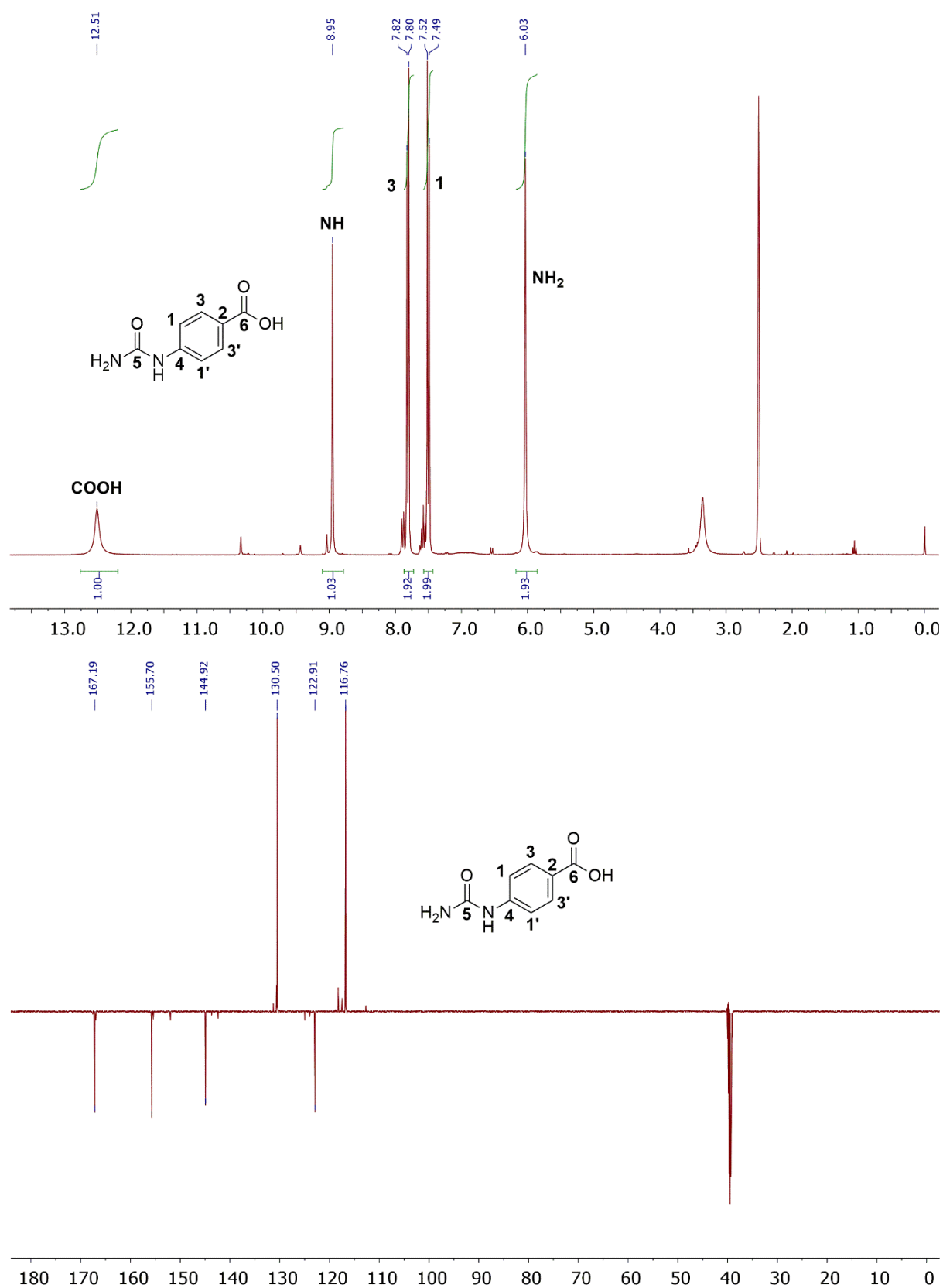


Figure 52: ^1H - and ^{13}C -NMR-spectrum of 4-ureidobenzoic acid (**287**) in DMSO-d_6 .

7. Analytical data and spectra

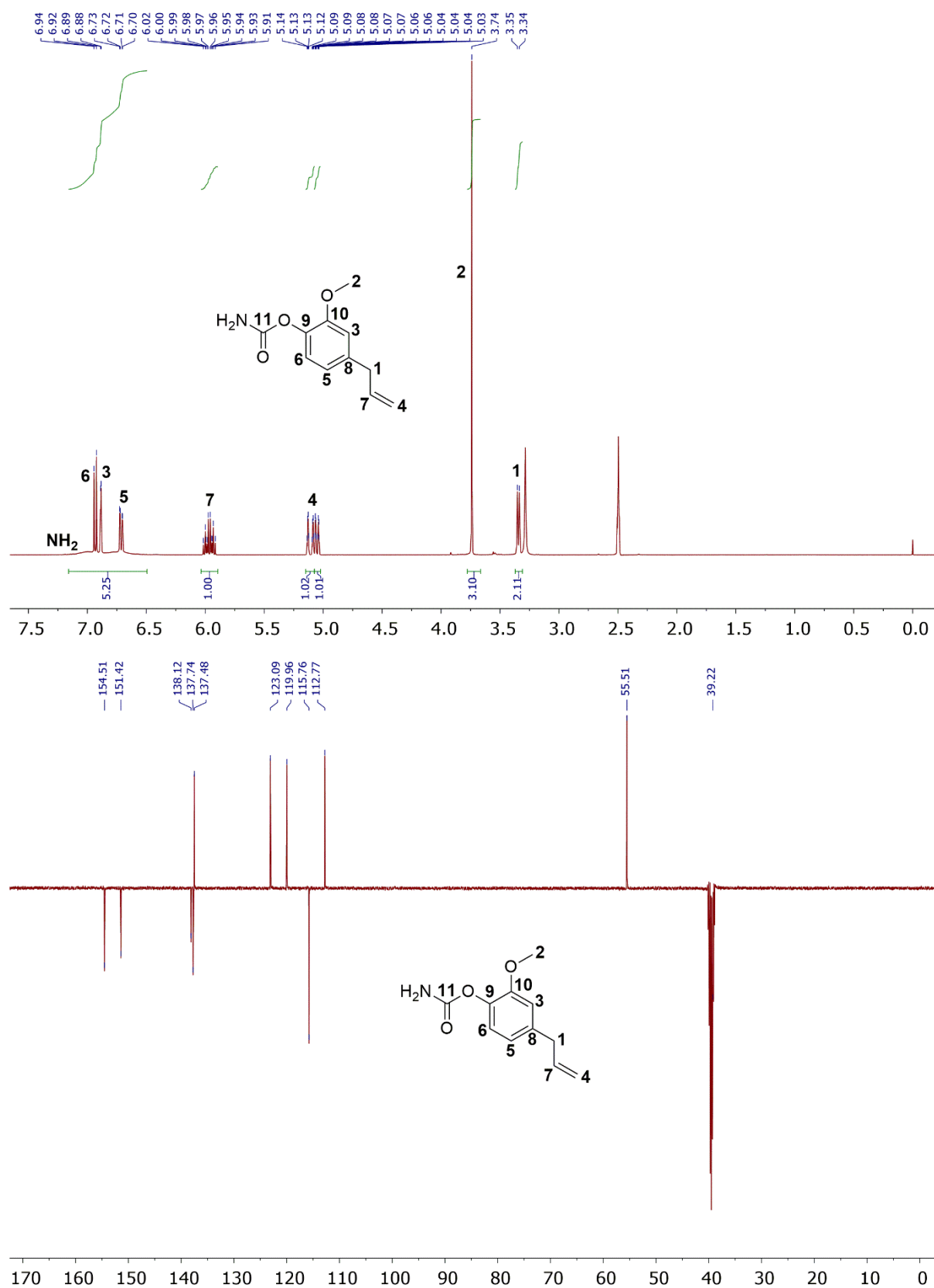


Figure 53: ^1H - and ^{13}C -NMR-spectrum of 4-allyl-2-methoxyphenyl carbamate (365) in DMSO-d_6 .

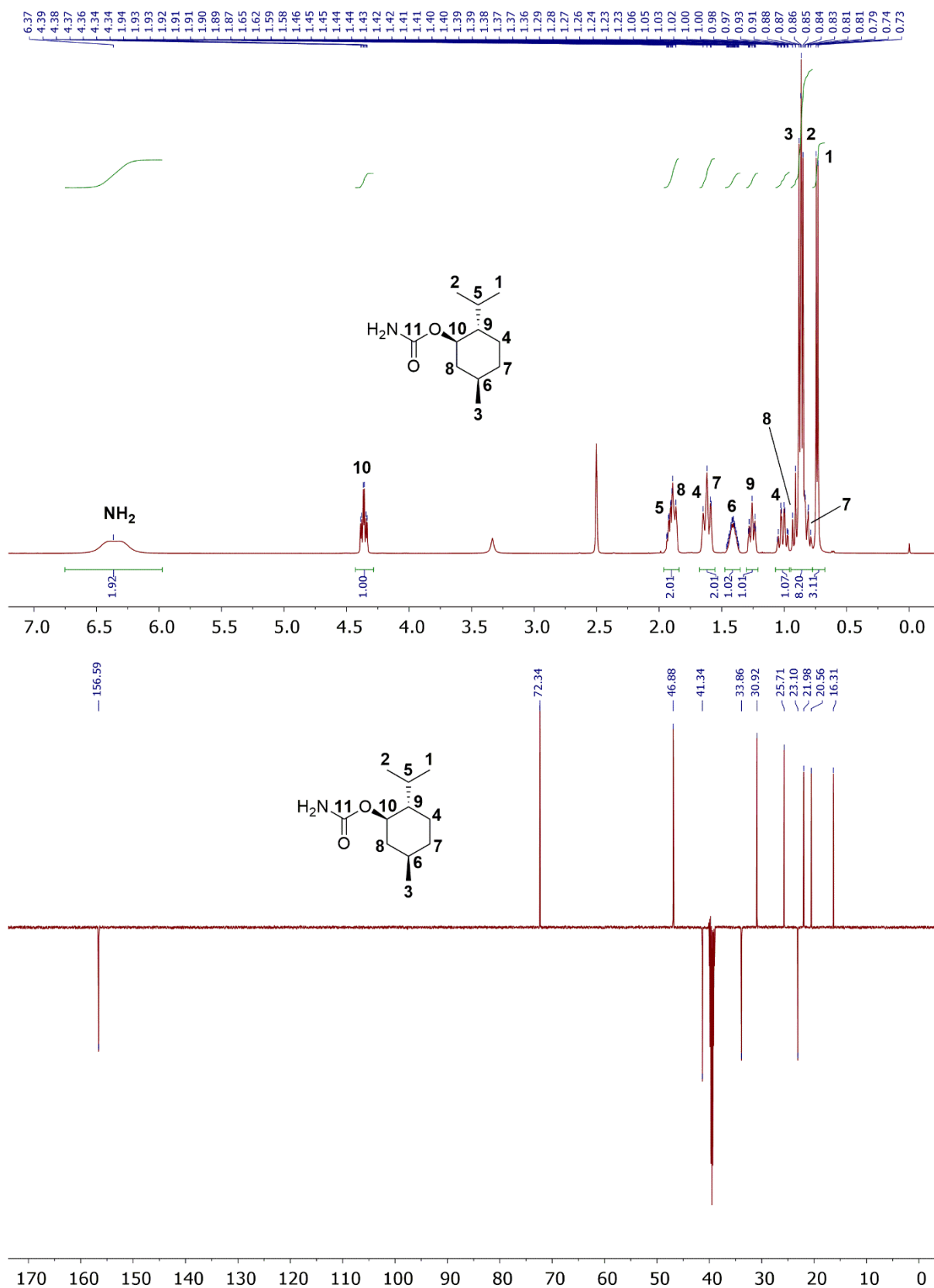


Figure S4: ¹H- and ¹³C-NMR-spectrum of (1*R*,2*S*,5*R*)-2-isopropyl-5-methylcyclohexyl carbamate (**367**) in DMSO-*d*₆.

7. Analytical data and spectra

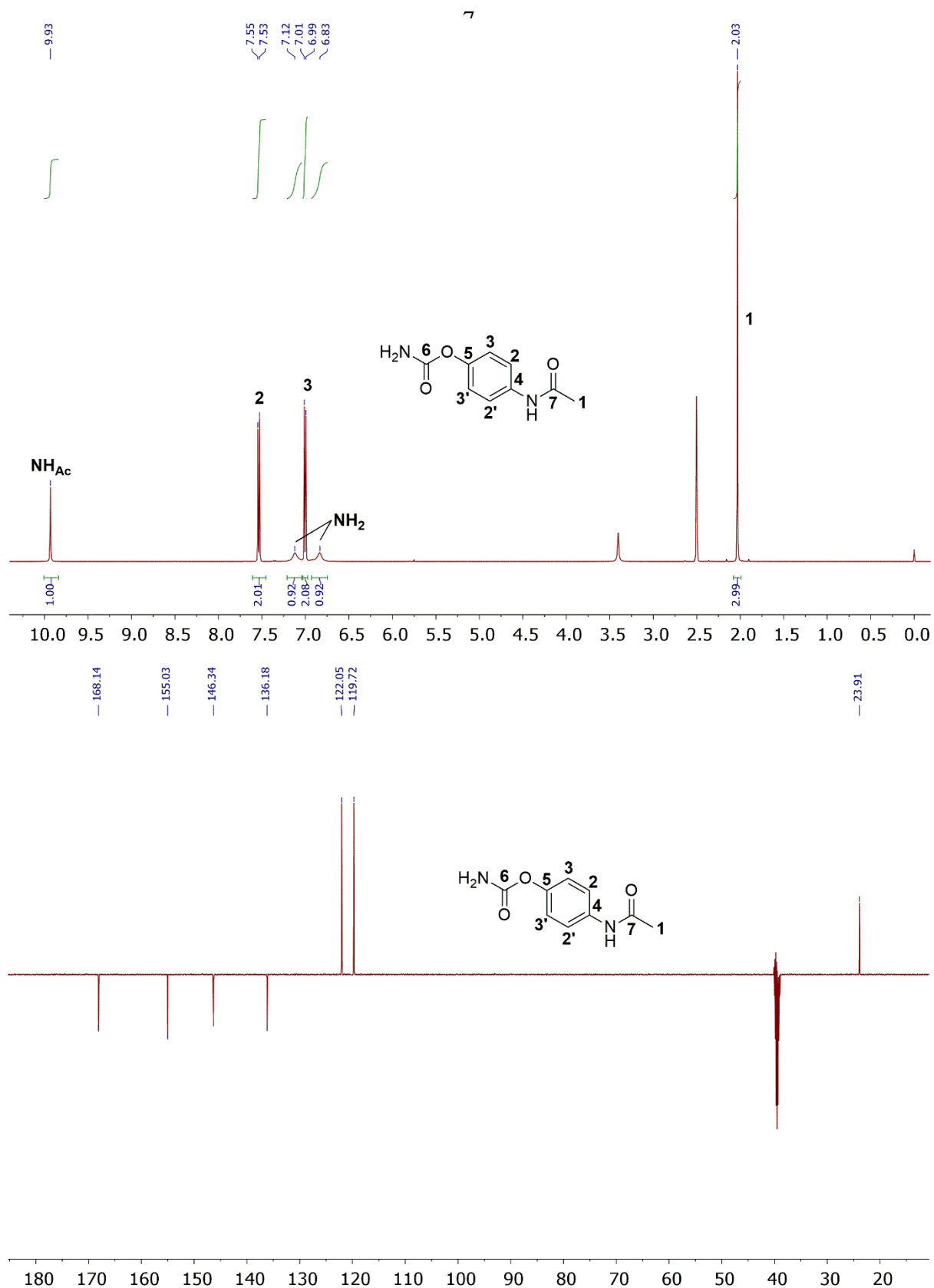


Figure 55: ¹H- and ¹³C-NMR-spectrum of 4-acetamidophenyl carbamate (**368**) in DMSO-d₆.

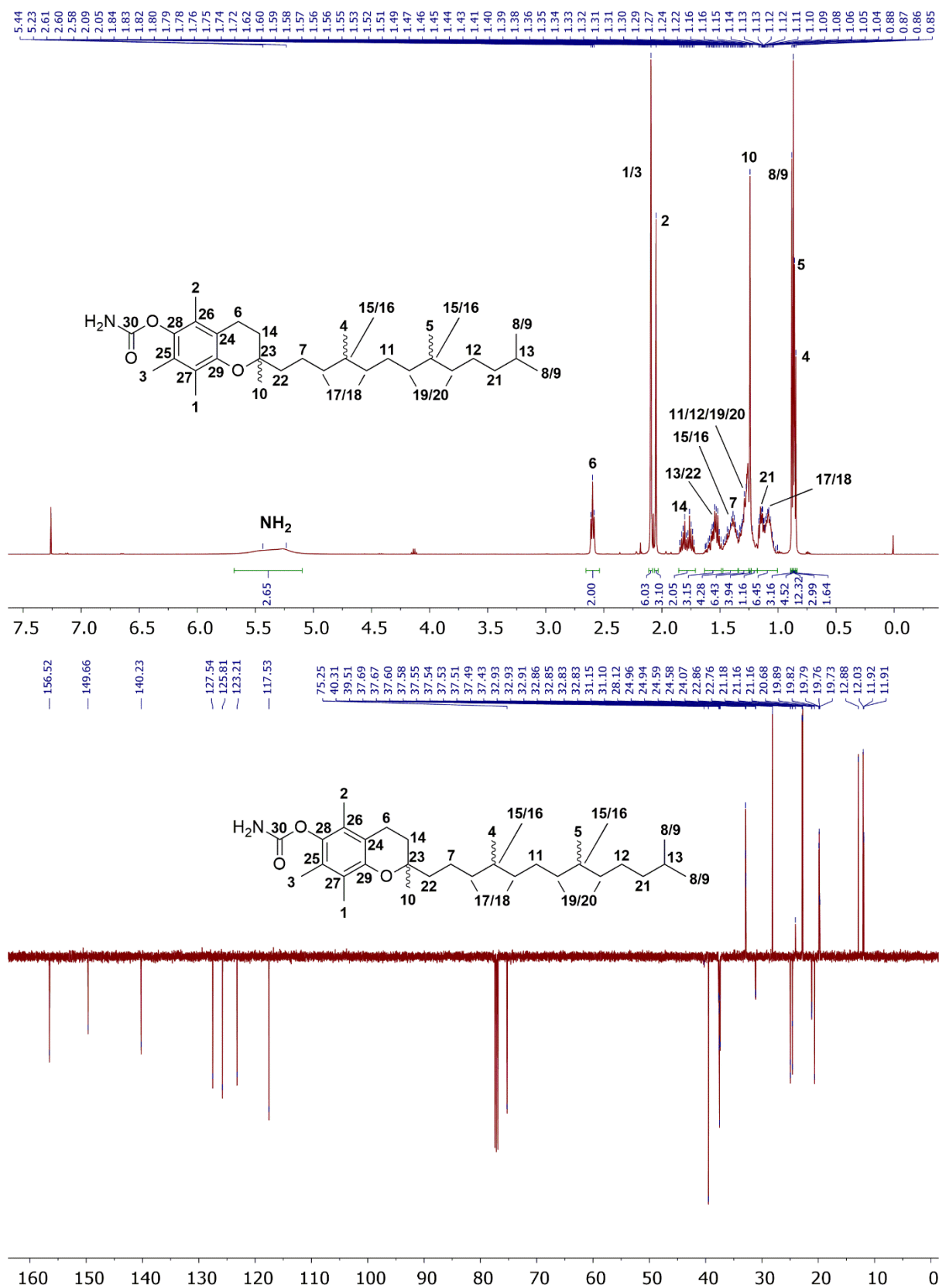
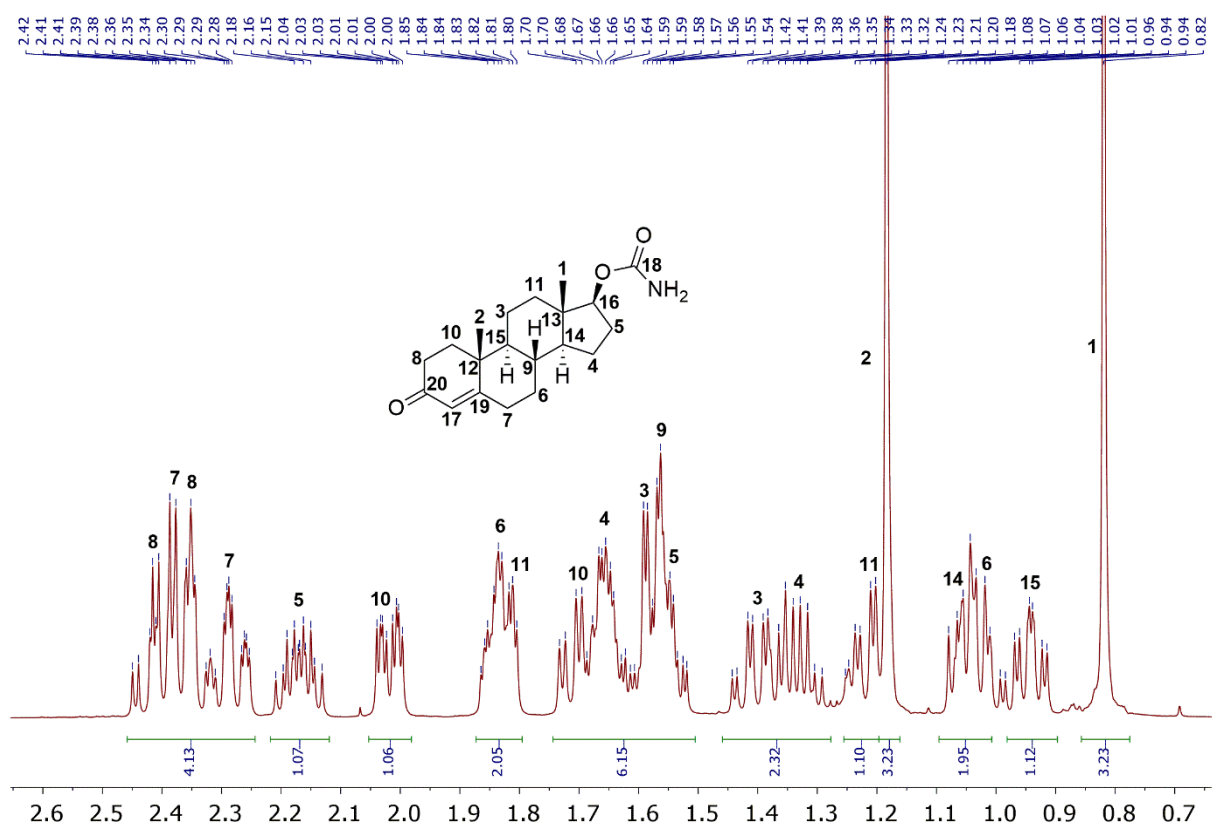
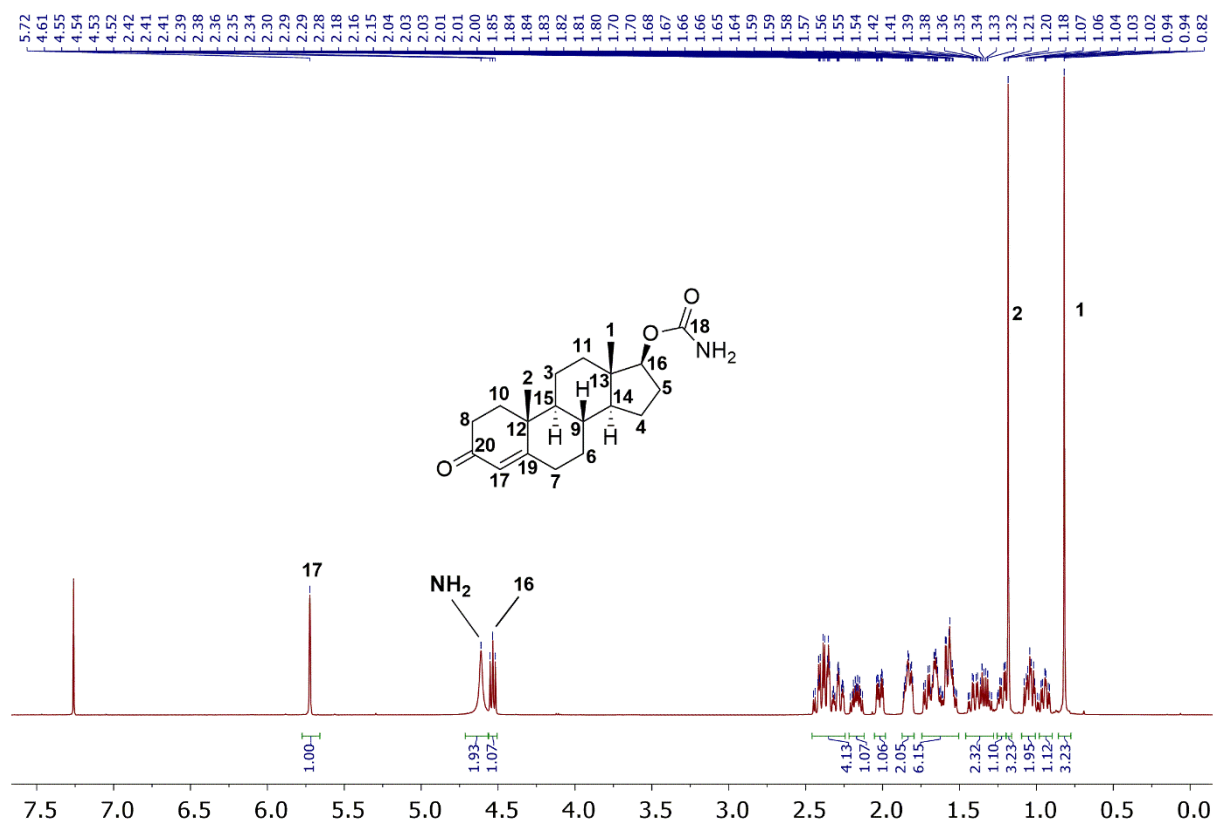


Figure 56: ^1H - and ^{13}C -NMR-spectrum of 2,5,7,8-tetramethyl-2-(4,8,12-trimethyltridecyl)chroman-6-yl carbamate (**363**) in CDCl_3 .

7. Analytical data and spectra



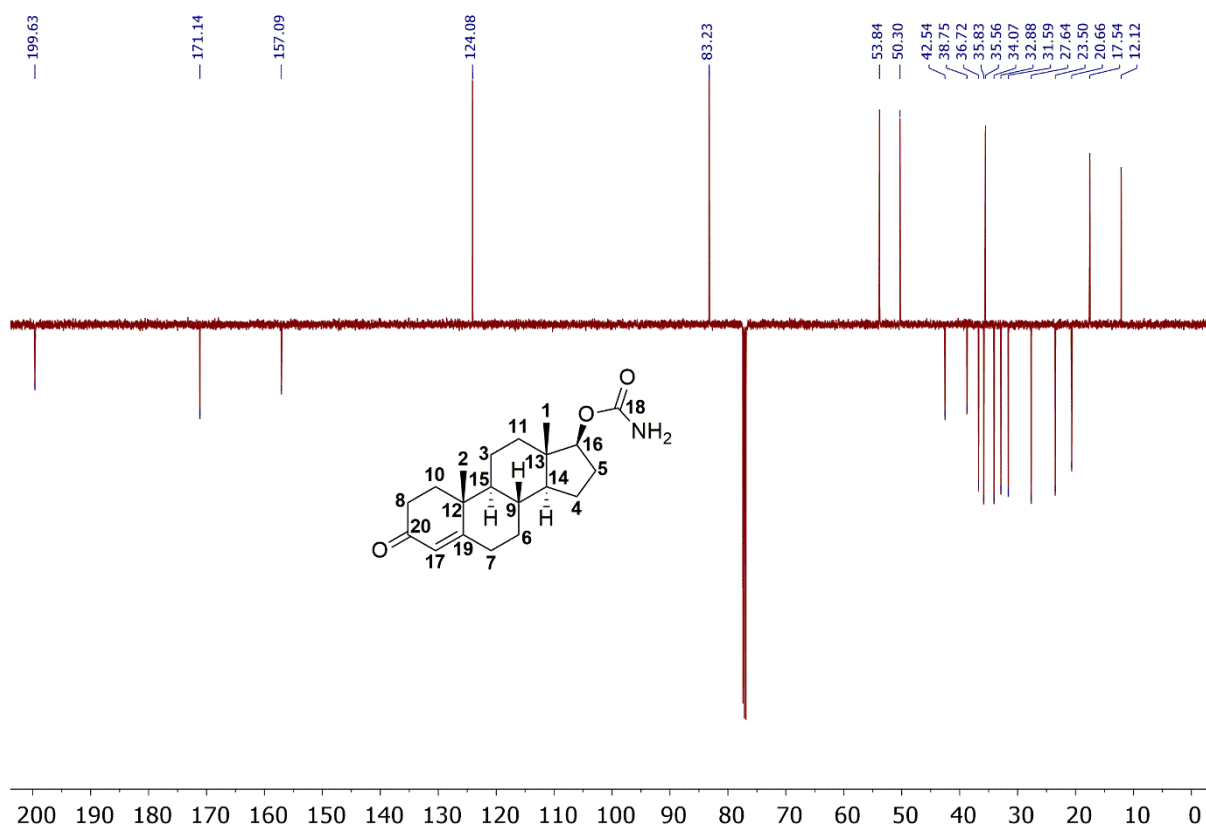
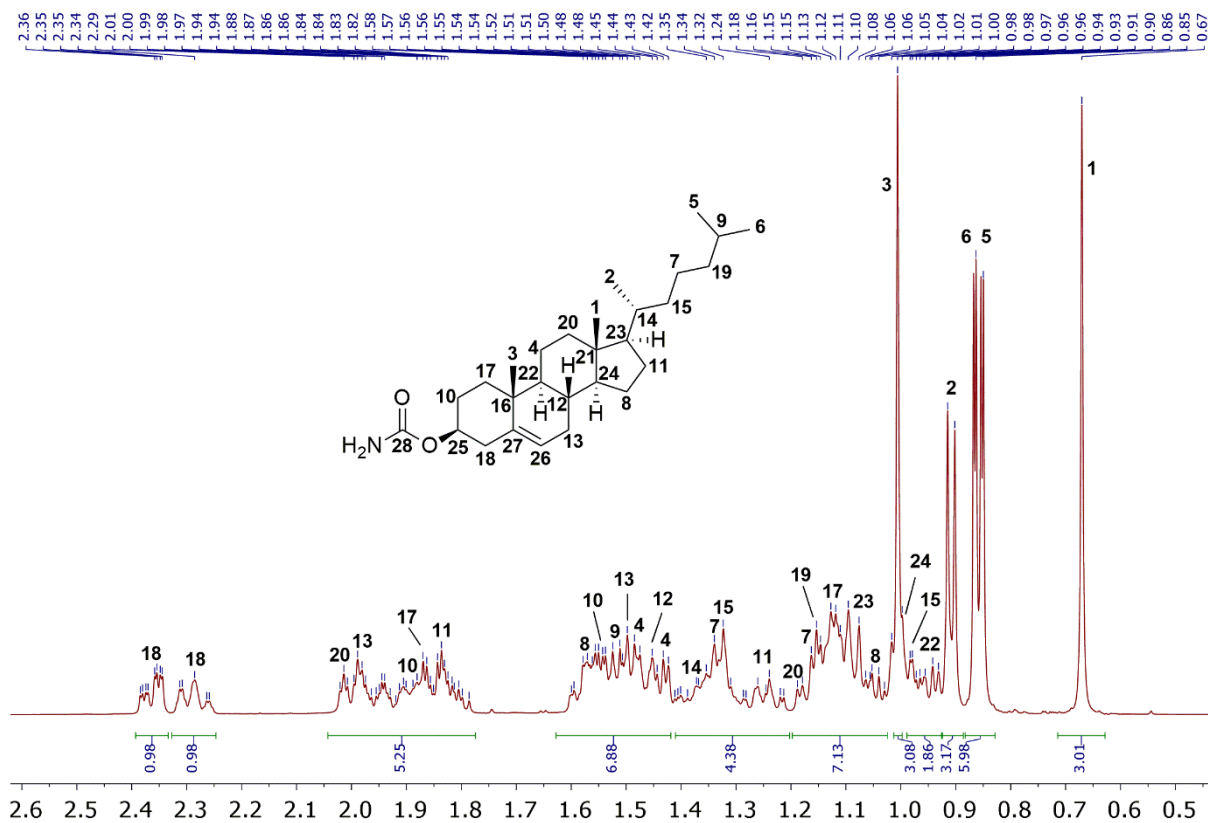
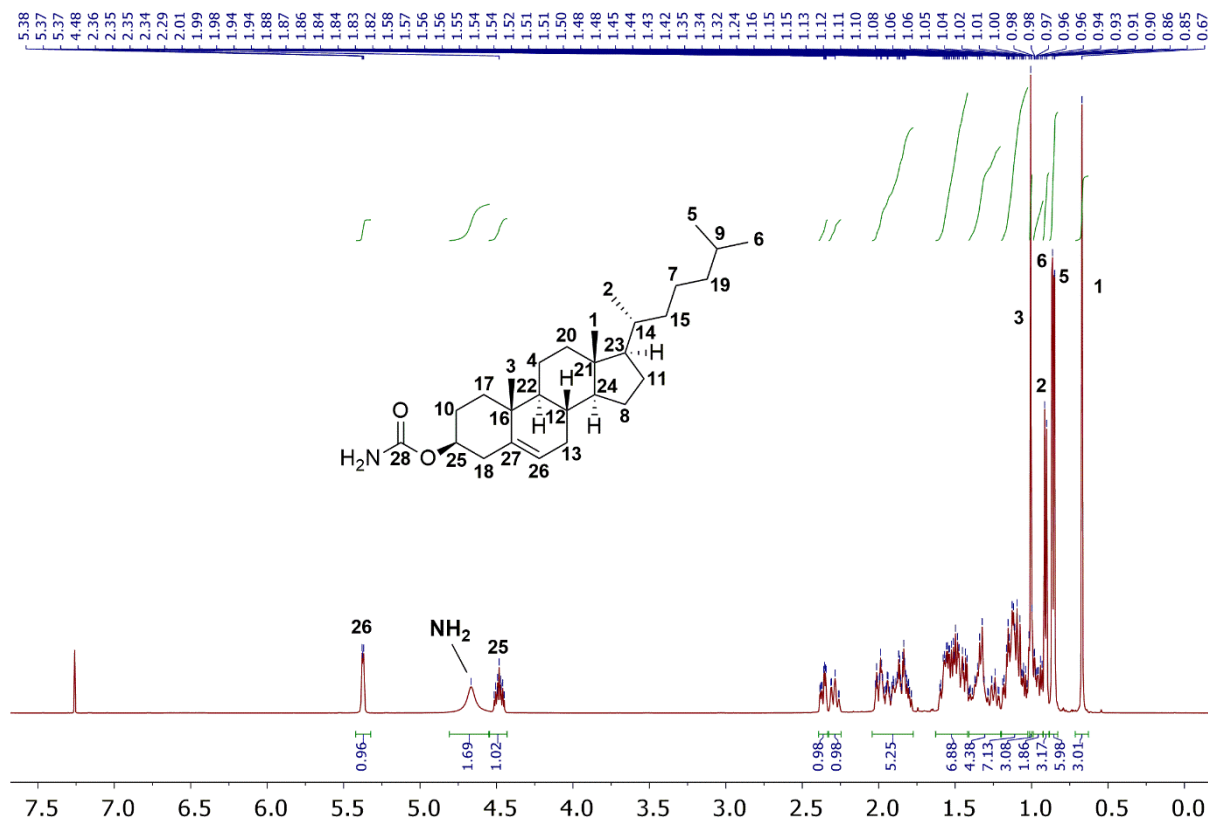


Figure 57: ^{13}C -NMR-spectrum of (8*R*,9*S*,10*R*,13*S*,14*S*,17*S*)-10,13-dimethyl-3-oxo-2,3,6,7,8,9,10,11,12,13,14,15,16,17-tetradecahydro-1*H*-cyclopenta[*a*]phenanthren-17-yl carbamate (**366**) in CDCl_3 .

7. Analytical data and spectra



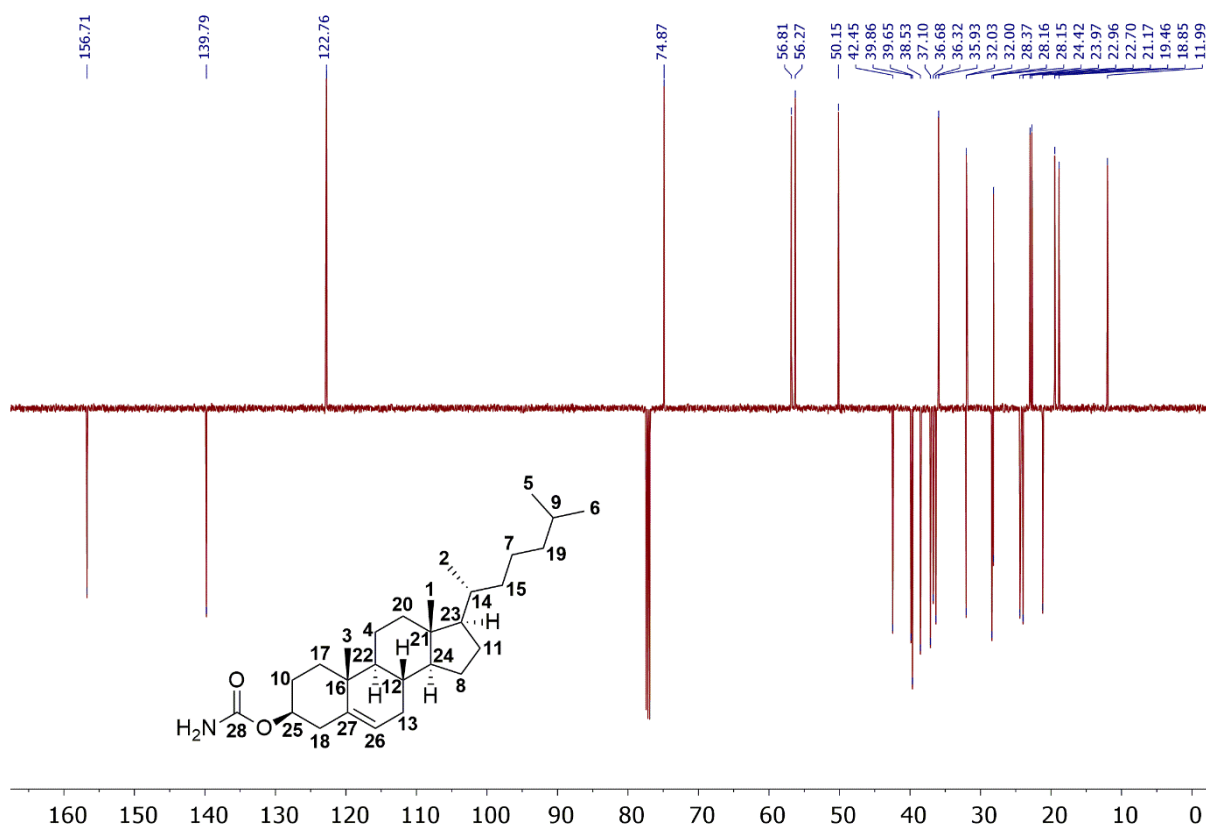


Figure 58: ^1H - and ^{13}C -NMR-spectrum of (3*S*,8*S*,9*S*,10*R*,13*R*,14*S*,17*R*)-10,13-dimethyl-17-((*R*)-6-methylheptan-2-yl)-2,3,4,7,8,9,10,11,12,13,14,15,16,17-tetradecahydro-1*H*-cyclopenta[*a*]phenanthren-3-yl carbamate (**364**) in CDCl_3 .

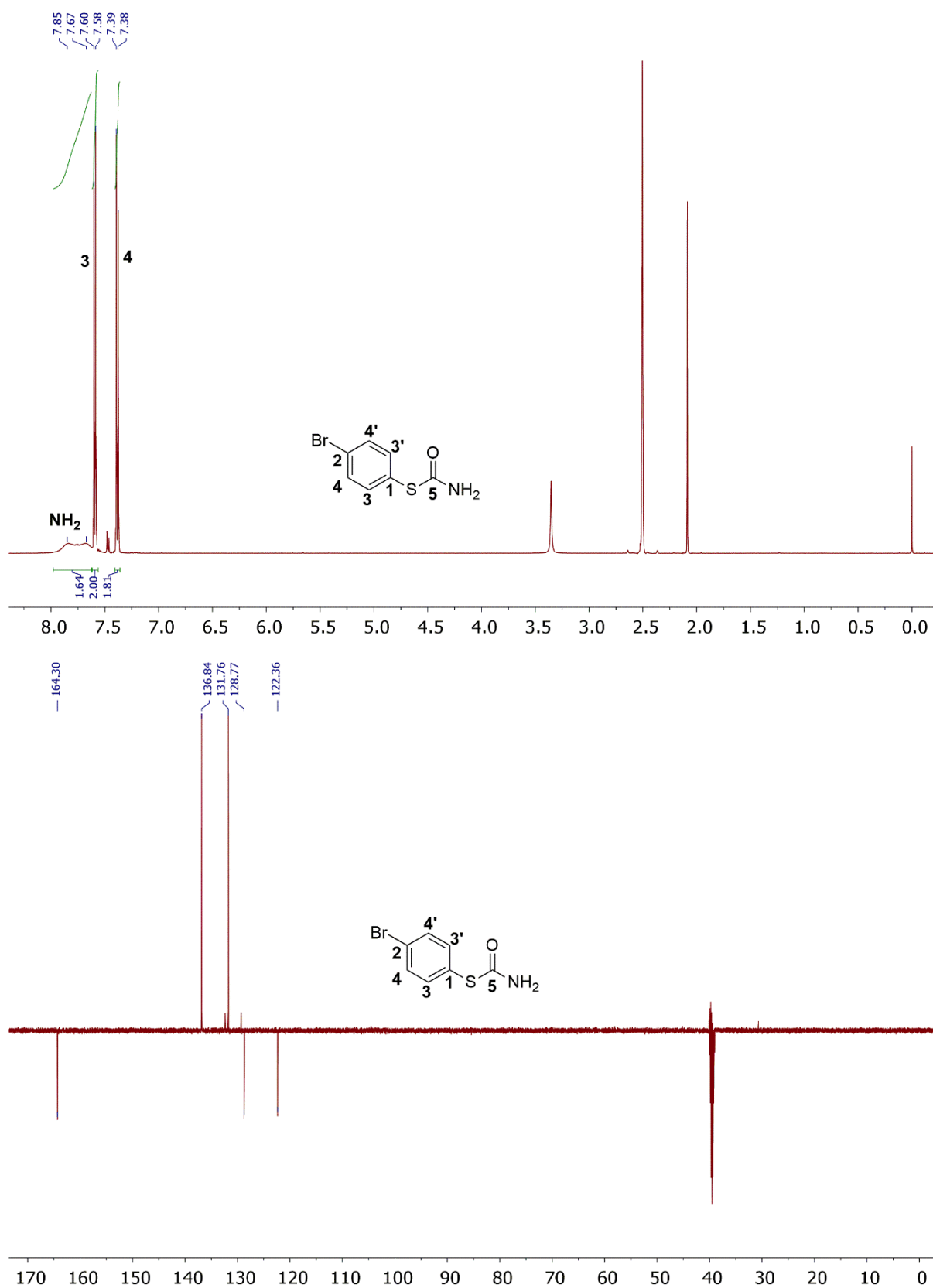


Figure S9: ^1H - and ^{13}C -NMR-spectrum of *S*-(4-bromophenyl) carbamothioate (**390**) in DMSO-d_6 .

7. Analytical data and spectra

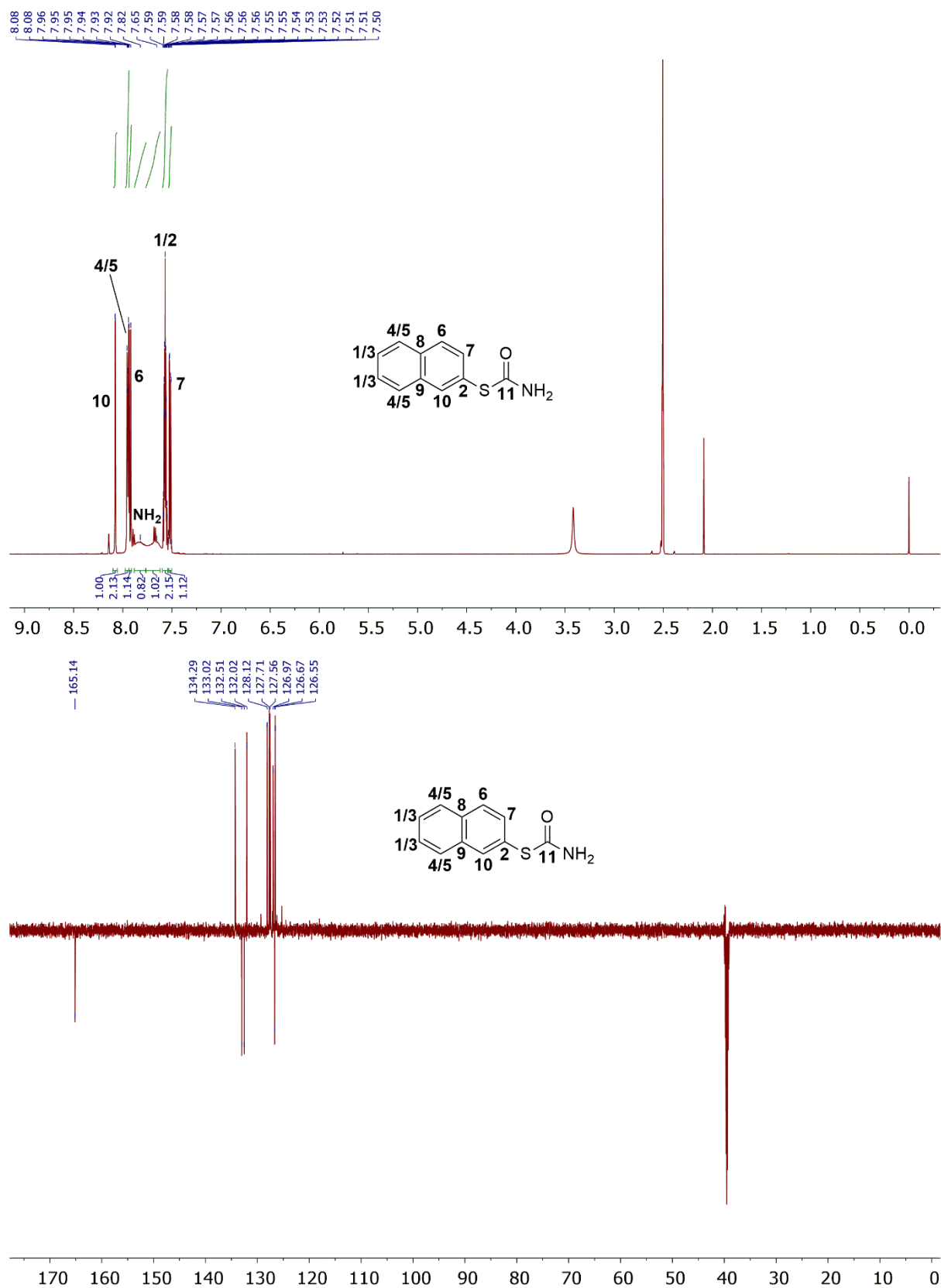


Figure 60: ¹H- and ¹³C-NMR-spectrum of *S*-naphthalen-2-yl carbamothioate (**391**) in DMSO-d₆.

7.1.2 Compounds protected by coumaranones

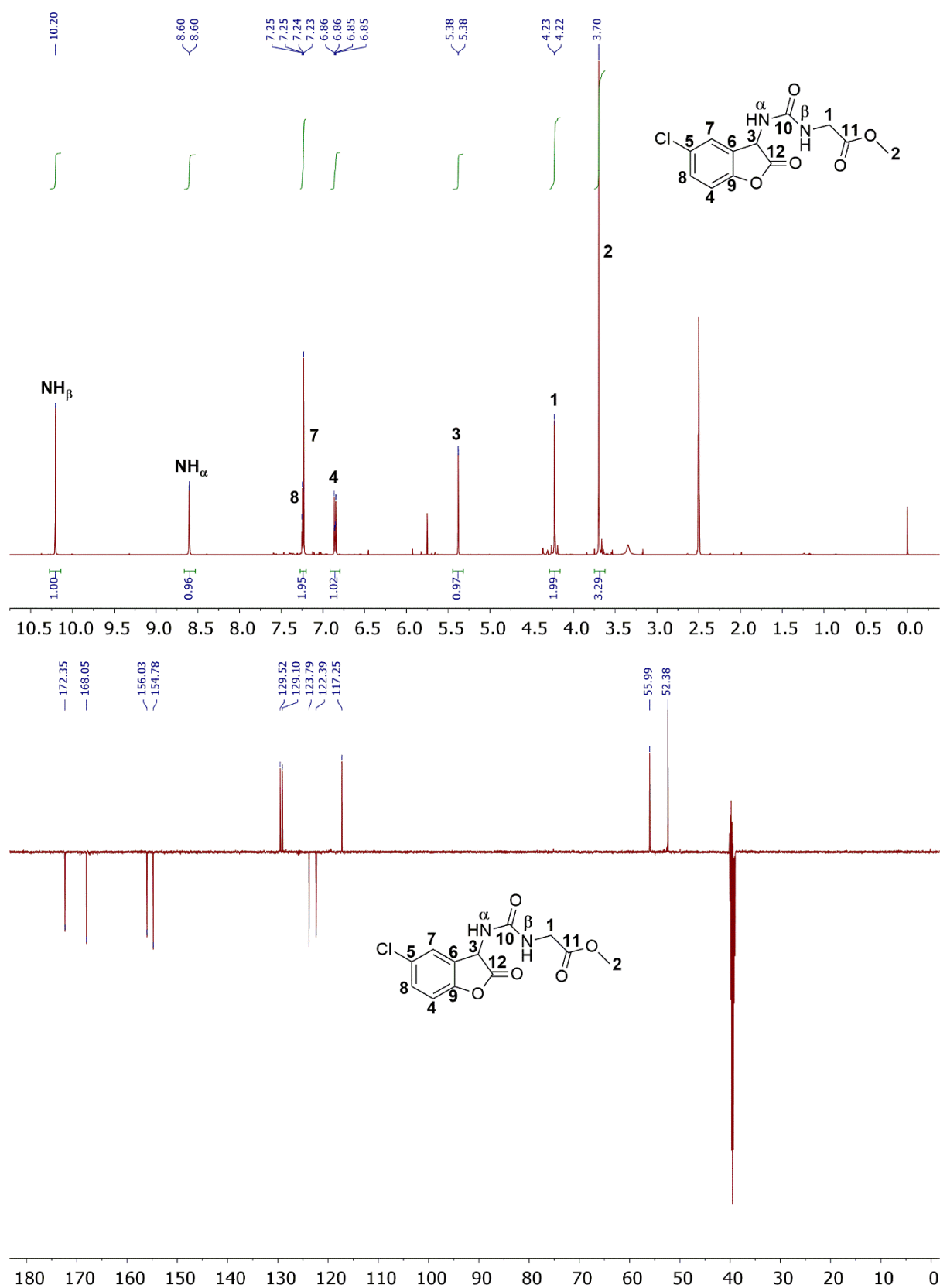


Figure 61: ¹H- and ¹³C-NMR-spectrum of methyl 2-(3-(5-chloro-2-oxo-2,3-dihydrobenzofuran-3-yl)ureido)acetate (**293**) in DMSO-d₆.

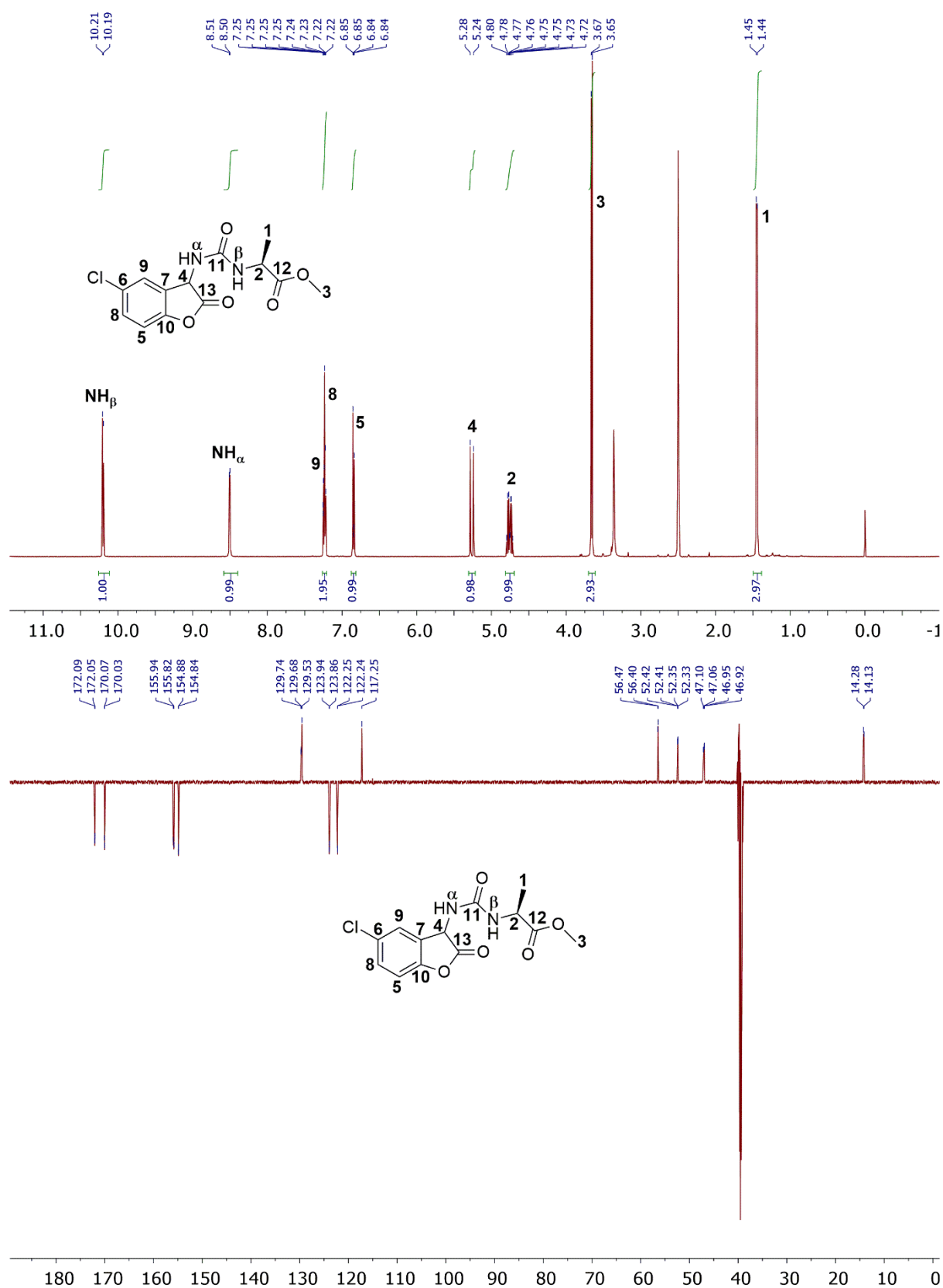


Figure 62: ^1H - and ^{13}C -NMR-spectrum of (2*S*)-methyl 2-(3-(5-chloro-2-oxo-2,3-dihydrobenzofuran-3-yl)ureido)propanoate (295) in DMSO- d_6 .

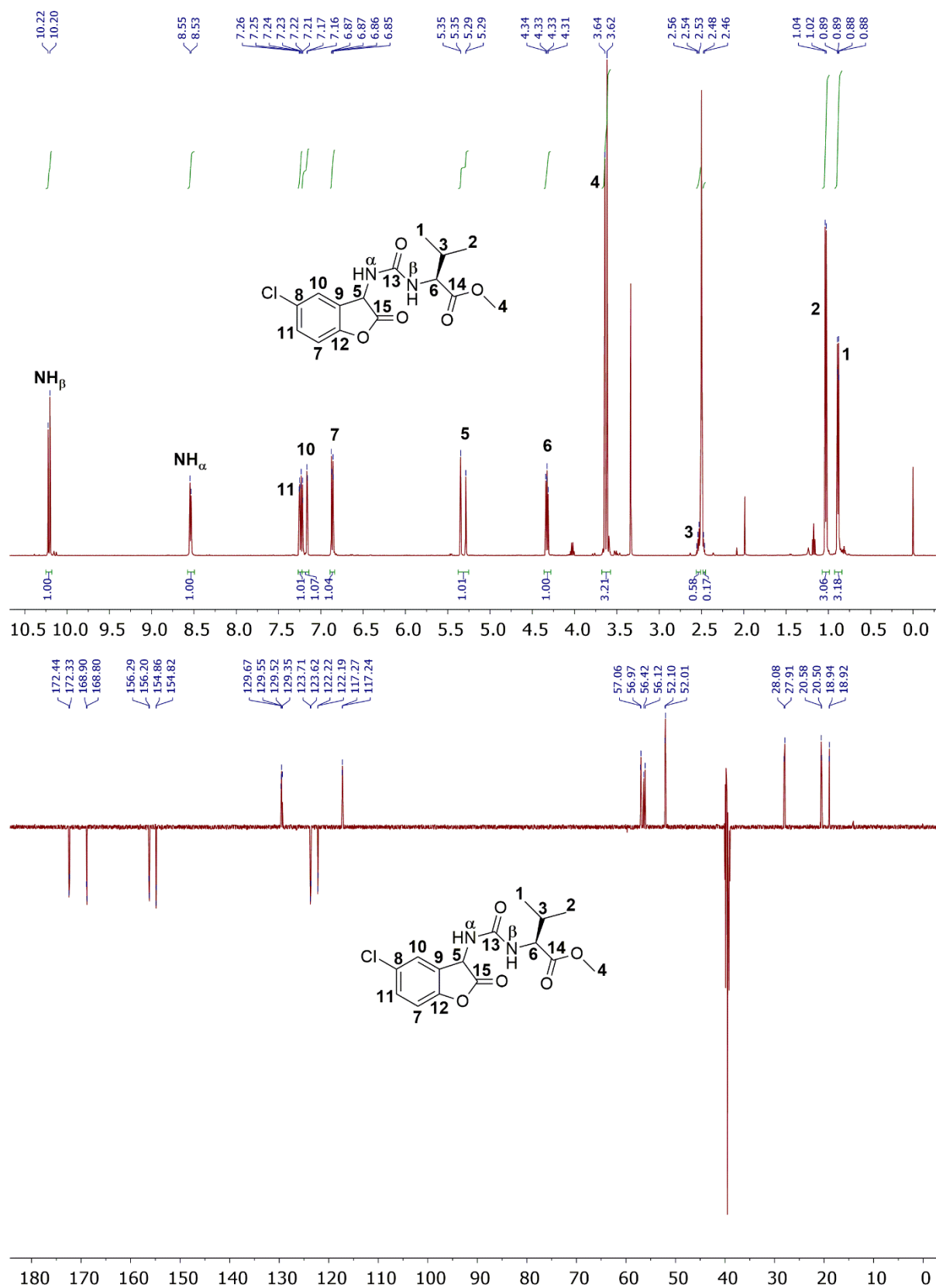
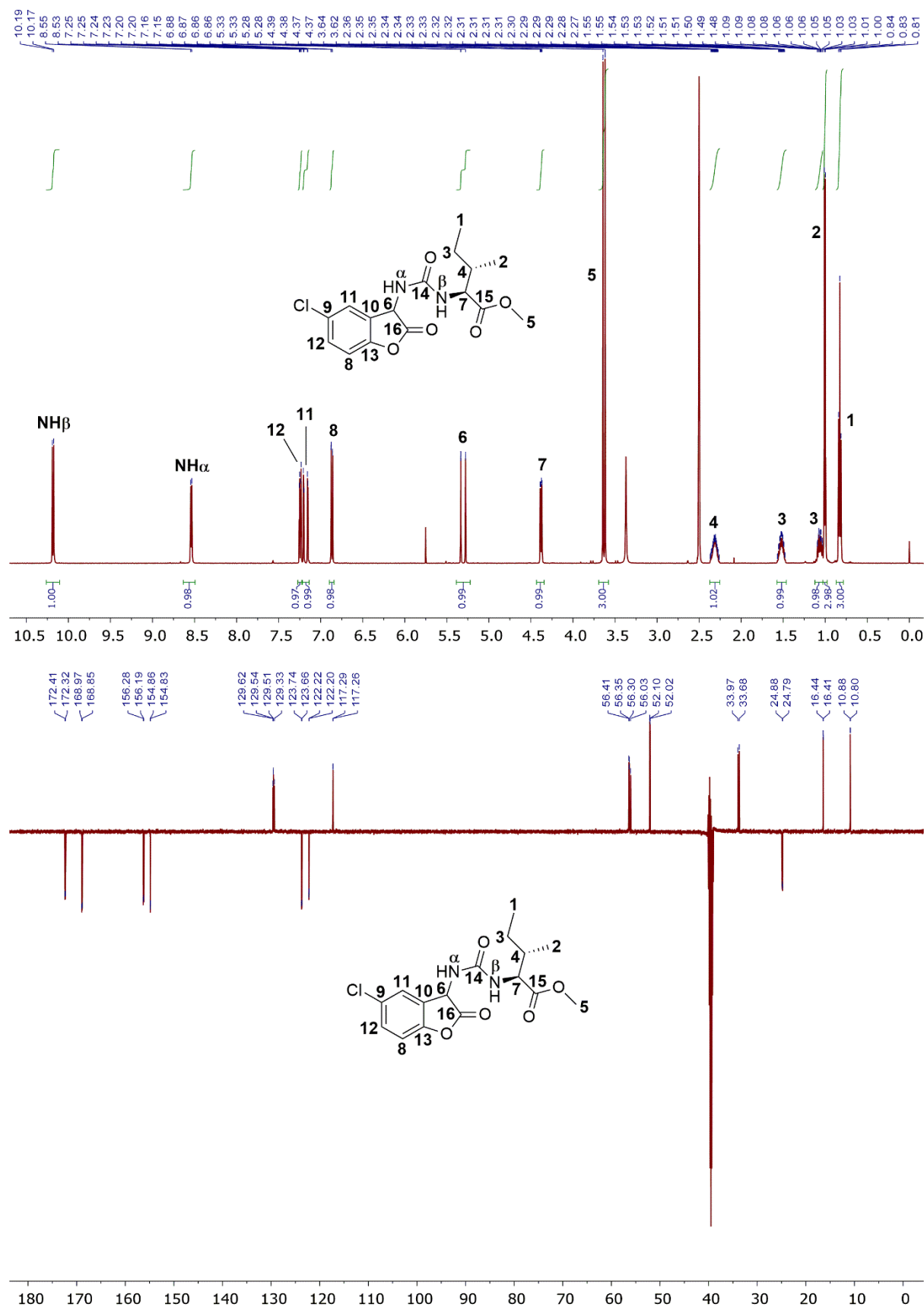


Figure 63: ¹H- and ¹³C-NMR-spectrum of (2*S*)-methyl 2-(3-(5-chloro-2-oxo-2,3-dihydrobenzofuran-3-yl)ureido)-3-methylbutanoate (**297**) in DMSO-*d*₆.



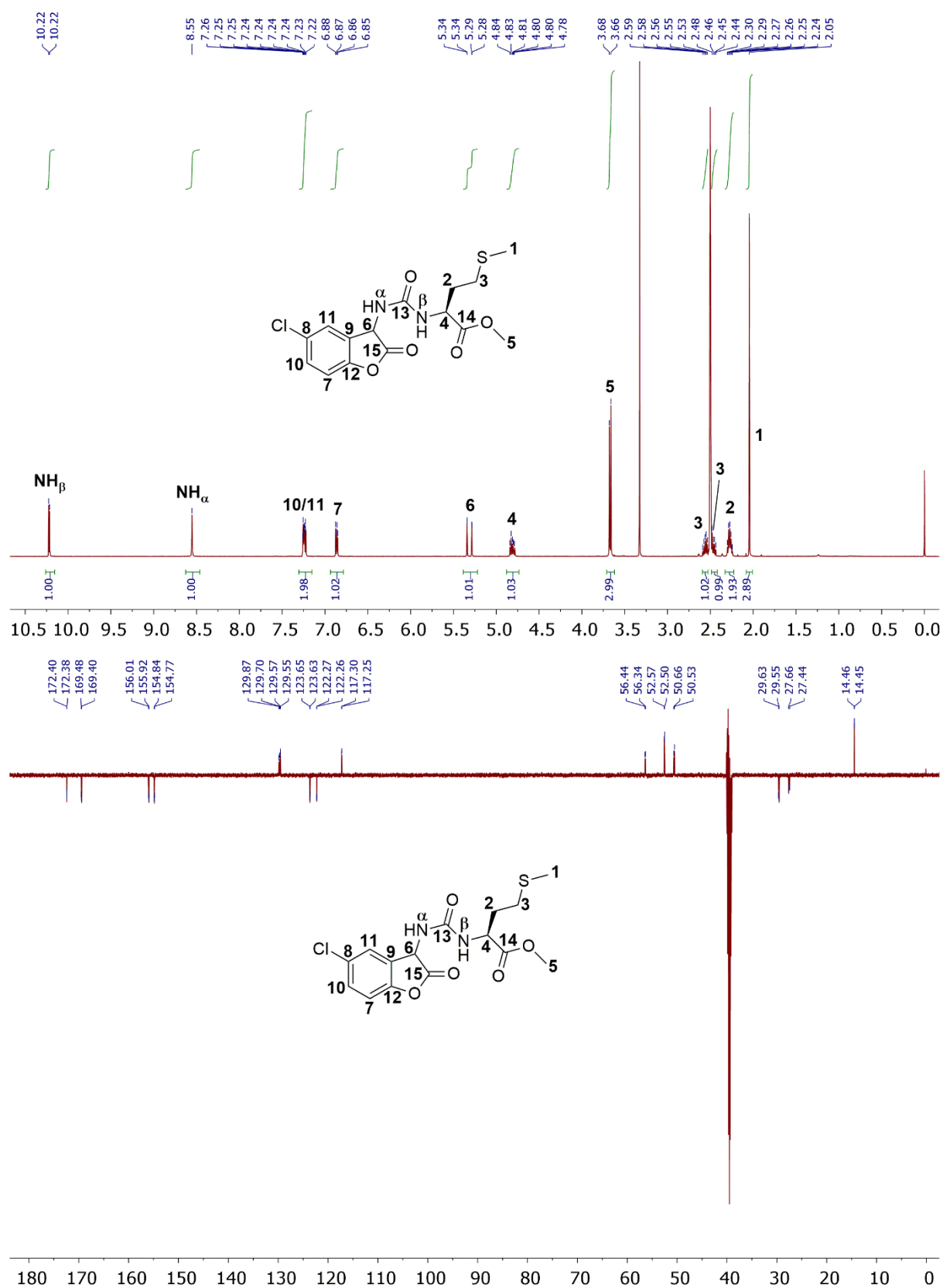


Figure 66: ¹H- and ¹³C-NMR-spectrum of (2*S*)-methyl 2-(3-(5-chloro-2-oxo-2,3-dihydrobenzofuran-3-yl)ureido)-4-(methylthio)butanoate (**303**) in DMSO-*d*₆.

7. Analytical data and spectra

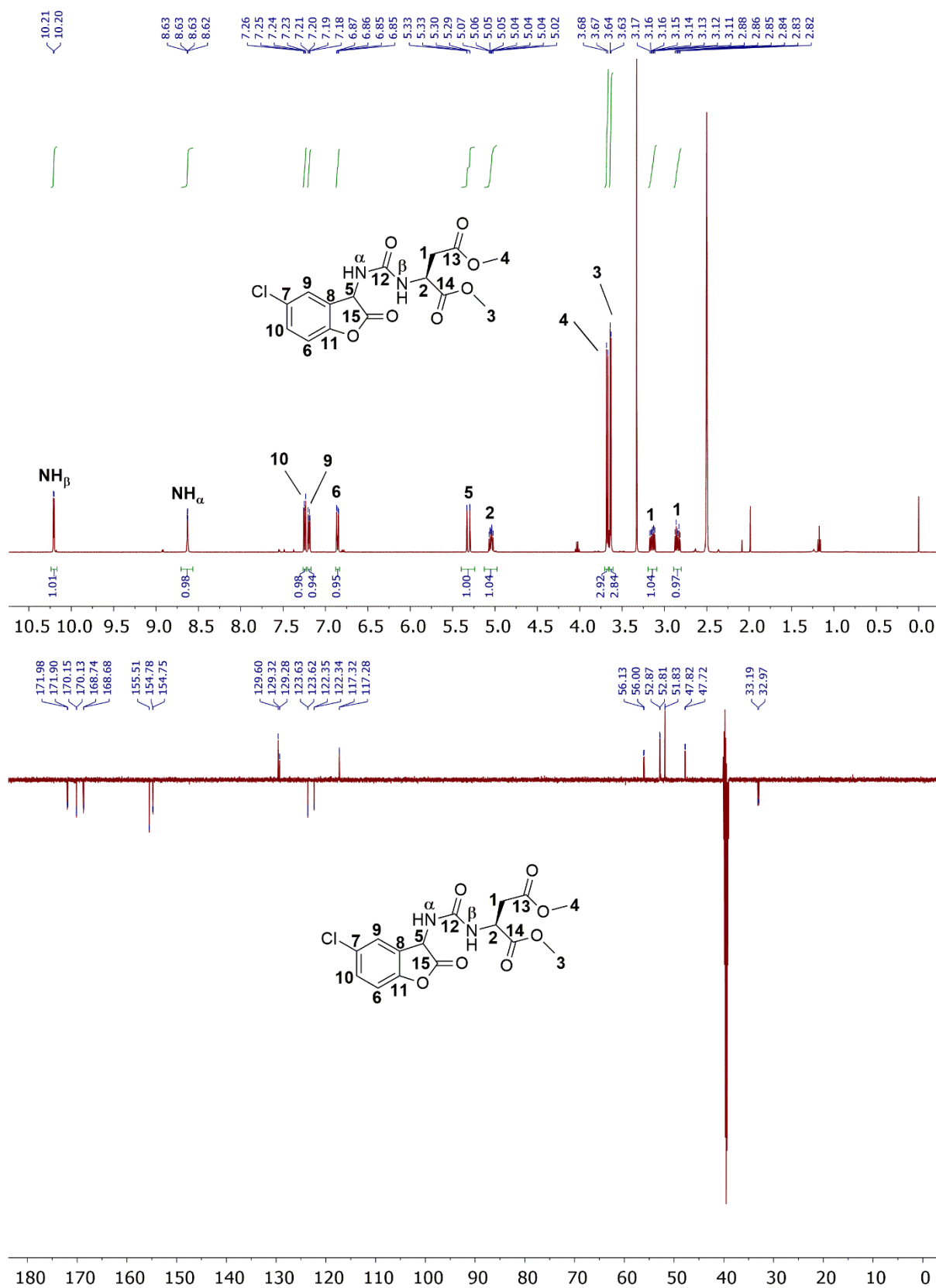


Figure 67: ^1H - and ^{13}C -NMR-spectrum of (2S)-dimethyl 2-(3-(5-chloro-2-oxo-2,3-dihydrobenzofuran-3-yl)ureido)succinate (305) in DMSO- d_6 .

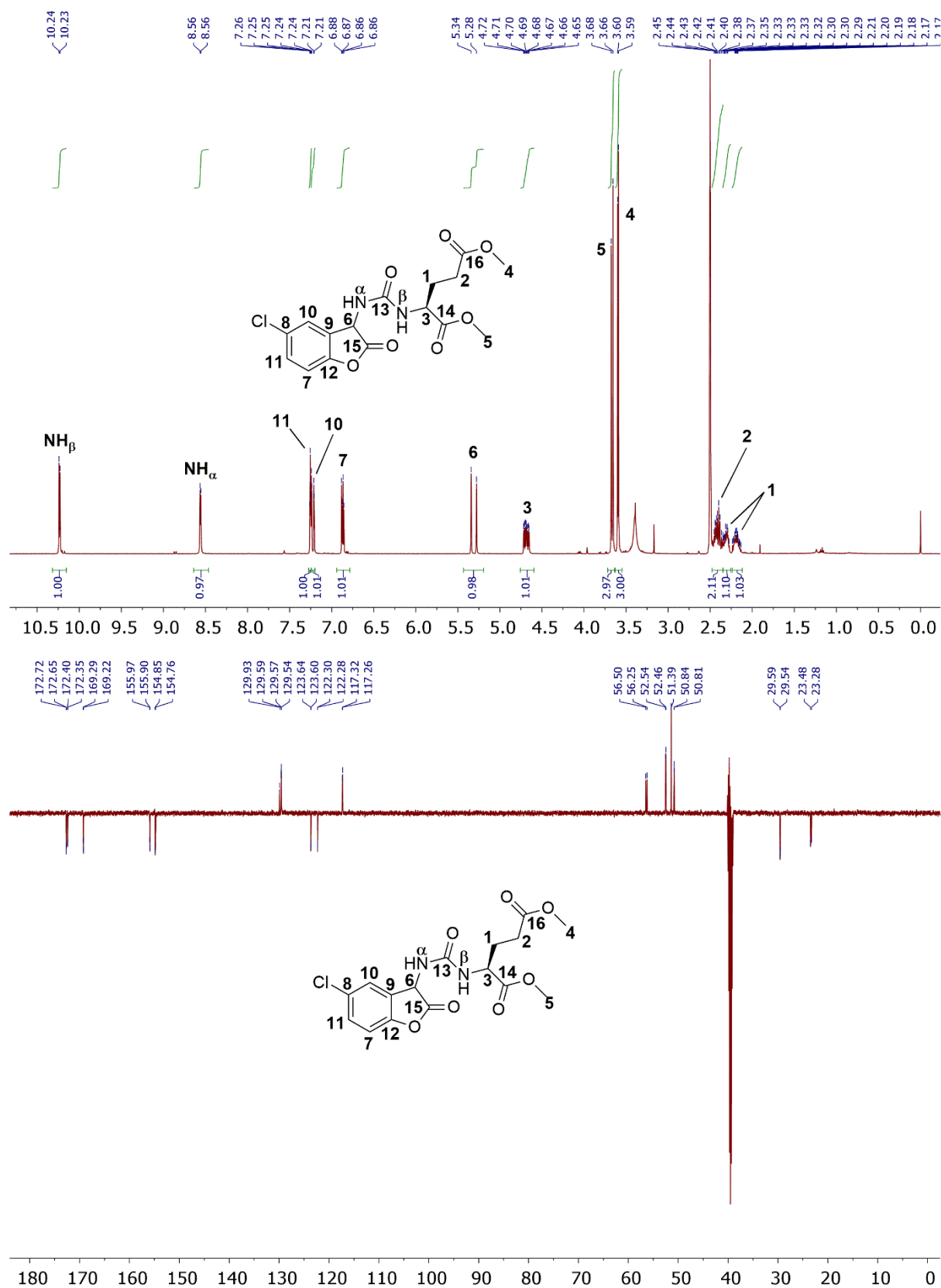


Figure 68: ^1H - and ^{13}C -NMR-spectrum of (2S)-dimethyl 2-(3-(5-chloro-2-oxo-2,3-dihydrobenzofuran-3-yl)ureido)pentanedioate (**307**) in DMSO-d_6 .

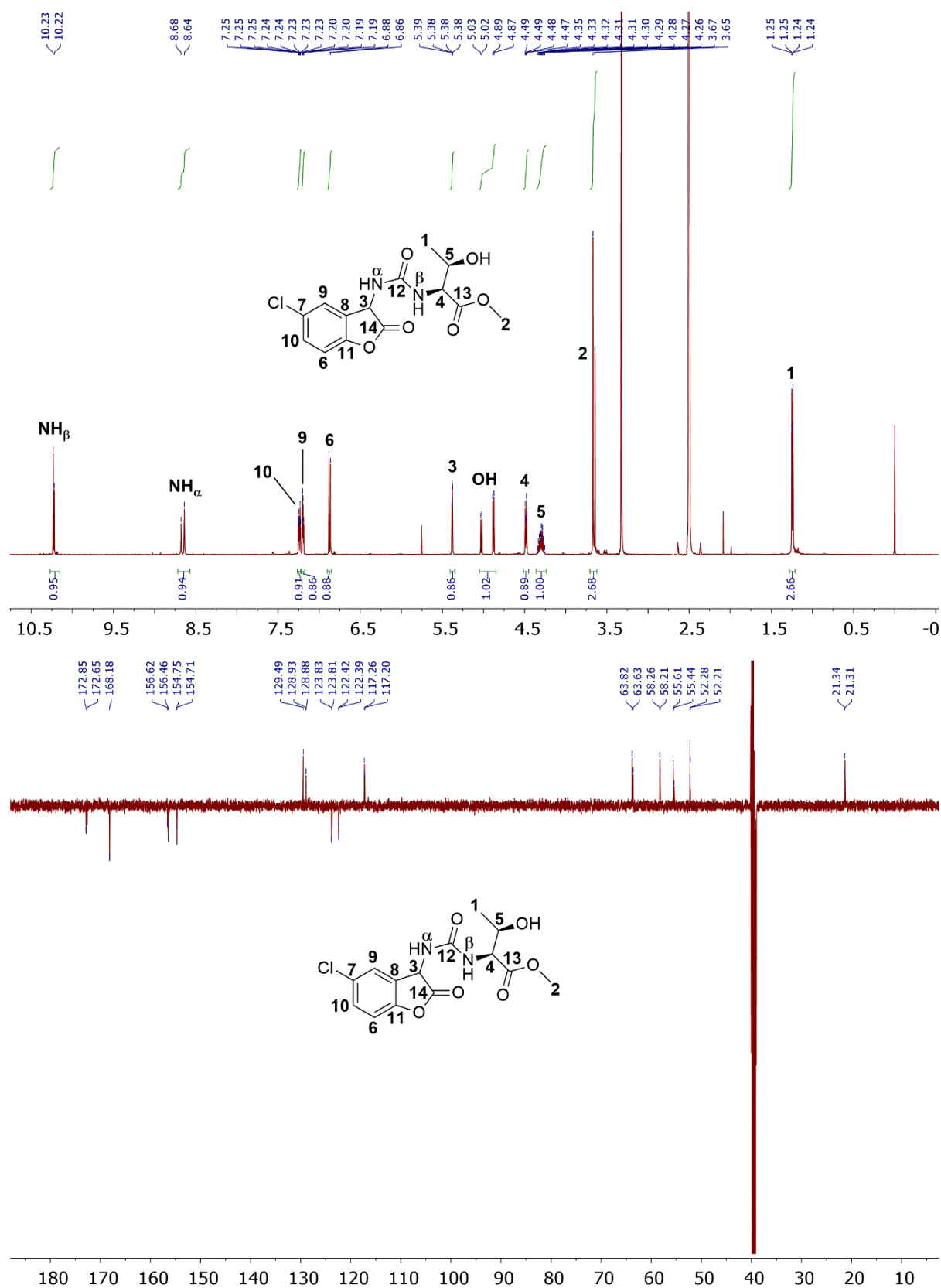
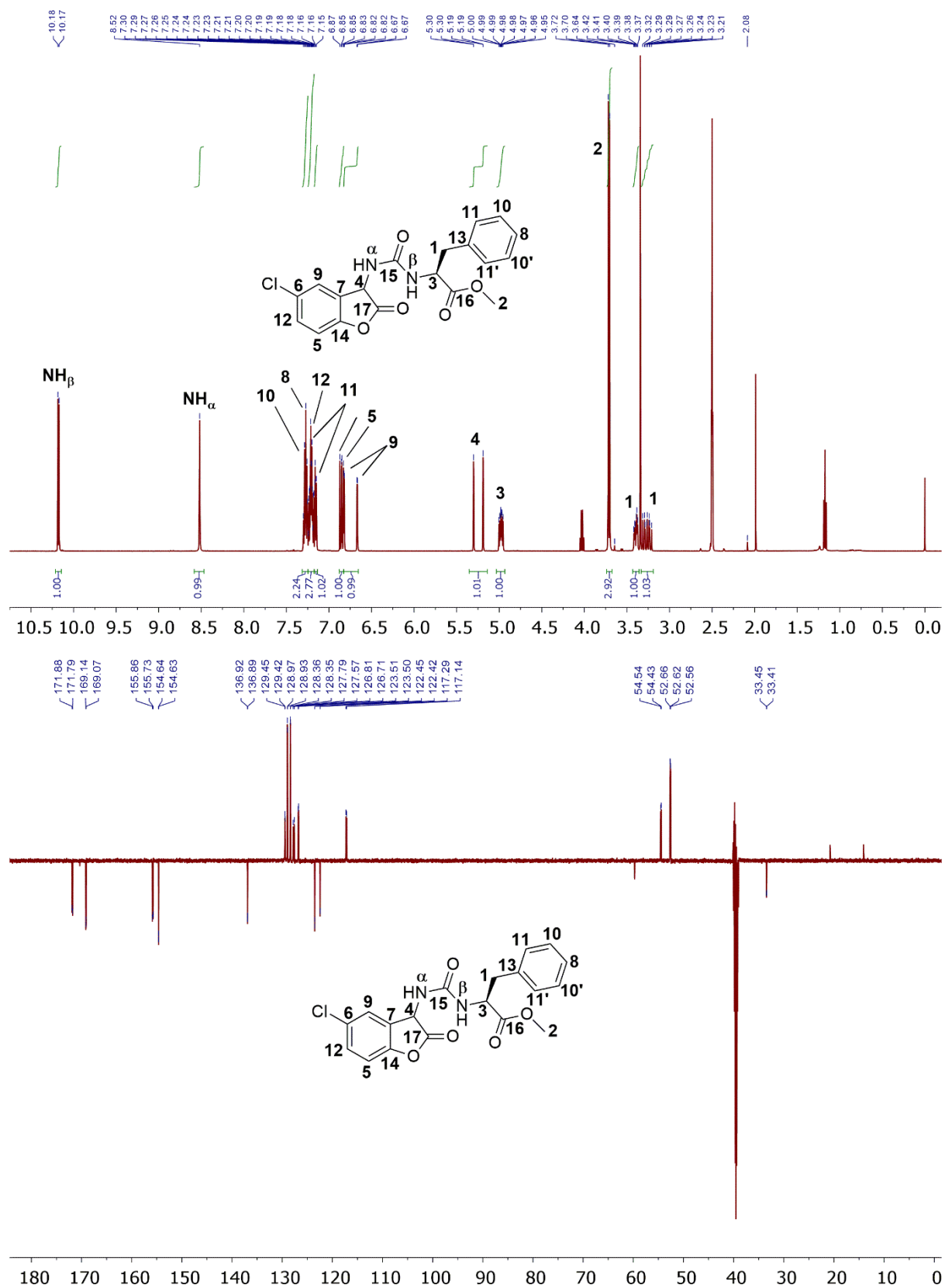


Figure 69: ¹H- and ¹³C-NMR-spectrum of (2*S*,3*R*)-methyl 2-(3-(5-chloro-2-oxo-2,3-dihydrobenzofuran-3-yl)ureido)-3-hydroxybutanoate (**309**) in DMSO-*d*₆.

7. Analytical data and spectra



7. Analytical data and spectra

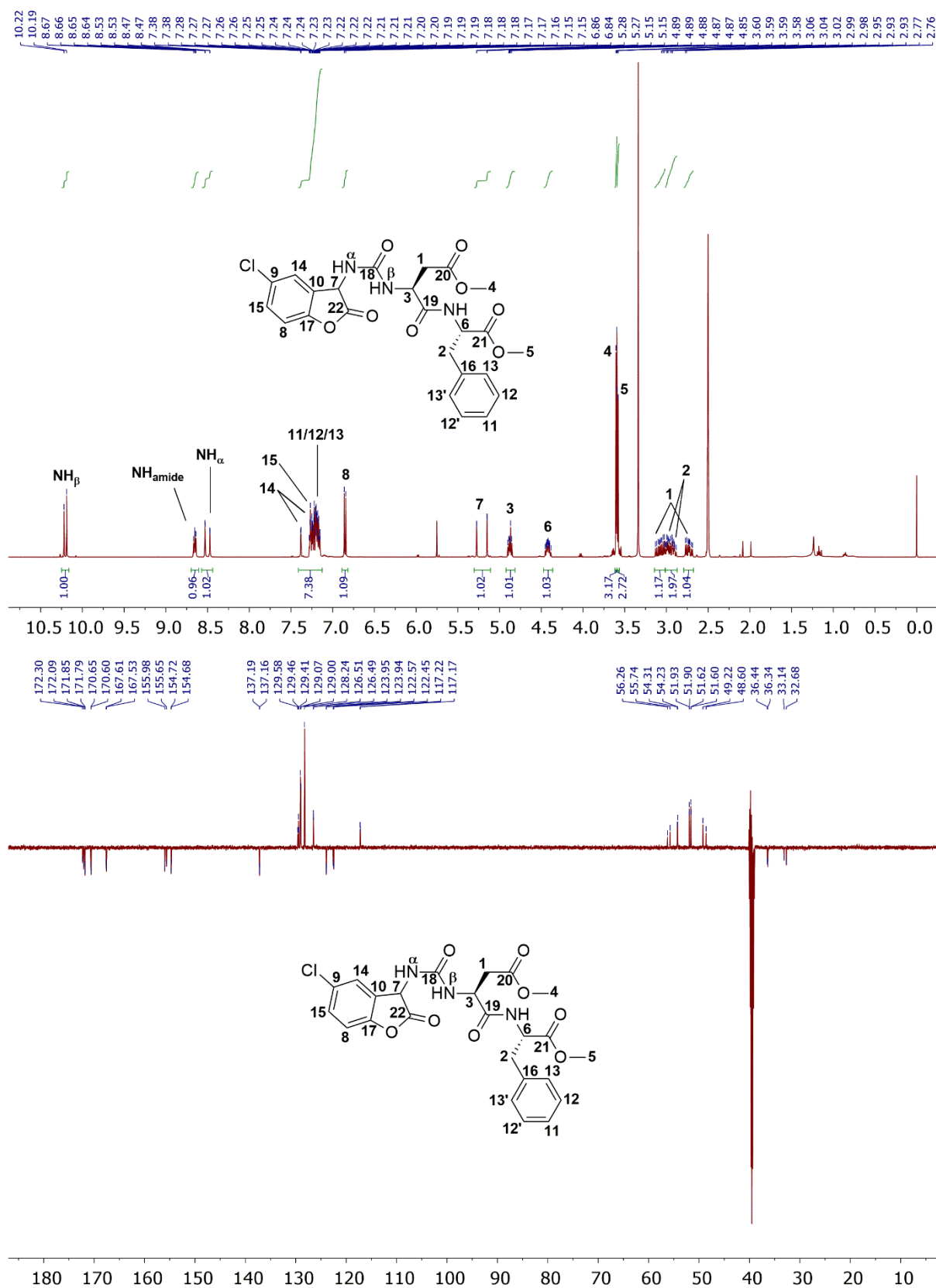


Figure 71: ¹H- and ¹³C-NMR-spectrum of (3*S*)-methyl 3-(3-(5-chloro-2-oxo-2,3-dihydrobenzofuran-3-yl)ureido)-4-(((*S*)-1-methoxy-1-oxo-3-phenylpropan-2-yl)amino)-4-oxobutanoate (**325**) in DMSO-d₆.

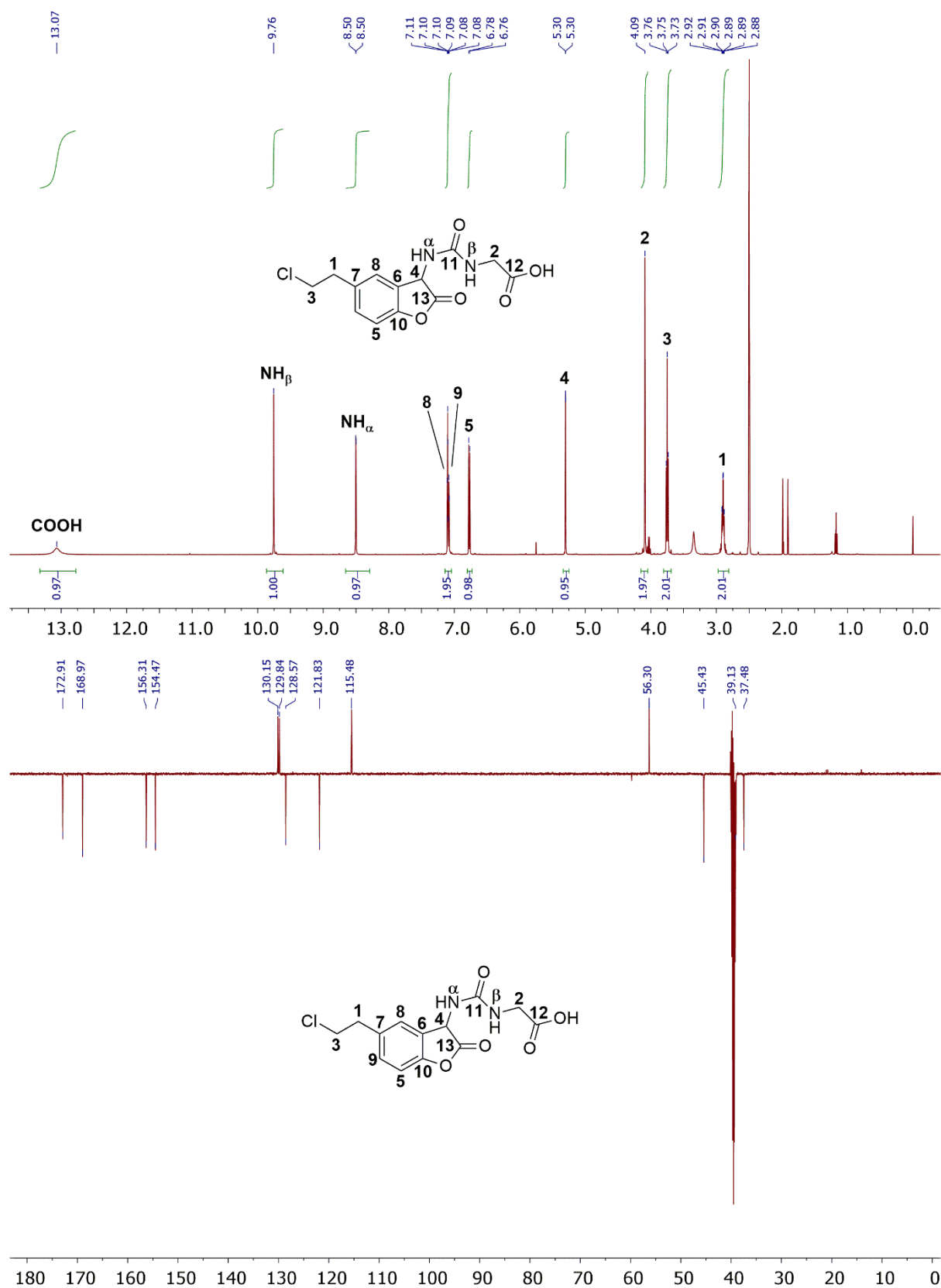


Figure 72: ^1H - and ^{13}C -NMR-spectrum of 2-(3-(5-(2-chloroethyl)-2-oxo-2,3-dihydrobenzofuran-3-yl)ureido)acetic acid (**294**) in DMSO-d_6 .

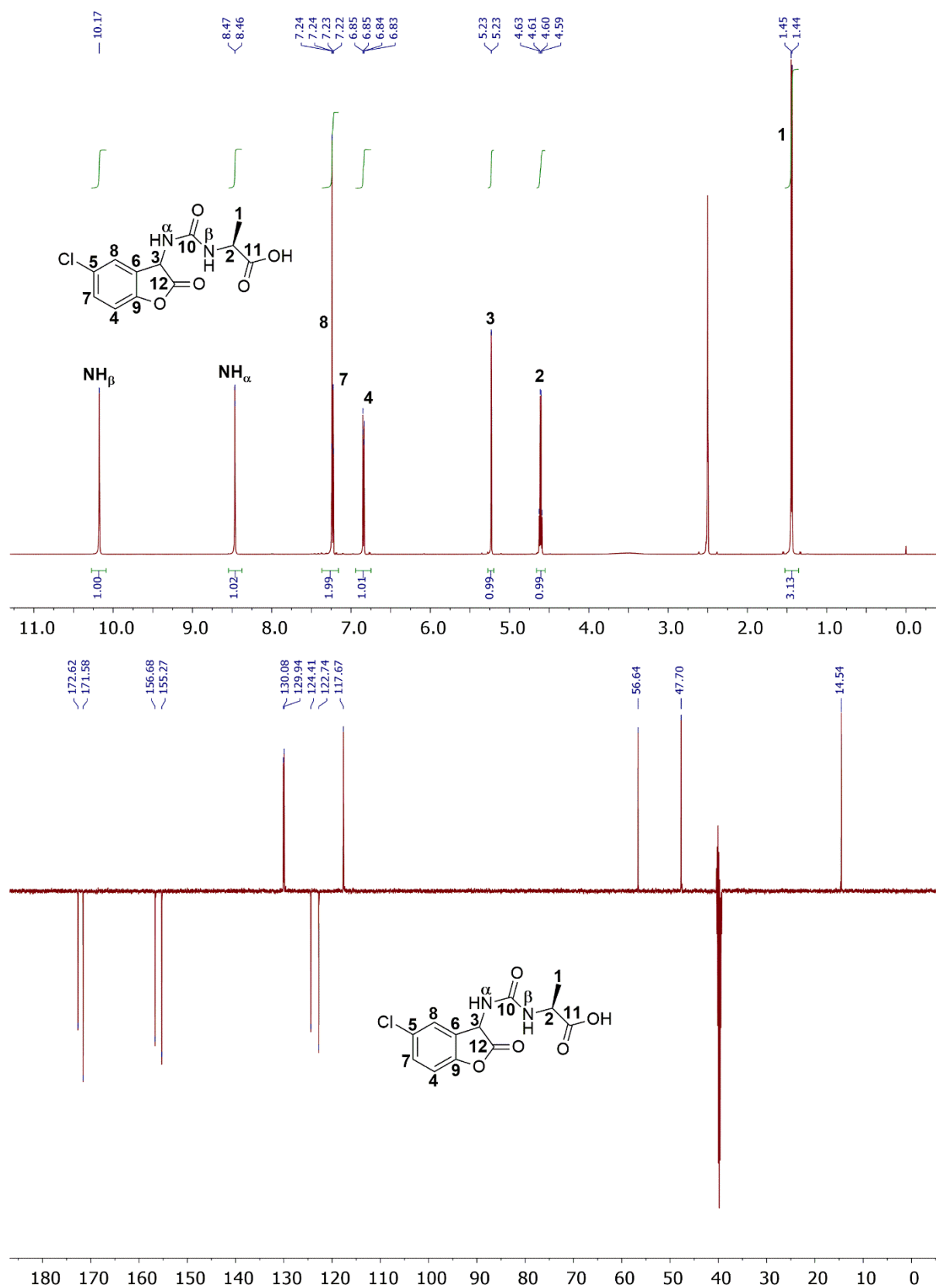


Figure 73: ¹H- and ¹³C-NMR-spectrum of (2S)-2-(3-(5-chloro-2-oxo-2,3-dihydrobenzofuran-3-yl)ureido)propanoic acid (**296b**) in DMSO-d₆.

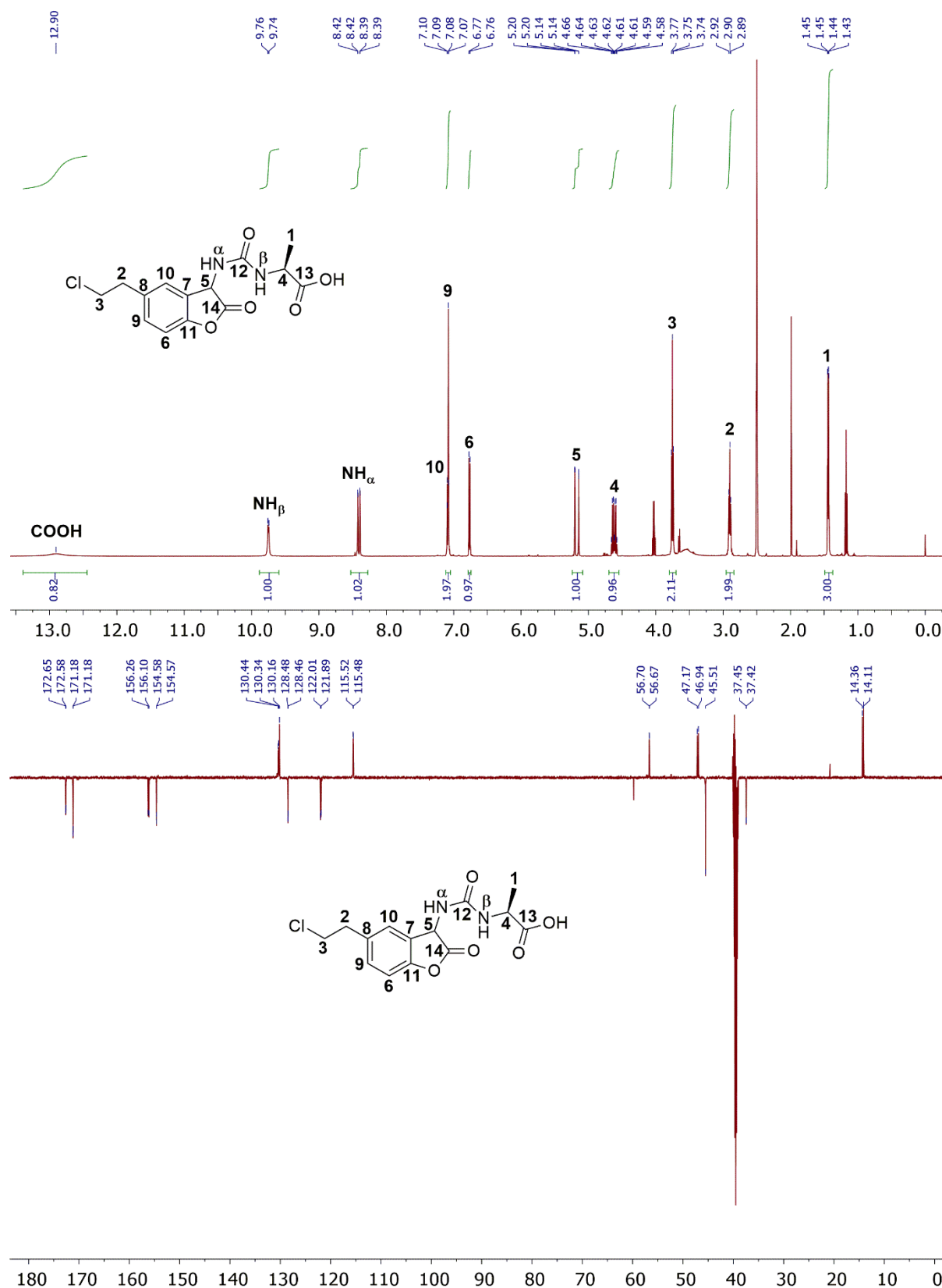


Figure 74: ¹H- and ¹³C-NMR-spectrum of (2S)-2-(3-(5-(2-chloroethyl)-2-oxo-2,3-dihydrobenzofuran-3-yl)ureido)propanoic acid (**296a**) in DMSO-d₆.

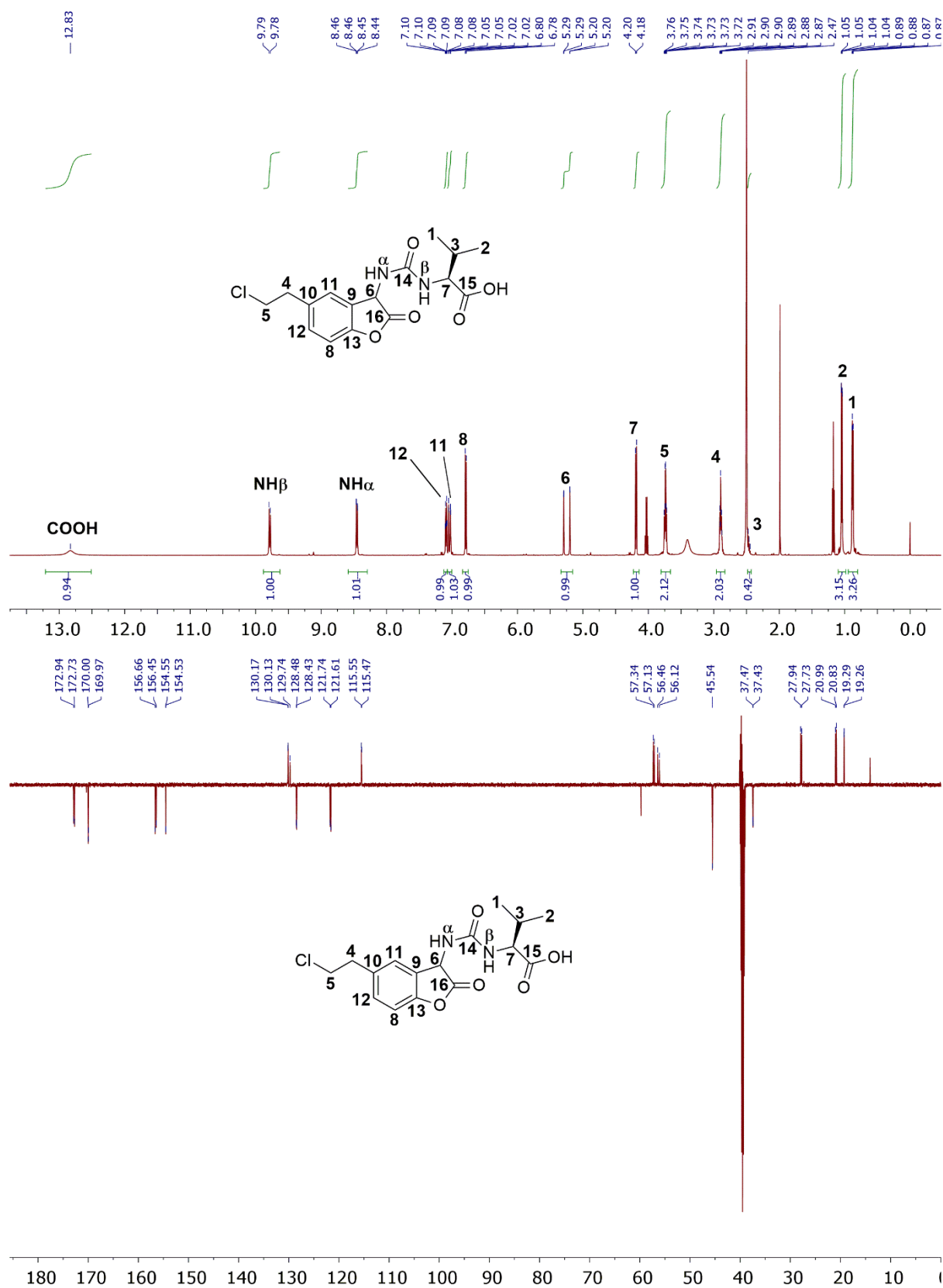


Figure 75: ^1H - and ^{13}C -NMR-spectrum of (2S)-2-(3-(5-(2-chloroethyl)-2-oxo-2,3-dihydrobenzofuran-3-yl)ureido)-3-methylbutanoic acid (**298**) in DMSO-d_6 .

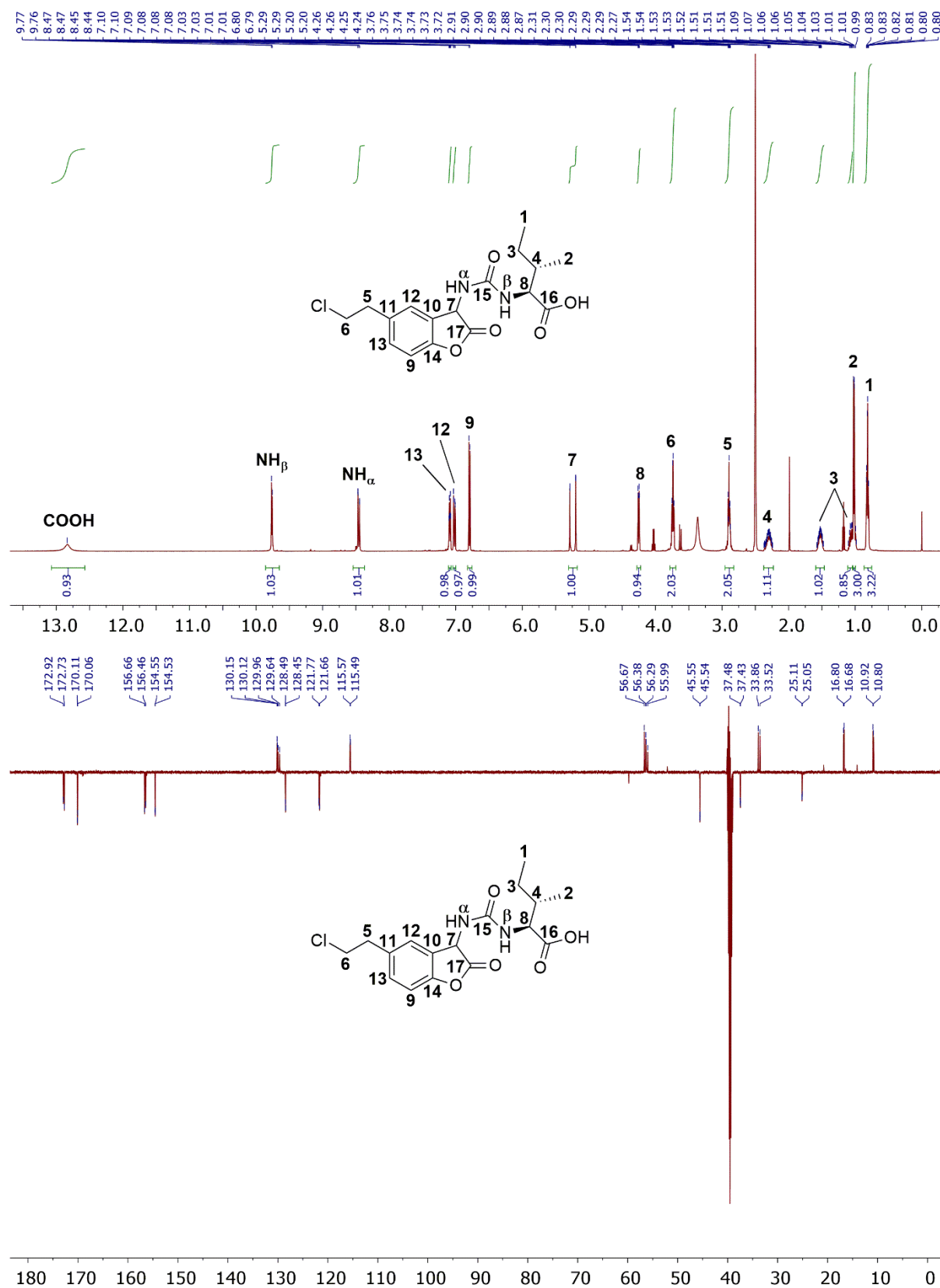


Figure 76: ^1H - and ^{13}C -NMR-spectrum of (2*S*,3*S*)-2-(3-(5-(2-chloroethyl)-2-oxo-2,3-dihydrobenzofuran-3-yl)ureido)-3-methylpentanoic acid (**300**) in DMSO-d_6 .

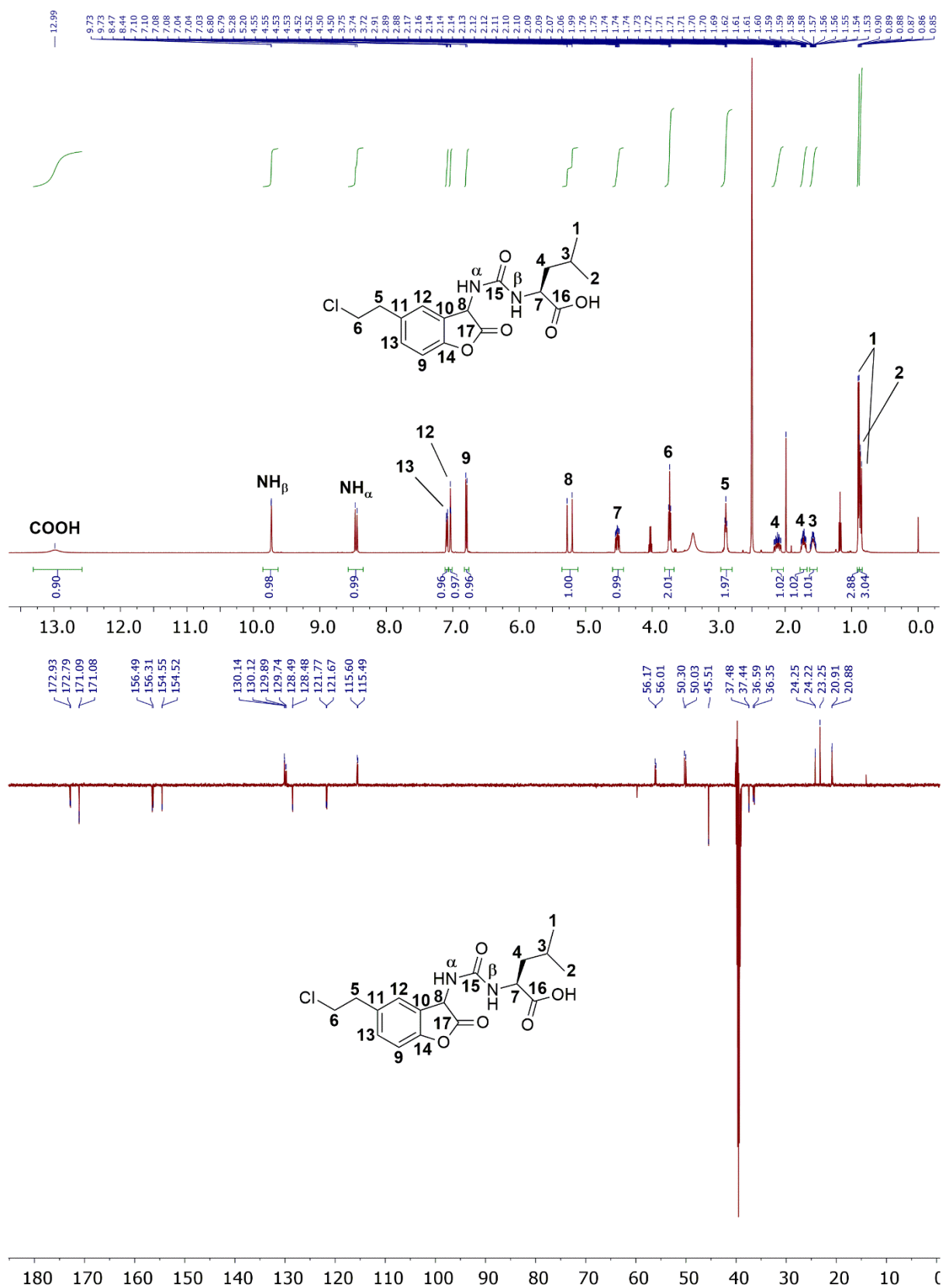


Figure 77: ^1H - and ^{13}C -NMR-spectrum of (2S)-2-(3-(5-(2-chloroethyl)-2-oxo-2,3-dihydrobenzofuran-3-yl)ureido)-4-methylpentanoic acid (**302**) in DMSO-d_6 .

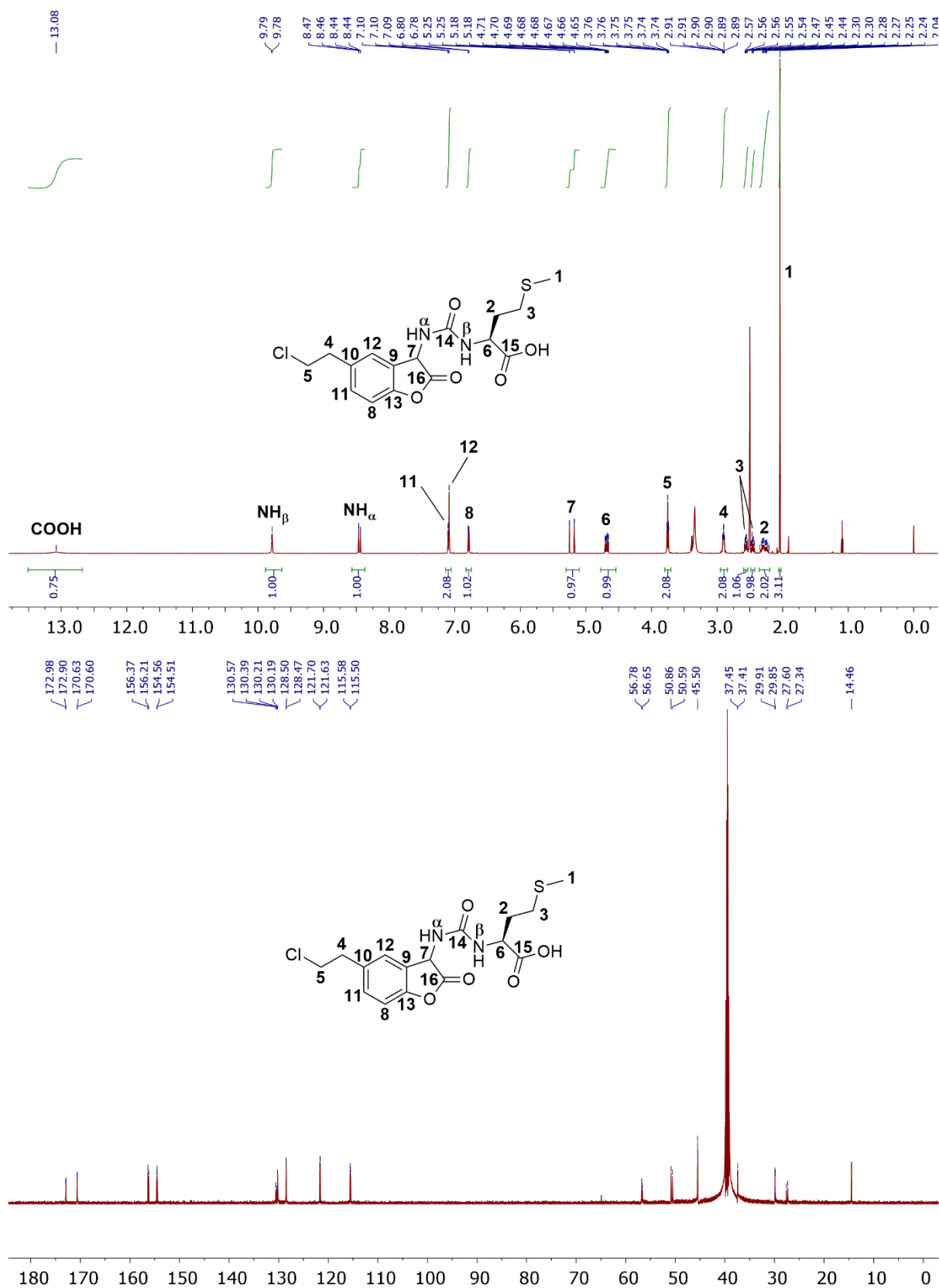


Figure 78: ¹H- and ¹³C-NMR-spectrum of (2S)-2-(3-(5-(2-chloroethyl)-2-oxo-2,3-dihydrobenzofuran-3-yl)ureido)-4-(methylthio)butanoic acid (**304**) in DMSO-d₆.

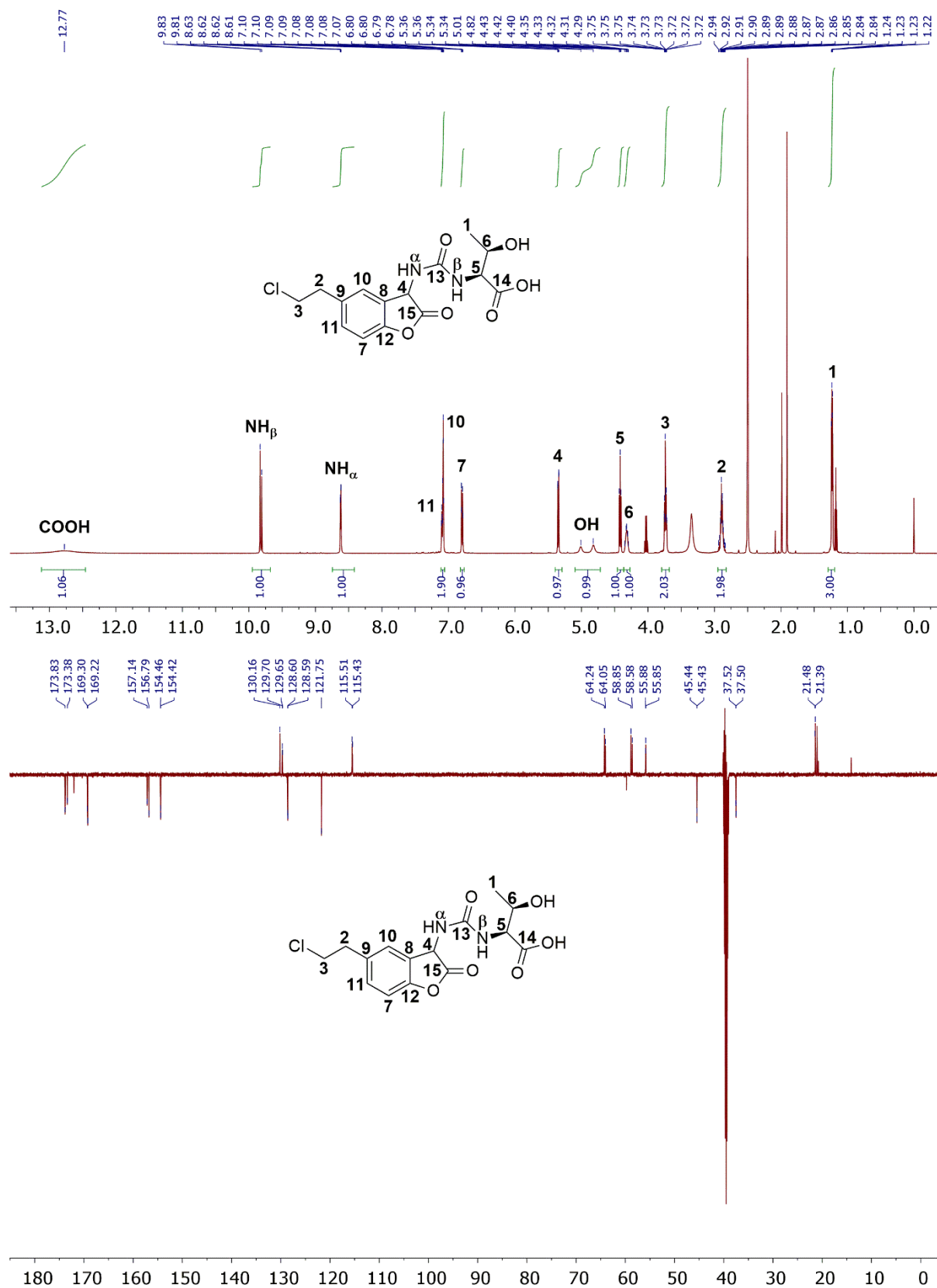


Figure 79: ¹H- and ¹³C-NMR-spectrum of (2*S*,3*R*)-2-(3-(5-(2-chloroethyl)-2-oxo-2,3-dihydrobenzofuran-3-yl)ureido)-3-hydroxybutanoic acid (**310**) in DMSO-d₆.

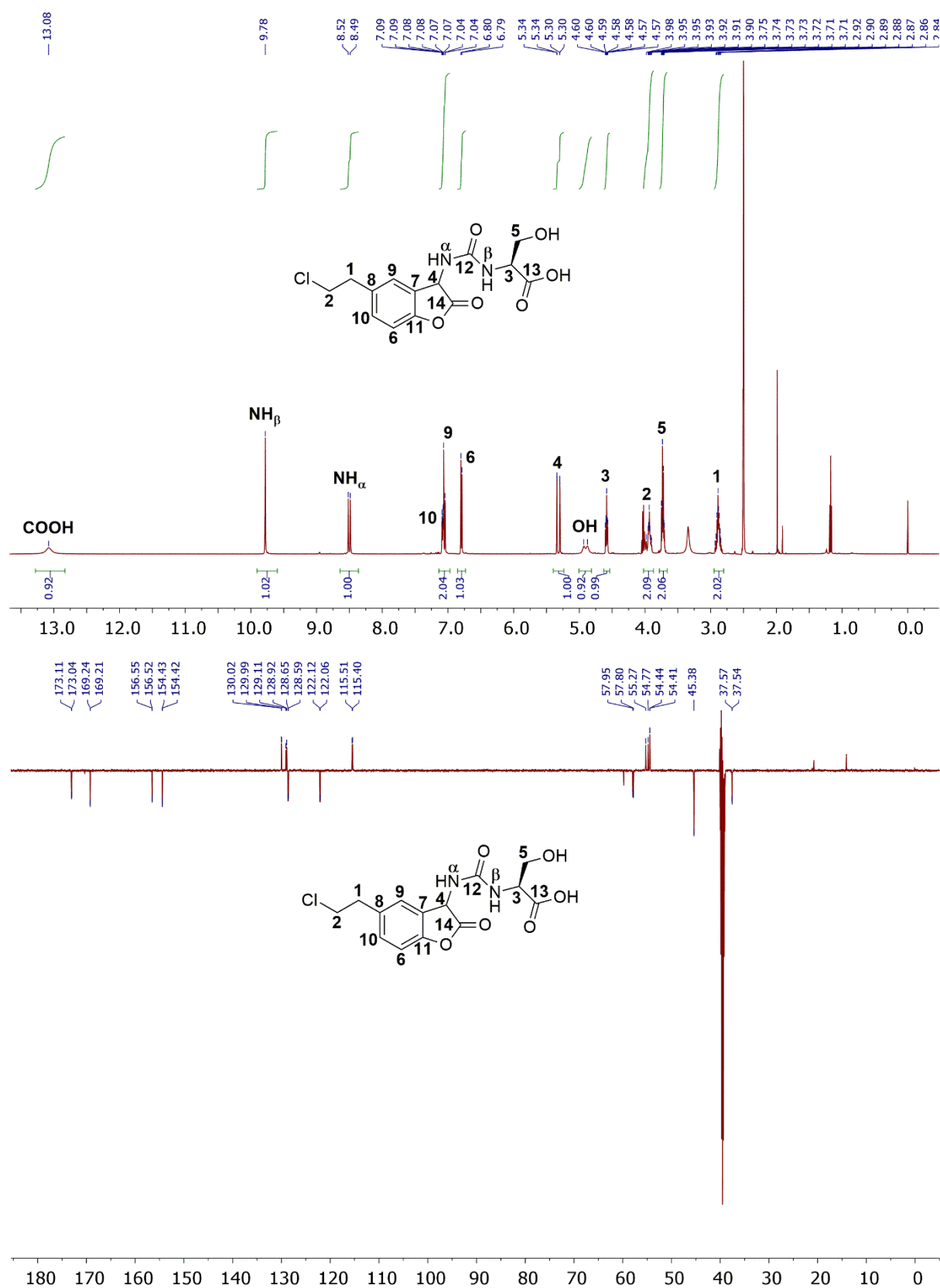


Figure 80: ^1H - and ^{13}C -NMR-spectrum of (2S)-2-(3-(5-(2-chloroethyl)-2-oxo-2,3-dihydrobenzofuran-3-yl)ureido)-3-hydroxypropanoic acid (**319**) in DMSO-d_6 .

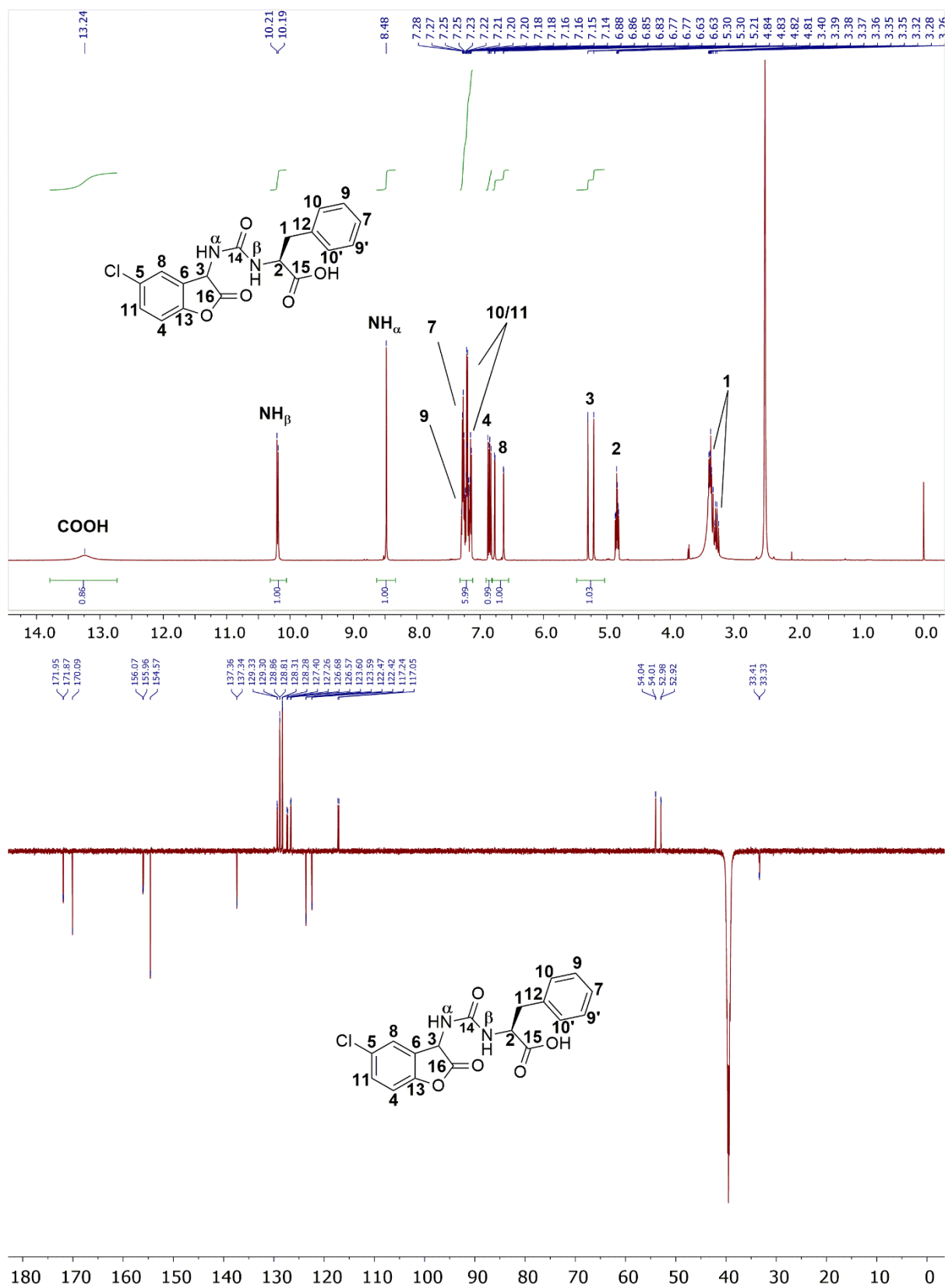


Figure 81: ¹H- and ¹³C-NMR-spectrum of (2*S*)-2-(3-(5-chloro-2-oxo-2,3-dihydrobenzofuran-3-yl)ureido)-3-phenylpropanoic acid (**314**) in DMSO-*d*₆.

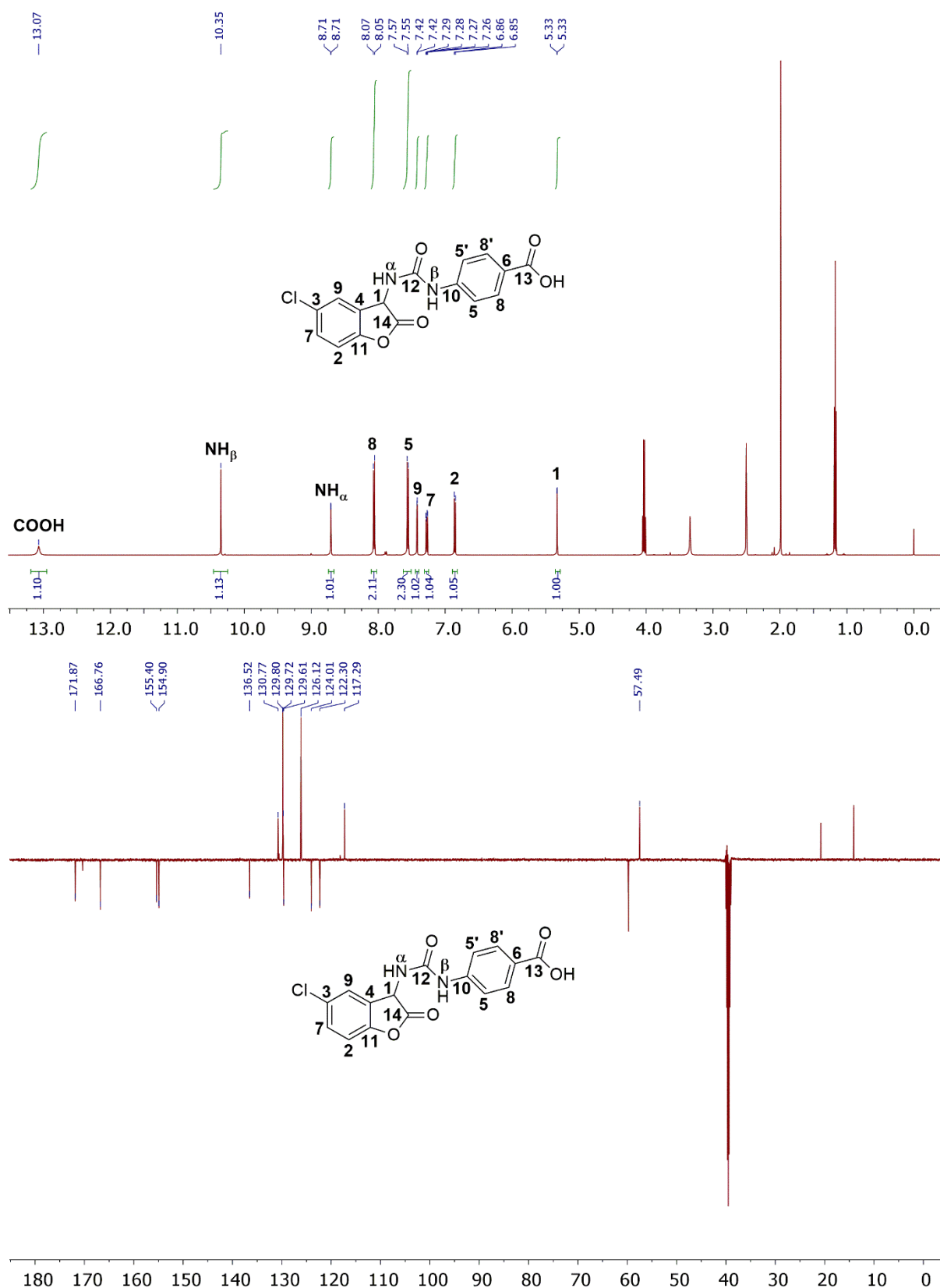


Figure 82: ¹H- and ¹³C-NMR-spectrum of 4-(3-(5-chloro-2-oxo-2,3-dihydrobenzofuran-3-yl)ureido)benzoic acid (**327**) in DMSO-d₆.

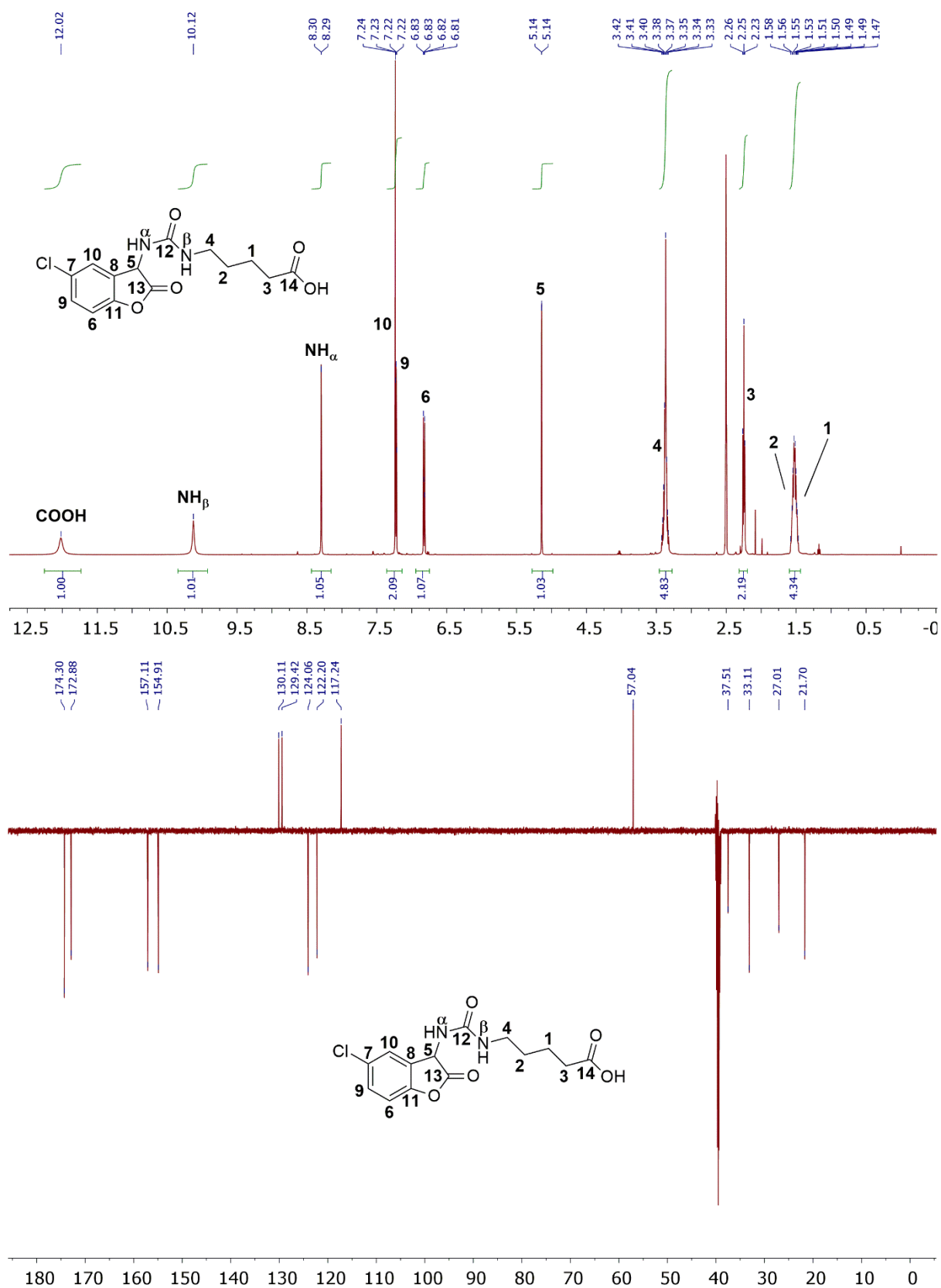


Figure 83: ^1H - and ^{13}C -NMR-spectrum of 5-(3-(5-chloro-2-oxo-2,3-dihydrobenzofuran-3-yl)ureido)pentanoic acid (328) in DMSO- d_6 .

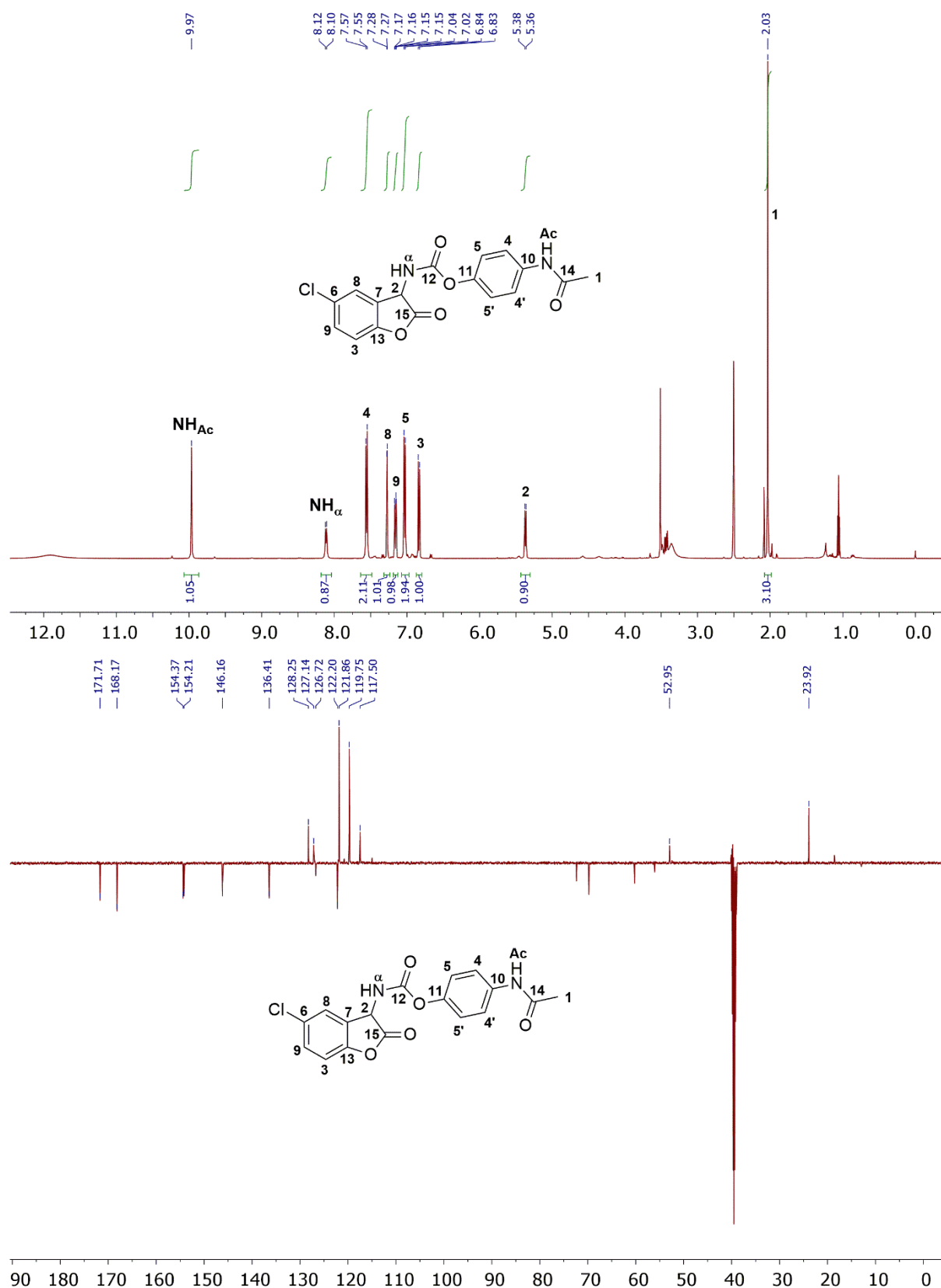


Figure 84: ^1H - and ^{13}C -NMR-spectrum of 4-acetamidophenyl (5-chloro-2-oxo-2,3-dihydrobenzofuran-3-yl)carbamate (**370**) in DMSO-d_6 .

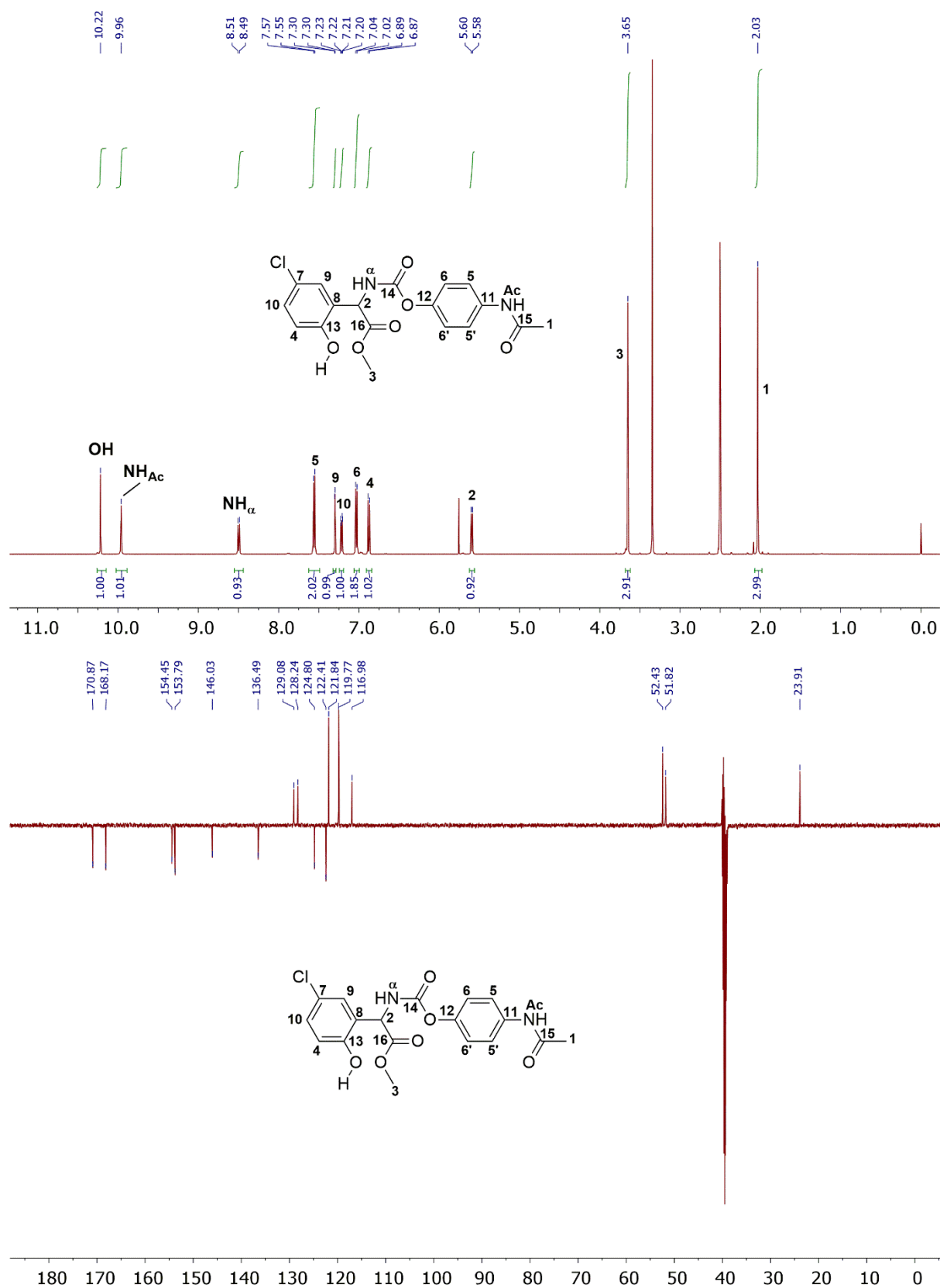


Figure 85: ^1H - and ^{13}C -NMR-spectrum of methyl 2-(((4-acetamidophenoxy)carbonyl)amino)-2-(5-chloro-2-hydroxyphenyl)acetate (**376**) in DMSO-d_6 .

7. Analytical data and spectra

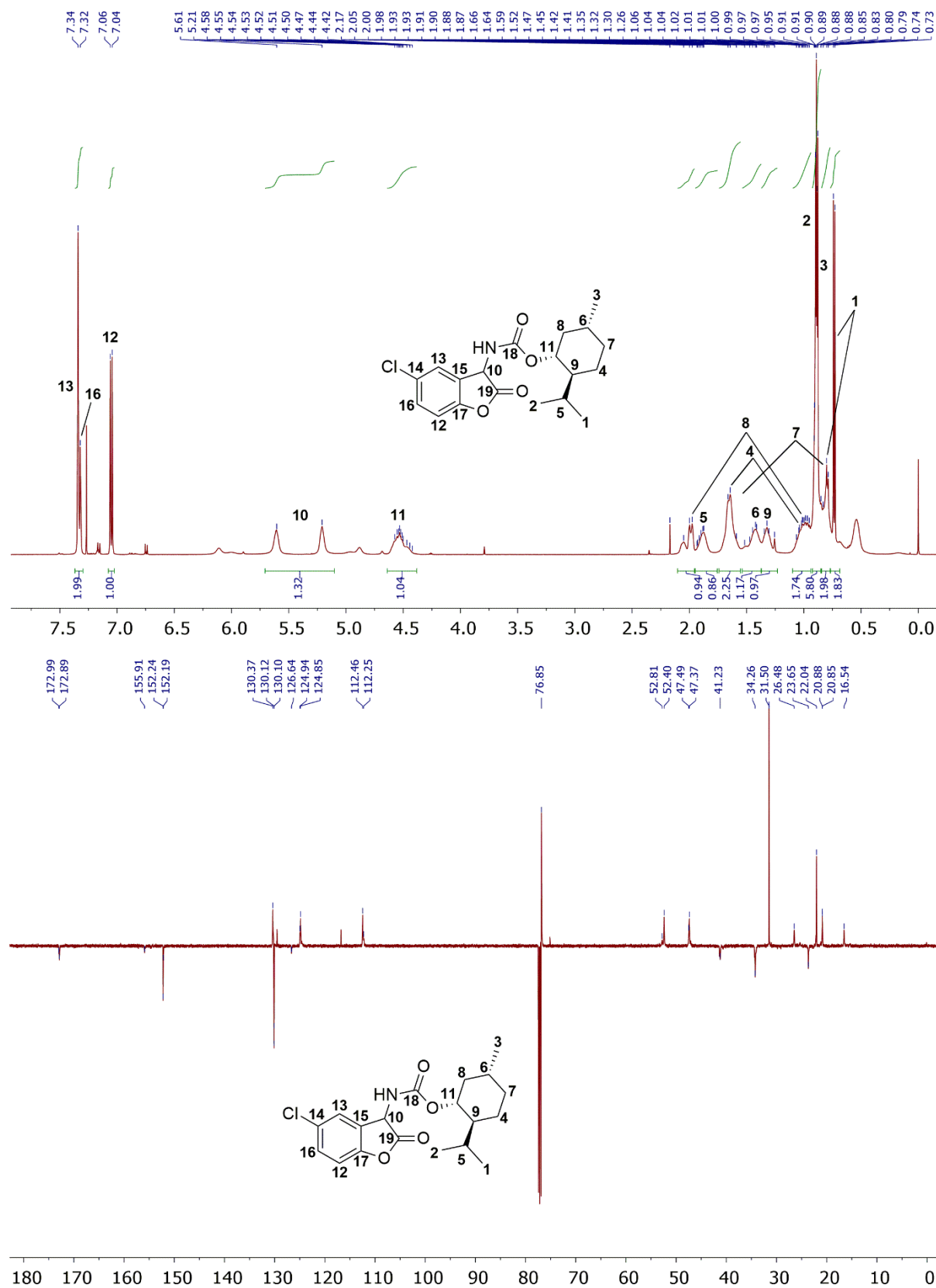


Figure 86: ¹H- and ¹³C-NMR-spectrum of (1*R*,2*S*,5*R*)-2-isopropyl-5-methylcyclohexyl (5-chloro-2-oxo-2,3-dihydrobenzofuran-3-yl)carbamate (**371**) in CDCl₃.

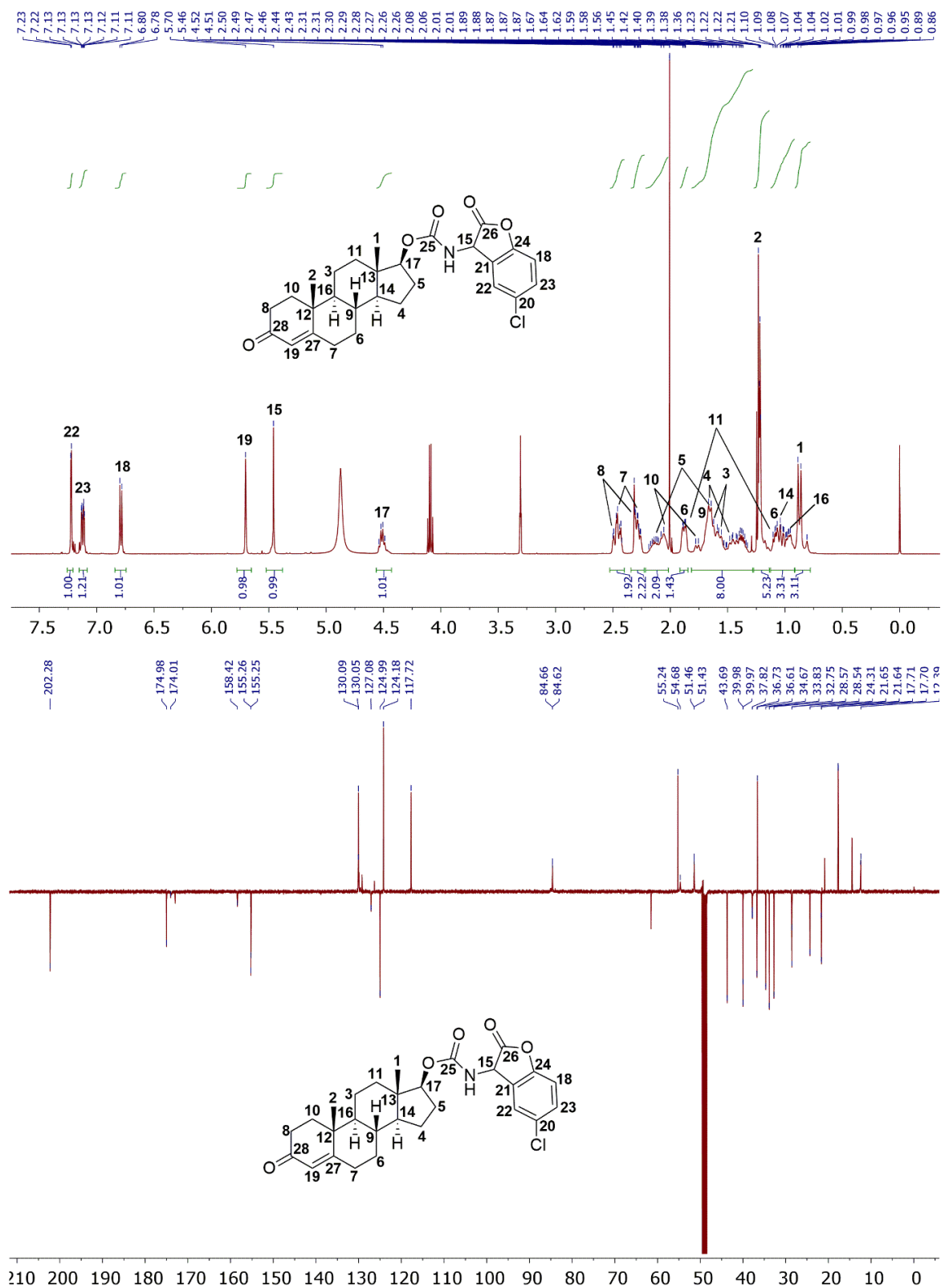


Figure 87: ^1H - and ^{13}C -NMR-spectrum of (8*R*,9*S*,10*R*,13*S*,14*S*,17*S*)-10,13-dimethyl-3-oxo-2,3,6,7,8,9,10,11,12,13,14,15,16,17-tetradecahydro-1*H*-cyclopenta[*a*]phenanthren-17-yl (5-chloro-2-oxo-2,3-dihydrobenzofuran-3-yl)-carbamate (**372**) in MeOD- d_3 .

7. Analytical data and spectra

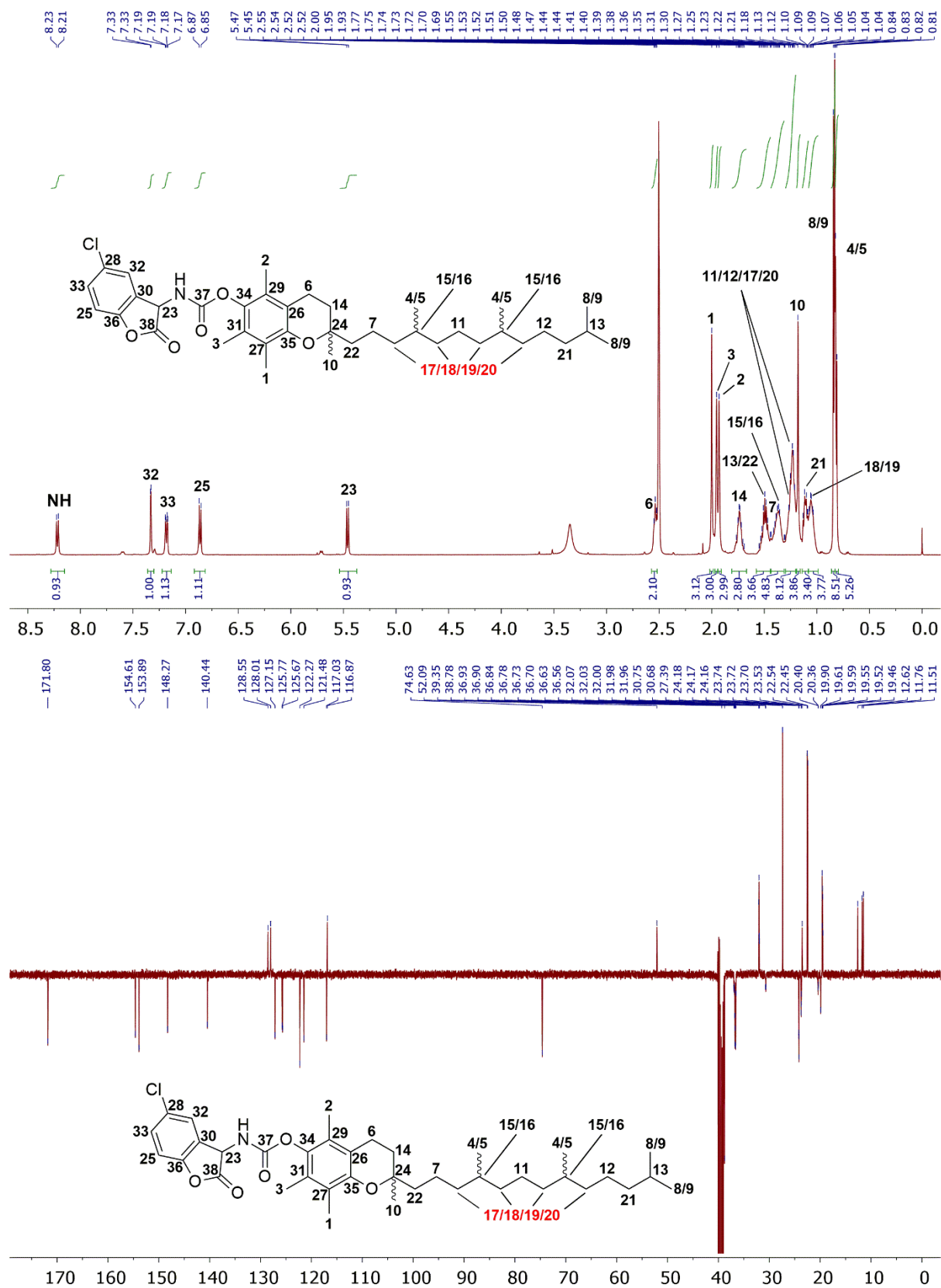


Figure 88: ^1H - and ^{13}C -NMR-spectrum of 2,5,7,8-tetramethyl-2-(4,8,12-trimethyltridecyl)chroman-6-yl (5-chloro-2-oxo-2,3-dihydrobenzofuran-3-yl)carbamate (**373**) in DMSO-d_6 .

7. Analytical data and spectra

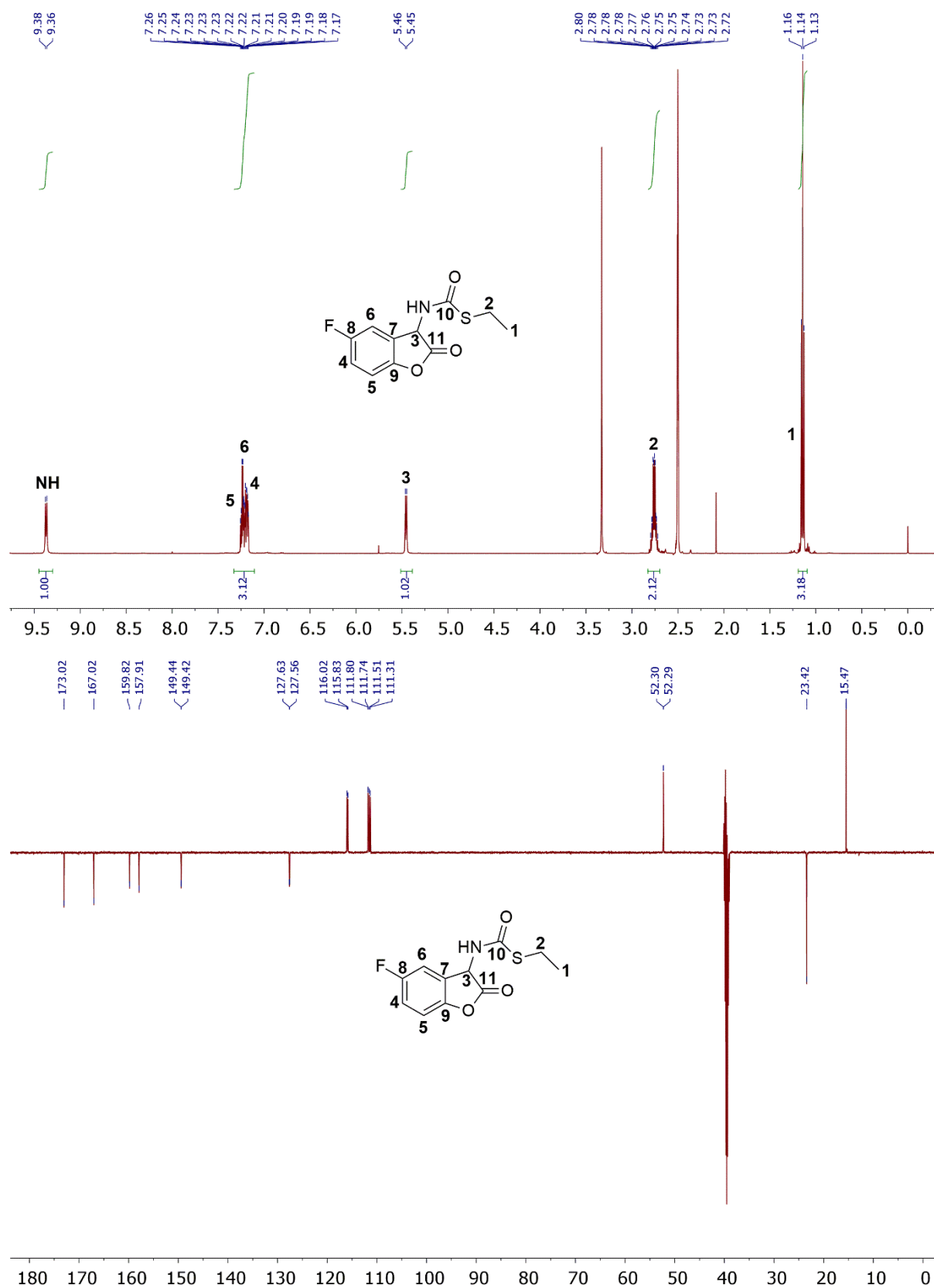


Figure 89: ^1H - and ^{13}C -NMR-spectrum of *S*-ethyl (5-fluoro-2-oxo-2,3-dihydrobenzofuran-3-yl)carbamothioate (**405**) in DMSO-d_6 .

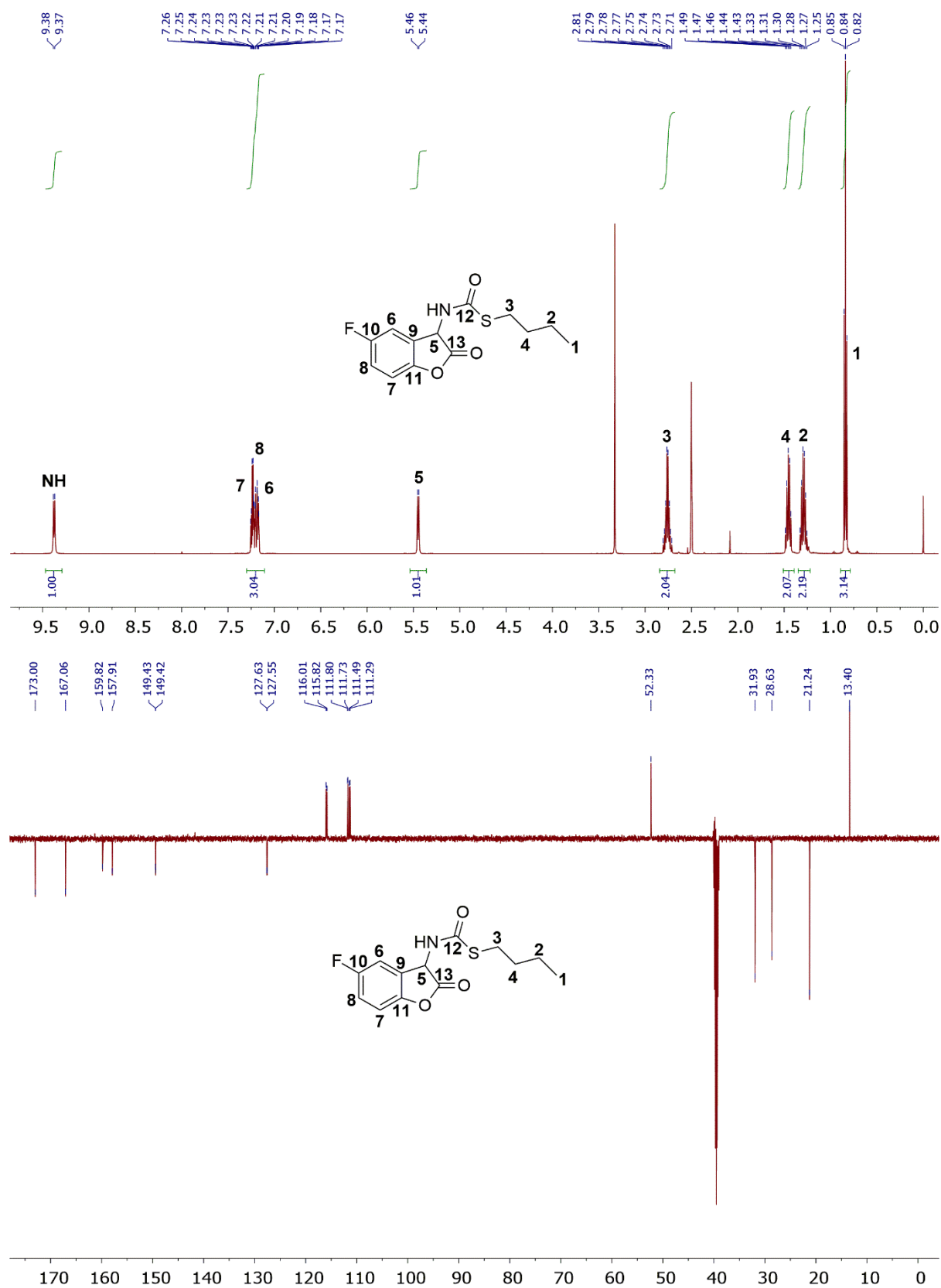


Figure 90: ¹H- and ¹³C-NMR-spectrum of *S*-butyl (5-fluoro-2-oxo-2,3-dihydrobenzofuran-3-yl)carbamothioate (**406**) in DMSO-d₆.

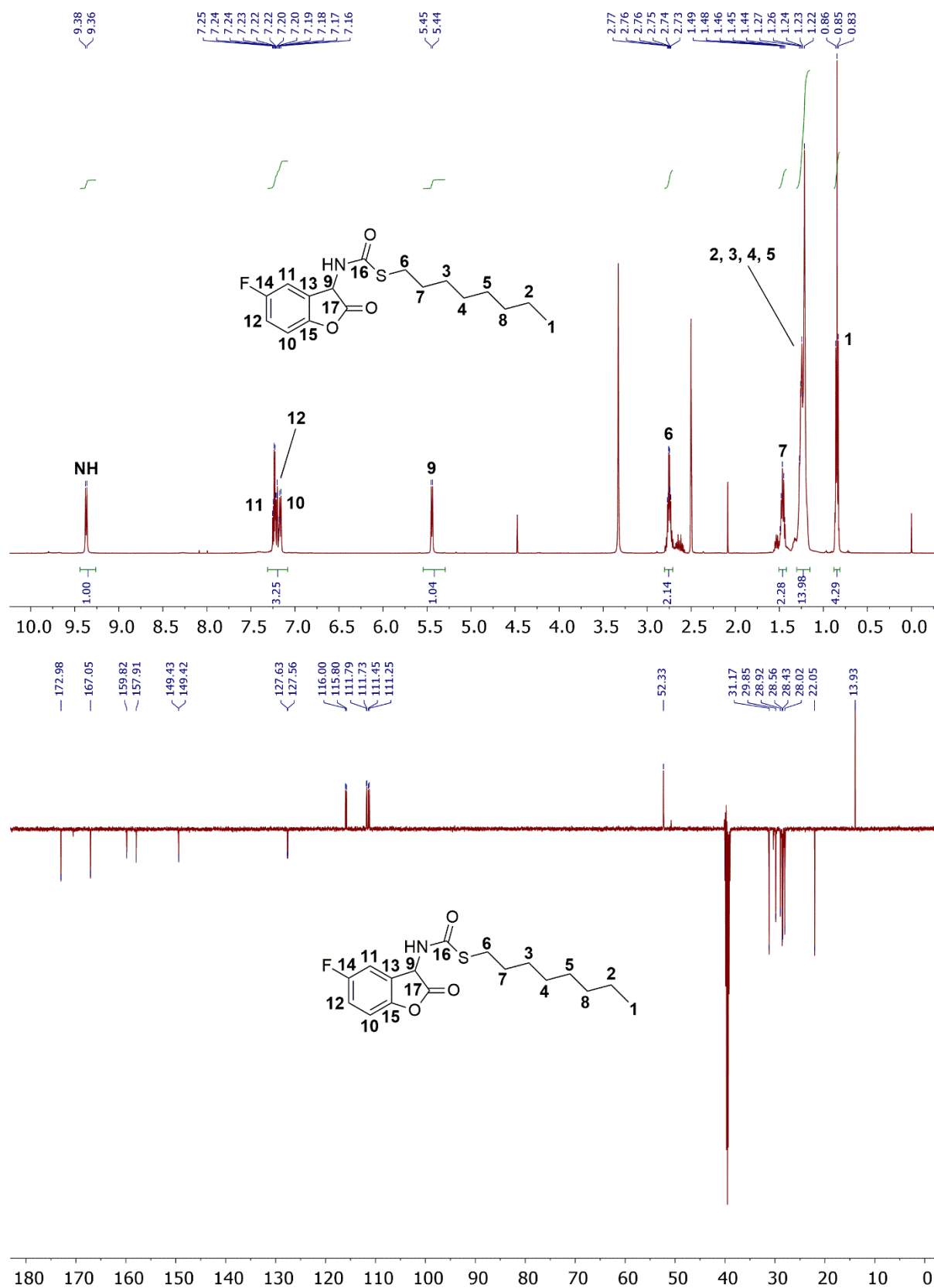


Figure 91: ¹H- and ¹³C-NMR-spectrum of *S*-octyl (5-fluoro-2-oxo-2,3-dihydrobenzofuran-3-yl)carbamothioate (**407**) in DMSO-d₆.

7. Analytical data and spectra

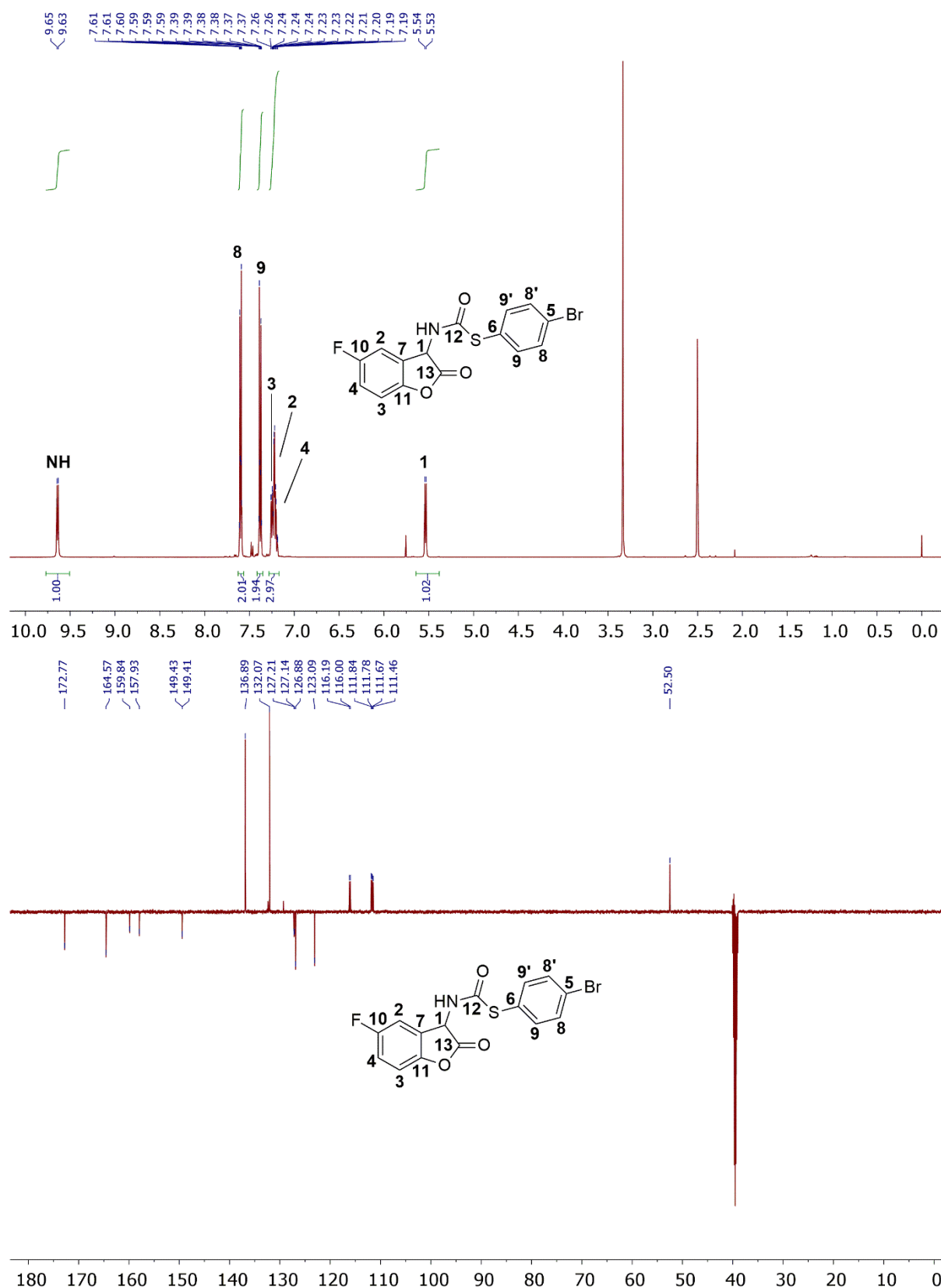


Figure 92: ¹H- and ¹³C-NMR-spectrum of *S*-(4-bromophenyl) (5-fluoro-2-oxo-2,3-dihydrobenzofuran-3-yl)carbamothioate (**403**) in DMSO-*d*₆.

7. Analytical data and spectra

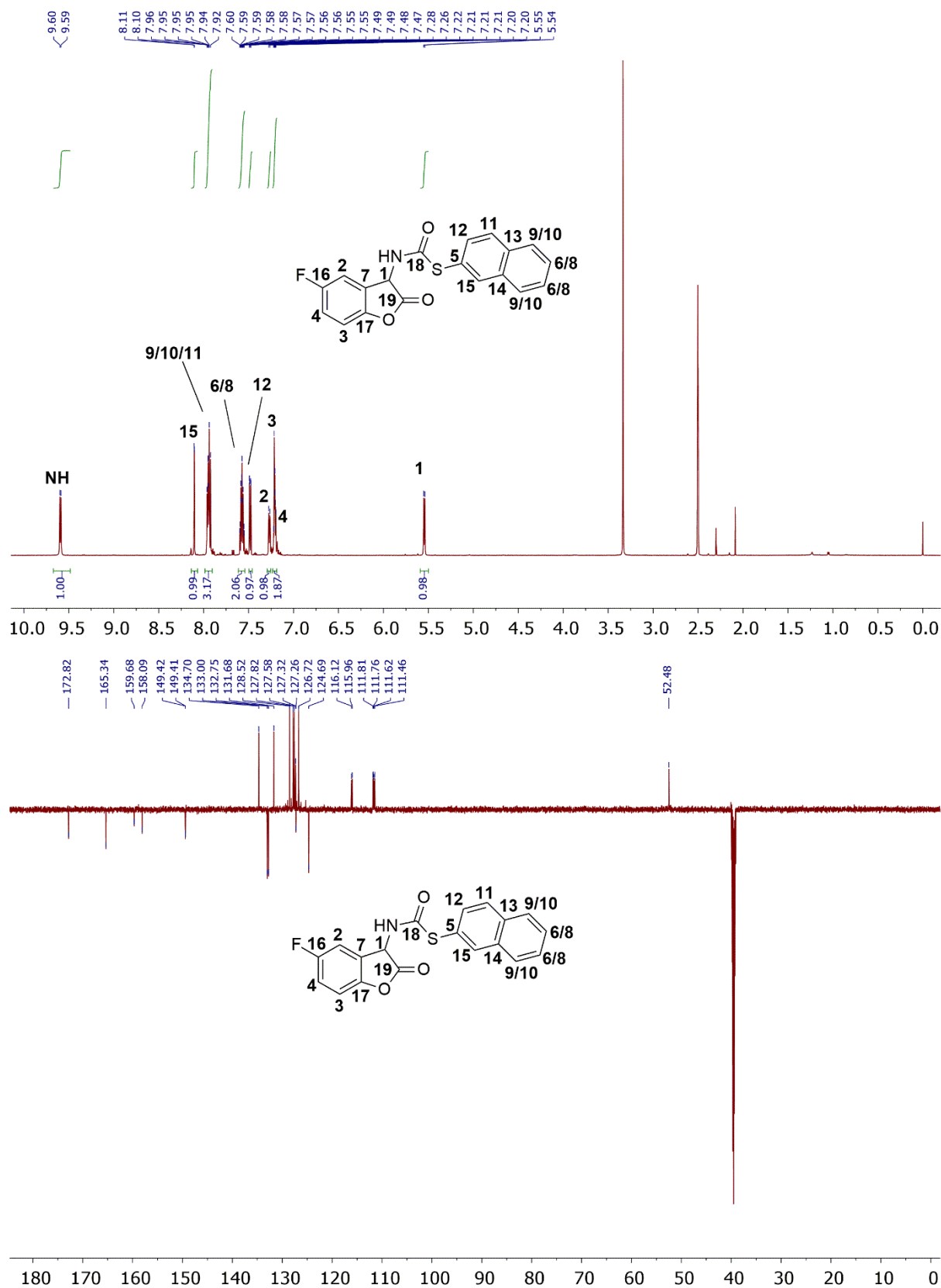
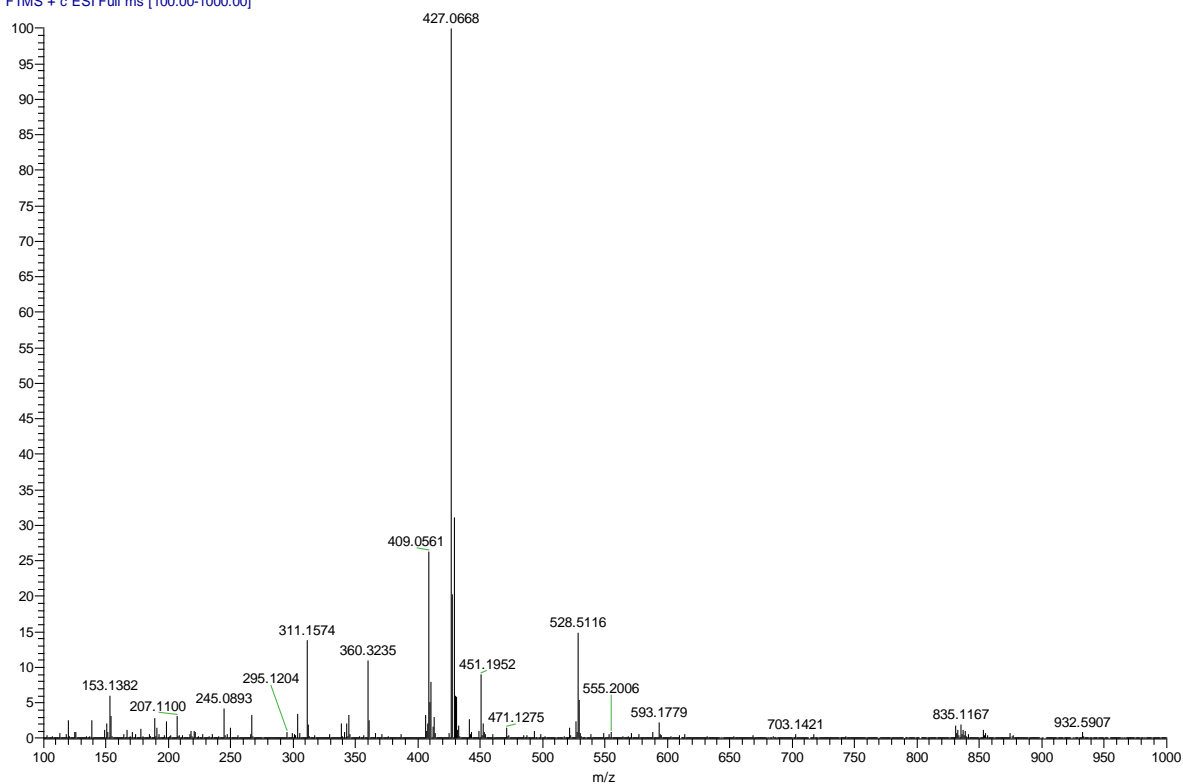


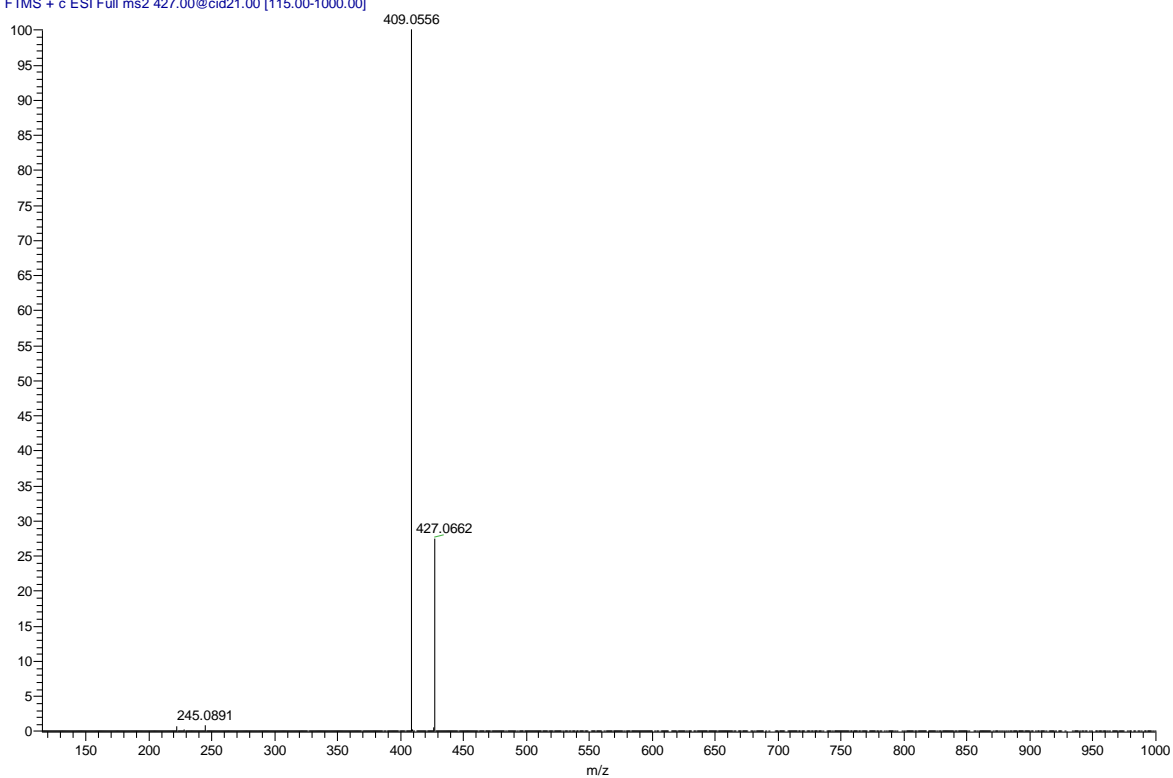
Figure 93: ^1H - and ^{13}C -NMR-spectrum of *S*-naphthalen-2-yl (5-fluoro-2-oxo-2,3-dihydrobenzofuran-3-yl)carbamothioate (404) in DMSO-d_6 .

7.1.3 Decomposition experiments

TML_284b #1-60 RT: 0.01-0.47 AV: 60 NL: 1.45E7
T: FTMS + c ESI Full ms [100.00-1000.00]



TML_284b@CID #1-58 RT: 0.01-0.64 AV: 58 NL: 4.07E6
T: FTMS + c ESI Full ms2 427.00@cid21.00 [115.00-1000.00]



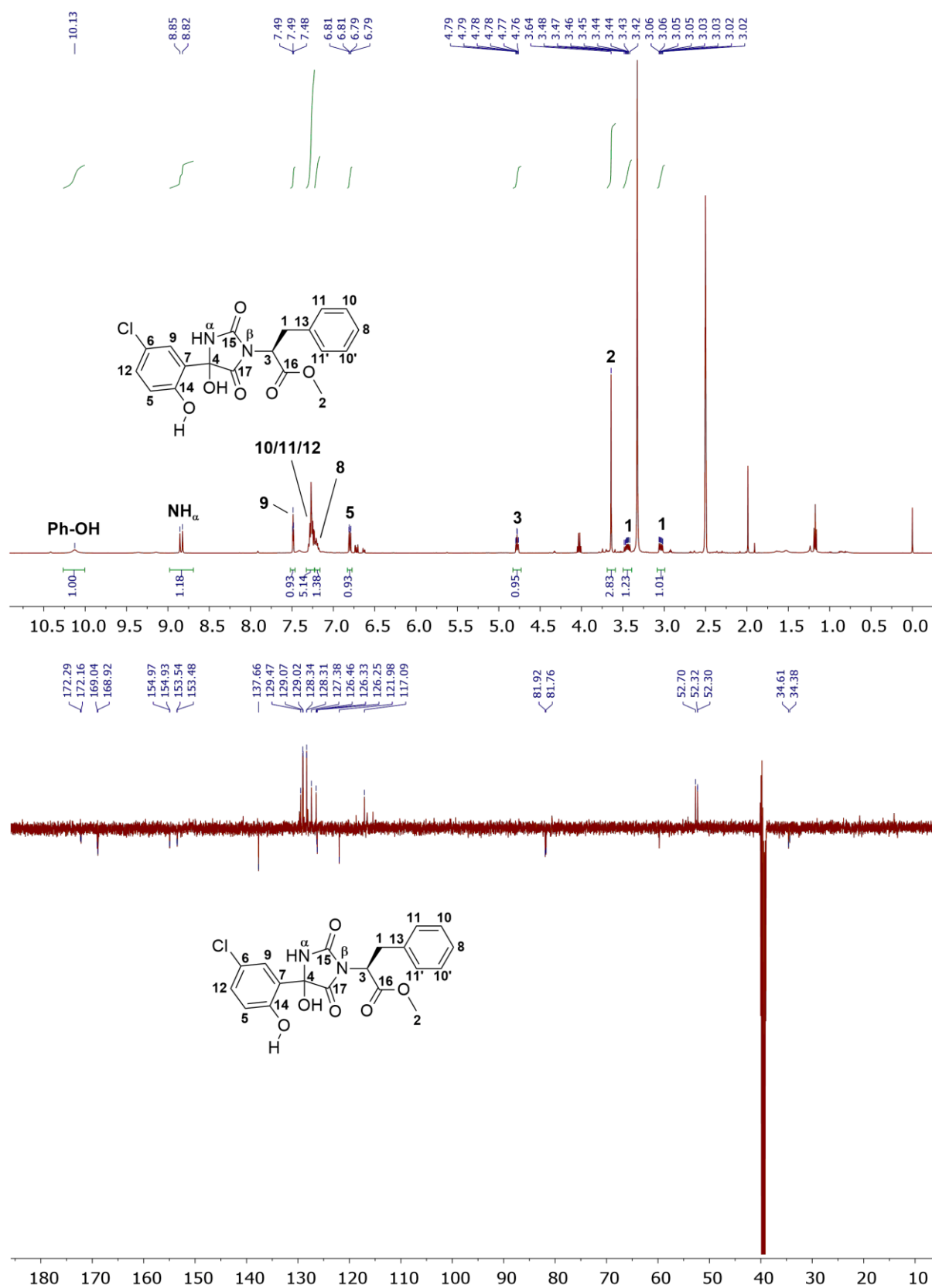


Figure 94: ESI-, ¹H- and ¹³C-NMR-spectrum of (2*S*)-methyl 2-(4-(5-chloro-2-hydroxyphenyl)-4-hydroxy-2,5-dioximidazolidin-1-yl)-3-phenylpropanoate (**329**) in DMSO-d₆.

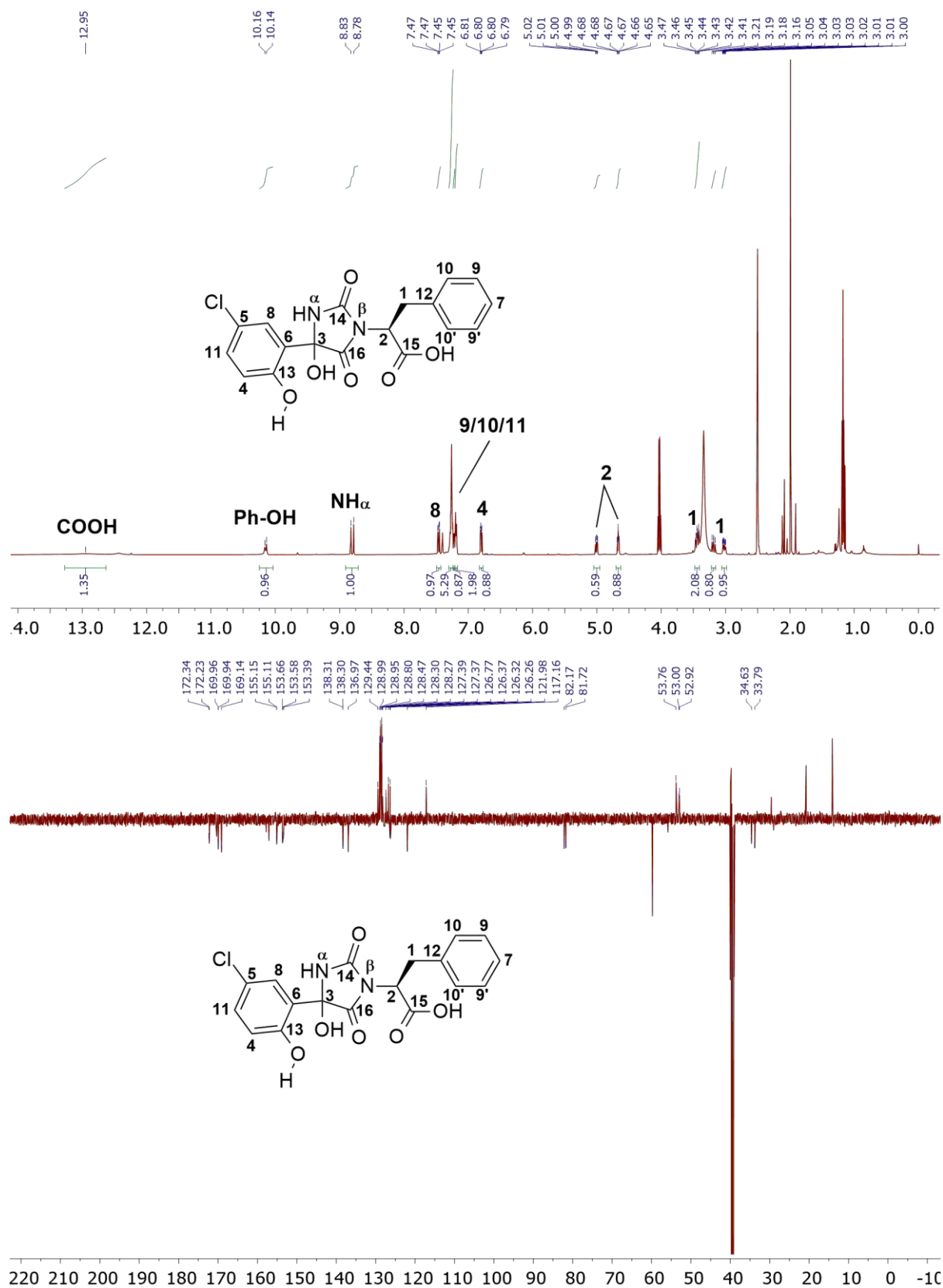


Figure 95: ¹H- and ¹³C-NMR-spectrum of (2S)-2-(4-(5-chloro-2-hydroxyphenyl)-4-hydroxy-2,5-dioximidazolidin-1-yl)-3-phenylpropanoic acid (**331**) in DMSO-d₆.

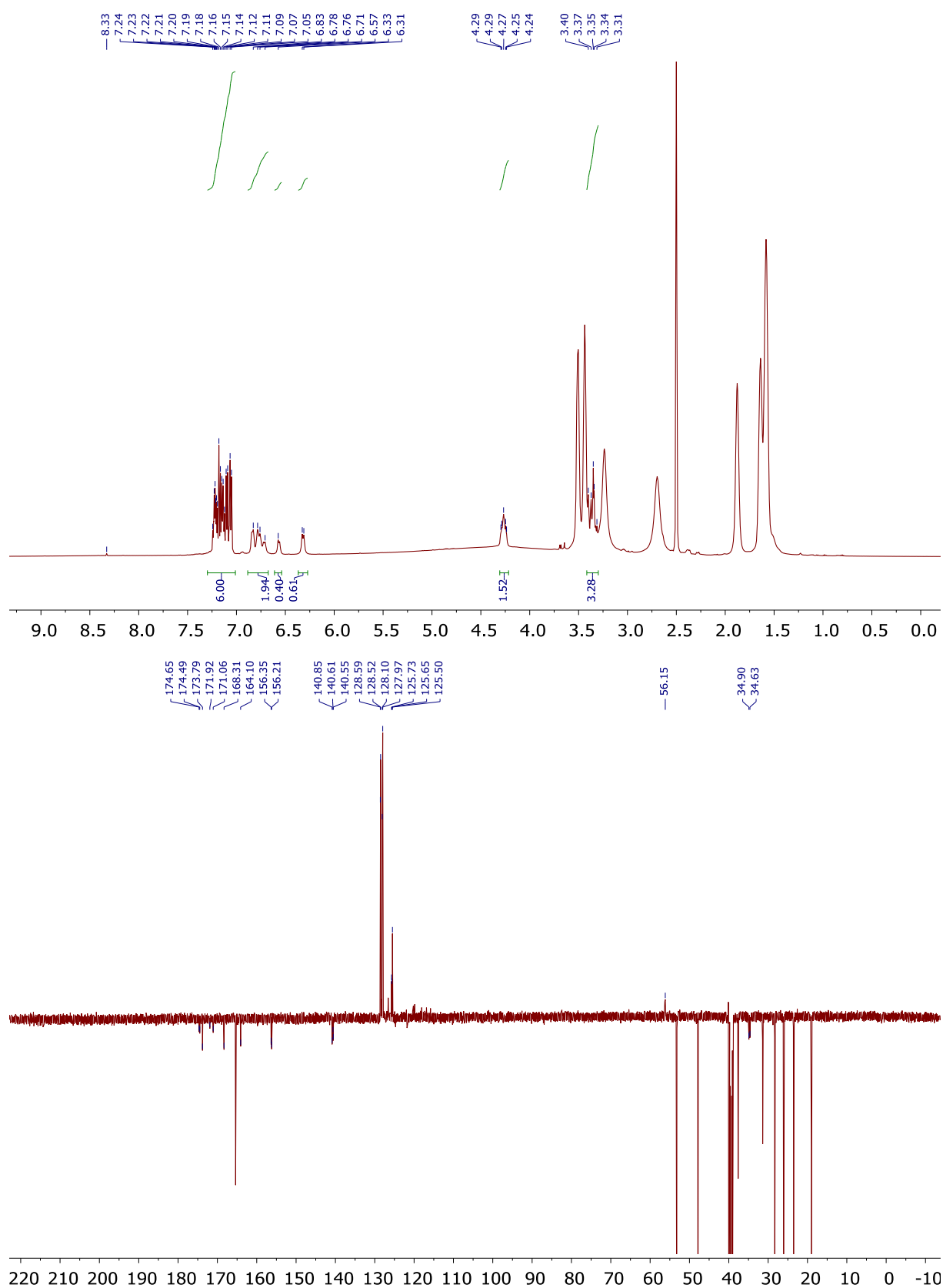


Figure 96: ¹H- and ¹³C-NMR-spectrum of (2*S*)-2-(4-(5-chloro-2-hydroxyphenyl)-4-hydroxy-2,5-dioximidazolidin-1-yl)-3-phenylpropanoic acid (**314**) in DMSO-*d*₆ before protonation (Contaminated with DBU).

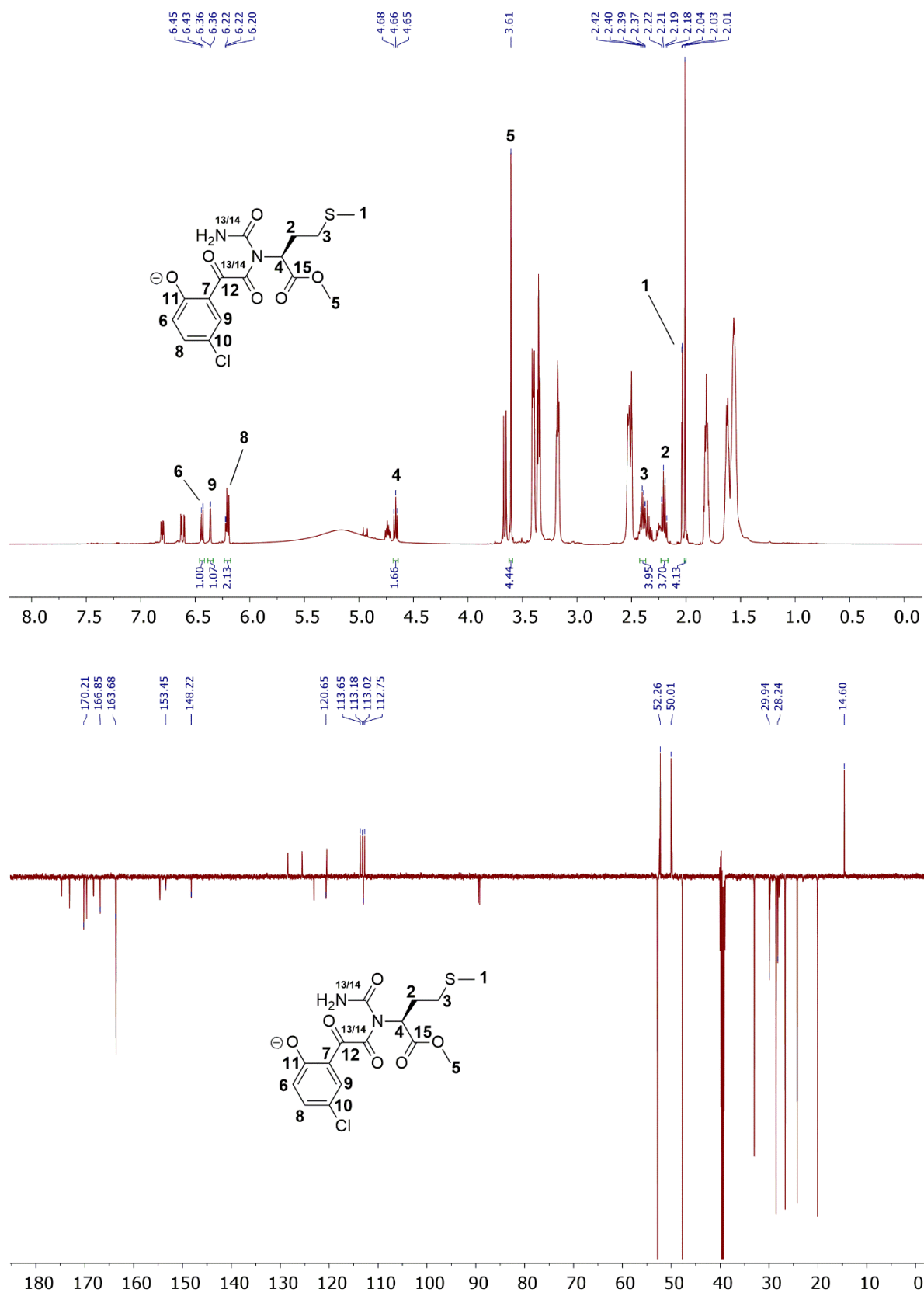


Figure 98: ^1H - and ^{13}C -NMR-spectrum of (*S*)-4-chloro-2-(2-(1-(1-methoxy-4-(methylthio)-1-oxobutan-2-yl)ureido)-2-oxoacetyl)phenolate (**333A**) in DMSO-d_6 .

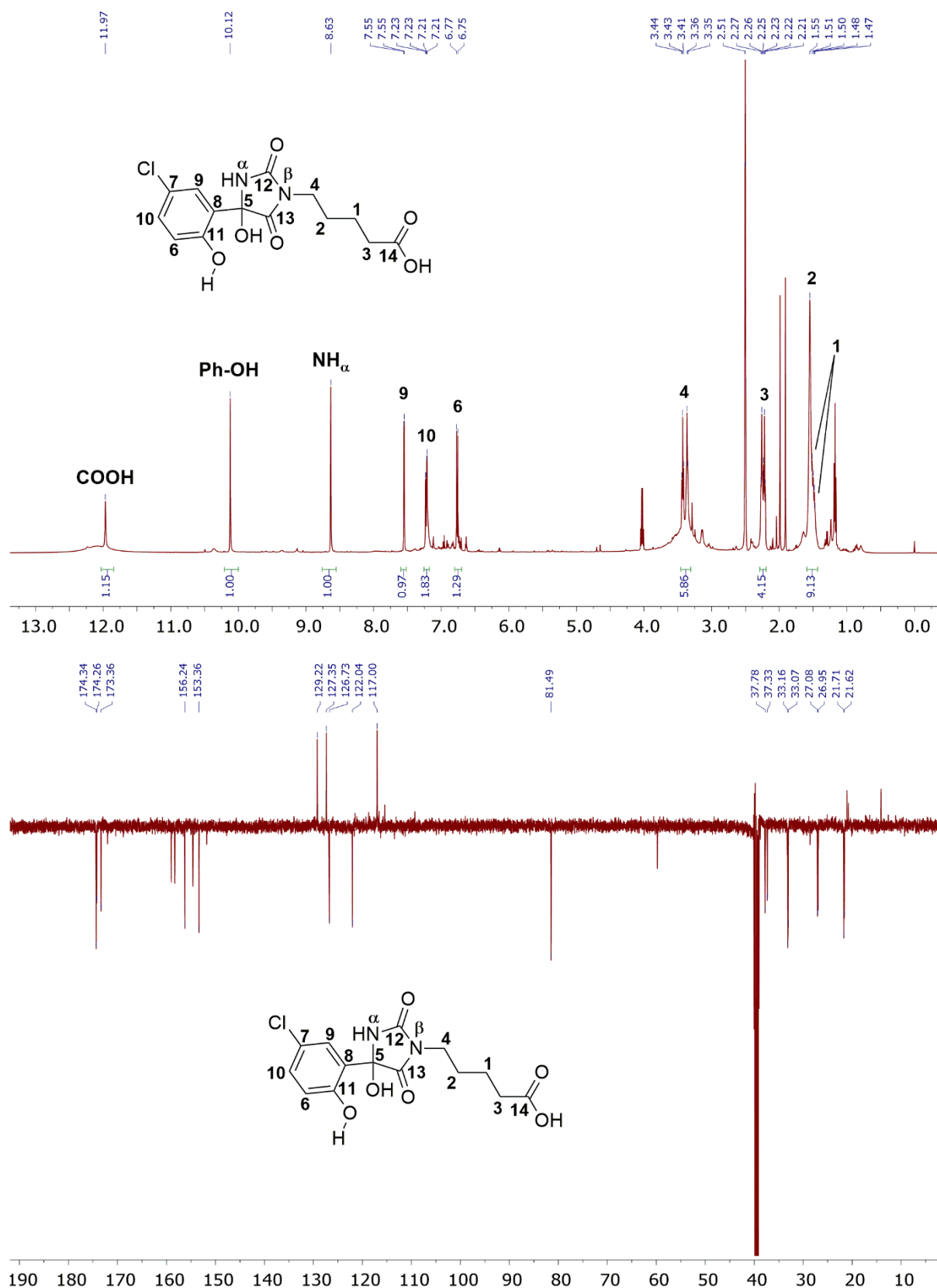


Figure 99: ¹H- and ¹³C-NMR-spectrum of 5-(4-(5-chloro-2-hydroxyphenyl)-4-hydroxy-2,5-dioximidazolidin-1-yl)pentanoic acid (**334**) in DMSO-d₆.

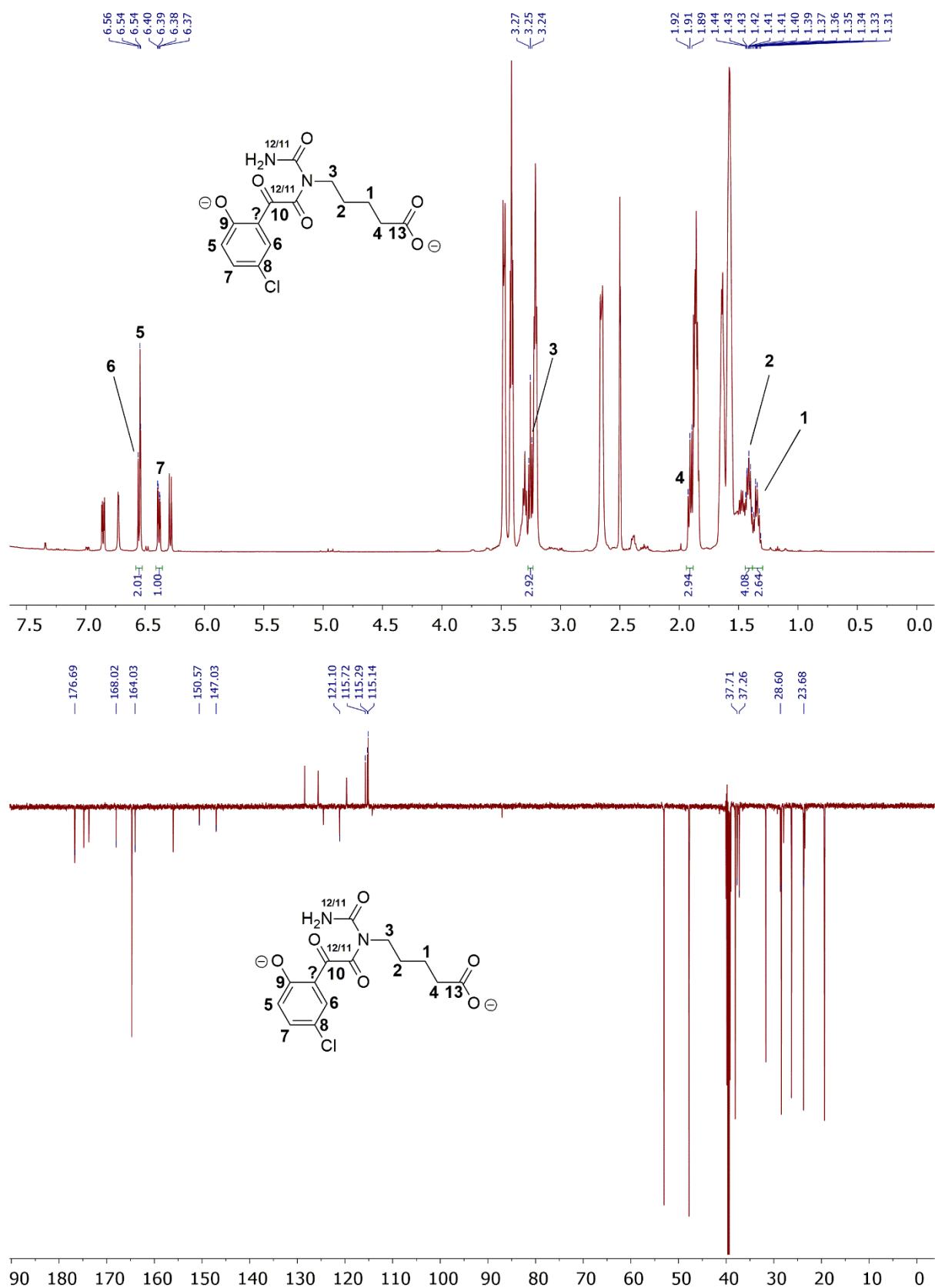


Figure 100: ¹H- and ¹³C-NMR-spectrum of 5-(N-carbamoyl-2-(5-chloro-2-oxidophenyl)-2-oxoacetamido)pentanoate (**335A**) in DMSO-d₆.

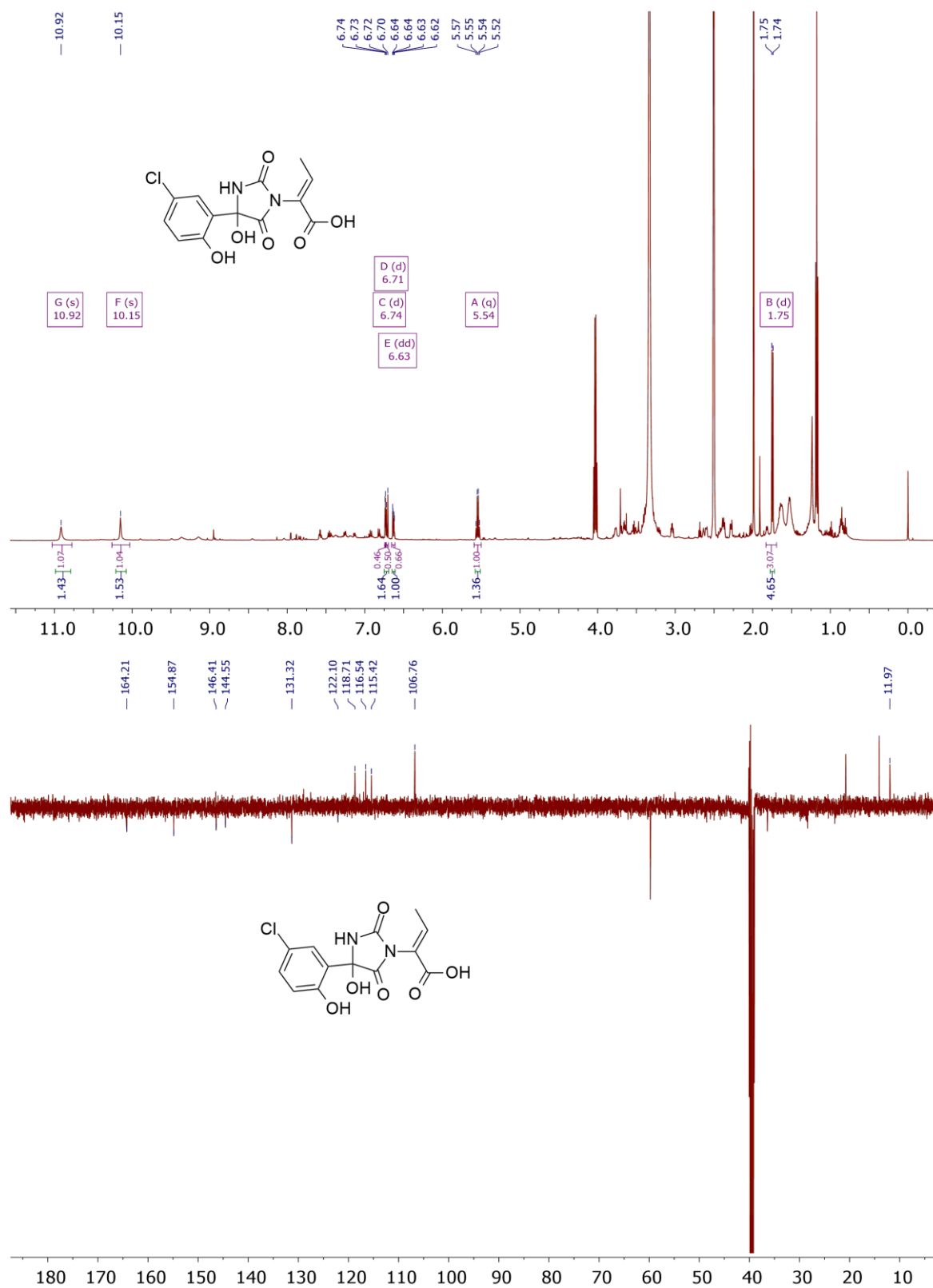


Figure 101: ¹H- and ¹³C-NMR-spectrum of the decomposition experiment of urea-coumaranone (**309**) in DMSO-d₆ (Contaminated with various byproducts). 2-(3-(5-chloro-2-oxo-2,3-dihydrobenzofuran-3-yl)ureido)but-2-enoic acid (**338**) is the assumed main product of the experiment after aqueous work-up.

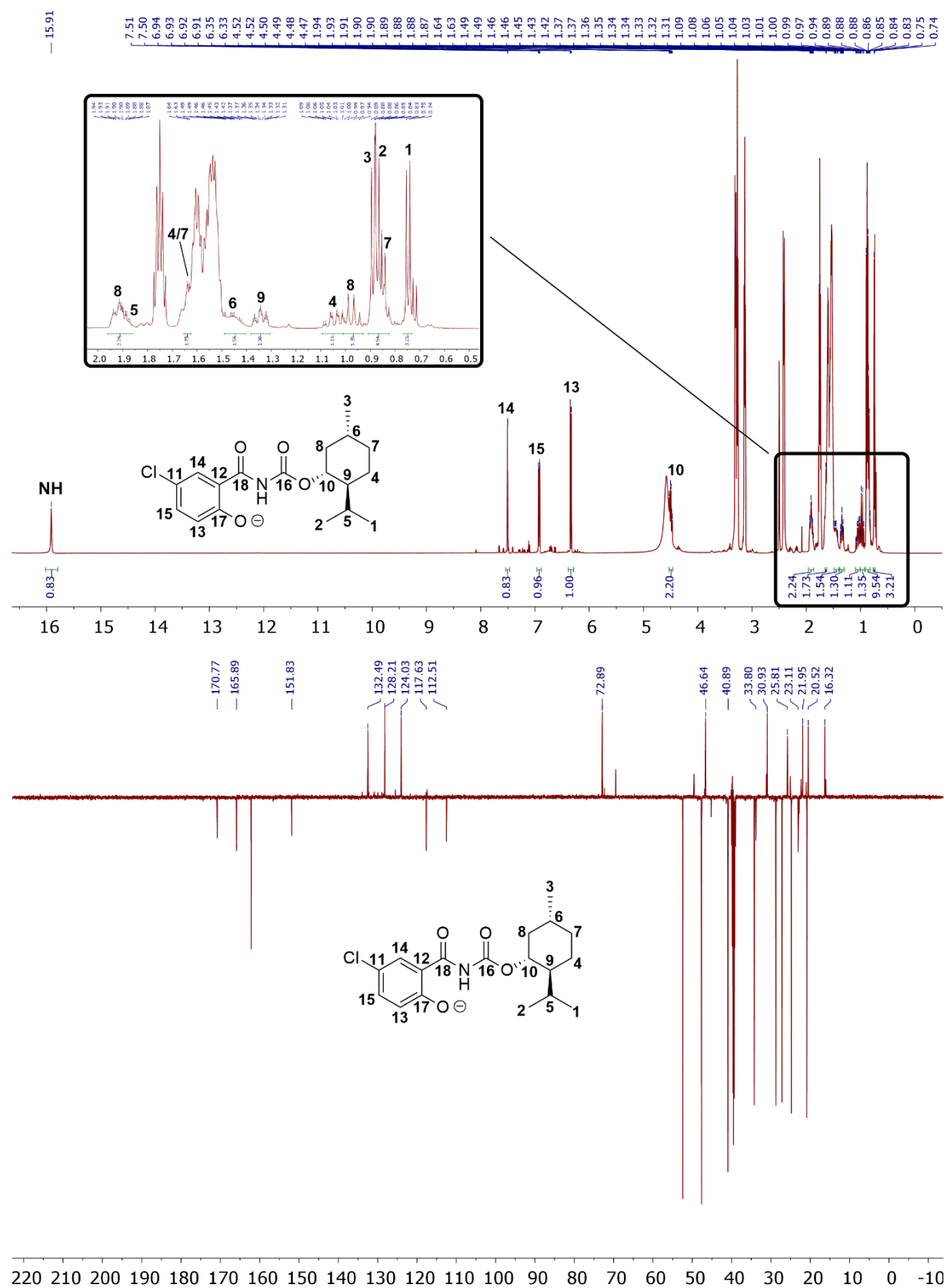


Figure 102: ¹H- and ¹³C-NMR-spectrum of 4-chloro-2-((((1*R*,2*S*,5*R*)-2-isopropyl-5-methylcyclohexyl)oxy)carbonyl)-carbamoylphenolate (**377A**) in DMSO-d₆ (Contaminated with DBU).

7.1.3 CL and photoluminescence spectra of coumaranone compounds

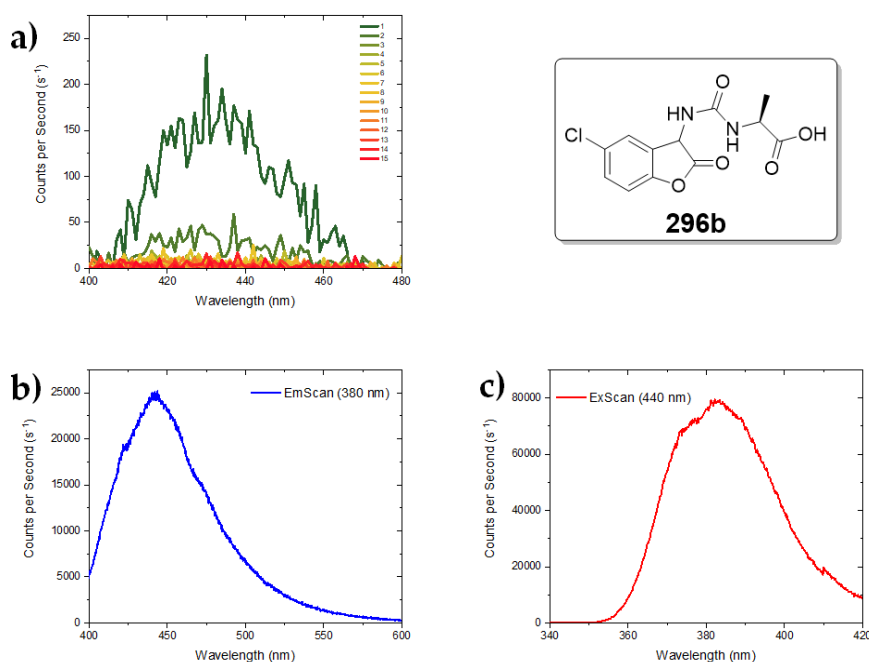


Figure 103: Emission and excitation spectra of **296b** in acetonitrile (every scan took 45 s): (a) emission scans of CL (i.e., without external excitation, Slit: 10), the arrow indicates the decrease in the CL; (b) emission scan of **296b** after CL was finished (external excitation $\lambda_{\text{Ex}} = 380$ nm, Slit: 0.7); (c) excitation scan of **296b** after CL was finished ($\lambda_{\text{Em}} = 440$ nm, Slit: 0.7).

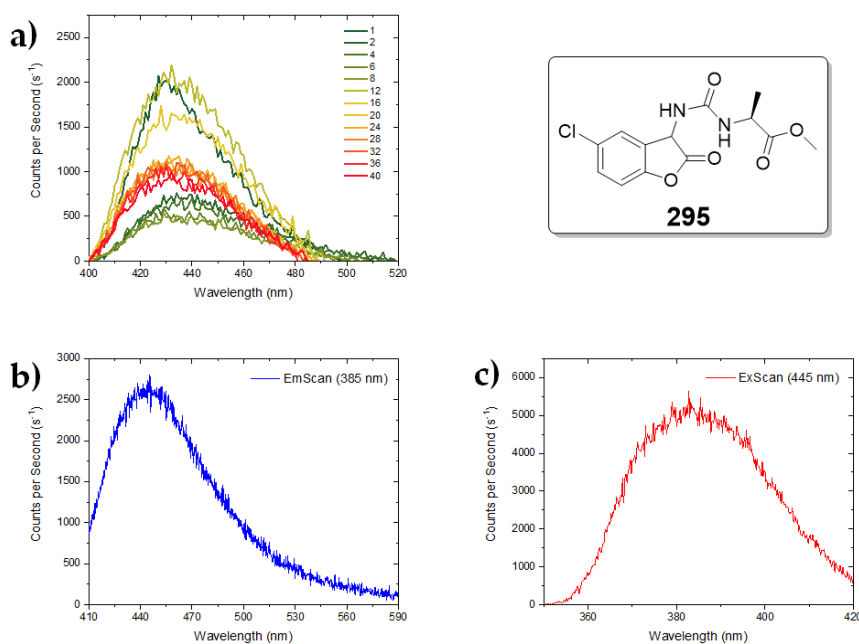


Figure 104: Emission and excitation spectra of **295** in acetonitrile (every scan took 45 s): (a) emission scans of CL (i.e., without external excitation, Slit: 10); (b) emission scan of **295** after CL was finished (external excitation $\lambda_{\text{Ex}} = 385$ nm, Slit: 0.4); (c) excitation scan of **295** after CL was finished ($\lambda_{\text{Em}} = 445$ nm, Slit: 0.4).

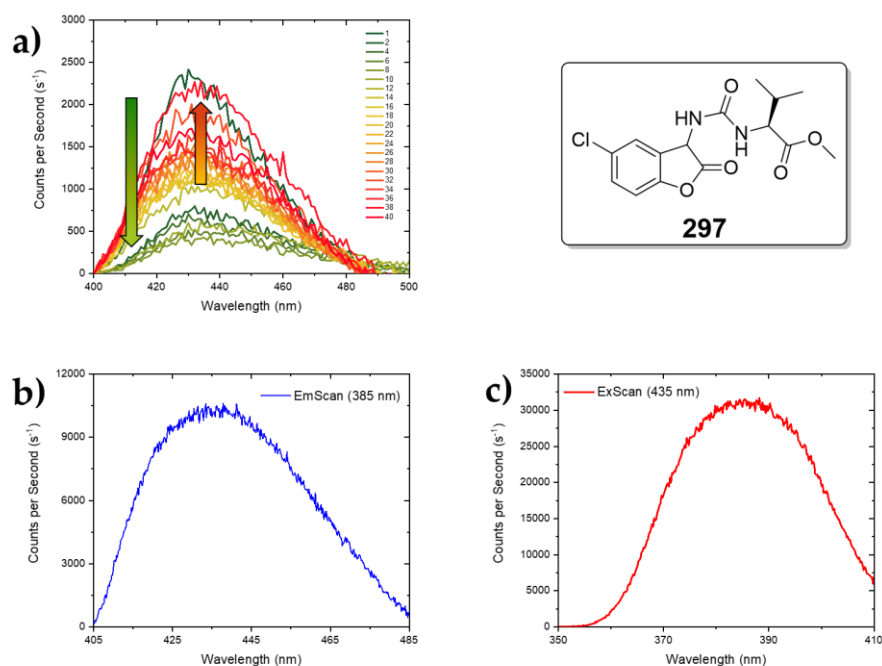


Figure 105: Emission and excitation spectra of **297** in acetonitrile (every scan took 45 s): (a) emission scans of CL (i.e., without external excitation, Slit: 10), the green red arrow indicates the decrease in CL after 10 scans. Starting from the 12th scan, the right red arrow indicates a new increase in CL; (b) emission scan of **297** after CL was finished (external excitation $\lambda_{\text{Ex}} = 385$ nm, Slit: 0.4); (c) excitation scan of **297** after CL was finished ($\lambda_{\text{Em}} = 435$ nm, Slit: 0.4).

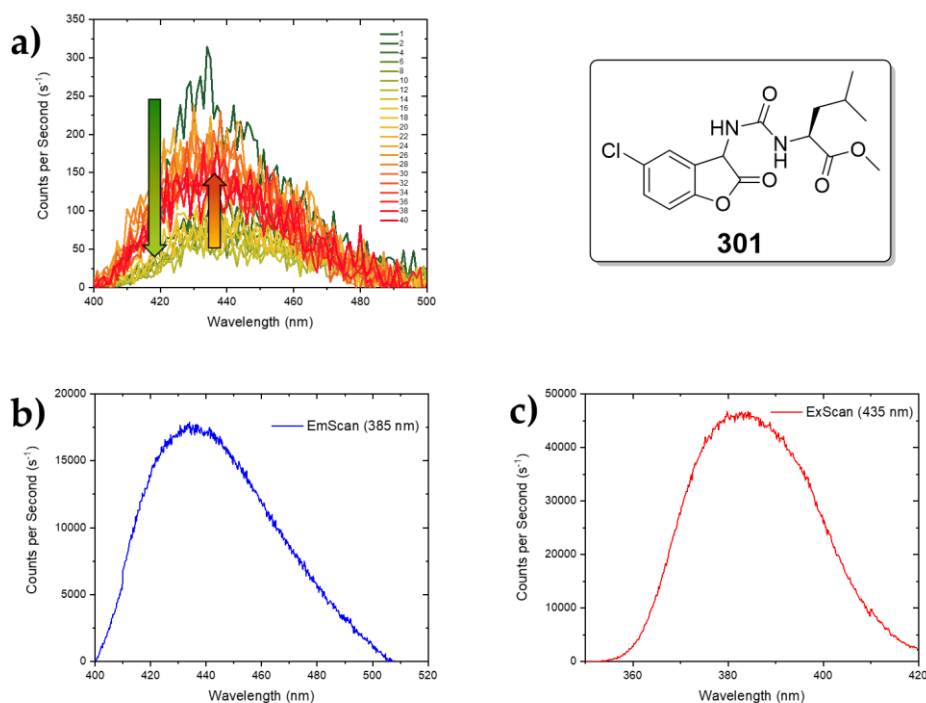


Figure 106: Emission and excitation spectra of **301** in acetonitrile (every scan took 45 s): (a) emission scans of CL (i.e., without external excitation, Slit: 10), the green red arrow indicates the decrease in CL after 12 scans. Starting from the 16th scan, the right red arrow indicates a new minor increase in CL; (b) emission scan of **301** after CL was finished (external excitation $\lambda_{\text{Ex}} = 385$ nm, Slit: 0.7); (c) excitation scan of **301** after CL was finished ($\lambda_{\text{Em}} = 435$ nm, Slit: 0.7).

8. Literature

- [1] T. W. Greene, P. G. M. Wuts, *Protective Groups in Organic Synthesis*, 5th Ed., John Wiley & Sons, Hoboken, NJ, **2014**.
- [2] P. J. Kociński, *Protecting Groups*, 3rd Ed., Thieme, NY, **2005**.
- [3] M. Schelhaas, H. Waldmann, "Protecting Group Strategies in Organic Synthesis", *Angew. Chem. Int. Ed. Engl.* **1996**, *35*, 2056–2083.
- [4] E. Fischer, *Untersuchungen über Kohlenhydrate und Fermente (1884 - 1908)*, Springer Verlag, Berlin, **1909**.
- [5] E. Fischer, *Untersuchungen über Kohlenhydrate und Fermente II (1908 – 1919)*, Springer Verlag, Berlin Heidelberg, **1922**.
- [6] E. Fischer, "Über die Verbindungen der Zucker mit den Alkoholen und Ketonen", *Chem. Ber.* **1895**, *28*, 1145–1166.
- [7] E. Fischer, "Verbindungen der mehrwertigen Alkohole mit den Ketonen", *Chem. Ber.* **1895**, *28*, 1167–1170.
- [8] E. Fischer, "Über Glucose-Aceton", *Chem. Ber.* **1895**, *28*, 2496–2497.
- [9] E. Fischer, "Teilweise Acylierung der mehrwertigen Alkohole und Zucker", *Chem. Ber.* **1915**, *48*, 266–275.
- [10] M. Schuler, A. Tatibouët, *Protecting Groups: Strategies and Applications in Carbohydrate Chemistry*, Wiley-VCH, Weinheim, Germany, **2019**.
- [11] E.-K. Kim, R. Krishnamurthy, "Synthesis of orotidine by intramolecular nucleosidation", *Chem. Commun.* **2015**, *51*, 5618–5621.
- [12] A. Robertson, R. Robinson, "Experiments on the Synthesis of Anthocyanins. Part V. A Synthesis of 3- β -Glucosidylpelargonidin Chloride, which is believed to be identical with Callistephin Chloride.", *J. Chem. Soc.* **1928**, 1460–1472.
- [13] R. B. Woodward, W. E. Doering, "The Total Synthesis of Quinine", *J. Am. Chem. Soc.* **1945**, *67*, 860–874.

- [14] R. B. Woodward, F. Sonderheimer, D. Taub, K. Heusler, W. M. McLamore, "The Total Synthesis of Steroids", *J. Am. Chem. Soc.* **1952**, *74*, 4223–4251.
- [15] R. B. Woodward, "Totalsynthese des Chlorophylls", *Angew. Chem.* **1960**, *72*, 651–662.
- [16] R. B. Woodward, "The Total Synthesis of Vitamin B₁₂", *Pure Appl. Chem.* **1973**, *33*, 145–178.
- [17] K. C. Nicolaou, E. J. Sorensen, *Classics in Total Synthesis*, Wiley-VCH, Weinheim, Germany, **1996**.
- [18] E. J. Corey, D. Seebach, "Carbanionen der 1,3-Dithiane, Reagentien zur C–C-Verknüpfung durch nucleophile Substitution oder Carbonyl-Addition", *Angew. Chem.* **1965**, *77*, 1134–1135.
- [19] E. J. Corey, D. Seebach, "Synthese von 1,n-Dicarbonylverbindungen mit Carbanionen der 1,3-Dithiane", *Angew. Chem.* **1965**, *77*, 1136–1137.
- [20] A. K. Banerjee, M. S. Laya, "Reagents for the preparation and cleavage of 1,3-dithiolanes", *Russ Chem. Rev.* **2000**, *69*, 947–955.
- [21] P. Kumar, R. S. Reddy, A. P. Singh, B. Pandey, "H-Y Zeolite, an Efficient Catalyst for Thioacetalization", *Tetrahedron Lett.* **1992**, *33*, 825–826.
- [22] E. C. Roos, P. Bernabé, H. Hiemstra, N. W. Speckamp, B. Kaptein, W. H. J. Boesten, "Palladium-Catalyzed Transprotection of Allyloxycarbonyl-Protected Amines: Efficient One-Pot Formation of Amides and Dipeptides", *J. Org. Chem.* **1995**, *60*, 1733–1740.
- [23] R. B. Merrifield, "Synthesis of a Tetrapeptide", *J. Am. Chem. Soc.* **1963**, *85*, 2149–2154.
- [24] R. B. Merrifield, "Automated Synthesis of Peptides", *Science* **1965**, *150*, 178–185.
- [25] M. Muttenthaler, G. F. King, D. J. Adams, P. F. Alewood, "Trends in peptide drug discovery", *Nat. Rev. Drug Discov.* **2021**, *20*, 309–325.
- [26] N. S. Isaacs, *Physical Organic Chemistry*, 2nd Ed., Addison Wesley Longman, Harlow, Essex, **1995**.
- [27] H. Kessler, R. Siegmeyer, "9-Fluorenylmethyl Esters as Carboxyl Protecting Group", *Tetrahedron Lett.* **1983**, *8*, 2555–2557.
- [28] K. Horita, T. Yoshioka, T. Tanaka, Y. Oikawa, O. Yonemitsu, "On the selectivity of deprotection of benzyl, mpm (4-methoxybenzyl) and dmpm (3,4-dimethoxybenzyl) protecting groups for hydroxy functions", *Tetrahedron* **1986**, *42*, 3021–3028.

- [29] R. Johansson, B. Samuelsson, "Regioselective Reductive Ring-opening of 4-Methoxybenzylidene Acetals of Hexopyranosides. Access to a Novel Protecting-group Strategy. Part 1", *J. Chem. Soc. Perkin Trans I* **1984**, 2371–2374.
- [30] R. A. W. Johnstone, A. H. Wilby, I. D. Entwistle, "Heterogeneous Catalytic Transfer Hydrogenation and its Relation to other Methods for Reduction of Organic Compounds", *Chem. Rev.* **1985**, 85, 129–170.
- [31] Y. Oikawa, T. Tanaka, K. Horita, O. Yonemitsu, "Selective hydrogenolysis of the benzyl protecting group for hydroxy function with raney nickel in the presence of the MPM (4-methoxybenzyl) and DMPM (3,4-dimethoxybenzyl) protecting groups", *Tetrahedron Lett.* **1984**, 25, 5397–5400.
- [32] T. B. Windholt, D. B. R. Johnston, "Trichloroethoxycarbonyl: a generally applicable protecting group", *Tetrahedron Lett.* **1967**, 2555–2557.
- [33] R. M. Jacobson, J. W. Clader, "New Alcohol Protecting Groups. β , β , β -Trichloroethoxymethyl Ethers", *Synth. Commun.* **1979**, 9, 57–62.
- [34] R. B. Woodward, K. Heusler, J. Gosteli, P. Naegeli, W. Oppolzer, R. Ramage, Ranganathan S., H. Vorbrüggen, "The Total Synthesis of Cephalosporin C.", *J. Am. Chem. Soc.* **1966**, 8, 852–853.
- [35] G. Oksdath-Mansilla, V. Hajj, D. M. Andrada, J. E. Argüello, J. Bonin, M. Robert, A. B. Peñéñory, "Photoremoval of protecting groups: Mechanistic aspects of 1,3-dithiane conversion to a carbonyl group", *J. Org. Chem* **2015**, 80, 2733–2739.
- [36] R. Gigg, C. D. Warren, "Use of the Allyl Ether as a Protecting Group in a New Synthesis of L-Lyxose", *J. Chem. Soc.* **1965**, 2205–2210.
- [37] R. Gigg, C. D. Warren, "The Allyl Ether as a Protecting Group in Carbohydrate Chemistry. Part II", *J. Chem. Soc.* **1968**, 1903–1911.
- [38] C. Rücker, "The Triisopropylsilyl Group in Organic Chemistry: Just a Protective Group, or More?", *Chem. Rev.* **1995**, 95, 1009–1064.
- [39] B. H. Lipshutz, J. J. Pegram, " β -(Trimethylsilyl)ethoxymethyl chloride. A new reagent for the protection of the hydroxyl group", *Tetrahedron Lett.* **1980**, 21, 3343–3346.
- [40] P. Sieber, "The 2-trimethylsilylethyl residue, a selectively cleavable carboxyl protecting group", *Helv. Chim. Acta* **1977**, 60, 2711–2716.

- [41] H. Gerlach, "2-(Trimethylsilyl)ethyl Esters as Carboxyl Protecting Group; Application in the Synthesis of (-)-(S)-Curvularin", *Helv. Chim. Acta* **1977**, *60*, 3039–3044.
- [42] L. A. Carpino, J.-H. Tsao, H. Ringsdorf, E. Fell, G. Hettrich, "The β -(trimethylsilyl)ethoxycarbonyl amino-protecting group", *J. Chem. Soc., Chem. Commun.* **1978**, 358–359.
- [43] C. Gioeli, N. Balgobin, S. Josephson, J. B. Chattopadhyaya, "2-(Trimethylsilyl)ethyl chloroformate: A convenient reagent for protection of hydroxyl function", *Tetrahedron Lett.* **1981**, *22*, 969–972.
- [44] D. Kadereit, H. Waldmann, "Enzymatic Protecting Group Techniques", *Chem. Rev.* **2001**, *101*, 3367–3396.
- [45] C. G. J. Verhart, G. I. Tesser, "New base-labile amino-protective groups for peptide synthesis", *Recl. Trav. Chim. Pays-Bas* **1988**, *107*, 621–626.
- [46] G. I. Tesser, I. C. Balvert-Geers, "The methylsulfonylethoxycarbonyl group, a new and versatile amino protective function", *Int. J. Pept. Protein Res.* **1975**, *7*, 295–305.
- [47] M. Patek, "Multistep deprotection for peptide chemistry", *Int. J. Peptide Protein Res.* **1993**, *42*, 97–117.
- [48] C. J. Moody, M. R. Pitts, "Indium as a Reducing Agent: Deprotection of 4-Nitrobenzyl Ethers and Esters", *Synlett* **1999**, 1575–1576.
- [49] R. W. Holley, A. D. Holley, "The Removal of *N*-*o*-Nitrophenoxyacetyl and *N*-Chloroacetyl Groups from Peptides", *J. Am. Chem. Soc.* **1952**, *74*, 3069–3074.
- [50] P. Wang, "Photolabile Protecting Groups: Structure and Reactivity", *Asian J. Org. Chem.* **2013**, *2*, 452–464.
- [51] C. G. Bochet, A. Blanc, Chapter 4, in *Organic Photochemistry and Photobiology*, 3rd Ed., CRC Press, Boca Raton, FL, **2012**.
- [52] P. Klán, T. Šolomek, C. G. Bochet, A. Blanc, R. Givens, M. Rubina, V. Popik, A. Kostikov, J. Wirz, "Photoremovable Protecting Groups in Chemistry and Biology: Reaction Mechanisms and Efficacy", *Chem. Rev.* **2013**, *113*, 119–191.
- [53] J. E. T. Corrie, A. Barth, V. R. N. Munasinghe, D. R. Trentham, M. C. Hutter, "Photolytic Cleavage of 1-(2-Nitrophenyl)ethyl Ethers Involves Two Parallel Pathways and Product Release Is Rate-Limited by Decomposition of a Common Hemiacetal Intermediate", *J. Am. Chem. Soc.* **2003**, *125*, 8546–8554.

- [54] Y. V. Il'ichev, M. A. Schwörer, J. Wirz, "Photochemical Reaction Mechanisms of 2-Nitrobenzyl Compounds: Methyl Ethers and Caged ATP", *J. Am. Chem. Soc.* **2004**, *126*, 4581–4595.
- [55] M. Gaplovsky, Y. V. Il'ichev, Y. Kamdzhilov, S. V. Kombarova, M. Mac, M. A. Schwörer, J. Wirz, "Photochemical reaction mechanisms of 2-nitrobenzyl compounds: 2-Nitrobenzyl alcohols form 2-nitroso hydrates by dual proton transfer", *Photochem. Photobiol. Sci.* **2005**, *4*, 33–42.
- [56] J. A. Barltrop, P. J. Plant, P. Schofield, "Photosensitive Protective Groups", *J. Chem. Soc. Chem. Commun.* **1966**, 822–823.
- [57] A. K. Singh, P. K. Khade, "3-Nitro-2-naphthalenemethanol: A photocleavable protecting group for carboxylic acids", *Tetrahedron* **2005**, *61*, 10007–10012.
- [58] A. Patchornik, B. Amit, R. B. Woodward, "Photosensitive protecting groups", *J. Am. Chem. Soc.* **1970**, *92*, 6333–6335.
- [59] A. Hasan, K.-P. Stengele, H. Giegrich, P. Cornwell, K. R. Isham, R. A. Sachleben, W. Pfeleiderer, R. S. Foote, "Photolabile Protecting Groups for Nucleosides: Synthesis and Photodeprotection Rates", *Tetrahedron* **1997**, *53*, 4247–4264.
- [60] M. C. Pirrung, L. Wang, M. P. Montague-Smith, "3'-Nitrophenylpropyloxycarbonyl (NPPOC) Protecting Groups for High-Fidelity Automated 5' → 3' Photochemical DNA Synthesis", *Org. Lett.* **2001**, *3*, 1105–1108.
- [61] V. Hagen, J. Bendig, S. Frings, T. Eckardt, S. Helm, D. Reuter, U. B. Kaupp, "Highly Efficient and Ultrafast Phototriggers for cAMP and cGMP by using Long-Wavelength UV/Vis-Activation", *Angew. Chem. Int. Ed.* **2001**, *40*, 1045–1048.
- [62] R. S. Givens, P. S. Athey, L. W. Kueper III, B. Matuszewski, J. -y. Xue, "Photochemistry of α -Keto Phosphate Esters: Photorelease of a Caged cAMP.", *J. Am. Chem. Soc.* **1992**, *114*, 8708–8710.
- [63] R. S. Givens, P. S. Athey, B. Matuszewski, L. W. Kueper III, J. -y. Xue, T. Fister, "Photochemistry of Phosphate Esters: α -Keto Phosphates as a Photoprotecting Group for Caged Phosphate", *J. Am. Chem. Soc.* **1993**, *115*, 6001–6012.
- [64] H.-Y. An, W. M. Kwok, C. Ma, X. Guan, J. T. W. Kan, P. H. Toy, D. L. Phillips, "Photophysics and Photodeprotection Reactions of *p*-Methoxyphenacyl Phototriggers: An Ultrafast and Nanosecond Time-Resolved Spectroscopic and Density Functional Theory Study", *J. Org. Chem.* **2010**, *75*, 5837–5851.

- [65] A. Banerjee, D. E. Falvey, "Direct Photolysis of Phenacyl Protecting Groups Studied by Laser Flash Photolysis: An Excited State Hydrogen Atom Abstraction Pathway Leads to Formation of Carboxylic Acids and Acetophenone", *J. Am. Chem. Soc.* **1998**, *120*, 2965–2966.
- [66] J. C. Sheehan, R. M. Wilson, "Photolysis of Desyl Compounds. A New Photolytic Cyclization", *J. Am. Chem. Soc.* **1964**, *86*, 5277–5281.
- [67] J. C. Sheehan, R. M. Wilson, A. W. Oxford, "The Photolysis of Methoxy-Substituted Benzoin Esters. A Photosensitive Protecting Group for Carboxylic Acids", *J. Am. Chem. Soc.* **1971**, *93*, 7222–7228.
- [68] M. C. Pirrung, J.-C. Bradley, "Dimethoxybenzoin Carbonates: Photochemically-Removable Alcohol Protecting Groups Suitable for Phosphoramidite-Based DNA Synthesis", *J. Org. Chem.* **1995**, *60*, 1116–1117.
- [69] J. F. Cameron, C. G. Willson, J. M. J. Fréchet, "Photogeneration of Amines from α -Keto Carbamates: Photochemical Studies", *J. Am. Chem. Soc.* **1996**, *118*, 12925–12937.
- [70] G. Papageorgiou, J. E. T. Corrie, "Synthesis and Properties of Carbamoyl Derivatives of Photolabile Benzoin", *Tetrahedron* **1997**, *53*, 3917–3932.
- [71] J. M. Peach, A. J. Pratta, J. S. Snaitha, "Photolabile Benzoin and Furoin Esters of a Biologically Active Peptide", *Tetrahedron* **1995**, *51*, 10013–10024.
- [72] M. C. Pirrung, T. Ye, Z. Zhou, J. D. Simon, "Mechanistic Studies on the Photochemical Deprotection of 3',5'-Dimethoxybenzoin Esters", *Photochem. Photobiol.* **2006**, *82*, 1258–1264.
- [73] H. Boudebous, B. Košmrlj, B. Šket, J. Wirz, "Primary Photoreactions of the 3',5'-Dimethoxybenzoin Cage and Determination of the Release Rate in Polar Media", *J. Phys. Chem. A* **2007**, *111*, 2811–2813.
- [74] M. Chensheng, W. M. Kwok, H.-Y. An, X. Guan, M. Y. Fu, P. H. Toy, D. L. Phillips, "A Time-Resolved Spectroscopic Study of the Bichromophoric Phototrigger 3',5'-Dimethoxybenzoin Diethyl Phosphate: Interaction Between the Two Chromophores Determines the Reaction Pathway", *Chem. Eur. J.* **2010**, *16*, 5102–5118.
- [75] R. S. Givens, C.-H. Park, "*p*-Hydroxyphenacyl ATP: A new Phototrigger", *Tetrahedron Lett.* **1996**, *37*, 6259–6262.
- [76] C. Ma, W. M. Kwok, W. S. Chan, Y. Du, J. T. W. Kan, P. H. Toy, D. L. Phillips, "Ultrafast Time-Resolved Transient Absorption and Resonance Raman Spectroscopy Study of the Photodeprotection

and Rearrangement Reactions of *p*-Hydroxyphenacyl Caged Phosphates", *J. Am. Chem. Soc.* **2006**, *128*, 2558–2570.

- [77] X. Chen, C. Ma, W. M. Kwok, X. Guan, Y. Du, D. L. Phillips, "A Theoretical Investigation of *p*-Hydroxyphenacyl Caged Phototrigger Compounds: An Examination of the Excited State Photochemistry of *p*-Hydroxyphenacyl Acetate", *J. Phys. Chem. A* **2006**, *110*, 12406–12413.
- [78] R. S. Givens, D. Heger, B. Hellrung, Y. Kamdzhilov, M. Mac, P. G. Conrad, E. Cope, J. I. Lee, J. F. Mata-Segreda, R. L. Schowen, J. Wirz, "The Photo-Favorskii Reaction of *p*-Hydroxyphenacyl Compounds Is Initiated by Water-Assisted, Adiabatic Extrusion of a Triplet Biradical", *J. Am. Chem. Soc.* **2008**, *130*, 3307–3309.
- [79] K. F. Stensrud, D. Heger, P. Šebej, J. Wirz, R. S. Givens, "Fluorinated photoremovable protecting groups: The influence of fluoro substituents on the photo-Favorskii rearrangement", *Photochem. Photobiol. Sci.* **2008**, *7*, 614–624.
- [80] P. G. Conrad, R. S. Givens, B. Hellrung, C. S. Rajesh, M. Ramseier, J. Wirz, "*p*-Hydroxyphenacyl phototriggers: The Reactive Excited State of Phosphate Photorelease", *J. Am. Chem. Soc.* **2000**, *122*, 9346–9347.
- [81] R. S. Givens, C.-H. Park, "New Photoactivated Protecting Groups. 6. *p*-Hydroxyphenacyl: A Phototrigger for Chemical and Biochemical Probes", *J. Am. Chem. Soc.* **1997**, *119*, 2453–2463.
- [82] R. S. Givens, M. Rubina, J. Wirz, "Applications of *p*-hydroxyphenacyl (*p*HP) and coumarin-4-ylmethyl photoremovable protecting groups", *Photochem. Photobiol. Sci.* **2012**, *11*, 472–488.
- [83] P. Klán, P. A. Pelliccioli, T. Pospíšil, J. Wirz, "2,5-Dimethylphenacyl esters: A photoremovable protecting group for phosphates and sulfonic acids", *Photochem. Photobiol. Sci.* **2002**, *1*, 920–923.
- [84] P. Klán, M. Zabadal, D. Heger, "2,5-Dimethylphenacyl as a New Photoreleasable Protecting Group for Carboxylic Acids", *Org. Lett.* **2000**, *2*, 1569–1571.
- [85] M. Zabadal, A. P. Pelliccioli, P. Klán, J. Wirz, "2,5-Dimethylphenacyl Esters: A Photoremovable Protecting Group for Carboxylic Acids", *J. Phys. Chem. A* **2001**, *105*, 10329–10333.
- [86] W. N. Atemnkeng, L. D. Louisiana, P. K. Yong, B. Vottero, A. Banerjee, "1-[2-(2-Hydroxyalkyl)phenyl]ethanone: A New Photoremovable Protecting Group for Carboxylic Acids", *Org. Lett.* **2003**, *5*, 4469–4471.

- [87] J. Literák, J. Wirz, P. Klán, "2,5-Dimethylphenacyl carbonates: A photoremovable protecting group for alcohols and phenols", *Photochem. Photobiol. Sci.* **2005**, *4*, 43–46.
- [88] L. Kammari, L. Plíštil, J. Wirz, P. Klán, "2,5-Dimethylphenacyl carbamate: A photoremovable protecting group for amines and amino acids", *Photochem. Photobiol. Sci.* **2007**, *6*, 50–56.
- [89] S.-S. Tseng, E. F. Ullman, "Elimination Reactions Induced by Photoenolization of *o*-Alky lbenzophenones", *J. Am. Chem. Soc.* **1976**, *98*, 541–544.
- [90] J. Pika, A. Konosonoks, R. M. Robinson, P. N. D. Singh, A. D. Gudmundsdottir, "Photoenolization as a Means to Release Alcohols", *J. Org. Chem.* **2003**, *68*, 1964–1972.
- [91] C. Ma, M. G. Steinmetz, Q. Cheng, V. Jayaraman, "Photochemical Cleavage and Release of Carboxylic Acids from α -Keto Amides", *Org. Lett.* **2003**, *5*, 71–74.
- [92] C. Ma, Y. Chen, M. G. Steinmetz, "Photochemical Cleavage and Release of Para-Substituted Phenols from α -Keto Amides", *J. Org. Chem.* **2006**, *71*, 4206–4215.
- [93] Y. Zhu, C. M. Pavlos, J. P. Toscano, T. M. Dore, "8-Bromo-7-hydroxyquinoline as a Photoremovable Protecting Group for Physiological Use: Mechanism and Scope", *J. Am. Chem. Soc.* **2006**, *128*, 4267–4276.
- [94] T. Furuta, Y. Hirayama, M. Iwamura, "Anthraquinon-2-ylmethoxycarbonyl (Aqmoc): A New Photochemically Removable Protecting Group for Alcohols", *Org. Lett.* **2001**, *3*, 1809–1812.
- [95] D. S. Kemp, J. Reczek, "New protective groups for peptide synthesis III The maq ester group mild reductive cleavage of 2-acyloxymethyleneanthraquinones", *Tetrahedron Lett.* **1977**, *18*, 1031–1034.
- [96] M.-G. Ren, N.-M. Bi, M. Mao, Q.-H. Song, "2-(1'-Hydroxyethyl)-anthraquinone as a photolabile protecting group for carboxylic acids", *J. Photochem. Photobiol. A* **2009**, *204*, 13–18.
- [97] J. -y. Yu, W.-J. Tang, H.-B. Wang, Q.-H. Song, "Anthraquinon-2-ylethyl-1',2'-diol (Aqe-diol) as a new photolabile protecting group for aldehydes and ketones", *J. Photochem. Photobiol. A* **2007**, *185*, 101–105.
- [98] T. Furuta, H. Torigai, M. Sugimoto, M. Iwamura, "Photochemical Properties of New Photolabile cAMP Derivatives in a Physiological Saline Solution", *J. Org. Chem.* **1995**, *60*, 3953–3956.
- [99] Y. Guo, Q. Song, J. Wang, J. Ma, X. Zhang, D. L. Phillips, "Unraveling the Photodeprotection Mechanism of Anthraquinon-2-ylmethoxycarbonyl-Caged Alcohols Using Time-Resolved Spectroscopy", *J. Org. Chem.* **2018**, *83*, 13454–13462.

- [100] S. Kitani, K. Sugawara, K. Tsutsumi, T. Morimoto, K. Kakiuchi, "Synthesis and characterization of thiochromone *S,S*-dioxides as new photolabile protecting groups", *Chem. Commun.* **2008**, 2103–2105.
- [101] Y. Zhang, H. Tanimoto, Y. Nishiyama, T. Morimoto, K. Kakiuchi, "Novel Photolabile Protecting Group for Phosphate Compounds", *Synlett* **2012**, 367–370.
- [102] C. Ma, Y. Zhang, H. Zhang, J. Li, Y. Nishiyama, H. Tanimoto, T. Morimoto, K. Kakiuchi, "Synthesis and Photochemistry of a New Photolabile Protecting Group for Propargylic Alcohols", *Synlett* **2017**, 28, 560–564.
- [103] J. A. Barltrop, P. Schofield, "Photosensitive Protecting Groups", *Tetrahedron Lett.* **1962**, 3, 697–699.
- [104] J. W. Chamberlin, "Use of the 3,5-Dimethoxybenzyloxycarbonyl Group as a Photosensitive *N*-Protecting Group", *J. Org. Chem.* **1966**, 31, 1658–1660.
- [105] H. E. Zimmerman, "Meta-Ortho Effect in Organic Photochemistry: Mechanistic and Exploratory Organic Photochemistry", *J. Phys. Chem.* **1998**, 102, 5616–5621.
- [106] P. Wang, A. Hu, Y. Wang, "Application of the Excited State Meta Effect in Photolabile Protecting Group Design", *Org. Lett.* **2007**, 9, 2831–2833.
- [107] W. Pengfei, H. Huayou, Y. Wang, "Novel Photolabile Protecting Group for Carbonyl Compounds", *Org. Lett.* **2007**, 9, 1533–1535.
- [108] H. Yang, X. Zhang, L. Zhou, P. Wang, "Development of a Photolabile Carbonyl-Protecting Group Toolbox", *J. Org. Chem.* **2011**, 76, 2040–2048.
- [109] P. Wang, L. Zhou, X. Zhang, X. Liang, "Facilitated photochemical cleavage of benzylic C-O bond. Application to photolabile hydroxyl-protecting group design", *Chem. Commun.* **2010**, 46, 1514–1516.
- [110] L. Zhou, H. Yang, P. Wang, "Development of Trityl-Based Photolabile Hydroxyl Protecting Groups", *J. Org. Chem.* **2011**, 76, 5873–5881.
- [111] H. Yang, L. Zhou, P. Wang, "Development of hydrophilic photolabile hydroxyl protecting groups", *Photochem. Photobiol. Sci.* **2012**, 11, 514–517.
- [112] P. Wang, W. Lu, D. Devalankar, Z. Ding, "Photochemical Formation and Cleavage of C-N Bond", *Org. Lett.* **2015**, 17, 170–172.
- [113] P. W. Atkins, J. de Paula, *Physikalische Chemie*, 5th Ed., Wiley-VCH, Weinheim, Germany, **2013**.

- [114] B. Valeur, M. N. Berberan-Santos, *Molecular Fluorescence: Principles and Applications*, 2nd Ed., Wiley-VCH & Co. KGaA, Weinheim, Germany, **2012**.
- [115] D. Wöhrle, M. W. Tausch, W.-D. Stohrer, *Photochemie: Konzepte, Methoden, Experimente*, Wiley-VCH, Weinheim, Germany, **1998**.
- [116] E. V. Anslyn, D. A. Dougherty, *Modern Physical Organic Chemistry*, 1st Ed., University Science Books, **2005**.
- [117] J. N. Demas, S. E. Demas, Luminescence, in *Reference Module in Chemistry, Molecular Sciences and Chemical Engineering*, Elsevier, Amsterdam, Netherlands, **2014**, pp. 1–35.
- [118] B. P. Chandra, A. S. Rathore, "Classification of Mechanoluminescence", *Crys. Res. Technol.* **1995**, *30*, 885–896.
- [119] H. Brandl, E. Täuscher, D. Weiß, "Triboluminescence: An almost forgotten light phenomenon", *Chem. Unserer Zeit* **2017**, *51*, 112–123.
- [120] T. Ishihara, K. Tanaka, K. Hirao, N. Soga, "Fracto-Luminescence of Rare Earth Element-Doped Hexacelsian (BaAl₂Si₂O₈)", *Jpn. J. Appl. Phys.* **1997**, *36*, 781–783.
- [121] N. A. Atari, "Piezoluminescence Phenomenon", *Phys. Lett.* **1982**, *90*, 93–96.
- [122] H. Frenzel, H. Schultes, "Lumineszenz im ultraschallbeschickten Wasser. Kurze Mitteilung", *Z. Phys. Chem.* **1934**, *27*, 421–424.
- [123] M. M. Richter, "Electrochemiluminescence (ECL)", *Chem. Rev.* **2004**, *104*, 3003–3036.
- [124] T. Wilson, J. W. Hastings, *Bioluminescence: Living Lights, Lights for Living*, Harvard University Press, Cambridge, MA, **2013**.
- [125] E. N. Harvey, *A History of Luminescence, from the Earliest Times until 1900*, American Philosophical Society, Philadelphia, PA, **1957**.
- [126] S. Albrecht, H. Brandl, T. Zimmermann, *Chemilumineszenz*, Hüthig Verlag, Heidelberg, Germany, **1996**.
- [127] J. Poisson, "Raphaël Dubois, from pharmacy to bioluminescence", *Rev. Hist. Pharm.* **2010**, *97*, 51–56.
- [128] H. D. Holland, "The oxygenation of the atmosphere and oceans", *Phil. Trans. R. Soc. B* **2006**, *361*, 903–915.

- [129] D. C. Catling, J. F. Kasting, *Atmospheric Evolution on Inhabited and Lifeless Worlds*, Cambridge University Press, Cambridge, UK, **2017**.
- [130] T. W. Lyons, C. T. Reinhard, N. J. Planavsky, "The rise of oxygen in Earth's early ocean and atmosphere", *Nature* **2014**, *506*, 307–315.
- [131] L. E. Orgel, "The origin of life-a review of facts and speculations", *Trends Biochem. Sci.* **1998**, *23*, 491–495.
- [132] D. E. Canfield, M. T. Rosing, C. Bjerrum, "Early anaerobic metabolisms", *Phil. Trans. R. Soc. B* **2006**, *361*, 1819–1836.
- [133] P. Sánchez-Baracaldo, T. Cardona, "On the origin of oxygenic photosynthesis and Cyanobacteria", *New Phytol.* **2020**, *225*, 1440–1446.
- [134] B. E. Schirrmeister, M. Gugger, P. C. J. Donoghue, "Cyanobacteria and the Great Oxidation Event: Evidence from Genes and Fossils", *Palaeontology* **2015**, *58*, 769–785.
- [135] G. P. Fournier, K. R. Moore, L. T. Rangel, J. G. Payette, L. Momper, T. Bosak, "The Archean origin of oxygenic photosynthesis and extant cyanobacterial lineages", *Proc. R. Soc. B* **2021**, *288*, 1–10.
- [136] S. H. D. Haddock, M. A. Moline, J. F. Case, "Bioluminescence in the Sea", *Annu. Rev. Mar. Sci.* **2010**, *2*, 443–493.
- [137] M. Vacher, I. Fdez Galván, B.-W. Ding, S. Schramm, R. Beraud-Pache, P. Naumov, N. Ferré, Y.-J. Liu, I. Navizet, D. Roca-Sanjuán, W. J. Baader, R. Lindh, "Chemi- and Bioluminescence of Cyclic Peroxides", *Chem. Rev.* **2018**, *118*, 6927–6974.
- [138] K. H. Nealson, J. W. Hastings, "Bacterial Bioluminescence: Its Control and Ecological Significance", *Microbiol. Rev.* **1979**, *43*, 496–518.
- [139] C. Hou, Y.-J. Liu, N. Ferré, W.-H. Fang, "Understanding Bacterial Bioluminescence: A Theoretical Study of the Entire Process, from Reduced Flavin to Light Emission", *Chem. Eur. J.* **2014**, *20*, 7979–7986.
- [140] G. Merényi, J. Lind, H. I. X. Mager, S.-C. Tu, "Properties of 4a-Hydroxy-4a,5-dihydroflavin Radicals in Relation to Bacterial Bioluminescence", *J. Phys. Chem.* **1992**, *96*, 10528–10533.
- [141] J. W. Eckstein, J. W. Hastings, S. Ghisla, "Mechanism of Bacterial Bioluminescence: 4a,5-Dihydroflavin Analogs as Models for Luciferase Hydroperoxide Intermediates and the Effect of Substituents at the 8-Position of Flavin on Luciferase Kinetics", *Biochemistry* **1993**, *32*, 404–411.

- [142] W. A. Francisco, H. M. Abu-Soud, A. J. Delmonte, D. A. Singleton, T. O. Baldwin, F. M. Raushel, "Deuterium Kinetic Isotope Effects and the Mechanism of the Bacterial Luciferase Reaction", *Biochemistry* **1998**, *37*, 2596–2606.
- [143] E. Brodl, A. Winkler, P. Macheroux, "Molecular Mechanisms of Bacterial Bioluminescence", *Comput. Struct. Biotechnol. J.* **2018**, *16*, 551–564.
- [144] P. Macheroux, K. U. Schmidt, P. Steinerstauch, S. Ghisla, P. Colepiccolo, R. Buntic, J. W. Hastings, "Purification of the yellow fluorescent Protein from *Vibrio fischeri* and Identity of the Flavin Chromophore", *Biochem. Biophys. Res. Commun.* **1987**, *146*, 101–106.
- [145] D. J. O'kane, V. A. Karle, J. Lee, "Purification of Lumazine Proteins from *Photobacterium leiognathi* and *Photobacterium phosphoreum*: Bioluminescence Properties", *Biochemistry* **1985**, *24*, 1461–1467.
- [146] J. Lee, D. J. O'kane, A. J. W. G. Visser, "Spectral Properties and Function of Two Lumazine Proteins from *Photobacterium*", *Biochemistry* **1985**, *24*, 1476–1483.
- [147] E. M. Maldonado, M. I. Latz, "Shear-Stress Dependence of Dinoflagellate Bioluminescence", *Biol. Bull.* **2007**, *212*, 242–249.
- [148] L. Wayne Schultz, L. Liu, M. Cegielski, J. W. Hastings, "Crystal structure of a pH-regulated luciferase catalyzing the bioluminescent oxidation of an open tetrapyrrole", *Proc. Natl. Acad. Sci. U.S.A.* **2005**, *102*, 1378–1383.
- [149] E. J. Buskey, E. Swift, "Behavioral Responses of Oceanic Zooplankton to Simulated Bioluminescence", *Biol. Bull.* **1985**, *168*, 263–275.
- [150] K. J. Fleisher, J. F. Case, "Cephalopod Predation Facilitated by Dinoflagellate Luminescence", *Biol. Bull.* **1995**, *189*, 263–271.
- [151] G. M. Hallegraeff, "A Review of Harmful Algal Blooms and Their Apparent Global Increase", *Phycologia* **1993**, *32*, 79–99.
- [152] F. D. Mello, N. Braidy, H. Marçal, G. Guillemain, S. M. Nabavi, B. A. Neilan, "Mechanisms and Effects Posed by Neurotoxic Products of Cyanobacteria/Microbial Eukaryotes/Dinoflagellates in Algae Blooms: a Review", *Neurotox. Res.* **2018**, *33*, 153–167.
- [153] L. E. Fleming et al., "Review of Florida red tide and human health effects", *Harmful Algae* **2011**, *10*, 224–233.

- [154] S. H. D. Haddock, M. A. Moline, J. F. Case, "Bioluminescence in the Sea", *Annu. Rev. Mar. Sci.* **2010**, *2*, 443–493.
- [155] H. Nakamura, Y. Kishi, O. Shimomura, D. Morse, J. W. Hastings, "Structure of Dinoflagellate Luciferin and Its Enzymic and Nonenzymic Air-Oxidation Products", *J. Am. Chem. Soc.* **1989**, *111*, 7607–7611.
- [156] P. D. Ngo, S. O. Mansoorabadi, "Investigation of the Dinoflagellate Bioluminescence Mechanism: Chemically Initiated Electron Exchange Luminescence or Twisted Intramolecular Charge Transfer?", *ChemPhotoChem* **2017**, *1*, 383–387.
- [157] G. S. Phun, D. Rappoport, F. Furche, T. R. Gibson, S. Tretiak, "Constructing the Mechanism of Dinoflagellate Luciferin Bioluminescence Using Computation", *J. Phys. Chem. Lett.* **2023**, *14*, 6001–6008.
- [158] M.-Y. Wang, Y.-J. Liu, "Theoretical Study of Dinoflagellate Bioluminescence", *Photochem. Photobiol.* **2017**, *93*, 511–518.
- [159] Y. Oba, C. V. Stevani, A. G. Oliveira, A. S. Tsarkova, T. V. Chepurnykh, I. V. Yampolsky, "Selected Least Studied but not Forgotten Bioluminescent Systems", *Photochem. Photobiol.* **2017**, *93*, 405–415.
- [160] V. B. Meyer-Rochow, S. Moore, "Biology of *Latia neritoides* Gray 1850 (Gastropoda, Pulmonata, Basommatophora): the only Light-producing Freshwater Snail in the World", *Int. Rev. gesamten Hydrobiol.* **1988**, *73*, 21–42.
- [161] O. Shimomura, *Bioluminescence: Chemical Principles and Methods*, World Scientific, Singapur, **2006**.
- [162] Y. Ohmiya, S. Kojima, M. Nakamura, H. Niwa, "Bioluminescence in the Limpet-Like Snail, *latia neritoides*", *Bull. Chem. Soc. Jpn.* **2005**, *78*, 1197–1205.
- [163] O. Shimomura, F. H. Johnson, Y. Kohama, "Reactions Involved in Bioluminescence Systems of Limpet (*Latia neritoides*) and Luminous Bacteria", *Proc. Nat. Acad. Sci. USA* **1972**, *69*, 2086–2089.
- [164] Y. Ohmiya, "Basic and Applied Aspects of Color Tuning of Bioluminescence Systems", *Jpn. J. Appl. Phys.* **2005**, *44*, 6368–6379.
- [165] N. S. Rodionova, E. Rota, A. S. Tsarkova, V. N. Petushkov, "Progress in the Study of Bioluminescent Earthworms", *Photochem. Photobiol.* **2017**, *93*, 416–428.

- [166] R. Bellisario, T. E. Spencer, M. J. Cormier, "Isolation and Properties of Luciferase, a Non-Heme Peroxidase, from the Bioluminescent Earthworm, *Diplocardia longa*", *Biochemistry* **1972**, *11*, 2256–2266.
- [167] J. D. F. Gilchrist, "Luminosity and its Origin in a South African Earthworm (*Chilota* sp.?)", *Trans R. Soc. S. Afr.* **1919**, *7*, 203–212.
- [168] H. Friend, "Luminous Worms", *Nature* **1919**, *103*, 446.
- [169] H. Ohtsuka, N. G. Rudie, J. E. Wampler, "Structural Identification and Synthesis of Luciferin from the bioluminescent Earthworm, *Diplocardia longa*", *Biochemistry* **1976**, *15*, 1001–1004.
- [170] N. G. Rudie, J. E. Wampler, "Earthworm Bioluminescence: Characterization of the luminescent Cell from *Diplocardia longa*", *Comp. Biochem. Physiol.* **1978**, *59A*, 1–8.
- [171] B. G. M. Jamieson, J. E. Wampler, "Bioluminescent Australian earthworms. Taxonomy and preliminary Report of Bioluminescence in the Gene *Spenceriella*, *Fletcherodrilus* and *Pontodrilus* (Megascolecidae: Oligochaeta)", *Aust. J. Zool.* **1979**, *27*, 637–669.
- [172] J. E. Wampler, B. G. M. Jamieson, "Earthworm Bioluminescence: Comparative Physiology and Biochemistry", *Comp. Biochem. Physiol.* **1980**, *66*, 43–50.
- [173] H.-M. Ke, I. J. Tsai, "Understanding and using fungal bioluminescence – Recent progress and future perspectives", *Curr. Opin. Green Sustain. Chem.* **2022**, *33*, 100570.
- [174] D. E. Desjardin, A. G. Oliveira, C. V. Stevani, "Fungi bioluminescence revisited", *Photochem. Photobiol. Sci.* **2008**, *7*, 170–182.
- [175] A. G. Oliveira, D. E. Desjardin, B. A. Perry, C. V. Stevani, "Evidence that a single bioluminescent system is shared by all known bioluminescent fungal lineages", *Photochem. Photobiol. Sci.* **2012**, *11*, 848–852.
- [176] P. J. Herring, "Luminous Fungi", *Mycologist* **1994**, *8*, 181–183.
- [177] Y. Oba, Y. Suzuki, G. N. R. Martins, R. P. Carvalho, T. A. Pereira, H. E. Waldenmaier, S. Kanie, M. Naito, A. G. Oliveira, F. A. Dörr, E. Pinto, I. V. Yampolsky, C. V. Stevani, "Identification of hispidin as a bioluminescent active compound and its recycling biosynthesis in the luminous fungal fruiting body", *Photochem. Photobiol. Sci.* **2017**, *16*, 1435–1440.
- [178] K. V. Purtov, V. N. Petushkov, M. S. Baranov, K. S. Mineev, N. S. Rodionova, Z. M. Kaskova, A. S. Tsarkova, A. I. Petunin, V. S. Bondar, E. K. Rodicheva, S. E. Medvedeva, Y. Oba, Y. Oba, A. S.

- Arseniev, S. Lukyanov, J. I. Gitelson, I. V. Yampolsky, "The Chemical Basis of Fungal Bioluminescence", *Angew. Chem.* **2015**, *127*, 8124–8128.
- [179] Z. M. Kaskova, et al., "Mechanism and color modulation of fungal bioluminescence", *Sci. Adv.* **2017**, *3*, e1602847.
- [180] A. A. Kotlobay, et al., "Genetically encodable bioluminescent system from fungi", *Proc. Natl. Acad. Sci. U.S.A.* **2018**, *115*, 12728–12732.
- [181] W.-X. Bi, J.-W. He, C.-C. Chen, R. Kundrata, X.-Y. Li, "Sinopyrophorinae, a new subfamily of Elateridae (Coleoptera, Elateroidea) with the first record of a luminous click beetle in Asia and evidence for multiple origins of bioluminescence in Elateridae", *Zookeys* **2019**, *864*, 79–97.
- [182] D. Kusy, J. W. He, S. M. Bybee, M. Motyka, W. X. Bi, L. Podsiadlowski, X. Y. Li, L. Bocak, "Phylogenomic relationships of bioluminescent elateroids define the 'lampyroid' clade with clicking Sinopyrophoridae as its earliest member", *Syst. Entomol.* **2020**, *46*, 111–123.
- [183] Y.-D. Li, R. Kundrata, E. Tihelka, Z. Liu, D. Huang, C. Cai, "Cretophengodidae, a new Cretaceous beetle family, sheds light on the evolution of bioluminescence", *Proc. R. Soc. B* **2021**, *288*, 20202730.
- [184] Y. Oba, D. T. Schultz, "Firefly genomes illuminate the evolution of beetle bioluminescent systems", *Curr. Opin. Insect Sci.* **2022**, *50*, 100879.
- [185] Y. Oba, K. Konishi, D. Yano, H. Shibata, D. Kato, T. Shirai, "Resurrecting the ancient glow of the fireflies", *Sci. Adv.* **2020**, *6*, eabc5705.
- [186] M. Kheirabadi, Z. Sharafian, H. Naderi-Manesh, U. Heineman, U. Gohlke, S. Hosseinkhani, "Crystal structure of native and a mutant of *Lampyrus turkestanicus* luciferase implicate in bioluminescence color shift", *Biochim. Biophys. Acta Proteins Proteom.* **2013**, *1834*, 2729–2735.
- [187] V. R. Viviani, Y. Ohmiya, "Bioluminescence Color Determinants of *Phrixothrix* Railroad-worm Luciferases: Chimeric Luciferases, Site-directed Mutagenesis of Arg 215 and Guanidine effect", *Photochem. Photobiol.* **2000**, *72*, 267–271.
- [188] Y. Ando, K. Niwa, N. Yamada, T. Enomoto, T. Irie, H. Kubota, Y. Ohmiya, H. Akiyama, "Firefly bioluminescence quantum yield and colour change by pH-sensitive green emission", *Nat. Photonics* **2008**, *2*, 44–47.
- [189] O. Shimomura, T. Goto, F. H. Johnson, "Source of oxygen in the CO₂ produced in the bioluminescent oxidation of firefly luciferin", *Proc. Natl. Acad. Sci. USA* **1977**, *74*, 2799–2802.

- [190] B. R. Branchini, C. E. Behney, T. L. Southworth, D. M. Fontaine, A. M. Gulick, D. J. Vinyard, G. W. Brudvig, "Experimental Support for a Single Electron-Transfer Oxidation Mechanism in Firefly Bioluminescence", *J. Am. Chem. Soc.* **2015**, *137*, 7592–7595.
- [191] J. A. Sundlov, D. M. Fontaine, T. L. Southworth, B. R. Branchini, A. M. Gulick, "Crystal structure of firefly luciferase in a second catalytic conformation supports a domain alternation mechanism", *Biochemistry* **2012**, *51*, 6493–6495.
- [192] V. N. Petushkov, M. A. Dubinnyi, A. S. Tsarkova, N. S. Rodionova, M. S. Baranov, V. S. Kublitski, O. Shimomura, I. V. Yampolsky, "A Novel Type of Luciferin from the Siberian Luminous Earthworm *Fridericia heliota*: Structure Elucidation by Spectral Studies and Total Synthesis", *Angew. Chem.* **2014**, *126*, 5672–5674.
- [193] V. N. Petushkov, N. S. Rodionova, V. S. Bondar, "Study of the Luminescence System of the Soil Enchytraeid *Fridericia heliota* (Annelida: Clitellata: Oligochaeta: Enchytraeidae)", *Dokl. Biochem. Biophys.* **2003**, *391*, 204–207.
- [194] M. A. Dubinnyi, Z. M. Kaskova, N. S. Rodionova, M. S. Baranov, A. Yu. Gorokhovatsky, A. Kotlobay, K. M. Solntsev, A. S. Tsarkova, V. N. Petushkov, I. V. Yampolsky, "Novel Mechanism of Bioluminescence: Oxidative Decarboxylation of a Moiety Adjacent to the Light Emitter of *Fridericia* Luciferin", *Angew. Chem.* **2015**, *54*, 7065–7067.
- [195] Y.-Q. Tang, Y.-J. Liu, "Theoretical study on bioluminescent mechanism and process of Siberian luminous earthworm *Fridericia heliota*", *J. Photochem. Photobiol. A* **2019**, *380*, 111870.
- [196] Y. Oba, S.-I. Kato, M. Ojika, S. Inouye, "Biosynthesis of luciferin in the sea firefly, *Cypridina hilgendorffii*: L-tryptophan is a component in *Cypridina* luciferin", *Tetrahedron Lett.* **2002**, *43*, 2389–2392.
- [197] J. G. Morin, A. C. Cohen, "It's all about sex: Bioluminescent courtship displays, morphological variation and sexual selection in two new genera of caribbean ostracodes", *J. Crust. Biol.* **2010**, *30*, 56–67.
- [198] O. Shimomura, "The discovery of aequorin and green fluorescent protein", *J. Microsc.* **2005**, *217*, 3–15.
- [199] B.-W. Ding, P. Naumov, Y.-J. Liu, "Mechanistic Insight into Marine Bioluminescence: Photochemistry of the Chemiexcited *Cypridina* (sea firefly) Lumophore", *J. Chem. Theory and Comput.* **2015**, *11*, 591–599.

- [200] P. Naumov, C. Wu, Y.-J. Liu, Y. Ohmiya, "Spectrochemistry and artificial color modulation of *Cypridina* luminescence: Indirect evidence for chemiexcitation of a neutral dioxetanone and emission from a neutral amide", *Photochem. Photobiol. Sci.* **2012**, *11*, 1151–1155.
- [201] O. Shimomura, F. H. Johnson, "Peroxidized coelenterazine, the active group in the photoprotein aequorin", *Proc. Natl. Acad. Sci. U. S. A.* **1978**, *75*, 2611–2615.
- [202] O. Shimomura, F. H. Johnson, "Mechanisms in the Quantum Yield of *Cypridina* Bioluminescence", *Photochem. Photobiol.* **1970**, *12*, 291–295.
- [203] S. V. Markova, E. S. Vysotski, "Coelenterazine-Dependent Luciferases", *Biochemistry* **2015**, *80*, 714–732.
- [204] O. Shimomura, F. H. Johnson, T. Masugi, "Cypridina Bioluminescence: Light-Emitting Oxyluciferin-Luciferase Complex", *Science* **1969**, *164*, 1299–1300.
- [205] E. V. Ereemeeva, S. V. Markova, W. J. H. Van Berkel, E. S. Vysotski, "Role of key residues of obelin in coelenterazine binding and conversion into 2-hydroperoxy adduct", *J. Photochem. Photobiol. B, Biol.* **2013**, *127*, 133–139.
- [206] F. Krafft, "Phosphorus. From elemental light to chemical element", *Angew. Chem.* **1969**, *8*, 660–671.
- [207] N. A. Giffin, J. D. Masuda, "Reactivity of white phosphorus with compounds of the p-block", *Coord. Chem. Rev.* **2011**, *255*, 1342–1359.
- [208] R. J. van Zee, A. K. Khan, "A Striking Deuterium Effect in Phosphorus Chemiluminescence. Identification of the Emitting Species", *J. Am. Chem. Soc.* **1974**, *96*, 6805–6806.
- [209] B. R. Radziszewski, "Untersuchungen über Hydrobenzamid, Amarin und Lophin", *Ber. Dtsch. Chem. Ges.* **1877**, *10*, 70–75.
- [210] M. Trautz, "Studien über Chemilumineszenz", *Z. Phys. Chem.* **1905**, *53*, 1–111.
- [211] M. Trautz, P. Z. Schorigin, "Ueber Chemilumineszenz", *Wiss. Photog. Photochem.* **1905**, *3*, 121–130.
- [212] K. Gleu, W. Petsch, "Die Chemilumineszenz der Dimethyl-diacridyliumsalze", *Angew. Chem.* **1935**, *48*, 57–59.
- [213] V. Herbert Otto Albrecht, "Über die Chemilumineszenz des Aminophthalsäurehydrazids", *Z. Phys. Chem.* **1928**, *136*, 321–330.

- [214] E. A. Chandross, "A new Chemiluminescent System", *Tetrahedron Lett.* **1963**, *12*, 761–765.
- [215] W. Adam, D. V. Kazakov, V. P. Kazakov, "Singlet-oxygen Chemiluminescence in Peroxide Reactions", *Chem. Rev.* **2005**, *105*, 3371–3387.
- [216] I. Bronstein, P. McGrath, "Chemiluminescence lights up", *Nature* **1989**, *338*, 599–600.
- [217] I. Bronstein, B. Edwards, J. C. Voyta, "1,2-Dioxetanes: Novel Chemiluminescent Enzyme Substrates. Applications to Immunoassays.", *J. Biolumin. Chemilumin.* **1989**, *4*, 99–111.
- [218] A. P. Schaap, H. Akhavan, L. Romano, "Chemiluminescent substrates for alkaline phosphatase: Application to ultrasensitive enzyme-linked immunoassays and DNA probes", *Clin. Chem.* **1989**, *35*, 1863–1864.
- [219] G. J. Lofthouse, H. Suschitzky, B. J. Wakefield, R. A. Whittaker, B. Tuck, "Synthesis and Chemiluminescent Reactions of Some 3-Alkoxy carbamoyl-benzo[*b*]furan-2(3*H*)-ones", *J. Chem. Soc. Perkin Trans. 1* **1979**, 1634–1639.
- [220] G. Zomer, *Chemiluminescence and Bioluminescence: Past, Present and Future*, RSC, Cambridge, UK, **2011**.
- [221] E. A. Chandross, F. I. Sonntag, "A Novel Chemiluminescent Electron-Transfer Reaction", *J. Am. Chem. Soc.* **1964**, *86*, 3179–3180.
- [222] J.-Y. Koo, G. B. Schuster, "Chemically Initiated Electron Exchange Luminescence. A New Chemiluminescent Reaction Path for Organic Peroxides.", *J. Am. Chem. Soc.* **1977**, *99*, 6107–6109.
- [223] J.-Y. Koo, S. P. Schmidt, G. B. Schuster, "Bioluminescence of the firefly: Key steps in the formation of the electronically excited state for model systems", *Proc. Natl. Acad. Sci. U. S. A.* **1978**, *75*, 30–33.
- [224] J.-Y. Koo, G. B. Schuster, "Chemiluminescence of Diphenoyl Peroxide. Chemically Initiated Electron Exchange Luminescence. A New General Mechanism for Chemical Production of Electronically Excited States", *J. Am. Chem. Soc.* **1978**, *100*, 4496–4503.
- [225] S. P. Schmidt, G. B. Schuster, "Dioxetanone Chemiluminescence by the Chemically Initiated Electron Exchange Pathway. Efficient Generation of Excited Singlet States", *J. Am. Chem. Soc.* **1978**, *100*, 1966–1968.
- [226] G. B. Schuster, "Chemiluminescence of Organic Peroxides. Conversion of Ground-State Reactants to Excited-State Products by the Chemically Initiated Electron-Exchange Luminescence Mechanism", *Acc. Chem. Res.* **1979**, *12*, 366–373.

- [227] W. Adam, M. Matsumoto, A. V. Trofimov, "Viscosity Dependence of the Chemically Induced Electron-Exchange Chemiluminescence Triggered from a Bicyclic Dioxetane", *J. Am. Chem. Soc.* **2000**, *122*, 8631–8634.
- [228] W. Adam, I. Bronstein, A. V. Trofimov, R. F. Vasil'ev, "Solvent-Cage Effect (Viscosity Dependence) as a Diagnostic Probe for the Mechanism of the Intramolecular Chemically Initiated Electron-Exchange Luminescence (CIEEL) Triggered from a Spiroadamantyl-Substituted Dioxetane", *J. Am. Chem. Soc.* **1999**, *121*, 958–961.
- [229] W. Adam, A. V. Trofimov, "The Effect of *meta* versus *para* Substitution on the Efficiency of Chemiexcitation in the Chemically Triggered Electron-Transfer-Initiated Decomposition of Spiroadamantyl Dioxetanes", *J. Org. Chem.* **2000**, *65*, 6474–6478.
- [230] E. L. Bastos, S. M. Da Silva, W. J. Baader, "Solvent Cage Effects: Basis of a General Mechanism for Efficient Chemiluminescence", *J. Org. Chem.* **2013**, *78*, 4432–4439.
- [231] H. Isobe, Y. Takano, M. Okumura, S. Kuramitsu, K. Yamaguchi, "Mechanistic Insights in Charge-Transfer-Induced Luminescence of 1,2-Dioxetanones with a Substituent of Low Oxidation Potential", *J. Am. Chem. Soc.* **2005**, *127*, 8667–8679.
- [232] L. H. Catalan, T. Wilson, "Electron Transfer and Chemiluminescence. Two Inefficient Systems: 1,4-Dimethoxy-9,10-diphenylanthracene Peroxide and Diphenoyl Peroxide", *J. Am. Chem. Soc.* **1989**, *111*, 2633–2639.
- [233] T. Wilson, "Comments on the Mechanisms of Chemi- and Bioluminescence.", *Photochem. Photobiol.* **1995**, *62*, 601–606.
- [234] Y. Takano, T. Tsunesada, H. Isobe, Y. Yoshioka, K. Yamaguchi, I. Saito, "Theoretical Studies of Decomposition Reactions of Dioxetane, Dioxetanone, and Related Species. CT Induced Luminescence Mechanism revisited", *Bull. Chem. Soc. Jpn.* **1999**, *72*, 213–225.
- [235] L. Yue, Y.-J. Liu, W.-H. Fang, "Mechanistic Insight into the Chemiluminescent Decomposition of Firefly Dioxetanone", *J. Am. Chem. Soc.* **2012**, *134*, 11632–11639.
- [236] L. Yue, Z. Lan, Y.-J. Liu, "The Theoretical Estimation of the Bioluminescent Efficiency of the Firefly via a Nonadiabatic Molecular Dynamics Simulation", *J. Phys. Chem. Lett.* **2015**, *6*, 540–548.
- [237] B.-W.- Ding, P.- Naumov, Y.-J. Liu, "Mechanistic Insight into Marine Bioluminescence: Photochemistry of the Chemiexcited *Cypridina* (Sea Firefly) Lumophore", *J. Chem. Theory Comput.* **2015**, *11*, 591–599.

- [238] C.-G. Min, P. J. O. Ferreira, L. Pinto da Silva, "Theoretically Obtained Insight into the Mechanism and Dioxetanone Species Responsible for the Singlet Chemiexcitation of Coelenterazine", *J. Photochem. Photobiol. B, Biol.* **2017**, *174*, 18–26.
- [239] L. Pinto Da Silva, C. M. Magalhães, D. M. A. Crista, J. C. G. Esteves Da Silva, "Theoretical modulation of singlet/triplet chemiexcitation of chemiluminescent imidazopyrazinone dioxetanone *via* C₈-substitution", *Photochem. Photobiol. Sci.*, **2017**, *16*, 897–907.
- [240] L. Pinto Da Silva, R. F. J. Pereira, C. M. Magalhães, J. C. G. Esteves Da Silva, "Mechanistic Insight into *Cypridina* Bioluminescence with a Combined Experimental and Theoretical Chemiluminescent Approach", *J. Phys. Chem. B* **2017**, *121*, 7862–7871.
- [241] C. M. Magalhães, J. C. G. Esteves da Silva, L. Pinto da Silva, "Study of coelenterazine luminescence: Electrostatic interactions as the controlling factor for efficient chemiexcitation", *J. Lumin.* **2018**, *199*, 339–347.
- [242] L. Delafresnaye, F. R. Bloesser, K. B. Kockler, C. W. Schmitt, I. M. Irshadeen, C. Barner-Kowollik, "All Eyes on Visible-Light Peroxyoxalate Chemiluminescence Read-Out Systems", *Chem. Eur. J.* **2020**, *26*, 114–127.
- [243] M. C. Cabello, F. H. Bartoloni, W. J. Baader, "An Update on General Chemiexcitation Mechanisms in Cyclic Organic Peroxide Decomposition and the Chemiluminescent Peroxyoxalate Reaction in Aqueous Media", *Photochem. Photobiol.* **2023**, *99*, 235–250.
- [244] M. Yang, J. Huang, J. Fan, J. Du, K. Pu, X. Peng, "Chemiluminescence for bioimaging and therapeutics: Recent advances and challenges", *Chem. Soc. Rev.* **2020**, *49*, 6800–6815.
- [245] M. M. Rauhut, L. J. Bollyky, B. G. Roberts, M. Loy, R. H. Whitman, A. V. Iannotta, A. M. Semsel, R. A. Clarke, "Chemiluminescence from Reactions of Electronegatively Substituted Aryl Oxalates with Hydrogen Peroxide and Fluorescent Compounds", *J. Am. Chem. Soc.* **1967**, *89*, 6515–6522.
- [246] M. M. Rauhut, B. G. Roberts, A. M. Semsel, "A Study of Chemiluminescence from Reactions of Oxalyl Chloride, Hydrogen Peroxide, and Fluorescent Compounds", *J. Am. Chem. Soc.* **1966**, *88*, 3604–3617.
- [247] M. M. Rauhut, "Chemiluminescence from Concerted Peroxide Decomposition Reactions", *Acc. Chem. Res.* **1969**, *2*, 80–87.

- [248] L. J. Bollyky, R. H. Whitman, B. G. Roberts, M. M. Rauhut, "Chemiluminescence from Reactions of Oxalic Anhydrides with Hydrogen Peroxide in the Presence of Fluorescent Compounds", *J. Am. Chem. Soc.* **1967**, *89*, 6523–6526.
- [249] S. S. Tseng, A. G. Mohan, L. G. Haines, L. S. Vizcarra, M. M. Rauhut, "Efficient Peroxyoxalate Chemiluminescence from Reactions of *N*-(Trifluoromethylsulfonyl)oxamides with Hydrogen Peroxide and Fluorescers", *J. Org. Chem.* **1979**, *44*, 4113–4116.
- [250] H. F. Cordes, H. P. Richter, C. A. Heller, "Mass Spectrometric Evidence for the Existence of 1,2-Dioxetanedione (Carbon Dioxide Dimer). A Chemiluminescent Intermediate", *J. Am. Chem. Soc.* **1969**, *91*, 7209.
- [251] R. Bos, N. W. Barnett, G. A. Dyson, K. F. Lim, R. A. Russell, S. P. Watson, "Studies on the mechanism of the peroxyoxalate chemiluminescence reaction: Part 1. Confirmation of 1,2-dioxetanedione as an intermediate using ^{13}C nuclear magnetic resonance spectroscopy", *Anal. Chim. Acta* **2004**, *502*, 141–147.
- [252] S. A. Tonkin, R. Bos, G. A. Dyson, K. F. Lim, R. A. Russell, S. P. Watson, C. M. Hindson, N. W. Barnett, "Studies on the mechanism of the peroxyoxalate chemiluminescence reaction. Part 2. Further identification of intermediates using 2D EXSY ^{13}C nuclear magnetic resonance spectroscopy", *Anal. Chim. Acta* **2008**, *614*, 173–181.
- [253] L. F. M. L. Ciscato, F. H. Bartoloni, E. L. Bastos, W. J. Baader, "Direct Kinetic Observation of the Chemiexcitation Step in Peroxyoxalate Chemiluminescence", *J. Org. Chem.* **2009**, *74*, 8974–8979.
- [254] F. H. Bartoloni, M. A. De Oliveira, L. F. M. L. Ciscato, F. A. Augusto, E. L. Bastos, W. J. Baader, "Chemiluminescence Efficiency of Catalyzed 1,2-Dioxetanone Decomposition Determined by Steric Effects", *J. Org. Chem.* **2015**, *80*, 3745–3751.
- [255] F. A. Augusto, A. Francés-Monerris, I. Fdez Galván, D. Roca-Sanjuán, E. L. Bastos, W. J. Baader, R. Lindh, "Mechanism of activated chemiluminescence of cyclic peroxides: 1,2-dioxetanes and 1,2-dioxetanones", *Phys. Chem. Chem. Phys.* **2017**, *19*, 3955–3962.
- [256] S. M. Da Silva, A. P. Lang, A. P. F. Dos Santos, M. C. Cabello, L. F. M. L. Ciscato, F. H. Bartoloni, E. L. Bastos, W. J. Baader, "Cyclic Peroxidic Carbon Dioxide Dimer Fuels Peroxyoxalate Chemiluminescence", *J. Org. Chem.* **2021**, *86*, 11434–11441.
- [257] A. J. Schmitz, *Ueber das Hydrazid der Trimesinsäure und der Hemimellithsäure*, PhD Thesis, Heidelberg University, Heidelberg, Germany, **1902**.

- [258] K. Gleu, K. Pfannstiel, "Über 3-Aminophthalsäure-hydrazid", *J. Prakt. Chem.* **1936**, *146*, 137–150.
- [259] W. Specht, "Die Chemilumineszenz des Hämins, ein Hilfsmittel zur Auffindung und Erkennung forensisch wichtiger Blutspuren", *Dtsch. Z. ges. gerichtl. Med.* **1937**, *28*, 225–234.
- [260] F. Proescher, A. M. Moody, "Detection of blood by means of chemiluminescence", *J. Lab. Clin. Med.* **1939**, *24*, 1183–1189.
- [261] M. Mayer, S. Takegami, M. Neumeier, S. Rink, A. Jacobi von Wangelin, S. Schulte, M. Vollmer, A. G. Griesbeck, A. Duerkop, A. J. Baumner, "Electrochemiluminescence Bioassays with a Water-Soluble Luminol Derivative Can Outperform Fluorescence Assays", *Angew. Chem Int. Ed.* **2018**, *57*, 408–411.
- [262] A. G. Griesbeck, Y. Díaz-Miara, R. Fichtler, A. Jacobi von Wangelin, R. Pérez-Ruiz, D. Sampedro, "Steric Enhancement of the Chemiluminescence of Luminols", *Chem. Eur. J.* **2015**, *21*, 9975–9979.
- [263] P. Khan, D. Idrees, M. A. Moxley, J. A. Corbett, F. Ahmad, G. Von Figura, W. S. Sly, A. Waheed, M. I. Hassan, "Luminol-Based Chemiluminescent Signals: Clinical and Non-clinical Application and Future Uses", *Appl. Biochem. Biotechnol.* **2014**, *173*, 333–355.
- [264] C. A. Marquette, L. J. Blum, "Applications of the luminol chemiluminescent reaction in analytical chemistry", *Anal. Bioanal. Chem.* **2006**, *385*, 546–554.
- [265] M. T. Beck, F. Joó, "Mechanism of the Reaction between Luminol and molecular Oxygen", *Photochem. Photobiol.* **1972**, *16*, 491–497.
- [266] Y. B. Tsaplev, A. V. Trofimov, "Chemiluminescence in the Auto-Oxidation of Luminol in Dimethyl Sulfoxide: Kinetic Effects of Alkalis, Quenching by Nitroblue Tetrazolium, and Elimination of Quenching by Hydrogen Peroxide", *Russ. J. Phys. Chem.* **2020**, *94*, 2369–2374.
- [267] J. Lind, G. Merényi, T. E. Eriksen, "Chemiluminescence Mechanism of Cyclic Hydrazides such as Luminol in Aqueous Solutions", *J. Am. Chem. Soc.* **1983**, *105*, 7655–7661.
- [268] G. Merényi, J. Lind, T. E. Eriksen, "Luminol Chemiluminescence: Chemistry, Excitation, Emitter", *J. Biolumin. Chemilumin.* **1990**, *5*, 53–56.
- [269] A. Giussani, P. Farahani, D. Martínez-Muñoz, M. Lundberg, R. Lindh, D. Roca-Sanjuán, "Molecular Basis of the Chemiluminescence Mechanism of Luminol", *Chem. Eur. J.* **2019**, *25*, 5202–5213.
- [270] E. H. White, M. M. Bursey, "Chemiluminescence of Luminol and Related Hydrazides: The Light Emission Step", *J. Am. Chem. Soc.* **1964**, *86*, 941–942.

- [271] P. D. Wildes, E. H. White, "Differences between Excited States Produced Chemically and Photochemically. Ion Pairs of Excited States Derived from Luminol", *J. Am. Chem. Soc.* **1973**, *95*, 2610–2617.
- [272] C. Tanaka, J. Tanaka, "Ab Initio Molecular Orbital Studies on the Chemiluminescence of 1,2-Dioxetanes", *J. Phys. Chem. A* **2000**, *104*, 2078–2090.
- [273] E. Rodríguez, M. Reguero, "The DDCI Method Applied to Reactivity: Chemiluminescent Decomposition of Dioxetane", *J. Phys. Chem. A* **2002**, *106*, 504–509.
- [274] P. Farahani, D. Roca-Sanjuán, F. Zapata, R. Lindh, "Revisiting the Nonadiabatic Process in 1,2-Dioxetane", *J. Chem. Theory Comput.* **2013**, *9*, 5404–5411.
- [275] L. De Vico, Y.-J. Liu, J. W. Krogh, R. Lindh, "Chemiluminescence of 1,2-dioxetane. Reaction mechanism uncovered", *J. Phys. Chem. A* **2007**, *111*, 8013–8019.
- [276] W. Adam, *Chemical and Biological Generation of Excited States*, Academic Press, Cambridge, MA, **1982**.
- [277] W. J. Baader, C. V. Stevani, E. L. Bastos, *The Chemistry of Peroxides*, John Wiley & Sons, Ltd., Hoboken, NJ, **2006**.
- [278] M. A. El-Sayed, "Spin-Orbit Coupling and the Radiationless Processes in Nitrogen Heterocyclics", *J. Chem. Phys.* **1963**, *38*, 2834–2838.
- [279] M. A. El-Sayed, "The Triplet State: Its Radiative and Nonradiative Properties", *Acc. Chem. Res.* **1968**, *1*, 8–16.
- [280] K. R. Kopecky, J. H. van de Sande, C. Mumford, "Preparation and Base-Catalyzed Reactions of Some β -Halohydroperoxides", *Can. J. Chem.* **1968**, *46*, 25–34.
- [281] K. R. Kopecky, C. Mumford, "Luminescence in the Thermal Decomposition of 3,3,4-trimethyl-1,2-dioxetane", *Can. J. Chem.* **1969**, *47*, 709–711.
- [282] J. H. Wieringa, J. Strating, H. Wynberg, W. Adam, "Adamantylideneadamantane peroxide, a stable 1,2-dioxetane.", *Tetrahedron Lett.* **1972**, *2*, 169–172.
- [283] S. Gnaim, A. Scomparin, S. Das, R. Blau, R. Satchi-Fainaro, D. Shabat, "Direct Real-Time Monitoring of Prodrug Activation by Chemiluminescence", *Angew. Chem.* **2018**, *57*, 9171–9175.

- [284] S. Gnaim, O. Green, D. Shabat, "The emergence of aqueous chemiluminescence: New promising class of phenoxy 1,2-dioxetane luminophores", *Chem. Comm.* **2018**, *54*, 2073–2085.
- [285] C. Peukert, S. Popat Gholap, O. Green, L. Pinkert, J. van den Heuvel, M. van Ham, D. Shabat, M. Brönstrup, "Enzyme-Activated, Chemiluminescent Siderophore-Dioxetane Probes Enable the Selective and Highly Sensitive Detection of Bacterial Pathogens", *Angew. Chem. Int. Ed* **2022**, *61*, 1–13.
- [286] B. Matuszczak, "Linear and Cyclic *N*-acetyl- α -aryl-glycines: Synthesis and Chemiluminescence Studies", *Monatsh. Chem.* **1996**, *127*, 1291–1303.
- [287] B. Matuszczak, "Zur Chemilumineszenz von *N*-Acyl- α -Arylglycinen: Anwendungsmöglichkeiten für die klinisch-chemische Analytik", *Pharmazie* **1996**, *51*, 862–865.
- [288] B. Matuszczak, "Linear and Cyclic *N*-Acyl- α -Arylglycines III. Synthesis and Chemiluminescence Studies of Naphthol and Phenanthrol Amidoalkylation Products", *Monatsh. Chem.* **1997**, *128*, 945–951.
- [289] B. Matuszczak, "Linear and Cyclic *N*-Acyl- α -Arylglycines. IV. Novel 3-Substituted 3-Acylaminobenzo[*b*]furan-2(3*H*)-ones: Synthesis and Chemiluminescence Studies", *J. Prakt. Chem.* **1998**, *340*, 20–25.
- [290] R. Krieg, B. Hoffmann, D. Weiß, C. Biskup, "First Synthesis of Highly Chemiluminescent Benzo[*b*]furan-2(3*H*)-ones Bearing a Urea Substructure", *Helv. Chim. Acta* **2019**, *102*, 1–20.
- [291] S. Schramm, D. Weiß, I. Navizet, D. Roca-Sanjuán, H. Brandl, R. Beckert, H. Görls, "Investigations on the synthesis and chemiluminescence of novel 2-coumaranones", *ARKIVOC* **2013**, 174–188.
- [292] S. Schramm, L. F. M. L. Ciscato, P. Oesau, R. Krieg, J. F. Richter, I. Navizet, D. Roca-Sanjuán, D. Weiss, R. Beckert, "Investigations on the synthesis and chemiluminescence of novel 2-coumaranones - II", *ARKIVOC* **2015**, *2015*, 44–59.
- [293] S. Schramm, I. Navizet, P. Naumov, N. K. Nath, R. Berraud-Pache, P. Oesau, D. Weiss, R. Beckert, "The Light Emitter of the 2-Coumaranone Chemiluminescence: Theoretical and Experimental Elucidation of a Possible Model for Bioluminescent Systems", *Eur. J. Org. Chem.* **2016**, *2016*, 678–681.
- [294] S. Schramm, I. Navizet, D. Prasad Karothu, P. Oesau, V. Bensmann, D. Weiss, R. Beckert, P. Naumov, "Mechanistic investigations of the 2-coumaranone chemiluminescence", *Phys. Chem. Chem. Phys.* **2017**, *19*, 22852–22859.

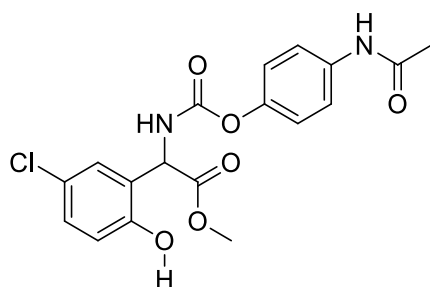
- [295] Schramm S, *Die Chemilumineszenz der 2-Coumaranone: Synthese, Lumineszenzmechanismus und Applikation*, PhD Thesis, Friedrich-Schiller University, Jena, **2016**.
- [296] C. Molinaro, P. G. Bulger, E. E. Lee, B. Kosjek, S. Lau, D. Gauvreau, M. E. Howard, D. J. Wallace, P. D. O'Shea, "CRTH2 antagonist MK-7246: A synthetic evolution from discovery through development", *J. Org. Chem.* **2012**, *77*, 2299–2309.
- [297] I. Nicolas, O. Jeannin, D. Pichon, M. Fourmigué, "Dibromohydantoins as halogen bond (XB) donors: a route toward the introduction of chirality in halogen bonded systems", *CrystEngComm* **2016**, *18*, 9325–9333.
- [298] K. Y. Chegaev, A. N. Kravchenko, O. V. Lebedev, Y. A. Strelenko, "New functional glycoluril derivatives", *Mendeleev Commun.* **2001**, *11*, 32–33.
- [299] A. N. Kravchenko, E. Y. Maksareva, P. A. Belyakov, A. S. Sigachev, K. Y. Chegaev, K. A. Lyssenko, O. V. Lebedev, N. N. Makhova, "Synthesis of 2-monofunctionalized 2,4,6,8-tetraazabicyclo[3.3.0]octane-3,7-diones", *Russ. Chem. Bull.* **2003**, *52*, 192–197.
- [300] T. Lippold, A. G. Griesbeck, R. Herzhoff, M. S. Wickleder, L. Straub, N. T. Flosbach, "5-Chlorocoumaranone-Conjugates as Chemiluminescent Protecting Groups (CLPG) and Precursors to Fluorescent Protecting Groups (FPG)", *Photochem* **2023**, *3*, 373–389.
- [301] L. Konnert, F. Lamaty, J. Martinez, E. Colacino, "Recent Advances in the Synthesis of Hydantoins: The State of the Art of a Valuable Scaffold", *Chem. Rev.* **2017**, *117*, 13757–13809.
- [302] R. Graf, "Umsetzungen mit *N*-Carbonyl-sulfamidsäure-chlorid, II) Alkohole und Phenole", *Chem. Ber.* **1963**, *96*, 56–67.
- [303] R. Young-Soy, U. Soo-Jong, J. Min-Sook, L. Joo-Dong, R. Hee-Chang, S. Jeong-Kuan, K. Hyo-Jung, K. Hyuk, J. Sung-Won, H. Hye-Sook, P. Si-Ho, K. Seong-Ho, *Retinol Derivatives and Process for Preparing Same*, **2002**, WO 02/057212 A1.
- [304] B. Loev, M. F. Kormendy, "An Improved Synthesis of Carbamates", *J. Org. Chem.* **1963**, *28*, 3421–3426.
- [305] V. Sanz, S. De Marcos, J. R. Castillo, J. Galbán, "Application of Molecular Absorption Properties of Horseradish Peroxidase for Self-Indicating Enzymatic Interactions and Analytical Methods", *J. Am. Chem. Soc.* **2005**, *127*, 1038–1048.

- [306] A. M. Azevedo, V. C. Martins, D. M. F. Prazeres, V. Vojinović, J. M. S. Cabral, L. P. Fonseca, "Horseradish peroxidase: A valuable tool in biotechnology", *Biotechnol. Annu. Rev.* **2003**, 9, 199–247.
- [307] K. Beyzavi, S. Hampton, P. Kwasowski, S. Fickling, V. Marks, R. Clift, "Comparison of horseradish peroxidase and alkaline phosphatase-labelled antibodies in enzyme immunoassays", *Ann. Clin. Biochem.* **1987**, 24, 145–152.
- [308] Y. P. Chau, K. S. Lu, "Investigation of the Blood-Ganglion Barrier Properties in Rat Sympathetic Ganglia by using Lanthanum Ion and Horseradish Peroxidase as Tracers", *Acta Anat.* **1995**, 153, 135–144.
- [309] J. E. Brunet, G. A. Gonzalez, C. P. Sotomayor, "Intremolecular Tryptophan Heme Energy Transfer in Horesradish Peroxidase", *Photochem. Photobiol.* **1983**, 38, 253–254.
- [310] D. G. Pina, A. V. Shnyrova, F. Gavilanes, A. Rodríguez, F. Leal, M. G. Roig, I. Y. Sakharov, G. G. Zhadan, E. Villar, V. L. Shnyrov, "Thermally induced conformational changes in horseradish peroxidase", *Eur. J. Biochem.* **2001**, 268, 120–126.
- [311] W. E. Blumberg, J. Peisach, B. A. Wittenberg, J. B. Wittenberg, "The Electronic Structure of Protoheme Proteins I. An Electron paramagnetic Resonance and optical Study of Horseradish Peroxidase and its Derivatives", *J. Biol. Chem.* **1968**, 243, 1854–1862.
- [312] M. J. Frisch, G. W. Trucks, H. B. Schlegel, G. E. Scuseria, M. A. Robb, J. R. Cheeseman, G. Scalmani, V. Barone, G. A. Petersson, H. Nakatsuji, X. Li, M. Caricato, A. V. Marenich, J. Bloino, B. G. Janesko, R. Gomperts, B. Mennucci, H. P. Hratchian, J. V. Ortiz, A. F. Izmaylov, J. L. Sonnenberg, D. Williams-Young, F. Ding, F. Lipparini, F. Egidi, J. Goings, B. Peng, A. Petrone, T. Henderson, D. Ranasinghe, V. G. Zakrzewski, J. Gao, N. Rega, G. Zheng, W. Liang, M. Hada, M. Ehara, K. Toyota, R. Fukuda, J. Hasegawa, M. Ishida, T. Nakajima, Y. Honda, O. Kitao, H. Nakai, T. Vreven, K. Throssell, J. A. , Jr. Montgomery, J. E. Peralta, F. Ogliaro, M. J. Bearpark, J. J. Heyd, E. N. Brothers, K. N. Kudin, V. N. Staroverov, T. A. Keith, R. Kobayashi, J. Normand, K. Raghavachari, A. P. Rendell, J. C. Burant, S. S. Iyengar, J. Tomasi, M. Cossi, J. M. Millam, M. Klene, C. Adamo, R. Cammi, J. W. Ochterski, R. L. Martin, K. Morokuma, O. Farkas, J. B. Foresman, D. J. Fox, *Gaussian 16*, Gaussian, Inc., Wallingford CT, **2016**.
- [313] A. D. Becke, "Density-functional thermochemistry. III. The role of exact exchange", *J. Chem. Phys.* **1993**, 98, 5648–5652.
- [314] G. A. Petersson, A. Bennett, T. G. Tensfeldt, M. A. Al-Laham, W. A. Shirley, J. Mantzaris, "A complete basis set model chemistry. I. The total energies of closed-shell atoms and hydrides of the first-row elements", *J. Phys. Chem.* **1988**, 89, 2193–2218.

- [315] M. D. Hanwell, D. E. Curtis, D. C. Lonie, T. Vandermeersch, E. Zurek, G. R. Hutchison, "Avogadro: an advanced semantic chemical editor, visualization, and analysis platform", *J. Cheminformatics* **2012**, *4*, 1–17.
- [316] J. Tomasi, B. Mennucci, R. Cammi, "Quantum Mechanical Continuum Solvation Models", *Chem. Rev.* **2005**, *105*, 2999–3093.

9. Appendix

9.1 Data of X-ray crystal measurements



376

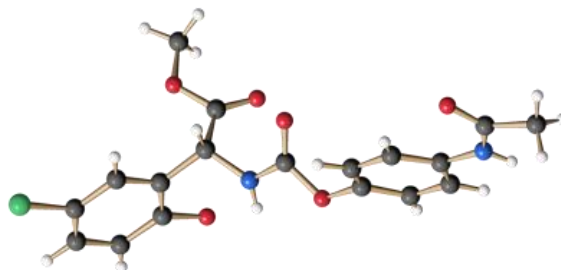
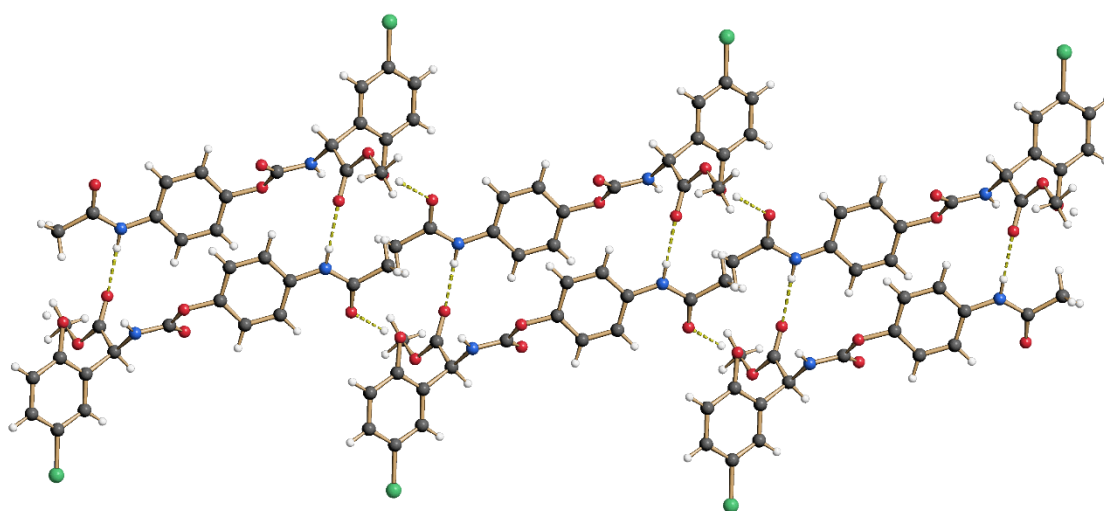


Table 100: Crystal data and structure refinement of **376**.

Moiety formula	$C_{18}H_{17}ClN_2O_6$
Formula weight	392.78
Temperature	100(2) K
Wavelength	1.54178 Å
Crystal system	Triclinic
Space group	P-1
Unit cell dimensions	$a = 7.4238(6)$ Å, $\alpha = 75.188(3)^\circ$.
	$b = 10.4320(9)$ Å, $\beta = 82.478(3)^\circ$.
	$c = 11.8407(10)$ Å, $\gamma = 87.684(3)^\circ$.
Volume	878.88(13) Å ³
Z	2
Density (calculated)	1.484 Mg/m ³
Absorption coefficient	2.285 mm ⁻¹
F(000)	408
Crystal size	0.100 x 0.030 x 0.020 mm ³
Index ranges	$-9 \leq h \leq 9$, $-12 \leq k \leq 12$, $-14 \leq l \leq 14$
Collected / Independent reflections	44702 / 3450 [R(int) = 0.0436]
Data / restraints / parameters	3450 / 0 / 258
Goodness-of-fit on F2	1.031
Final R indices [I > 2σ(I)]	R1 = 0.0335, wR2 = 0.0878
R indices (all data)	R1 = 0.0347, wR2 = 0.0890
Largest diff. peak and hole	0.396 and -0.298 e.Å ⁻³



10. Erklärung zur Dissertation

Gemäß der Promotionsordnung vom 12. März 2020

Hiermit versichere ich an Eides statt, dass ich die vorliegende Dissertation selbstständig und ohne die Benutzung anderer als der angegebenen Hilfsmittel und Literatur angefertigt habe. Alle Stellen, die wörtlich oder sinngemäß aus veröffentlichten und nicht veröffentlichten Werken dem Wortlaut oder dem Sinn nach entnommen wurden, sind als solche kenntlich gemacht. Ich versichere an Eides statt, dass diese Dissertation noch keiner anderen Fakultät oder Universität zur Prüfung vorgelegen hat; dass sie - abgesehen von unten angegebenen Teilpublikationen und eingebundenen Artikeln und Manuskripten - noch nicht veröffentlicht worden ist sowie, dass ich eine Veröffentlichung der Dissertation vor Abschluss der Promotion nicht ohne Genehmigung des Promotionsausschusses vornehmen werde. Die Bestimmungen dieser Ordnung sind mir bekannt. Darüber hinaus erkläre ich hiermit, dass ich die Ordnung zur Sicherung guter wissenschaftlicher Praxis und zum Umgang mit wissenschaftlichem Fehlverhalten der Universität zu Köln gelesen und sie bei der Durchführung der Dissertation zugrundeliegenden Arbeiten und der schriftlich verfassten Dissertation beachtet habe und verpflichte mich hiermit, die dort genannten Vorgaben bei allen wissenschaftlichen Tätigkeiten zu beachten und umzusetzen. Ich versichere, dass die eingereichte elektronische Fassung der eingereichten Druckfassung vollständig entspricht.

Teilpublikationen:

T. Lippold, A. G. Griesbeck, R. Herzhoff, M. S. Wickleder, L. Straub, N. T. Flosbach, "5-Chlorocoumaranone-Conjugates as Chemiluminescent Protecting Groups (CLPG) and Precursors to Fluorescent Protecting Groups (FPG)" *Photochem* **2023**, 3, 373-389.

Datum, Name und Unterschrift

30.10.2023, Tim Michael Lippold,



11. Curriculum vitae

Tim Lippold

Chemiker (M.Sc.)

Nationalität: deutsch

Geboren am 15. Dezember 1990 in Neuss, Deutschland

BERUFLICHER WERDEGANG

05/2019 – Heute

WISSENSCHAFTLICHER MITARBEITER

- Universität zu Köln
- Übungsgruppenleiter für organische Chemie
- Betreuung von organisch-chemischen Praktika

02/2017 – 06/2017
08/2015 – 01/2016

STUDENTISCHE HILFSKRAFT

- Universität zu Köln
- Wissenschaftliche und analytische Arbeit im Arbeitskreis von Dr. Nils Schlörer
- Betreuung von organisch-chemischen Praktika

08/2013 – 09/2013
03/2012 – 09/2012

LABORASSISTENT

- Silesia Gerhard Hanke GmbH & Co. KG
- Zusammenstellung von Aromen nach Rezeptvorlage
- Sensorische Schulung
- Einführung in SAP®ERP

07/2010 – 07/2011

ZIVILDienst

- Lukaskrankenhaus, Neuss
- Zentralsterilisation
- Einwöchiges Seminar zur politischen Bildung in Trier

AUSBILDUNG

Seit 05/2019

CHEMIE PROMOTION

- Universität zu Köln; Betreuer: Prof. Dr. Axel G. Griesbeck
- Thema: Protection and release of small molecules via chemiluminescent protection groups (CLPG)

04/2016 – 02/2019

CHEMIE MASTER

- Universität zu Köln
- Abschlussnote: 1.3 (6 Semester)

10/2012 – 06/2016

CHEMIE BACHELOR

- Universität zu Köln
- Abschlussnote: 1.9 (7 Semester)

08/2001 – 06/2010

ABITUR

- Gymnasium Norf, Neuss; Abitur mit Latinum, Abschlussnote: 2.7

1997 – 2001

GRUNDSCHULAUSBILDUNG

- St. Peter Grundschule Rosellen, Neuss

KONFERENZBEITRÄGE

- [1] 27. Lecture Conference on Photochemistry (GDCh), 2020, Online-Konferenz, Poster.
- [2] International Chemical Congress of Pacific Basin Societies, 2021, Online-Konferenz, Poster.
- [3] 28th IUPAC Symposium on Photochemistry, 2022, Amsterdam, Niederlande, Poster.
- [4] 28. Lecture Conference on Photochemistry (GDCh), 2022, Düsseldorf, Deutschland, Poster.
- [5] 31st International Conference on Photochemistry, 2023, Sapporo, Japan, Vortrag.

VERÖFFENTLICHUNGEN

- [1] A. G. Griesbeck, B. Goldfuss, C. Jäger, T. Lippold, M. Kleczka, "Strong Asymmetry in the Peroxide Bifurcation Mechanism: The Large-Group Effect in the Singlet Oxygen Ene Reaction with Allylic Alcohols" *ChemPhotoChem* **2017**, 1, 213-221.
- [2] M. Atar, B. Öngel, H. Riedasch, T. Lippold, J. M. Neudörfl, D. Sampedro, A. G. Griesbeck, "Intra- and Intermolecular Fluorescence Quenching of Alkylthio-Substituted Phthalimides by Photoinduced Electron Transfer: Distance, Position and Conformational Dependence" *ChemPhotoChem* **2020**, 4, 89-97.
- [3] T. Lippold, J. M. Neudörfl, A. G. Griesbeck, "New Acridone- and (Thio)Xanthone-Derived 1,1-Donor-Acceptor-Substituted Alkenes: pH-Dependent Fluorescence and Unusual Photooxygenation Properties" *Molecules* **2021**, 26, 3305.
- [4] T. Lippold, A. G. Griesbeck, R. Herzhoff, M. S. Wickleder, L. Straub, N. T. Flosbach, "5-Chlorocoumaranone-Conjugates as Chemiluminescent Protecting Groups (CLPG) and Precursors to Fluorescent Protecting Groups (FPG)" *Photochem* **2023**, 3, 373-389.

AUSZEICHNUNGEN UND ZUSATZQUALIFIKATIONEN

Fortbildung „Lehren und Lernen im Labor“, Mai, 2015, Köln.

GMP-Grundlagenkurs, August 2021 (inklusive Zertifikat).

Preis der Lehre: Chemie-Seminar für Mediziner, WS22/23, Köln.

ORT, DATUM

Tim Lippold

Köln, 30.10.23

